Investigating the expression and function of Complement Receptor 1 (CR1) on iPS derived microglia

Bethany Jane Marshall Shaw

Thesis presentation for the degree of Doctor of Philosophy (Medicine)

2022

i) Acknowledgments

Firstly, I would like to express my gratitude to the UKDRI for funding this project and for being an excellent centre to work in. I would also like to thank Professor Paul Morgan for giving me the opportunity to undertake my PhD in his lab and for all the support and guidance given throughout my project. I would like the thank Professor Nick Allen for his support with iPS culture work and and Professor Phil Taylor for their advice and support. Additionally, I would like to thank Dr. Kimberly Jones for iPS neuronal protein samples, Dr. Nina Storbel for her iPS neuronal RNA and Dr. Jincy Winston for her support in iPS astrocyte culturing. Thanks to Dr Emma Cope for her assistance in the CRISPR.

From the stem cell team I would like to thank Emily, Nina, Elisa and Jincy who offered an essential supportive network which without would have made this project even more challenging. I am incredibly grateful for all the support given from going over data together to our social diners and for the occasional weekend cell feeds. From the complement group I would like to thank Sarah, Rob and Wiola for always offering a helping hand. Thank you to Dina and Megan for their positive encouragement and brightening up the harder lab days. I would like to offer a special thanks to Nikoleta, for her incredible knowledge, endless encouragement, and constant support.

I would like to thank the YYMCA- Roanne, Pete, Jack, Owen, Ed and Barbara who helped reduce some of the PhD stresses with much cheese, wine and Strongbow dark fruits. Without their support and friendship, I might have gone insane. Thanks to KAB, who have been with me since the beginning of my scientific journey, from undergraduate to the end of my thesis they have been an essential support network and without whom I would be lost. Thanks to Tara for being always supportive.

I am extremely grateful to the support from my mum, Jane, who suffered through many long phone calls and responded with only praise and encouragement. I would like to thank my brother, Ross for his support.

ii) Summary

Objectives: GWAS has identified the gene encoding Complement receptor 1 (CR1/CD35) as a high risk locus for the development of Alzheimer's disease (AD)[1–3]. CR1 is a receptor and regulator of the complement system, involved in immune complex handling and as co-factor for Factor I (FI) mediated breakdown of C3b[4,5]. Studies of expression of CR1 within the CNS have been contradictory, some reporting no expression[1,5–7]. We aimed to investigate the expression of CR1 on CNS cells using induced pluripotent stem cells (iPSC) differentiated to glia. To confirm expression and test function, CR1 KO iPS clones were generated and differentiated.

Methods: iPSC were differentiated to microglia and astrocytes using adaptions of published protocols. Expression of CR1 transcript was tested with RT-qPCR and protein using immunofluorescence and western blotting. CR1 was knocked out using CRISPR Cas9. CR1 KO and CR1 WT iPS lines were differentiated to microglia for testing in functional assays, including phagocytosis of pH-Rodo e-coli bioparticles and pro-inflammatory transcript response following acute LPS stimulation.

Results: CR1 was expressed on iPS microglia but not on iPS astrocytes. CR1 KO clones were generated and differentiated to microglia. Acute LPS stimulation of CR1 KO and CR1 WT iPS microglia revealed significantly less TNFα and IL-6 transcript in KO compared to WT cells. In phagocytosis assays, CR1 KO microglia showed a significant reduction in uptake of e-coli bioparticles compared to CR1 WT when the particles were serum opsonised but not in the absence of opsonisation or when the serum source was depleted of FI.

Conclusions: We demonstrate that CR1 is expressed on iPS-derived microglia confirmed by CRISPR KO. Functional assays showed an impact of CR1 expression on key iPS microglia functions that are relevant to AD pathology. Together the data provide a starting point to understanding how CR1 variants impact AD pathogenesis.

iii) Abbreviations

ΔΔCT	Delta Delta cycle threshold
AD	Alzheimers Disease
ACH	Amyloid Cascade Hypothesis
ACM	Astrocyte Conditioned Media
ACTβ	Actin β
ADAM10	A Disintegrin and metalloproteinase domain-containing protein 10
ADF	Advanced DMEM/F12 supplemented
AGM	Aorta-Gonad Mesonphros
AICD	Amyloid Precursor Protein intracellular Domain
ALS	Amyotrophic Lateral Sclerosis
AMD	age-dependent macular degeneration
AP	Alternative Pathway
APC	Astrocyte precursor cell
Apoe	Apolipoprotein
APP	Amyloid precursor protein
ASC	Apoptosis-associated speckle like protein containing a CARD
Aβ	Amyloid-β
BACE1	Beta-Secretase 1
BIN1	Bridging Integrator 1
BMP4	Bone Morphogenetic Protein 3
BSA	Bovine Serum Albumin
C1	Complement factor 1
C1INH	Complement Inhibitor
C1INH	Complement Inhibitor
C2	Complement factor 2
C3	Complement factor 3
C4	Complement factor 4
C3	Complement factor 3
C4	Complement factor 4
C5	Complement factor 5
C6	Complement factor 6
C7	Complement factor 7
C8	Complement factor 8
C9	Complement factor 9
CAA	Cerebral amyloid angiopathy
CCP	Complement Control Protein
CD11b	Cluster of differentiation 11b
CD14	Cluster of differentiation 14
CD200	Cluster of differentiation 200
CD200R	Cluster of differentiation 200 Receptor
CD68	Cluster of differentiation 68
CDK5	Cyclin dependent Kindase
cDNA	Complementary DNA

Clu	Clusterin
CNS	Central Nervous System
CNTF	Ciliary Neurotrophic factor
CP	Classical pathway
CR1	Complement Receptor 1 (CD35)
CR2	Complement Receptor 2
CR3	Complement Receptor 3
CR4	Complement Receptor 4
CRISPR	Clustered Regularly Interspaced Palidromic Repeats
crry	Complement receptor 1 related protein y
CSF	Cerebral spinal fluid
CVF	Cobra Venom Factor
CX3CR1	C-X3-C Motif Chemokine Receptor 1
Cyto-D	Cytochalasin D
DDD	dense deposit disease
DEAE	Diethylaminoethyl chromotography
dH_20	Distilled water
DKK1	Dickkopf WNT signalling Pathway Inhibitor 1
DNA	Deoxyribonucleic acid
DSB	Double Stranded Break
EAAT2	Excitatory Amino Acid Transporter 2
EB	Embryo Body
ECL	Enhanced Chemiluminescence
EGF	Epidermal Growth Factor
EJ	Exon Junction
ELISA	Enzyme-Linked Immunosorbent Assay
EMP	Erythro Myeloid Precursor
EOAD	Early Onset Alzheimer Disease
FB	Factor B
FD	Factor D
FGF_2	Fibroblast Growth Factor
FH	Factor H
FI	Factor I
GAPDH	Glyceraldehyde-3-Phosphate Dehydrogenase
GFAP	Glial Fibrillary Acidic Protein
GM-CSF	Granulocyte-Macrophage colony stimulating factor
gRNA	guide RNA
GWAS	Genome Wide Association Studies
HDR	Homology Directed Repair
HPRT	Hypoxanthine Phosphoribosyltransferase 1
Iba-1	Ionized calcium binding adaptor molecule 1
HRP	Horse radish Peroxidase
ICM	Inner Cell Mass
IHC	ImmunoHistoChemistry
IL-1β	Interleukin 1 β

IL-3	Interleukin
IL-34	Interleukin 34
IL-6	Interleukin 6
INPP5D	Inositol Polyphosphate-5-Phosphatase D
iPS Pre	iPS Precursor cells
iPSC	Induced Pluripotent Stem Cell
KO	Knock Out
LCIB	Live Cell Imaging Buffer
LHR	Long Homologous Repeat
LOAD	Late Onset Alzheimer Disease
LP	Lectin Pathway
LPS	Lipopolysaccharide
MAC	Membrane Attack Complex
MASP	Mannan-binding lectin serine protease
MBL	Mannose Binding Lectin
MCI	Mild Cognitive Impairment
MCP	Membrane Cofactor Protein
M-CSF	Macrophage Colony Stimulating Factor
mRNA	Messager Ribonucelo acid
MS	Multiple Sclerosis
NFT	Neurofibril tangles
NFκB	Nuclear Factor Kappa B
NHEJ	Non homologous End Joining
NHS	Normal Human Serum
NLRP3	NLR Family Pyrin Domain Containing 3
NMD	Nonsense Mediated Decay
NLR	Nod Like Receptor
NOS	Nitric Oxide Synthesis
NSAIDs	Non-Steroidal anti inflammatory drugs
OCT	Octamer-binding Transcription Factor 2
P2RY12	Prionogenic Receptor
PBS	Phosphate Buffered Saline
PCR	Polymerase Chain Reaction
PDL	Poly-D-Lysine
PenStrep	Penicillin and Dihydrostreptomycin
PET	Positron Emission Topography
PRR	Pattern Recognition Receptor
PSEN	Presenilin
PTC	Premature Termination Codon
RCA	Regulators of Complement Activation
RI	Rock Inhibitor (Y27632)
RIPA	Radioimmunoprecipitation Assay buffer
RNA	Ribonucleic acid
RNP	Ribonucleoprotein
RT-Qpcr	Reverse Transcriptase PCR
SCF	Stem Cell Factors
SCR	Short Consensus repeats
sCR1	soluble CR1

SDHA	Succinate Dehydrogenase Complex Flavoprotein Subunit A
SDS	Sodium Dodecyl Sulphate
SNP	Single Nucleotide Polymorphism
SSEA3	Stage-Specific Embryonic Antigen 3
TALEN	Transcription activator-like effector nucleases
TGFβ	Transforming Growth Factor Beta
TLR	Toll Like Receptor
TMEM119	Transmembrane Protein 119
TNFα	Tumor Necrosis Factor alpha
TP	Terminal Pathway
TREM2	Triggering Receptor Expressed On Myeloid Cells 2
TUNEL	Terminal Deoxynucleotidyl Transferase dUTP nuck end labelling
UBC	Ubiquitin C
VEGF	Vascular Endothelial Growth Factor A
VTN	Vitronectin
YS	Yolk Sac
ZFN	Zinc Finger Nucleases

Table of Contents

1.0 Introduction

1.1 Dementia

Dementia was first accepted as a medical disorder in 1798, when French physician Phillipe Pinel published his classification of mental disorders[1,3]. In this, he gives one of the first descriptions of dementia and is often credited with coining the term. Derived from Latin, dementia can be broken down to its prefix *'de-'* meaning 'out' , *'ment'* referring to 'the mind' and *'-ia-'* being used when referring 'to a state', translating *dementia* to 'a state out of one's mind'[1,3]. Although this accurately reflects the observed symptoms of end stage dementia it does not reflect the progressive disease process'. Therefore, a better description for dementia would be 'a slow deterioration of cognitive capabilities, that is a direct result of disease processes in the brain'[1,3–5].

Dementia can present itself through various symptoms, depending on the causative disease and disease progression. The most common symptom is a loss of memory, with individuals not recognizing familiar places or people. However symptoms can include loss of other cognitive and psychological capabilities including; disorientation, difficulty in completing familiar tasks, trouble following conversation or difficulties with spatial awareness and motor function[3]. With time these symptoms become increasingly severe and frequent, ultimately resulting in a patient being unable to care for themselves[1,3]. An example of this deterioration is mapped throughout the Shakespeare tragedy, King Lear, in which the old king is considered to present symptoms of dementia[6,7]. During the play King Lear is shown to erupt into uncontrollable rages, make multiple irrational decisions, have displays of confusion, several visual hallucinations and significant memory loss, accumulating in a confused mad king who proclaims, 'who is it, that can tell me who I am?' This decline and subsequent loss of self is typical in dementia[6,7].

Dementia can be a result of multiple neurological disorders. In the King Lear example, his symptoms are thought to be inspired by Lewy Body dementia[6,7]. This makes up the second most common dementia-causing disease and results from aggregation of protein deposits called Lewy Bodies that disrupt the brain network[8,9]. However, there are multiple other diseases which can result in dementia including, but not limited to; Parkinson's Disease, HIV, head trauma, B12 deficiency and Vascular Picks disease[1]. The most common of these is Alzheimer's disease[2,10,11].

1.2 Alzheimer's Disease

Alzheimer's disease (AD) makes up 60%-70% of 50 million global dementia cases. In the UK the number of people diagnosed with AD between 2005 and 2016 increased by 115% and is expected to continue to climb[12]. Most of these cases occur post age 65 and are diagnosed as Late Onset Alzheimer's Disease (LOAD), while 5% of these occur before 65, diagnosing these patients with Early Onset Alzheimer's Disease (EOAD)[13].

The first known recorded case of AD was of Auguste Deter, a 51-year-old woman who was admitted into Frankfurt's psychiatric hospital under the care of physician Alois Alzheimer[2,14]. Over time she had become increasing paranoid and erratic, and by the time of admission had serious memory loss and difficulties in performing routine tasks like preparing meals. Admitted in 1901, Auguste was treated in the hospital until her death, 4 years later, after which histology was performed on her brain. This identified plaques throughout the cerebral cortex and thick fibrils which accumulate in normal

appearing cells until the nucleus and cytoplasm seemingly disappear, indicating cell death[2,14]. These fibrils and plaques have since been established as hallmark characteristic in the AD brain and it is now known the plaques consist of amyloid β (Aβ) while the thick fibrils within cells are hyperphosphorylated tau tangles[2,10,13,14]. These discoveries were made several years after the first description of AD.

A break-through in AD research came in 1984 when George Glenner identified Aβ protein in angiopathic blood vessels of individuals with AD and Down's syndrome[15,16]. This indicated a link between AD and Down's syndrome, a neurodevelopment disease resultant from trisomy of chromosome 21, which led to the identification of chromosome 21 as an interesting avenue to research[17,18]. This avenue of research was supported by observations of some families having multiple AD cases, implying AD followed an autosomal dominant inheritance pattern[17]. Subsequently Aβ was identified in plaques and in 1987 the precursor to which, Amyloid Precursor Protein (APP), was cloned and shown to localize to chromosome 21[2,19,20]. Further sequencing studies, using a Nottinghamshire family with multiple cases of EOAD, led to the identification of a mutation at codon 717 on the *APP* [2,20]. Since then, two additional genetic mutations have been identified to increase risk of EOAD. Loss of function mutations on Presenilin 1 (*PSEN1* – chromosome 14) and Presenilin 2 (*PSEN2* – chromosome 1) were associated with increased risk of EOAD both which are found outside of chromosome 21 but have functions relating to APP processing[2,20].

The identification of three risk genes related to Aβ production strengthens a central amyloid role in AD pathogenesis. Indeed, early AD research mostly focused on Aβ production, resulting in the generation of a proposed amyloid cascade hypothesis (ACH)[13,19,21–23]. Originally published by Selkoe and Hardy, the ACH begins with deposition of amyloid, assigning it as the central causative element in AD[13,19,21–23]. In this cascade it is hypothesized that abnormal deposition of insoluble Aβ build up into plaques which triggers the formation of second core pathology, neurofibrillary tangles (NFT)[23]. NFT are made up of hyperphosphorylated tau, which accumulates inside the cell, disrupting cellular functions and resulting in cell death[23].

1.3 Amyloid in AD pathogenesis

A central role of Aβ in AD pathology has been shown by multiple researchers. Injection of Aβ oligomers intraventricularly into healthy mice resulted in significant memory impairments[24]. Mice showed a reduced capacity for memory encoding and consolidation but not recall, similar to disruptions seen in the early stages of EOAD[24]. This effect is strengthened by the rescue of memory impairment following treatment with a monoclonal antibody against Aβ, 4G8[24]. Indeed, multiple animal models for AD have been generated mainly by expressing human genes for APP for PSEN1 which result in amyloid pathology alongside cognitive impairments[25]. This strengthens a central role for Aβ in AD pathology.

Aβ is produced following sequential cleavage of APP. APP is a transmembrane glycoprotein which has multiple physiological functions, including neurotrophic and synaptogenesis events, with upregulation of APP being recorded during neuronal maturation[26]. APP also produces multiple biological active fragments which engage in a range of physiologically important roles, some of which are still being uncovered[26].

Processing of APP utilizes three key proteinases; α secretase (mainly ADAM10), β secretase (BACE1 and BACE2) and γ secretase (PS1 and PS2 encoded by *PSEN1/2*).[26,27] APP is initially processed by α and β secretases at the extracellular domains, producing soluble APP derivates (APPα or APPβ) alongside α/β carboxyl terminal fragments (CTF). [26,28] Γ secretase then cleaves APP at the carboxyl terminus to

produce APP intracellular domain (AICD) with an additional substrate, depending on the sequence of processing[26,28]. When γ secretase acts in concert with α secretase it produces the small 3kDa protein p3, however when following β secretase Aβ fragments of various sizes are generated, this pathway is summarized in figure 1.1[26,28].

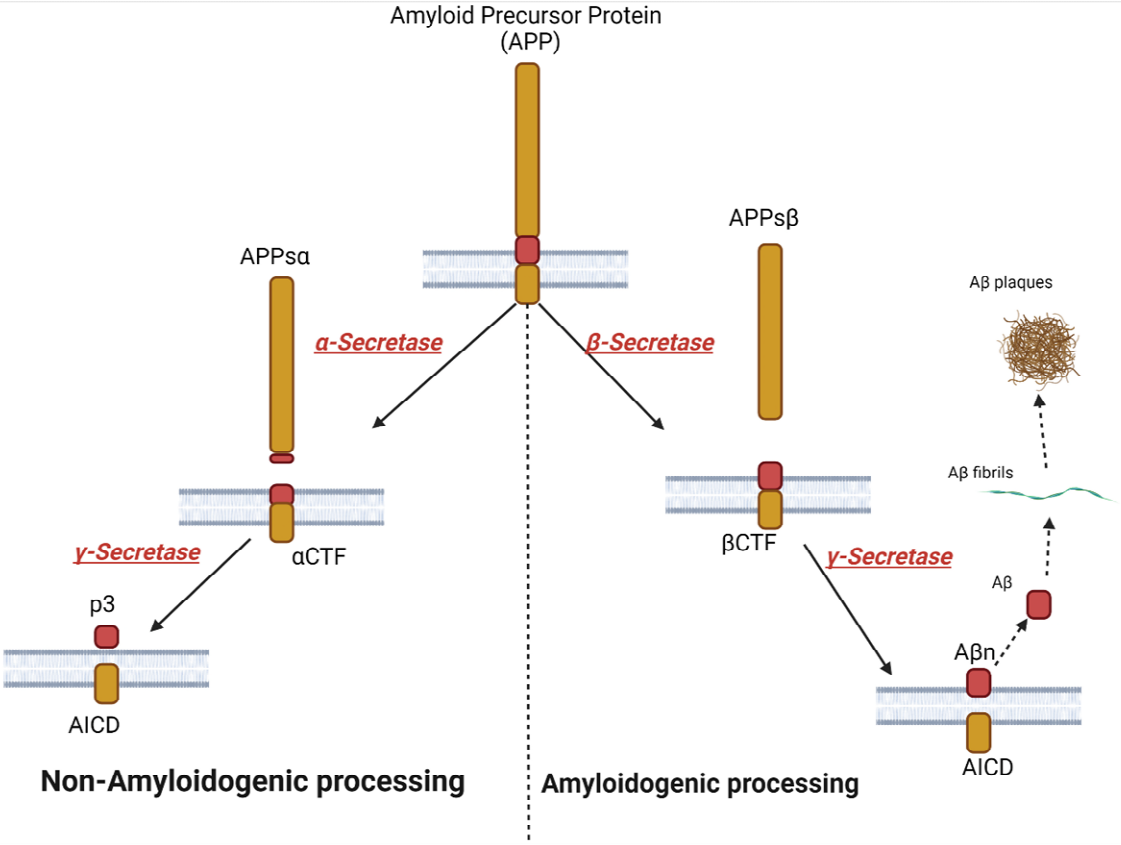

Figure 1.1 Amyloid Processing
Amyloid precursor protein (APP) can be processed by non-amyloidogenic processing which is cleaved sequentially by α-secretase followed by γ-secretase producing APPsα, P3 fragments. Alternatively, APP can be processed via amyloidogenic processing with action first by β secretase followed by γ- secretase producing APPsβ and Aβ fragments which form fibrils that aggregate to form Aβ plaques. In AD excess Aβ is produced. Created with BioRender.com[26,28].

Multiple Aβ fragments can be produced, varying between 38-42 amino acids, with the larger fragments being more hydrophobic and therefore more prone to aggregation[26,29]. The larger Aβ42 is the predominant peptide in AD, due to genetic mutations in γ secretases reducing the carboxyl peptide cleavage[30]. In AD the ratio of Aβ42 to Aβ40 (which is the predominant peptide in non-AD individuals) is altered, resulting in more hydrophobic Aβ fragments with a higher propensity for self-aggregation and oligomer formation[26,29]. The importance of this cleavage pattern was highlighted following the identification of protective missense mutation A673T[31]. This lies within the second amino acid of the Aβ peptide region of APP, within close proximity to the proteolytic site for BACE1[31]. Presence of A673T results in a 40% reduction of amyloidogenic peptide production and a reduced risk of developing AD[31,32]. Indeed, significantly reduced age-related cognitive decline is observed in individuals with the mutation[31,32]. Contrasting to this are data collected from individuals with one of the characterized APP AD risk variants, A673V, which codes for a single amino acid change at the same site as A673T mutation[33]. The result of this is instead increased BACE1 cleavage, producing more amyloidogenic peptides and plaques with an increased risk for AD[33].

Although it is undeniable that Aβ is central in AD pathology, more recent research has moved away from the ACH and the thinking of Aβ as the triggering cause of AD pathology. This follows multiple inconsistencies in Aβ research and the failure of several Aβ targeted therapies in clinical trials. Indeed, amyloid PET imaging reveals the presence of amyloid plaques in up to 47% of cognitively healthy individuals[34]. One cohort, following a group of nuns, revealed at least a third to fulfill the neuropathological criteria for AD without presenting any significant cognitive impairments up until their last assessment[35]. This questions why Aβ build up is pathological only in AD cases, suggesting that the amyloid plaques may not be the central mechanism for the subsequent pathology. Supporting this is the temporal and spatial mismatch observed between amyloid plaques and NFTs during disease progression[36,37]. Imaging has shown amyloid plaques to first appear in neocortical regions before spreading to limbic and subcortical areas[34]. However, tau has been shown to first appear in the trans-entorhinal cortex and then spreads to paralimbic and neocortical areas[34]. This questions the ACH proposal of Aβ being the central mechanism that causes tau pathology and has directed research to explore a third core characteristic of AD in neuroinflammation[38–40].

1.4 Inflammation in AD

Initial acute inflammation is a neuroprotective process, designed to reduce damage to cells by production of a plethora of pro- and anti-inflammatory molecules[41]. When the equilibrium of these products is disrupted chronic inflammation occurs[41]. Chronic inflammation is seen in a variety of neurodegenerative diseases, including Parkinson's disease (PD), multiple sclerosis (MS) and amyotrophic lateral sclerosis (ALS)[41].

Many studies now highlight chronic inflammation as a fundamental aspect of AD pathogenesis. Since the 1980s, reports have shown the presence of inflammatory markers and activated immune cells surrounding amyloid plaques in the AD brain[38,42,43]. This is further supported by the presence of multiple inflammation markers within the cerebrospinal fluid (CSF) of individuals with AD or mild cognitive impairment (MCI)[44,45]. A relationship between the presence of these markers and development of MCI to AD has since been observed, although this remains controversial. A key study supporting a central role of inflammation in AD came from a large epidemiological study which followed long term non-steroid anti-inflammatory drugs (NSAIDs) users[46,47]. Those who were chronic NSAID takers had shown ~50% reduced risk for developing LOAD. This is supported by multiple animal studies which show AD transgenic models to have reduced pathology and cognitive impairments following long term treatment of NSAIDS[38,44,46]. Common NSAID, ibuprofen, was given to a tau AD mouse model over a 6 month time course[48,49]. This treatment significantly reduced Aβ pathology, the number of activated immune cells, the number of dystrophic neurites and the expression of inflammatory markers[48,49]. Furthermore, mice showed improved performance in open field behavior tests[48]. Despite these promising results, trials for NSAIDs in humans have provided unclear data, with no convincing evidence for the beneficial use being found[46]. It has been suggested that this treatment is only effective as an early intervention and made further difficult by poor diagnostic tools for confirming AD[46].

Regardless, these findings suggest a central neuroinflammatory role in AD. However, unlike other risk factors for AD, inflammation is unlikely to occur in isolation but alongside other AD pathologies and risk factors. Indeed, much evidence has shown inflammation to exacerbate Aβ and tau pathologies. For instance, elevated levels of the pro-inflammatory cytokine interleukin-1 (IL-1) has been shown to increase APP and therefore Aβ load[44,50]. Another pro-inflammatory cytokine, IL-6, has been shown to stimulate the activation of CDK5, a kinase which is known to 15pprox.1515phorylated tau[51]. This

provides a link to seemingly separate key pathologies and has shifted the focus of AD research to the potential role of inflammation. As the brain is separated from the peripheral immune system by the blood brain barrier (BBB) this has focused research on central nervous system (CNS) resident immune cells; astrocytes and microglia[38,41].

1.4.1 Astrocytes

Astrocytes are star-like supporting cells, which exist in a heterogenous population throughout the brain parenchyma[52]. They have a range of roles from maintaining homeostasis to neurotransmitter uptake and recycling, gliotransmitter release, modulation of synaptic activity, maintenance of the blood brain barrier and inflammation[52]. Astrocytes are known to exist in the brain in two main states, quiescent and activated. The presence of activated astrocytes is observed in multiple brain disorders. AD amyloid plaques are often accompanied by a cluster of reactive astrocytes, which have processes which penetrate into the plaques[53]. Activated astrocytes have been shown to follow the distribution of plaques throughout the association cortex of AD patients, with the number of reactive astrocytes increasing with disease progression. Some investigations, using Terminal Deoxynucleotidyl Transferase dUTP nuck end labelling (TUNEL) and caspase 3 immunohistochemistry on patient post-mortem samples reported the presence of apoptotic astrocytes[54,55]. Although this has not be replicated in subsequent studies, other investigators have noted the presence of astrocytic markers such as GFAP in the CSF of AD patients leading them to suggest the presence of astrocytic apoptosis in AD pathology[56]. How these activated astrocytes contribute to the ongoing deterioration in AD is still under investigation.

1.4.2 Microglia

Microglia are the primary immune cells of the CNS and are responsible for multiple homeostatic functions. Physiologically, microglia are highly ramified with processes that continuously extend and retract in the brain parenchyma, surveying for any subtle changes in the CNS microenvironment[44]. Upon detection of a pathological insult, such as cell debris or abnormal protein aggregates, microglia become activated[57]. Once activated, microglia undergo morphological changes, becoming round amoeboid cells with increased phagocytic capacity and production of inflammatory mediators, including cytokines and chemokines[44,57,58]. Numerous studies have shown Aβ in various forms to activate microglia, inducing release of cytokines including tumor necrosis factor α (TNF-α) and nitric oxide (NO), which are increased within the AD brain[44,57,58].

Activation of microglia is referred to as microgliosis. Initial observations made by Alois Alzheimer revealed the presence of microgliosis around amyloid plaques[38,59]. This observation has been replicated in multiple studies, in multiple models[38]. Initially, microgliosis was considered a consequence of amyloid pathology, however recent evidence suggests these microglia could be playing an active role in plaque formation[58,60]. One lab observed that microglia surround deposits which they suggested forms a protective barrier around the amyloid plaques, compacting the amyloid fibrils into one dense core[60]. This would prevent the addition of new Aβ into existing plaques, reducing axonal dystrophy[60]. This was mostly observed in early stage plaques[60]. However, contrary reports show microglia surrounding amyloid deposits to contribute to the formation and growth of plaques[61]. Two photon microscopy on the brains of the Aβ-overexpressing AD transgenic mouse model showed microglia engulfment of Aβ[61]. This results in clusters developing within the microglia, causing cell death and subsequent release of Aβ into the extracellular space[61]. These contradictory actions highlight the unknowns of microglial function in AD pathology.

One essential hallmark of inflammation is the production of chemokines and cytokines[38]. Production of cytokines by microglia is stimulated following the activation of pattern recognition receptors (PRR) or via activation of the inflammasome[62]. Lipopolysaccharide (LPS), a common *in vitro* stimulator derived from gram negative bacteria cell walls, activates microglia through interaction of Toll Like Receptors (TLR)s[62–64]. TLRs are PPRs, LPS specifically activate TLR2 and/or TLR4[63,65]. This leads to activation of nuclear factor kappa B (NFκB), a transcription factor which modulates the expression of multiple immune and inflammatory mediators and stimulates the secretion of pro-inflammatory cytokines such as IL-8[62]. TLR4 has also shown to activate the inflammasome, which is an inducible multiprotein complex which contributes the inflammation, the most researched inflammasome is NLRP3 [66,67]. The inflammasome consists of a sensor protein e.g. NLRP3 and an adaptor protein, apoptosis associated-speck like protein (ASC)[66,67]. The ASC recruits and activates caspases including pro-caspase-1, which when stimulated induces the cleavage of pro-IL-1β and pro-IL-18 producing activated IL-1β and IL-18, which further stimulate the production of more cytokines[66,67]. Activation of the Inflammasome is still not fully characterized however canonical activation requires two independent, co-concomitant signals, one priming[68]. *In vitro* treatment of LPS and Aβ fibrils has shown to be sufficient to activate the inflammasome[68]. Despite this, LPS has been shown to be capable of activating the inflammasome to some extent through non-canonical activation pathways[69].

Activation of the inflammasome is shown in AD through increased caspase-1 within the frontal cortex of AD patients[68]. Additionally, genetic deletion of NLRP3 in AD mouse models showed reduced levels of IL-1β and Aβ pathology which correlated with improved cognitive results[68,70,71]. Cytokine TNFα is of particular interest in LOAD research and has been shown to be elevated in the CSF of LOAD patients compared to healthy controls[72]. Indeed, animal data implies the chronic production of TNFα throughout the course of disease[72]. Genetic deletion of TNFα receptor, TNF-RIII, in several mouse models of AD showed reductions in brain inflammation and Aβ burden[73]. This is replicated following the treatment with TNFα inhibitor, Infliximab, approved by the FDA for treatment of peripheral inflammatory conditions, such as Crohn's disease[74]. Intracerebral administration of Infliximab into 12 month APP/PS1 AD mouse models (which present Aβ and tau pathology) results in a rapid, but transient, reduction in Aβ load and tau hyperphosphorylation[75].

Genetics have provided further support for a central microglial role in LOAD pathology. Genome-wide association studies (GWAS) scan the genomes of multiple individuals with particular phenotypes for common variants[76–79]. This allows for the detection of mostly single nucleotide polymorphisms (SNPs) associated with phenotypes or pathologies[79]. Multiple GWAS studies for LOAD have been performed, revealing >50 risk loci which can be used, in combination with environmental factors, to predict an individual's risk for developing LOAD termed their polygenic risk score[80]. The strongest identified risk is variations with the *APOE* isoform[81]. Indeed, *APOE* has long been associated with AD pathology, with those homozygous for the ε4 allele to have a 15-fold increased risk to developing LOAD[82]. Figure 1.2 summarizes key genetic hits associated with AD, highlighting that genes which confer higher disease severity are rarer within the population. Pathway analysis on GWAS hits has revealed many of these genetic loci to converge on cholesterol metabolism and immune response pathways[77,83]. This further implicates microglia-centric pathways in the pathogenesis of LOAD, supporting a central role for inflammation and immunity on LOAD pathology. One of the strongest immune pathways related to risk of LOAD is the complement system[77,83].

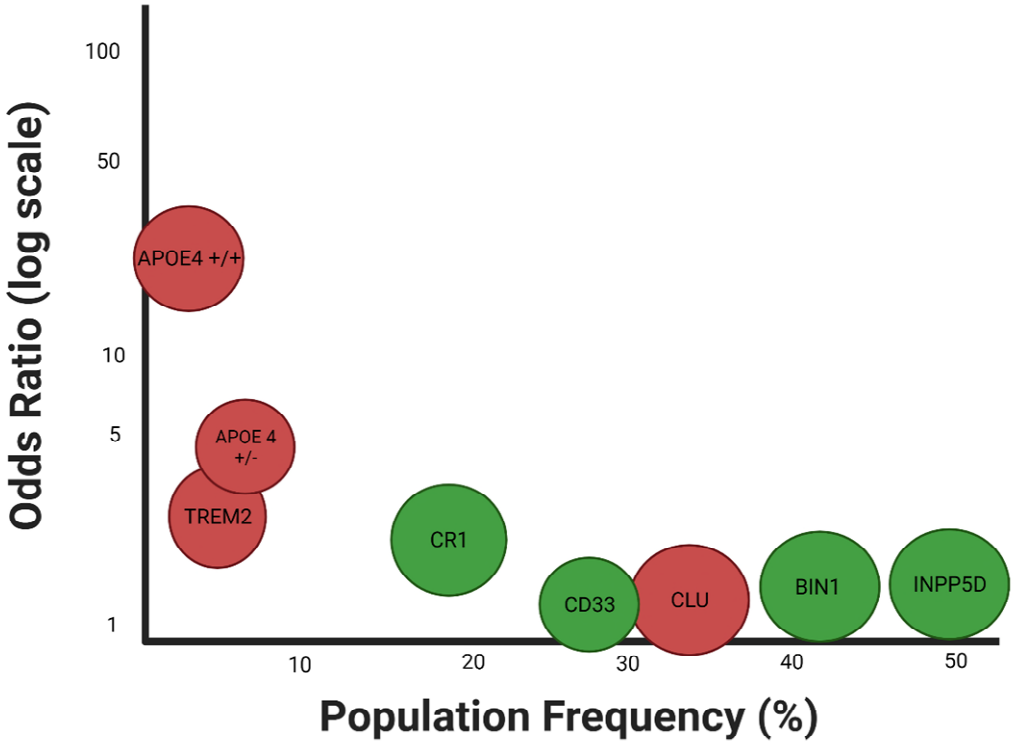

Figure 1.2: Rare and common AD risk variants
Genetic factors with lower risk are more common and associated with lower disease severity. Hits identified with GWAS show low odds ratio while APOE represents the biggest hit. Created with BioRender.com and based of [84]

1.5 The Complement System

The complement system was first detected in the 1880's following the injection of microbes into experimental animals[85–87]. This revealed the presence of antibacterial substances within the serum of animals, which are now referred to as antibodies[85–87]. Water separation of antibacterial serum produces two precipitates; a protein fraction and a soluble protein fraction[87]. In 1891, Buchner and colleagues showed the combination of these fractions was required for the previously observed antibacterial function, while separation removed the antimicrobial activity[85,87]. Additionally, they observed the soluble fraction of serum from animals injected with microbes could be replaced with th18pprox.le fraction of serum of animals that had not been injected and still possess low level natural antibacterial activity[81]. Bordet identified the presence of two substances within the serum of animals injected with microbes; the first existing prior to injection while the second being induced by the microbe. The former of these fractions was shown to be heat labile, completely losing its antimicrobial ability after a 30 minute incubation at 56^{o}C which was regained following addition of fresh serum from an un-injected animal[85,87]. This fraction was termed alexin, the Greek of which means 'to ward off' and is what we now refer to as complement[85–87]. Experiments spanning the next 70 years have revealed complement to include a series of sequentially activated proteins spread across three pathways, which is summarised in figure 1.3[87].

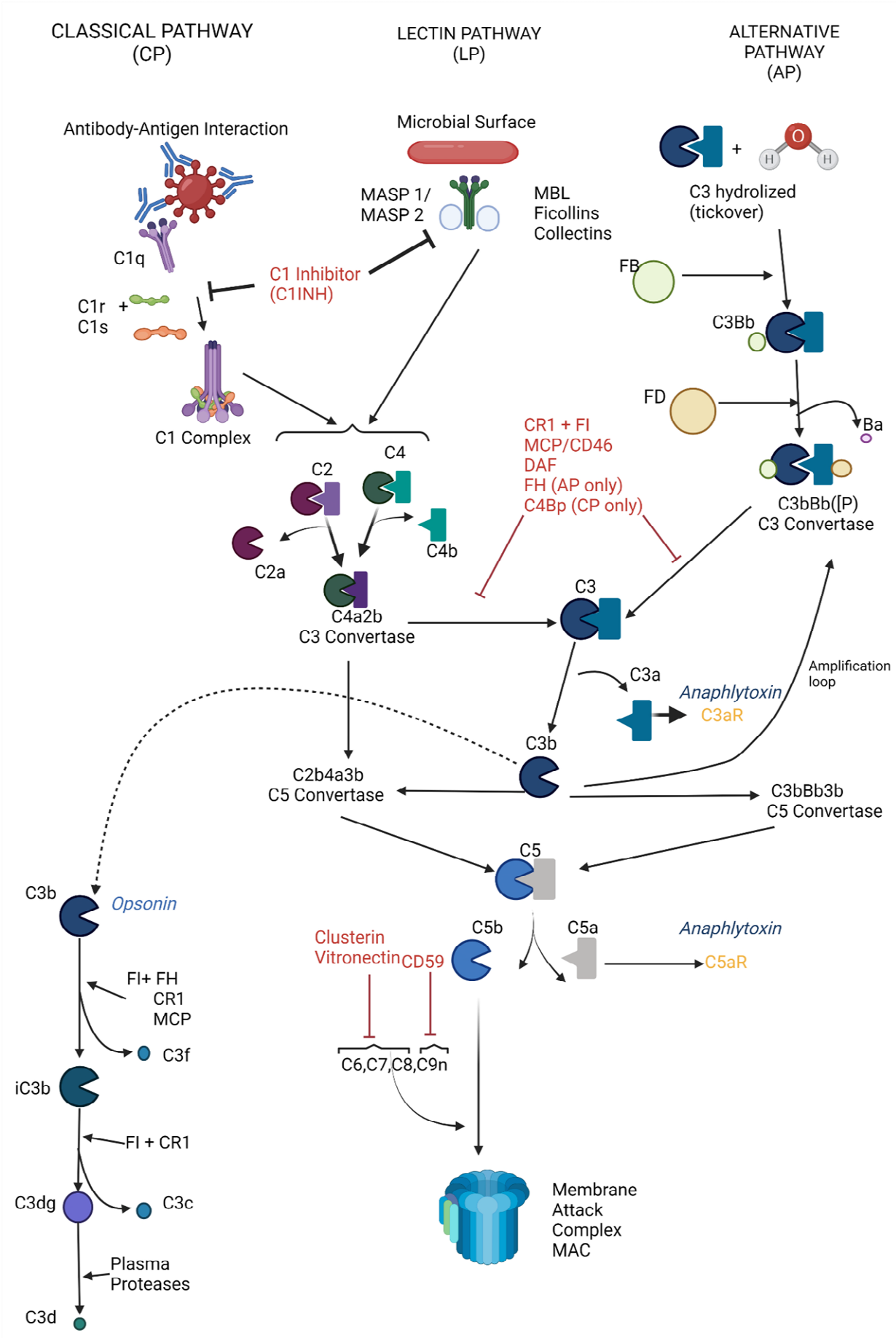
CLASSICAL PATHWAY (CP)
LECTIN PATHWAY (LP)
ALTERNATIVE PATHWAY (AP)
Antibody-Antigen Interaction
Microbial Surface
MASP 1/ MASP 2
MBL
Ficollins
Collectins
C3 hydrolized (tickover)
C1q
C1 Inhibitor (C1INH)
C1r + C1s
FB
C3Bb
FD
Ba
C1 Complex
C2
C4
C4b
C2a
C4a2b C3 Convertase
CR1 + FI
MCP/CD46
DAF
FH (AP only)
C4Bp (CP only)
C3bBb([P) C3 Convertase
C3
C3a
Anaphlytoxin
C3aR
Amplification loop
C3b
C2b4a3b C5 Convertase
C3bBb3b C5 Convertase
C5
C3b
Opsonin
Clusterin
Vitronectin
CD59
C5b
C5a
Anaphlytoxin
C5aR
FI+ FH
CR1
MCP
C3f
iC3b
FI + CR1
C3dg
C3c
C6,C7,C8,C9n
Plasma Proteases
C3d
Membrane Attack Complex MAC

Figure 1.3: Complement Cascade (Classical/Alternative/Lectin pathway)
Complement can be enacted through three pathways which are triggered following detection of different stimuli. All three pathways converge on C3 The red text represents inhibitors. Created with BioRender.com and using [86].

1.5.1 The Classical Pathway (CP)

The Classical Pathway (CP) is activated following the detection of antibody-antigen complexes. Antibodies display an Fc region to the environment which can be detected by complement C1q[85,87]. Binding of C1q initiates a series of enzymatic reactions we now recognise as the CP[85,87]. In total, 11 proteins are involved in the CP, named in order of discovery they follow a pattern of: C1, C4, C2, C3, C5-C9[85,87]. Throughout the cascade several biologically active fragments are generated which are involved in chemotaxis, vasodilation and opsonization with the final reactions of the cascade producing a cell lysis complex referred to as the membrane attack complex (MAC)[86].

In the mid-1920s, several complement components were identified. Brand showed the two fractions produced from dialyzing serum could not lyse antibody-coated erythrocytes independently but could when added sequentially[85,87]. His experiments revealed addition of the precipitated fraction (he termed euglobulin) interacted with antibodies. This interaction was required to precede the addition of the second soluble fraction (he termed pseudoglobulin) [85,87]. These fractions were later renamed to midpiece (what we now know is C1) and endpiece (what we now know as C2). Since, diethylaminoethyl (DEAE) chromatography experiments have revealed C1 component to consist of three separate proteins which are known as C1q, C1r and C1s[88,89].

Identification of a third complement component, C3, was shown by Omorkow in 1911, and Ritz in 1912. Utilising antibody-coated sheep erythrocytes, they showed lysis to be triggered following the addition of guinea pig serum[87]. This lysis was blocked following addition of cobra venom factor (CVF), which is now known to be a structural and functional analogue for complement C3[90]. Indeed, CVF is capable of binding with factor B to form a C3 convertase, causing depletion of C3[90,91]. A similar experimentation model was used to identify C4, instead lysis was blocked following the addition of ammonium indicating the presence of a component sensitive to ammonia[92].

Although these factors had been uncovered, their sequence of action was obscured until 1954, in which Mayer applied a range of experimental procedures to determine the sequential pathway shown in figure 1.3[85]. Activation of the CP is initiated by the binding of C1q to the Fc portion of a bound antibody. Binding of C1q autoactivates pro-enzyme C1r, which cleaves and activates serine protease C1s to form the C1 esterase complex[88]. C1 reacts with C4, in a calcium-dependent reaction, to produce fragments C4a and C4b[85,93]. C4b can then attach to the surface of the activator, allowing for C2 to be cleaved, in the presence of magnesium, to produce C2a and C2b. C4a and C2b form C4aC2b, a CP C3 convertase[85,86,93]. This cleaves C3 into fragments C3a and C3b, each with individual complement activities. C3b is a common complement opsonin, binding to a pathogen to signal for its removal by immune cells. C3b also binds to the C3 convertase to form C4aC2bC3b also referred to as C5 convertase. This cleaves C5 into C5a and C5b. C5a, along with C3a, are anaphylatoxins which can bind to C5aR or C3aR respectively to recruit immune cells to a site of damage[86]. C5b continues the cascade into the terminal pathway (TP). This includes the formation of the multiprotein MAC, which inserts itself into microbial membrane to trigger lysis. The MAC is assembled on the membrane sequentially with C5b, C6, C7, C8 and C9[85,86].

1.5.2 The Alternative Pathway

Originally the AP was named the properdin pathway and was first observed by Pillemer following an unsuccessful attempt to purify C3[85,94]. Due to the observation that adding zymosan to plasma, in the presence of high temperatures, magnesium ions and at pH7, reduces serum C3 it was hypothesised that yeast absorbs C3, meaning C3 could be purified from the complex, however, this failed[87]. Pillemer suggested this to be due to the presence of a previously unknown serum protein binding to zymosan, in which he named properdin. Indeed, depletion of properdin from serum resulted in a loss of antibacterial action[94,95]. This led to the hypothesis that properdin activates C3 by the binding of pathogens in the absence of antibodies[85,87]. At the time this was highly controversial, with subsequent experiments confirming properdin to activate complement, independent of antibodies[85,87]. However, it has since been shown that the AP is initiated by spontaneous hydrolysis of serum C3 and properdin is now considered as a C3 convertase rather than a linker for pathogen and complement[96].

Current understanding of the AP evolves around the presence of auto-complement activation by the 'tick-over' of spontaneous hydrolysis of C3 to form C3(H_20)[96,97]. Following this factor B (FB) binds to the C3(H_20), resulting in a conformation change causing cleavage of factor D (FD) which produces fluid phase AP C3 convertase[87,98]. This cleaves C3 into C3a and C3b. C3b and FB can bind to form more C3 convertases, resulting in a positive amplification loop of complement activation which requires tight regulation[87,97,98].

1.5.3 The Lectin Pathway

Several publications from the 1970s had reported activation of C1 in serum in the absence of any antibodies[87,99]. Binding of C1 and complement activation was observed following the addition of RNA tumour virus' in the presence of lipid A- a component of salmonella LPS[87,100]. This led to the discovery of the third complement pathway, which is activated following the interaction of pathogens and naturally occurring carbohydrate-binding proteins, known as lectins. Lectins such as mannose binding lectin (MBL) and ficolins recognise bound carbohydrates, initiating the lectin pathway (LP)[87,99,101].

The LP was differentiated from the CP following evidence of activation occurring in the absence of C1q. Furthermore, C1q and MBL were shown to be highly structurally similar[102]. It is now known that cell-bound MBL forms a complex with two dimers of MBL-associated serine proteases (MASPs); MASP1 and MASP2. Autoactivation of MASP1 triggers MASP2, which then cleaves C4 and C2 to produce C4a, C4b, C2a and C2b and the C4a2b C3 convertase is generated and the pathway from this point is the same as the CP[101,103].

1.5.4 Regulators of complement

Together the three pathways of complement make up a vital part of innate immunity, crucial in defending the body, however these effects can potentially be damaging to surrounding host cells if not controlled. The CP and LP is dependent on activation by the presence of a foreign body but under some circumstances (e.g. tissue ischaemia), both pathways can become extensively activated and result in injury to the host[86]. Even more vital for regulation is the AP, which is spontaneously activated in a constant tick-over and loss of regulation of the amplification loop results in rapid damage to surrounding host cells. Therefore, the complement system contains essential regulators which exist in the bodily fluids (like plasma) or attached on the surfaces of host cells[85–87]. These regulators are required to minimise damage to self and regulate the role of complement.

Several factors, mostly in the fluid-phase, control the activation of the complement system. C1INH (C1-Inhibitor) is one such. Present in the plasma, C1INH irreversibly binds and inactivates C1r and C1s

(of the CP) or MASP1 and MASP2 (of the LP) thereby inhibiting the initial activation of complement[85,87]. Like other complement regulators, C1INH has alternative functions, also inhibiting factor XIIa of the clotting system, which interacts with the coagulant system[104]. Other plasma regulators include complement factor H (FH) and complement factor I (FI) which predominantly regulate the AP. FI is a serine protease, capable of inactivating C3b to inactive iC3b in the presence of a co-factor (e.g. CD46, MCP, CR1 and FH), FI can further degrade iC3b to C3dg and C3c in the presence of other co-factors. One of these co-factors is FH. FH predominantly competes with FB to bind C3b when acting with FI to cleave C3b[100,101]. FH also decreases the stability of the C3bBb convertase, regulating the AP amplification loop production of C3b[100,101]. It is important to note FI has additional action in cleaving component C4b and C4bC2a convertase of the LP in the presence of C4-binding protein[100,101].

Additionally, complement regulators include; CR1 (CD35), CD55 (DAF), CD46 (MCP) and CD59 (protectin)[85,105–107]. MCP acts as a cofactor for FI in the cleavage of C3b but is only capable of protecting the cell it is expressed on, offering a selective protection[100,101]. This is also true for CR1, which can act alongside FI in the cleavage of C3b and has an additional function in accelerating the decay of C3 convertase of all pathways[108]. More information on the role of CR1 in this pathway is in section 1.5.7. DAF also works to destabilise the C3 convertase by accelerating its dissociation[100,101].

CD59 is separated from the other regulators as it is responsible for controlling the terminal complement pathway by regulating the generation of the MAC. This action is performed by inhibiting C9 from associating with CD5b-8 which prevents the C5b-9 pore to properly form[109]. Generation of the MAC can also be controlled by fluid phase regulators clusterin (CLU) and vitronectin (VTN), which interfere with the assembly of the complex. VTN, preferentially binds to C5b-7 and interacts with C9, forming sC5B-9, which is inhibited from polymerization and its proper function[85,106]. VTN also functions outside of complement, primarily in cell attachment and cell spreading[85,87]. CLU, has a more limited role acting at the level of C7 to prevent it from insertion into the cell membrane[110].

Together these regulatory proteins control complement from excess activation and auto-injury and lack of this control can result in pathologies, such as those present in age-dependent macular degeneration (AMD), which has been attributed in part to uncontrolled complement activation in the Bruch's membrane of the retina[111]. This was observed following the identification of AMD-associated factor H gene polymorphism (H402Y). H402Y affects the surface binding function of FH, affecting FH's ability to regulate AP activation on host[111]. The defective surface binding by FH in this instance aids in the pathology of AMD and is also present in other disorders such as dense deposit disease (DDD) which similar pathology is observed in the glomerular basement membrane of the kidney[111,112].

1.5.5 Complement and AD

A role for complement in AD has been shown since the 1990's, with immunohistochemistry (IHC) data indicating the presence of multiple complement factors in close proximity to Aβ plaques[113–116]. LOAD post-mortem tissue of varying Braak stages indicate high levels of early complement components: C1q, C4d, C3d at the earlier stages of disease with increased later complement components, C5b-C9, appearing at later Braak stages[117,118]. Furthermore, analysis of CSF from AD patients indicates reduced C1q protein level and elevated C3 levels compared to healthy controls[119–121]. Enriched C3 protein was shown particularly at a stage of disease with tau pathology, consistent with other recordings showing C3 to be elevated in response to tau pathology[122].

Animal models have also provided important tools for understanding the potential role of complement in LOAD pathogenesis and have unveiled a complicated story. Immunohistochemistry

(IHC) data for complement dysregulation shown in human AD brains has been recaptured in various animal models[123,124]. Crossing of LOAD animal models with complement deficiencies or with complement blocking treatments has provided support for a central complement role in LOAD pathogenesis. For instance, crossing of C3-deficient animals with amyloidosis mouse models PS2APP and tau pathology mouse model TauP301S shows a rescue of plaque associated synapse loss in the PS2APP model and reduced neuronal loss and brain atrophy in TauP301S, indicating improvements in behavioural and neurophysical measurements[125]. Another group showed that the C5aR antagonist could reduce fibrillar amyloid deposits and activated glia in two separate LOAD mouse models (Tg2576 and 3xTg) with a significant reduction in hyperphosphorylated tau in the latter[126,127]. This implicates complement in multiple LOAD hallmarks.

One of the key focuses on the role of complement in LOAD has been on synaptic refinement. Synapse loss is considered a strong pathological correlate for cognitive decline in AD patients and is one of the first signs of disease in demented and mildly cognitively impaired patients[128]. Studies focusing on the developing rodent visual system indicate a central role for complement components, C1q, C3 and CR3 in the tagging and subsequent removal of synapses. Inhibition of these factors in AD animal models reduces the number of activated glia and reduces synaptic loss[129,130]. It has now been show that C1q associates with synapses, tagging them for removal by CR3 expressing microglia. The role for CR3 in this process is supported by treatment of Aβ oligomers to LOAD animal models to induce synaptic loss. When Aβ oligomers were injected into CR3 knockout (KO) animals significantly less synaptic loss was observed compared to CR3 WT animals[131].

More recently complement has been linked to AD via GWAS which identify rare genetic polymorphisms linked to specific phenotypes. GWAS highlighted many genes linked to immunity and inflammation with risk for developing AD, including two key complement gene loci, Clusterin (*CLU*) and complement receptor 1 (*CR1/CD35*)[132–134].

1.5.6 Clusterin (CLU/APOJ)

CLU, also known as APOJ, is the third-most associated risk gene for LOAD and acts as a regulator for the terminal complement pathway which generates the MAC[135]. GWAS identified three SNPs within the *CLU* gene to be significantly associated with AD, all three of which are non-coding[133,136,137]. Currently, little information is available on how this SNP affects CLU protein, although one SNP, rs1113600 has been shown to be associated with increased CSF Tau levels in AD patients through interaction with another GWAS hit, *BIN1*[138].

1.5.7 Complement receptor 1 (CR1/CD35)

CR1 is a regulatory receptor within the complement system[134,137]. CR1 binds opsonizing fragments C3b and C4b. The primary role of CR1 is as a co-factor for FI-mediated cleavage of C3b and C4b to iC3b and C4c respectively. Additionally, CR1 has a Decay Accelerating Activity (DAA) for both classical and alternative C3 and C5 convertases[139,140]. Cleavage of CR1 also produces soluble CR1 (sCR1), which is a potent local inhibitor of complement activity[141–143].

1.5.7.1 Structure of CR1

CR1 is a linear transmembrane glycoprotein. Encoded on chromosome 1, region q32, *CR1* is within a genetic cluster of Regulatory Complement Activation proteins (RCA) which also includes *MCP* and

DAF[86,108,144]. In all three of these proteins, the extracellular portion consists of independent domains termed short consensus repeats (SCR). These are also termed sushi domains and complement control proteins (CCP) within the literature[86,102,108]. The number of SCRs in each RCA differ; MCP and DAF occupy the lower end with up to 4 SCR while the largest form of CR1 can have up to 44 SCRs[108,134]. Each SCR is made up on 59-75 amino acids, with a high conservation of hydrophobic amino acids between SCRs[108,145,146]. Each repeating structure contains 4 cysteine and 1 tryptophan residue, with the first and third cysteine making a di-sulphide bridge and the second and fourth another. Together this creates a hydrophobic core within each SCR[108,145,146].

Within CR1 the SCRs, all except the 2 carboxyl terminal SCRs, make up larger units termed Long Homologous Region (LHR)[108,147]. Each LHR consists of 7 SCRs, as shown in figure 1.4. The most common form of CR1 consists of 30 SCRs into 3 LHR units labelled LHRA-D. Each LHR confers a function of CR1, with LHR-A SCRs 1-3 being the main site of CR1 DAA activity and a C4b binding site[140,145]. The second and third active sites, in LHR-B (SCR8-10) and LHR-C (SCR 15-17) respectively are highly homologous, and have high binding affinity for C3b/C4b fragments[140,145]. Point mutations within sites 2 and 3 have shown the importance of ionic charge in binding to opsonins; with a loss of binding correlating with increased negative charge and the converse being shown[140,145]. The final LHR-D is thought to have a low affinity for C1q and MBL[140,145,148,149]. LHR-D is also thought to be the area involved with antigens for knop blood variant, one of the three polymorphisms of CR1[150]. The structures of CR1 is shown in figure 1.4.

Within the population, four size alleles of CR1 have been identified, each with varying numbers of LHR units summarised as shown in figure 1.4[108,141,146]. These are genetic allotypes, which are produced from differences in transcript, rather than post-translational modification. The two most common are CR1 F (4 LHR) and CR1 S (5 LHR) and make up 83% and 15% respectively of CR1 within a Caucasian population[141]. Slightly different gene frequencies are seen between races with Mexican cohorts showing CR1-F to make up 82% with CR1-S 11% however in all cohorts CR1 F and CR1 S are the most common[86]. These two alleles are flanked by rarer variants named; CR1-F' (3 LHR) and CR1-D (6 LHR)[108,141]. The functional implications of the variance in LHR domains is currently unclear.

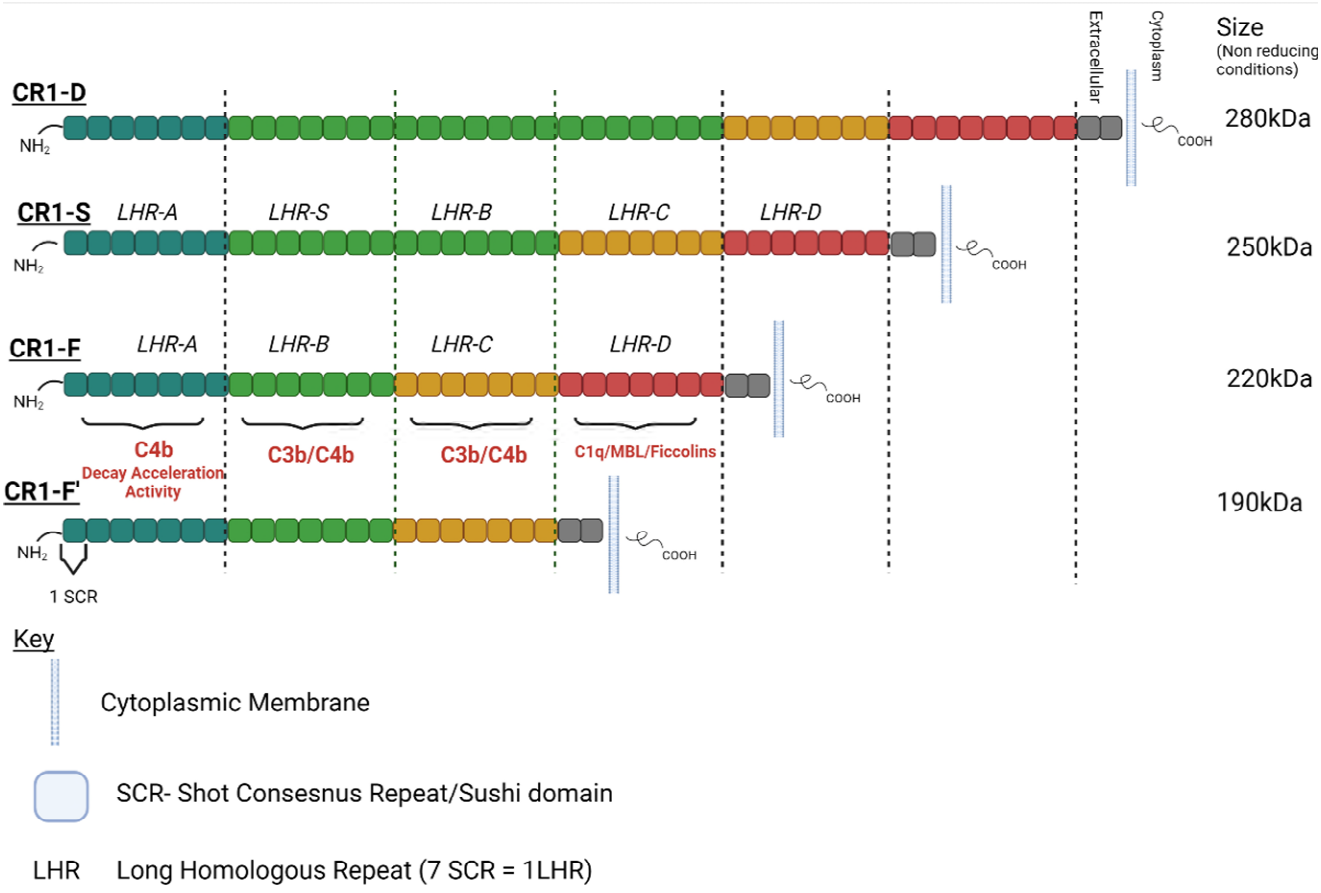

Figure 1.4: CR1 structure and size polymorphism
Complement Receptor 1 is made up of long homologous repeats (LHR), which in turn is made up of 7 short consensus repeats (SCR). Each LHR makes a binding site. Four separate size polymorphisms of CR1 exists which differ in number of LHR. The most common size's are CR1-S which has 5 LHR and CR1-F which has 4 LHRs. The most common size polymorphism- CR1-F- has the relevant functions of each LHR which is similar for all other size polymorphism.. Created with BioRender.com and using [146]

In addition to size polymorphism variations, HINDIII restriction fragment length polymorphism in CR1 has been identified[108]. This corresponds to an SNP within intron 27 of CR1[151,152]. This has shown the presence of a HINDIII site to correlate with copy number of CR1 present on erythrocytes[151]. Two alleles have shown to exist–- the low (L) and high (H). Individuals homozygotic for the L polymorphism show <200 copies of CR1 on erythrocytes, significantly lower than those homozygotic for the H polymorphism[151,152].

A third genetic polymorphism of CR1 has been shown through the presence of different knops blood antigens[150]. This has shown to be important in rosette formation of infected and uninfected red blood cells in malaria, with a correlation between density and severity of disease shown[150].

1.5.7.2 Expression of CR1

Around 90% of CR1 is found on erythrocytes and other circulating cells, such as macrophages, B cells, subsets of T cells and neutrophils[86,153]. CR1 is also found on non-circulating cells, such as follicular dendritic cells and macrophages of the adrenal gland, however its expression within the CNS remains elusive[141].

The human protein atlas can be used when investigating the expression of human transcripts and proteins in a range of tissues and species[154]. It utilises transcriptomic and proteomic data in multiple sample tissues, their data for the expression of *CR1* shows a low detection of mRNA in multiple brain areas with little to no amounts of CR1 protein detected[155]. A deeper look at this shows the largest mRNA signal to come from the pons/medulla closely followed by the hippocampal formation, amygdala, and hypothalamus. A further look at available *in situ* data shows low amounts of *CR1* message within the cerebral cortex, all of which came from neuronal cells with no co-localization of *CR1* with glial cells[141]. This is supported by post-mortem analysis of the choroid plexus, which showed CR1 to only be present on neurons and blood cells, an alternative study also investigating the choroid plexus saw only phagocytic Kolmer cells to stain positive for CR1 and observed no neuronal staining[141,146,156]. More recent immunohistochemistry saw CR1 detection on both neuronal and astrocytic cells on MS and healthy tissue, however pre-absorption of the antibody with CR1 protein showed only the astrocytic staining to be specific to CR1[141,157]. This was later supported with primary astrocytic cultures and astrocyte cell lines with consistent findings indicating astrocyte line T193 to express CR1 protein[141,157]. Another astrocyte cell line, T109, failed to support this[157]. Only one immunohistochemistry study identified CR1 on human microglia cells[141]. Together this presents an unclear, inconsistent story on the CNS expression of CR1.

1.5.7.3 Functions of CR1

Primarily CR1 is a receptor for C3 fragment, C3b. C3b is a common opsonin, which coats the surface of immune complexes to signal for their removal. In the periphery, this is referred to as 'immune adherence'. Previous studies have shown Aβ in the plasma to be coated by C3b, which is detected by erythrocyte CR1 allowing for the transportation of opsonised Aβ from the blood to the liver[114]. Here, Aβ is transferred from erythrocyte to hepatic macrophages for destruction[114,158]. However, when CR1 is present with FI, C3b is converted to iC3b, a ligand for phagocytosis receptor CR3. The presence of opsonin increases the detection and uptake of toxins[108,134]. This function is summarised in figure 1.5, A secondary function of CR1 is in regulatory dissociation of C3 and C5 convertases of the CP and AP, this function also requires FI[134,140].

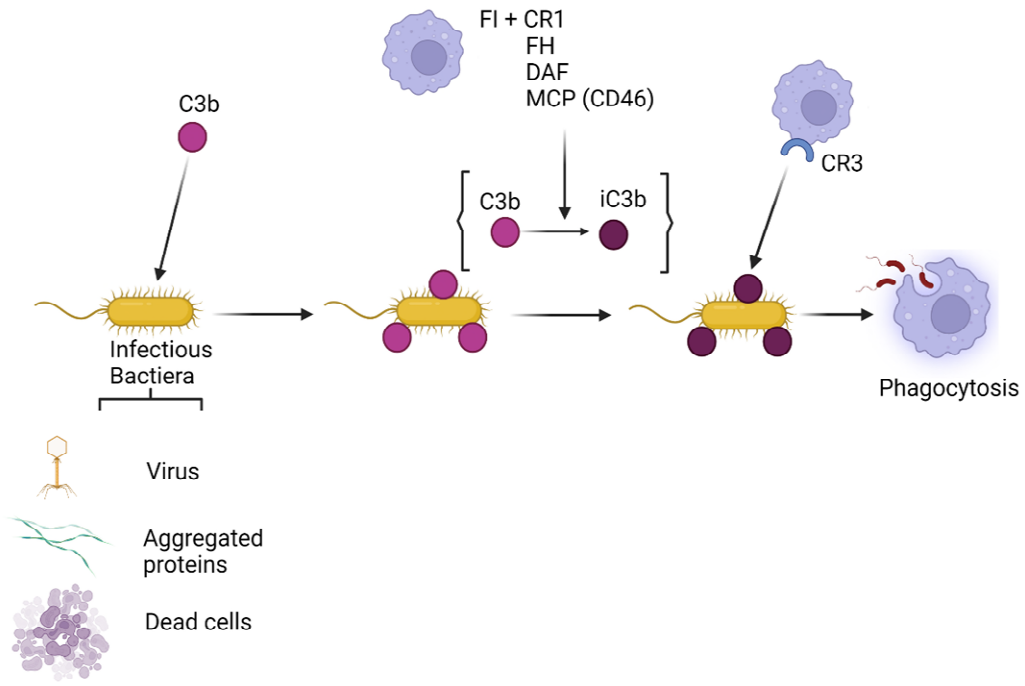

Figure 1.5: Function of CR1
C3 fragment C3b is produced following C3 convertase action on C3. C3b is an opsonin which covers infectious elements like bacteria or virus' as well as dead cells and aggregated/misfolded proteins. C3b is then converted to IC3b with CR1 and FI. IC3b is the ligand for CR3, a phagocytosing receptor found on microglia cells. This allows for the coated molecule to be removed and phagocytosed. Created with BioRender.com[157].

1.5.7.4 Soluble CR1

Proteolytic cleavage of CR1 produces soluble CR1 (sCR1) which is present at low concentrations in the plasma, ~ 50ng/ml[141]. sCR1 consists of the extracellular SCRs from CR1 and is a local potent inhibitor of complement[143]. Previous studies have shown treatment with sCR1 to be beneficial for systemic lupus erythematosus (SLE) and glomerulonephritis as an anti-inflammatory[143].

1.5.7.5 Crry

Studying CR1 in animal models is complicated by the lack of CR1 in non-human primates and rodents. Non-human animals have an additional gene , CR1-related protein y, Crry. Sequence homology analysis of human *CR1*, indicates the closest ortholog to be complement related protein y (*Crry*), see figure 1.6. The sequence and functions of Crry and human CR1 are shown to be very similar, with the exception of Crry being much smaller than human CR1[159,160]. Indeed, *Crry* is considered the evolutionary precursor to human *CR1*, with its knockout from mice resulting in embryonic lethality[159,161]. Despite these similarities, Crry fails to recapitulate the full function and capacity of human CR1, greatly limiting experimental models for the study of CR1. Although some useful data has been generated for Crry function in mouse models, it is important to be aware of the caveats of this

work and to repeat data on human models[159,162]. This is made possible by the newly developed Jackson lab mouse models which express human CR1[163].

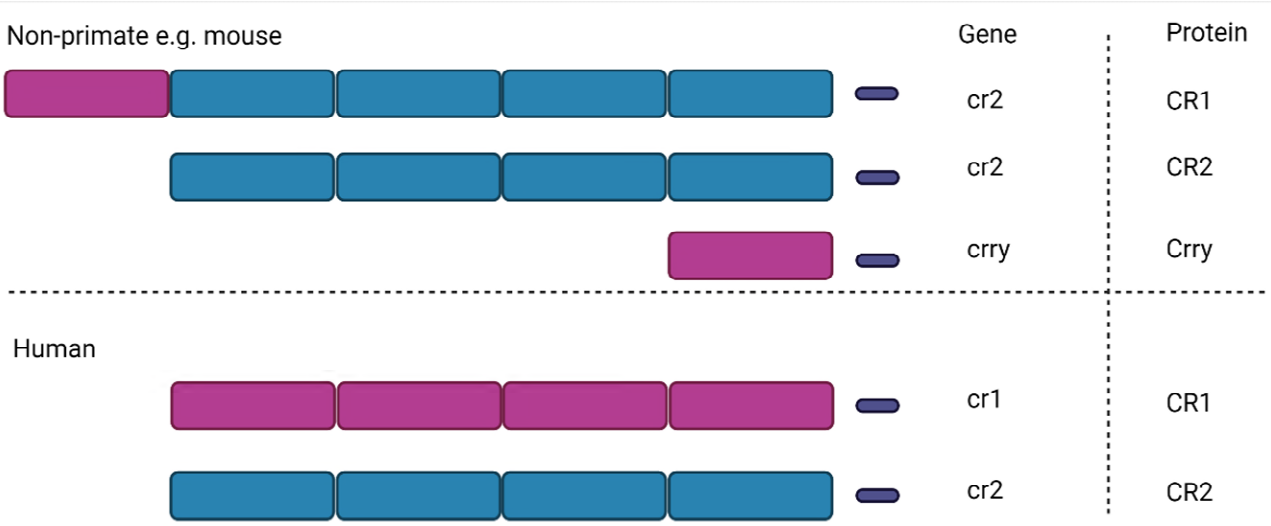

Figure 1.6: Difference of CR1 and murine crry genetic locations
Purple blocks denote common sequences in Crry and human CR1 proteins while blue blocks represent common sequences between human and mouse CR2 proteins. In humans CR1 and CR2 is encoded on two separate genes to produce two separate proteins. However, in non-primates such as mice, CR1 and CR2 is encoded on the same gene, cr2 to produce proteins CR1 and CR2. Created with BioRender.com and [163,164]

1.5.7.6 Genetic association of CR1 with AD

As previously mentioned, the *CR1* locus has been implicated in AD pathogenesis through large independent GWAS studies[133,134,165]. The first study to link the *CR1* locus to AD risk was shown through the Genetic and Environmental Risk in AD Consortium 1 (GERAD1) study and was confirmed in Lambert et al[78,166]. The Lambert et al study revealed 11 SNPs across multiple gene loci shown to be associated with AD. This included two SNPs within CR1[166]. The first of these is rs6646401, which had an odds ratio (OR) of 1.21 and p value of 3.5×10−9, and the second being rs3818361 which had an OR of 1.19 and p=8.9×10−8[165,167]. Both of these SNPs are within 1.27kb of the size polymorphism linkage disequilibrium site[166]**.** Individuals possessing rs6646401 have a 14% likelihood of expressing the shorter CR1-F size allele[141].

GWAS studies have identified other *CR1* SNPs as relevant research targets in the pathology of LOAD. However, much variation has been observed between different ethnic populations. Following this, SNP rs6656401 and rs391936 have been confirmed as AD risk SNPs in France, Belgium, Finland, Italy, Spain, USA, UK, The Netherlands, Germany and Han Chinese populations[168–172]. Other SNPs rs6701713, rs4844610 rs1408077 and rs6701710 have shown significance in Western populations but not in other ethnic groups, such as the Han Chinese or Korean cohorts[173]. Contrary to this, rs116806486 and rs6691117 have been associated with AD in Han Chinese people but not found in other races[174]. These differences could be due to heritability of the disease or possibly methodological differences. In order to ascertain the genetic risk of CR1 in AD, large, sufficiently powered studies of varying populations are required in addition to provide a comprehensive summary of the current genetic hits.

Preliminary associations between GWAS CR1 SNP hits and AD pathological traits have been explored. One study separated AD patients from those with cerebral amyloid angiopathy (CAA), a disease commonly occurring alongside AD and associated with build-up of amyloid in blood vessels[175].

Separation of these similar disorders revealed *CR1* variant rs6656401 to be significantly related to recurrence of CAA and the severity of vascular amyloid deposition. This is supported by others who utilised autopsy samples from healthy elderly subjects to show an association of rs6656401 with increased severity of vascular amyloid deposition[175]. Additionally, this CR1 SNP was still found to be significantly related to LOAD patients, even after the removal of patients exhibiting CAA. This indicates this *CR1* SNP encodes for risk for LOAD and CAA independently[175]. Furthermore, this implies a relation of rs6656301 to common pathological hallmark, Aβ. However, this requires further investigation to confirm. Another study investigated the relationship of CR1 SNP with LOAD cognitive symptoms focusing on rs4844609. This revealed a significant association between rs4844609 and a decline in episodic memory and increase in neuropathological features of LOAD patients. They further showed this effect to be modulated by *APOE* status, indicating a common pathway for ApoE and CR1[147]. Non-coding SNP, rs6656401 has shown to be associated with increased cognitive decline in LOAD patients across episodic memory, semantic memory, perceptual speed and visuospatial ability[147]. Interestingly this same SNP has been linked to smaller local grey matter volume in the entorhinal cortex of healthy individuals[176]. A similar effect has been shown in those with anther CR1 SNP, rs1408077, which has been related to significant reductions in entorhinal cortex thickness[177]. It has been hypothesised that these alterations may make individuals more susceptible to developing LOAD later in life. Moving forward, more in-depth investigations into associations of CR1 SNP and AD phenotypes is required to aid in understanding how CR1 may be implicated in disease.

1.5.7.7 Potential roles for CR1 in AD

There are several mechanisms in which CR1 may increase susceptibility to AD. One of these is in the clearance of Aβ in the periphery and directly within the brain. The capacity of CR1 to generate iC3b from C3b may affect the capacity for phagocytosis. Indeed, isolated rat microglia and showed phagocytosis of Aβ and opsonised dextran beads to be reduced when added alongside a Crry blocking antibody[162]. The similarity between crry and CR1 implicate this as a possible role of CR1 in human cells, implicating CR1 in phagocytosis.

The importance of CR1 in complement regulation is shown through Crry knock out animal studies, which show animals to have reduced serum C3 and FB[178]. This was hypothesised to be due to chronic AP activation depleting available C3. Interestingly, the AP has been specifically linked to AD pathology with increased mRNA for FB, FI and FH associated with AD brain samples relative to non-demented individuals[179]. This indicates overactivation of the AP in AD, in which CR1 might be implicated. Uncovering any CR1 SNP associations with AP protein/transcript in brain samples could aid in understanding this relationship. Contrary to this, studies on AD mouse model, with human amyloid precursor protein (hAPP) transgenic mice showed inhibition of the complement system to increase plaque and neurodegeneration, while addition of C3 reduced plaque load[125]. These results point to a protective role of complement activation in this model of AD.

Some evidence for a role of CR1 in tau pathology has been shown. Unpublished data from the Haroutunian lab showed a correlation of CR1 mRNA and NFT tangle and phosphorylated tau abundance[180]. Others have shown *Crry-/-* mice to have a strong and significant reduction in tau phosphorylation at serine 235 site, a site for hyperphosporylation of tau[164].

The mechanisms for CR1's action within AD requires much research. The first part of this is confirming the expression of CR1 within the CNS followed by investigating how CR1 may be involved in key functions and how AD related SNPs impact this. However, investigation of CR1 is complicated by the lack of human CR1 within animal models (the previously mentioned Jackson CR1 mice have only

recently been developed). Furthermore, there is a low availability for human primary cells and the currently available brain cell line models are known to have multiple problems, for instance human microglia cell line, HMC3, has shown to have low phagocytic capacity[181]. These issues are overcome by the availability of stem cell models, which can now be derived from adult somatic cells. This provides a human cell model which can be manipulated to a range of CNS cell types.

1.6 Stem Cells

Stem cells are self-renewing pluripotent cells, which are able to differentiate into any cell type[182]. Embryonic stem cells (ESC) were the first available stem cell model which are derived from the inner cell mass (ICM) of the blastocyte[183]. The blastocyte, generated from the fusion of sperm and ovum during fertilisation, is made up of two distinct cells types: the ICM and the trophectoderm (TE)[184]. The TE develops to form extraembryonic structures which support the development of the embryo, such as the placenta. As the TE becomes more specialised, the ICM cells remain undifferentiated and fully pluripotent. If allowed to continue through embryogenesis, germ layers: endoderm, mesoderm and th30pprox.30rm are formed, each gives rise to differentiated cells and tissues of the developing organism, this is summarised in figure 1.7[184]. ESCs were first successfully collected from the ICM separately by Martin and Evans during the 1980s. Previously, many had failed to achieve this due to a lack of cells available in the ICM at the time of harvest. Evans et al (1981) overcame this by delaying blastocyte implantation[185]. This allowed for inner cells to accumulate. Alternatively, Martin (1981) utilised a carcinoma cell line to produce conditioned media which was then used to culture ICM cells on a layer of feeder cells[186]. In both methods, ESC capable of forming teratomas of all three germ layers was shown[187].

Induced pluripotent stem cells (iPSC) were later developed from adult somatic cells by Takahasi and Yamanaka in 2006[188]. It was shown that the introduction of key pluripotent transcription factors by retroviral transduction into mouse embryonic fibroblasts reprogrammed them to pluripotent stem cells[188]. This was quickly adapted for use in human somatic cells, beginning with skin fibroblasts, and has now been expanded to multiple tissues, such as blood. The transcription factors identified as sufficient to induce this change are referred to as the Yamanaka factors and include: *Oct4, Sox3, Klf4* and *Myc*, this is summarised in figure 1.7[188,189]. iPSC cells confirmed by the presence of pluripotent transcription factors in addition to other pluripotent markers: nanog, *Lin28, SSEA3, TRA1-60* and *REX1*[188,190,191].

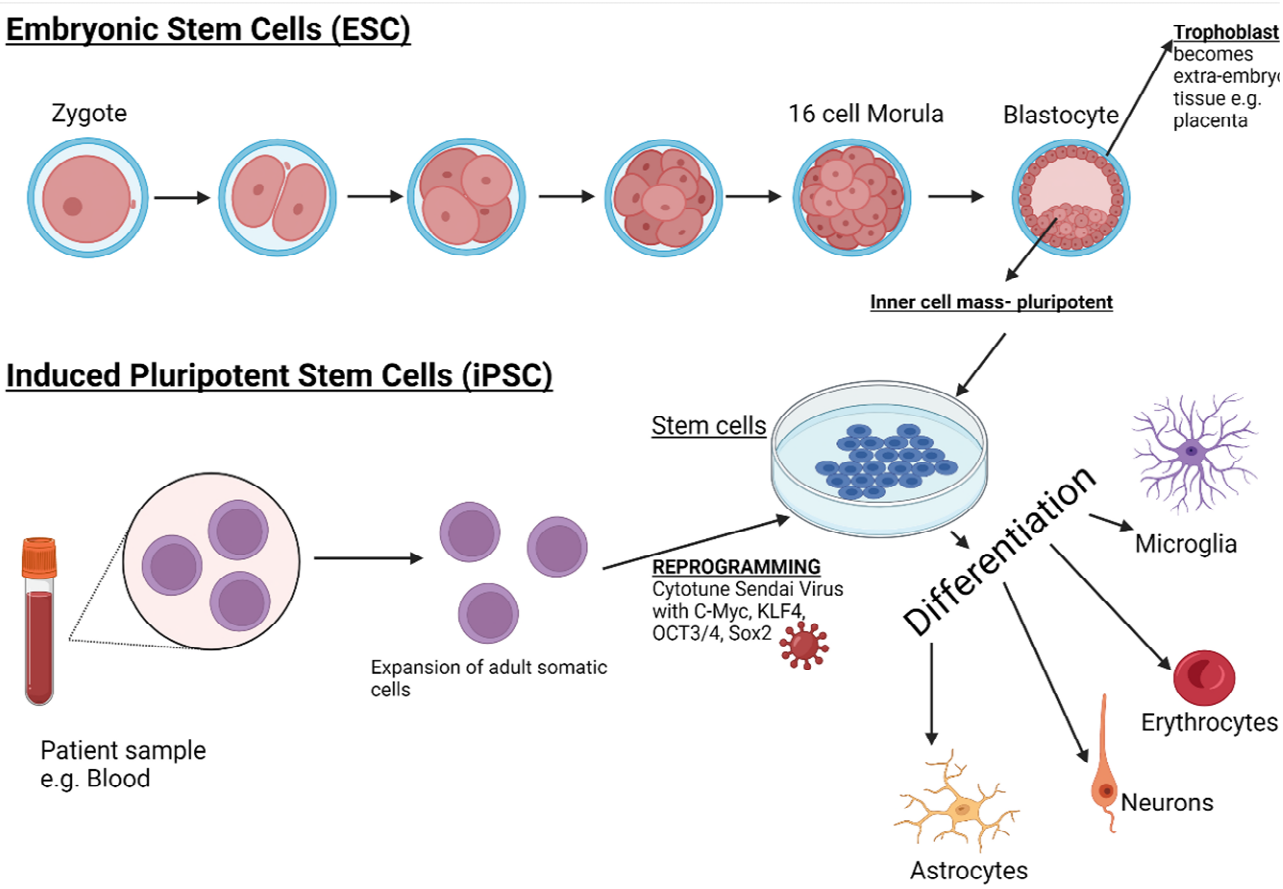

Figure 1.7: Generation of embryonic stem cells and induced pluripotent stem cells *Embryonic stem cells (ESC) are produced from the inner cell mass of the blastocyte which is produced once the zygote contains 123 inner cells. Induced pluripotent stem cells (iPSC) are produced from adult somatic cells which can be derived from skin cells or from the blood. These cells are then expanded before being transfected with cytotune sendai virus with pluripotent genes such as C-Myc, KLG3, OCT3/4 or SOX2. ESC and iPSC can then be differentiated to any cell type. Created with BioRender.com and* [192].

Since 2006, an explosion of methods for the generation of various cells has been published. Differentiation to a desired cell type is performed by mimicking the growth factor gradients present *in utero*. This directs pluripotent cells towards the desired cell type. This has hugely impacted biological sciences, particularly neuroscience, which until this point had relied on animal models, primary cells and cell lines. Established protocols for the generation of astrocytes, neurons, pericytes, oligodendrocytes, endothelial cells and microglia are now available[57,193–199].

Use of iPS microglia are of highly valuable models. As previously mentioned, microglia are highly reactive cells which react to subtle changes in the micro-environment. Isolation of primary microglia from the pathological human brain or from rodent models often results in activation[57]. Similarly, cell lines for studying microglia, such as the human HMC3 line, have multiple problems. For instance, HMC3 cells have shown to have a reduced phagocytic capacity and low CD11b presence, two key characteristics of functional microglia[181]. Stem cells offer a unique and valuable alternative model for studying microglia. Despite this, differentiation to microglia cells proved to be one of the most difficult cells to differentiate to, with the first protocol not published until 2016[200]. These problems were due to the origin of microglia being obscured, a prerequisite for directed differentiation.

1.6.1 Microglia Ontogeny

The ontogeny of microglia was previously a controversial subject. Originally microglia were thought to be neuro-ectoderm in origin, with astrocytes, neurons and microglia thought to be derived from the same progenitors. Indeed, neurons and astrocytes are produced from a common neuro-ectoderm pathway, however this does not include microglia. Evidence for this difference was first provided by PU.1 knockout animal models, were shown to be absent of microglia[201]. *PU.1* is an essential transcription factor for the generation of monocytes, suggesting that microglia are instead derived from hematopoietic cells[201]. This was supported by evidence showing similar morphological features between microglia and macrophages in addition to similar expression of multiple markers such as CD11b[57].

Haematopoiesis in embryogenesis occurs in two major sites in two waves: the extra-embryonic yolk sac (YS) and the fetal liver[202,203]. The first wave of haematopoiesis, primitive hemopoiesis, is initiated in the YS, shortly after gastrulation producing erythrocytes and macrophages. In mice this initiates around embryonic day 7 (E7). Primitive macrophages appear in the blood islands of the yolk sac, in mice around the ninth day of gestation. These macrophages spread to various tissues, including the brain, through the early circulatory system. These primitive macrophages penetrate the developing tissue where they continue to proliferate until they colonize the whole tissue[204]. These cells are referred to as 'fetal macrophage populations.' Following E8.5 in mice, a new wave of hematopoietic progenitors is generated in the aorta, gonads and mesonephros (AGM) region.[202,204] These progenitors colonize the fetal liver, which becomes the dominant hematopoietic organ producing hematopoietic cells including monocytes. This is referred to as definitive haematopoiesis. It has been shown primitive haematopoiesis relies on PU.1 but it is independent of Myb while the opposite is true for definitive haematopoiesis[204]. This supports that YS- derived macrophages constitute a separate population of cells to those produced in the definitive wave of haematopoiesis. It was conclusively documented that microglia progenitors were present in the brain in mice around E9/E9.5, this in combination with PU.1 KO animal studies suggests microglia to be derived from YS-macrophages. Since, lineage tracing studies have confirmed microglia to be derived from YS-macrophages which penetrate the brain prior to the formation of the blood brain barrier[204,205].

1.6.2 Directed differentiation to iPS Microglia

Protocols for the generation of iPS microglia first produce embryonic macrophages and skew them towards a microglia phenotype. During 2016-2017, several protocols for the generation of microglia were published[57]. No consensus on the methodology for iPS- or ESC-derived microglia has been made with protocols using a variety of culture media and conditions. Some similarities exist between protocols, with some first generating 3D embryo body (EB) organoids while others use multiple media changes on a monolayer of cells[57]. Despite this difference, multiple similarities exist across the protocols; for instance, the use of some growth factors, such as bone morphogenetic protein 3 (BMP-4), which encourages differentiation towards mesodermal lineage. Incubation of BMP-4 and other growth factors, such as vascular endothelial growth factor A (VEGF) (which is necessary for haematopoiesis) produces YS-like cysts from eBs[197,206–208].

Stem cell technology offers many advantages such as a readily available source of microglia which can be derived from patients of the disorder investigated. Furthermore, with the advance of genetic editing tools, such as CRISPR Cas9, stem cells offer the opportunity to produce genetically informative models. CRISPR/Cas9 is a bacterial adaptive immune system which can be used to produce high efficiency edits in cells. CRISPR–- standing for Clustered Regularly Interspaced Short Palindromic Repeats–- is a system in which bacterium integrate edits of infective viral DNA adjacent to sequences

for cas endonucleases[209,210]. This allows a bacterium to express the cas protein and integrated DNA. The integrated DNA acts as a guid–, so if the bacteria is infected again, it can recognise the protein and the cas endonuclease can be directed to its specific site and bind to produce a double stranded break (DSB). This would disrupt production of the protein to provide protection from the invading pathogen[210,211]. This system has been optimised for use in the lab, allowing researchers to generate knock outs, add sections into a gene or even make single nucleotide changes. Compared to alternative genetic machinery tools, such as zinc fingers, CRISPR offers a highly efficient, highly selective tool allowing for specific locations to be targeted[210]. Furthermore, the expanse of CRISPR tools offers a range of additional functions including timed genetic edits.

Despite the benefits of stem cells, they still come with many unknowns and difficulties. For instance, clones have been shown to vary greatly between one another with some more prone to spontaneous differentiation events than others. Furthermore, cells produced in this method are mono-cultures containing only one cell type. This has been shown to alter differentiation due to reliance of cell-cell signalling in these events. Resolving these issues will include the generation of more protocols for co-cultures or 3D organoid cultures. Organoids, also referred to as 'mini-brains' can contain astrocytes, neurons and microglia providing a 3D cell environment for the research of brain cells[212].

1.7 Aims and Objectives

The overarching hypothesis of this thesis is that CR1 is involved in LOAD pathology by action within the CNS, most likely through its complement regulatory and opsonin-binding functions. In order to investigate this, iPS cells were differentiated into iPS microglia. Differentiation to microglia required some optimisation to select the optimal differentiation protocol for subsequent assays. Following this, iPS microglia were characterized for expression of CR1 at the transcript and protein level using a range of techniques. CR1 KO iPS clones were then generated using CRISPR/Cas9 machinery. Once confirmed for the absence of CR1 protein, comparisons between CR1 WT and CR1 KO iPS microglia functions were made. This provides evidence for the expression of CR1 on CNS iPS models and offers tools and prelimary data to begin uncovering how CR1 is implicated in cellular function.

Summary of the aims are as follows:

- To optimise and characterize directed differentiation from iPS to iPS microglia cells
- Characterize iPS microglia for expression of CR1
- Characterize iPS astrocytes for astrocytic markers and expression of CR1
- Generate CR1 KO iPS clones using CRISPR Cas9
- Perform prelimary functional assays on how CR1 affects microglia role
- Characterise the relative expression of complement in iPS cortical neurons, iPS astrocytes and iPS microglia

2.0 Materials and Methods

2.1 Materials

All cell culture consumables are in table 2.1, antibodies in table 2.2 , kits used in table 2.5 followed by general consumables in table 2.6 and Fluidigm consumables in table 2.7. Tables 2.3 and 2.4 show information on in house antibodies used in this thesis. Any buffers or medium recipes are in the relevant section. All RT-QPCR primers are in appendix 1.

2.1.1 Tissue Culture Reagents

Component	Use in this work	Supplier	Catalogue number
E8 flex basal media	Undifferentiated iPS media	Life Technologies	A2858501
Advanced DMEM/F12 (ADF)	Astrocyte conditioned media base media	Gibco	12634010
XVIVO-15	Differentiation base media	Scientific Laboratory Supplies	LZBE02-060Q
Glutamax (100x 200mM L-gluatmine)	Support cell survival	Thermo Fisher	35050-038
Penicillin/Streptomycin 5,000U/ml	Antibiotic	Gibco	15070063
ß-mercaptoethanol	Helps to maintain levels of oxygen radicals	Life Technologies	31350
1% vitamin A neurobrew	Supplement for iPS astrocyte maintenance	Miltenyi Biotech	130-093-566
Y-27632 dihydrochloride (Rock Inhibitor RI) Stock conc = 1mM	Supplement which supports single cell iPS survival	Tocris	1254
Vitronectin (VTN)	Undifferentiated iPS coating	Gibco	A31804
ReLesR	Gently passaging reagent	Stem Cell Technologies	05872
Fibronectin	iPS microglia coating	Merck Millipore	FC010-5MG
Matrigel	iPS astrocyte coating	Corning	11573560
Poly-D-Lysine	Coating for glass	Gibco	A3890401
BMP-4	Growth Factor	PeproTech	120-05ET
SCF	Growth Factor	PeproTech	300 07
VEGF	Growth Factor	PeproTech	100-20
IL-3	Growth Factor	PeproTech	200 03
MCSF	Growth Factor	PeproTech	300-25
CHIR99021	Growth Factor	Sigma Aldrich	SML1046-5MG
DKK1	Growth Factor	R&D	5439-DK-010/CF

IL-6	Growth Factor	Gibco	PHC0061
FGF_2	Growth Factor	Peprotech	100-18B
EGF	Growth Factor	Sigma Aldrich	SRP3027
CNTF	Growth Factor	Thermo Fisher	PHC7015
PBS pH 4	To wash cells	Gibco	10010015
Trypan Blue	Cell counting dye	Thermo Fisher	15250061
Formalin	Fixative	Merck	HT501128
Aggrewell-800	Plate used to make embryo bodies (EB)	Stem cell technology	34850
Accutase	Cell passaging reagent	Thermo Fisher	A1110501
Cryostor	Cell storage medium	Merck	C2874
1X TrypLE	iPS dissociation reagent for EB generation	Gibco	12604013

Table 2.1 Consumables for cell culture

2.1.2 Antibodies

Component	Use in this work	Supplier	Catalogue number
CD45 conjugated to FITC	Confirm myeloid cell signature in precursors for microglia differentiation	BioLegend	982316
FITC isotype control	Isotype control	BioLegend	981802
CD14 conjugated to APC	Confirm myeloid cell signature in precursors for microglia differentiation	BioLegend	325607
APC Isotype control	Isotype control	BioLegend	400121
CD11B conjugated toBrilliant Violet	Confirm myeloid cell signature in precursors for microglia differentiation	BioLegend	301323
Brilliant Violet Isotype control	Isotype control	BioLegend	400157
Oct4 primary antibody	Undifferentiated iPS cell marker	Abcam	ab200834
Sox2 primary antibody	Undifferentiated iPS cell marker	Abcam	ab03690
Tra1-60 primary antibody	Undifferentiated iPS cell marker	Abcam	Ab16388
CD45 primary antibody	Myeloid cell marker	Abcam	ab30470
CD14 primary antibody	Myeloid cell marker	Abcam	ab183322
CD11b primary antibody	Myeloid cell marker	Abcam	ab8878
Iba-1 primary antibody	Microglia cell marker	Abcam	ab178680
Tmem119 primary antibody	Microglia cell marker	Abcam	ab185333

CX3CR1 primary antibody	Microglia cell marker	Abcam	ab51668
CD68 primary antibody	Microglia cell marker	Abcam	ab201340
GFAP primary antibody	Astrocyte cell marker	Dako	Z0334
ALDH1 primary antibody	Astrocyte cell marker	Abcam	ab177463
IgG control	Isotype control		
Alexa Fluor goat anti Rat 594	Secondary antibody	Invitrogen	A-11007
Alexa Fluor goat anti Mouse 594	Secondary antibody	Invitrogen	A11005
Alexa Fluor goat anti Rabbit 488	Secondary antibody	Invitrogen	A11008
Alexa Fluor goat anti Mouse 488	Secondary antibody	Invitrogen	A-10680
Alpha Tubulin WB control	Protein loading control	Abcam	ab7291
CR1	Gene of interest	Abcam	ab212311
CR1 MBI38 anti Mouse	Gene of interest	Made in-house	See 2.1.2.1
CR1 MBI35 anti Mouse	Gene of interest	Made in-house	See 2.1.2.1
Poly CR1 anti Rabbit	Gene of interest	Made in-house	See 2.1.2.1

Table 2.2: Antibodies

2.1.2.1 In house antibody information

Multiple antibodies for a range of complement proteins have been generated in house. For some of these antibodies the production and screening methods have been published[213–215]. The generation of antibodies against CR1 was done by Dr. Claire Harris while C3 antibodies were generated by multiple lab members.

2.1.2.1.1 Summary of antibody production:

Monoclonal antibodies (mab) against CR1 were produced in WT mice while C3 monoclonal antibodies were made using C3 KO mice. Mice were immunised subcutaneously with recombinant proteins (CR1 50-100µg; C3- 50-100µg) in complete Freund's adjuvant (CFA; Sigma). Animals were boosted twice with protein in incomplete Freund's adjuvant (IFA; Sigma) at intervals between 2 and 4 weeks. Serum samples were collected and used to screen for production of antibodies against the immunised protein. The best responders were boosted for a fourth time and then were humanely sacrificed, and the spleens dissected. Splenocytes were collected and fused with SP2 mouse myeloma cells. Cells were incubated under standard tissue culture (TC) conditions until visible clones were present within the well and supernatant was collected. Fused cells could be frozen and stored as backup stocks for later revival if antibody stocks were running low.

Polyclonal antibodies were generated in young adult New Zealand white rabbits. Rabbits were immunised with CR1 proteins and C3 proteins (50-100µg) in CFA. They were then boosted with protein

in IFA at weeks 4 and 5. Around week 6, a 10ml test bleed was collected to test for antibody production. If positive, rabbits were exsanguinated, and antiserum was acquired.

Antibodies underwent multiple rounds of screening using recombinant proteins in an enzyme-linked immunosorbent assay (ELISA) like protocol outlined in previous papers[213–215]. In-house antibodies were used as they offer an efficient and cost reducing reagent. Although CR1 antibodies had been carefully screened by lab members, additional images were captured using a commercial CR1 antibody. Furthermore, pre-absorption staining was performed. For this method, antibody was incubated with excess sCR1 protein (section 2.2.5.5) to reveal loss of staining. These additional steps provide support for the specificity of the CR1 antibodies to CR1. An additional western blot is provided in figure 2.1 which shows in house antibody MBI38 to bind to CR1 protein, revealing no additional or unspecific bands. This provided further support for the antibodies specificity in addition to blot shown in figure 2.7. The protocol for the western blot (WB) is available in section 12.2.7.

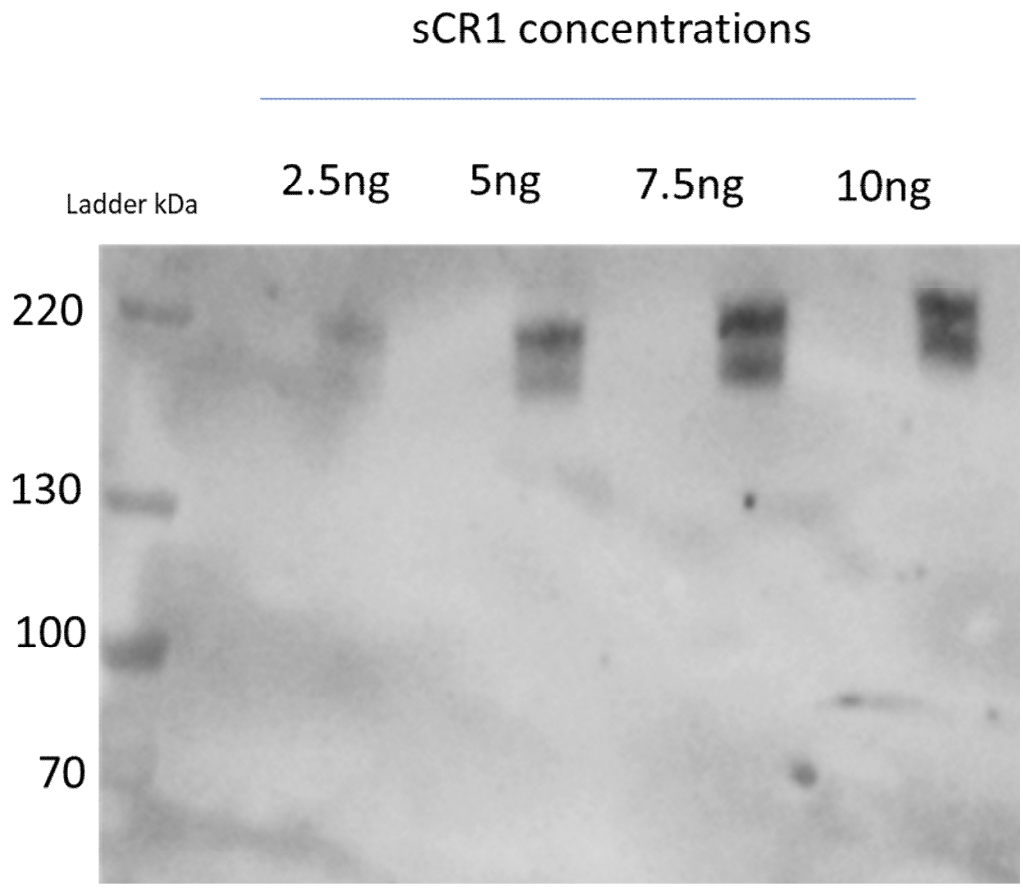

Figure 2.1 Western blot of increasing concentrations of CR1 protein with in house antibody MBI38. This was repeated once.

2.1.2.1.2.CR1 antibody information

In-house CR1 antibody label	*Isotype*	*Host*
MBI-38	*IgG1*	*Anti-Mouse*
MBI-35	*IgG1*	*Anti-Mouse*
Poly-CR1		*Anti-Rabbit*

Table 2.3 Summary of in house CR1 antibodies

2.1.2.1.3 C3 antibody information for ELISA

Antibody	*Use in this work*
Poly anti C3	*Capture antibody*
Antibody PC3- HRP	*Detection antibody- conjugated to HRP*

Table 2.4 Summary of in house C3 antibodies

2.1.3 Kits

Component	Use	Supplier	Catalogue number
Power up SYBR green	RT-qPCR fluorescent reagent	Applied Biosystems	A25778
High-Capacity RNA-to-cDNA™ Kit	Generating cDNA from RNA	Thermo Fisher	4387306
RNAeasy mini-kit	RNA extraction kit	Qiagen	74104
P3 Primary cell 4D-Nucleofecter kit	Nucleofection kit	Lonza	V4XP-3032
Pierce Micro BCA assay kit	Protein quantification kit	Thermo Fisher	23235
QIAquick PCR purification	PCR purification kit	Qiagen	28104

Table 2.5: Kits

2.1.4 General Consumables

Component	Use in this work	Supplier	Catalogue number
Lipopolysaccharide	Endotoxin for stimulation	Sigma Aldrich	L2654-1MG
DuoKit IL-1β	ELISA	R&D	DY201
DuoKit CCL_2	ELISA	R&D	DY279-05
FITC conjugated Amyloid β	Oligomer amyloid β used for phagocytosis	Anaspec	AS-60479-01
DAPI	Nuclear stain	BioLegend	422801
Cytochalasin D	Phagocytosis inhibtor	Sigma Aldrich	C8273-1MG
pHrodo red E.coli bioparticles	E-coli bioparticles used for phagocytosis	Life Technologies	P35361
Live Cell Imaging Solution	Clear solution for live cell imaging	Life Technologies	A14291DJ
96-well black-walled µ-clear microplates	Imaging	Griener	655094
Normal Goat Serum	Blocking reagent	Dako	X0907/X0903
RIPA buffer	Protein extraction	Thermo Fisher	89900
Qiazol	RNA extraction reagent	Qiagen	79306
Glycogen	RNA extraction-Qiazol	Thermo Fisher	R0561
BSA	Protein for blocking buffers	Thermo Fisher	B14
ECL	Activate western blot for detection	Merck	GERPN2106
Sodium Azide	RNA extraction-Qiazol	Thermo Fisher	15835188
EDTA	Flow buffer	Thermo Fisher	17892
Chloroform	RNA extraction-Qiazol	Merck	67-66-3
Fluorsave	Mountant	VWR	345789
OPD Tablets	ELISA substrate for HRP colour change	Thermo Fisher	34006
CR1 Protein	Used for pre-absorption in staining	Sigma	
C3 Protein	Used for standards in C3 ELISA	Comptech	A138
SYBR safe	Stain to visualise agarose gel	Invitrogen	10328162
Agarose	Used to make up gel to run PCR samples		16500500
GoTaq Master mix	Master mix for PCR	Promega	M7122 17919

Acrylamide	Used to make gels for running protein	Thermo Fisher	J66184.A1
TEMED	Used to make gels for running protein	Invitrogen	17919
SDS	Used to make gels for running protein	Invitrogen	15525017
Page ruler ladder 10-250kDa	Western blot ladder	Thermo-Fisher	26620
HRP conjugated secondary ab Goat anti mouse	Secondary antibody for western blot	Invitrogen	62-6520
Tween-20	Used for buffers in staining and western blotting	Themo Fisher	003005
Maxisorp plate	ELISA plate	Thermo Fisher	44-2404-21
PhosStop	Supplement for protein extraction	Merck	4906845001
Tris Base	Base of buffers	Thermo Fisher	17926
Proteinase K	DNAse extraction	Thermo Fisher	25530031
dNase 1	To remove DNA from RNA samples	Invitrogen	18068015

Table 2.6: General Lab consumables

2.1.5 High-Throughput qPCR consumables

Component	Use	Supplier	Catalogue number
Reverse Transcription master mix	Generate cDNA	Fluidigm	100-6297
Pre-amplification master mix	Preamplification mixture	Fluidigm	100-5580
Exonuclease	To end the preamplification reaction	BioLabs	M0293L
Flex 6 Delta gene sample reagent	Used to dilute samples	Fluidigm	100-7673
Flex 6 IFC	Fluidics chip used to optimise DNA concentration for 6 samples and 6 primers	Fluidigm	100-6308
DNA Binding dye	Required to load samples	Fluidigm	100-7609
Assay Loading Reagent	Required to load primers	Fluidigm	100-7611
Control Line Fluid	Required to activate the fluidic	Fluidigm	100-4058
DNA Suspension Buffer (TE buffer)	Suspend DNA and make dilutions	Thermo Fisher	12090015
sssoFast Eva Green	RT-qPCR fluorescent reagent	Biorad	1772-5211
96.96 IFC	96 sample, 96 primers fluidics chip	Fluidigm	BMK-M-96.96

Table 2.7 High-throughput RT-QPCR Fluidigm consumables

2.2 Methods

2.2.1 Cell culture

Cells were maintained using aseptic techniques and incubated in a humidified incubator set to 37°C, 5% CO_2.

2.2.1.1 Maintenance of undifferentiated KOLF2 Induced Pluripotent Stem Cells (iPSC)

KOLF2 human stem cell line is a commercial line purchased from HipSci (the human-induced pluripotent stem cell initiative; Sanger institute) They were reprogrammed using Cytotune 1, Sendai virus transfection by the company. More information is available online at HipSci.com (https://www.hipsci.org/lines/#/lines/HPSI0114i-kolf_2).

KOLF2 iPS cells were cultured in feeder free conditions and maintained in Essential 8 flex media (E8). Cells were passaged when 60% confluent using 1ml of cell passaging reagent ReLeSR per well. ReLeSR encourages the gentle detachment of cells and if used correctly will not detach any cells undergoing spontaneous differentiation. Optimal detachment required the cells to be incubated with ReLeSR at 37°C for 3 minutes. After incubation ReLeSR was aspirated, and cells collected in E8 media, being careful to not break up colonies. Cells were then plated onto pre-prepared vitronectin (VTN) coated plates. Vitronectin coating was performed using VTN diluted in PBS at 1:100, 1ml of this was used per well of a 6 well plate and incubated at room temperature for 1 hour. iPS colonies grow in large round colonies. If colonies became overgrown and began to touch, spontaneous differentiation occurs. Cells begin to morphologically change becoming more spiked as shown in figure 2.1.

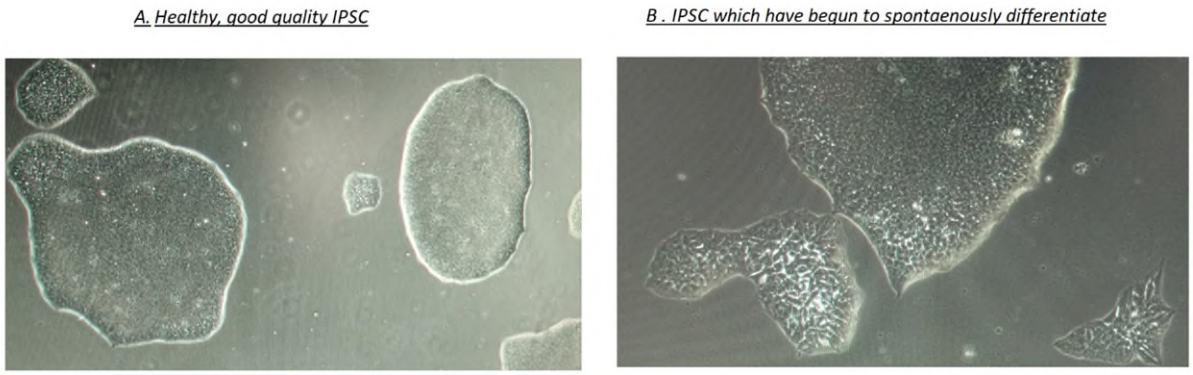

Figure 2.1: Light images of iPS colonies
Healthy pluripotent cells are shown on the left and the beginnings of spontaneously differentiation on the right.

2.2.1.2 Freezing and Thawing undifferentiated iPS cells

Undifferentiated iPS cells were frozen when 80% confluent. Cells were detached using ReLeSR, as above, and were collected in 1ml of commercial cryopreservation media Cryostor rather than E8. Cells were frozen in a -80°C freezer overnight using a cryopreservation Mr. Frosty container and were then transferred into the liquid nitrogen for long term storage.

Plating fresh vials of frozen cells required quick thawing with a water bath. Once thawed, cells were collected in pre-warmed E8 and centrifuged in a 15ml falcon tube at 400g for 5 minutes. Medium was

aspirated, and the pellet resuspended with 1ml of pre-warmed E8 media and plated onto VTN pre-coated plates.

2.2.1.3 Directed differentiation to generate iPS microglia precursors

iPS cells were differentiated to microglia-like cells following two separate protocols, the first is labelled 'the monolayer method' and is adapted from Takata et al 2017 while the second is referred to as 'the Embryo Body (EB)method' and is adapted from Haenseler et al 2017[197,207]. Both produce floating precursor cells (iPS Pre), positive for CD11b, CD14 and CD45.These cells were harvested weekly and plated for terminal differentiation to microglia-like cells, positive for markers Tmem119 and CX3CR1. Differentiation to microglia cell type was the same regardless of protocol used and is outlined in section 2.2.4.

A brief comparison of the iPS microglia and practicality of these two methods are discussed in chapter 3.3. It was decided to continue with the EB method as these cultures were more efficient and produced cells for longer.

2.2.1.3.1 Monolayer method

The monolayer method is adapted from protocol published in Takata et al 2017[197]. This utilises a large range of growth factors which are exchanged every 2 days for the first 15 days and then maintained in SF Diff supplemented media until iPS Pre production finishes. Exchanging the media on a 2D culture produces dense structures which later form transparent cysts. Eventually large, round iPS pre cells were produced which could be harvested for terminal differentiation.

2.2.1.3.1a) Media for the monolayer method

Media used throughout the protocol are as follows:

StemPro media: this is the base media which is supplemented with growth factors according to the day of the differentiation. Table 2.1 shows the recipe for a 500ml bottle of media while table 2.2 shows the growth factor supplementation.

Component	**Final Concentration in 500ml media**
StemPro-34	500ml bottle
StemPro-34 Supplement	As supplied
Human Transferrin	200µg/ml
Glutamax	2mM
Ascorbic Acid	0.05mM
PenStrep	1:100

Table 2.8: STEMPRO recipe

Day	Media name:	Growth factors- concentration
1	A	BMP-4 : 5ng/ml VEGF : 50ng/ml CHIR99021: 2µM
3	B	BMP-4 : 5ng/ml VEGF: 50ng/ml FGF2: 20ng/ml
5	C	FGF2: 5ng/ml VEGF:15ng/ml
7-11	D	VEGF: 10ng/ml FGF2: 10ng/ml SCF: 50ng/ml DKK1: 30ng/ml IL6 : 10ng/ml IL-3 : 20ng/ml
13-15	E	FGF: 10ng/ml SCF: 50ng/ml IL-6: 10ng/ml IL-3 : 20ng/ml

Table 2.9: Supplementation of growth factors into STEMPRO in the monolayer method

SF Diff: Following 15 days in supplemented Stempro cells are moved into SF Diff media, the recipe is shown in table 2.10.

Component	Amounts (ml)
IMDM with Glutamax	375ml
F12 Media	125ml
N2	5ml
B27	5ml
PenStrep	5ml
BSA	250µl
Make up 49 ml aliquots then add:	
mCSF	50ng/ml

Table 2.10 SF DIFF media recipe

2.2.1.3.1b) Protocol for monolayer method

Undifferentiated iPS cells were grown on VTN in E8, as previously mentioned. When 70% confluent, cells were split using ReLeSR and counted. Roughly, $1X10^5$ cells were plated in E8 onto Matrigel (diluted 1:100 in PBS) in a 6-well plate. Matrigel coating used 1ml of Matrigel/well and required incubation at 37^oC for 20-30 minutes. The following day, E8 was replaced with supplemented StemPro media, beginning with media A supplemented with 5ng/ml BMP4, 50ng/ml VEGF and 2µM CHIR99021. On day 3, media A was exchanged for media B supplemented with 5ng/ml BMP4, 50ng/ml VEGF and 20ng/ml FGF_2. On day 5, media was exchanged to media C which removes the BMP4 and reduces concentrations of VEGF to 15ng/ml and FGF_2 to 5ng/ml from media B. This was changed to media D on day 7 which was supplemented with 10ng/ml VEGF, 50ng/ml SCF, 10ng/ml FGF_2, 30ng/ml DKK1, 10ng/ml IL-6 and 20ng/ml IL-3 and was changed every 2 days until day 11. On day 13 media E was added to cultures, this included 10ng/ml FGF_2, 50ng/ml SCF, 10ng/ml IL-6 and 20ng/ml IL3. On day 15

media was changed to SF Diff supplemented with 50ng/ml mCSF, this was changed every 5 days until the end of the culture.

During the differentiation , iPS cells grow on top of one another and eventually begin to produce cystic yolk-sac- like structures. From day 15 onwards large round iPS precursors can be seen attached to the monolayer, and within 3 weeks these cells detach and can be collected for terminal differentiation. Terminal differentiation is conducted as described in section 2.2.4. All media used in this protocol are shown in tables 2.8, 2.9 and 2.10.

2.2.1.3.2 EB method

2.2.1.3.2a) Media

Medium preparation used throughout the EB protocol are as follows:

EB 3G: Embryo Body differentiation media, in table 2.11

Component	**Final Concentration in 50ml**
E8	50ml- base media
BMP-4	50µg/ml
VEGF	50µg/ml
SCF	20µg/ml
RI	1µM

Table 2.11: EB 3G recipe for the EB protocol

Factory Media: Once EBs are ready, they are transferred to a flask with factory media, shown in table 2.12.

Component	**Add to 500ml**
XVIVO-15	500ml base media
PenStrep	50U/ml
Glutamax (100X)	1:100 (2mM)
	Make up 49ml aliquots and then add:
mCSF	100ng/ml
IL-34	25ng/ml

Table 2.12: Factory media

2.2.1.3.2b) Protocol for EB method

Undifferentiated iPS cells were grown in E8 media on VTN. Once 90% confluent EBs were generated. Three EB methods were trialed to find the most efficient and replicable method. The first used direct lifting of colonies. For this, 1ml of warmed Accutase was added to cells and incubated at 37^{o}C for 2-3 minutes. Colonies were gently detached using a 1ml pipette into 2ml of E8 3G media, being careful to try and not break up colonies. The lifted colonies were kept in a 6 well plate overnight in 2ml EB 3G. The next day firm EBs could be seen and media was replaced with fresh EB 3G. Media exchange was done every second day for 6 days. Following day 6, EBs were transferred to flasks and termed ‘factories’. Factories were fed with factory media.

The second EB method used a hanging droplet protocol. For this, cells were detached using 1ml of Accutase per well of cells and collected in 1ml of E8 3G media supplemented with PFA. Cell droplets of 20µl were pipetted onto the lid of a 10cm dish and the base was then filled with PBS. The lid was then carefully placed on the dish and kept in the incubator overnight. The next day round Ebs could be seen inside each individual droplet. These are collected and transferred to a low attachment 6 well plate with 6ml of EB 3G per well. Media was changed every 2 days for 6 days. Following day 6, EBs were transferred into flasks and termed 'factories', and were fed with factory media.

The final EB method used an Aggrewell-800, which is a-24 well plate with 300 indents within each well. This allows for an EB to be generated in each indent with up to 24 lines per plate. Prior to EB generation, the aggrewell plate was prepared. For this, 1ml of rinse solution was added per well and the plate centrifuged at 3000g for 3 minutes. Rinse solution was then removed, and the well was washed with PBS. 1ml of 2X EB 3G was then added to wells and the plate was kept in the incubator while the cells were prepared. Cells from 2-3 confluent wells were collected using 1ml of prewarmed TrypLE per well. This was incubated at 37^{o}C for 5 minutes. Cells were collected using PBS and diluted in PBS at 1:10 ratio of TrypLE to PBS so for 3 wells, 3ml of TrypLE was used which was diluted to 30ml with PBS. Cells were counted and then centrifuged at 400g for 5 minutes. The solution was aspirated and cells were res-suspended in E8 flex media to a final concentration of 4X10^{6}/ml. 1ml of cells was then plated into a well of the Aggrewell. The Aggrewell was centrifuged at 300g for 3 minutes with the deacceleration brake on. Cells were evenly distributed across the indents of the well. The Aggrewell was kept in the incubator overnight, the next day EBs could be seen in each indent. A 75% media change was conducted every day for 6 days, this included careful removal of 1ml of media from the well and replacing it with 1ml of EB 3G media. This was repeated to generate a 75% media change. After day 3, EBs were plated across 3 wells of a low attachment 6 well-plate with 6ml of EB 3G media per well. After 4 days, EBs were transferred into flasks and termed 'factories' and fed with factory media.

For all factories, 8 EBs were using a T25 flask while 15 EBs for a T75 flask. While in factories, factory media (table 2.12) was used to maintain the EBs and was exchanged weekly. In the first few weeks EBs began to attach to the bottom of the flask and produced a skirt of endothelium around them. Dense EBs then formed yolk-sac like cystic structures. After 2 weeks in factories, large round cells with filipodia could be seen stuck to the endothelium. By week 3 these cells detached, becoming free floating in the flask. These cells are referred to as iPS precursors (iPS pre) and are the cells collected for terminal differentiation to iPS microglia. Collection was done during the weekly factory feed, with the collected media being centrifuged at 400g for 3 minutes and the cell pellet used for subsequent differentiation, as described in section 2.2.4. Factories were produced for up to 6-8 weeks and were later discarded using bleach. Media used for this protocol are shown in table 2.11 and 2.12.

2.2.1.4 Directed differentiation to iPS microglia

2.2.1.4.a) Media:

Terminal differentiation was done in either XVIVO supplemented media, as is used in McQuade et al 2018, or in-house produced astrocyte conditioned media (ACM)[208]. The recipe for XVIVO terminal media is in table 2.13 and the protocol for ACM production is in section 2.2.3.3.

Terminal differentiation XVIVO media:

Component	**Add to 500ml**
XVIVO-15	500ml base media
PenStrep	50U/ml
Glutamax	1:100 (2mM)
	Make up 49ml aliquots and then add:
GM-CSF	10ng/ml
IL-3	100ng/ml

Table 2.13: XVIVO terminal media recipe

2.2.1.4b) Protocol:

iPS pre were collected weekly and resuspended in the relevant media, this was either supplemented XVIVO in table 2.13 or in-house generated ACM. Cells were plated onto 1ng/ml fibronectin in the numbers stated in table 2.14. iPS microglia were differentiated for 10 to 14 days in the relevant media. Figure 2.2 shows iPS microglia differentiating over 14 days in ACM. This shows cells begin to develop processes around day 6.

Table 2.14: Cell plating numbers and ACM volumes in different plate types

Vessel type	**Number of cells per well (aprox.)**
Coverslip (24 well plate)	20,000-40,000
Opera Phenix plate	10,000
96 well plate	20,000 – 40,000
24 well plate	150,000 100,000
12 well plate	200,000
6 well plate	400,000

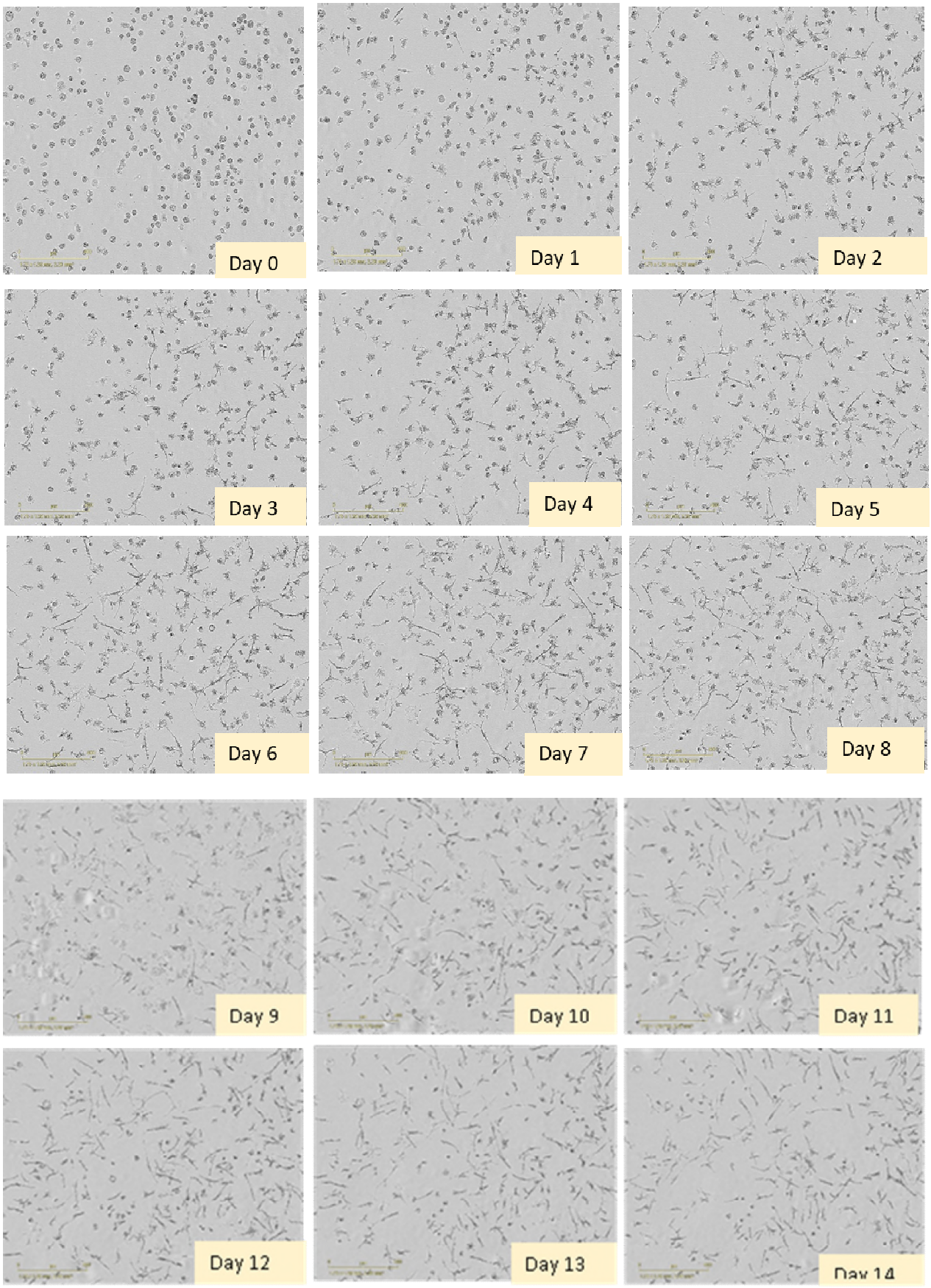

Figure 3.2 Differentiation to iPS microglia cells over 14 days in ACM. Images were taken on the IncuCyte using a 40x lens. Cells could be used for downstream experiments from day 10.

If cells were plated onto glass, either on coverslips or on opera phenix plates, Poly-D-Lysine (PDL) coating was required. PDL coating was performed in advance by incubating at room temperature for 1 hour. After this, glass covers were washed three times with distilled water and left overnight in the hood to dry. Coverslips were coated in a 24-well plate. PDL plates were kept in parafilm at RT for no longer than 5 weeks.

2.2.1.5 Culture and expansion of iPS astrocytes

2.2.1.5a) Media

NEF media: Astrocyte Precursor Cells (APC) media in table 2.8

Component	Final Concentration in 500ml
Advanced DMEM/F12	**/**
Pen/Strep	**5ml 50U/ml**
Glutamax	1:100 (2mM)
	Prepare aliquots of 49ml and add:
NeuroBrew with Vit A	1% (w/v)
EGF	20ng/ml final conc
FGF	20ng/ml final conc

Table 2.14: NEF media for APC expansion and culturing

CNTF Media: Astrocyte terminal differentiation media in table 2.13

Components	**Final Concentration in 500ml**
Neurobasal-A	N/A
Pen/Strep	50U/ml
Glutamax	1:100 (2mM)
Prepare 49ml aliquots and add:	
Neurobrew with Vit A	1ml
CNTF	10ng/ml

Table 2.15: CNTF terminal differentiation to iPS astrocytes

2.2.1.5b) Protocol

Astrocyte differentiation was done by Dr Jincy Winston using ApoE3 KOLF2 iPS cells following a protocol adapted from Serio et al 2012. Astrocyte precursor cells (APC) were generated at a late stage of the differentiation and could continue to expand for up to 10 passages. APC were cultured in NFT media on a T75 flask pre-coated with Matrigel by coating for 30 minutes at 37^{o}. Media was exchanged every second day and as these cells were proliferating, they were split every week using warmed Accutase. Once 60% confluent, media was exchanged to CNTF terminal differentiation media. iPS astrocytes were fully differentiated in 14 days. Once fully differentiated media was exchanged to advanced DMEM/F12 (ADF) and fed every second day. Figure 2.3 shows phase images of APC and iPS astrocytes.

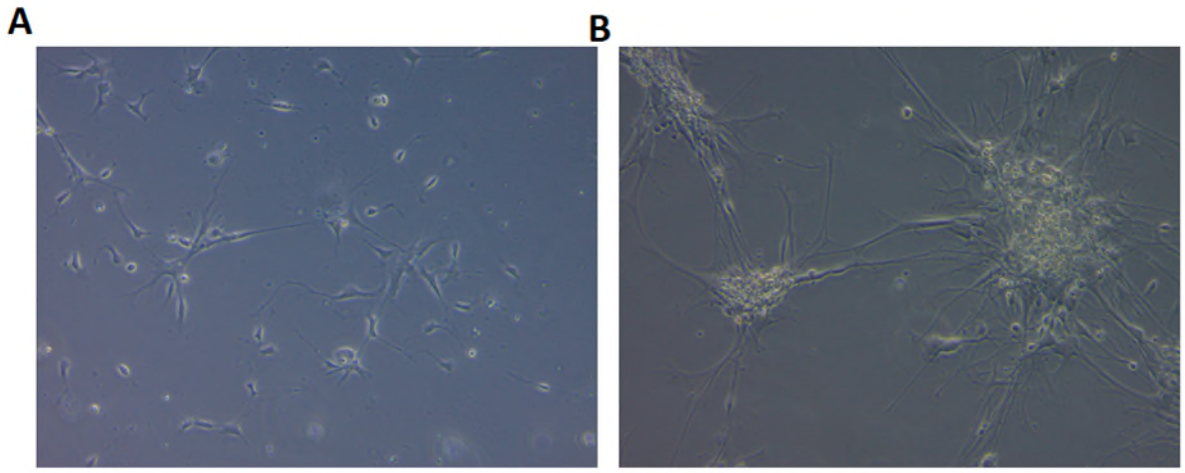

Figure 2.3: Phase images of iPS astrocytes.
A: iPS APC, B: Fully differentiated iPS astrocytes

2.2.1.6. Collection of Astrocyte Conditioned Media (ACM*)*

ACM was generated from fully differentiated iPS astrocytes, 1 week following the CNTF terminal differentiation. For ACM production, iPS astrocytes were differentiated in a T175 flasks. ADF supplemented with 1% (w/v) vitamin A neurobrew was the base media for ACM. Media was removed from iPS astrocytes and replaced with supplemented ADF for 48 hours. Media was collected and immediately frozen at -80^{o}C. After 6-8 harvests of ADF, aliquots were thawed and combined to generate one batch. Controlling between batches was performed by diluting the ACM in ADF so the final concentration of CCL_2 was 1mg/ml CCL_2, as has been done in previous papers. CCL_2 was measured using an ELISA (R&D).

2.2.2 Genetic manipulation with CRISPR Cas9

2.2.2.1 Protocol for CRISPR KO induction

Undifferentiated iPS cells were grown to 70-80% confluency and pre-treated with 1µM rock inhibitor in E8 for at least 30 minutes before Cas9 transfection. For each transfection, one 6cm dish coated in VTN was used. VTN was prepared as described in section 2.1.1.1, 3ml of this solution was incubated on a single 6cm dish for 1 hour in room temperature.

As this is a knock-out (KO), 2 guide RNA (gRNA) were needed to guide the Cas9 enzyme to the specific edit site, sequences are shown in table 2.16. Cas9 is an endonuclease which causes a double DNA break. Transfection was performed using a ribonucleoprotein (RNP) method which includes 200pmol fluorescent tracer RNA (tRNA) and 200pmol guide RNA (gRNA). The RNP was made up in 4.5µl duplex buffer and heated at 95^{o}C for 2 minutes, then cooled on the bench top at room temperature. Following this the RNP complex is added to 24.4pmole of cas9 protein. This was incubated at room temperature for 10-20 minutes. During this incubation, cells were prepared.

Cells were detached using 1ml of prewarmed Accutase per well. Once detached, cells were collected and centrifuged at 400g for 3 minutes. The pellet was then resuspended in 2ml E8 media supplemented with 1mM rock inhibitor to a final concentration of 1µM. Cells were pipetted up and

down into a single cell suspension and counted using a haemocytometer. Counts of 200,000 cells were used per nucleofection. The P3 nucleofection Lonza kit was used, the first step of this was to add 16.4µl P3 buffer to 3.6µl of the resuspended cells. Cells were then added to a well of a 16 well cuvette, being careful no bubbles were formed. The Cas9 RNP mix was then pipetted on top of the cells, mixing by pipetting up and down gently. Nucleofection was done by electroporation using the Amaxa-4D machine. Following electroporation, cells were transferred from the cuvette onto the coated 6cm dish in E8 supplemented with rock inhibitor within 10 minutes of the nucleofection. The dish was left in the incubator, and cells were fed every second day. Once colonies were visible, single colonies could be picked into 96-well plates and used for screening. CR1 KO was performed alongside Dr. Emma Cope.

Forward gRNA	Reverse gRNA
GTCAATGCAATGCCCCAGAATGG	GAGTCAGACCTGACCACGAT

Table 2.16: CRISPR guide RNA sequences

2.2.2.2 Screening transfected colonies with PCR

To identify positive clones for both heterogenous and homogenous CRISPR edits, polymerase chain reaction (PCR) was performed on individual colonies. Colonies were picked from a 6cm dish into a 96-well plate, with one colony/well. Once these had grown, they were split into another 96-well plate, mirroring the first plate. One plate was then used for PCR, and DNA was extracted using the proteinase K method (see 2.2.3 for DNA extraction protocol). The other 96-well plate was used to grow the colonies so any positive clones could be frozen, expanded and stored in -80^{o}C short term and liquid nitrogen for long term storage.

Primers for this PCR are in table 2.17. A PCR reaction mix was made up using GoTaq green buffer (Promega) with 2mM of 25M MgCl (10mM), GoTaq enzyme (Promega), DNA (in 1:10 dilution of Tris buffer), dNTP mix (at 10mM each nucleotide), 1:20 primer and made up to 25µl with nuclease free water. Samples were run on an 2% (w/v) agarose gel at 100V for 20-30 minutes.

PCR purification was performed on samples using the Qiagen PCR purification kit and sent to Eurofins for subsequent sequencing.

Forward Primer	Reverse Primer
CTGTAATCCCAGCTACTCAGGAA	ATACTGTTAATCAAACGGTCCAC

Table 2.17: Screening primer sequences

2.2.3 PCR to characterize CR1

2.2.3.1 DNA extraction

Lysis Buffer:

Component	Volume
H_20	50ml
1M Tris pH9	34ml
0.05M EDTA	2.5ml
10% (w/v) SDS	1ml
5M NaCL	155µl

Table 2.18 Ingredients for DNA extraction buffer.

200µl of proteinase K (stock concentration was 0.4mg/ml) was added to 10ml of lysis buffer, recipe in table 2.18. Lysis buffer was directly added onto the well, in a 96-well plate, 50µl was used per well. This was incubated at 60°C for up to 4 hours or overnight, if overnight the plate was placed in a humidified box. Once incubated, lysed DNA was collected and diluted with 10mM Tris pH8.0. This was incubated at 95°C for 30 minutes to heat inactivate the proteinase K. 1µl of DNA was used for PCR reactions.

2.2.3.2 Junction Fragment PCR

A total of 10ng DNA was added to a final volume of 10ul alongside 2.5mM nucleotides, 0.5 units GoTaq DNA polymerase and 10µM primers. Primers were taken from Kucukkilic et al 2018, see table 2.19[216]. These primers were designed flanking the intronic region of the extra LHR in the longer CR1-S isoform and are illustrated in figure 2.4.

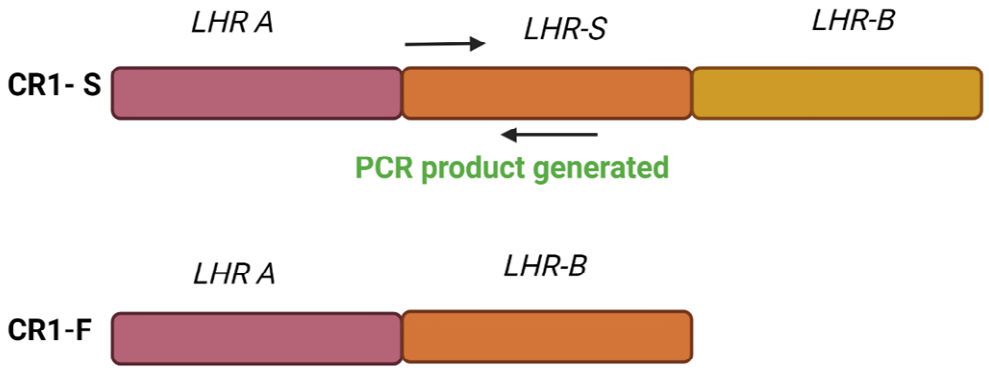

Figure 2.4: Junction Fragment PCR primer amplification.
Primers are designed to target the intronic regions in-between LHRA and LHRS on the larger CR1-S allele therefore products are only seen when CR1-S at 1500kb but no band with CR1-F allele. The figure was created with BioRender.com and[216].

The amplification used a touchdown PCR shown in table 2.20. This begins with a denaturation step at 95°C for 2 minutes. This was followed by 20 cycles of: 95°C for 30s, 70°C for 30s (with temperature decreasing in increments of 0.5°C to a final temperature of 60°C) and 70°C for 30s. This was then followed by a round of 15 cycles of: 95°C for 30s, 60°C for 30s and 70°C for 30s. A final incubation of 70°C of 5 minutes was performed. Final products were run on a 2% agarose gel with SYBR safe for 10 minutes at 100V.

Forward	Reverse
5'-AATGTGTTTTGATTTCCCAAGATCAG-3'	5'-CTCAACCTCCCAAAGGTGCTA-3'

Table 2.19: Primers for junction fragment PCR [216]

95°C	2 minutes	

95°C	30s	20 cycles
70°C (Decrease by 0.5°C till 60°C)	30s	
70°C	30s	
95°C	30s	15 cycles
60°C	30s	
70°C	30s	
70°C	5minutes	

Table 2.20: Junction fragment PCR protocol

2.2.3.2 HINDIII Density Polymorphism PCR

To assess the CR1 density polymorphism, a previously published restriction fragment length polymorphism (RFLP) method was used. This followed a PCR amplification followed by a HINDIII restriction enzyme digestion. Genomic DNA was extracted as previously described in section 2.2.3.1. The PCR mix was made up using 2X GoTaq master mix, 10µM of each PCR primer (shown in table 2.21) and 100ng of genomic DNA made up to a final volume of 50µl with distilled water. DNA was quantified using a nanodrop. PCR protocol is shown in table 2.22. This follows an initial denaturation step of 95°C for 2 minutes followed by 30 cycles of 95°C for 30s, 60°C for 30s and 72°C for 30s and then a final extension step of 72°C for 5 minutes. A portion of the PCR product was digested with 100 units of HINDIII restriction enzyme for 1 hour at 37°C. This was inactivated by heating at 60°C for 60 minutes. Digested products were analysed on a 1% (w/v) agarose gel including control samples of each genotype as kindly gifted from Professor Santiago Rodriguez de Cordoba. The gel was stained with SYBR safe gel stain and visualised with UV light. Those homozygous for high-density CR1 alle (HH) showed a product at 1.8kb while those homozygous for low density CR1 allele (LL) show two bands at 1.3 and 0.5kb.

Forward Primer	Reverse Primer
5'–CCTTCAATGGAATGGTGCAT–3'	*5'–CCCTTGTAAGGCAAGTCTGG–3'.*

Table 2.21: Density polymorphism primers

95°C	2 minutes	
95°C	30s	30 cycles
60°C	30s	
72°C	30s	
72°C	5 minutes	

Table 2.22: Density polymorphism PCR protocol

2.2.4 RNA extraction and RT-QPCR

Initially RNA was extracted using a Qiagen RNAeasy mini kit, however due to poor quality and quantity, an alternative Qiazol method was trialed. Nanodrop was used to measure the quantity and quality of RNA. Quality was measure in 260:230 and 260:280 ratios which for RNA should be 2.0-2.2 and >2.0 respectively. Figure 2.5 is a comparison of RNA collected from both methods, showing the Qiazol

method to produce more and better quality RNA. However, RNA still showed to be of lower quality than required which can cause issues with data generation downstream.

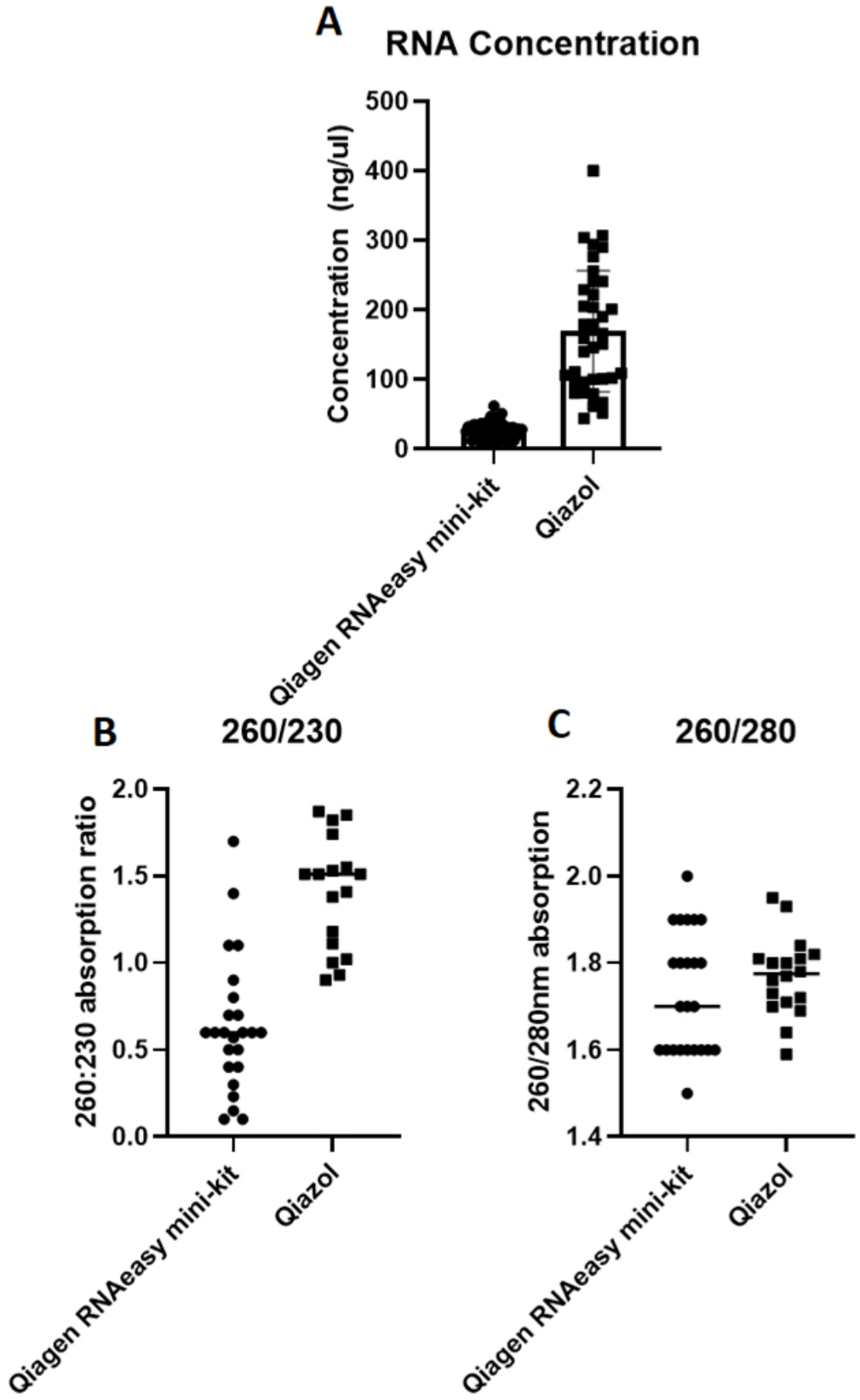

Figure 2.5: Comparison of RNA quantity and quality from two different methods using the nanodrop. *A) Concentration of RNA ng/ul B) the 260:230 ration allows for detection of other substrates such as salts and should be*

around 2.0 for RNA. C) the 260:280 ratio allows for detection of contaminating nucleotides and for RNA should be between 2.0-2.2.

2.2.4.1 RNA extraction using Qiagen mini-RNAeasy kit

RNA was extracted from cells and lysed using RLT buffer (RNAeasy mini kit, Qiagen). Total RNA was extracted according to the manufacture protocol and total RNA quantified using nanodrop.

This included initial lysing of the cells using 350µl RLT buffer. Lysate was collected and 350µl of 70% (w/v) ethanol was added. This was transferred to a RNeasy spin column and centrifuged for 15s at 8000g and the flow through discarded. 700µl of provided RW1 buffer was added to the column and centrifuged at 8000g for 15s and the flow through discarded. Buffer RPE was added at 500µl and centrifuged for 1 minute at 8000g, and the flow through discarded. An additional 500µl RPE buffer was added and centrifuged at 8000g for 2 minutes and the flow through discarded. An additional drying step was performed by column for 2 minutes at 8000g discarding any flow through. Finally, 30µl of provided RNA free water was added to the filter in the column. This was spun at 8000g for 1 minute and the flow through collected, transferred to a labelled Eppendorf tube. RNA was stored at -80^{o}C.

2.2.4.2 RNA extraction using Qiazol method

Media was aspirated from cells, and two PBS washes were performed to remove any remaining media from the well. Qiazol was added directly to the cells in the well, pooling 500µl for one sample. For microglia, 4 wells of a 12-well plate were pooled together. These samples could then be stored at -80^{o}C for further extraction later on or the extraction could be continued from this point. Samples were allowed to sit for 5 minutes, reaching room temperature. Tubes were inverted occasionally during this time. 100µl of Chloroform was added per sample, this was left at room temperature for 5 minutes during which time a clear separation could be seen. Separation was made clearer following a 15-minute centrifuge step at 2000g at 4 degrees. Theaqueous phase was then transferred to a new tube. Glycogen was added at 1.5ul/sample followed by 250µl of Isopropanol and 1ml of ethanol. This was then centrifuged for 10 minutes at 6000g, at 4^{o}C. Supernatant was then removed and a second ethanol wash step was performed . Following the second wash, the pellet was air dried until no liquid was visible. To ensure no ethanol remained in the sample, a short spin at 300g for 3 minutes was performed, and any remaining liquid was removed. When it was clear that no liquid remained, the pellet was resuspended in 12-20µl of nuclease free H20 and incubated on a heat block at 65^{o}C for 10 minutes. Once extracted, RNA samples were analysed using the nano-drop and stored at -80^{o}C.

2.2.4.3 DNase treatment

Deoxyribonuclease 1 (DNase 1) was used to digest any single or double stranded DNA within the sample. This was performed post RNA extraction. DNase treatment was performed in duplicate using 0.5ml RNAse free microcentrifuge tubes. While on ice 1µg RNA, 1µl of 10X DNASE reaction buffer and 1µl DNase 1 were added and made up to 10µl with distilled water. Tubes were incubated at room temperature for 15 minutes. Inactivation was performed by addition of 1µl of a 25mM EDTA solution and heating at 65^{o}C for 10 minutes. This RNA then underwent reverse transcription to generate cDNA.

2.2.4.4 cDNA generation

The Thermofisher one step cDNA kit was used to make cDNA for RT-QPCR reactions. Depending on the quantity of RNA extracted, 1µg-250ng was used to make cDNA to a final 9µl volume. Components were added together as in table 2.23, with 2X RT buffer, 20X enzyme mix and up to 9µl of RNA sample and made up to a final volume of 20ul with nuclease free water. This was briefly centrifuged at 400g for 5 minutes before being put into a thermocycler. The mixture was heated for 1 hour at 37^{o}C then at 95^{o}C for 5 minutes and held at 4^{o}C. cDNA was then diluted to a final concentration of 200ng DNA using distilled water.

Component	Volume (µl)
2X RT Buffer	10µl
20X Enzyme mix	1µl
RNA sample	Up to 9µl
Nuclease free water	Up to 20µl
Total	20µl

Table 2.23: cDNA master mix volumes

2.2.4.5 Power Up Sybr Green RT-QPCR

For RT-qPCR, 1µl of 200ng diluted cDNA was used in a 20µl reaction with 5µl SYBR green, 1µl optimised primer mix and dH_20 was added to a final volume of 20µl. RT-qPCR was carried out on CFX connect real time system (Biorad) or a Quantstudio 7 (Thermofisher). Primers were designed on primer blast, with Tm between 55-62^{o}C. Established efficiency of each primer was recorded, if the efficiency was too high, primer concentration was decreased. Additionally, no RT controls (samples that did not undergo reverse transcription) were run to ensure primers amplify along an exon-exon junction so final CT values do not include genomic DNA amplification.

Relative gene expression values were generated using the ΔΔCT method which shows expression first relative to a house keeping gene, GADPH, and secondly to a particular condition e.g. comparing microglia-like cells to iPS cells. The ΔΔCT is explained in section 2.2.11.1. Appendix 1 contains all the primer sequences used.

2.2.4.6 High-Throughout RT-QPCR using Fludigidm

RNA was collected, as previously described. cDNA was generated using the Fluidigm kit. For this 100ng of total RNA and random hexamers were added to the Fluidigm Reverse Transcription Master Mix kit. Prior to use in the high throughput array a preamplification step is required. For this 1.25ul of each cDNA was mixed with Preamp Master mix and 0.5ul of the pooled gene primers (500nM final concentration per primer). Preamplification was performed as described in table 2.24, beginning with a 2 minute 95^{o}C denaturation step and 10 cycles of 15s at 95^{o}C and 4 minutes at 50^{o}C. The number of cycles was experimentally determined prior to running test sameples. Appendix 2 shows the raw CT values from Fluidigm run.

95^{o}C	**2 minutes**	
95^{o}C	15 seconds	10 cycles
60^{o}C	4 minutes	

Table 2.24 Preamplification run

Following preamplification, samples underwent an Exonuclease I step to remove any remaining primers from the preamplification. Diluted Exo 1 at 4U/µl was added to 5µl pre-amplified reaction and digested at 37°C for 30 minutes followed by an inactivation incubation at 80°C for 15 minutes. The subsequent pre-amplified product was diluted to 1:5 using TE buffer.

The high throughput qPCR was performed on a Fluidigm 96.96 Dynamic Array IFC chip, this is formatted for 96 samples and 96 genes. Before primer and sample mixtures were added to the IFC inlets, the IFC was primed. Control line fluid was injected into the 2 accumulators on the chip and the priming script ran on the Biomark HD Real-time PCR system.

The primer reaction and assay mixes were prepared in 96-well PCR plates using the 96.96 Dynamic Array DNA binding Dye and Assay loading reagents kits. For the primer mixture, forward and reverse primers were combined and added to loading reagent and TE DNA suspension buffer as in table 2.22. The plate was then briefly vortexed and centrifuged at 1000g for 1 minute, then a 5µl volume of each mix was loaded into the respective inlets with a multichannel pipette. The sample reaction was prepared in a 96-well plate with the pre-amplified, Exo-1 treated, cDNA, SsoFast Evan Green supermix and 20X DNA binding Dye as in table 2.23. This was centrifuged at 1000g for 1 minute and 5µl was loaded into the fluidic microwells using a multichannel pipette. The chip was placed into the HX controller for automatic loading and mixing. Following loading, the chip was moved to the Biomark HD real time PCR System and cycling program GE Fast 96x96 PCR+Melt v2 was selected. Analysis was performed using BioMark Gene Expression Data Analysis software. This analyses each data point to generate a 'pass' or 'fail' CT score. Failed points presented poor melt curves, indicating low Tm or non-specific amplification. These points were removed from the data, and the remaining CT values downloaded from the software. Gene expression values are generated as log2 expression counts, converted from Ct values by ΔΔCT analysis. Appendix 1 contains all the primer sequences used.

2.2.5 Immunostaining

2.2.5.1 Antibodies

All antibodies used for immunofluorescence are summarised in table 2.25.

Target gene	Host	Dilution	Role
Oct-3	Anti-Rabbit	1:200	Pluripotent markers- transcription factor
SOX2	Anti-Rabbit	1:200	Pluripotent markers- transcription factor
Tra1-60	Anti-Rabbit	1:50	Pluripotent markers- membrane
SSEA4	Anti-Mouse	1:200	Pluripotent markers- membrane
CD45	Anti -mouse	1:100	Haemopoietic marker
CD11B	Anti-Rat	1:100	Haemopoietic marker
IBA-1	Anti-Rabbit	1:100	Microglia marker
CX3CR1	Anti-Rabbit	1:100	Microglia marker

TMEM119	Anti-Rabbit	1:100	Microglia marker
CD68	Anti-mouse	1:100	Microglia marker
GFAP	Anti- Rabbit	1:1000	Astrocyte marker
CR1 (commercial)	Anti- mouse	1:100	Gene of interest
CR1 (MBI-35)	Anti- mouse	1:100	Gene of interest
CR1 (MBI-38)	Anti-Mouse	1:100	Gene of interest
CR1 (PolyCR1)	Anti-Rabbit	1:100	Gene of interest
AF 488 Rb	Goat anti rabbit	1:400	Secondary
AF 488 Ms	Goat anti mouse	1:400	Secondary
AF 594 Rb	Goat anti rabbit	1:400	Secondary
AF 594 Ms	Goat anti mouse	1:400	Secondary
AF 594 Rat	Goat anti rat	1:400	Secondary

Table 2.25: Antibodies used for immunostaining
Alexa Fluor (AF), Mouse (Ms), Rabbit (Rb).

2.2.5.2 Non-adherent IF

For non-adherent cells staining, cells were collected and counted before being fixed in 200µl 4% (w/v) paraformaldehyde (PFA). Following this, two 3-minute washes in 200µl PBS were performed. On the last wash, cells were split into a 15ml falcon tube with roughly 20,000 cells in 200µl 0.1% (w/v) BSA/PBS per tube. Cells were then transferred onto a slide which was centrifuged using a cyto-spinner at 300g for 10 minutes. Once finished, a circle was drawn around the cells using a mako water repellent pen. This was left to dry for 10 minutes at room temperature before the staining protocol was performed. First cells were blocked in blocking buffer. A 50ml volume of intracellular staining blocking buffer consisted of 1.5ml BSA, 1ml goat serum and 50µl Triton-X in 47.5ml PBS, while the extracellular blocking buffer contained just 1.5ml BSA and 1ml goat serum in 47.5ml PBS. Blocking was performed for 1 hour at room temperature before being removed from the slide. This was replaced with blocking buffer supplemented with primary antibody to an optimised concentration, see table 2.25, and incubated at 4^{o}C overnight. The next day, primary antibody was removed and 3 washes of 200µl PBS were performed. After this incubation, secondary antibody diluted to 1:400 in blocking buffer was added for 1 hour at room temperature in the dark. This was followed by 3 washes in PBS. DAPI was then added at 1:1000 in blocking buffer and left for 10 minutes in the dark. After this, 3 more PBS washes were done. Coverslips were mounted onto the slides and stored at 4^{o}C. These were visualised within 3 weeks of staining on the confocal Zeiss spinning disc microscope.

2.2.5.3 IF of cells grown on coverslips

Coverslips were pre-treated with PDL and the appropriate cell coating for the cell type growing i.e. undifferentiated cells on VTN. Once cells were ready for staining, they were fixed with 4% (w/v) PFA at 10 minutes in room temperature. Fixative was removed and three PBS washes performed. Blocking buffer, as in section 2.4.2, was used and incubated on cells for 1 hour at room temperature, followed by 3 PBS washes. Primary antibody was added to the appropriate blocking buffer at the optimised

concentrations and the samples were incubated at 4°C overnight. The next day primary antibody was removed and 3 PBS washes performed. Secondary antibody was then added at 1:400 to blocking buffer and incubated on cells for 1 hour in the dark. Following this, secondary antibody was removed and 3 PBS washes performed. Following this, DAPI in 1:1000 blocking buffer was added for 10 minutes in the dark at room temperature. The coverslip was then removed from the well using forceps and mounted on a slide using Fluorsave mounting media. Slides were stored at 4°C and visualised within 3 weeks of staining on the confocal Zeiss spinning disc microscope.

2.2.5.4 Live cell Immunostaining

Once cells were ready for staining, media was aspirated and cells washed twice with cold PBS. This was followed by a short blocking step using extracellular blocking buffer for 20 minutes at 4°C. Primary antibody was added to the blocking buffer and incubated for a further 30 minutes, keeping cells on ice at all times. Primary antibody was then aspirated and quickly washed for 2 minutes twice using cold PBS before the addition of secondary antibody diluted in blocking buffer. This was incubated for a further 30 minutes, on ice in the dark. Once complete, media was aspirated and cells were fixed for 10 minutes using 4% (w/v) PFA. Cells were then treated with DAPI for 10 minutes before being mounted onto coverslips using Fluorsave mounting media and visualised on the Zeiss Spinning Disc microscope.

2.2.5.5 Pre-absorption of primary antibody

Primary antibody, 1mg/ml MBI38, was preabsorbed with CR1 protein at a stock concentration of 1mg/ml. Three times the concentration of sCR1 protein was used to ensure all available antibody epitopes were saturated. Therefore, 6µg of CR1 protein was incubated with 2µg MBI38 for 30 minutes on a roller at room temperature. Staining was then continued as described before and visualized on a confocal Zeiss spinning disc microscope.

2.2.6 Flow Cytometry

2.2.6.1 Antibodies:

Target	Fluorophore	Concentration
CD45	FITC	1:40
CD14	APC	1:40
CD11b	Brilliant Violet	1:40

Table 2.26: Flow Cytometry antibodies

Flow cytometry was used to characterise iPS microglia precursor cells. Cells were counted and split into groups of 30,000 – 50,000 cells/well in a 96-well plate. The plate was spun at 300xg for 3 minutes and media removed. Cells were resuspended in 200µl of 0.1% (w/v) BSA in PBS with 5µl of the conjugated antibody or the isotype-matched control. This was incubated on ice for 20 minutes in the dark or for 1 hour at room temperature in the dark. Following staining cells, the plate was spun at 300g for 5 minutes and cells resuspended in 200µl of 0.1% (w/v) BSA in PBS and transferred to a flow cytometry tube. Fluorescence was measured using a BD LSR Fortessa and analysed using FlowJo software. Antibodies used are listed in table 2.26.

12.2.7 Western Blot

2.2.7.1 Protein extraction

2.2.7.1.1 From cells in culture

Protein was extracted using commercially purchased RIPA buffer supplemented with 1 PhosSTOP tablet into 10ml of RIPA, to protect the lysate against dephosphorylation. The volume of RIPA used depended on cell type. For undifferentiated iPS cells, 1ml was used per $1X10^6$ cells while for iPS microglia, 300µl was used on 400,000 cells (1 well of a 6-well plate, table 2.14). Buffer was incubated on cells for 20 minutes on ice, after which the well was scraped to collect as much lysate as possible. This was transferred into a 15ml falcon tube which was centrifuged at 14,000g for 15 minutes at 4^oC. Buffer was aspirated, removing any cell debris and the protein was stored at -80^oC.

2.2.7.1.2. Generating ghost pellets

Protein was prepared from blood cells collected from individuals in the lab. In accordance with the human tissue act, consent forms were signed prior to collection, see appendix 3, and protein was immediately extracted so the blood was not stored. These pellets were used as controls in western blot loading. Multiple samples were prepared to provide a single batch stock that would last for a long period of time.

To prepare the sample, 100µl of blood was added to 900µl sterile PBS which was centrifuged at 100g for 5 minutes at 4^oC. Excess liquid was removed. This was repeated three times. Lysing was performed by addition of 900µl H_20 which was centrifuged at 100g for 5 minutes at 4^oC. This was repeated 3-5 times or until the pellet appeared pink-white.

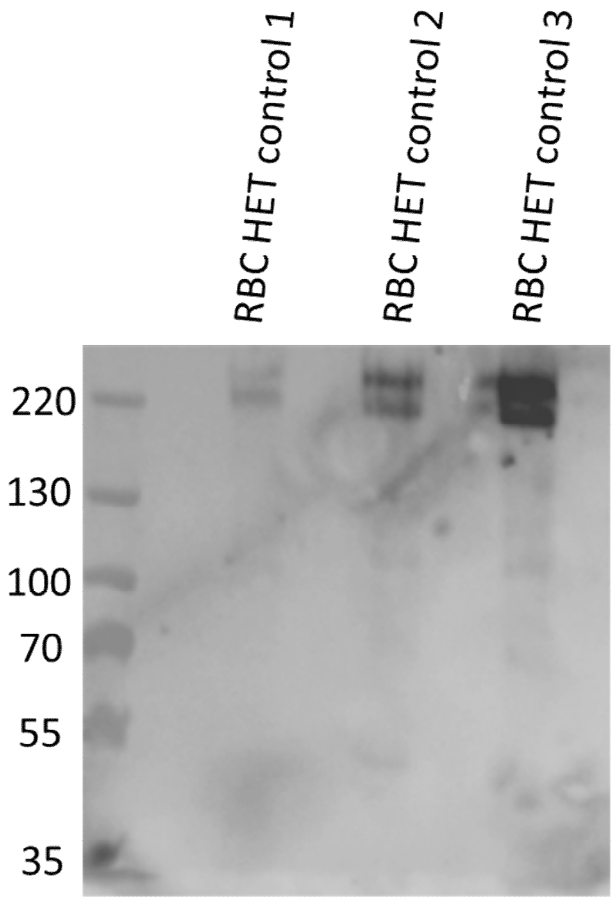

Figure 2.7 Western blot for RBC ghost pellets with in house antibody MBI38
This reveals two CR1 bands, one for CR1F and another for CR1S at the expected molecular weight in 3 biological replicates of ghost pellets. This was repeated once.

2.2.7.2 Protein Quantification

Protein quantification was conducted using the Pierce Micro BCA assay kit. This kit includes 3 components; Reagents A-C, which were used to make up the Working Solution (WS). Making up the WS required the following steps:

Step 1: Calculating the total WS required

(# standards + # samples) × (# replicates) × (volume of WS per sample) = total volume WS required

Typically, 9 standards were used with 2 replicates using 1ml WS per sample. In an example with 3 samples being tested the equation would resemble:

(9 standards + 3 samples) x (2 replicates) x (1ml of WS per sample) = 24ml WS required.

Step 2: Making up the WS

For this a ratio of 25:24:1 of the reagents A: B: C is used respectively.

Following from the example above:

24 ml would use 12.01ml reagent A, 11.5ml reagent B and 0.4ml reagent C

First, 1ml of WS was aliquoted into 1.5ml Eppendorf tubes, then 1µl of sample and standard was added to the WS in duplicate. Tubes were incubated at 60^{o}C for 1 hour. Following this, 200µl of each sample was pipetted into a 96-well plate. Absorbance was measured at 593nm using a plate reader. Standards were used to generate a standard curve an example is shown in figure 2.6 below. Protein concentrations for each sample were interpolated from the standard curve using Graphpad software.

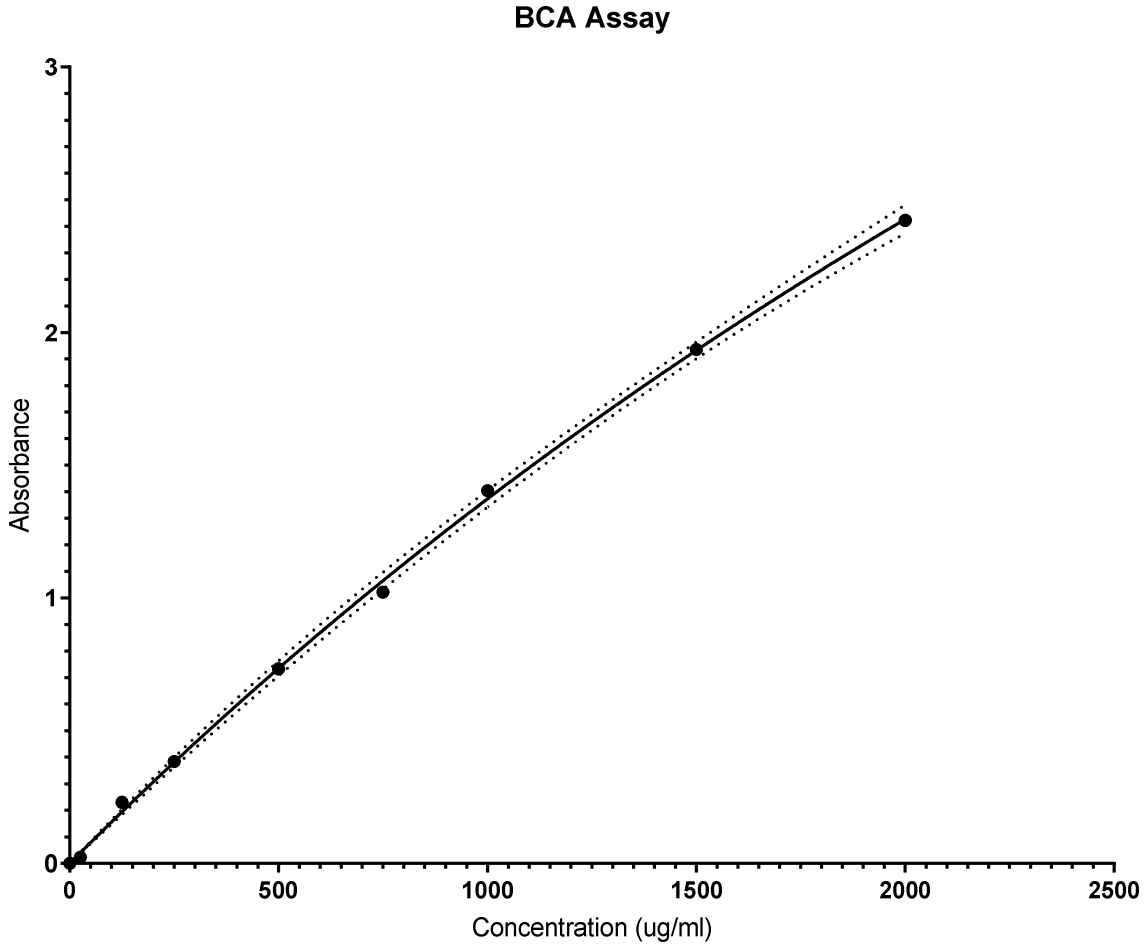

Figure 2.6 An example standard curve for protein quantification

2.2.7.3 Making gels

2.2.7.3.1 Buffers

Buffer	Composition
Lower Buffer	46.76 Tris-Base, 1g SDS made up in 250ml ddH_20 pH 8.8
Upper Buffer	15.13g Tris-Base, 1g SDS in 250ml ddH_20 pH 6.8

Table 2.27 Table of buffer recipies for making up gels

Lower gel:

Components	For 1, 7.5% gel (ml)
Lower Buffer	1.875
40%(w/v) Acrylamide/Bis	1.4
DdH_20	4.105
10%(w/v)Ammonium persulphate	0.075
TEMED	0.0075

Table 2.28: Lower gel recipe

Upper gel:

Components	For 1, 5% gel (ml)
Upper Buffer	0.6
40%(w/v) Acrylamide/Bis	0.313
DdH_20	1.597
10%(w/v) Ammonium persulphate	0.025
TEMED	0.0025

Table 2.29 Upper gel recipe

2.2.7.3.2 Protocol

SDS gels were made in-house following the recipe above. All CR1 westerns were run on a 7.5% lower gel, 5% upper gel.

Lower gel was made first in a 50ml falcon tube and pipetted into the cassette up until the fourth marking on the cassette. 1ml of 100% Isopropanol was pipetted on top of this to prevent formation of bubbles within the gel This was left at room temperature, undisturbed for 30 minutes or until the gel has set. The isopropanol was poured of and two washes of distilled H_20 was performed to ensure all isopropanol was removed. Following, this the upper buffer was made in a 50ml falcon tube and pipetted on top of the lower buffer to the cassette was filled, a comb was added on top of this so to create wells for sample addition. This was left at room temperature for 20 minutes or until set. Once set, the gel was either used straight away of wrapped in wet tissue paper and stored at 4^oC for up to 1 week.

2.2.7.4 Gel Electrophoresis

2.2.7.4.1 Buffers

Buffer	Ingredients for IL (except Loading Buffer=
Loading Buffer (for non-reducing)	3ml 20% SDS to 3.75ml 1M Tris, 9mg Bromophenol blue and 4.5ml glycerol
10X Running Buffer	30.3g Tris, 144.1g Glycine, 10g SDS (pH8.3)
1X Running Buffer	100ml 10X Running Buffer, 900ml DH20
10X Transfer Buffer	800ml DH_20, 24.2g Tris Base and 150.1g of Glycine
1X Transfer Buffer	100ml 10X Transfer Buffer, 200ml Methanol, 700ml DH20.
Wash Buffer	PBST 0.05% (w/v)
Blocking Buffer	PBST + 5% (w/v) Semi-skinned milk
Antibody buffer	PBST 3% (w/v) BSA

Table 2.30: Gel electrophoresis buffers

2.2.7.4.2 Protocol

30µg of samples were prepared in a 5X Non-Reducing Loading Buffer, see table 2.30. Samples were then boiled at 100^{o}C for 10 minutes. Once boiled, samples were loaded in the gel, alongside PageRuler Ladder. The tank was filled with 1X running buffer, see table 2.30. The gel was run for 1 hour at 120V. After running, proteins were transferred from the gels onto a nitrocellulose membrane. This was performed using a transfer sandwich prepared in order of: sponge - filter paper - gel – nitrocellulose membrane – filter paper – sponge. The transfer sandwich was placed back in the tank and this was filled with 1X transfer buffer. This was run uninterrupted for 10V at 1 hour. Following transfer, the membrane was blocked using blocking buffer for 1 hour at room temperature. Once blocking was complete, primary antibody was supplemented in antibody buffer and incubated on the membrane overnight at 4^{o}C. The following day, primary antibody solution was removed, and the membrane washed three times using wash buffer. Once washed, secondary horseradish peroxidase (HRP)-conjugated antibody was added to antibody buffer at 1:1000. This was incubated on the membrane at room temperature for 1 hour. Three more washes with wash buffer were performed. Enhanced chemiluminescence (ECL),a chemiluminescent substrate for the detection of HRP, was made up and added onto the membrane to allow for detection of protein. ECL consists of two substrates which are added 1:1. Once prepared, the ECL is added onto the membrane for 1-2 minutes and then removed. Membrane was then imaged using the Syngene imager. After visualisation membranes could be stained using ponceau S stain. For this, the membrane was washed three times with water before being submerged in ponceau S stain for 15 minutes while being constantly agitated. This was then washed three more times with water allowing protein to be visible on the membrane.

2.2.8 Enzyme Linked Immunosorbent Assay (ELISA)

2.2.8.1 Buffers

Buffer	Recipe
Washing buffer	In 50ml PBS, add 50µl of Tween-20 to make a 0.1% solution
Blocking buffer	In 50ml PBS, add 50µl BSA.
Stop solution	In 500ml of water add 50ml Sulfuric acid to make a 10% stop solution

Table 2.31 ELISA buffers

2.2.8.2 Range of ELISA standards

ELISA	Range of standards used
IL1β	3.9 – 250pg/ml
CCL_2	15.6 – 1000 pg/ml
C3	0.016 - 1µg/ml

Table 2.32 Ranges of ELISA standards

2.2.8.3. Commercial ELISA protocol

Quantitative sandwich ELISA kits for cytokines IL-1β and CCL ₂ were purchased from R&D. The first step was to coat MaxiSorp 96-well plates (Nunc) with capture antibody, which was left overnight at 4^{o}C. The following day, capture antibody was removed and 3 washes were performed with wash buffer. Wells were then blocked for 1 hour at room temperature using 200µl of blocking buffer per well. After blocking, the samples and standards were added in a volume of 100µl per well. Standards were prepared following the manufacturer's instructions, ranges for these ELISAs are in table 2.32. Samples were added undiluted, following results from an initial optimization run. To optimize sample dilutions, a range of dilutions in blocking buffer were investigated to find the optimal dilution for detection within the standards' range. Standards and samples were incubated for 2 hours at 4^{o}C. After this incubation the samples and standards were aspirated and five washes in wash buffer were performed. Detection antibody was added for 1 hour at room temperature. This was then followed by 3 washes in washing buffer. 100µl of HRP- Streptavidin solution was added for 30 minutes at room temperature. Following this incubation, HRP antibody was removed and three washes with wash buffer were performed. 100µl of OPD solution swa then added per well. OPD solution was prepared as per the manufacturer's instructions with 1 gold tablet added to 30ml of water followed by the addition of the silver tablet 10 minutes later. This reaction was allowed to develop for up to 10 minutes before 100µl of stop solution was pipetted on top. This resulted in a colorimetric reaction which can be detected on a plate reader at 450nm. Standard curves were generated with absorbance on the y axis against the concentration on the x axis. This allows for sample concentration to be read from the standard curve. Each sample was run in duplicate.

2.2.8.4 In house ELISA protocol

C3 ELISA antibodies were generated in-house, information for this is available in section 2.1.1.1.2. Initially MaxiSorp plates were coated with detection antibody at 5µg/ml. Plates were incubated overnight at 4^{o}C. The following day, antibody was removed and blocking buffer, recipe in table 2.32, was added for 1 hour at room temperature. After blocking, blocking buffer was removed and washed with washing buffer (table 2.32). Standards and samples were added in a 100µl volume per well and allowed to incubate for 2 hours at 4^{o}C. After incubation, three washes were performed. Next, detection antibody conjugated with HRP was prepared in blocking buffer at 1:500 from a 1.49mg/ml stock with 100µl added per well. This was incubated for 1 hour at room temperature. This was then removed, and wells were washed three times with washing buffer. OPD solution was prepared as described above, 100µl per well was added triggering a colour change reaction. This was stopped by addition of 100µl stop solution. This resulted in a colorimetric change which was detected at 450nm on a plate reader. Samples were run in duplicate and analyzed using standard curves.

2.2.9 Functional Assays

2.2.9.1 Phagocytosis

Phagocytosis was performed on the IncuCyte which is capable of phase, red and green imaging. Ph-rodo conjugated beads allows for a fluorescent dye to be activated in the presence of an acidic pH. Therefore, when bioparticles are ingested within the acidic lysosome a colour signal will be released, detection of this gives a reading for bioparticle uptake. As complement is the central pathway being investigated, pH-rodo e-coli bioparticles were opsonised prior to phagocytosis.

2.2.9.1.1 Preparation of serum for opsonisation

Human serum was obtained from consenting individuals in the lab. Following the human tissue act guidelines, sample was not stored.

FI depleted serum was generated by Dr Wiola Zelek who depleted all FI from collected serum using a column depletion method.

2.2.9.1.2 Opsonisation of bioparticles

Opsonisation was performed using human serum and depleted human serum and added to bioparticles at a 1:3 ratio. This was then incubated at 37^{o}C for 1 hour. Following this, the sample was centrifuged at 400g for 3 minutes at 4^{o}C. Two washes with dH_20 were performed to ensure all serum was removed. On the last spin, the pellet was reconstituted in Live Cell Imaging Solution (LCIS). This was sonicated for 30 minutes with 30, 30s pulses.

2.2.9.2 E. coli bioparticle phagocytosis

iPS microglia were differentiated on Greiner 96-well plates with 10,000 cells per well in ACM for 10 days. Once differentiated, cells were imaged in the phase and red channel to obtain a reliable measurement of number of cells/well and any cell autofluorescence. Beads were prepared as described in the opsonisation section in a total of 200µl LCIS. While beads were in the sonicator, inhibitors and dyes were added to the cells. Inhibitor, Cytochalasin D (Cyto-D), was added to a final concentration of 1µM into the appropriate control wells and incubated on the cells for 40 minutes at 37^{o}C. Cytochalasin D is an actin inhibitor, which will prevent the cells from phagocytosing the cargo. After the incubation, media was removed from the cells and one wash with LCI was performed. Finally, 200µl of LCIBS was added back into each well, and Cytochalasin D treatment added back into the appropriate wells. Beads were added at 0.025mg/ml/well. The plate was then centrifuged at 400g for 3 minutes. This was then imaged on the IncuCyte, imaging every 30 minutes for a total of 4 hours at 20X using phase and green channels. Datum was analysed using the IncuCyte mask, which used the phase image to detect the cells, this allowed for unwanted artifacts to be excluded in the final analysis. Once the mask was set, readings for the integrated intensity of red fluorescence to be generated for each time point, this was plotted against time to give a time course of bioparticle uptake. An example of the selection mask is shown in figure 2.7.

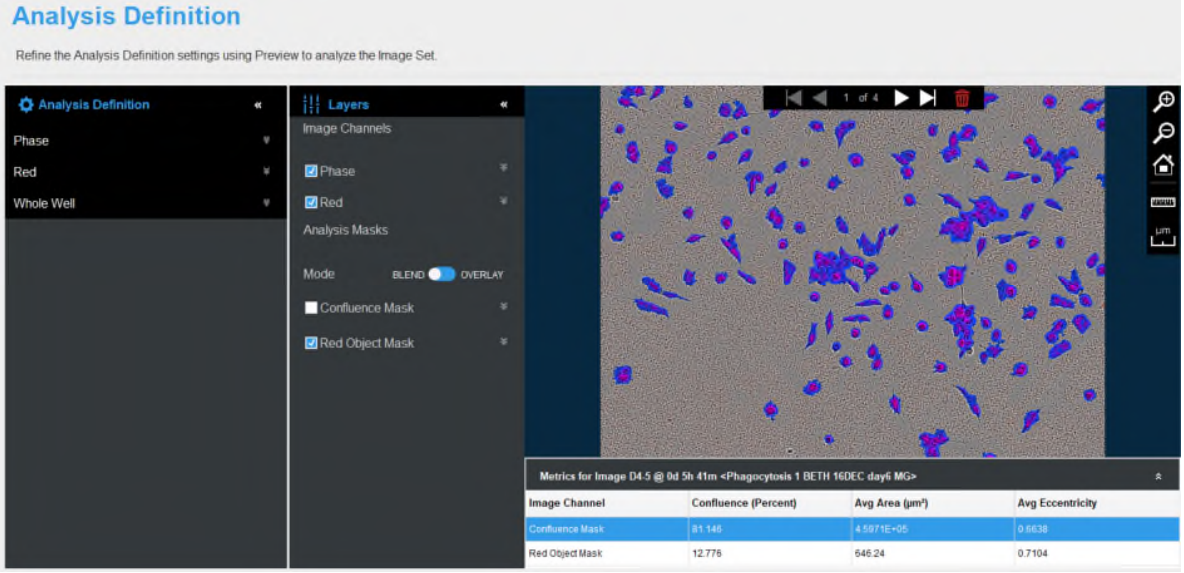

Figure 2.7: Screenshot of mask selection in IncuCyte analysis software.

2.2.9.3 Stimulation of iPS microglia

Microglia were stimulated with lipopolysaccharide (LPS), a component of the gram-negative bacterial cell wall. LPS at 100ng/ml was added directly into the well and supernatant/RNA collected after 8 and 24 hours as described before.

2.2.10 Analysis

All graphs and statistical analysis were generated using GraphPad prism 9. RNA used in Fluidigm experiments were all from one differentiation but from multiple different harvests. Cells were taken and differentiated from as early as harvest 2. Future work would not differentiate precursor cells to microglia until at least harvest 4.

2.2.10.1 ΔΔCT analysis of RT-qPCR data

RT-qPCR was analyzed using the ΔΔCT methods. For Fludigim values, analysis was performed using the Fluidigm R package while non-RT-qPCR data was calculated manually. The ΔΔCT method generates fold change in expression plotted on a $\log_2$ scale, the methodology is explained below.

The output in RT-qPCR assays is the cycle threshold (CT). This indicates the number of cycles taken to reach a threshold. First the ΔCT was generated by subtracting the CT values of the gene of interest from the CT values of the housekeeper genes (or the mean of the housekeepers). Next, the ΔCT of condition A is subtracted from the ΔCT of condition B, this compares one condition to another. These values were then transformed by log2 to get fold change. The equations are as followed:

Calculating the ΔCT:

CT (gene of interest) – CT (housekeepers) = ΔCT

e.g.

(CT of CR1) – (CT of housekeeper GAPDH) = ΔCT

Calculating the ΔΔCT:

ΔCT (condition 1) - ΔCT (condition 2) = ΔΔCT

e.g.

ΔCT of stimulated data for CR1 - ΔCT of non-stimulated data for CR1 = ΔΔCT

2.2.10.2 Analysis of immunofluorescence

Immunofluorescence images were analyzed compared to secondary only controls. These controls had no primary antibody added, only secondary. All images are shown in relation to the fluorescence shown in the secondary only control. These images are shown in the first panel of every immunofluorescence figure to provide support for the images shown. Analysis was done using Zen 3.1 (Zeiss). A biological repeat refers to a separate terminal differentiation however a technical repeat refers to cells from the same harvest.

2.2.10.3 Statistical Analysis

Statistical analysis was carried out using GraphPad Prism 9.0 software. Statistical analysis was performed on ΔΔCT RT-qPCR data. This first step of this required the normalcy to be investigated using the Shapiro-Wilk test. If P <0.05 then the dataset failed the normalcy test and was not normally distributed however if P >0.05 then the dataset was found to be normally distributed. If the data was normally distributed and had only one gene of interest then a t test was used. However, if the data was normally distributed but had multiple genes of interest to be compared, then a multiple t-test with Holm-Sidak post hoc multiple comparison was used. If the data failed the Shapiro-Wilk test then it was not normally distributed or was not powerful enough. In this circumstance, when comparing only one gene, a Mann Whitney test was used. However, to compare multiple genes together with data that was not normally distributed then a multiple Mann Whitney test with post hoc Sidak-Bonferonni multiple comparison was used. The one exception to this is figure 4.5, in which a Kruskal Wallis test with post hoc Dunnets multiple comparison was used, this data was non-parametric therefore an ANOVA was not used. Asterisks represent statistical significance using GraphPad prism suggested values, these are: ** P< 0.05; ** P < 0.01; *** P<0.001; ****P<0.0001* for this. If found to be not significant no asterisk is labelled as P >0. 05.

For other data sets, a Shapiro Wilk test was first performed. If P <0.05 then the dataset failed the normalcy test however if P >0.05 then the dataset was found to be normally distributed. If this passed this test then an ANOVA with Tukey post hoc corrections was used. If it did not pass this, then a Kruskal Wallis test with post hoc Dunnets multiple comparison was used. Asterisks represent statistical significance using GraphPad prism suggested values, these are: ** P< 0.05; ** P < 0.01; *** P<0.001; ****P<0.0001* for this. If found to be not significant, no asterisk is labelled, as P >0.05.

Statistics used are noted in the figure legends for clarity.

3.0 Characterizing the differentiation of iPSC to iPS microglia

3.1 Introduction

Microglia are responsible for maintaining a healthy micro-environment by engaging in phagocytosis and inflammatory process[217]. These cells are highly mobile and when not activated have been shown to be continuously extending and retracting their processes in non-overlapping regions[218,219]. Their multiple processes feel the environment for ligands, such as LPS. Upon detection of a 'trigger', microglia adopt an activated phenotype, becoming amoeboid, round cells, and resulting in the secretion of inflammatory components into the surrounding milieu. Microglia are also essential in the engulfment of unwanted molecules and particles through phagocytosis and endocytosis[218,220–222]. Our understanding of microglia functions has largely been informed by primary cells and cell line models studies in vitro. Multiple protocols are available for the extraction of primary microglia from rodents, which offers a genetically homogenous pathogen free population with tightly controlled post-mortem delay for microglial extraction[57]. However, the evolutionary divergence from rodents to humans limits the translation of rodent microglia studies to the clinic. Furthermore, inbreeding of animal models reduces variability of microglia populations[57,223]. These concerns are by-passed by the extraction of microglia from human tissue which offers a genetically variable pool of microglia[57]. However, due to difficulty of obtaining "healthy" brain tissue, microglia are usually only available from already pathological tissue[194]. Additionally, unlike with rodents, extraction of human microglia inevitably offers less control over antemortem conditions which could impact on the resultant microglia phenotype. Indeed, a significant positive correlation has been reported between CD11b expression (a marker of immunoreactivity) in grey matter microglia and post-mortem delay[57]. An alternative model is available through use of microglial cell lines, the most common being mouse Bv2 and human HMC3 cells[57]. These cell lines were generated using viral transduction of oncogenes, such as v-myc, resulting in highly proliferative cells useful for downstream experiments[57,181]. These easily maintainable cells provide a useful experimental model. However, recent studies have shown that cell lines differ genetically and functionally from primary microglial human HMC3 cells have a notably reduced phagocytic capacity compared to primary microglial cells[57,181,223]. The recent availability of stem cell models has offered an advantageous new in vitro method for the study of microglia which enable detailed mechanistic studies.

Stem cells are proliferating pluripotent cells, which can be manipulated towards any cell type[57]. Multiple protocols for the generation of a range of cell types have been described with well-defined methods for the differentiation to neuroectoderm-derived brain cells such as neurons, astrocytes and oligodendrocytes[57,192]. However, it wasn't until the end of 2016 that the first protocol for generating human iPS microglia-like cells was published[57]. This was due to lack of information on the embryonic origin of microglia, a prerequisite for the directed differentiation of hPSC. It is now known that microglia cells are derived from erythromyeloid precursors (EMP) which are secreted from the yolk sac during primitive hematopoiesis[218,224,225]. Secreted EMPs migrate to the brain, before the development of the blood brain barrier, where they continue to differentiate to microglia cell type[218]. Protocols for generating iPS microglia aim to recapitulate these early embryonic events by timed exposure to specific growth factors and small molecules[57]. However, the protocols published differ

substantially regarding use of which growth factors and the timing of the exposure periods[57]. Furthermore, many of these protocols utilize mechanical manipulators and fluorescence cell sorting to enrich the production of progenitor cells[194].

The aim of this chapter is to optimize the production of microglia-like cells from the commercially available iPS KOLF2 cell line following an adapted version of the protocols published in Haenseller et al 2017 and Takata et al 2017. The most significant change made in the protocols was moving towards ACM as an alternative terminal differentiation media.

3.2 Results

3.2.1 Culture and confirmation of pluripotent iPS cells

KOLF2 iPS cells are a commercially available pluripotent stem cell line derived from skin tissue of a male donor. They are a commonly used cell line with a known genetic mutation in development gene ARID2. This has since been corrected and these cells are available at HipSci, however this correction was done after this work had begun therefore the cells, I used still possess the genetic abnormality.

iPS cells were cultured in E8 flex medium, containing growth factor FGF_2. iPS cells were harvested at passage 26 and a cell bank was generated from this for future use. Previous karyotype testing, performed by Prof. Nick Allen, had been conducted on these cells showing no trisomy or unexpected abnormalities. Pluripotency was confirmed by the expression of key pluripotent markers. KOLF2 cells were shown to be positive for transcription factors SOX2 and OCT4 in addition to pluripotent surface marker SSEA4. Figure 3.1 shows representative images of immunofluorescence confocal staining for these three markers on KOLF2 cells. Analysis of images was done using secondary only controls, which are present in the first panel.

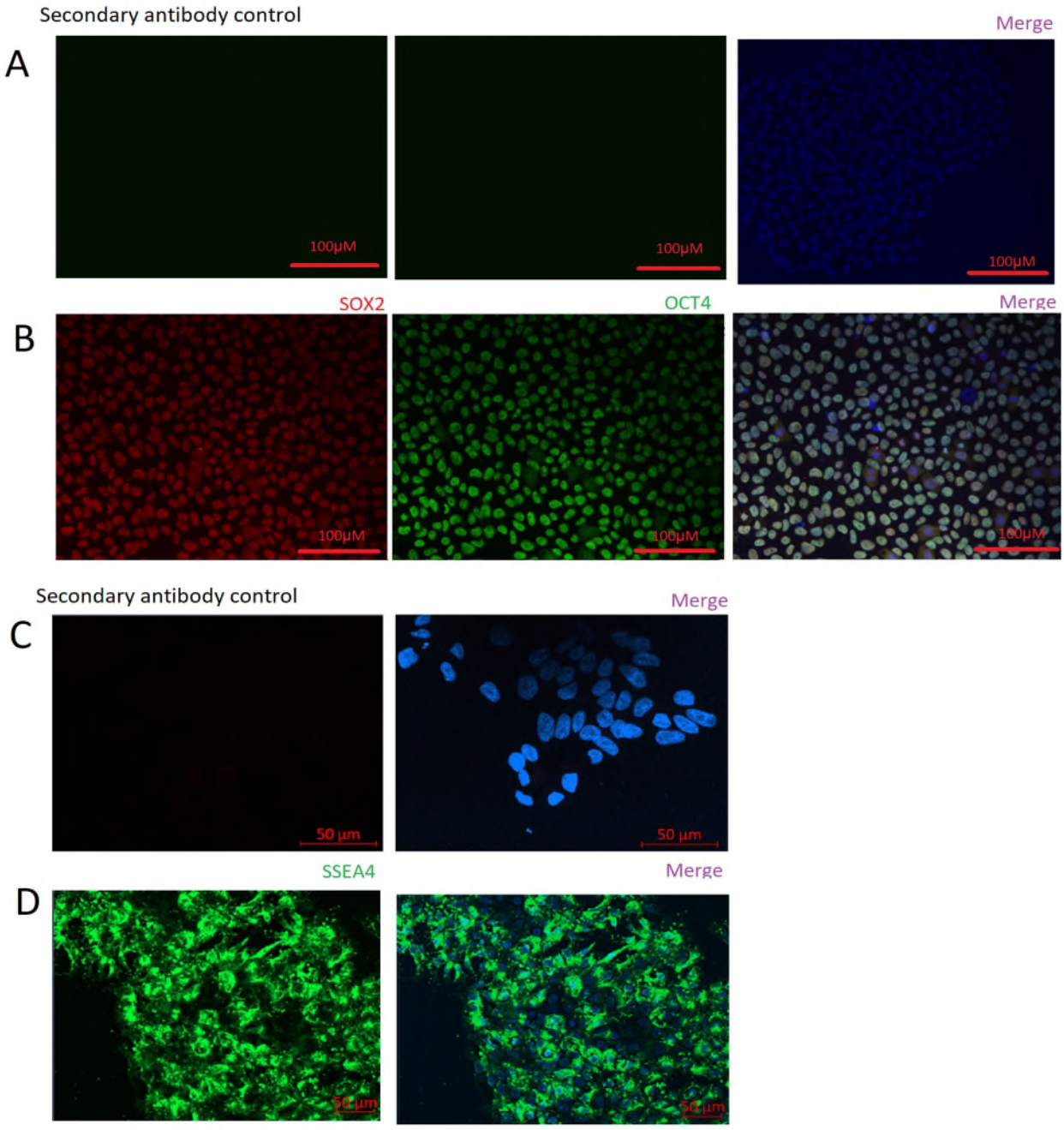

Figure 3.1: Undifferentiated iPS cells stain positively for pluripotent markers
A) Secondary antibody staining control images for image B, B) Images taken on the Zies spinning disc microscope show undifferentiated iPS cells are positive for pluripotent transcription factors SOX2 and OCT4. This shows all cells to be positive for these key transcription markers which are solely located within the nucleus. C) Secondary antibody staining control for images shown in panel C, D) Combined Z stack images of extracellular pluripotent SSEA4 staining on undifferentiated iPS cells taken on the Zeiss spinning disc. Staining for surface marker appeared slightly more variable than that for the transcription markers, but most cells show to be positive for this marker. These images are representative images from at least 3 biological and 2 technical repeats.

3.2.2 Directed differentiation to iPS microglia following an EB based method.

An embryonic body (EB) based protocol, adapted from Haenseller et al 2017[207] was chosen to generate iPS microglia. The schematic in figure 3.2 shows the adapted protocol followed; like the original protocol, EB organoids were generated from healthy iPS cells and incubated in E8 flex media

supplemented with 50ng/ml Bone Morphogenic Protein 4 (BMP4), 50ng/ml Vascular Endothelial Growth Factor (VEGF) and 20ng/ml Stem Cell Factor (SCF) and is referred to as EB 3G. EB were fed every second day for 6 days, with the first 24 hours including 10µM of rock inhibitor (Y-27632), which encourages cell survival. Over the 6-day incubation, EB become denser in the centre and the beginnings of cystic structures start to become visible. On day 7 EB were collected, and 60 EB / T75 flask were plated in XVIVO supplemented with 50ng/ml Macrophage Colony Stimulating Factor (M-CSF) and 25ng/ml Interleukin-3 (IL3), at this stage cultures are termed factories. EBs adhere to the flask within a week, producing a skirt of endothelial cells surrounding it. Yolk sac-like cyst become clearly visible from the EBs and within 2 weeks iPS microglia precursor cells (iPS Pre) can be seen attached to the endothelium. iPS pre were easily identifiable as large round cells with clear filopodia which gradually detach so they are free floating in the media. These cells are harvested weekly for terminal differentiation into iPS microglia by culturing in-house produced astrocyte conditioned medium (ACM); this is the major adaption from the original Haenseller et al 2017 protocol which used XVIVO supplemented with GM-CSF and IL-34. ACM was generated from iPS astrocytes differentiated following a protocol published in Serio et al 2012. Confirmation of astrocytic phenotype is shown in figure 3.8 and 3.9 and the protocol for producing ACM is discussed in section 3.4.2.1 Terminal differentiation in ACM was conducted over 10 days, with no change of media over this time. Microglia-like morphology was observable from day 2 in ACM.

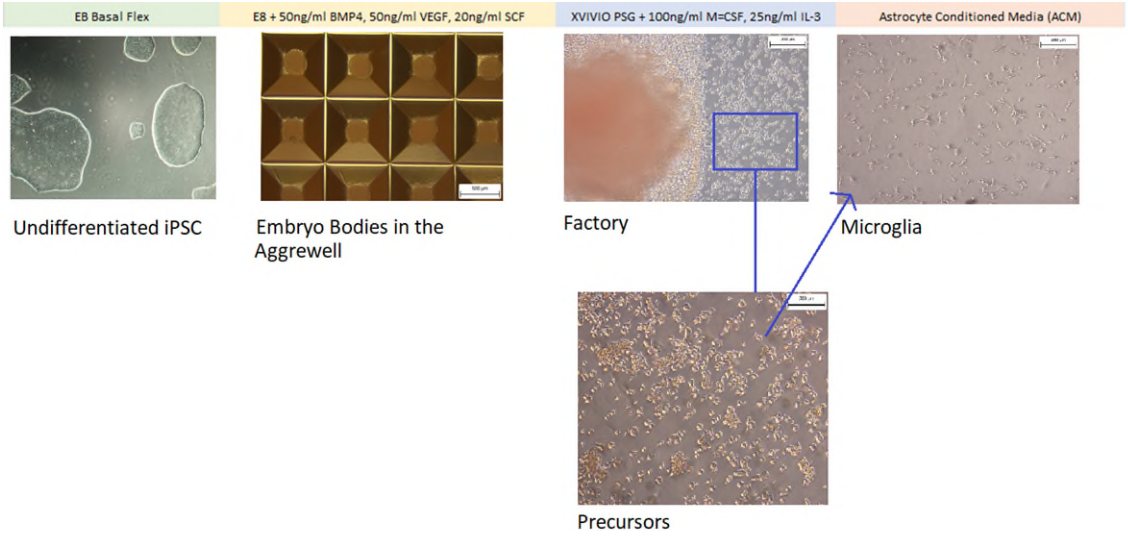

Figure 3.2: Schematic of iPS differentiation to iPS microglia following EB differentiation *Undifferentiated iPS cells were grown in E8 flex media. EBs were made using an Aggrewell-800 and incubated for 6 days in EB 3G which is supplemented with growth factors BMP4, VEGF and SCFs. After 6 days EBs are plated in a flask with XVIVO supplemented with mCSF and IL3.. EBs take around a week to attach to the flask and over the course of the next few weeks begin to become more cystic producing yolk sac like structures with an endothelium skirt around, as can be shown in the image labelled 'factory'. It. . iPS precursors begin to appear attached on the endothelium. After 3-4 weeks iPS precursors can be seen free floating in the flask. These cells were collected weekly and plated in ACM. After 10 days these cells become ramified microglia-like cells.*

Generation of EB is considered the bottleneck for successful differentiation; therefore, three methods were trialled to ensure heterogenous, consistent Ebs were generated. The first protocol utilised a suspension culture method in which iPS colonies were gently dissociated using Tryple, encouraging whole colonies to lift of the plate. Overnight incubation in EB 3G with 10µM rock inhibitor allowed for organoid formation, with many colonies rounding of as is shown in figure 3.3a). However, this

method produced highly inconsistent EB which varied considerably in size. Second method utilised a hanging droplet protocol. Here iPS were dissociated, counted and re-suspended in EB 3G with 10µM rock inhibitor and poly vinyl acetate (PVA) to a concentration of 10,000 cells/ml. Droplets of 20µl were pipetted onto the lids of 10cm dishes, around 20-30 droplets could fit on one dish lid. This lid was placed back onto the dish which had a layer of water; the set-up is shown in figure 3.4b). After overnight incubation, EB were clearly visible within each droplet and could be collected to continue the treatment in EB 3G. This consistently produced uniform EB of a defined size; however, this technique was impractical for generating large number of EB of multiple genotypes. Finally, a trans-well aggrewell method was performed using an Aggrewell800. These plates consists of 24 wells, each containing 300 small indents which can contain 1 EB each. For each aggrewell plate, 4 million healthy IPS cells were re-suspended in EB 3G with rock inhibitor, pipetted into one aggrewell and briefly centrifuged. Under the light microscope, clumps of cells were seen in each indel; after 24 hours in the incubator these formed into clear Ebs as shown in figure 3.3c). This final method was practically simple, producing 300 EB/well of uniform defined size; hence, this method was chosen for continued production of Ebs.

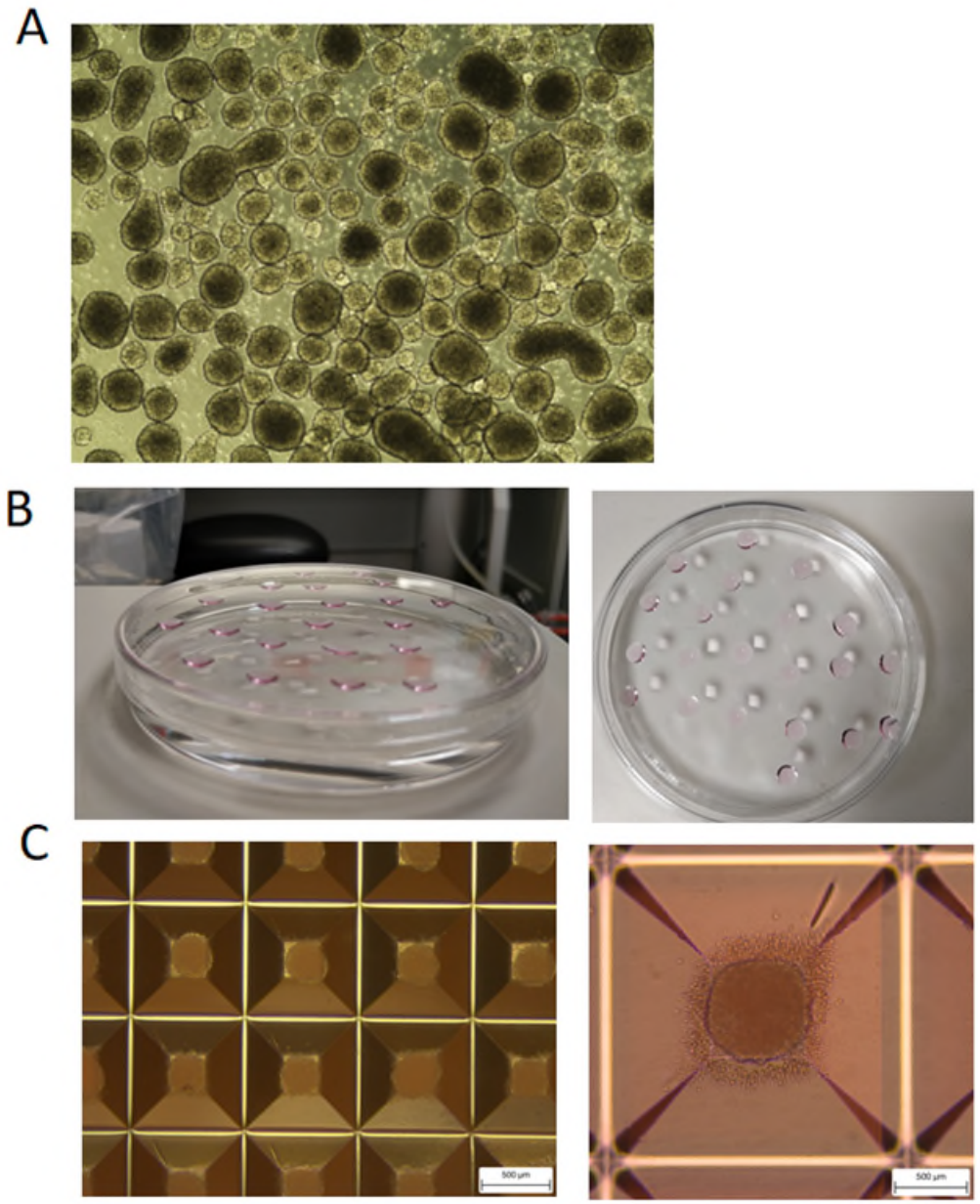

Figure 3.3: Alternative methods for generating embryo bodies
A) EB's generated by using a harsh detachment agent. EB differed in size but a large central density can be seen in most of them. This is a common feature in EB nearer the end of EB 3G incubation. B) A hanging droplet method was used by generating droplets containing cells in EB 3G supplemented with PVA. These droplets are pipetted onto the lid of a 10cm dish which was carefully placed back onto the dish which had a small amount of water covering the base, this prevents evaporation of the media bubbles. When placing the lid on the dish it is important to make sure the droplets on the lid are not disturbed.. C) Aggrewell900 was used to generate 300 EB of a defined size.

Once EB had been successful generated and incubated for the appropriate amount of time, they were plated to produce factories. After 2-3 weeks, round precursor cells were clearly visible floating in the media, these were characterized by RT-qPCR, immunofluorescence, and flow cytometry for key hematopoietic markers CD45 and CD14 and the integrin CD11b. Variations in markers CD14 and CD11b was seen across harvests; however, these markers remained sufficiently consistent to confirm the successful production of iPS pre.

Figure 3.4 indicates the change in three key hematopoietic markers message normalised to housekeepers SDHA, HPRT, GAPDH and ACTB and relative to expression in undifferentiated IPS cells.

This shows a significant increase in all three haemopoietic markers: CD11B (P=0.023), CD14 (P=0.019) and CD45 (P=0.006) in iPS precursors differentiated from undifferentiated iPS cells. The biggest increase is seen in CD11B, an integrin of phagocytosis complement receptor, CR3.

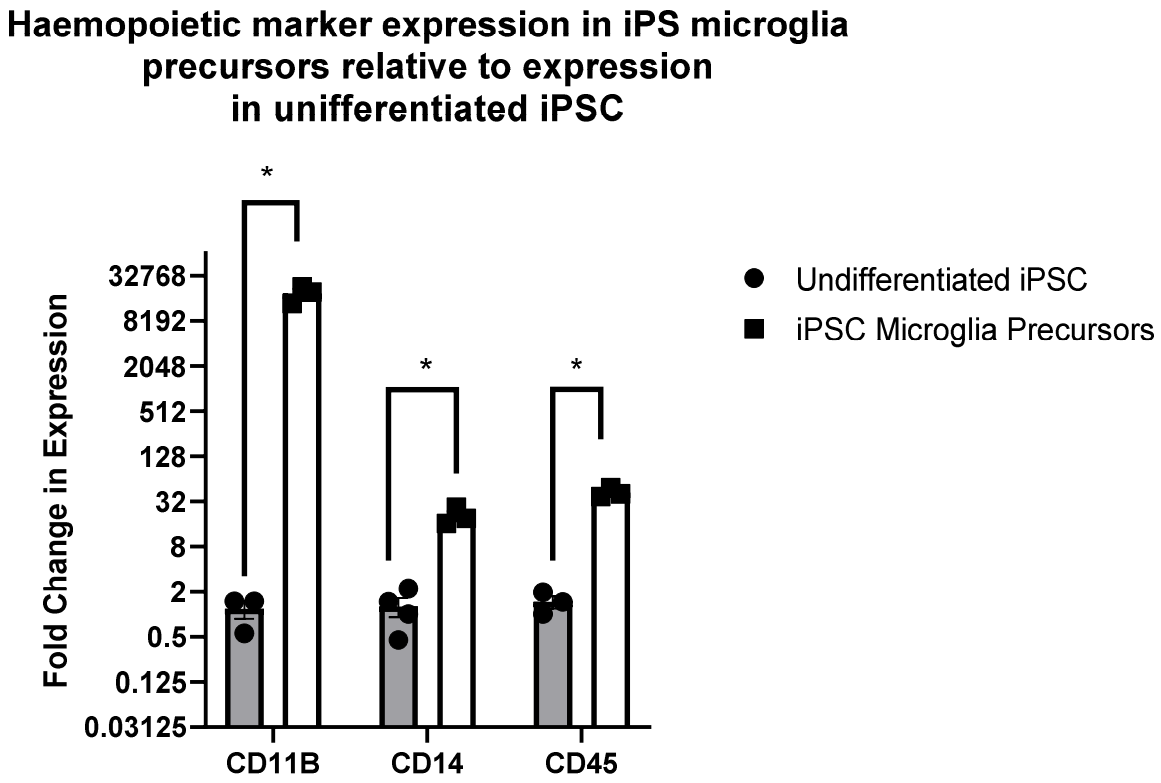

Figure 3.4: Expression of haematopoietic marker messages in iPS pre was increased compared to the expression in undifferentiated iPS cells.

*Significant upregulation of three hematopoietic markers CD14 (P= 0.019), CD11b (P=0.023) and CD45 (P=0.006) was increased when differentiated to iPS microglia precursors from undifferentiated iPS cells. This shows CD11b, an intergrin of CR3, to have the biggest increase. This confirms the differentiation towards haemopoietic cell types. Error bars represent the SD. A multiple unpaired t-test with post hoc Holm-Sidak multiple comparison with significance set at: * P< 0.05; ** P < 0.001; *** P<0.001; ****P<0.0001.*

Protein characterisation supported the message data in figure 3.4. Immunofluorescence in figure 3.5 shows iPS pre to express protein markers CD11B and CD45. CD45 was shown across the membrane while CD11b was shown to be present in clumps on the cell surface.

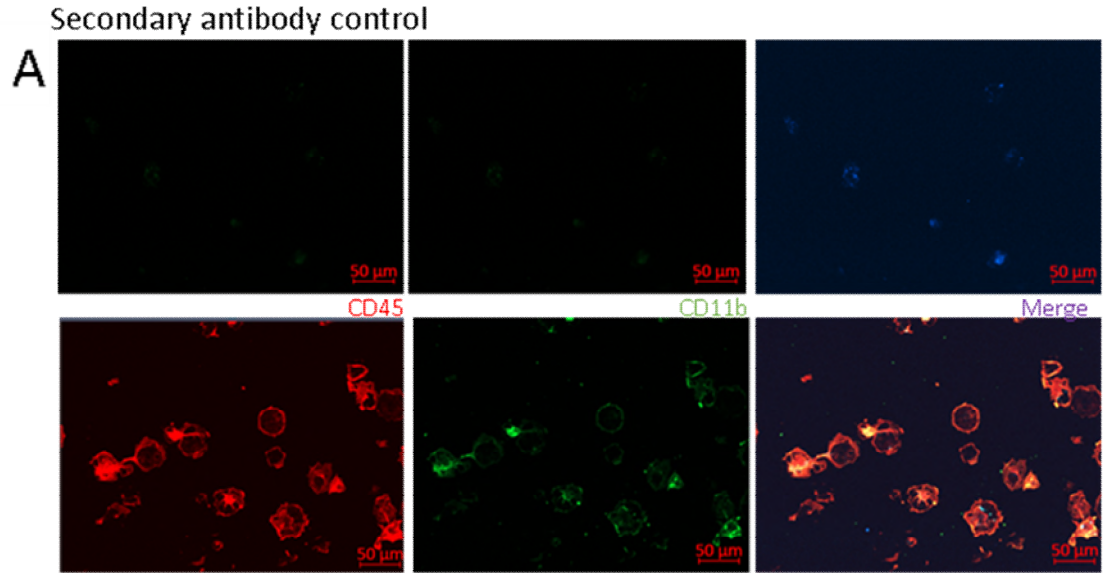

Figure 3.5: iPS precursor confocal staining with hematopoietic markers CD11b and CD45.
A) Secondary antibody only control B) Confocal images indicate positive staining for hematopoietic markers CD45 and CD11b, both key myeloid cell markers. Images were captured on Zeiss spinning disc confocal microscope. These images are representative images from at least 3 biological and 2 technical repeats.

Flow cytometry further supported this, showing positive shifts for the expression of hematopoietic markers CD45 and CD14. Flow cytometry was used to confirm presence of myeloid iPS precursors and was conducted on the first harvest of every factory.

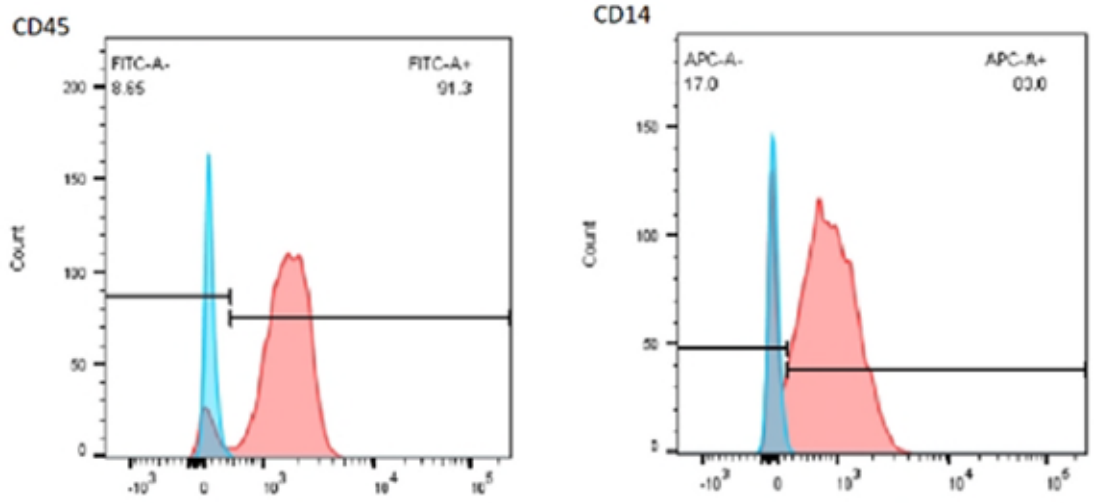

Figure 3.6: iPS pre characterised with hematopoietic markers CD14 and CD45 with flow cytometry
The blue peak is the isotype control while the red peak is the antibody bound peak. iPS pre show a positive shift for hematopoietic markers CD14 (83%) and CD45 (91%) which show a positive shift. CD45 antibody was conjugated to PE fluorophore while the CD14 antibody was conjugated to an APC fluorophore. Flow cytometry for myeloid markers was run on the first harvest of every factory to ensure cells expressed key hematopoietic markers. Isotype control information is in section 2.1.2. Therefore, this was ran at across minimum of 4 factory set ups and twice within each factory run.

Once cells had been confirmed to express hematopoietic markers they were plated in ACM and after days 10-14 show a microglia phenotype. Confirmation for successful differentiation to iPS microglia is shown in figure 3.7 which shows cells are positive for microglia marker CX3CR1 and lysosomal marker CD68.

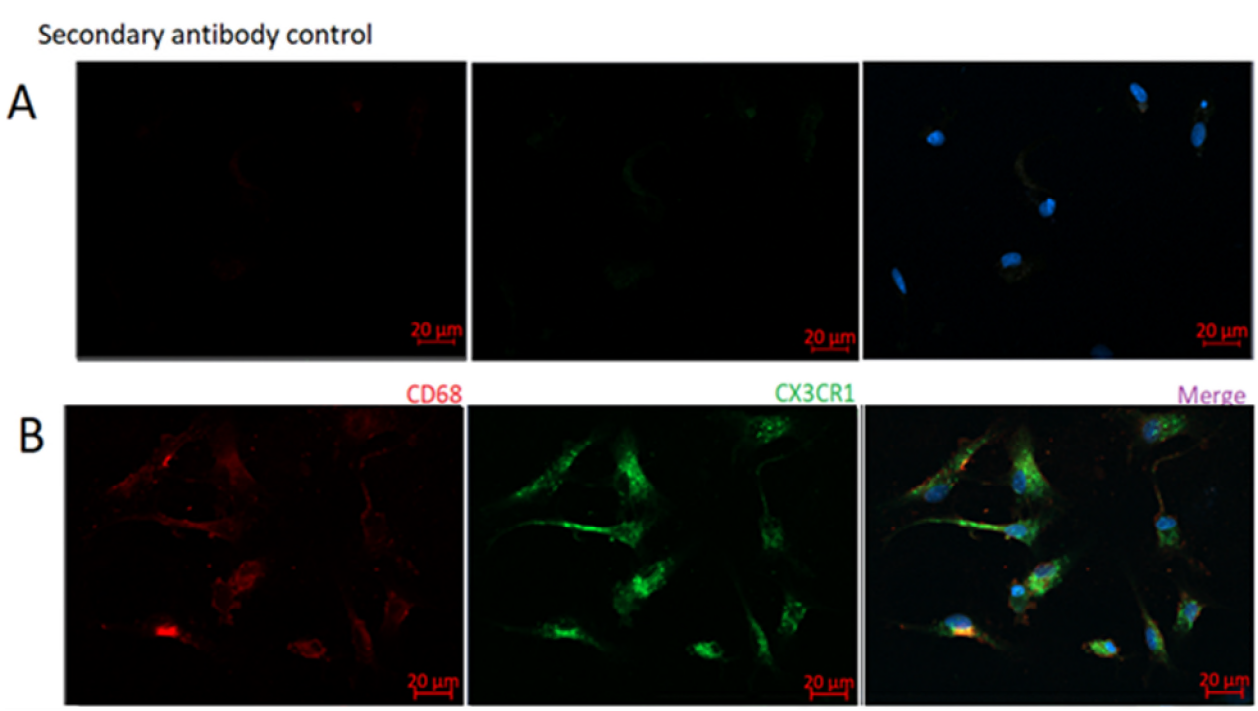

Figure 3.7: Representative images of iPS microglia staining showing cells are positive for microglia marker CX3CR1 and CD68.

A) Secondary antibody only control B) Z stacks combined show cells are positive for expression of CX3CR1 and CD68. All images were taken on Zeiss spinning disk. These images are representative images from at least 3 biological and 3 technical repeats.

3.2.3 Optimization of terminal differentiation

3.2.3.1 Optimization of coating materials

Precursors were collected weekly and plated for terminal differentiation to microglia-like cells. Originally this process was performed on extracellular matrix, Matrigel (1:100; Coring), which is a commercially available matrix comprising Lamin, collagen and nidogen. However, it was noticed that many cells detach between days 10-14 of terminal microglia differentiation , reducing the number of microglial cells produced for downstream assays. An alternative extracellular coating matrix, fibronectin, was tested alongside a no-coating condition in hope of increasing final microglia yield.

Images of differentiating cells were captured on the IncuCyte at day 5 and 10 (figure 3.7a-c). Images from day 10 indicate few cells remaining in the Matrigel and non-coating conditions with many more cells present in the fibronectin (1:100; Merck) coated group. This was supported by quantification of the change in confluency between the 10 and 5 day time points (figure 3.7d), which shows the largest reduction in cell number when plated on Matrigel. Analysis reveal the change in confluency of iPS microglia grown on fibronectin to be significantly lower than when plated on the other two conditions: no coating ($p= 0.0237$) and Matrigel ($p=0.0077$). Therefore, fibronectin offered the optimal coating for the most iPS microglia survival.

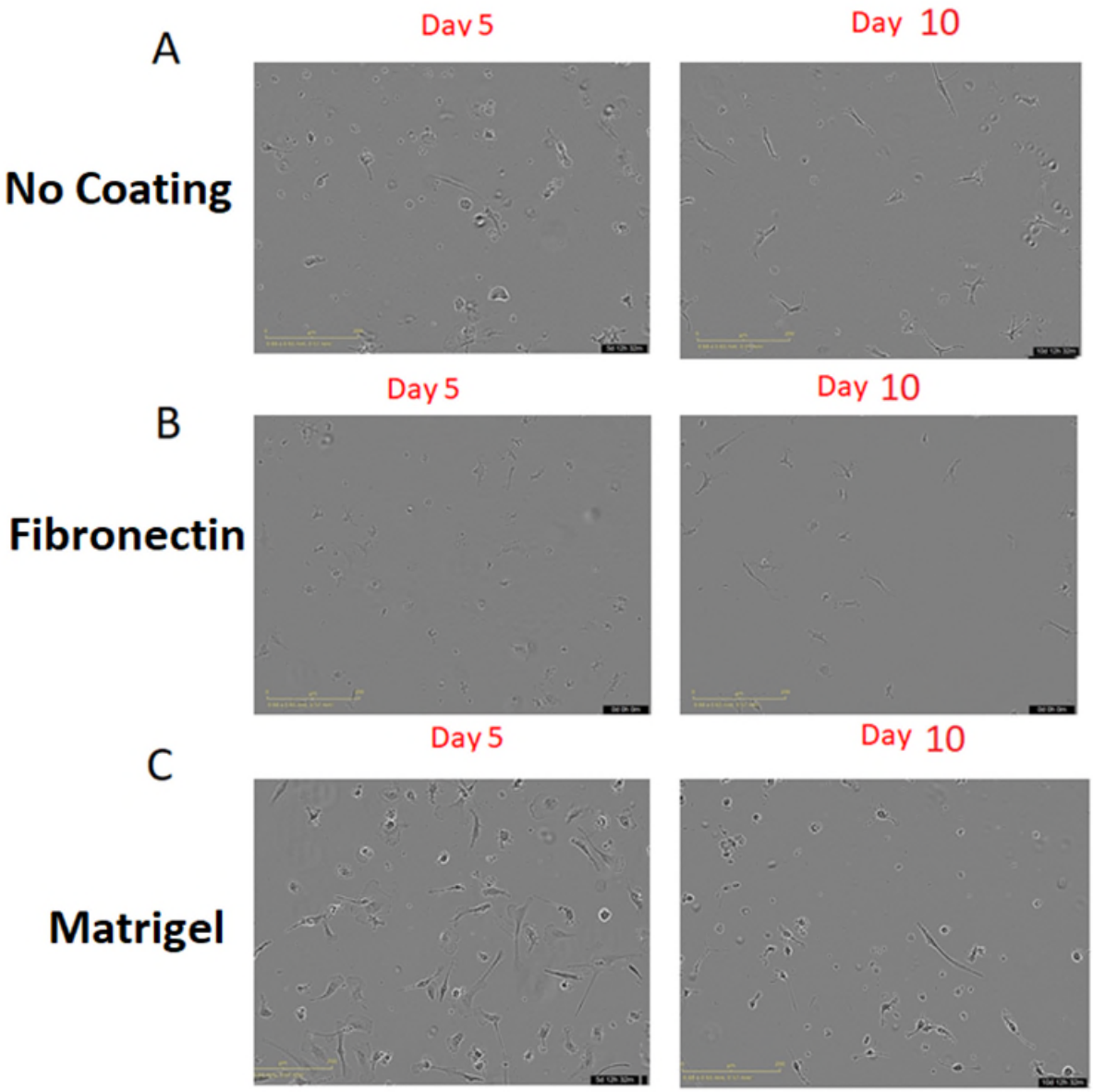
A
Day 5
Day 10
No Coating
B
Day 5
Day 10
Fibronectin
C
Day 5
Day 10
Matrigel

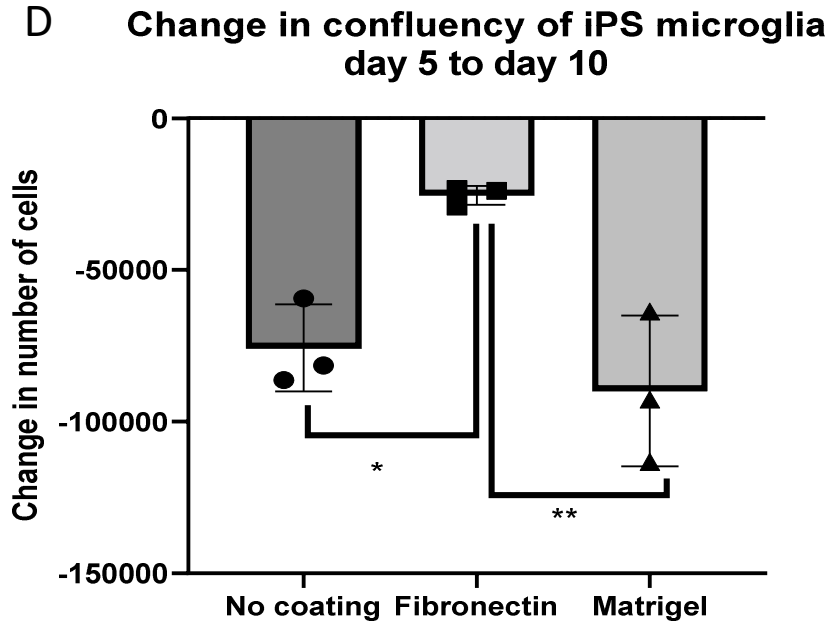

Figure 3.7: Optimisation of coating for terminal differentiation to iPS microglia *A-C) IncuCyte images taken at day 5 post plating and day 10 post plating. By day 5 cells appear to have stuck down and started differentiating, however fewer cells are present in the day 10 image, with the biggest change observable in no-coating and Matrigel coating. D) Quantification of change in confluency of cells and subsequent morphological characterisation. This reveals lowest reduction in cell number from day 10-5 is seen in Fibronectin coating which was significantly lower than the change in confluency from the other conditions, no-coating (p=0.0237) and Matrigel (p=0.0077) conditions. Each point on the graph represents an average of 3 wells from one plate therefore this data represents three biological replicates in triplicate. Error bars are SD values. A one way ANOVA with Tukey multiple comparison was performed with significance set at: . * P< 0.05; ** P < 0.01; *** P<0.001; ****P<0.0001. If found to be not significant, no asterisk is labelled, and P >0.05.. Cells were all taken from one harvest and were terminally differentiated simultaneously.*

3.2.3.2 Optimization of terminal media

In addition to adapting the extracellular matrix, the medium used during the terminal differentiation phase was optimized and compared to the original published media, which was XVIVO supplemented with 10ng/ml Granulocyte-macrophage colony stimulating factor (GM-CSF) and 100ng/ml interleukin-34 (IL-34) for 10-14 days[194,207].

3.2.3.2.1 Generation of in-house ACM

In-house ACM was produced from APOE3 IPS astrocytes differentiated by Dr Kimberly Jones (Nick Allen lab) following a protocol published by Serio et al 2013[226]. Astrocyte precursor cells (APC) were produced following ectoderm induction alongside neuronal precursor cells (NPC). A pure population of APCs was produced by CD44 FACs sorting; figure 3.8 shows an example image of APC cells. When at 60% confluent terminal differentiation, medium was added and left until full differentiation into iPS astrocytes in 14 days. Initially, APC cells continue to expand; however, after several days, cell nuclei began to clump together with large process' extending between them. Once fully differentiated, iPS astrocytes can be maintained for several months and continue to mature across the first few weeks. Confirmation of iPS astrocyte phenotype is shown in figure 3.8 and figure 3.9. Conditioned media was produced by addition of ADF supplemented with 2% (w/v) Neurobrew with Vit A on mature astrocytes for 2 days, then harvested. Multiple collections were pooled together to form a single batch which was batch-controlled with a CCL_2 ELISA and diluted to a final concentration of CCl_2 1ng/ml

to minimize the effects of different batches. ACM was stored at -80^{o}C for long time storage. To ensure cells were astrocytic, characterization for key astrocytic markers was conducted using RT-qPCR, western blot and immunofluorescence. Figure 3.9 shows significant increases of three astrocytic marker transcript in iPS astrocytes compared to undifferentiated iPS cells; GFAP (P=0.00048), EAAT2 (P=0.0125) and S100β (P=0.00048).

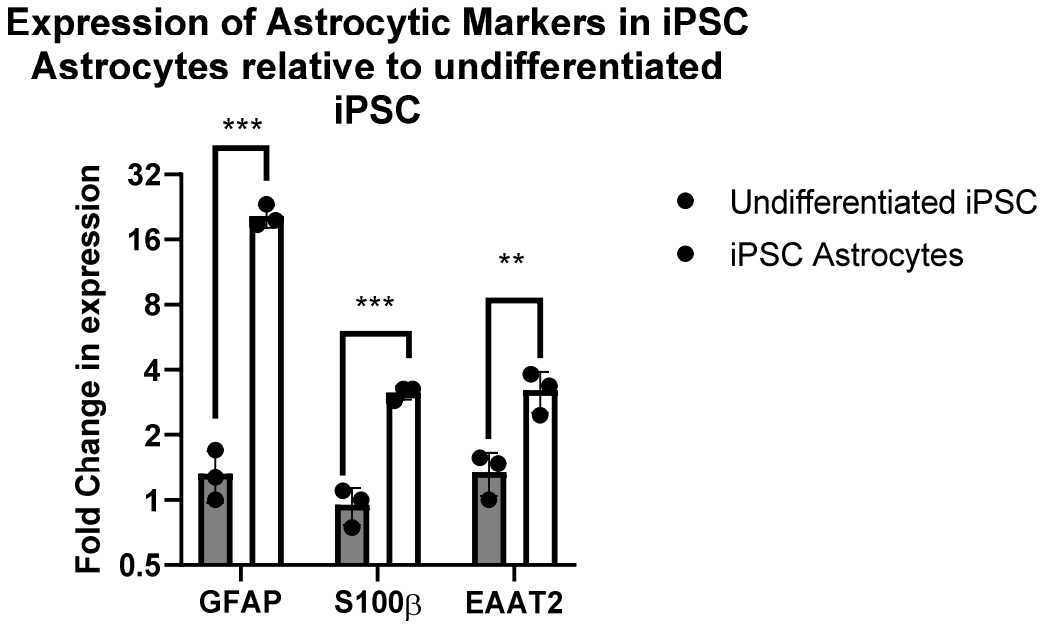

Figure 3.9: Expression of astrocytic marker messages in iPS astrocytes was s80ignificantly increased compared to the expression in undifferentiated iPS cells.

*Significant upregulation of three astrocytic markers GFAP (P= 0.00048), S100β (P=0.00048) and EAAT2 (P=0.0125) was increased when differentiated to iPS astrocytes from undifferentiated iPS cells. This confirms the differentiation towards astrocytic-like cells. Error bars represent the SD. . A multiple unpaired t-test with post hoc Holm-Sidak multiple comparison with significance set to: * P< 0.05; ** P < 0.01; *** P<0.001; ****P<0.0001.*

Characterisation of iPS astrocytes for GFAP protein expression is shown in figure 3.10. Immunofluorescence in 3.10A shows bright green GFAP staining throughout the cell. This was confirmed with western blotting, which revealed iPS APC and iPS astrocytes produced a strong band for GFAP at 50kDa.

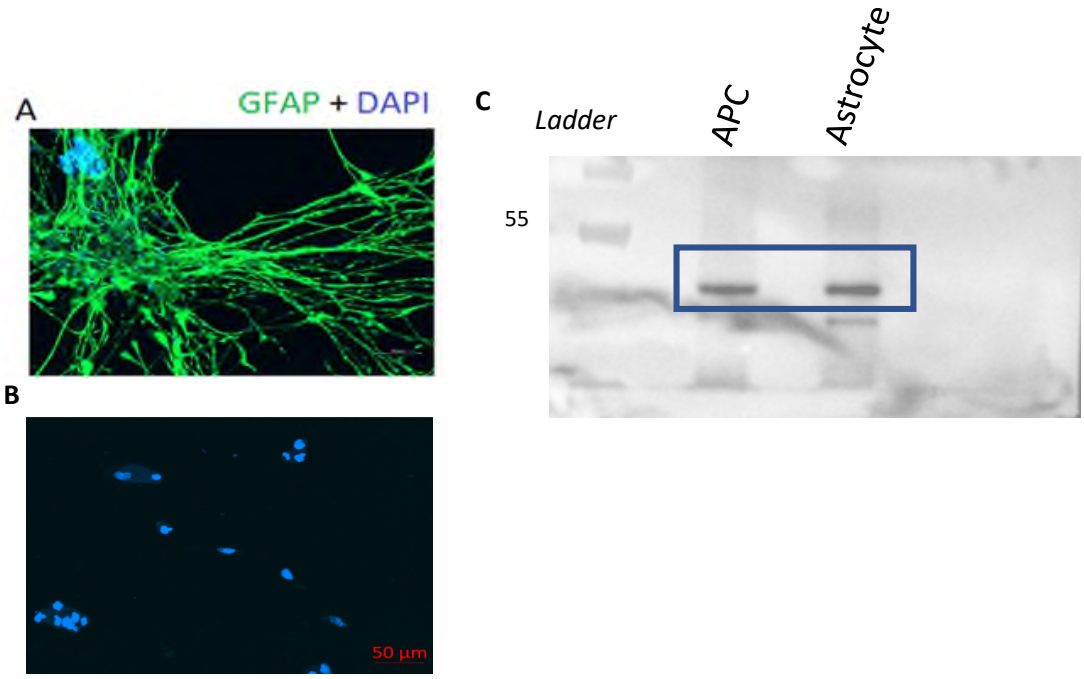

Figure 3.10: Confirmation of astrocytic protein in iPS astrocyte with immunofluorescence and western blot *A) Immunofluorescence of IPS astrocytes shows bright AF488 staining with GFAP primary, DAPI shows the clustering of cell bodies. This represents 3 biological repeats. B) This is the secondary only control for A. C) A western Blot with 20µg of APC and Astrocyte protein show bands as expected at 50kDa for GFAP. A gradient gel was used, with upper 7.5% and the lower 5% acrylamide. Immunofluorescence was performed on a Zeiss spinning disk confocal microscope. This is representative of 2 biological repeats*

An ACM batch was prepared by the pooling of 6-7 harvests of conditioned media. Each batch was stored at -80°C after batch testing using an ELISA for astrocyte secretion marker CCL_2, as has been previously reported[227]. A dilution factor for each batch was generated from this ELISA so that final concentration of CCL_2 was 1ng/ml. Additional control of batch variability was achieved by limiting use of each batch to one set of experiments i.e. all iPS microglia used to generate the data for CR1 expression data in chapter 2 was done using Batch B of ACM.

Over the course of this project three ACM batches were generated. Figure 3.11 shows that CCL_2 concentration varied between batches, producing different dilution factors. Additionally, early, and late ACM were tested, these samples were collected during the first collection of Batch C (Early ACM) and during the last collection of batch C (late ACM) prior to pooling. This revealed a notably reduced CCL_2 concentration in the late ACM compared to the early ACM, suggesting that variations of CCL_2 expression occurred with maturation of cells.

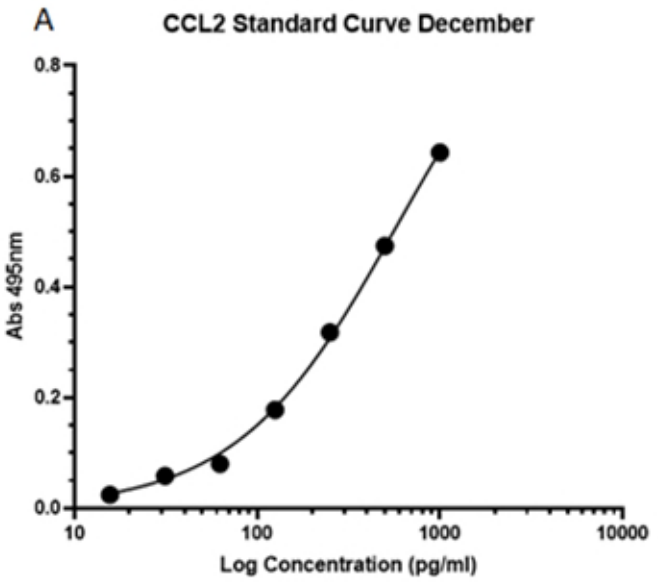

B

CCL2	Concentration (pg/ml)	Dilution to 1ng/ml
Batch A	1625	3:2
Batch B	1900	1:1
Batch C	5000	1:4
Early ACM	5000	N/A
Late ACM	2600	N/A

Figure 3.11: CCL_2 ELISA for ACM batch control
A) Standard curve of CCL_2 ELISA, B) Table of results for three batches used including CCL2 concentration (pg/ml) and dilution used so that final concentration is 1ng/ml.

A C3 ELISA was carried out on batch B and batch C. This was done because C3 secretion is reported to increase in activated astrocytes, allowing a preliminary comparison of astrocytic activation states[157]. Figure 3.12 shows that amounts of C3 differed between batches with Batch B containing 9µg/ml compared to Batch C with only 3.8µg/ml, suggesting that the ACM produced in Batch B was produced from more activated cells. Comparison of early and late ACM from the same batch revealed a difference of 0.3µg/ml, suggesting only small changes across the same harvest.

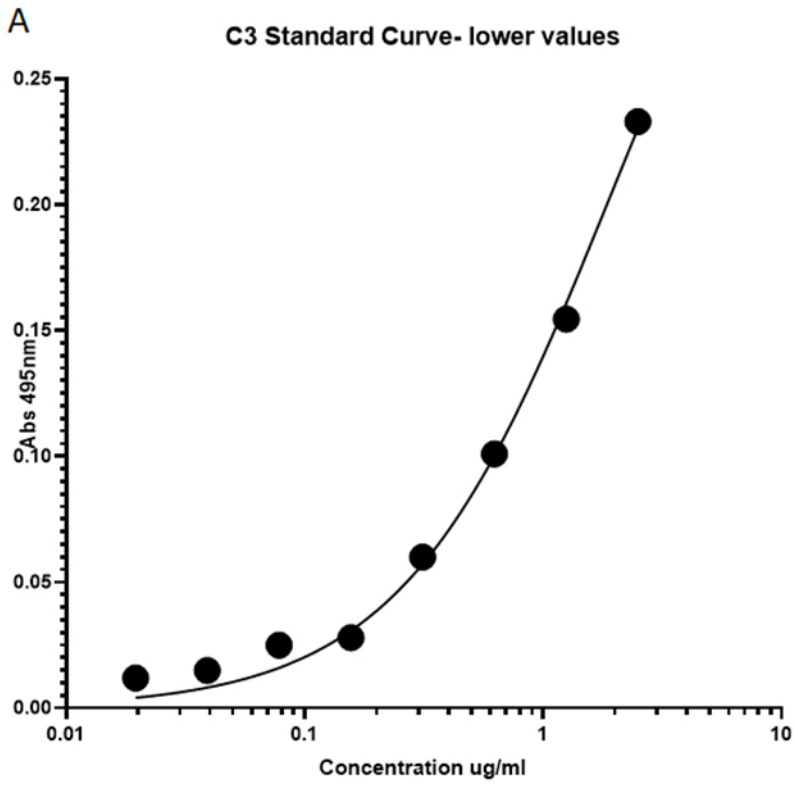

B

C3	Concentration (ug/ml)
Batch B	9
Batch C	3.8
Early ACM	3.2
Late ACM	3.5

Figure 3.12: C3 ELISA in ACM
A) standard curve of C3 ELISA, B) Table indicating differences of two batches of ACM and early and late collection of ACM from Batch C of ACM.

iPS pre were differentiated in Batch A and Batch B simultaneously and assessed for microglia markers using immunofluorescence to compare the resultant cells and the effect of batch. Figure 3.13 shows that cells in these different medium batches stained positive for microglia markers CX3CR1 and CD68. However, clearer, brighter staining for both markers was seen with Batch A, particularly in CD68 which is notably dimmer in cells grown in batch B.

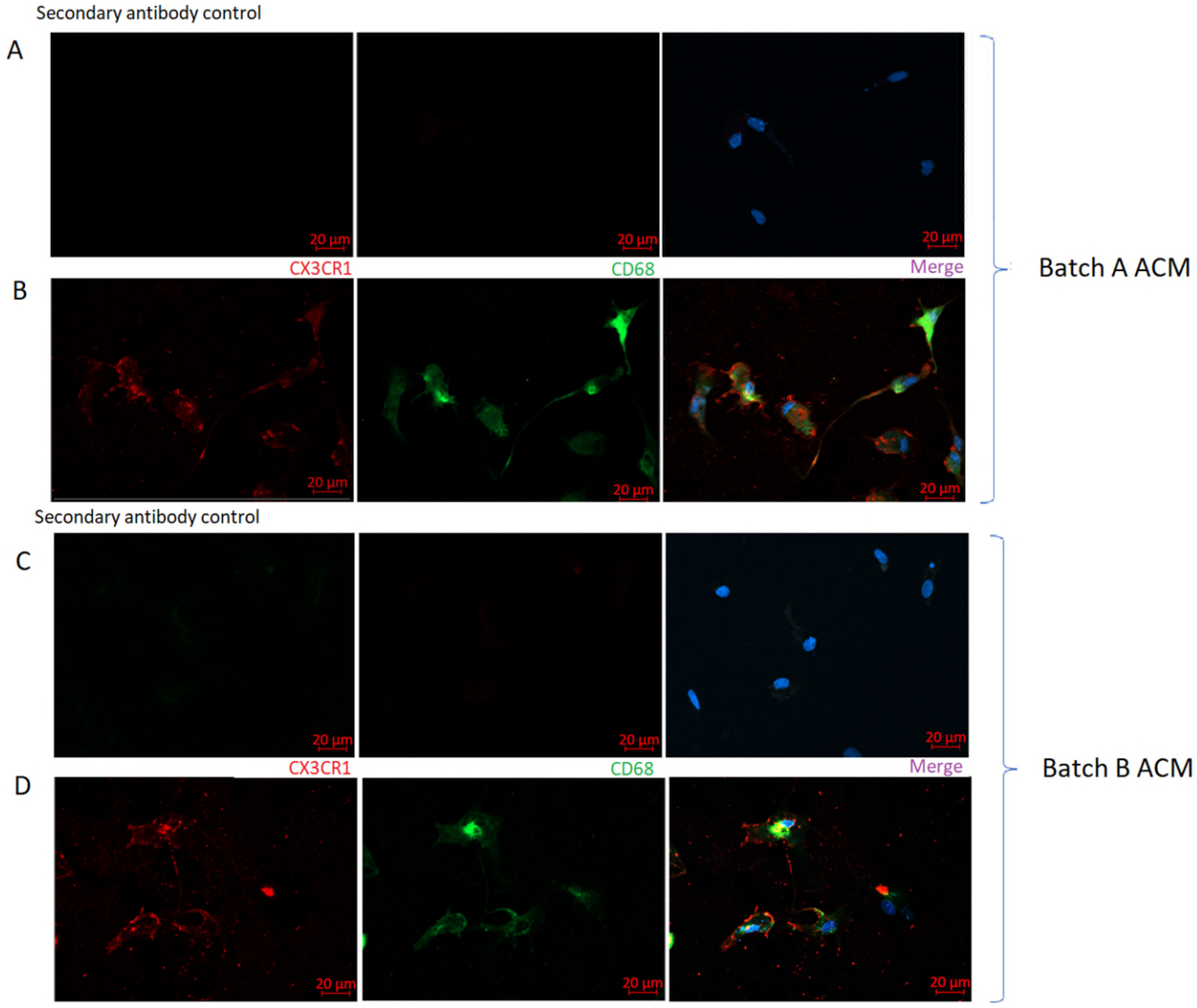

Figure 3.13: Immunofluorescence of microglia markers CX3CR1 and CD68 on iPS microglia differentiated in two separate ACM batches.
A) Secondary antibody controls for iPS microglia differentiated in batch A ACM. B) Cells were differentiated in batch A of ACM were positive for markers microglia specific marker CX3CR1 and lysosomal marker CD68 C) Secondary antibody control for iPS microglia differentiated in batch B of ACM.D) Cells were differentiated in Batch B of ACM showing cells to be positive for expression of CX3CR1 and CD68. All images were Z stacks captured on Zeiss spinning disc confocal microscope. These images are representative images from at 1 biological with 2 technical repeats.

3.2.3.2.2 Comparison of supplemented XVIVO and ACM differentiated iPS microglia

A brief morphological comparison of iPS microglia differentiated in ACM or supplemented XVIVO was performed. Figure 3.14 shows phase images of iPS microglia generated in the two media. This shows XVIVO grown cells to be large with visible vacuoles throughout the cell body compared to precursors (from the same harvest) which were differentiated in ACM. XVIVO microglia appeared to have few processes with many of the cells having a bi-polar shape. Conversely, ACM iPS microglia were much smaller, without the vacuoles within the cell, and were more branched compared to those differentiated in XVIVO supplemented media. This indicates morphological differences between the two terminal differentiation medias however, this is not sufficient information to determine the most 'micoglial-like' differentiation media.

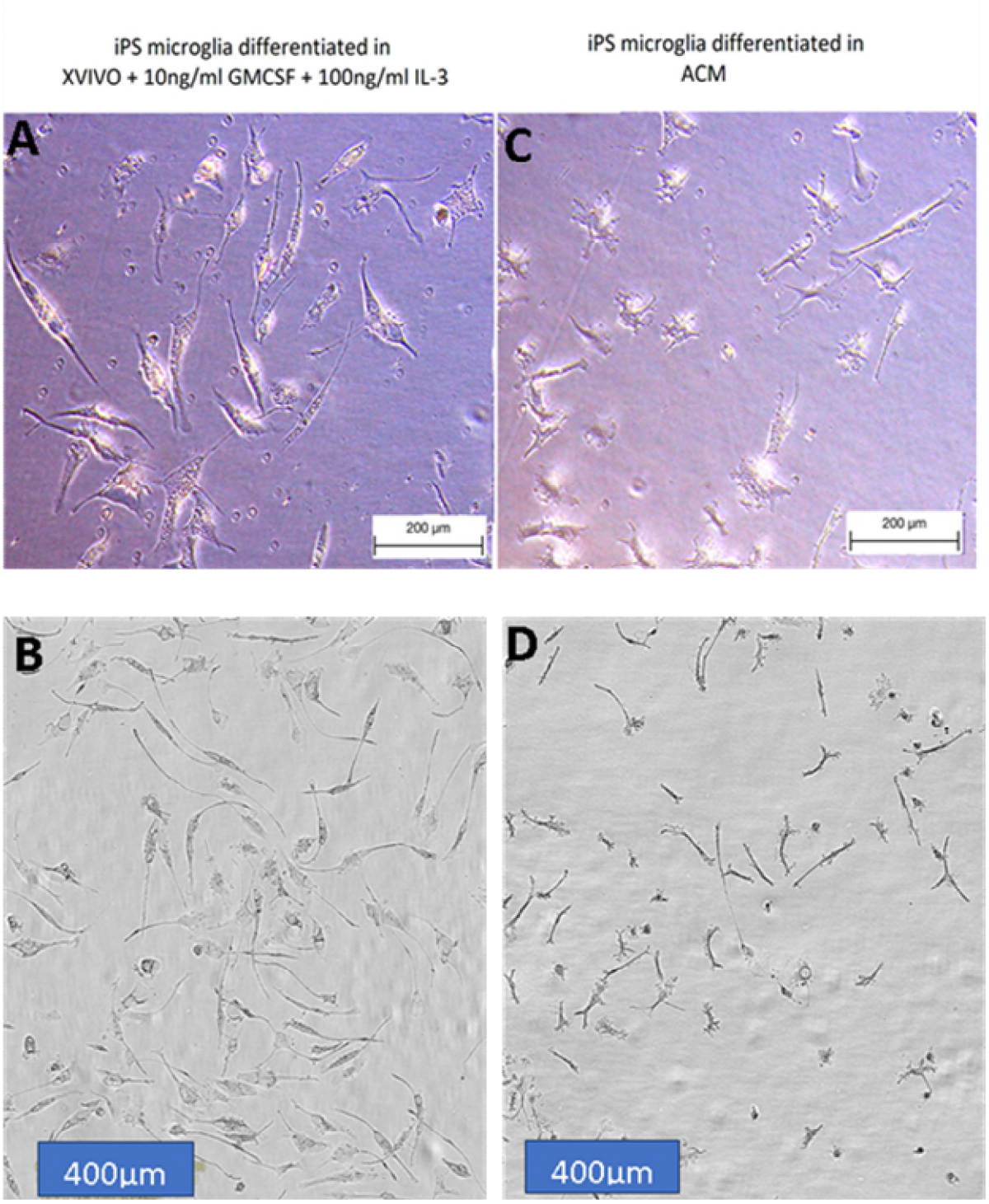

Figure 3.14: Phase microscope images of iPS microglia differentiated in supplemented XVIVO and in-house generated ACM.
A) The image on the left shows iPS microglia differentiated in XVIVO media supplemented with 10ng/ml GMCSF and 100ng/ml IL-3. This shows cells with some process' with large vacuoles decorating the cell body of the cells. This was taken on a light microscope using a 40X lens B) The image below also shows XVIVO grown iPS microglia but taken on the incucyte using a 20X lens. This shows the same cell morphology with long, bi-polar cells. C) The image on the right shows iPS microglia differentiated in in-house generated ACM. Cells appear smaller compared to those in image A and many show highly processed cells. Furthermore cells appear to be absent of the vacuoles seen in image A. This image was taken on a light microscope using a 40X lens. D) This image was taken on the IncuCyte using a 20X lens and shows cells to be smaller than that in B. These images represent 2 biological repeats and 4 technical repeats.

RT-qPCR was used to investigate the expression of key microglia markers in cells differentiated in both media. Figure 3.15a shows iPS XVIVO microglia to have an increase in expression of P2RY12, IBA-1 and CX3CR1 relative to undifferentiated IPS cells when normalised to a single housekeeper,

SDHA. Figure 3.15b shows ACM iPS microglia had a significant increase in microglia markers IBA-1 (P=0.0121), P2YR12 (P=0.0285) and CX3CR1 (P=0.0166) relative to undifferentiated iPS cells. Figure 3.15b is normalised to multiple housekeepers and is generated using Fluidigm.

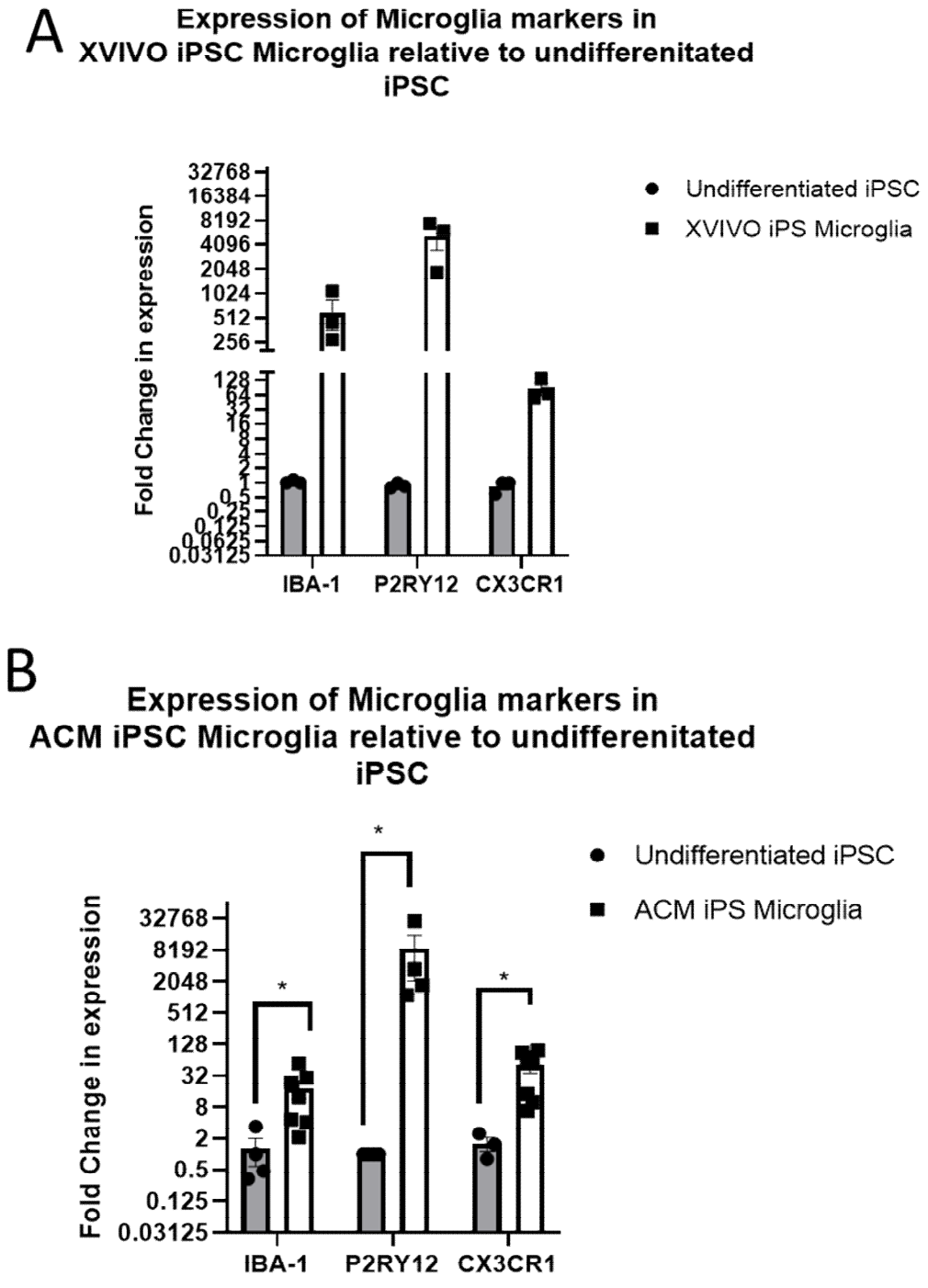

Figure 3.15: Expression of microglia marker message in microglia differentiated in XVIVO and ACM compared to the expression in undifferentiated iPS cells.

A) Microglia markers IBA-1, P2RY12 and CX3CR1 were not significantly increased in iPS microglia differentiated in XVIVO media supplemented with IL-3 and M-CSF. This was run on a quant studio 7 RT-qPCR machine and is normalised to one housekeeper-SDHA. Error bars represent the SD. Multiple Mann Whitney with Holm-Sidak multiple comparison post hoc was performed. B) A significant upregulation of IBA-1 (P=0.0121), PRY12 (P=0.0285) and CX3CR1 (P= 0.0166) was shown in

*iPS microglia differentiated in ACM relative to undifferentiated iPS expression. This was ran on the fluidigm and is normalised to 5 hourskeepers- SDHA, HPRT, ACTINB, GAPDH and UBC. Error bars represent the SD. Multiple Mann Whitney with Holm-Sidak multiple comparison post hoc was performed with significance set to: * P< 0.05; ** P < 0.01; *** P<0.001; ****P<0.0001. Absence of asterisk indicates no significant difference with P > 0.05.*

Expression of microglia proteins was assessed using immunofluorescence for markers CD45, CD11b and CD68. Figure 3.16 shows CD45 staining in clusters on the cell surface of ACM microglia but appeared more evenly distributed across the larger XVIVO cells. A similar effect was seen with CD11B, with faint clusters on the cell body of ACM iPS microglia while XVIVO iPS microglia showed brighter expression of CD11b throughout the cell.

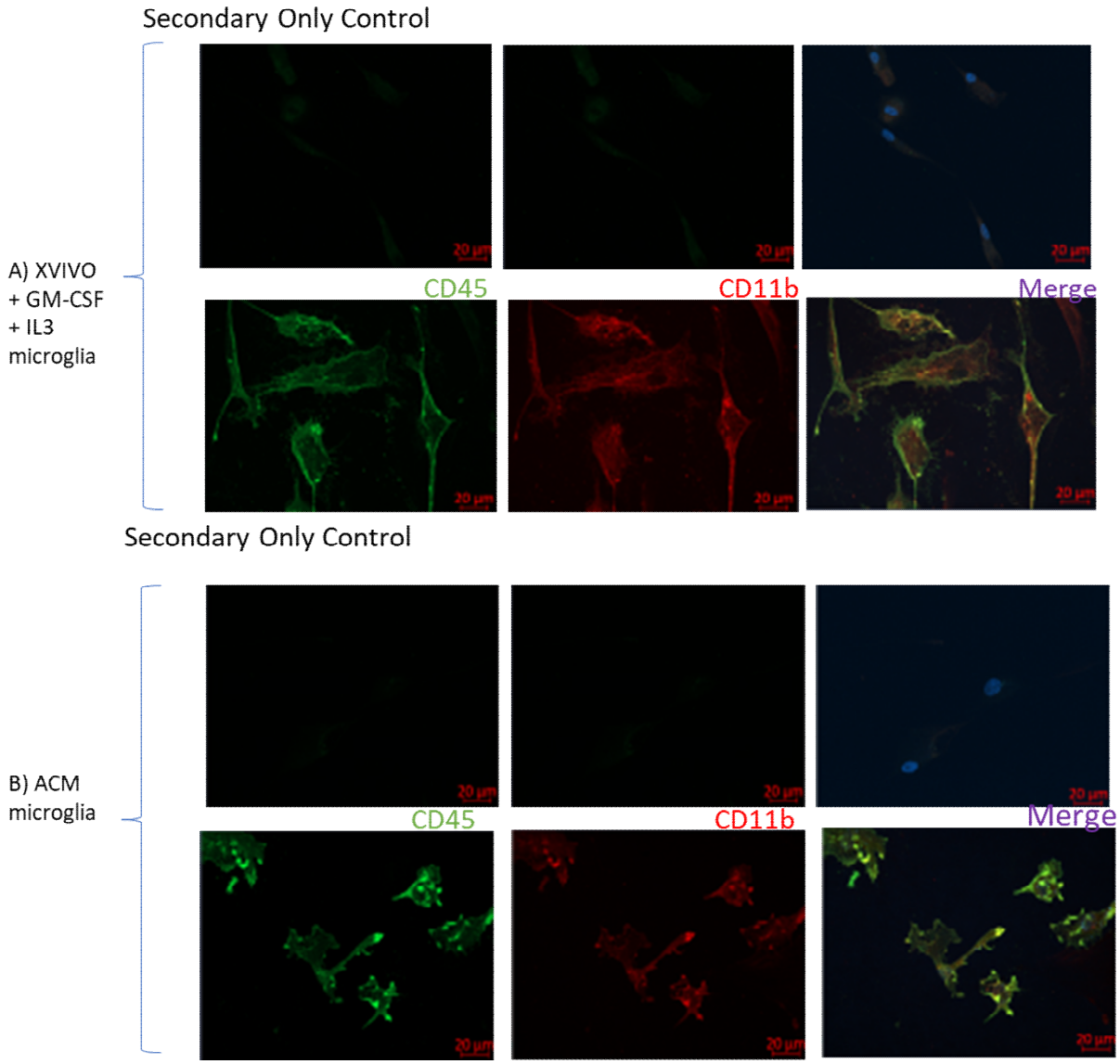

Figure 3.16: Immunofluorescence of markers CD45 and C11b on iPS microglia differentiated in supplemented XVIVO and ACM.

A) XVIVO differentiated iPS microglia are positive for microglia markers CD11b and CD45. Expression of CD45 appears to be spread throughout the cell, while CD11b appeared to be mostly around the extensions B) ACM differentiated iPS microglia shows CD11b to be expressed in large clumps over the cell surface, staining brightly, CD45 appears much fainter in comparison but is present mostly on the cell body. All images were captured on Zeiss spinning disc confocal microscopy. These images are representative images from at 1 biological and 2 technical repeats.

3.2.4 Functional characterization of ACM EB microglia

RNA was collected from activated iPS microglia and RT-qPCR performed for markers of cell activation. This panel includes two pro-inflammatory cytokines, Tumor Necrosis Factor (*TNFα*) and Interleukin-6 (*IL-6*), and inflammasome markers Nodd-LPR pyrin domain containing protein 3 (*NLRP3)* and activation transcription factor Nuclear-kappa light chain enhancer of activated B cells (*NFκB*). All four of these markers indicate activation of microglia.. Figure 3.19 shows changes in transcript for these four markers in iPS microglia stimulated with 100ng/ml of LPS for 6 hours. This reveals significant increases in pro-inflammatory cytokines with IL-6 (P=0.0047) increased 20-fold and TNFα (P=0.0001) increased 156-fold following LPS treatment. This indicates iPS microglia to elicit a pro-inflammatory response , a core role of microglia *in vitro.*

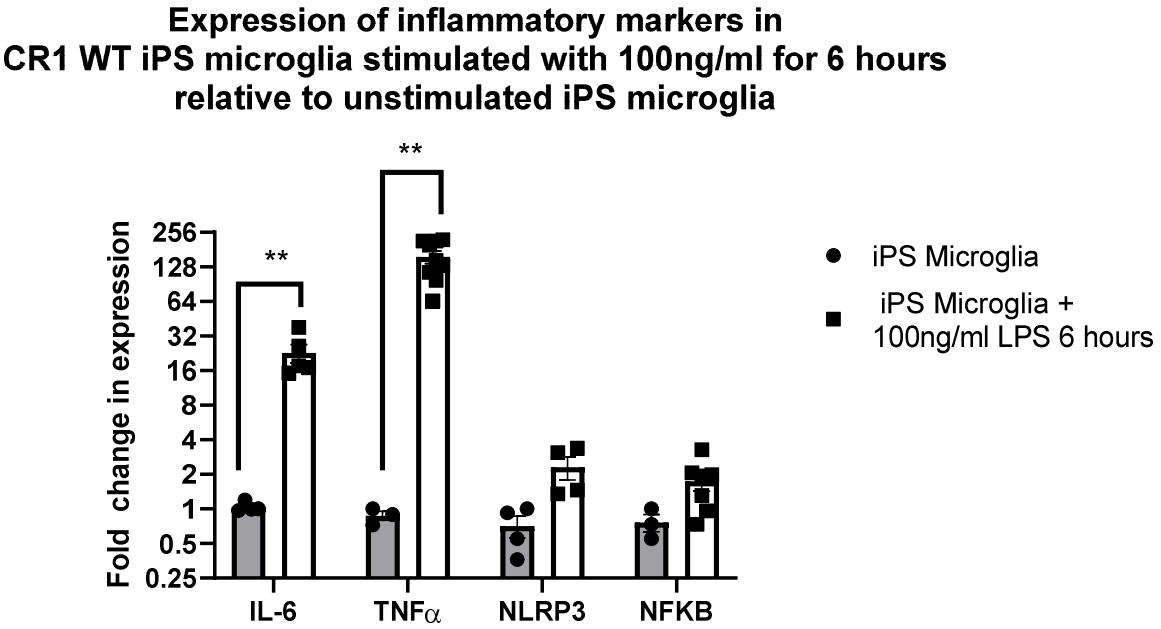

Figure 3.19: Message expression of inflammatory cytokines in iPS microglia stimulated with 100ng/ml LPS for 6 hours was increased compared to expression in unstimulated iPS microglia but no significant change in inflammasome NLRP3 or activation transcription factor, NFKB, was shown.
*Significant upregulation of two inflammatory cytokines IL-6 (P= 0.0047) and TNFα (P=0.0049) was observed following 6 hours of 100ng/ml LPS activation in iPS microglia. Transcription factor NFKB and inflammasome sensor NLRP3 were not significantly increased with 6 hours of LPS stimulation. Error bars represent the SD. Statistics were performed using the multiple Mann Whitney test with Holm Sidak multiple comparison with significance set to * P< 0.05; ** P < 0.01; *** P<0.001; ****P<0.0001. Absence of asterisk indicates no significant difference with P > 0.05. This was produced using the Fluidigm and normalised to 5 housekeepers.*

Another essential role for microglia is the phagocytosis of foreign particles. An *in vitro* phagocytosis assay was performed using pH-Rodo conjugated E.coli bioparticles, as described in section 2.2.9.1. This allowed for red fluorescence to be emitted when beads were phagocytosed and entered the acidic lysosomal compartment, therefore only phagocytosed beads fluoresce. Figure 3.20A shows increase in red fluorescence over 6 hour assay period with increased red fluorescence in phase images of figure 3.19a). This effect was blocked with addition of cytoskeleton inhibitor, cytochalasin D at

10µM. Figure 3.20B shows quantification of this data, with total integrated red intensity plotted on the y with time (minutes) on the x. The integrated red intensity was calculated by the IncuCyte analysis software and normalized to total number of cells, also calculated by the IncuCyte. Statistical analysis revealed significant increase of red fluorescence over 6 hours p=0.0034.

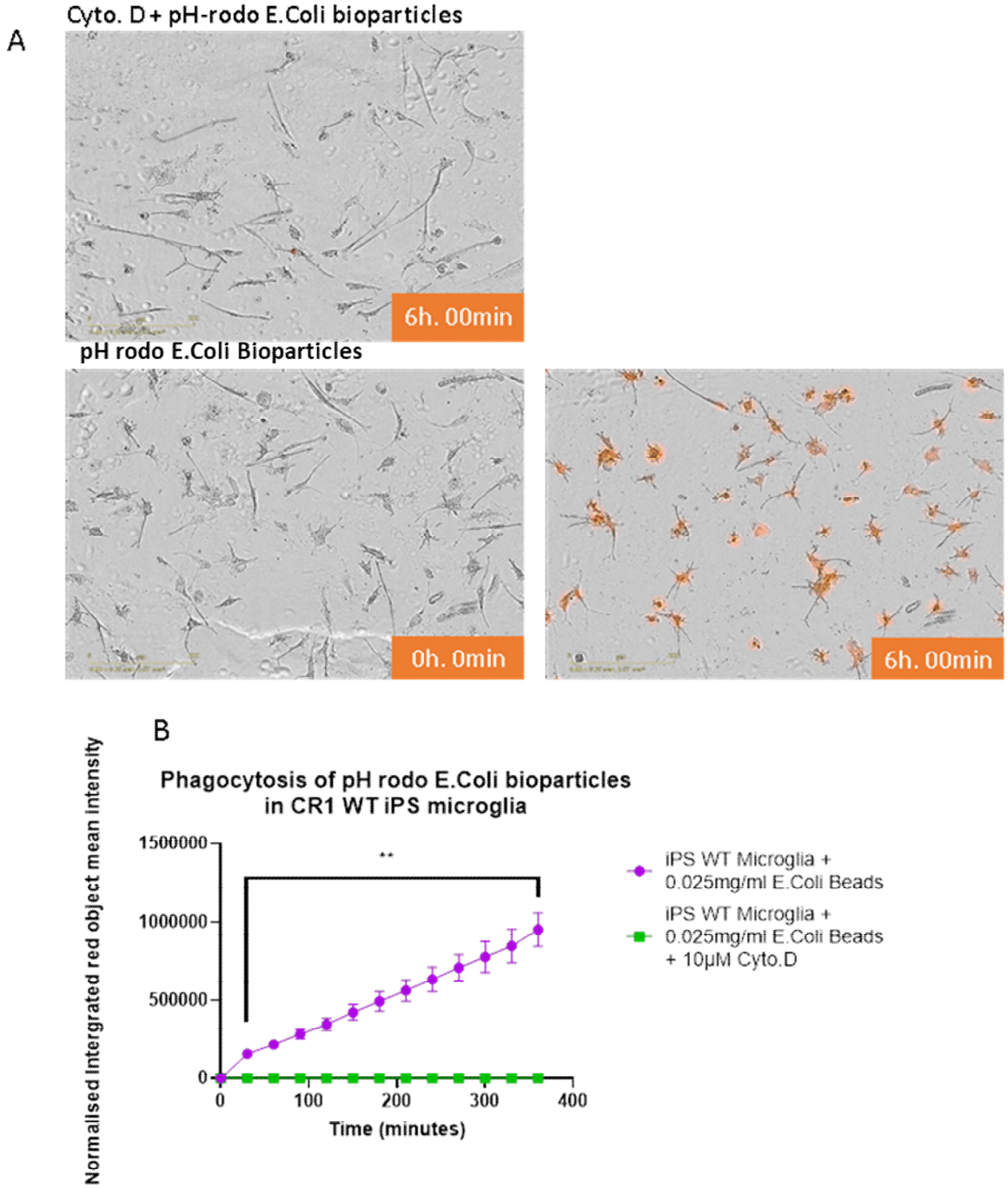

Figure 3.20: ACM iPS successfully phagocytose Ph-Rodo E-coli bioparticles
A) Images from the Incucyte of bioparticle ingestion. The first panel shows the Cyto D. control wth no red fluorescence in the iPS microglia at the last 6 hour time point. The panel underneath show an increase in red fluorescent from the 0 hours and 6 hour time point indicating bioparticle ingestion by iPS microglia. The yellow bar on the bottom left shows scale bar to 400µm. B) Quantification of integrated Red Object was normalised to cell counts which were measured using the IncuCyte confluency mask. This shows increase in fluorescence over 6 hours (360 minutes). Control group with phagocytosis inhibitor, cyochalsain

*D, showed no change in red fluorescence. An ANOVA from time point 1 to time point 13 revealed the increase in red fluorescence in the absence of Cyto-D to be significant (P=0.0034) with significance set to: * P< 0.05; ** P < 0.01; *** P<0.001; ****P<0.0001. for this P >0.05. Data was collected as described in section 2.1.1.9 and was measured using the IncuCyte. Data in this figure shows three technical repeats from cells collected on the same harvest. However this is representative of 3 biological repeats.*

3.2.5 Direct differentiation to IPS microglia using a monolayer protocol

Differentiation through the previously described EB protocol was generally consistent; however a failure in the differentiation occurred in the course of the work, meaning no iPS microglia were produced. While trouble shooting this problem, a monolayer differentiation protocol was trialed as a secondary solution. It was later discovered that failure of the EB method was due to faulty growth factor batches and was remedied by a change in supplier from Biolegend to Gibco. Differentiation by an alternative method offered the opportunity to select the optimal differentiation strategy for subsequent experimentation.

The monolayer method was adapted from the original protocol by Takata et al 2017[197]. Summarized in figure 3.21, this method utilized more complex media changes, with additional growth factors. Additionally, EBs were not generated during this protocol, instead cells were differentiated in a 2D layer and is referred to as the monolayer protocol.

For successful differentiation, a very low number of starting iPSC are required, roughly 100 cells/cm² in 1 well of a 6 well plate. Initially, use of higher numbers resulted in a failure of differentiation in most cases, with the cells peeling of the bottom of the well before completing the protocol. The first treatment was performed in media supplemented with hematopoietic growth factors BMP4 (5ng/ml) and VEGF (50ng/ml) alongside WNT activator CHIR99021 (2µM). After 2 days in this medium, cells proliferated to cover the bottom of the well producing denser patches across the layer. The next medium change, on day 3, saw the replacement of CHIR99021 with FGF2 (20ng/ml). After large cystic structures are observed growing from dense patches of cells. The third medium, added on day 5 removed the BMP4 and reduced the concentration of VEGF to 15ng/ml; cultures showed a growth of these cystic structures during this time. This medium was changed 2 days later to one supplemented with VEGF (10ng/ml), FGF2 (10ng/ml), SCF (50ng/ml), IL-6 (10ng/ml), IL-3 (20ng/ml) and DKK1 (30ng/ml) which cultures were fed with for 4 days, changing media on the second day . During this media change, around day 10, multiple cells began to appear within the supernatant including ruffled precursors which could be seen attached to the less dense cell patches. It was noted that most cells were spotted around the edges of the well. At day 13 the media was changed for one supplemented with FGF2 (10ng/ml), SCF (50ng/ml), IL-3 (20ng/ml) and IL-6 (10ng/ml) for another 2 days before the final media change on day 15. The final media used is supplemented with CSF1R ligand M-CSF (100ng/ml) and IL-3 (25ng/ml) and is changed weekly. Precursors were seen floating in the supernatant after two weeks in this media. During this time the well fills with round ruffled precursors, very similar to those produced by the factories in the EB protocol. These were carefully collected and terminally differentiated to IPS microglia in ACM, as previously described. Precursors were collected weekly, for around 2 months after which cells began to detach and die in the dish.

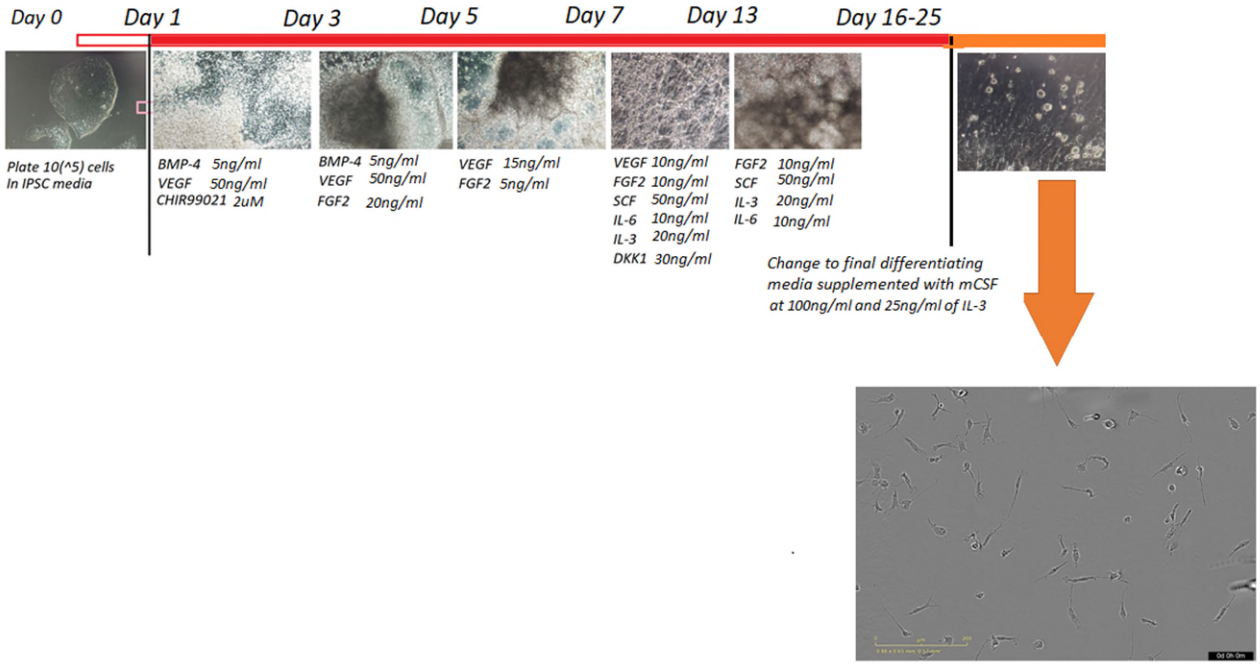

Figure 3.21: Schematic of differentiation to iPS microglia following the monolayer differentiation *Media supplemented with growth factors mentioned above are added at specific time points, cells begin to change quickly starting to produce yolk-sac like cystic structures by day 3. iPS Pre cells are seen stuck to the endothelium early on, around day 10, these begin to detach into the media between days 16-25, typically around day 21 however some detached earlier on. These cells are collected for terminal differentiation using ACM and fibronectin.*

IPS precursor identity of cells produced in the monolayer protocol was confirmed with flow cytometry for three hematopoietic markers CD14, CD11B and CD14. Monolayer iPS PRE produced a positive shift in all three hematopoietic markers (Figure 3.22). The largest shift was for CD14 with a smaller shift in CD45 and CD11b. It is important to note that fewer cells were collected weekly with this protocol than when differentiated through the EB based method.

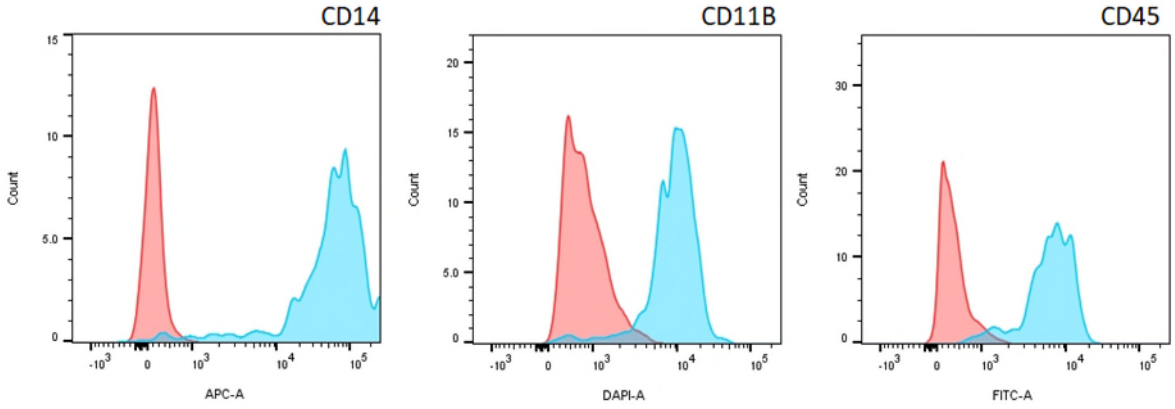

Figure 3.22: iPS Pre are characterised with hematopoietic markers with flow cytometry *The red peak represents the isotype control while the blue the antibody treated cells. Cells show a positive shift for all three hematopoietic markers with 88% of cells positive for CD14, CD11b 86% positive and 60% positive for CD45. Flow was run on the first harvest of each differentiation before plating for terminal differentiation. Flow was performed on the Fortessa BD. This was repeated every monolayer set up when precursors were obvious within the media.*

iPS monolayer microglia grown in ACM were characterized for microglia markers IBA-1 and CD45 using immunofluorescence. Figure 3.23 shows cells brightly stained for IBA-1 and CD45 with expression of IBA-1 mostly in clumps on the cell body and CD45 throughout the cells.

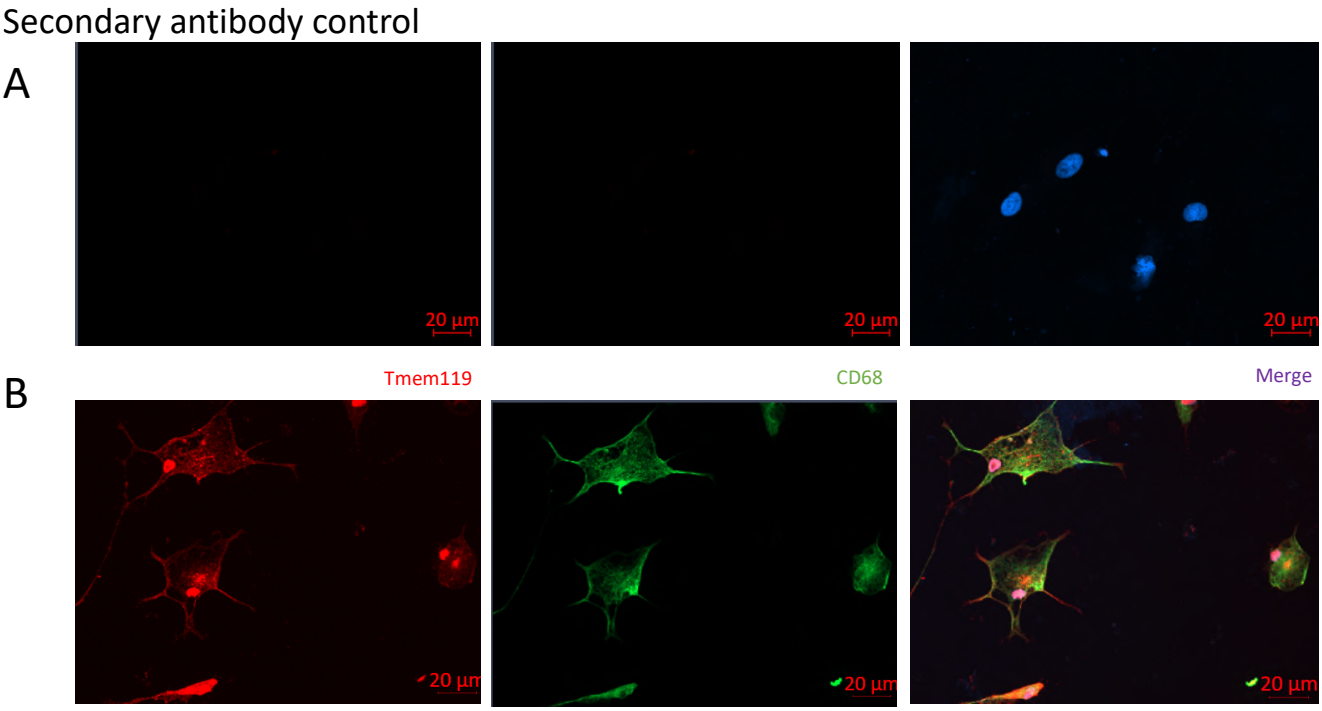

Figure 3.23: Monolayer iPS Microglia differentiated in ACM were positive for microglia markers IBA-1 and CD45
A) Secondary antibody control B) iPS microglia differentiated in ACM were positive for microglia markers IBA-1 and CD45. IBA-1 appear mostly in the process while CD45 is more evenly distributed throughout the cell. Images taken on Zeiss confocal microscope. These images are representative images from at 2 biological and 3 technical repeats.

Although this protocol successfully produced microglia which positively stained for microglia markers, an additional cell type was observed growing alongside the iPS microglia. These cells were flat and continued to proliferate throughout the well over the course of ACM treatment. In some cultures, these cells took over the whole well, meaning they were no longer useable for downstream experiments. The origin and phenotype of these contaminating cells remains unclear however the morphology appears to be similar to that of fibroblast cells. A phase image in figure 3.24 shows a well with multiple of these flat cells, which grow underneath the iPS microglia, they appear fainter than the differentiating cells but are clearly spread out underneath them. The black arrow points to one such cell.

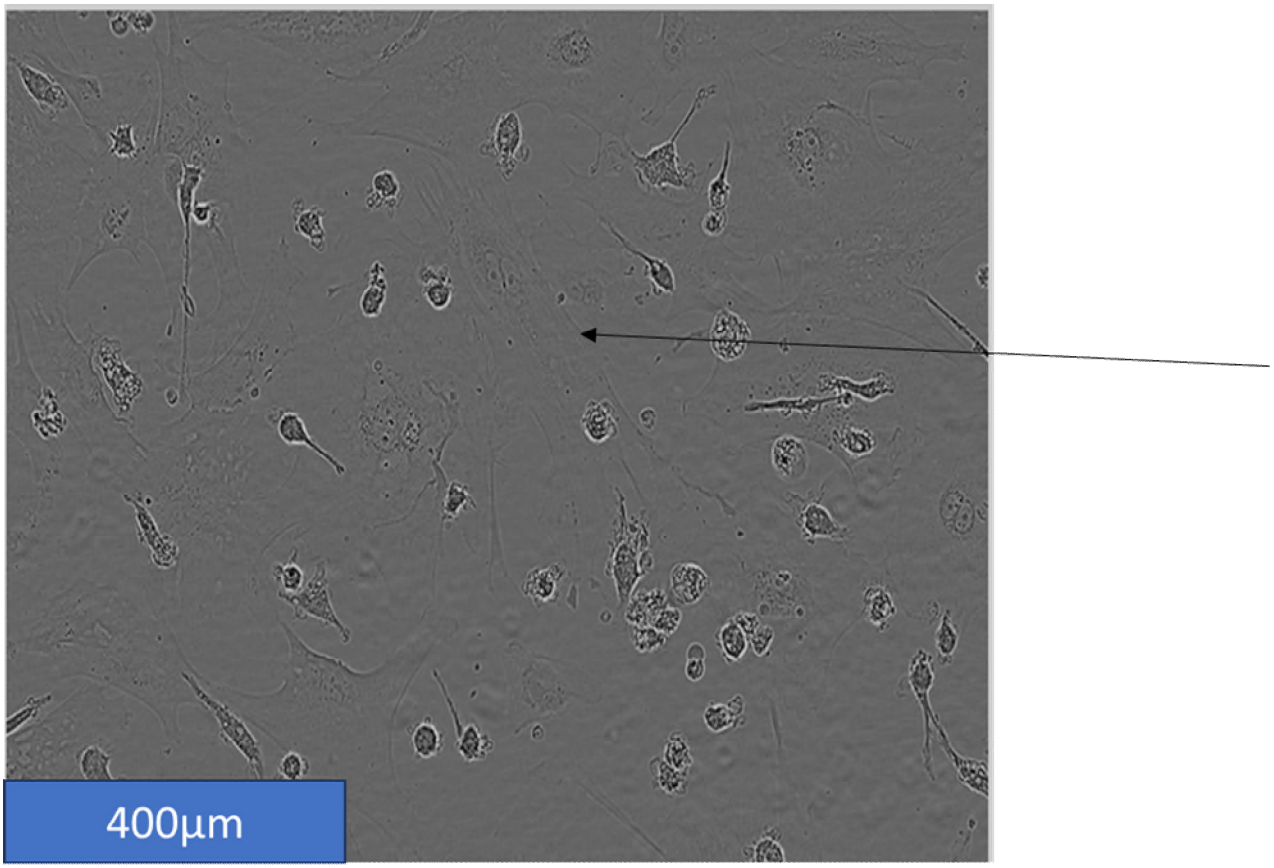

Figure 3.24: Contaminating cells were consistently seen in monolayer cultures
An image captured on the IncuCyte shows iPS microglia with the contaminating cells growing underneath it. These cells appear flat and spread throughout the culture, one of these cells are pointed out with a black arrow. These cells were seen in multiple cultures, taking over the whole well. Although no extensive characterisation was performed the morphology of these cells highly resemble that of fibroblast cells. This is a representative image of something that was observed in multiple plates.

3.3 Discussion

In vitro study of microglia has presented multiple difficulties due to the immune privileged nature of the CNS and high reactivity of these cells. Indeed, even differentiation of iPS into microglia was difficult due to controversies on the ontogeny of microglia cells[194,225]. It is now understood microglia derive from erythro-myeloid precursors produced during primitive haematopoiesis, an early embryonic event[38,224]. Directed differentiation with iPSC attempt to recapitulate these events with the use of defined medias to mimic concentration gradients present in utero.

In the work described in this Chapter, iPS cells were successfully differentiated to an iPS microglia phenotype following two adapted published protocols. The resulting iPS microglia displayed robust expression of key essential microglia markers at the transcript and protein level. iPS microglia derived from the EB protocol were shown to engage in characteristic microglia functions such as producing a pro-inflammatory response following LPS challenge and phagocytosis of e-coli beads

In both protocols described in this Chapter, a yolk-sac-like structure is developed following the addition of growth factor BMP-4, used to push cells towards a mesodermal lineage[194]. Large round precursors, with filipodia are produced from this cyst and were confirmed as hematopoietic cells by flow cytometry for key markers CD14 and CD45, as in the original protocols[228,229]. Flow cytometry revealed cells harvested through the differentiations had variations in CD14 and CD11b expression. Both of these haemopoietic markers are functional, CD11b being an integrin of phagocytosis receptor CR3 and CD14 acts as co-receptor with LPS detector TLR4. A more extensive quality control panel of markers would be useful in the characterisation of these myeloid precursors. These might include alternative hematopoietic markers such as CD43, which is used in some protocols to FACs sort iPS pre to produce purer cultures. Alternatively CD235a, a marker found specifically on EMPs secreted during primitive haematopoiesis waves could be useful in confirming successful differentiation and provide more robust characterization of iPS pre[230]. Precursors were collected weekly and terminally differentiated to iPSC microglia using in-house ACM which produced ramified cells within 10 days.

In-house ACM was produced from APOE3 iPS astrocyte cultures with multiple harvests generating a batch. This was a key change made from the original published EB protocol which utilised XVIVO-15 supplemented with GM-CSF and IL-34 to generate iPS microglia. The importance of IL-34 in the differentiation of microglia has been shown through characterisation of IL-34 null mice, which fail to produce microglia[194]. Although IL-34 is primarily produced by neuronal cells in the brain, alternative ligand M-CSF is produced by glia such as astrocytes and can interact with the essential receptor CSF1R to provide necessary cues for microglia development and differentiation[231]. Therefore, although IL-34 is not supplemented into ACM, it is likely that m-CSF present within the media fulfils this requirment[232]. Indeed, use of both media produced branched cells, positive for microglia markers CD11b and CD68. Movement to an alternative terminal media was prompted following the generation of currently unpublished RNA transcript data within the lab, which revealed that iPS microglia differentiated in supplemented XVIVO media possessed higher expression of message for activation markers. Indeed, cells produced with supplemented XVIVO showed activation transcript levels similar to those seen in cells grown in ACM after LPS stimulation. This “pre-activated” phenotype is supported by increased CD68 immunofluorescence in XVIVO iPS microglia, shown in figure 3.17, although this requires confirmation in a more quantitative method such as western blotting or an ELISA for common pro-inflammatory cytokines such as TNFα. It is unclear what would cause baseline activation when differentiated in this media. One possibility could be the addition of GM-CSF, which is a common pro-inflammatory molecule produced following toll-like receptor 4 stimulation[233]. This is supported by

culturing of primary microglia with GM-CSF which in some cases was shown to transition primary microglia to a more dendritic-cell like phenotype with altered immune properties[233,234].

Another possibility for the production of activated microglia could be due to the absence of certain factors rather than the presence. It is well known that neuronal and astrocytic cells secrete multiple inhibitory signals to maintain microglia homeostasis in vitro. Within the brain a precise signalling of secreted factors is shown to be essential in maintaining a homeostatic microglia phenotype, one such is the binding of neuronal CD200 to microglial CD200R which provides a constant inhibitory signal[235]. Antibody inhibition of CD200R has shown to increase activation markers CD11b and CD45 on isolated primary microglia[235]. Indeed, studies of impact of multiple media on the survival of animal postnatal and adult microglia show ACM to produce the most viable cells; these studies distinguished the presence of TGFβ, M-CSF and cholesterol as essential factors in the maintenance of microglia[231]. A complete biochemical characterisation of ACM is required to fully understand the components which may influence microglia differentiation. Mass spectrometry of multiple ACM batches could help in revealing the key secreted factors present, which would also provide much needed information on variation between batches, beginning with characterisation for TGFβ, M-CSF and cholesterol.

ACM was batch controlled with use of a CCL2 ELISA following protocols present in the literature[227]. Despite batch controlling, microglia produced in different batches showed noticeably different marker expression and pattern as shown in figure 3.13. These variations are unsurprising as APC cells continue to proliferate during the first few days of terminal differentiation. Therefore, it is hard to gauge an accurate estimate of number of cells used to collect each batch of ACM from. This is further confounded by the continued maturation of cultures over time, with many showing increase of GFAP expression after several weeks of astrocyte cultures. Use of a more extensive batch control through additional ELISAs for C3 and TGFβ could partially aid this. Regardless, terminal differentiation into microglial phenotype requires much research to fully develop an optimal media. Use of defined media supplemented with a range of growth factor combinations including IL-34, TGFβ, M-CSF, CD200 and cholesterol would be one approach. Performing single cell transcriptomic of cells differentiated in media of different combinations could reveal essential information on necessary components for generating the most microglia-like cell.

In addition to characterisation of the terminal differentiation media, an analysis of extracellular matrix was conducted. This was performed as multiple precursors during the course of differentiation would detach, resulting in low cell number for subsequent experiments. Matrigel, a mixture of multiple extracellular components such as laminin and collagen IV is used in the original Haenseller et al 2017 protocol[207]. However, fibronectin was found to maintain cultures better; previous studies have shown that fibronectin alongside fractalkine receptor CX3CR1, influences microglia colonization in the brain[236].

After several months of successful IPS microglia differentiation following the adopted Haenseller et al 2017 protocol, production of iPS precursors began to decline until cultures completely failed and no precursors could be generated. Trouble-shooting this included multiple lines of action including modulation of EB incubation time, improvement of EB towards a more homogenous production method and modulation of the number of EBs in each factory. The failure to differentiate cells was later revealed to be rooted in defective growth factors and was amended with a change of growth factor supplier. Alongside trouble shooting, an alternative microglia differentiation protocol was trialled. The second method followed a protocol published by Takata et al 2016, which unlike the EB method, did not require the production of 3D structures but rather encouraged generation of yolk-sac like structures in a 2D monolayer utilising a larger range of growth factor supplemented medias. Some critical growth factors remained consistent between the two methods, such as BMP4 which

encourages movement towards mesodermal lineage and VEGF which is essential for the production of hematopoietic lineage cells[194,206]. Ligands for the key microglial differentiation receptor CSFR, are seen in both protocols through M-CSF and IL-34, both of which are essential for production of microglia-like cells. Genetic knock out of either of these factors significantly reduces microglia in animals, with CSFR knock out animals having >99% of microglia depleted[218]. Despite these similarities, the second monolayer method had additional factors to mimic a closer resemblance to the effects seen in utero. One important difference is in the addition of CHIR99021 and DKK1 which modulate WNT signalling. The WNT pathway is a signal transduction pathway which in the embryo is important in cell fate specification, cell proliferation and cell migration[197,230]. CHIR99021 acts as an agonist for the WNT pathway, working by activation of G3K3B, and is introduced to the culture at day 1 before its removal at day 3. DKK1 is a WNT pathway antagonist and is added at day 6-10 of differentiation. This switching on and then off, of the pathway mimics the shift seen during embryonic development thereby generating a specific directed differentiation[230]. The EB method cystic yolk-sac like structures are visible which produce morphologically similar precursors, which express the same surface markers.

Although both protocols produced microglia positive for key markers, it was decided to move forward with the EB method. This was due to increased efficiency of cell production and longer survival of cultures with this method. Furthermore, contaminating non-microglial cells were often produced alongside iPS microglia when following the monolayer methods. These cells were large and flat and continued to proliferate, in some cases taking over the whole well, preventing use of these cells for subsequent work. A full characterisation of what these cells are has not been completed; however, removal of these cells following CD11b MACs bead sorting was observed. Literature research on the possible origin of these cells supports them as being endothelial fibroblast cells. This would be intuitive due to the importance of endothelial KDR+ cells within the yolk sac in vitro, necessary to support the differentiation of hematopoietic cells. Confirmation of this could be performed using a KDR antibody in addition to the absence of CD71, which is often used to confirm the presence of hematopoietic endothelium cells[237]. Alternatively, single cell transcriptomics may aid in uncovering the phenotype of these contaminating cells.

Within this chapter the protocols used to generate iPS microglia for subsequent work are described, justifying key adaptions made from the original protocol. Cells produced clearly possess key microglia characteristic markers including Tmem119, and also engage in essential microglial function such as phagocytosis supporting directed differentiation to a microglia phenotype.

4.0: Expression of Complement Receptor 1 in iPS-derived glial cells

4.1 Introduction

Complement Receptor 1 (CR1/CD35) is a multifunctional complement regulator. Primarily, CR1 is a receptor of C3 and C4 opsonising fragments, C3b and C4b respectively, which decorate the surface of debris, signalling them for removal[86]. Other complement opsonising factors including initiating elements C1q and MBL, have also been shown to bind to CR1, in addition to a number of other ligands, including Aβ and Epstein Barr virus[102,141,158]. Indeed, erythrocyte CR1 has been shown to directly bind Aβ in the circulation and transport it to the liver for degradation by resident macrophages, illustrating a role for CR1 in peripheral Aβ clearance that may be of relevance to LOAD[114,158]. In addition, CR1 works to supress amplification of the complement cascade by performing co-factor function with the complement enzyme FI to cleave C3b to its inactive iC3b form, preventing it from being recruited into a functional C3 convertase; CR1 also aids in accelerating the decay of classical and alternative pathway C3 and C5 convertases[86,141].

Most of the CR1 in the body is found on erythrocytes and other circulating cells such as B cells, T cells, macrophages, and neutrophils[141]. Genome wide association studies (GWAS) investigating common hits for LOAD have highlighted SNP within the CR1 gene as increasing the risk for developing LOAD[134,136,138]. One such hit is rs6656401, a SNP found in an intronic region of CR1; 86% of individuals who possess a A/A genotype also possess the longer CR1-S allele. Indeed, those with A/A are shown to have a 2.5-fold increased risk of developing LOAD while those who express G/A genotype have an 1.8 fold increase compared to those with the non-risk G/G genotype[141,238] It is currently unclear the mechanisms for which these alterations in CR1 increase risk for development of LOAD[138]. In fact, even the expression of CR1 within the CNS remains unclear and debated, with some studies identifying CR1 only on astroglia, while others have found it to be expressed only on neuronal and microglia cells, while some others claim it to be completely absent from the CNS[141,157,172]. Clarifying this confusion is the first hurdle in understanding the role of CR1 within LOAD pathology.

The aim of this chapter is to investigate whether iPS -derived microglial cells express CR1 transcript and protein. To achieve this, all stages along the EB differentiation pathway were tested first for CR1 transcript using RT-qPCR and then for CR1 protein using immunofluorescence and western blotting using well characterized in-house antibodies against CR1. Additionally, this chapter aims to assess two other CNS cell types for CR1 expression, namely iPS-derived astrocytes and iPS-derived immature cortical neurons.

4.2 Results

4.2.1 CR1 transcript and protein expressed at different stages along the EB differentiation

4.2.1.1 Genomic analysis of CR1 allele expression in KOLF2 demonstrate homozygotic expression of the short CR1-F allele

KOLF2 iPS cells are a commercially available cell line available from HipSci, reprogrammed from a male donor's skin sample. Genomic information of these cells is available through the HipSci website, this revealed the nucleotide sequence of CR1 at the site of rs6656401 SNP in KOLF2 cells to possess a G/G genotype at this position. This suggests the presence of homozygotic CR1-F isoform[141]. This was confirmed using a previously published PCR, which uses primers designed to bind to an intronic region unique to the larger CR1-S isoform[216]. Therefore, the presence of a single band at 1.5kBp indicates the expression of CR1-S isoform while the absence of a band indicates the expression of CR1-F isoform. Figure 4.1 shows control DNA, from blood cells of consenting donors, and DNA from 3 KOLF2 undifferentiated iPSC. Control DNA was selected from protein sample pre-screened for CR1 isoform using western blot by Dr. Nikoleta Daskoulidou. The S/S control show a clear band at 1.5kBp, the F/S control a fainter band at 1.5kBp and the F/F control showed no band at all. This is due to the amplified region only being present in CR1-S isoform. KOLF2 iPS cells showed no band in any of the repeats, showing they possess homozygotic CR1-S in these cells. This is confirmed at the protein level using a western blot in figure 4.11.

In addition to size polymorphism, KOLF2 cells were analysed for the copy number variation polymorphism using a HIND III PCR protocol. Controls were kindly gifted by Prof Santiago Rodriguez de Cordoba (Madrid). Control cells homozygous for the H/H genotype produce a single band at 550KBp while homozygous L/L cells have a single band at 500kBp and heterozygotic lines generate both bands. Figure 4.2b shows three biological replicates of KOLF2 iPS DNA demonstrating that they have a single band at 550Kbp, identifying them as possessing the H/H copy number variation polymorphism.

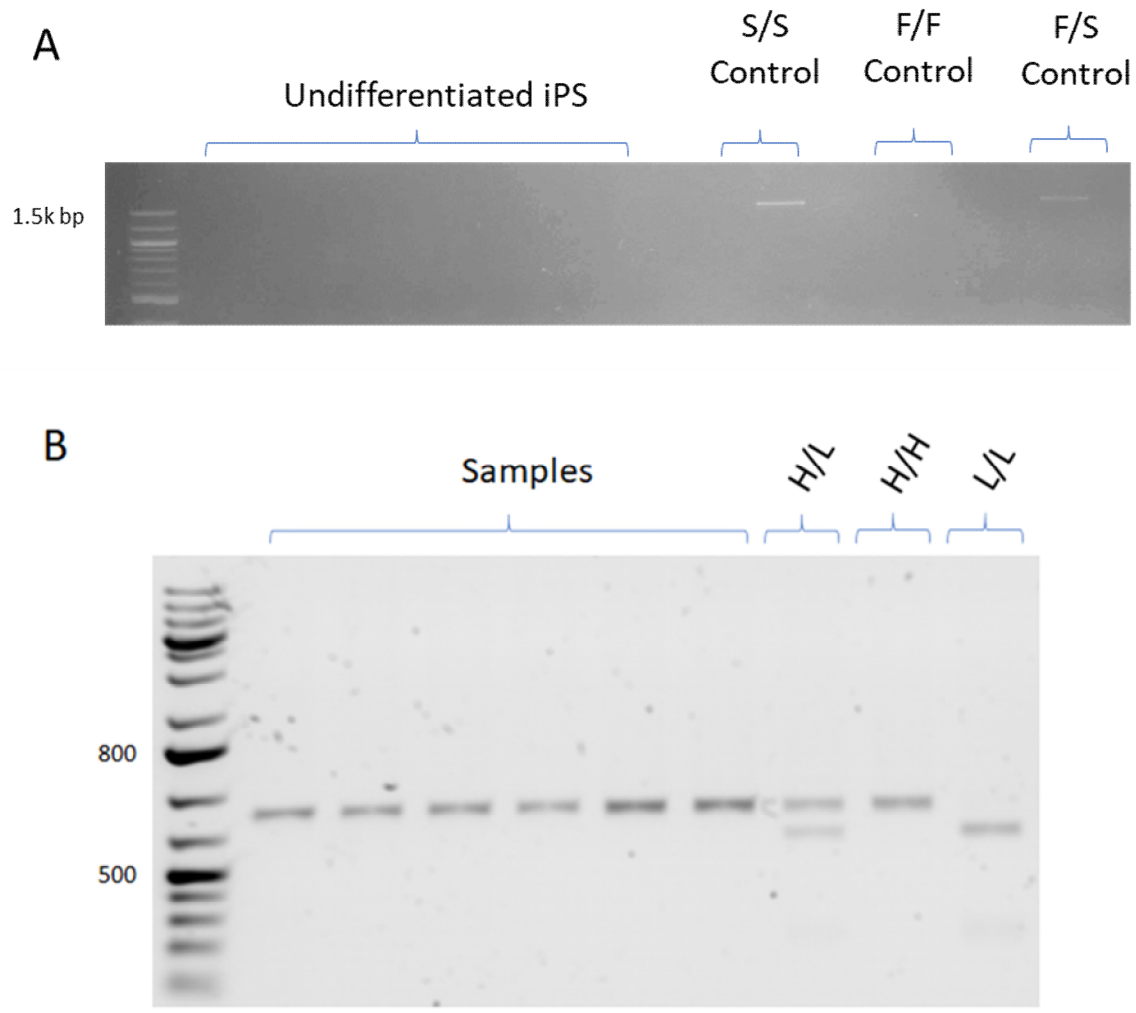

Figure 4.1: Identification of genomic CR1-F allele in iPS KOLF2 cell line. *A) Junction Fragment PCR was performed which allows for identification of size polymorphism within samples by amplification of an intronic region only found in the longer CR1-S form. Control samples, generated in house,, reveal only those homozygotic for the longer isoform to produce a band at 1.5kBp, with heterozygotic control showing a fainter band while homozygotic CR1-F producing no band. Three biological replicates or KOLF2 iPS DNA, ran in duplicate reveal no bands to be present supporting the presence of shorter CR1-F size polymorphism. B) HIND III Copy number variation was investigated using an established PCR protocol, controls were run showing a higher band in H/H lines and a lower with L/L. Heterozygotic controls show 2 bands at both weights. Three biological replicates of KOLF2 DNA were run in duplicate revealing them to posses H/H density polymorphism.*

4.2.1.2 Undifferentiated iPS cells express CR1 transcript but not protein.

RT-qPCR was used to investigate the expression of CR1 transcript in undifferentiated iPS cells. Figure 4.2 shows an amplification plot, with the number of cycles along the x axis, and delta normalized reporter (Rn) on the y. The (Rn) is the subtraction of the equipment's baseline Rn from the experimental Rn value, giving a measurement of amplification signal. Figure 4.2 shows threshold is at CT value 38 for CR1 in undifferentiated iPS KOLF2 cells, this indicates a very low expression of CR1 RNA in undifferentiated iPS cells.

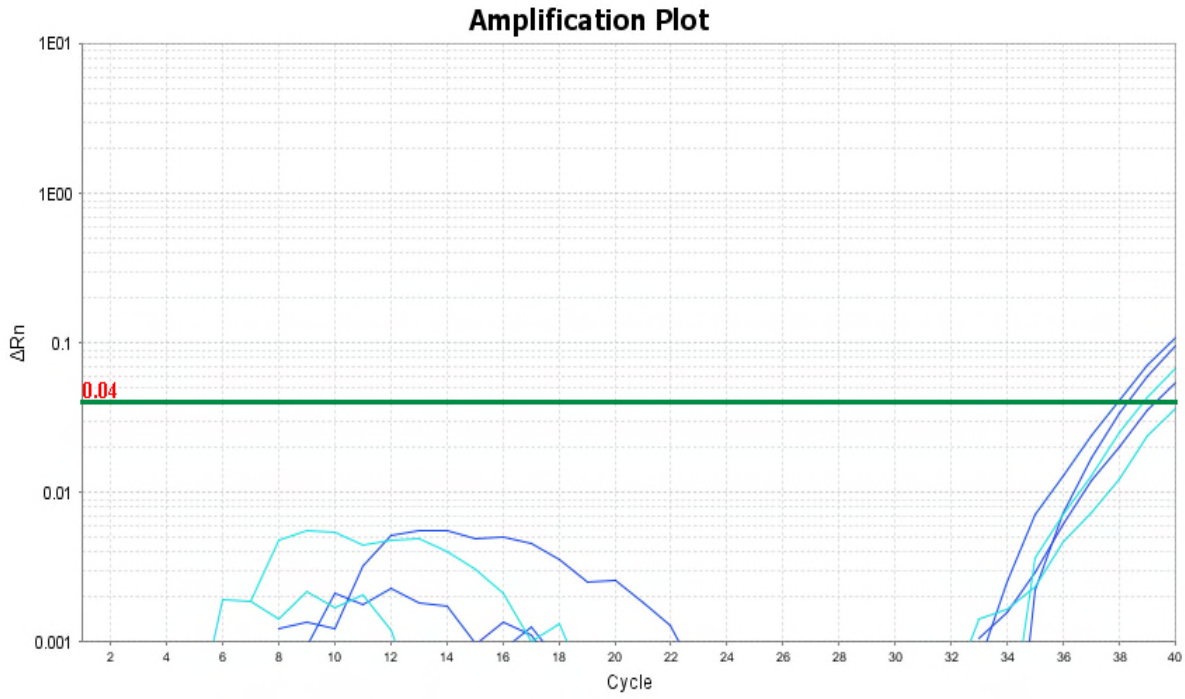

Figure 4.2: Undifferentiated iPS cells amplified CR1 transcript in QPCR analysis *Shows the amplification plot of undifferentiated iPS cell RNA with CR1 primers, the cycle threshold (CT) is the number of cycles needed before the threshold (marked by the horizontal green line) is reached, so the higher the number of cycles the lower the expression of mRNA. This plot indicates CT of undifferentiated iPS cells to be high, around 37-38, for CR1.*

Despite the identification of transcript in undifferentiated iPS cells, protein was not detected as shown by lack of signal in immunofluorescence in figure 4.3 and western blotting in figure 4.4. This is most likely due to differences in the techniques, RT-qPCR includes multiple amplifications of the cDNA thus increasing the detection threshold. On the other hand, protein investigation techniques are bluntly checking the presence or absence of a protein.

Figure 4.3 shows co-staining of undifferentiated iPS cells with three pluripotency markers and three in-house CR1 antibodies. This reveals bright pluripotent fluorescence with antibodies against Tra1-60, SSEA4 and OCT4. CR1 showed no staining with all three antibodies, indicating cells to be positive for pluripotency markers but negative for CR1 protein expression.

Secondary antibody control

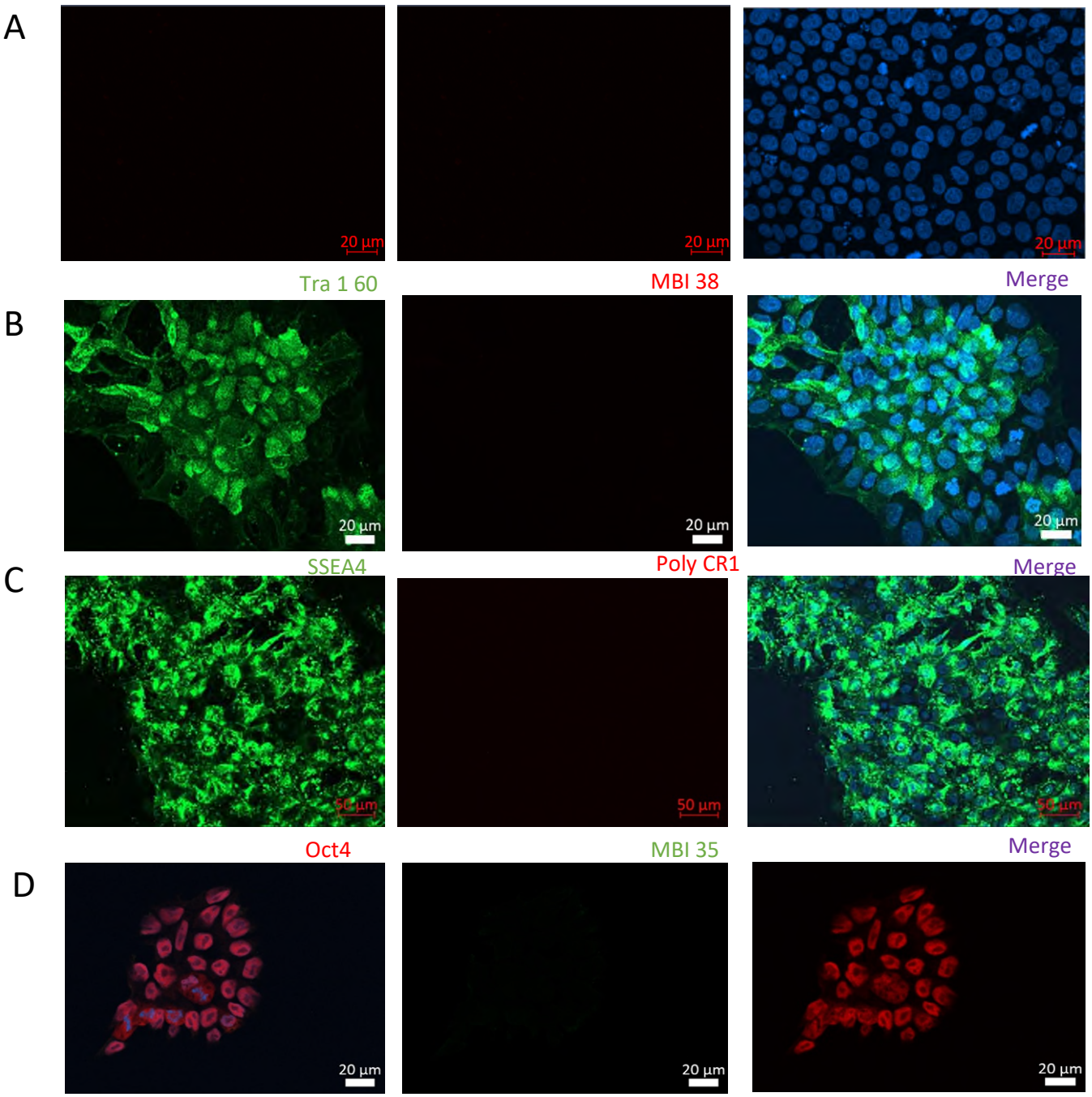

Figure 4.3: Immunofluorescence of undifferentiated iPS cells shows the absence of CR1 with and without pluripotent markers.

A) Se Pluripotent marker Tra1-60 shows bright green staining across all the plated cells within the colony however no fluorescence is detected with MBI-38 CR1 antibody staining. B) Pluripotent marker SSEA4 shows a speckled positive pattern of staining in all cells plated but no CR1 was detected with PolyCR1 antibody. C) Pluripotent transcription factor OCT4 shows positive nuclear stain in cells while no CR1 staining with in-house MBI-35 antibody. All images were taken on Zeiss spinning disc confocal microscope. Different scale bars are from exporting from different computers.

Western blotting confirmed the absence of CR1 in undifferentiated iPS cells. Figure 4.4 shows three biological replicates of undifferentiated iPS KOLF2 protein alongside CR1 heterozygotic red blood cell

a control protein. The in-house monoclonal antibody MBI-35 detected a clear visible band at the expected 220kDa in the red blood cell control and a fainter band for the larger CR1 250kDa. No bands were visible in any of the undifferentiated cell samples.

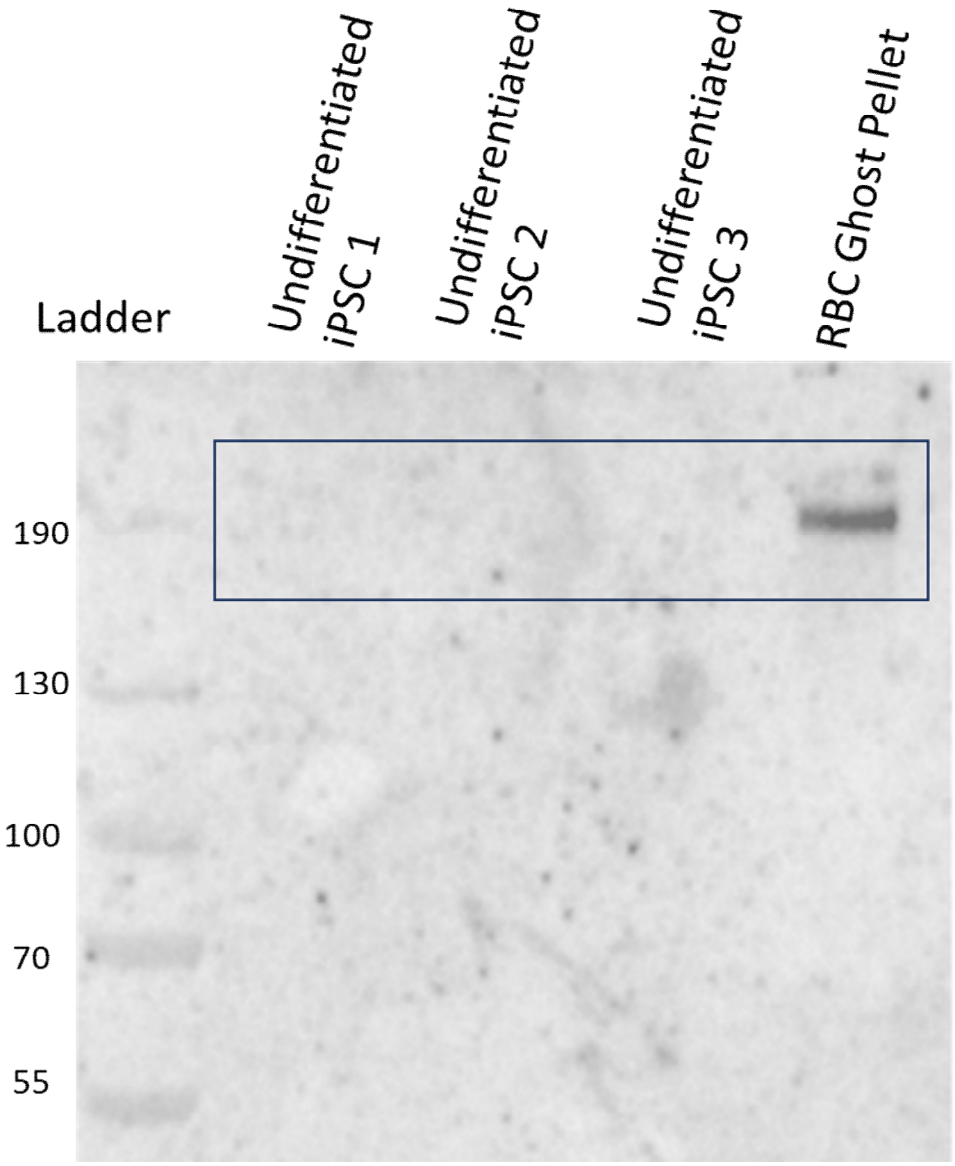

Figure 4.4: Western Blot analysis of three biological replicas of KOLF2 iPS show no CR1 band.
Control red blood cell protein shows a clear band at 220kDa and a fainter upper band at 250kDa for the two CR1 sizes within the sample. However, 30µg of undifferentiated KOLF2 iPS cell lysates showed no bands. In-house MBI-35 antibody was used. Three biological replicates were ran on this blot with and is one of two technical replicates.

4.2.1.3 CR1 transcript and protein was expressed in iPS microglia precursor cells and IPS microglia cells

RNA extracted at different points in the microglia differentiation reveal significant 29-fold upregulation of CR1 transcript in iPS precursors (P=0.037) and 57-fold upregulation in iPS microglia (P=0.0049) relative to expression in undifferentiated iPS cells. Figure 4.5 also shows a 4.5-fold (P=0.0025) significant increases in CR1 transcript in iPS microglia stimulated with 100ng/ml of LPS for

6 hours relative to unstimulated controls. This indicates that activation of microglia with LPS increases CR1 message.

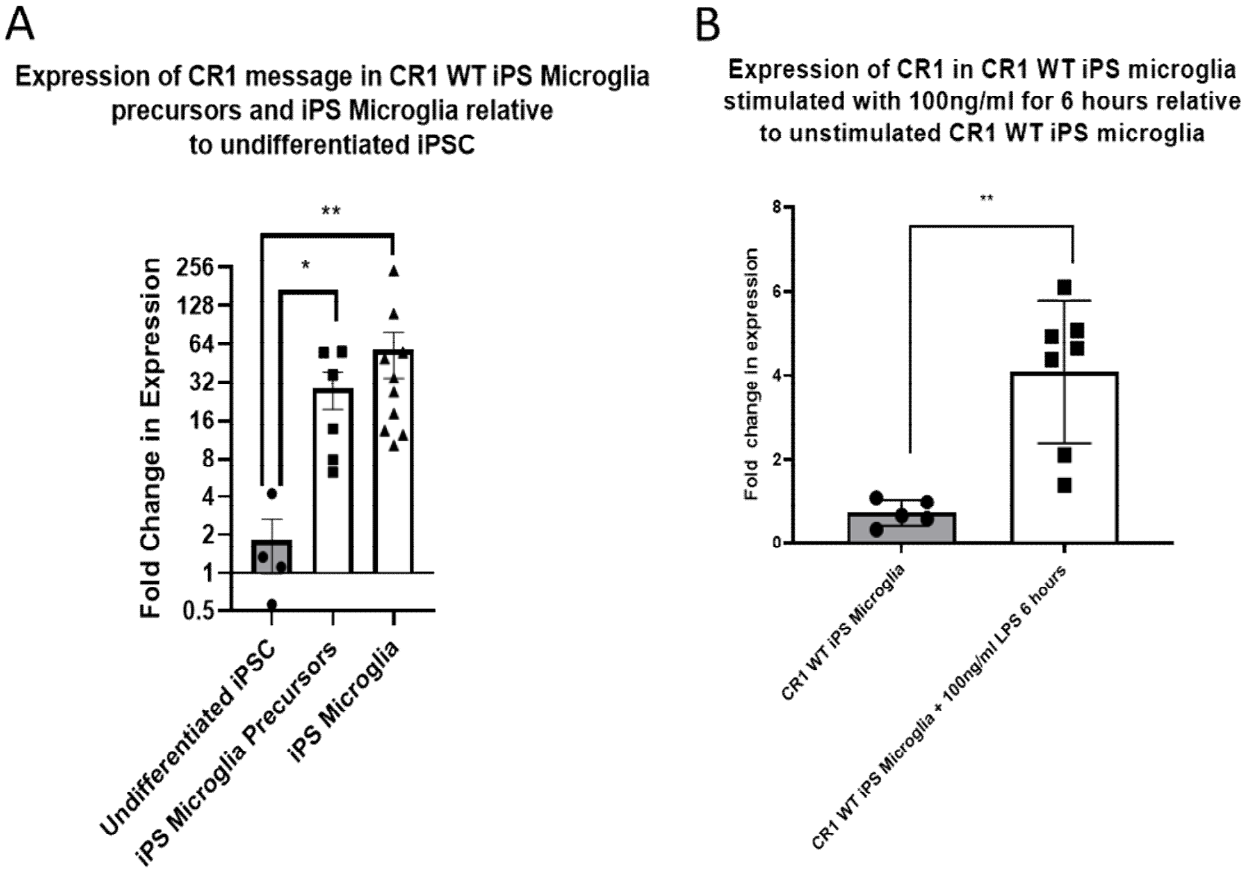

Figure 4:5: Message expression of CR1 increased in iPS precursor and iPS microglia relative to undifferentiated iPS cells and was significantly increased when iPS microglia were stimulated with 100ng/ml LPS for 6 hours *A) Significant upregulation of CR1 was shown in iPS precursors (p=0.037) and iPS microglia (P = 0.0049) relative to undifferentiated iPS cells. B) Expression of CR1 was significantly increased in iPS microglia (P=0.0025) when stimulated with 100ng/ml LPS for 6 hours relative to expression in unstimulated iPS microglia. Error bars represent the SD. For graph A, Kruskal-Wallis test with Dunns post hoc was performed while for data in graph B a Mann Whitney test was performed. For both graphs significance was set at * P< 0.05; ** P < 0.01; *** P<0.001; ****P<0.0001.*

Immunofluorescence identified surface expression of CR1 on iPS pre, showing punctate staining of CR1 alongside hematopoietic markers CD45, with two monoclonal in-house antibodies. Figure 4.6 shows staining around the edges of the cells, although it is important to note cells were attached to the slide using a slide spinner causing them to flatten which might disrupt distribution in staining.

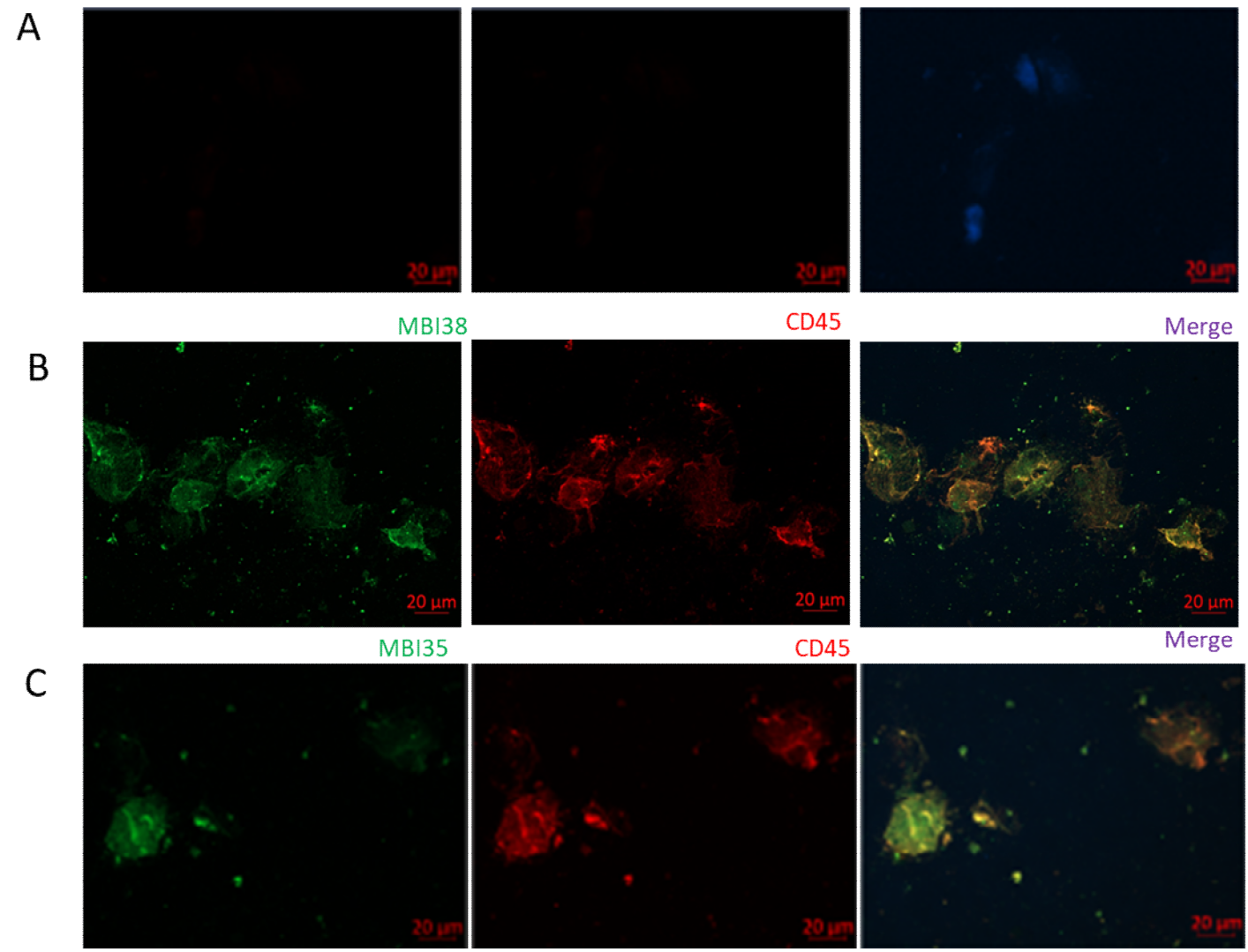

Figure 4.6: Immunofluorescence of iPS microglia precursor cells, generated by the EB method, shows expression of CR1 and hematopoietic marker, CD45.
A) iPS microglia precursors indicate the expression of CR1 protein using in house MBI-35 and are positive for hematopoietic marker CD45. B) Another monoclonal antibody MBI-38 stained positive, CR1 expression looks clustered on the surface of the cell in different locations to CD45 in the merge. All images are confocal images taken on a Zeiss spinning disk microscope. These are representative images from 3 biological repliactes.

Figure 4.7 shows staining of iPS microglia using three in-house CR1 antibodies and one commercial CR1 antibody. Figure 4.7A shows the secondary control for images B-D. Figure 4.7B shows iPS microglia to stain positive for CR1 using in-house MBI-38 antibody. Expression is shown mostly around the cell body of cells with some positive staining seen extending along the process. This expression pattern is also seen with MBI-38 in figure 4.7C which shows that cells are strongly positive for microglia CR1 with staining mostly on the cell body. Figure 4.7D, shows staining with polyCR1 in house antibody. PolyCR1 staining shows CR1 to be present in clusters on the surface of the cells, concentrated mostly on the cell body with some clusters on the process. In addition to CR1 staining these panels show cells to be positive for microglia markers CX3CR1 (B and C) and C68 (D). This shows cells to express microglia markers in addition to CR1. In addition to in house antibody staining a commercial abcam CR1 antibody was tested. These images were taken on a Olympus fluorescent microscope, with the secondary

antibody control shown in panel D. Figure 4.7E shows microglia to be positive for CR1 using this antibody. Like the panels above, staining appears to be mostly concentrated on the cell body with little staining seen on the process. These cells also stained positive for CX3CR1 however their morphology looks slightly different compared to images in panels A-D, this is most likely due to them being derived from an earlier differentiation batch while optimisation of the differentiation was still on-going.

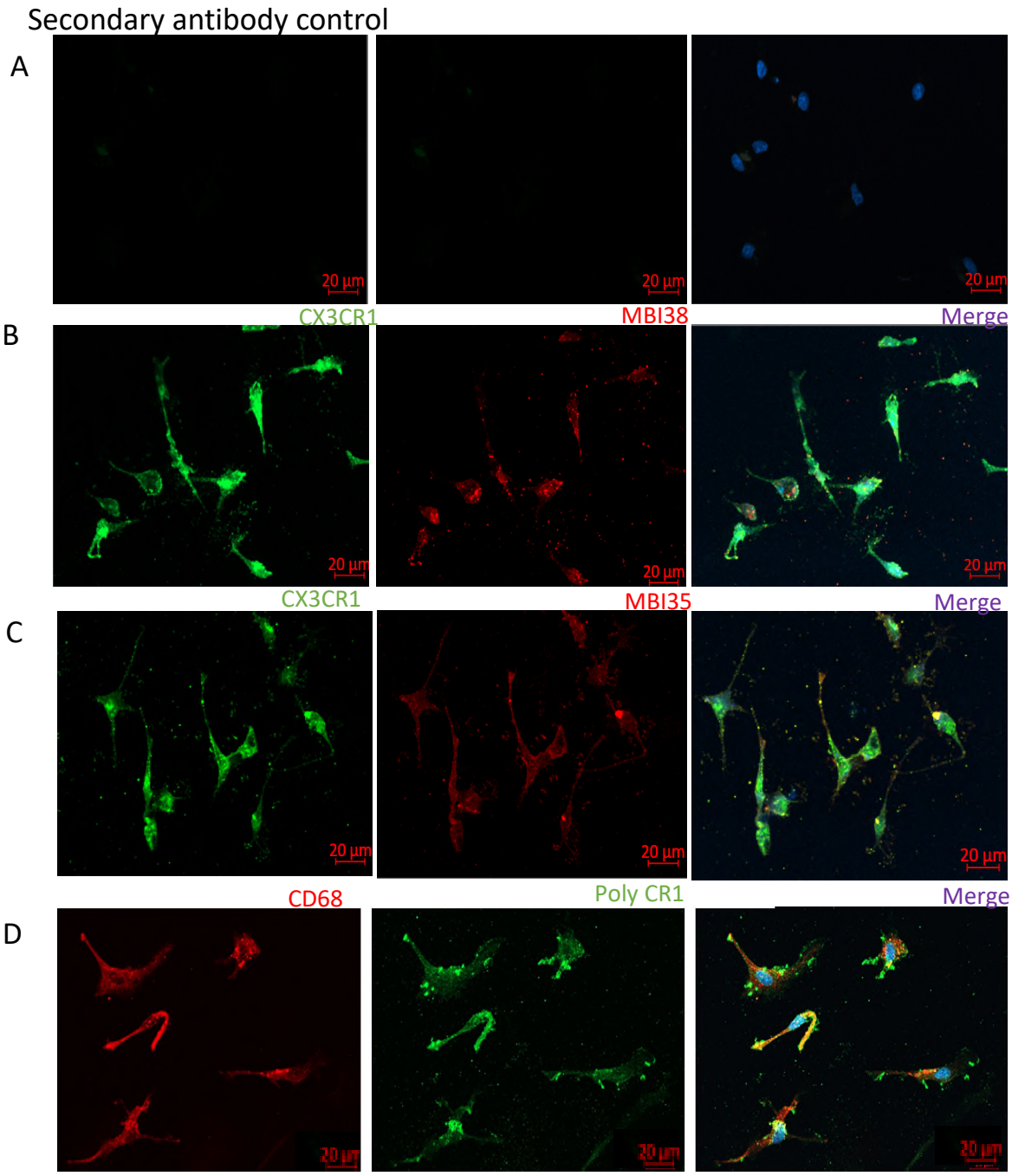

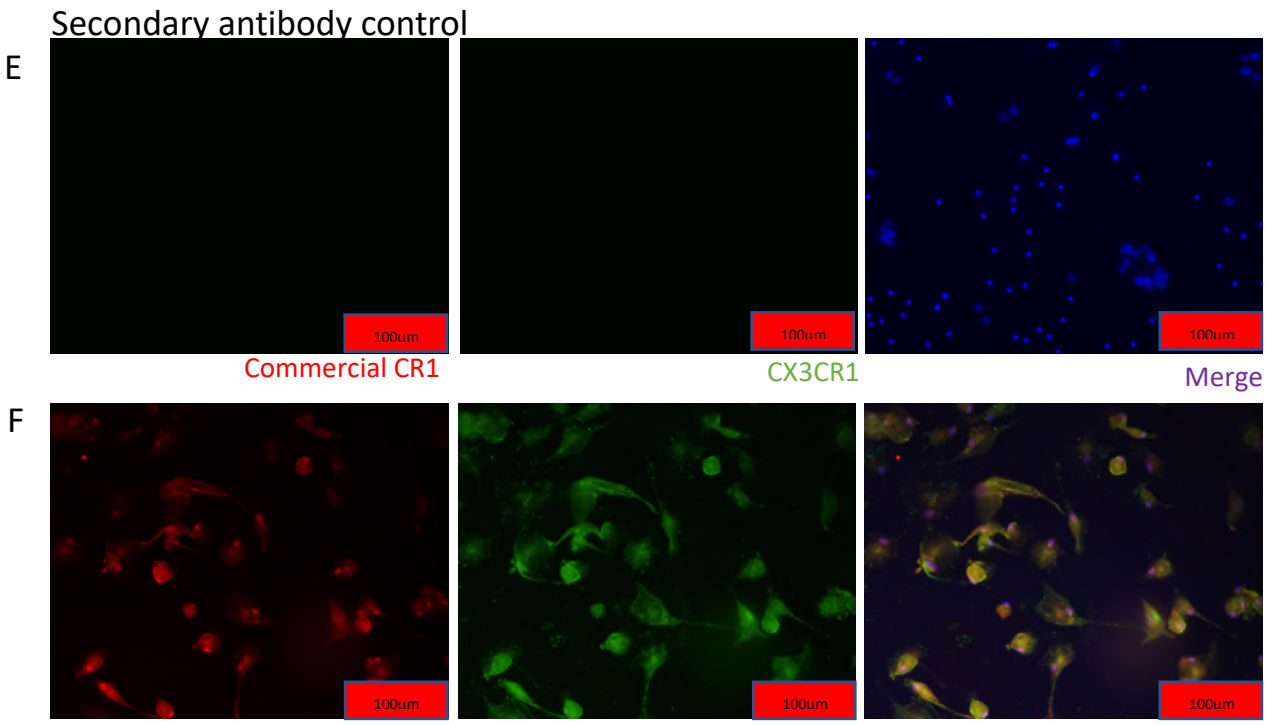

Figure 4.7: Immunofluorescence of iPS microglia differentiated in ACM by the EB method show expression of CR1. *Panels A-D were taken on the Zeiss spinning disc confocal microscope while panesl E-F were taken on the Olympus fluorescent microscope. A) This is a secondary antibody control for images shown in B-D. B) Cells show positive expression for CR1 using MBI38 in-house antibody and microglia marker CX3CR1. C) Cells are positive for CR1 using MBI-35 in house antibody and microglia marker CX3CR1. D) PolyCR1 shows clustered expression of CR1 on the surface of the cells alongside activation marker CD68. E) Secondary only antibody control for F, F) iPS microglia were positive for CR1 when using a commercial CR1 antibody. Images A-D are representative images from a minimum of 3 biological repeats for each antibody while images E-F are representative images from 2 biological replicates.*

Live staining was performed in which fixation was added after antibody incubation which was performed on ice. This ensures no permeabilization of the membrane has occurred through the fixation process which could lead to non-specific fluorescence. Figure 4.8 shows live staining with microglia marker CX3CR1 and CR1 antibody MBI-35, which was performed on ice to prevent ingestion of antibodies. This demonstrates bright staining for both markers CX3CR1 and CR1, indicating that both are present on the membrane of cells.

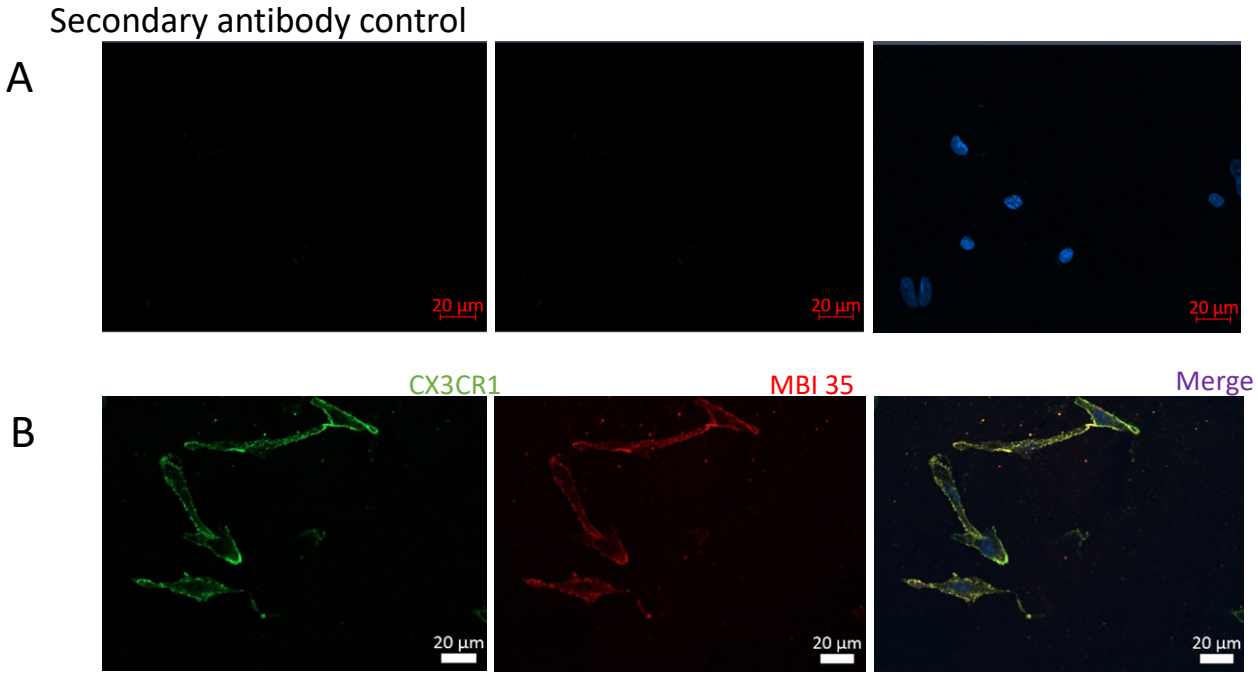

Figure 4.8: Live immunofluorescence of iPS microglia with no fixative shows CR1 on the surface of iPS microglia *A) In-house monoclonal MBI-38 and CX3CR1 are both on the surface, B) In-house monoclonal MBI-35 show iPS microglia positive for CR1, these cells are also positive for microglia marker CX3CR1. All images are confocal images taken on a Zeiss spinning disk microscope. These are representative images for 3 biological repliactes.*

The specificity of staining for CR1 on iPS microglia was confirmed by performing a pre-absorption of the CR1 antibodies prior to staining. This adds some supporting information of the specificity of for the in house antibodies to bind to CR1. This method (section 2.2.5.5.) incubation excess CR1 protein with antibody MBI35 so that antibody binding sites are saturated with protein. This prevents the antibody from binding to any CR1 on the cells. Figure 4.9 shows this incubation eliminated staining for CR1, which was seen without antibody reabsorption.

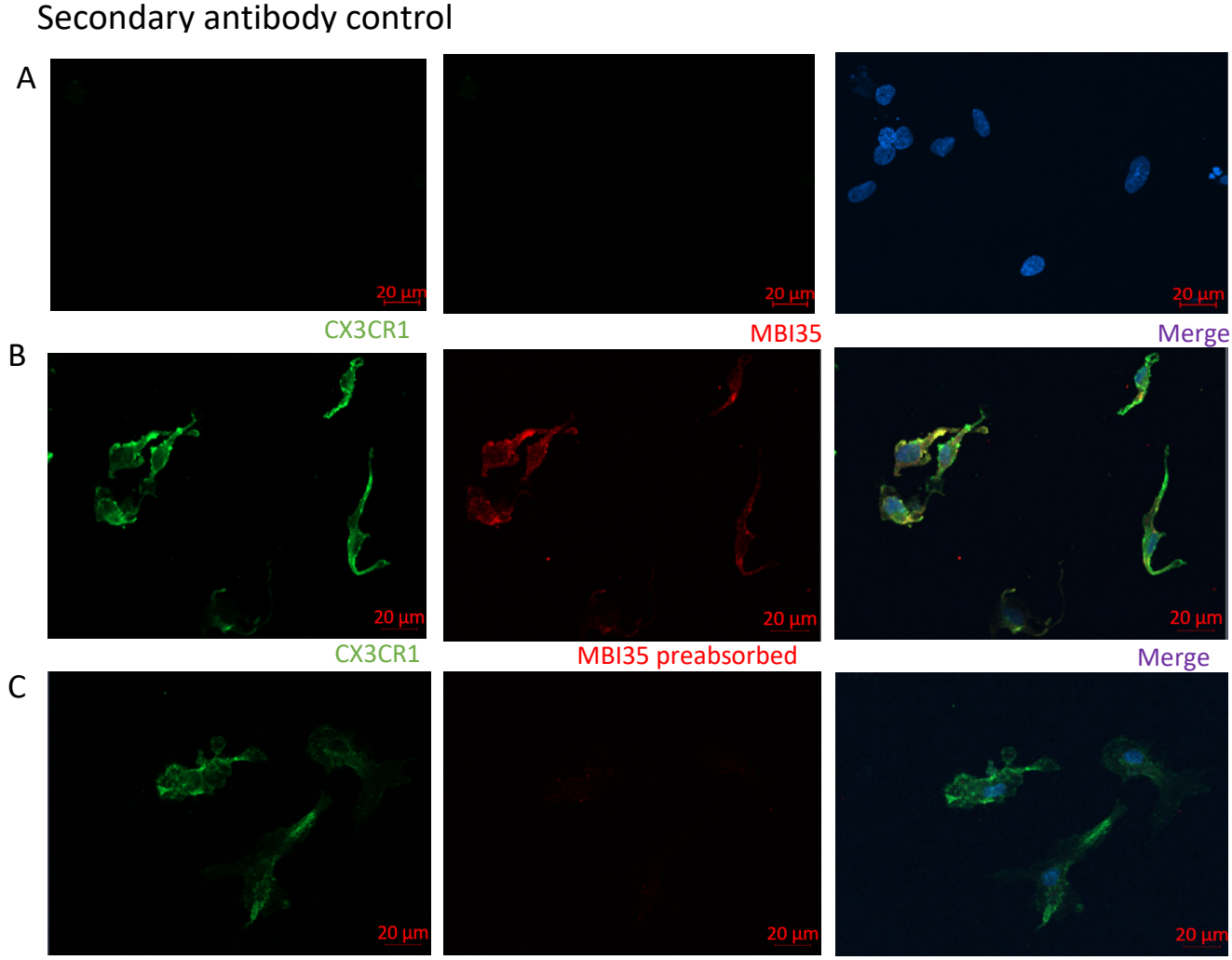

Figure 4.9: Pre-absorption of CR1 on iPS microglia confirm CR1 specific binding.
A) Confocal staining of iPS microglia with in-house antibody MBI-35 showing positive expression of CR1. B) When monoclonal MBI-35 was pre-absorbed with excess CR1 protein staining was completely lost. This indicates specificity of the antibody used against CR1. All images are confocal, taken on a Zeiss spinning disc microscope. This representative of one biological repeat and two technical repeats, staining was performed in parallel.

In addition to staining, western blotting was used to confirm the presence of CR1 on iPS microglia. Cell lysate, a total of 30µg of protein, was loaded for undifferentiated iPS, iPS Pre and iPS microglia, separated on SDS-PAGE, western blotted and probed with MBI-35 antibody. Figure 4.10 shows two clear bands in heterozygous (CR1-F/CR1-S) red blood cell control, with a larger and smaller CR1 bands at 220kDa and 250KDa. Undifferentiated iPS cells showed no band but a clear band at 220kDa was present in iPS Pre and iPS microglia. Control marker GAPDH was used as a protein loading control for the iPS lanes. This shows that CR1 protein is present in iPS pre and iPS microglia but not undifferentiated iPS cells; the data also confirm that KOLF2 cells are homozygous for the smaller CR1-F polymorphic variant, as suggested by genomic examination in figure 4.1. Densitometry was not performed as different cell types will have differing levels of control protein, protein control in this instance is to show the presence of protein.

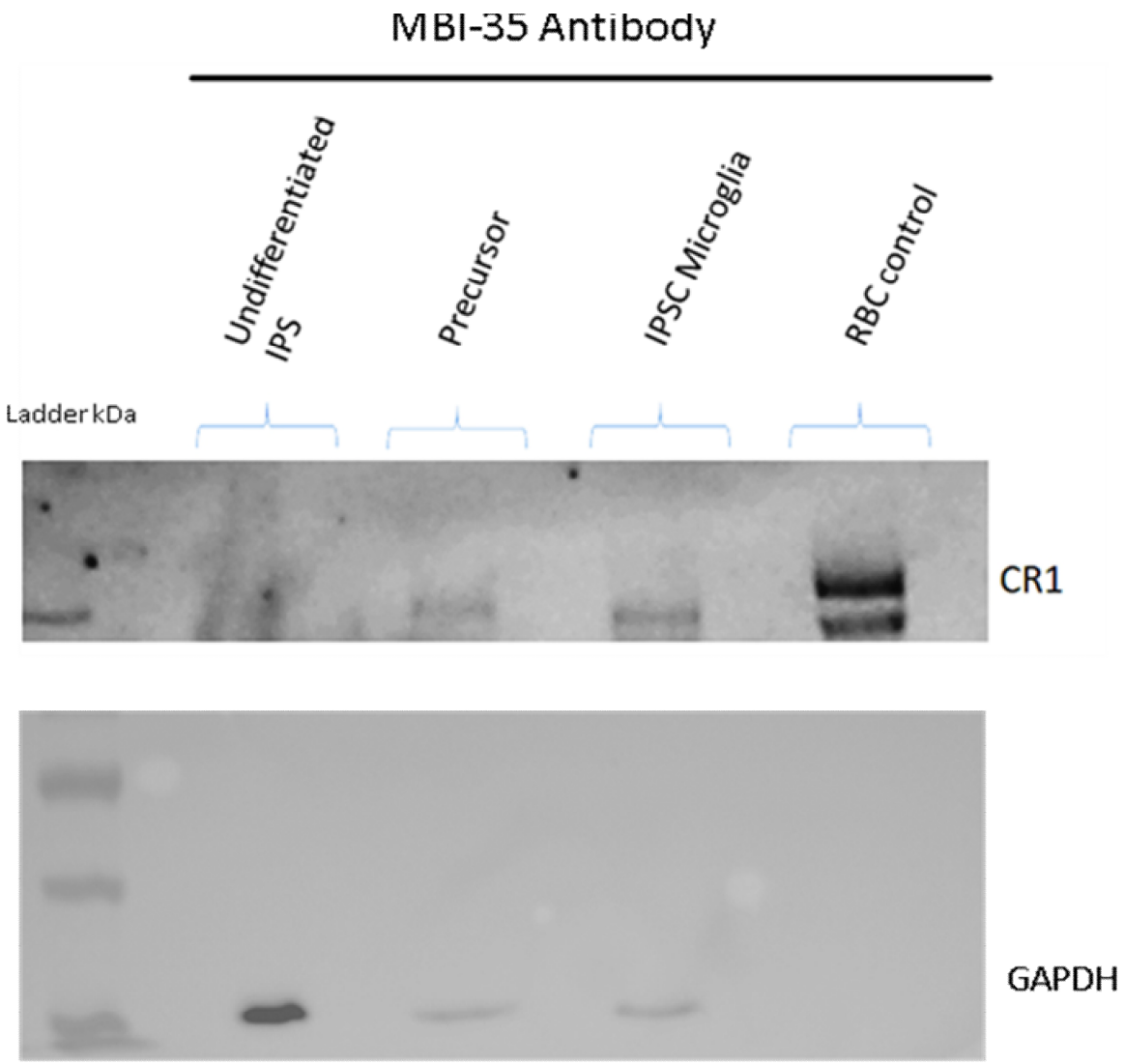

Figure 4.10: Western Blot shows KOLF2 express CR1-F protein in iPS microglia precursors and iPS microglia. *MBI-35 in house monoclonal antibodies show red blood cell control has a CR1-F and CR1-S heterozygote band. iPS precursors and iPS microglia both show bands at CR1-F genotype. Undifferentiated IPS shows no band at CR1. GAPDH was used as a loading control, undifferentiated iPS shows a strong band while iPS precursors and iPS microglia show similar protein control band, lesser than undifferentiated iPS. This was reproduced twice.*

4.2.1.4 CR1 is expressed in microglia iPS cells produced by EB and monolayer methods.

All cells mentioned in this chapter up to this point were differentiated following an EB based method [207]; in order to further confirm the presence of CR1 on iPS microglia, another iPS microglia differentiation protocol was followed, the monolayer method (Takata et al. 2017) as discussed in the previous chapter (chapter 3.0). These alternatively differentiated cells were assessed for expression of CR1 and microglia marker TMEM119 by immunofluorescence. Figure 4.11 shows monolayer-differentiated iPS microglia stained for microglia marker TMEM119 and CR1 using MBI-38. Although some background is visible in CR1 channel, clear staining on the cell membrane is visible confirming these iPS microglia also express CR1 on their surface.

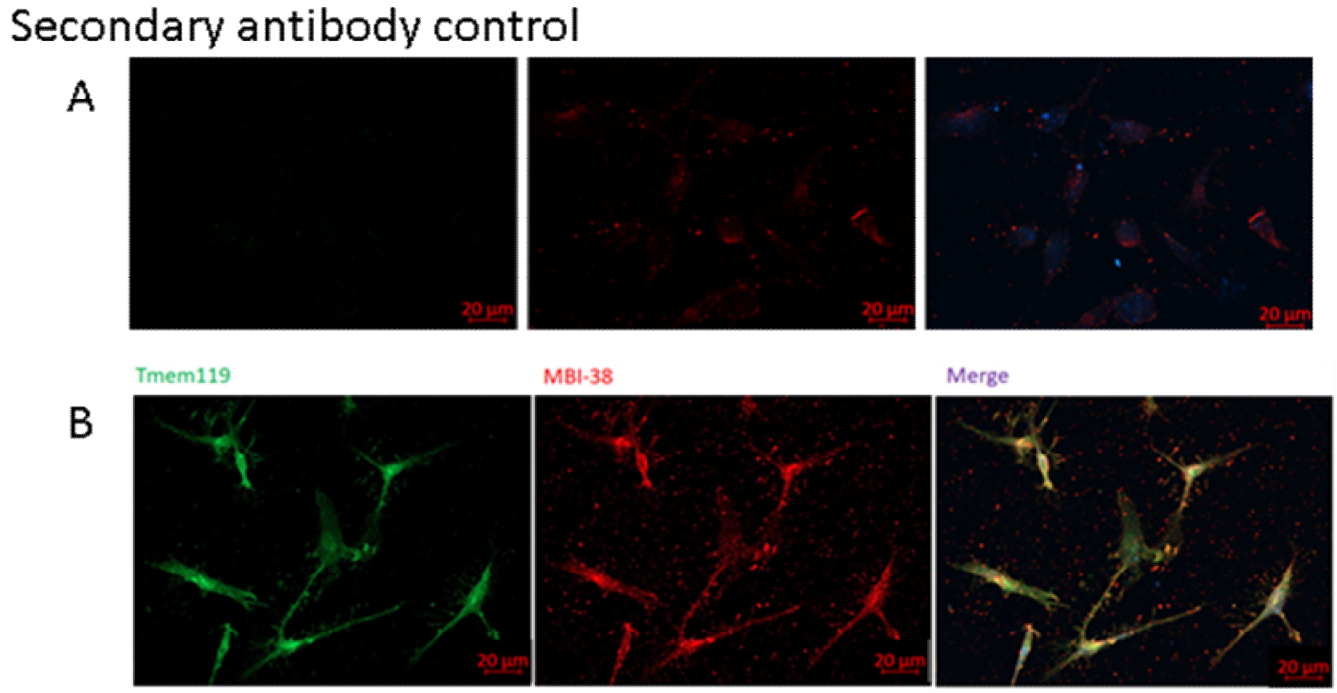

4.11 CR1 protein is expressed in cells produced by the monolayer method.
A) Secondary only control B) Monolayer microglia differentiated in ACM, shows cells to be positive for CR1 with MBI-38 and the microglial marker Tmem119. All images are confocal images taken on a Zeiss spinning disk microscope. These images are representative of 2 biological repeats.

In addition to variations in iPS differentiation methods, alternative terminal differentiation methods within the EB differentiation protocol were tested, discussed in more detail in the previous chapter (chapter 3.0). In all previous figures, including figure 4.11, cells were differentiated using in-house generated astrocyte conditioned media (ACM). However, this is an adaption from the original protocol (Haenseler et al. 2017) which differentiated cells in XVIVIO medium supplemented with growth factors GMCSF and IL34 [207]. As this is the medium more widely used by other labs it was important to confirm the expression of CR1 on microglia differentiated in this way. Figure 4.12 shows both cells differentiated in ACM and in XVIVIO medium stained with PolyCR1 and lysosomal marker CD68. Figure 4.12B shows punctate CR1 staining across the cells in the single colour channel. CD68 staining was very bright on these cells making it difficult to discern CR1 stain in the merged images, but close inspection of the merge shows some areas of CR1 staining distinct from the bright CD68 stain. The data indicates CR1 to be present on XVIVIO differentiated iPS microglial cells.

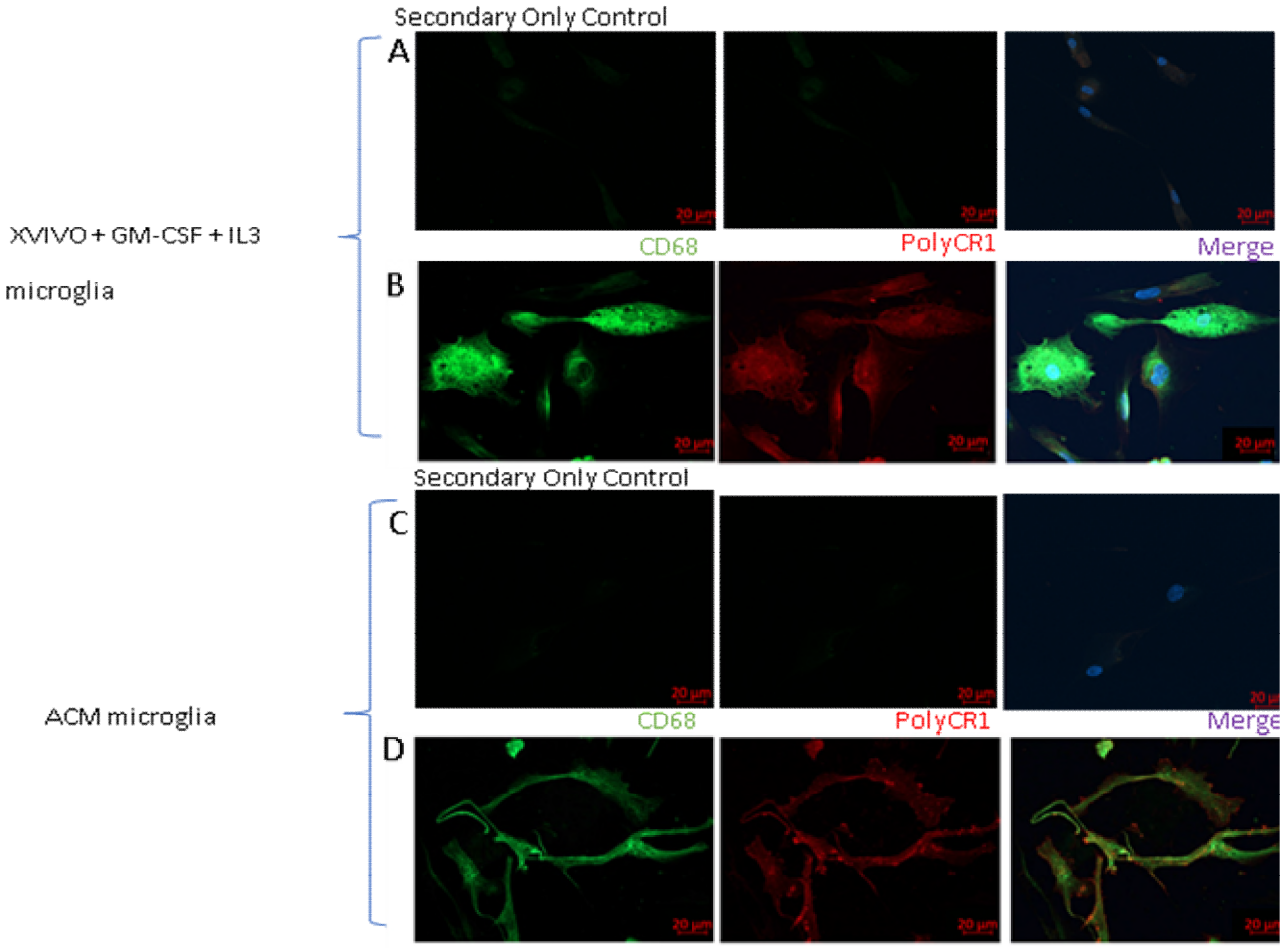

Figure 4.12: Staining with PolyCR1 on *iPS microglial cells* ***differentiated in XVIVO supplement media and ACM cells show both are positive for CR1.***
A & B) XVIVO grown iPS microglia A) Secondary only control while B) Staining with Poly CR1 shows staining throughout the cell with brighter staining for activation marker CD68. C&D) ACM grown iPS microglia C) Secondary only control B) PolyCR1 stainng shows clusters of CR1 throughout the cell with brighter staining for activation marker CD68. All images are confocal images taken on a Zeiss spinning disk microscope. Staining for ACM cells was repeated multiple times, these are representative images from at least 4 biological repeats while XVIVO images are representative of only 2 biological repeats. Staining was only performed in parallel once.

4.2.2 CR1 transcript and protein not found in other iPS CNS cells.

4.2.2.1 iPS astrocytes

iPS astrocytes were generated following adaption from two protocols and were differentiated by Dr. Kimberly Jones[239,240]. mRNA was extracted for RT-qPCR. No amplifications amplification for CR1 in three biological replicates of iPS astrocytes was observed. Figure 4.13a shows that the amplification of CR1 did not reach a threshold indicating no amplification of CR1; this is supported by figure 4.13B which shows that the melting curve did not amplify any product. Final confirmation is shown in figure 4.13C) in which PCR product was ran on an agarose gel; there were no specific bands in three iPS biological replicates, while a positive control THP-1 post PCR product showed a clear band at 200bp.

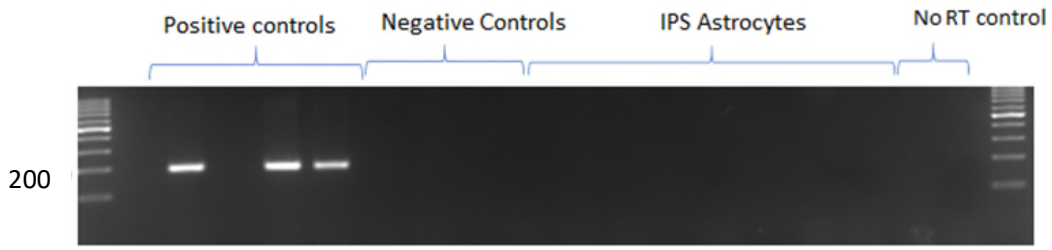

Figure 4.13: No amplification of CR1 transcript was seen with astrocyte mRNA
RT-qPCR products were ran alongside positive controls (THP-1 cells) which showed a band at the expected 200bp. Negative controls (SH-SY5Y, a neuronal cell line) showed no bands, neither did three biological repeats of iPS astrocytes. No RT control confirms the absence of contamination. This was repeated twice on the quant studio 7 RT-qPCR machine.

Protein expression in iPS astrocytes was investigated using immunofluorescence in figure 4.14. Staining with MBI35 shows the absence of CR1 while staining with astrocytic marker GFAP shows bright astrocytic process' throughout the cells.

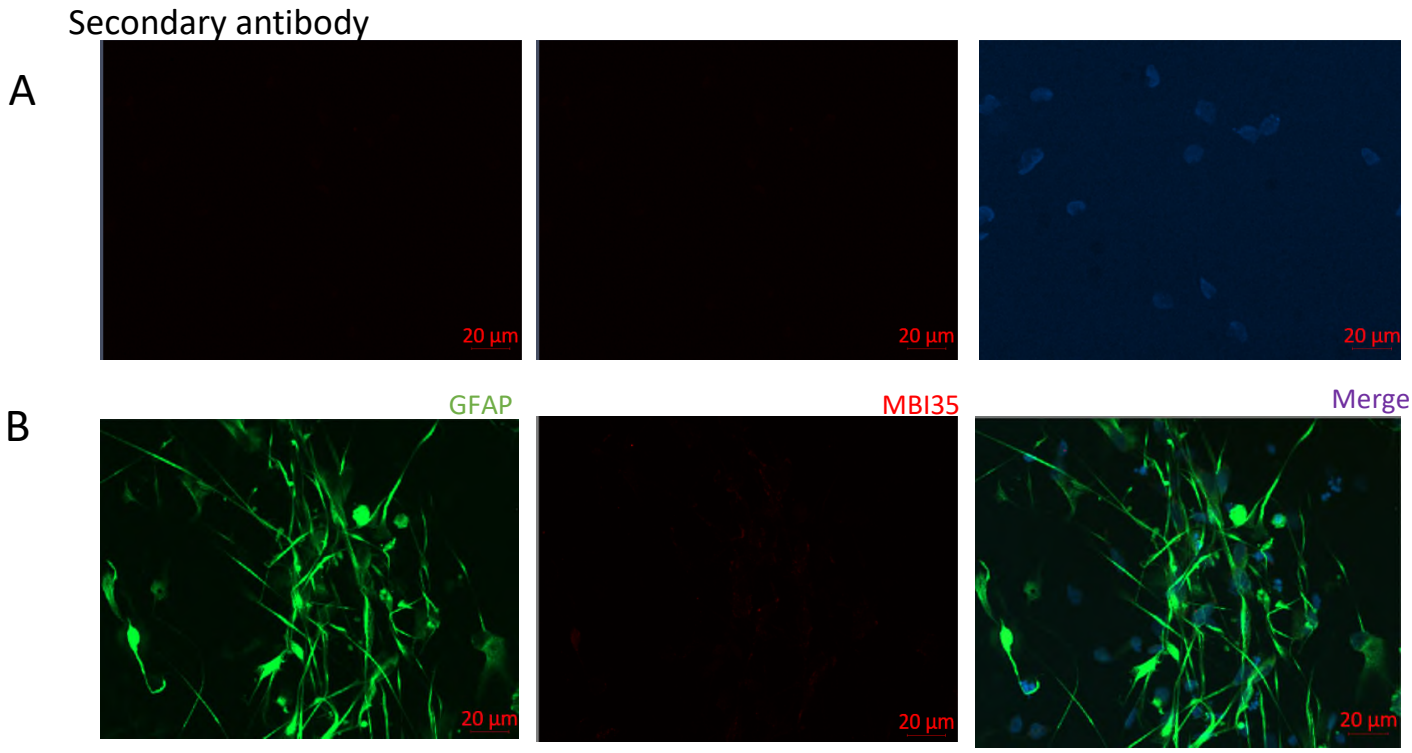

Figure 4.14: Immunofluorescence shows absence for CR1 protein on iPS astrocytes with 2 monoclonal in-house antibodies.
A) Secondary only control B) iPS astrocytes are brightly positive for GFAP throughout the cell while no staining is visible with MBI-36. All images are confocal images taken on a Zeiss spinning disk microscope. Representative images from two biological repeats.

Western blot was performed to confirm the absence of CR1 protein in iPS astrocytes and iPS astrocyte precursor cells (APC). Figure 4.15 shows that MBI-38 detected no bands in iPS APC and iPS

astrocytes while heterozygotic red blood cell control showed two clear bands. This was performed with MBI-38 antibody. Additionally, the bottom of the membrane was stained for astrocytic marker GFAP, showing a band at 50kDa and confirming that protein was loaded in each well and expressed a key astrocytic marker. No GFAP band was visible in red blood cell control.

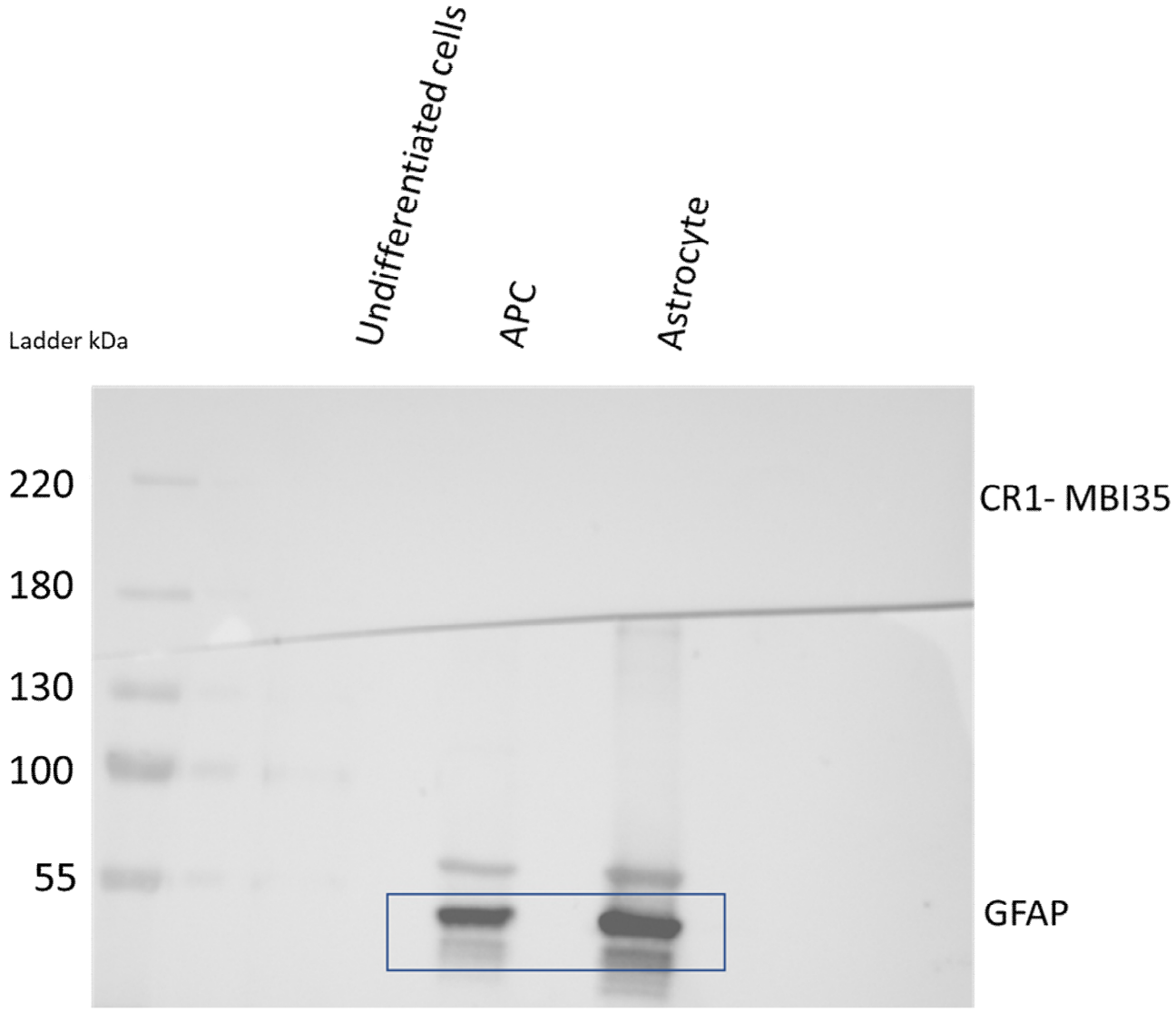

Figure 4.15: Western Blot shows no band for CR1 in iPS astrocytes precursor cells or IPS precursors.
30µg of iPS APC and iPS astrocyte protein was loaded, as calculated by BCA assay. Staining with MBI-38 anti-CR1 showed the absence of CR1 while staining with anti-GFAP shows a clear band at 50kDa. Red blood cell (RBC) controls showed heterozygotic expression for CR1 but did not express astrocytic marker GFAP. This was only repeated once.

4.2.2.2 Immature iPS cortical neurons showed no protein expression of CR1.

Immature cortical neuronal protein was gifted from the Allen lab in three biological replicates. These cells had not yet developed spontaneous current or expression of NeuN and are therefore referred to as immature cortical neurons. Figure 4.16 shows loading of 40µg of protein and staining of westerns with MBI-38; no CR1 bands were detected in these cells; the red blood cell control shows two CR1 bands.

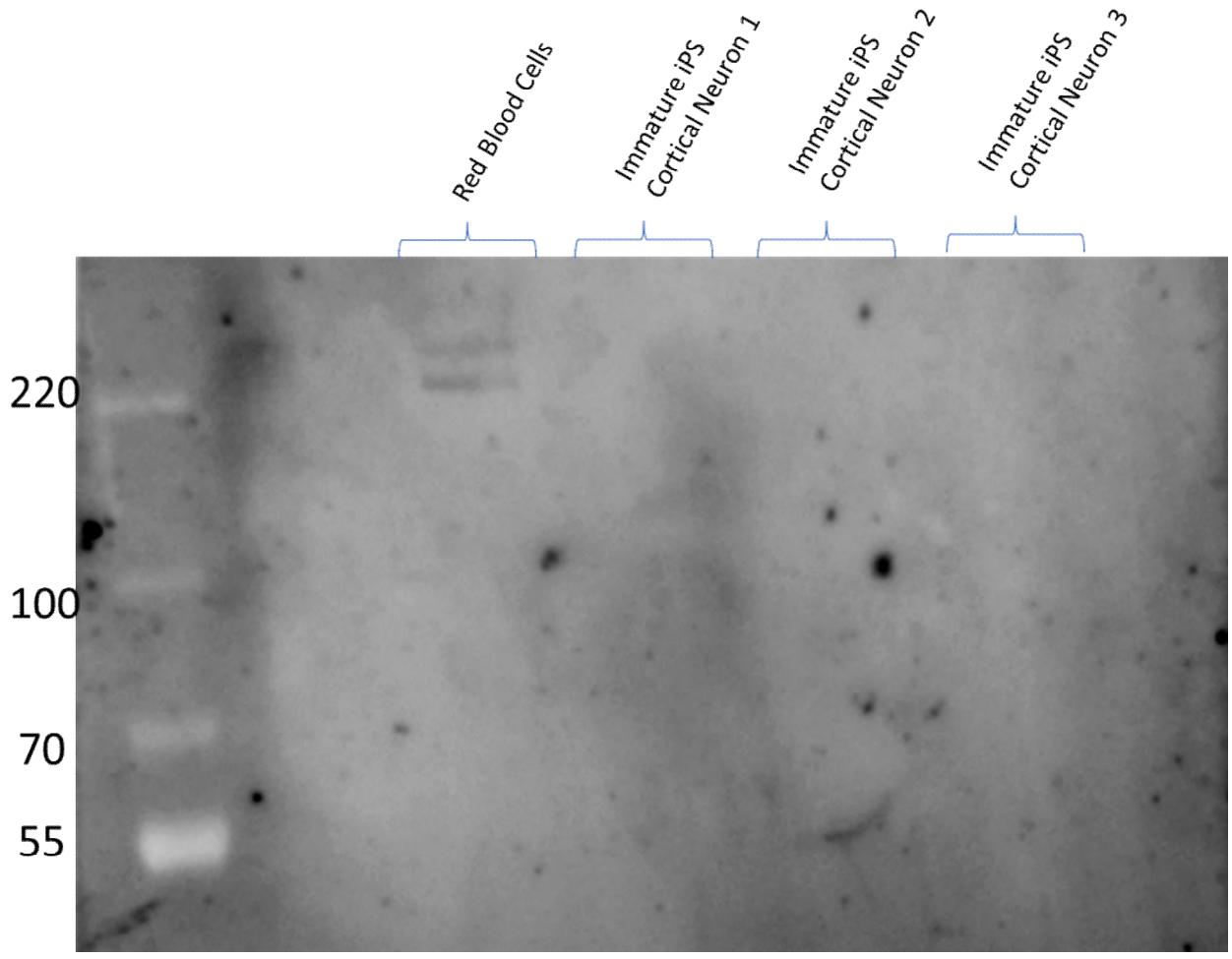

Figure 4.16: Western Blot with CR1 MBI38 shows no bands with 3 biological repeats of immature cortical neurons. *Immature cortical neurons showed no expression of CR1 in three biological replicates while red blood cell control was heterozygotic for CR1 indicated by the presence of two bands.*

4.3 Discussion

The work in this chapter confirms the expression of CR1 on the surface of iPS-derived microglia and their precursors when differentiated by two separate protocols in two separate terminal differentiating mediums. Absence of CR1 on iPS-derived astrocytes and immature cortical neurons was also recorded.

CR1 message was investigated using RT-QPCR, this revealed expression of CR1 transcript in iPS microglia and immediate precursors, with higher expression in fully differentiated iPS microglia. Activation of iPS microglia with LPS caused a small increase in CR1 transcript. Microglial expression of complement factors such as C1q, have been shown to shown to increase substantially following microglia stimulation with LPS[241]. Furthermore, investigations using primary rat microglia showed upregulation of the rodent CR1 orthologue, Crry, following LPS and Aβ stimulation, with slightly higher expression following addition of Aβ[162]. Increased expression of CR1 may, in addition to increasing receptor availability, enhance regulation of complement locally, thus reducing damage to self-cells. Investigating how iPS microglia alter expression at the protein level with a range of relevant stimuli is required.

RT-qPCR for *CR1* transcript on the undifferentiated KOLF2 cells produced a signal, albeit at high CT value, indicating very low transcript expression; despite this CR1 protein was not detected on undifferentiated KOLF2 when investigated. This mismatch is likely due to the sensitivity of RT-qPCR which involves several amplification events, unlike protein characterisations which bluntly examines whether the product is present or not. Therefore, it is plausible that CR1 protein is expressed on KOLF2 but expression is extremely low, to the extent where it is undetectable with the chosen protein methods. Alternatively, some of the cells used for RNA collection might have undergone some spontaneous differentiation; however, this was repeated multiple times with results remaining consistent making this possibility quite unlikely.

Detection of CR1 protein was performed using two techniques, western blot and immunofluorescence using three well characterised in-house CR1 antibodies. Staining of iPS microglia and their immediate precursors reveal CR1 to be clustered on the surface of cells. Confirmation of specificity was provided by showing that pre-absorption of the antibody with CR1 protein abrogated staining in immunofluorescence. Pre-absorption represents an essential staining control when proof of expression is sought; indeed, a previous report of CR1 staining in human brain samples reported neuronal expression, though this remained following antibody pre-absorption thus likely non-specific due to cross-reactivity with other molecular structures[141]. Furthermore, this provides some support of the specificity of the in-house antibodies used. Clustering of CR1 has previously been described on other cell types and suggested to be important for CR1 functions[151]. Previous label fracture studies identified human erythrocytes to have 8-20 clusters of CR1 each made up of multiple CR1 receptors[151,242]. Polymorphonuclear leukocytes showed less clustering of CR1 than erythrocytes but clustering was observed[151]. The cell surface expression of CR1 was confirmed by use of live staining, performed on ice to prevent engulfment of probes. Further confirmation was derived from staining of CR1 with a commercially purchased CR1 antibody alongside CX3CR1. Like staining with in-house antibodies, CR1 was shown to predominantly in the cell body, fainter than the fluorescence from microglia markers. However, it was harder to observe the speckled pattern of CR1 in these images,

this is most likely due to these images not being confocal but just being of one plane. Future work should expand with alternative commercial antibodies to produce more comparative images. Regardless, staining with commercial antibody supports the expression of CR1 on iPS microglia.

Western blotting was used to further test CR1 expression; iPS microglia and the immediate precursors were both positive, giving a single band congruent with the CR1F variant, as predicted from available information on the KOLF2 iPS line from which they were derived. Future confirmation of CR1 protein expression on iPS microglia should be provided using ELISA with an IP step prior to addition onto the assay. Utilising supernatant in the ELISA allows for detection of sCR1, a local but potent inhibitor of complement produced by the shedding of CR1 from the membrane[142]. Previous studies have reported a significant increase in CR1 shedding into plasma in those with AD risk loci rs6656401 and rs4844609 but with no relation to cognitive decline[141]. Another study revealed elevated CSF levels of sCR1 in patients with mild cognitive impairment who later went on to develop AD compared to those that did not[121]. Investigating how the polymorphism of CR1 may be implicated in altered CR1 shedding at the cellular level of homeostatic and activated cells could reveal an alternative mechanism for action for CR1 in pathogenesis of LOAD. Furthering this, it would be intriguing to know the subsequent effect of locally elevated sCR1 to subsequent complement action, this could be performed with measurements of C3 and its fragments in the brain or CSF.

Previous published work on human brain and/or isolated brain cells and/or cell lines has reported that CR1 is expressed on astrocytes and/or neurones. For astrocytes, studies utilising astrocytic cell lines have yielded contradictory data with one line, T190, showing presence of CR1 protein while other lines were negative[141]. Other investigations using primary astrocytic cell cultures and healthy and MS brain tissue samples supported positive CR1 staining on primary astrocytes[141,157]. To test this, the same assays described above for iPS microglia expression were used to investigate the expression of CR1 on iPS astrocytes. No expression of CR1 at the protein or transcript level was detected in this cell type, contradicting some of the published data. It is possible that the iPS astrocytes used in this study are not sufficiently mature to provide conclusive findings. Unlike iPS models of microglia, astrocytes continue to mature with increased culture time with cells showing an increased expression of astrocytic marker GFAP with longer culturing. Moving forward, iPS astrocytes should be kept in culture for longer before being used to investigate whether they begin to express CR1 later in culture. Furthermore, astrocytes can exist within a range of activation states within the brain, isolation from primary cell culture or post-mortem study could lead to activation of astrocytes, altering their expression and skewing results; it is plausible that activated astrocytes express CR1. Future iPS astrocyte work should inspect multiple activation states using common stimulators such as PMA and LPS to assess whether these induce or alter expression of CR1. Additionally, co-culture work with astrocytes and microglia would provide a more physiological model as multiple studies have highlighted the importance of astrocytic-microglia cross talk in physiological conditions[243,244]. Indeed, some of the cross-talk involves the complement activation product C3a[245].

The use of ACM is an important part of the differentiation; however, storage, generation and characterisation of ACM can provide multiple problems which are resolved by the live co-culturing of cells[243,245]. In addition to iPS astrocytes, iPS cortical neurons were investigated for protein expression of CR1. iPS neurone protein extracts were kindly gifted from Dr. Kimberly Jones of the Allen lab; these were derived from iPS neurons which had not yet begun to produce spontaneous currents, a central role for cortical neurons. No CR1 protein was detected by western blotting of these homogenates but the insensitivity of this method and the immaturity of the cells used mean that the data provided in this chapter are not conclusive regarding expression of CR1 on neurons.

Prior to starting the work described in this chapter, a literature search for expression of CR1 was performed; this revealed a small number of results, many of which were conflicting. The publicly available Allen brain atlas, which provides data on the expression of multiple genes across the body. reported low CR1 transcript expression across multiple brain areas including the cerebral cortex, amygdala and hippocampus[154]. Additional In-situ staining of multiple human post-mortem samples from different aged individuals reported very low CR1 expression restricted to neuronal cells and neutrophils [155]. However, neither source provides any data for the protein expression of CR1 with the CNS. Other labs have described the presence of CR1 transcript in phagocytic Kolmer cells of the choroid plexus and ependymal cells, the latter only during bacterial meningitis[144,246]. This was not replicated in subsequent studies using normal, MCI and AD brains which failed to produce a band for CR1 in western blot analysis[141]. It was suggested this was due to low sensitivity and specificity of antibodies used which failed to detect low levels of protein. The rodent analogue of CR1, Crry, was expressed on isolated rat microglia; however, this is not sufficient to support expression of CR1 on human microglia because there are important functional and genetic differences between the two genes[162].

iPS cells offers a unique human model to study expression of CR1 and multiple markers in microglia and other brain cell types, including mature cortical neurons and oligodendrocytes, work that is needed to fully understand the distribution of CR1 in brain and guide studies in human brain samples. They also provide a perfect test bed for discovering the impact of AD associated CR1 variants, notably the CR1-S variant, in brain cell function. This work successfully confirms presence of CR1 on iPS microglia and iPS precursors. Moving forward the use of tri-cell organoids, could hugely help in deciphering the expression patterns of CR1 in fully mature microglia and other brain cells; cells grown in a 3D system produce more physiologically relevant models that may help in identifying the brain cell types demonstrating CR1 expression, essential for understanding how it may alter immune functions and impact the dysregulation seen in the early stages of AD pathology.

5.0- Generating and characterising CR1 KO iPS clones

5.1 Introduction:

Complement Receptor 1 (CR1) is a regulatory receptor in the complement cascade[86]. Genome-wide association studies (GWAS) have identified single nucleotide polymorphisms (SNP) within CR1 that increase an individual's risk for developing late onset Alzheimer's disease (LOAD)[247]. How CR1 is implicated in LOAD pathogenesis and the effects of each SNP on expression and function of CR1 are unknowns.

Investigating the role of CR1 in the CNS presents multiple complications, including obtaining appropriate models to investigate it. Primary human brain cells are difficult to obtain, often only available after surgical or post-mortem removal from patients who already present pathology within the CNS. Furthermore, removal of cells from the complex brain parenchyma shifts them from their physiological state; particularly vulnerable to this are the CNS immune cells, microglia. Microglia are highly reactive to subtle changes within the micro-environment and change in this triggers cell activation. Animal models offer different complications, primarily as murine CR1 is produced differently from human CR1, exhibiting a different expression and distribution. Humans possess separate genes for the generation of CR1 and CR2 while mice generate both from a single gene by making alternatively spliced transcripts[162]. Complement related protein y (crry) is considered a closer orthologue to human CR1 in protein sequence and function. Indeed, sequence homology has identified CR1 to have evolved from the crry gene[164]. Genetic modifications to rodent crry provides additional challenges, with homozygous knock outs being embryonically lethal, thought to be due to uncontrolled complement activation in the developing embryo and placenta[164,248]. The alternative splicing and difficulty in generating knock out models hinders the use of rodents for investigating the expression and function of CR1. These issues are overcome by the generation of human brain cell models utilising induced pluripotent stem cells (iPSC). Generation of human IPS brain cells, allows for the expression of CR1 to be determined and functional analysis of how CR1 may be implicated in key functional process. Additionally, IPS cells can be derived from patients, with known CR1 SNPs or isoforms or can be genetically modified so to investigate specific genetic effects on differentiated cells.

Genetically altered cells are highly useful to study a multitude of biological functions. In particular, genetic knock out (KO) lines are valuable in uncovering the role of various genes in different systems. This is commonly done by introduction of a double stranded break (DSB) in the DNA, resulting in a frame shift of the RNA which is statistically likely to include introduction of a premature termination codon (PTC)[249]. Upon detection of a PTC during translation, nonsense mediated decay (NMD) is triggered resulting in destruction of the transcript so no protein can be generated[249–251]. Various protocols have been developed to generate KOs mostly by adapting restriction enzymes, which are bacterial endonucleases capable of producing DSB in specific locations. Adaptions of this using zinc finger motifs and transcription activator like effectors improves the specificity of cuts but still provides a limited editing efficiency[252,253]. More recently developed is CRISPR, a bacterial immunity system which has been modified for use in the lab.

CRISPR was first identified in 1987 in E-coli. Repeating palindromic regions separated by non-repeating DNA sequences, called spacers, were identified adjacent to well conserved genes referred to as CRISPR associated genes (Cas genes) in bacterial cells[209,210]. Spacers within this motif have been shown to originally derive from phages or other infectious agents, with bacteria integrating these sequences into their own genome following infection. Upon subsequent infection from a phage, Cas enzymes and spacer regions are transcribed. The spacer sequence is then utilised as a target for binding of Cas enzymes to specific genes in the infecting phage genome. Like restriction enzymes, Cas enzymes are endonucleases capable of generating DSB. Generation of DSB in these sequences is used to prevent production of phage mRNA to protect cells against infection[209,210]. Since its identification in bacteria, CRISPR has been engineered for laboratory use.

CRISPR provides a uniquely specific DNA binding model, which allows for any gene in the genome to be selected and targeted for editing. Experimentally this is done by the provision of guide RNAs (gRNA) which interact with Cas enzymes as the spacer product in bacteria would. gRNA is designed to a specific area of interest and is made up of two parts; CRISPR RNA (crRNA) and trans activated RNA (tracrRNA). The crRNA is the pre-designed 17-20bp sequence specific to the target DNA and the tracrRNA acts as a scaffold to the Cas endonuclease. There are several critical factors to consider when designing the grRNA, and there are several available Cas nucleases, each of which can only bind to the DNA in the presence of a PAM (protospacer adjacent motif) site. Each Cas has a specific PAM and is one limitation of the CRISPR system, however this is in part overcome by a wide range of available Cas proteins. The most commonly used is Cas9 from S. pyogenes which binds 3bp upstream to its PAM site, 5'-NGG-3'[210].

CRISPR offers a robust genetic manipulation tool with minimal off-target effects which has been extensively adapted to fulfil a range of biological experiments. Following the identification of CR1 as a LOAD genetic risk factor, increased interest in its contribution to CNS cell function has occurred. CRISPR technology offers a unique tool to uncover these possible roles. For this reason, CR1 KO CRISPR clones were generated in IPS cells and differentiated to IPS microglia. This chapter describes the generation of three homozygous CR1 KO lines and their complete characterisation for expression of CR1. Additionally, I show that CR1 KO IPS microglia still possess microglial morphology and markers, demonstrating that CR1 KO had little effect on differentiation.

5.2 Results:

5.2.1 CR1 KO strategy

Knock out (KO) of CR1 was performed using SpCas9 enzyme with two guide RNAs designed to bind to a region within exon 2 of CR1. As multiple transcripts of CR1 exist it is important that the designed complex targets an area in all possible CR1 transcripts, therefore an early exon was selected. Specific guides with a predicted efficiency of over 60% were selected using Deskgen online tool (now called Synthego -a CRISPR designing tool), with each binding near a PAM site (-NGG). Snapgene software (genetic imager; San Diego) was used to map the CRISPR design. Figure 5.1a) shows the genomic CR1 sequence with the intronic and exonic nucleotides and amino acid sequence underneath. Guide RNA are shown by the red text, as labelled, with the black labels indicating screening primers, which flank the edit; use of these guides would remove a section of 145bp from the CR1 gene. Figure 5.1b) shows the resultant sequence with the 145bp edit removed; this was done to ensure that this edit would produce a PTC, marked by * in the translation sequence. In order to trigger nonsense-mediated decay (NMD), PTC must be within the exon and at least 50bp from the exon-exon junction[249]. Figure 5.1b) indicates that this CRISPR design would introduce a PTC into an appropriate site in exon 3, which should be sufficient to trigger NMD.


A
Screening primer
CTGTAATCCCAGCTACTC
GGTAGATGACCTGAGGTCAGGAGTCGAGACCAGCCTGGCCAACATGGTAAAACCCCATCTCTACTAAAAATACGAAAATTAGCCAGGTGTGGTGGTGGGCACCTGTAATCCCAGCTACTC
CCATCTACTGGACTCCAGTCCTCAGCTCTGGTCGGACCGGTTGTACCATTTTGGGGTAGAGATGATTTTTATGCTTTTAATCGGTCCACACCACCACCCGTGGACATTAGGGTCGATGAG
Val Asp Asp Leu Arg Ser Gly Val Glu Thr Ser Leu Ala Asn Met Val Lys Pro His Leu Tyr Lys Tyr Glu Asn Pro Gly Val Val Val Gly Thr Cys Asn Pro Ser Tyr Ser
3165 3170 3175 3180 3185 3190 3195 3200
Screening primer
AGGAA
AGGAAGCTGAGGTAAGGACAATTGCTTGAACCCAAGAGGCGGAGGTTGCAGTGAGCCAAGATAGCGCCACTGCACTCCAGCCTGGGTGATGGAGCCAGTCTCCGTCTCAAAAAAGAAAAA
TCCTTCGACTCCATTCCTGTTAACGAACTTGGGTTCTCCGCCTCCAACGTCACTCGGTTCTATCGCGGTGACGTGAGGTCGGACCCACTACCTCGGTCAGAGGCAGAGTTTTTTCTTTTT
Gly Ser Gly Lys Asp Asn Cys Leu Asn Pro Arg Gly Gly Gly Cys Ser Glu Pro Arg Arg His Cys Thr Pro Ala Trp Val Met Glu Pro Val Ser Val Ser Lys Lys Lys Lys
3205 3210 3215 3220 3225 3230 3235 3240
Guide 1
GTCAATGCAATGCCCCAGAATGG
AAAAAGTATGGTAATTTCTCCATTAACTTTGATGCTTCTATGGTCTTGATCTCCAGGTCAATGCAATGCCCCAGAATGGCTTCCATTTGCCAGGCCTACCAACCTAACTGATGAATTTGA
TTTTTCATACCATTAAAGAGGTAATTGAAACTACGAAGATACCAGAACTAGAGGTCCAGTTACGTTACGGGGTCTTACCGAAGGTAAACGGTCCGGATGGTTGGATTGACTACTTAAACT
Exon 2
DELETION
Lys Ser Met Val Ile Ser Pro Leu Thr Leu Met Leu Leu Trp Ser Ser Pro Gly Gln Cys Asn Ala Pro Glu Trp Leu Pro Phe Ala Arg Pro Thr Asn Leu Thr Asp Glu Phe Glu
3245 3250 3255 3260 3265 3270 3275 3280
GTTTCCCATTGGGACATATCTGAACTATGAATGCCGCCCTGGTTATTCCGGAAGACCGTTTTCTATCATCTGCCTAAAAAACTCAGTCTGGACTGGTGCTAAGGACAGGTGCAGACGTAA
CAAAGGGTAACCCTGTATAGACTTGATACTTACGGCGGGACCAATAAGGCCTTCTGGCAAAAGATAGTAGACGGATTTTTTGAGTCAGACCTGACCACGATTCCTGTCCACGTCTGCATT
Exon 2
DELETION
Phe Pro Ile Gly Thr Tyr Leu Asn Tyr Glu Cys Arg Pro Gly Tyr Ser Gly Arg Pro Phe Ser Ile Ile Cys Leu Lys Asn Ser Val Trp Thr Gly Ala Lys Asp Arg Cys Arg Arg Lys
3285 3290 3295 3300 3305 3310 3315 3320
GAGTCAGACCTGACCACGAT
Guide 2
GTAACTCTGGAGTGGGAACCCCCCTGTTAGTCAAACATCTGTAAGATCTGATTCAATTTGTTCAAATTTTGTAACTGAGTTGCATATGACAATTAGTTTGCCAAGGTGCAATACATATGA
CATTGAGACCTCACCCTTGGGGGGACAATCAGTTTGTAGACATTCTAGACTAAGTTAAACAAGTTTAAAACATTGACTCAACGTATACTGTTAATCAAACGGTTCCACGTTATGTATACT
Leu Trp Ser Gly Asn Pro Pro Val Ser Gln Thr Ser Val Arg Ser Asp Ser Ile Cys Ser Asn Phe Val Thr Glu Leu His Met Thr Ile Ser Leu Pro Arg Cys Asn Thr Tyr Glu
3325 3330 3335 3340 3345 3350 3355 3360
ATACTGTTAATCAAACGGTTCCAC
Screening Primer
GAATTATTCTTGTAGATCATACCTTGTTACTGCTTTGAGTTCCTGGCGCCTTCATTAAAAGTTTATTTCATGAGAAACAGTCATTGCAGGACATGATTGAGGGAAAATCCCCATTCACTG
CTTAATAAGAACATCTAGTATGGAACAATGACGAAACTCAAGGACCGCGGAAGTAATTTTCAAATAAAGTACTCTTTGTCAGTAACGTCCTGTACTAACTCCCTTTTAGGGGTAAGTGAC
Asn Tyr Ser Cys Arg Ser Tyr Leu Val Thr Ala Leu Ser Ser Trp Arg Leu His Lys Phe Ile Ser Glu Thr Val Ile Ala Gly His Asp Gly Lys Ile Pro Ile His Trp
3365 3370 3375 3380 3385 3390 3395 3400
GGGGTCTCCCATTTTCATGACTAAAATTAAGTAATGAATGACTTGGGACAAGAAAGAGAAGTGGATTAAATAACTAAAAGATGTGACAATCTTGGGCTTTGAGATCTTTGGATTATACCA
CCCCAGAGGGTAAAAGTACTGATTTTAATTCATTACTTACTGAACCCTGTTCTTTCTCTTCACCTAATTTATTGATTTTCTACACTGTTAGAACCCGAAACTCTAGAAACCTAATATGGT
Gly Ser Pro Ile Phe Met Thr Lys Ile Lys Met Thr Trp Asp Lys Lys Glu Lys Trp Ile Lys Leu Lys Asp Val Thr Ile Leu Gly Phe Glu Ile Phe Gly Leu Tyr Gln
3405 3410 3415 3420 3425 3430 3435 3440
GTTGAATTGAATTACAGATAATAACAAAGTTTACATTTTTCTGGGAGGCATAATATGGGGATGAAACAGATCTGAAAGGAAAGTTTTTTTTGAAAGGGAGCTGATCCTGAGGCAGTCTGG
CAACTTAACTTAATGTCTATTATTGTTTCAAATGTAAAAAGACCCTCCGTATTATACCCCTACTTTGTCTAGACTTTCCTTTCAAAAAAAACTTTCCCTCGACTAGGACTCCGTCAGACC
Leu Asn Ile Thr Asp Asn Asn Lys Val Tyr Ile Phe Leu Gly Gly Ile Ile Trp Gly Asn Arg Ser Glu Arg Lys Val Phe Phe Glu Arg Glu Leu Ile Leu Arg Gln Ser Gly
3445 3450 3455 3460 3465 3470 3475 3480
TGAGTTTCCTCAAGGTAGCAAAATCTGTGGAACCATCAGAACTGCGTGTGTTCCTCAGTAAGCTACAGGCAGGTTGAGACCTTATGTACTAAAAAAGTTTTTAGTTTACTCTACTTGGC
ACTCAAAGGAGTTCCATCGTTTTAGACACCTTGGTAGTCTTGACGCACACAAGGAGTCATTCGATGTCCGTCCAACTCTGGAATACATGATTTTTTTCAAAAATCAAATGAGATGAACCG
Glu Phe Pro Gln Gly Ser Lys Ile Cys Gly Thr Ile Arg Thr Ala Cys Val Pro Gln Ala Thr Gly Arg Leu Arg Pro Tyr Val Leu Lys Lys Val Phe Ser Leu Leu Tyr Leu Ala
3485 3490 3495 3500 3505 3510 3515 3520
TCCAAAATTCTGTTTCTTTCCTGTAGGTAAATCATGTCGTAATCCTCCAGATCCTGTGAATGGCATGGTGCATGTGATCAAAGGCATCCAGTTCGGATCCCAAATTAAATATTCTTGTAC
AGGTTTTAAGACAAAGAAAGGACATCCATTTAGTACAGCATTAGGAGGTCTAGGACACTTACCGTACCACGTACACTAGTTTCCGTAGGTCAAGCCTAGGGTTTAATTTATAAGAACATG
Exon 3
Pro Lys Phe Cys Phe Phe Pro Val Gly Lys Ser Cys Arg Asn Pro Pro Asp Pro Val Asn Gly Met Val His Val Ile Lys Gly Ile Gln Phe Gly Ser Gln Ile Lys Tyr Ser Cys Thr
3525 3530 3535 3540 3545 3550 3555 3560

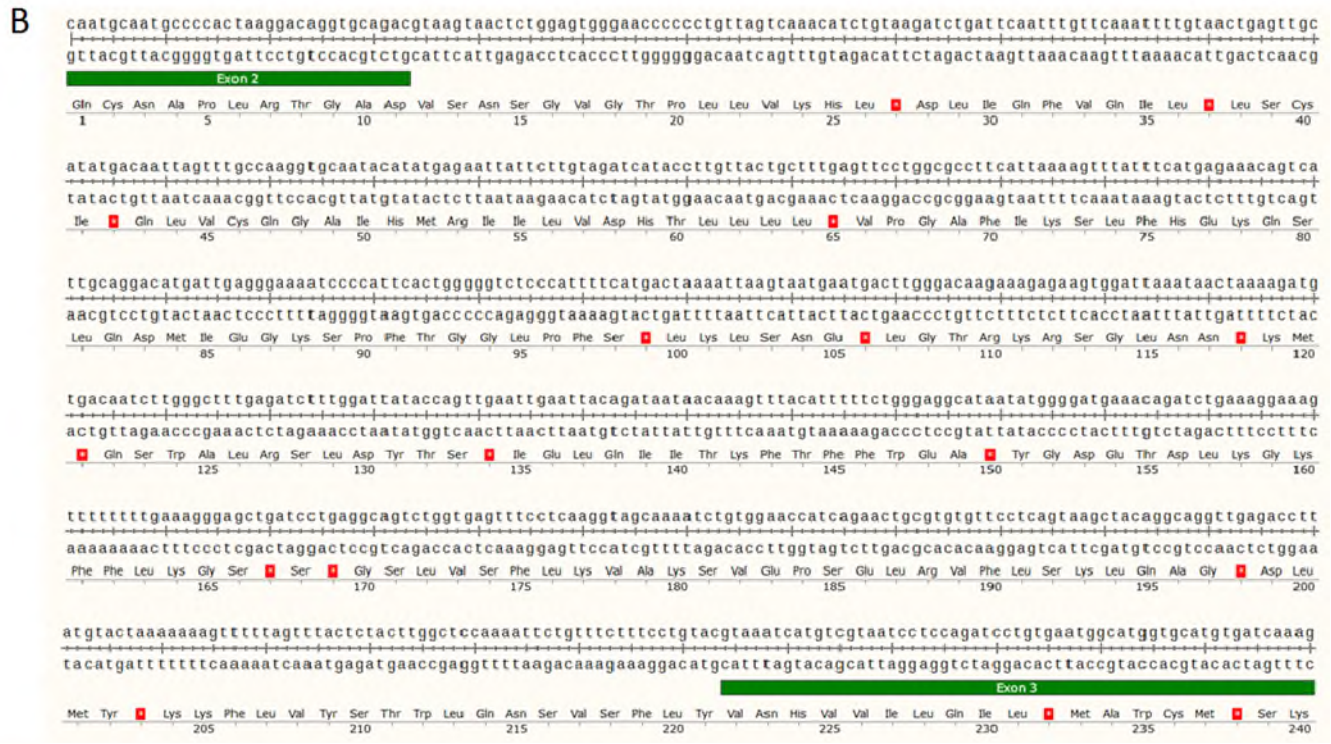

Figure 5.1: Schematic of CRISPR KO design on exon 2 of CR1. *Snap-gene was used to map the genomic sequence of CR1. The two strands represent each strand of DNA while underneath shows the corresponding translation of the sequence. Exons were marked onto the transcript. A) Shows the KO plan, two guides which bind within exon 2 of CR1 were selected and are marked with red writing. In between these two sites lies the deleted site of 145bp. Flanking this are the two screening primers used to identify whether the area had been deleted or not, these are in black writing and annotated 'screening primers', these were also the primers used to generate sequencing data. B) CR1 genomic DNA with the expected site cut out. This illustrates KO of this size is sufficient to cause a frame shift in the translation and introduce premature stop codons to trigger nonsense mediated decay to KO the protein.*

5.2.2. Generating CR1 KO iPS clones

Post-CRISPR screening was performed using PCR primers flanking the edit shown in figure 5.1a. This allow for identification of clones which successfully take up the CRISPR complex and edit, producing CR1 transcript 145bp smaller than the non-edited CR1. Single colonies were picked and expanded in 96 well plates and DNA collected. Figure 5.2a) shows the initial screen, in which non-edited cells produced a single band at 733bp, such as clone D2, while cells which had the 145bp edit in both strands produced a single lower band at 588bp, two such clones are clear in figure 5.2a), D8 and G3. Several heterozygous clones were generated, shown by the presence of both bands, including D3, C7, C9, E5, F2, G2 and G4. Figure 5.2a) shows an unclear result with clone C3; subsequent PCR analysis revealed this to be a homozygous knock out, as shown in figure 5.2b). After the initial screen, sub clones were picked to ensure KO efficiency within the culture. After these were picked, grown and frozen to make stocs. DNA was collected and re-analysed in the screening PCR to confirm the presence of the edit. Figure 5.2b) shows 7 subclones of each homozygous KO with heterozygous D3 clone between each homozygotic clone. PCR screening confirmed the 3 heterozygotic CR1 KO clones; C3, D8 and G3.

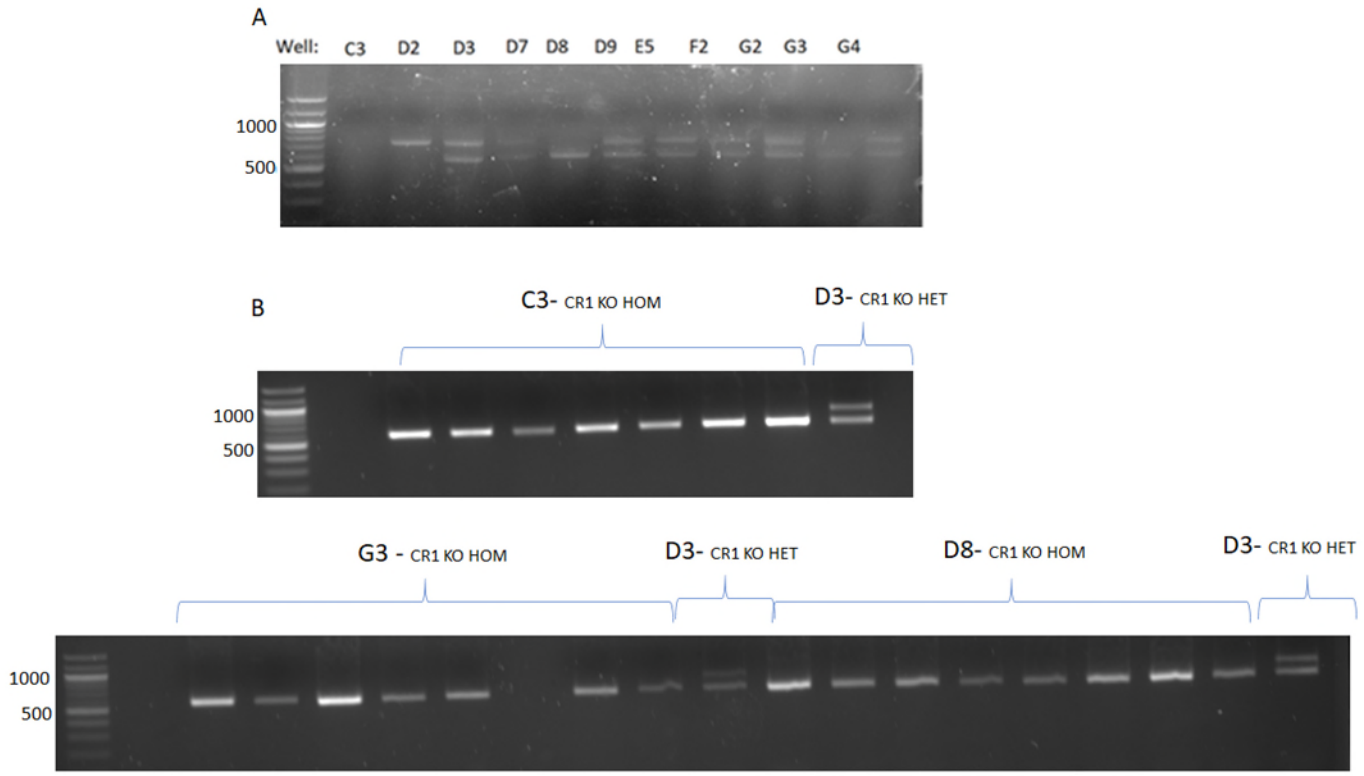

Figure 5.2: Three clones had CR1 KO out homozygotic, several heterozygotic KO were generated. *A) The original PCR screen, the well is noted at the top. D2 is the WT, with one larger band, D3, D9, E5, F2, G2, G4 were all heterozygotic KO with 2 bands visible and three homozygotic KO are seen; C3, D8 and G3. B) Shows subclones PCR of each of the three homozygotic KO, clones were picked from each KO, grown and DNA extracted from them. 6-8 repeats for each three were run with a heterozygotic KO (D3) in between to confirm each band represents the lower weight.*

Sequencing was performed for each homozygotic KO. Post-PCR product was sent to Sanger for direct sequencing. Results in figure 5.3 show sequencing data for each clone. Raw data is presented graphically, along with the three nucleotide sequences. The first line of this is the CR1 template sequence (FASTA sequence) with the following two rows being the amplified product of each clone, one for each chromosomal copy. In all three clones, binding of the enzyme with the first guide is as expected, this is true for the second guide in D8 (figure 5.3a) and C3 (figure 5.3b) clones; however, for clone G3 (figure 5.3c) binding seems to have shifted downstream. All three clones showed different edits, with D8 being the cleanest with no insertion of nucleotides between the two cuts. C3 and G3 are less clean with multiple nucleotides randomly incorporated within the break.

The sequenced product was checked in Snapgene to produce a translation sequence to investigate whether a reading frame shift had occurred, and a PTC introduced. Figure 5.3d) shows that the translation of each clone did cause a frame shift; D8 and G3 present the same frame shift, with the addition of PTC within exon3 of both chromosomes. C3 appeared quite different due to an insertion of nucleotides (around 60) meaning a larger exon 2 was generated; however, the introduction of a PTC was still recorded. Both copies revealed the same edit for all three clones.

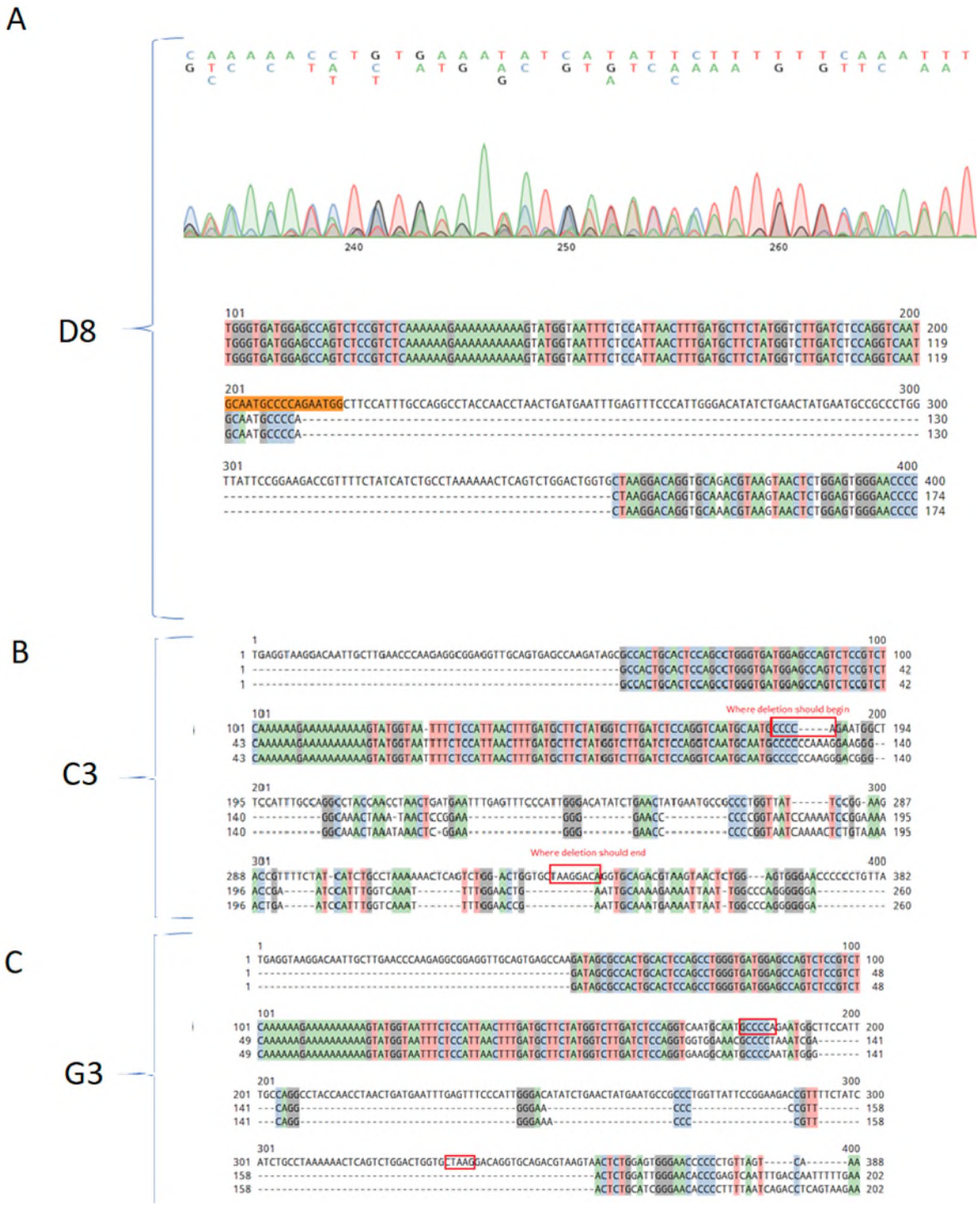
A
D8
B
C3
C
G3
Where deletion should begin
Where deletion should end

Figure 5.3: Sequencing data confirms 145bp edit within exon 2 and the subsequent translational changes due to this edit in three homozygotic clones.
A-C) Shows sequencing report. The top image shows the fluorescent chart with the subsequent parts representing the read data. In each image the top nucleotide line shows the input template sequence with the two underneath each strand from the clone, as labelled on the left (A-D8, B- G3 and C- C3). The orange highlighted region on the first line, either by an orange highlight or red box represents where the first KO guides should bind. D) Shows the translational changes generated from the sequenced data, each has a frame shift and corresponding change in nucleotides. The red boxes correspond to STOP codosn, each of the three clones has an introduced PTC. Sequencing was sent of twice with two different DNA collections.*

In addition to ensuring that the designed edit had occurred, it was important to show no off target edits had occurred. The guides selected had only one potential off target site in the nearby CR1L gene. Primers were designed flanking where this edit would exist and a PCR screen performed. Figure 5.4 shows four controls, HMC3 (microglia cell line), unedited KOLF2 line and two WT clones, B7 and D2 which had gone through the CRISPR; all four generated a single product at 450bp. Three homozygotic KO lines alongside this showed the same product indicating no change in CR1L had occurred post CRISPR. Any other off target edits were within CR1 itself.

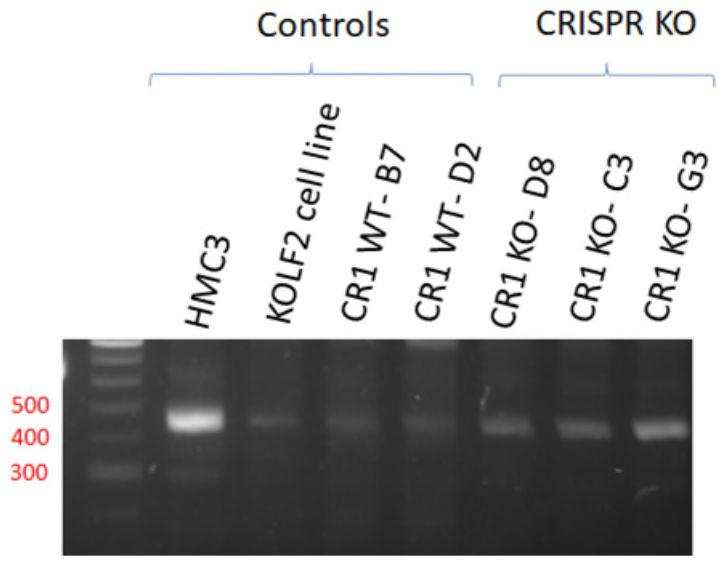

Figure 5.4: CR1 KO off target analysis shows CR1L to be unchanged in CR1 KO.
Four controls were run to ensure no edit had occurred. This included microglia cell line HMC3, parent KOLF2 cell line which had not undergone the CRISPR and two WT clones which did not incorporate the edit post CRISPR, B7 and D8. All show a single band at 450bp. The three homozygotic edit clones were ran alongside this each showing the same single band at 450bp indicating no edit at this position of CR1L had occurred. This is from two technical repeats.

In addition to ensuring no off target effects had occurred, copy number variation for other genomic alterations were investigated. Passaging of iPS cells can result in genetic alterations such as copy

number changes or trisomy. In order to ensure no genetic alterations, which may skew downstream assays, a screen was performed. DNA from cells was isolated alongside the generation of new factories, ensuring that DNA checked was from the same passage as cells used to generate data. An Illumina Global Screening Array was utilised, making comparisons in DNA to the reference genome GRCh37 / hg19. PennCNV software (https://penncnv.openbioinformatics.org/en/latest/) was used to identify any deletions or duplications within the genetic material; however, this is limited to only very large edits. The screen produced in figure 5.5 was compared to earlier runs for the parent cell line KOLF2, which had been submitted for analysis after the cell line had arrived. This allowed for any changes from passaging to be identified.

Figure 5.5 shows that no trisomy had occurred in any clones; however, two duplications and three deletions were present in all clones alongside an additional duplication in WT clones KOLF2 and D2. The common duplications and deletions were found in the initial KOLF2 screen, indicating they were not generated due to passaging through the course of this project. This is not true for the 20q.11.21 duplication seen in KOLF2 or D2 which is a new edit acquired during the course of experimentation. Its presence on KOLF2 cells, which did not undergo CRISPR, shows that this is not an effect of CRISPR.

Sample ID	CR1 Genotype	**3p14.2** *61136894-61905527*	**3p13** *72288657-72424795*	**6p22.3** *15509133-15722102*	**9q33.1** *119244942-119374306*	**18q22.1** *62115075-62264706*	**20q11.21** *30011117-30409363*
KOLF2	WT	Duplication	Deletion	Deletion	Deletion	Duplication	Duplication
D2	WT	Duplication	Deletion	Deletion	Deletion	Duplication	Duplication
B7	WT	Duplication	Deletion	Deletion	Deletion	Duplication	No CNV
D8	HOM KO	Duplication	Deletion	Deletion	Deletion	Duplication	No CNV
G3	HOM KO	Duplication	Deletion	Deletion	Deletion	Duplication	No CNV
C3	HOM KO	Duplication	Deletion	Deletion	Deletion	Duplication	No CNV

Figure 5.5: Copy Number Variant Analysis
Analysis of all clones showed a variaty of duplications and deletions, but all samples are consistent except for in 20q11.21 which is a duplication seen only in KOLF2 and D2 WT cells. No trisomy has been identified.

5.2.3 Characterizing CR1 KO iPS clones

RT-qPCR was used to investigate the presence of *CR1* message in CR1 KO iPS microglia. Figure 5.6 shows the ΔΔCT of the data with cells normalised to housekeeper SDHA and relative to CR1 expression in undifferentiated iPS cells of the corresponding genotype. This shows significant reduction in CR1 transcript in iPS precursors (P=0.028) and in iPS microglia (P=0.0007).

.

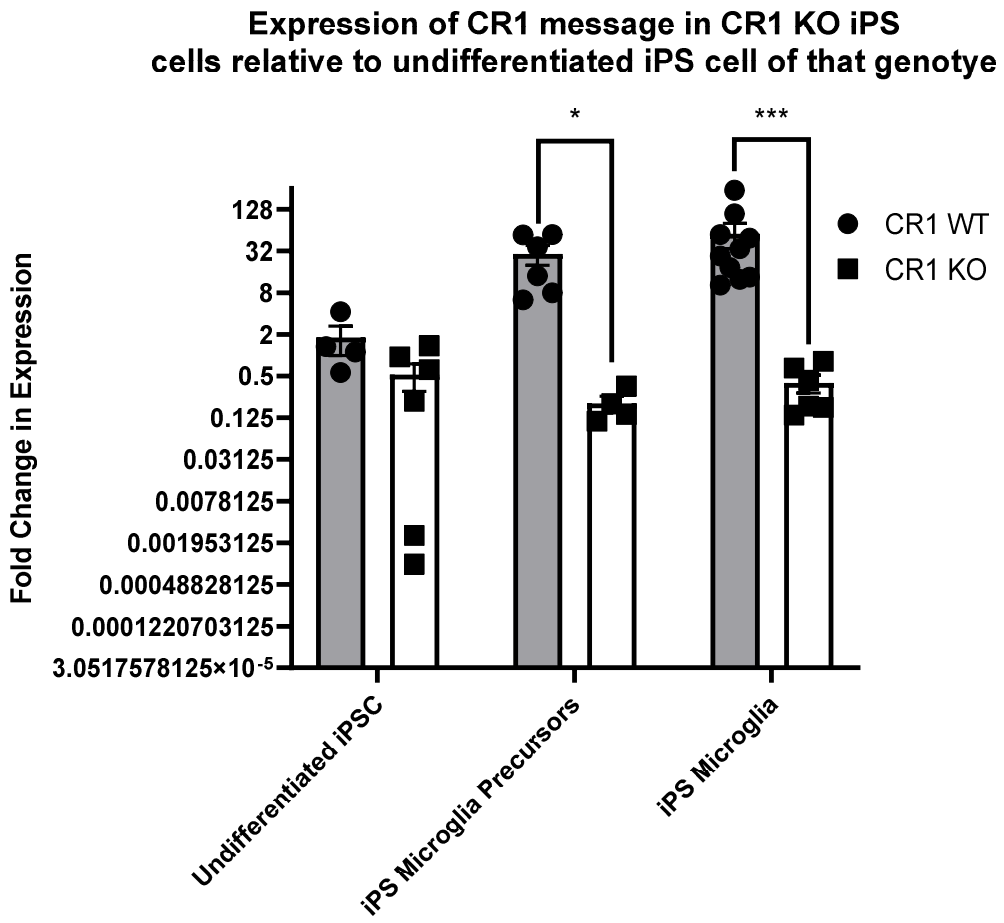

Figure 5.7: Expression of CR1 message was significantly reduced in CR1 KO iPS precursors and iPS microglia relative to expression of CR1 in CR1 WT iPS precursors and CR1 WT iPS microglia when relative to expression in undifferentiated iPS cells.

*Significant downregulation of CR1 was shown in CR1 KO iPS precursors (p=0.028) and iPS microglia (P = 0.0007) compared to expression in CR1 WT iPS microglia. Error bars represent the SEM. A multiple Mann-Whitney test with post hoc Holm-Sidak multiple comparison was performed with significance set at * P< 0.05; ** P < 0.01; *** P<0.001; ****P<0.0001. Absence of asterisk indicates no significant difference with P > 0.05.*

Protein expression was investigated using western blotting (figure 5.8) and immunofluorescence (figures 5.9, 5.10). Western blot was performed with in-house antibody MBI-35. Figure 5.8 shows red blood cell lysate control produced two bands at ~220kDa and 250kDa due to the donor being heterozygotic for CR1F and CR1S. CR1 WT KOLF2 iPS microglia cells showed a single band at 220kDa demonstrating that they expressed CR1F; the band was absent in all three iPS microglia CR1 KO clones. GAPDH loading control run on the same blot showed a clear band at 35kDa in all iPS microglia protein samples, indicating similar amount of protein loaded in the CR1 KO samples. However, no band for GAPDH was seen in the CR1 WT protein. A ponceau stain, performed after antibody induction, reveal a bubble over the expected GAPDH band in CR1 WT protein. The ponceau stain also confirms the presence of protein in all 4 lanes.

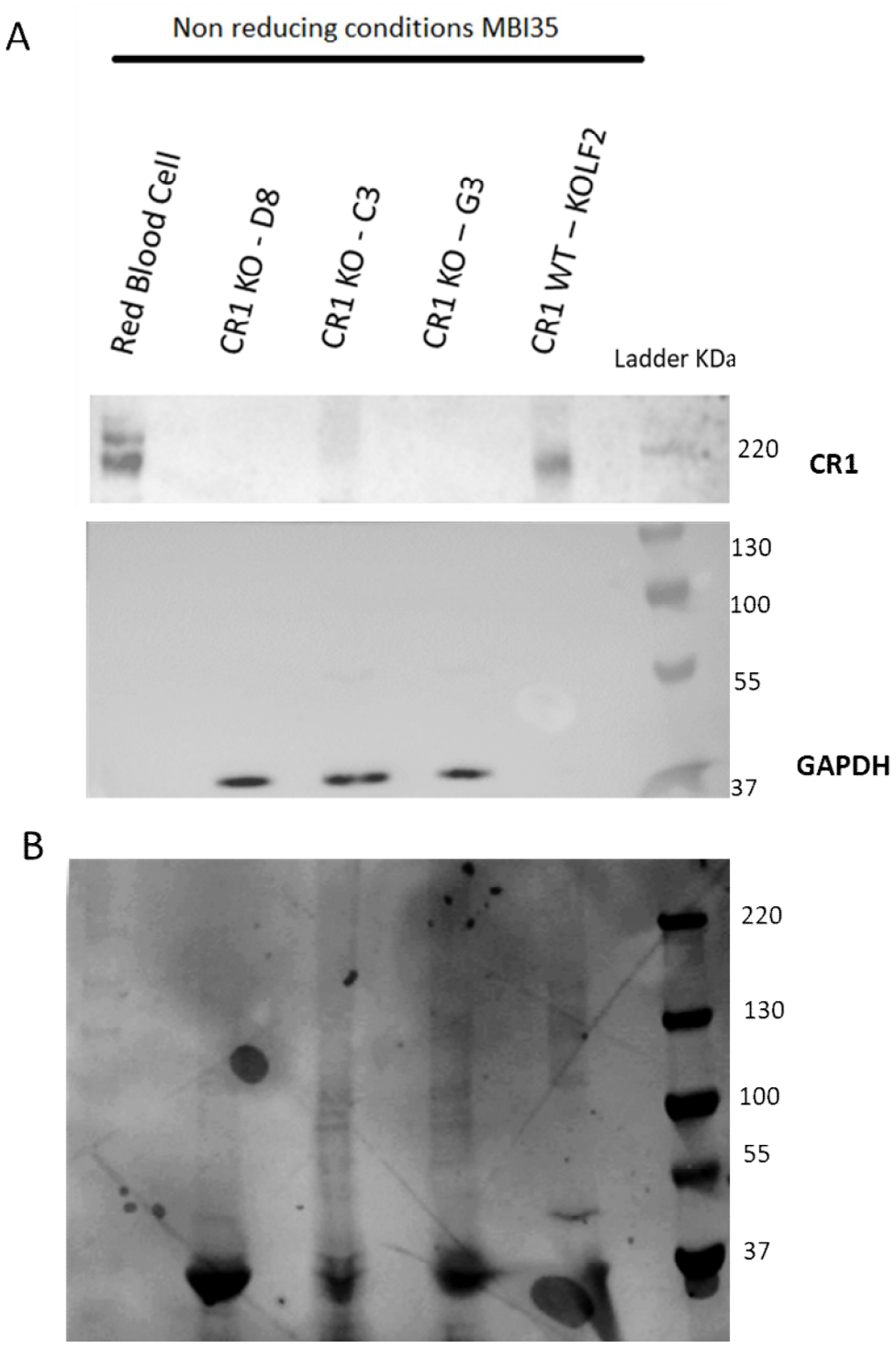

Figure 5.8: Western Blot of CR1 KO fully differentiated to iPS microglia showed no protein bands with MBI-35 *Red blood cell control showed two heterozygotic CR1 bands and the CR1 WT IPS microglia showed one clear band at CR1-F. The three KO showed no bands, indicating the absence of CR1 protein. GAPDH control showed similar loading of all three cells however the GAPDH was not clear in the CR1 WT. However, a band can be seen in earlier blot in figure 4.10 in which the same biological sample shows a clear band for CR1 and GAPDHB) After transferring the gel was stained with ponceau S to reveal protein bands on the membrane. This was performed after staining and shows that protein was loaded for all wells and that there was a bubble over the expected band for GAPDH probably caused during transfer. Bands in RBC are extremely faint. This represents only 1 biological and technical repeat.*

Confocal microscopy showed that all KO clones were positive for microglia marker CD11b but negative for CR1 using monoclonal MBI-38. CD11B staining showed that the cells are highly ramified, with microglia-like morphology (figure 5.9).

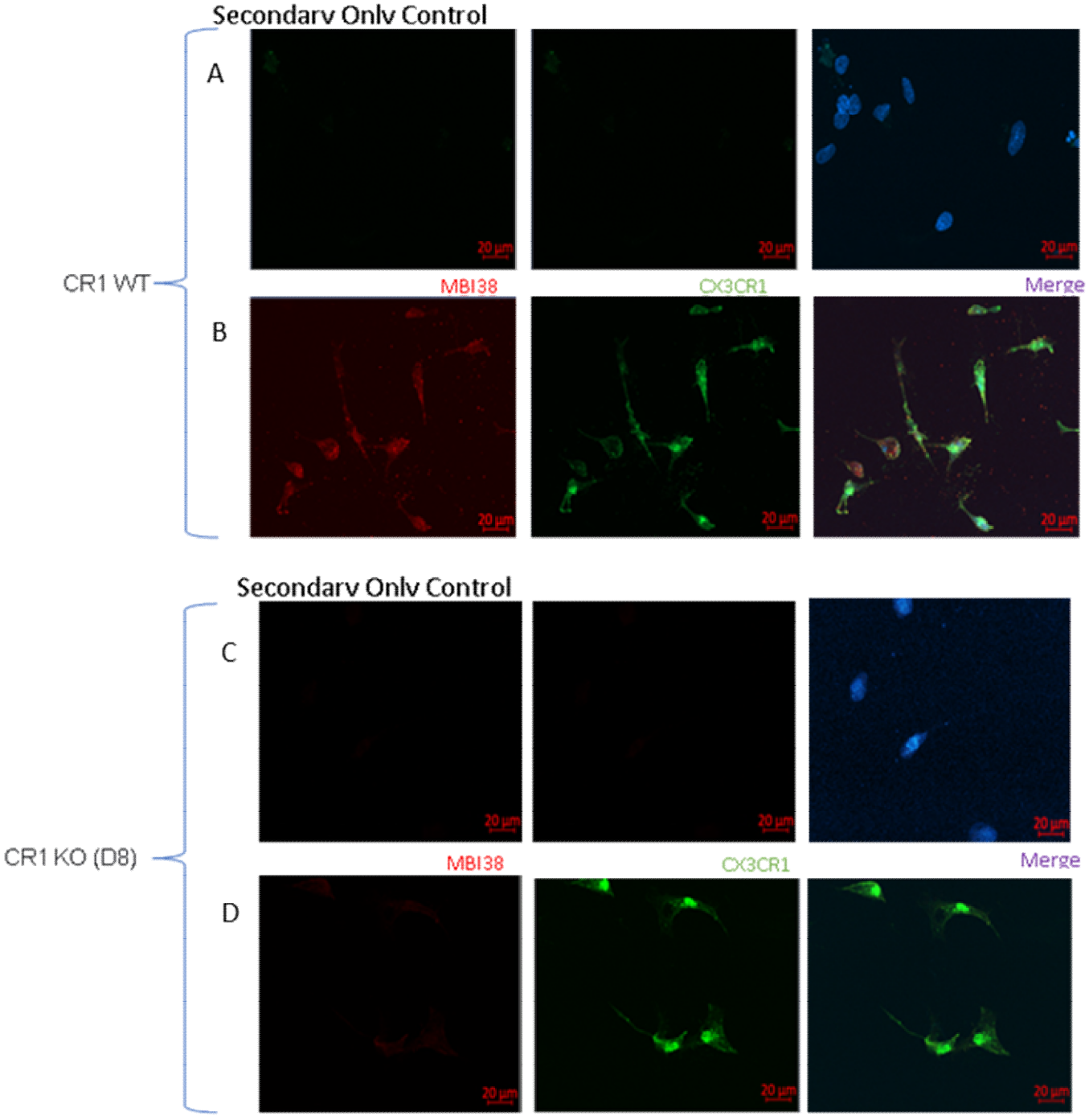

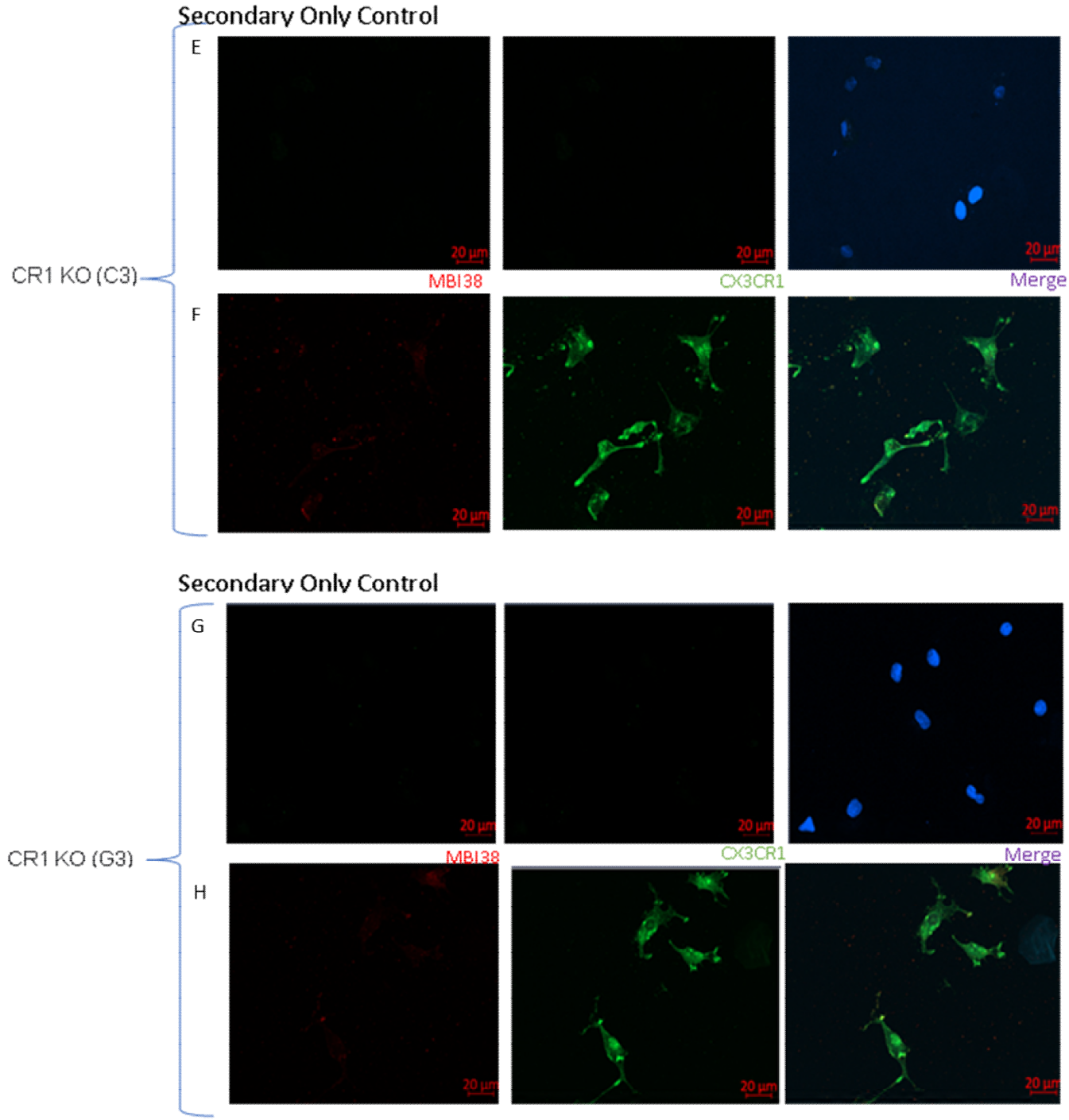

Figure 5.9: Imaging of three KO homozygote clones showed no staining with in-house CR1 antibody MBI-38.
A & B) CR1 WT clone D2 A) Secondary only control B) CR1 WT microglia are positive for CR1 and integrin CD11b. C & D) CR1 KO clone C3 microglia C) Secondary only control D) C3 microglia do not stain positive for CR1 with MBI-38 but do stain positive for CD11B, which is a microglia marker and part of complement receptor CR3 E & F) Shows CR1 KO G3 microglia E) Secondary only control, F) G3 clones do not have any staining with CR1 MBI-38 but do stain positive for CD11B presenting a highly ramified morphology. G & H) CR1 KO clone D8 microglia, G) Secondary only control H) G3 showed background for CR1 with MBI-38 but no clear staining was observed cells were positive for CD11B. These images are representative of 3 biological repeats.

To confirm surface localisation of the markers, live staining was performed, fixing cells after antibody incubation on ice to ensure no antibody internalisation. Figure 5.10 illustrates that two clones, D8 and C3, stained positively for microglia marker IBA-1 but are absent for any CR1 staining.

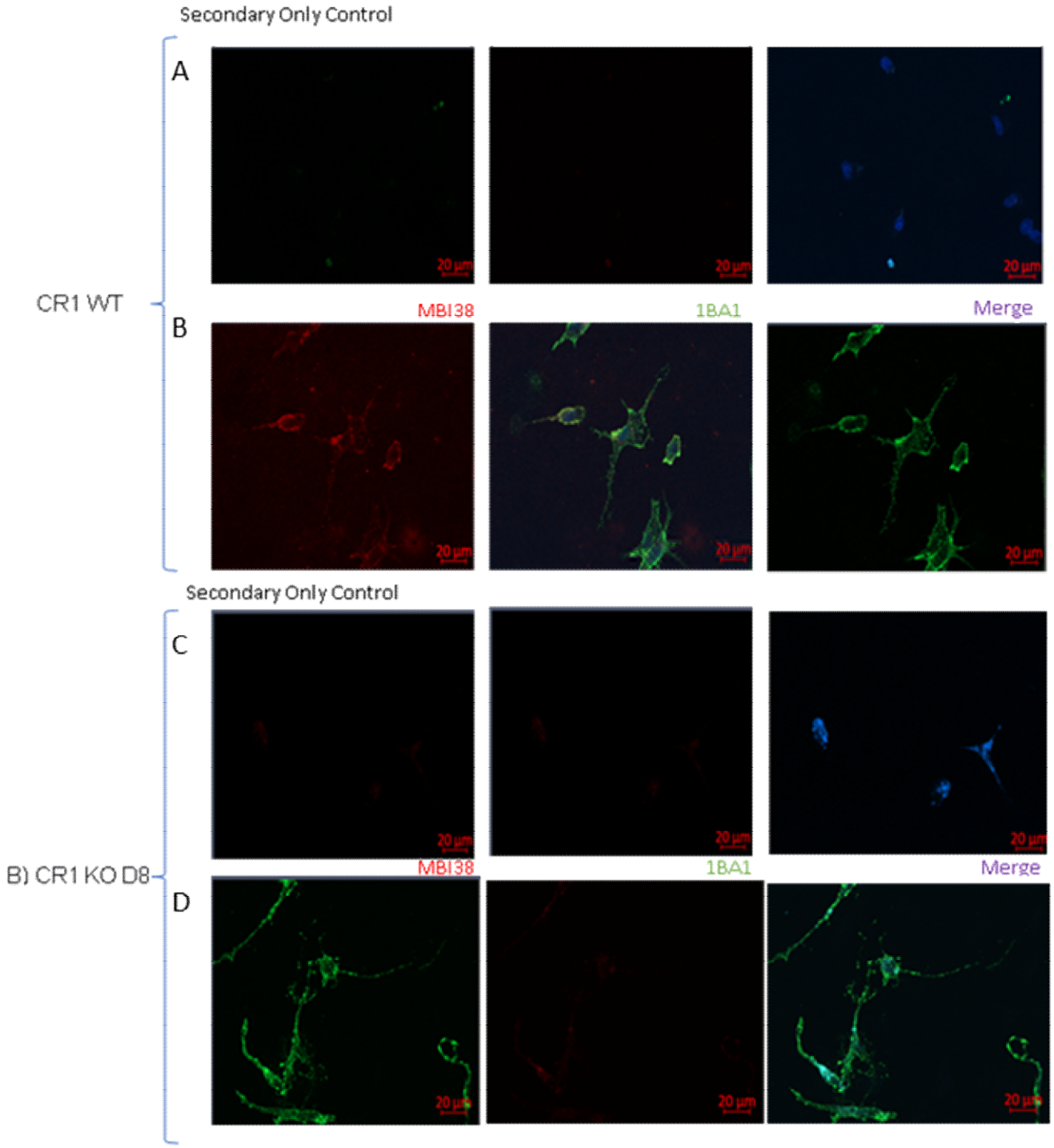

Figure 5.10: No CR1 was observed in two CR1 KO clones when stained without fixing but was shown on CR1 WT clone. *A) CR1 WT clone D2 showed positive staining for CR1 with MBI38 B) KO clone D8 showed no staining with CR1 with MBI-38 but did stain positive for macrophage marker IBA-1. C) No CR1 was observed but clear IBA-1 staining is shown.*

RT-qPCR was used to test expression of key microglial markers. Figure 5.11 shows ΔΔCT analysis of three key markers in CR1 KO iPS microglia relative to expression in CR1 WT iPS microglia. This reveals no significant difference between expression in IBA-1, PRY12 and CD11b.

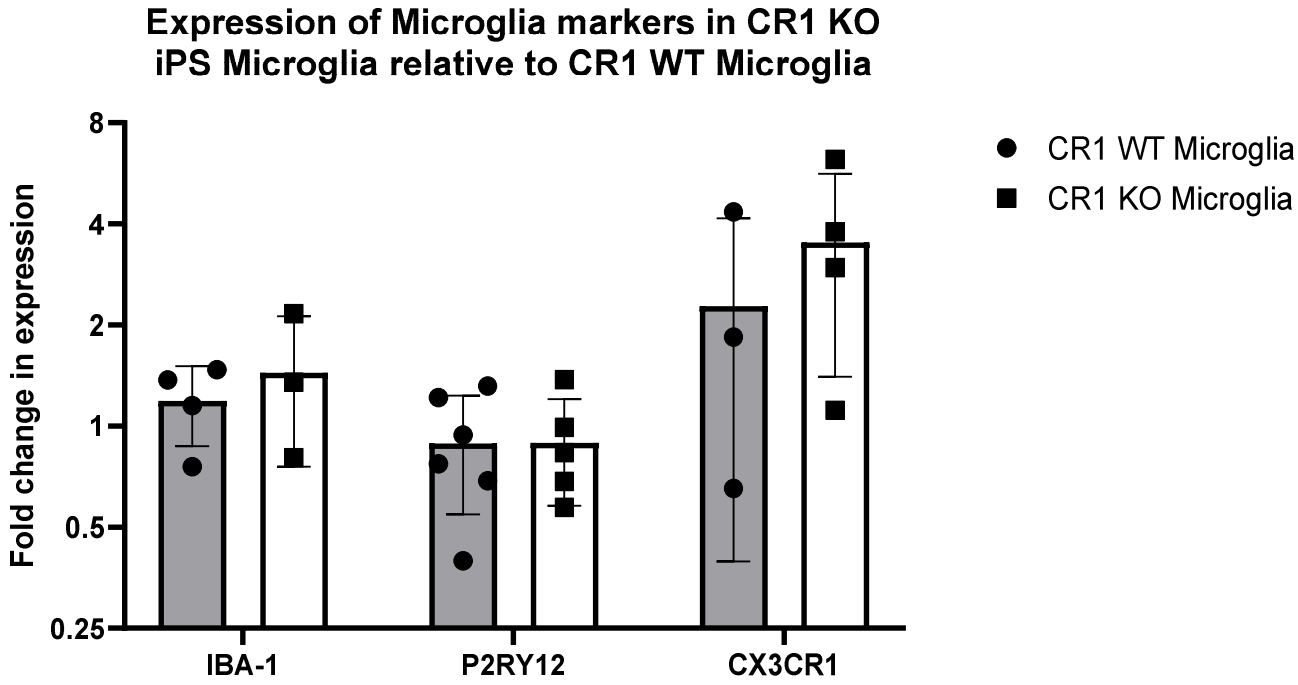

Figure 5.10: No significant difference of microglia marker expression was shown in CR1 KO iPS microglia when relative to expression in CR1 WT iPS microglia.
*Expression of microglia markers in CR1 KO iPS markers was not significantly different to the expression in CR1 WT iPS microglia. Error bars represent the SD. A multiple Mann-Whitney test with post hoc Holm-Sidak multiple comparison was performed with significance set at * P< 0.05; ** P < 0.01; *** P<0.001; ****P<0.0001. Absence of asterisk indicates no significant difference with P > 0.05.*

5.3 Discussion

Three homozygotic CR1 KO iPS clones were successfully generated and characterised using CRISPR spCas9. Knock out clones were identified with an initial PCR screen and subclones picked and ran in parallel to ensure no contamination with other genotypes had occurred and to produce a bank of subclones for subsequent work. Homozygotic KO clones (D8, C3 and G3) and two WT non-edited clones (D2 and B7) were expanded and taken forward.

All clones taken forward had no off-target effects as confirmed by PCR. Primers used in figure 5.3 were designed flanking the potential site of edit and revealed no change in *Cr1L* to have been generated. Low off target effects is a major benefit of CRISPR technology over other genetic tools such as ZFN and TALEN which are known to occasionally result in unplanned edits[252]. CRISPR efficiency is partly modulated by the method of machinery introduction. For the generation of KO, use of ribonucleoprotein (RNP) complex is sufficient[194]. The RNP consists of a fluorescent trans activating CRISPR RNA (tracrRNA) which hybridizes to the guide RNA (gRNA) and Cas protein, providing a linker for the two machineries (the guide RNAs and the Cas endonuclease)[209]. Introduction via RNP allows for the degradation and removal of cas by the cell. More complicated CRISPR edits (such as those introducing a specific nucleotide change that require a template) can require insertion of the machinery into a vector such as a plasmid[210,211]. In this circumstance the cas is continuously produced, increasing on-target efficiency and off-target binding.

Uptake of the RNP complex was encouraged by electroporation, once transported into the nucleus, guides can directly bind to the complementary region of interest, directing the cas9 endonuclease with it[194,209,210]. The Cas protein (in this case spCas9) binds to 3 bp upstream of its relevant PAM site (in this case -NGG) where it causes a DSB[210]. The DNA then attempts to repair itself with endogenous repair mechanisms such as non-homologous end joining (NHEJ) or homology directed repair (HDR)[194,209,210]. NHEJ is an error prone mechanism in which the cell attempts to repair a break in the DNA with insertion of random available nucleotides[194,209,210]. This results in a transcript with some indels inserted or lost around a point of edit, which is likely to result in a frame shift mutation[209,210,252]. Following a frame shift mutation, it is statistically likely that at some point an addition of PTC will occur, which is sufficient to trigger nonsense mediated decay (NMD) pathways[249,251,254].

NMD is a translation coupled protective mechanism, physiologically used to stop the generation of nonsense mRNA and faulty proteins[249–251,254]. One mechanism to trigger NMD is detection of an PTC. However, in order for NMD to be triggered it is vital PTC are distinguished from normal wild type stop codons[249]. This mechanism occurs differently across species, in mammals this event has shown to be linked to the proximity of the PTC and the exon junction complex (EJC). The EJC are added to pre-mRNA, after splicing, and lie 20-24 nucleotides upstream to exon-exon junctions[249,250]. When PTC lie 50-55 base pairs upstream of the final exon-exon junction NMD can be triggered[250]. Alternatively, addition of PTC in front of an intron has also shown to be sufficient to trigger NMD, following the observation of degradation when introns are artificially inserted after a normal stop codon[250]. The introduction of a PTC was investigated in CR1 KO clones, as shown in figure 5.2. Clones were sequenced following a pre-PCR screen using direct sanger sequencing. This indicated the generation of an edit of varying sizes in all three homozygotic KO clones. Clone D8 showed a clear cut in the expected region, with no additional indel insertion. However, clones C3 and G3 show a more complicated product with multiple different indels inserted in between the breaks. These sequences were then checked for frame shift mutations and changes in the reading frame, shown in figure 5.2d.

Indeed, all three showed a frame shift of translation. Despite different transcripts, translation of D8 and G3 indicate the same product is generated with a PTC added within exon 3, in a sufficient position to trigger NMD. However, clone C3 produced a different translation product, conserving more of exon 2 due to a higher number of random indels being added. Regardless, a PTC is observed upstream of the exon-exon junction indicating despite these differences the edit should be sufficient to degrade CR1 message before translation. This is an important indicator for the success of the CRISPR KO, particularly important prior to differentiation of cells but is not sufficient to confirm the absence of CR1 in differentiated cells which required message and protein analysis. Previous studies investigating the efficiency of CRISPR saw that KO of 193 transcripts in different cell lines resulted in 1/3 of them to still produce the target protein, albeit the majority of them truncated or non-functional[255]. They owed these alteration to either exon skipping or translation re-initiation[255]. Therefore, characterisation of differentiated IPS cells for the absence of CR1 was performed using a range of techniques; RT-qPCR, immunofluorescence (fixed and live) and western blotting.

Protein characterisation revealed the absence of CR1 protein on CR1 KO cells, with western blotting producing no bands when 30ug of D8, G3 and C3 are loaded but WT D2 retaining a single band at 190kDa. This shows CR1 KO has been successful, providing further support to the expression of CR1 on iPS microglia. Data on transcript provided a more complicated story. RT-qPCR analysis revealed amplification of transcript to still occur, although at a lesser amount that in WT cells. Initially it was proposed that primers bind before the edit. However, mapping of the primer revealed this to not be the case. The presence of transcript is likely due to NMD occurring during translation, occurring when the PTC is detected in the already formed transcript[251,254]. Therefore, message is still generated but then degraded, meaning primers can still bind to the Cr1 message. The lower amount of transcript in CR1 KO is due to some message being degraded which would not occur in CR1 WT clones. This has been reported in previous reports which state different efficiencies for NMD between different cells and for different edits[255]. Therefore, presence of transcript does not necessarily suggest the production of protein in this instance.

Alongside confirmation of CR1 KO, cells were characterized for the successful differentiation to iPS microglia. Previous animal studies investigating the murine orthologue for CR1, showed KO of crry to be embryonically lethal, triggering maternal complement attack on the developing foetus[161,164,248]. Back crossing of crry-/- onto other complement backgrounds including C4 depletion, FH (Factor H) depletion and C5 depletion was used and revealed C4 depletion to offer no protection, C5-/- only a weak protection but FH -/- to completely protect the embryos indicating activation to be mostly in dependant on alternative pathway[248]. The embryos were further rescued by back-crossing onto a C3 depleted genetic background or treatment of C5 antibody inhibitors during foetal development[178]. Examination of crry-/- pups which survived revealed no obvious phenotypes however microglia appeared primed, an interesting observation in the context of LOAD[164]. Therefore, it was important to ensure CR1 KO did not have an effect on differentiation or subsequent microglia phenotype, although it is important to note this is unlikely as failures in crry-/- models is considered an effect of excess complement attack on the placenta. For this reason, initial differentiations included CR1 KO het clones so to ensure cells could indeed differentiate and to provide an intermediatory phenotype for comparison. Indeed, homozygotic and heterozygotic CR1 KO clones were successfully differentiated to an iPS microglia phenotype. Immunofluorescence staining confirmed all cells to express microglia marker CD11B and IBA-1. Additional transcript data revealed homozygous CR1 KO clones to generate transcript for multiple microglia markers confirming the successful differentiation to iPS microglia.

iPS cells are particularly vulnerable to genomic changes through passaging. Illumina Global Screening Array was used to identify large copy number variants in 3 CR1 WT clones, 5 of which had gone through the CRISPR; 2 wildtypes (D2 and B7), and 3 homozygotic CR1 KO clones (D8, C3 and G3). The DNA extraction was done alongside generation of cells, to ensure the passage checked was consistent with the passage used to generate the majority of data. Examination of 6 clones showed no trisomy of any chromosomes but did see 3 duplications and 2 deletions, consistent in all clones. These changes were all consistent with previous passages ran through this CNV check, supporting no additional changes occurred when passaging the cells for this work. Despite this there is one exception in clones D2 and KOLF2 which show a separate duplication at 20q11.21. This duplication is unsurprising as the international stem cell initiative saw this amplification in 20% of 125 human embryonic stem cell lines and in 18% of iPSC and is commonly seen in human cancers suggesting this results in an increase proliferative phenotype[256,257]. Previous iPS researchers reveal the 20q11.21 location to contain sequences for three genes; ID1, HMI3 and Bcl-xl, they revealed duplication in this area to not affect protein expression of ID1 and showed HM13 have a limited function not related to differentiation of iPS cells, it is unclear how this could affect differentiated cell function.

Knock out of CR1 provides a useful tool in confirming the expression of CR1 on IPS microglia. Additionally, they are a good model for understanding some potential functional roles of CR1 on cells. However, it is important to remember that KO is a blunt model, not physiologically relevant to LOAD pathology. Future work should look to generate isogenic IPS lines of different CR1 isoforms so to study to specific effect of size allele on microglia function. Additional SNPs which have been flagged through LOAD GWAS could provide a more targeted interest, for example, rs484460 which lies within LHRD and is associated with cognitive disruption in patients could be generated with the introduction of a pre-designed template[76]. However, this could provide difficulties due to the highly homologous nature of CR1 but could be overcome with use of adapted cas proteins such as cas nikases. Nikases would produce a single break, using four of these could increase target specificity in targeting. Alternatively editing cells which posses the long CR1-S form so to produce CR1-F may be provide a model useful to pull apart the effect of SNP highlighted in LOAD[210]. Regardless, blunt KO of CR1 is extremely useful in first confirming expression of CR1 on different CNS cell types and as a beginning look at how CR1 may be involved in basic cellular functions.

6.0 Functional comparison of CR1 WT and CR1 KO iPS microglia

6.1 Introduction

The complement system refers to a series of >30 proteins which interact together through three main pathways: the CP, the AP and the LP[85,86]. The majority of peripheral complement is synthesized by hepatocytes in the liver, with the exception of factors C1q, properdin and C7 which are predominantly produced by leukocytes, and factor D which is synthesised by adipose tissue[138]. Hepatic-derived complement proteins circulate in the plasma, allowing them to penetrate tissues to mediate complete immune defence. However, a smaller scale but likely important local production of complement occurs in extrahepatic tissues and organs[258,259]. Evidence for this is shown through transplant studies, which implicate the kidneys as the secondary major complement source, showing a single donated kidney makes up around 5% of circulating C3[260]. Indeed, extrahepatic complement sources are thought to constitute ~10% of circulating complement proteins[258]. Recently evidence for local CNS complement synthesis has been demonstrated alongside an emerging role for complement in a number of neurological diseases[138,261].

Unlike most other organs, the brain exists in an immune privileged environment in which the blood brain barrier (BBB) closely restricts the movement of cells and plasma proteins, including complement proteins[138,262]. Despite this, there is growing evidence for a role of complement in the CNS, indicating local production of complement proteins. The brain cellular source for each component remains mostly elusive with data from primary cells and cell lines currently providing the majority of data. This has revealed that most complement components are synthesized within the CNS, with transcript data of human primary oligodendrocytes revealing the presence of all CP and TP components[263]. A human oligodendrocyte cell line (HOG cells) supports this, adding expression data for complement regulators such as CD59, decay accelerating factor (DAF), membrane cofactor protein (MCP/CD46) and C1-inhibitor (C1INH)[144]. This regulator expression was mirrored in a human astrocyte cell line which also expressed receptor for C5a (C5aR)[246,264]. Similarly, human neuronal cells have been shown to express message for the majority of complement components including C4, C9, C1q, FH, C1INH, C3, C6 and Factor B (FB)[265]. Mapping the presence (or absence) of complement receptors and regulators could provide essential information into individual brain cell roles in the CNS complement system. Additionally, this will indicate whether certain cell types have increased vulnerability to complement attack, which would exacerbate pathology in some diseases. This is of particular interest as complement has been indicated in AD by multiple methods.

A role for complement in AD pathology has been shown by increased presence of message and protein of AP components in post-mortem tissue from AD patients compared to non-demented controls[266]. Key AP proteins, FB, FI and FH were increased in AD brain tissue compared to non-demented tissue, implicating upregulation of the AP in AD[266]. However, the most convincing evidence for a causative role of complement in AD is derived from GWAS studies which show CR1/CD35 to be a high impact risk factor for developing LOAD.

CR1 is a complement receptor and regulator, capable of binding the opsonizing fragments C3b, C4b and C1q. Primarily, CR1 is a co-factor for FI in the breakdown of C3b to iC3b, the former being a ligand for phagocytosis receptor CR3. CR1 and FI also work together in the accelerated decay of C3 and C5 convertases of the classical and alternative pathways. These two functions act to keep the complement system in check[86]. Initial GWAS studies identified two SNPs of CR1 associated with AD.

Coding SNP rs4844609 results in a single amino acid change, T1610S, in a region reported to bind C1q; indeed increased C1q binding has been shown in the presence of this SNP[102,141]. The presence of this SNP in LOAD patients associated with increased neuropathological features and decline in episodic memory relative to individuals with mild cognitive impairments, in an Apoe dependent fashion[141]. The second SNP, rs6656401, lies within an intronic region and is strongly associated with the CR1 length polymorphism. Additional SNPs in CR1 have since been implicated in AD through different cohorts, for example, Han Chinese populations show associations with CR1 SNPs rs116806486 and rs669117 but these do not reach significance in other populations[138,267] How these polymorphisms alter CNS cell function in physiological and pathological conditions remains unclear. Initial studies have utilized murine microglia cells, which express the CR1 orthologue Crry, to indicate a role for CR1 in microglia functions. These show Crry involvement in microglial uptake of Aβ oligomers and production of pro-inflammatory cytokines following LPS and Aβ stimulation[162]. However, these studies have not been replicated on human models.

The first aim of this chapter was to generate relative complement transcript expression data in three iPS brain cell lines using high-throughput RT-QPCR. The same technique was then used to compare complement expression at baseline and after LPS stimulation in CR1 WT iPS microglia and CR1 KO iPS microglia. Functional assays then focused on microglia specific roles. This included comparing production of pro-inflammatory cytokine transcript after LPS stimulation and phagocytosis of e-coli bioparticles in multiple opsonization conditions.

6.2 Results

6.2.1 High-throughput QPCR

A Fluidigm 96.96 microfluidics chip was used to conduct high-throughput RT-qPCR on a range of RNA samples extracted from CR1 WT and CR1 KO iPS microglia, unstimulated and stimulated with 100ng/ml LPS for 6 hours, iPS astrocytes and iPS cortical neurons. A large panel of primers was used covering a range of categories, including: i) differentiation genes to confirm cell phenotypes (data in previous chapters); ii) A panel of activation markers including 2 pro-inflammatory cytokines and, iii) complement factors and regulators. Data was analyzed using Fluidigm RT-QPCR analysis software producing relative fold changes following the ΔΔCT method. ΔΔCT first normalizes data to housekeepers, in this instance multiple housekeepers were used, including: SDHA, HPRT, UBC, ACTB and GAPDH, summarized as 'multiple housekeepers' in the text below. The second part of ΔΔCT analysis is comparing normalized data to expression in another condition or cell type, which is specified for each data set in the heading of each graph. All RNA was DNAse treated to eliminate contaminating DNA, and primers were designed across an exon-exon junction to ensure they did not amplify genomic DNA.

6.2.1.1. Complement transcript in iPS microglia relative to undifferentiated iPS cells

Figure 6.1 shows expression of most complement factors to not be significantly up regulated through the differentiation of iPS cells to iPS microglia.. This is most likely due to large variance in the values, skewing the data which could be improved by increasing the power of the experiment. Similarly, complement regulators and receptors showed no significant increases in transcript expression with differentiation to iPS microglia. The exception to this is CR1 which is significantly increased (P=0.0027).

A

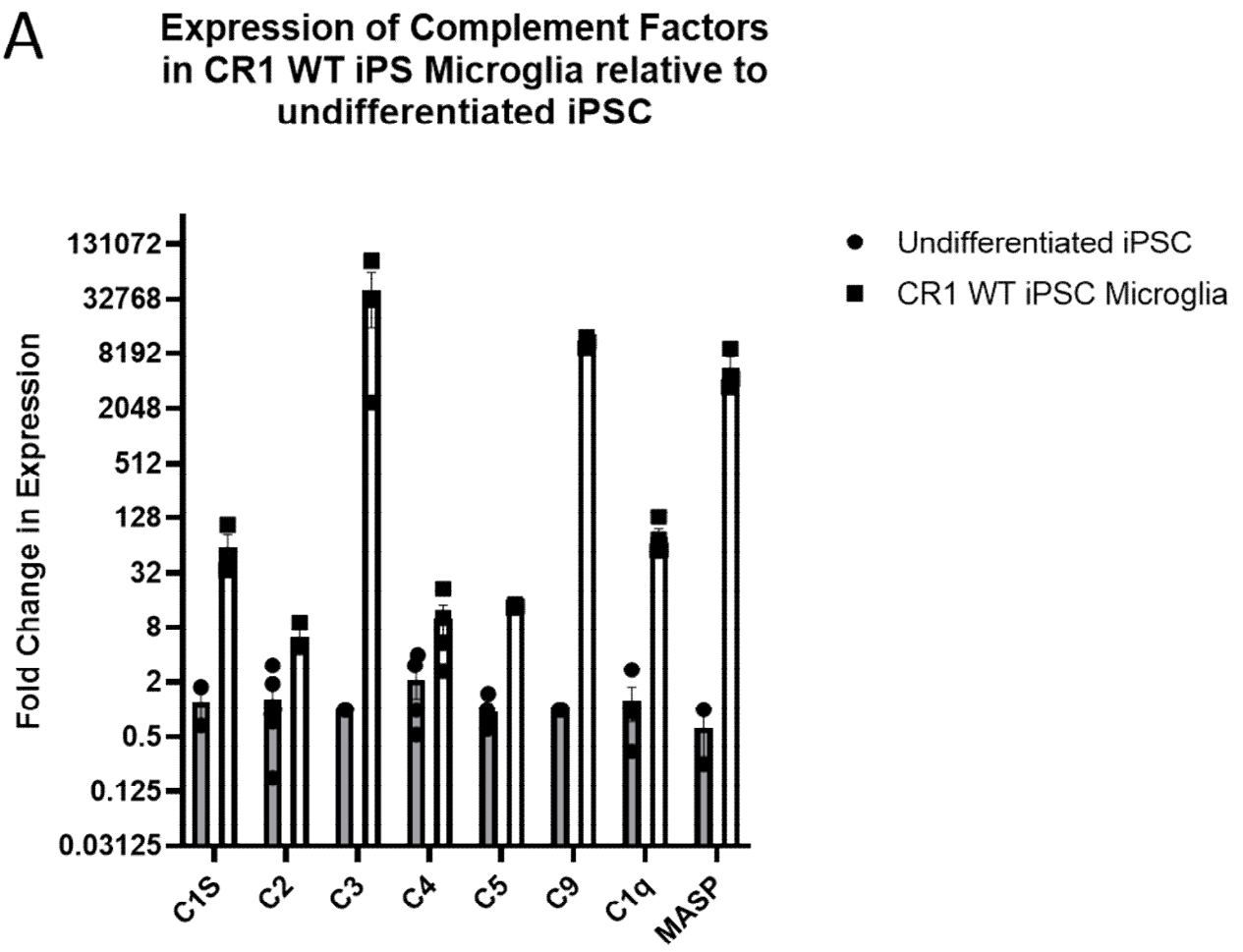
Expression of Complement Factors in CR1 WT iPS Microglia relative to undifferentiated iPSC
Fold Change in Expression
131072
32768
8192
2048
512
128
32
8
2
0.5
0.125
0.03125
C1S
C2
C3
C4
C5
C9
C1q
MASP
Undifferentiated iPSC
CR1 WT iPSC Microglia

B

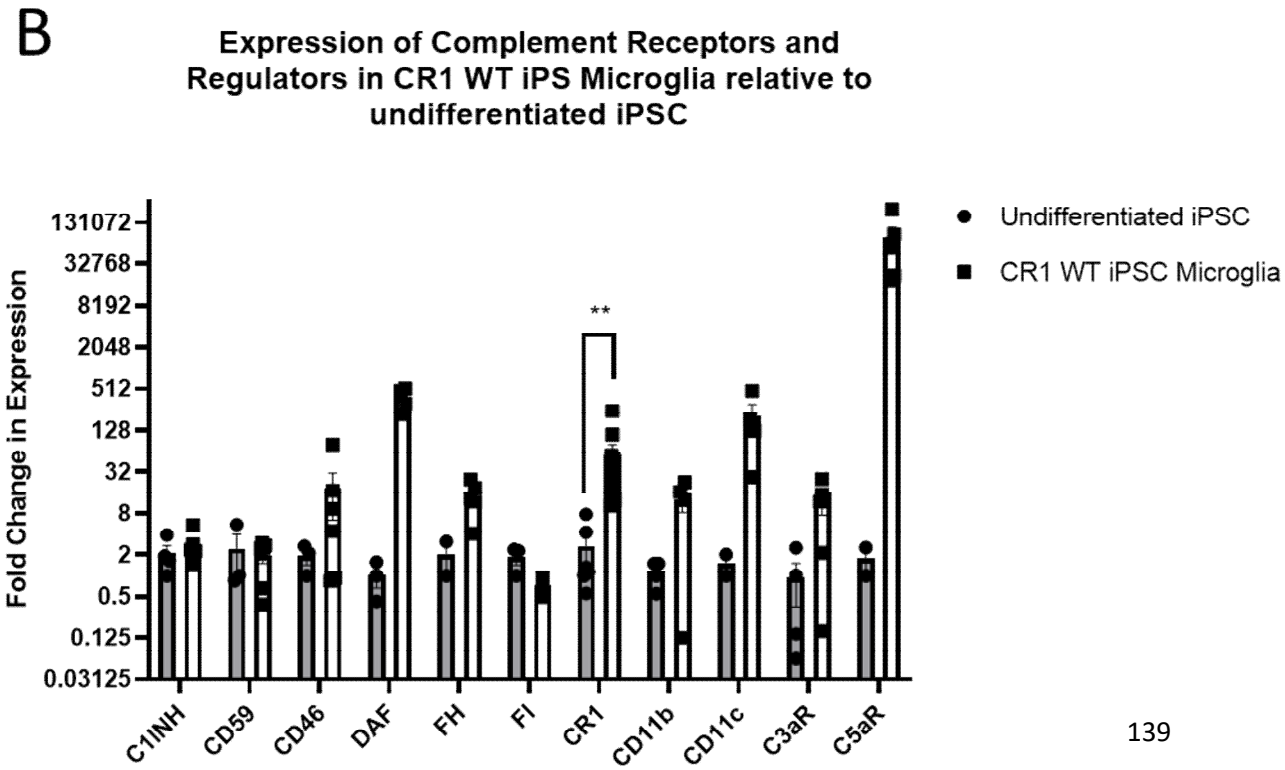
Expression of Complement Receptors and Regulators in CR1 WT iPS Microglia relative to undifferentiated iPSC
Fold Change in Expression
131072
32768
8192
2048
512
128
32
8
2
0.5
0.125
0.03125
**
C1INH
CD59
CD46
DAF
FH
FI
CR1
CD11b
CD11c
C3aR
C5aR
Undifferentiated iPSC
CR1 WT iPSC Microglia

Figure 6.1: Complement factor, receptor and regulator message expression in iPS microglia relative to expression in undifferentiated iPSC.

*A) Expression of complement factors reveal no significant changes in expression with differentiation to iPS microglia. Lack of significant findings is likely due to increased variability of data points which is discussed in section 6.3 of this chapter. B) Expression of most complement receptors and regulators in iPS microglia were not significant when relative to undifferentiated iPS cells, with the exception of CR1 which (P = 0.0027). Lack of significant findings is likely due to increased variability of data points which is discussed in section 6.3 of this chapter. Error bars represent the SD. A multiple Mann-Whitney test with post hoc Holm-Sidak multiple comparison was performed with significance set at * P< 0.05; ** P < 0.01; *** P<0.001; ****P<0.0001. Absence of asterisk indicates no significant difference with P > 0.05.*

As the complement system is primarily an immune/inflammatory pathway, changes of complement transcript after 6-hour 100ng/ml LPS treatment was measured. Figure 6.2 shows change in complement factors (figure 6.2a), regulators and receptors (figure 6.2b) in stimulated CR1 WT iPS microglia relative to unstimulated CR1 WT iPS microglia.

Complement factors showed small changes in transcript in stimulated iPS microglia relative to unstimulated iPS microglia but none of these changes were significantly different. Similarly, complement receptors and regulators expression in stimulated iPS microglia shows slight differences compared to non-stimulated iPS microglia however none reached significance. The one exception to this is CR1 which was significantly upregulated 4 fold (P=0.024).

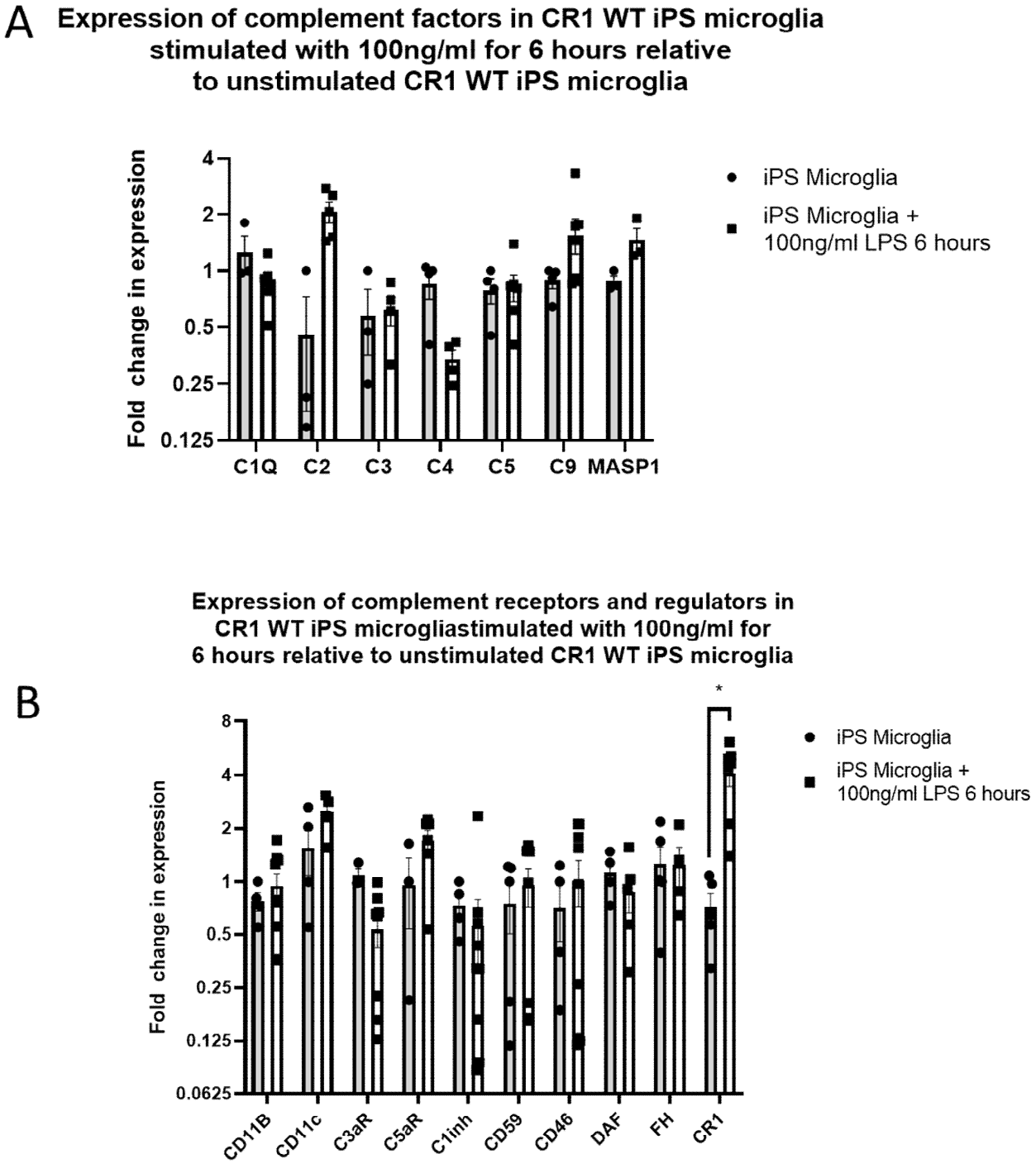

Figure 6.2: Complement factor, receptor and regulator message expression iPS microglia stimulated with 100ng/ml LPS for 6 hours relative to unstimulated iPS microglia.

A) Expression of complement factors reveal no significant changes in expression with stimulation of iPS microglia with LPS. B) Expression of most complement receptors and regulators in iPS microglia were not significant when relative to undifferentiated iPS cells, with the exception of CR1 which (P = 0.024). Error bars represent the SD. A multiple Mann-

*Whitney test with post hoc Holm-Sidak multiple comparison was performed with significance set at * P< 0.05; ** P < 0.01; *** P<0.001; ****P<0.0001. Absence of asterisk indicates no significant difference with P > 0.05.*

6.2.1.2 Comparison of CR1 WT and CR1 KO iPS microglia complement transcript expression

Figure 6.3 shows change in expression of complement component transcript at baseline in CR1 KO iPS microglia relative to CR1 KO undifferentiated cells. All complement factors were increased with differentiation, as was seen in CR1 WT microglia in figure 6.1. Complement factor C4 message was significantly increased 32-fold (P=0.016) and C9 was significantly increased by 8192-fold (P=0.035). No other changes in complement factor were significantly changed. Similarly, no significant changes in complement regulators and receptors were observed with differentiation of CR1 KO iPS cells to iPS microglia.

A

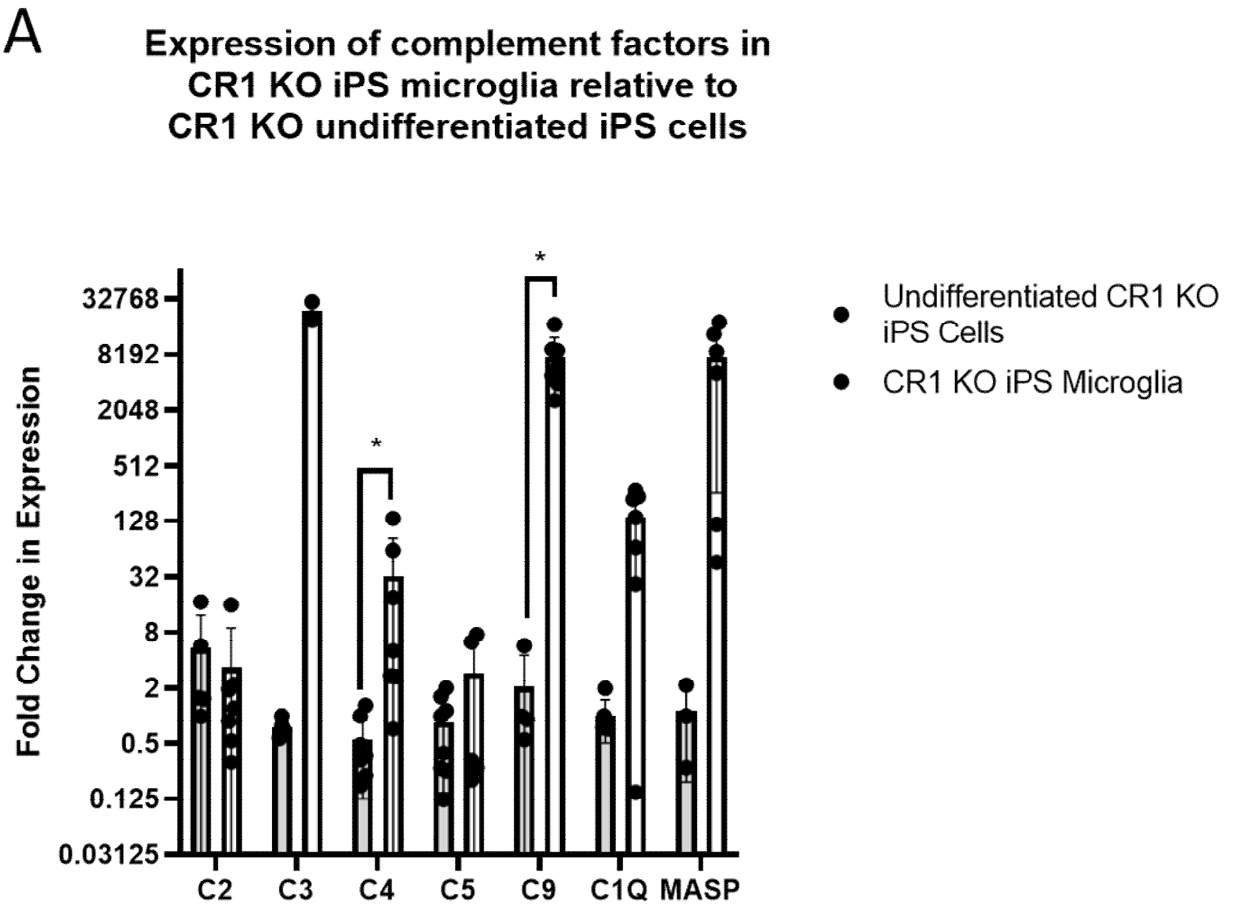
Expression of complement factors in CR1 KO iPS microglia relative to CR1 KO undifferentiated iPS cells
Fold Change in Expression
32768
8192
2048
512
128
32
8
2
0.5
0.125
0.03125
*
*
C2
C3
C4
C5
C9
C1Q
MASP
Undifferentiated CR1 KO iPS Cells
CR1 KO iPS Microglia

B

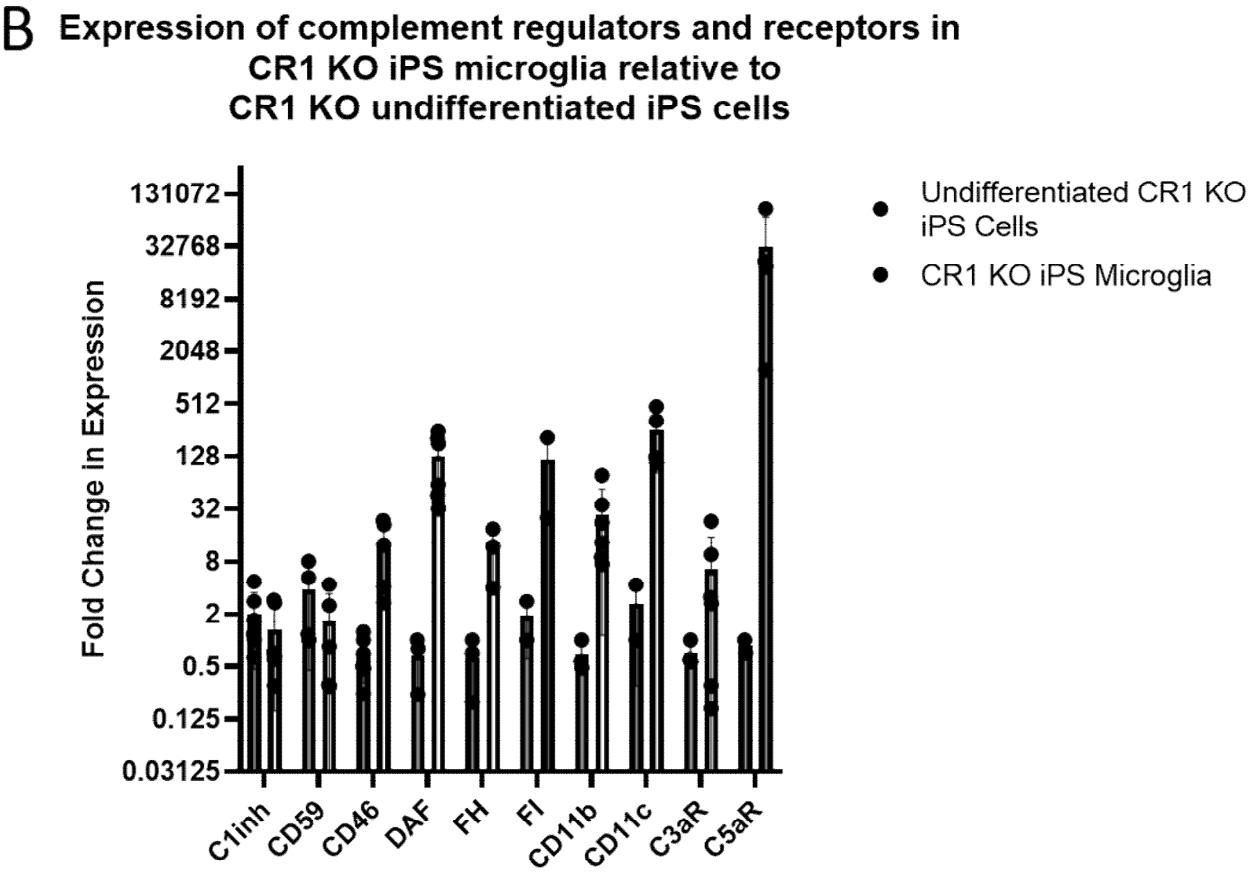
Expression of complement regulators and receptors in CR1 KO iPS microglia relative to CR1 KO undifferentiated iPS cells
Fold Change in Expression
131072
32768
8192
2048
512
128
32
8
2
0.5
0.125
0.03125
C1inh
CD59
CD46
DAF
FH
FI
CD11b
CD11c
C3aR
C5aR
Undifferentiated CR1 KO iPS Cells
CR1 KO iPS Microglia

Figure 6.3: Complement factor, receptor and regulator message expression in CR1 KO iPS microglia relative to expression in CR1 KO undifferentiated iPSC.

*A) Expression of complement factors show significant increases in C4 (p=0.016) and C9 (P=0.035) in CR1 KO iPS microglia relative to undifferentiated CR1 KO iPS cells. B) Expression of most complement receptors and regulators in CR1 KO iPS microglia were not significant relative to CR1 KO undifferentiated iPS cells. Error bars represent the SD. A multiple Mann-Whitney test with post hoc Holm-Sidak multiple comparison was performed with significance set at * P< 0.05; ** P < 0.01; *** P<0.001; ****P<0.0001. Absence of asterisk indicates no significant difference with P > 0.05.*

Figure 6.4 shows the expression of complement in CR1 KO iPS microglia relative to expression of complement in CR1 WT iPS microglia. This revealed no significant differences in complement factor, receptor, or regulator expression between CR1 WT iPS microglia and CR1 KO iPS microglia.

A

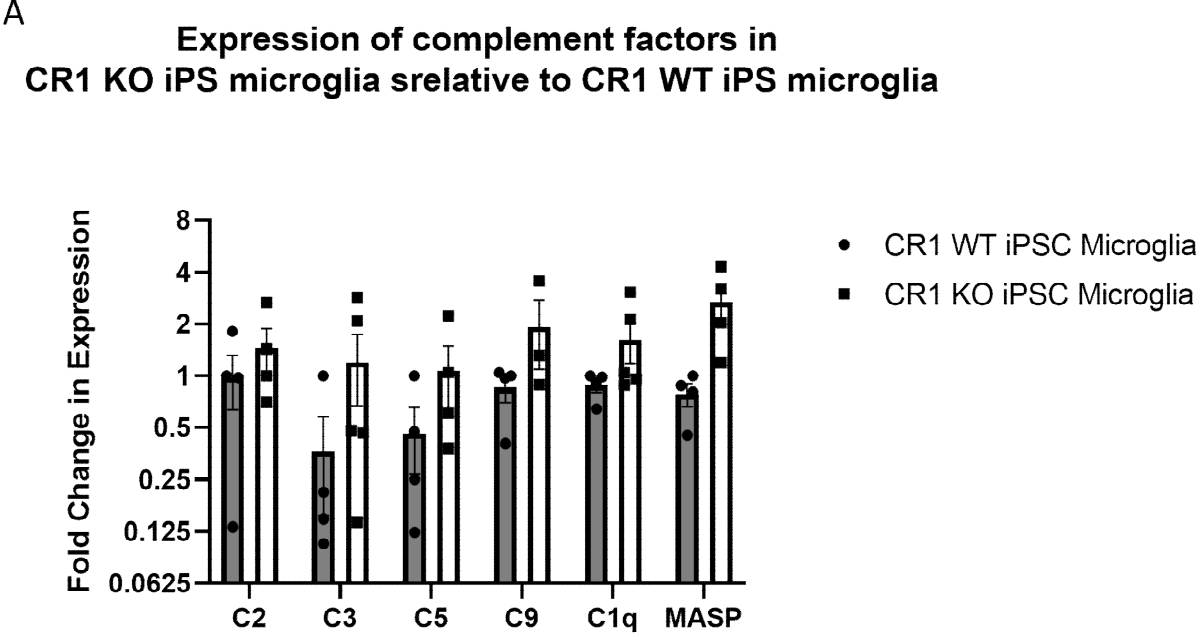

B

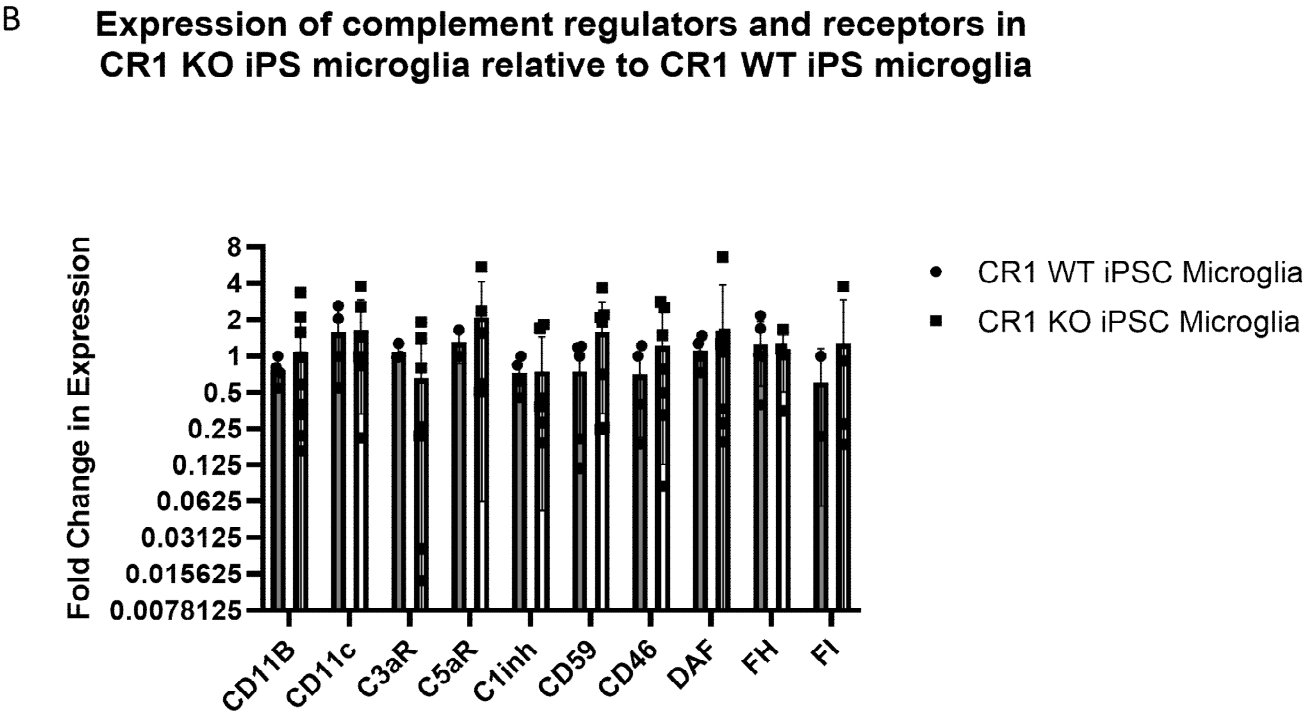

Figure 6.4: Complement factor, receptor and regulator message expression in CR1 KO iPS microglia relative to CR1 WT iPS microglia

*A)Expression of complement factors reveal no significant changes in expression between CR1 KO and CR1 WT iPS microglia. B) Expression of complement receptors and regulators CR1 KO iPS microglia were not significantly different than expression in CR1 WT iPS microglia. Error bars represent the SD. A multiple Mann-Whitney test with post hoc Holm-Sidak multiple comparison was performed with significance set at * P< 0.05; ** P < 0.01; *** P<0.001; ****P<0.0001. . Absence of asterisk indicates no significant difference with P > 0.05.*

CR1 KO iPS microglia were stimulated with LPS alongside CR1 WT iPS microglia. Figure 6.5a shows changes in complement factor expression in CR1 KO iPS microglia differentiated from undifferentiated CR1 KO iPS cells. This revealed a significant upregulation of complement factor C5 which was upregulated 7-fold (P=0.005) however no other complement factor was significantly altered when CR1 KO iPS microglia were stimulated with LPS. Figure 6.5b shows only C1inh was significantly upregulated 3-fold (P=0.02) while no other regulators and receptors changes reached significance.

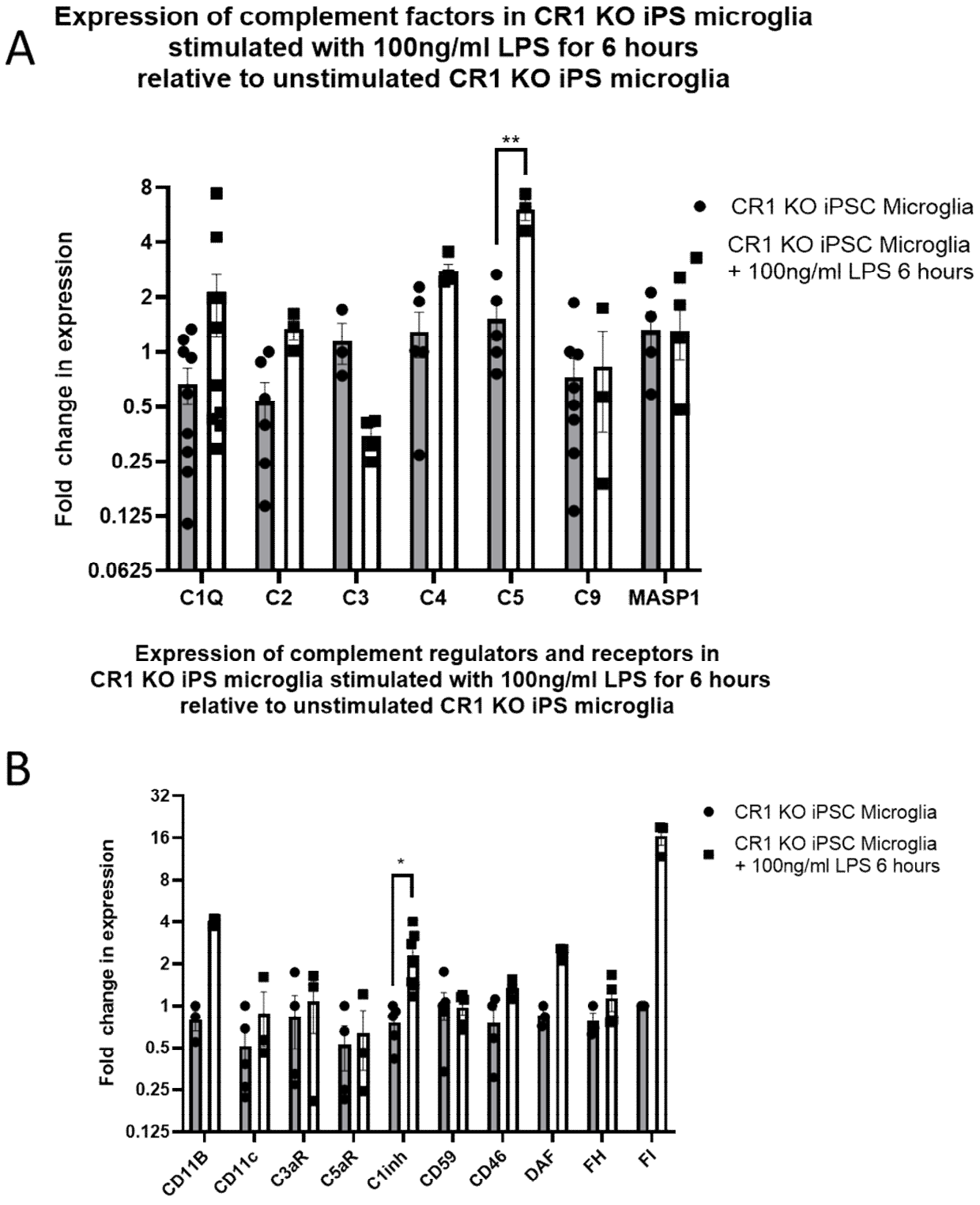

Figure 6.5: Complement factor, receptor and regulator message expression in CR1 KO iPS microglia stimulated with 100ng/ml LPS for 6 hours relative to unstimulated CR1 KO iPS microglia

A) Expression of most complement factors reveal no significant changes in expression when CR1 KO iPS cells are stimulated with LPS. Exception to this is C5 which was significantly upregulated (P = 0.005). B) Expression of most complement receptors and regulators in stimulated CR1 KO iPS microglia were not significant when relative to unstimulated CR1 KO iPS

*microglia. The exception to this is C1inh (P=0.02) which is significantly upregulated. Error bars represent the SD. A multiple Mann-Whitney test with post hoc Holm-Sidak multiple comparison was performed with significance set at * P< 0.05; ** P < 0.01; *** P<0.001; ****P<0.0001. Absence of asterisk indicates no significant difference with P > 0.05.*

Comparison of transcript levels in LPS-stimulated CR1 KO versus CR1 WT is shown in figure 6.6. This reveals two factors to be significantly reduced in activated CR1 KO iPS microglia compared to CR1 WT iPS microglia; C1q which was downregulated 77% (P=0.017) and C3 which was downregulated 75% (P= 0.03). Other complement factor C4 was significantly upregulated 3.1-fold (P=0.017). No significant changes in complement regulators and receptors were detected.

A

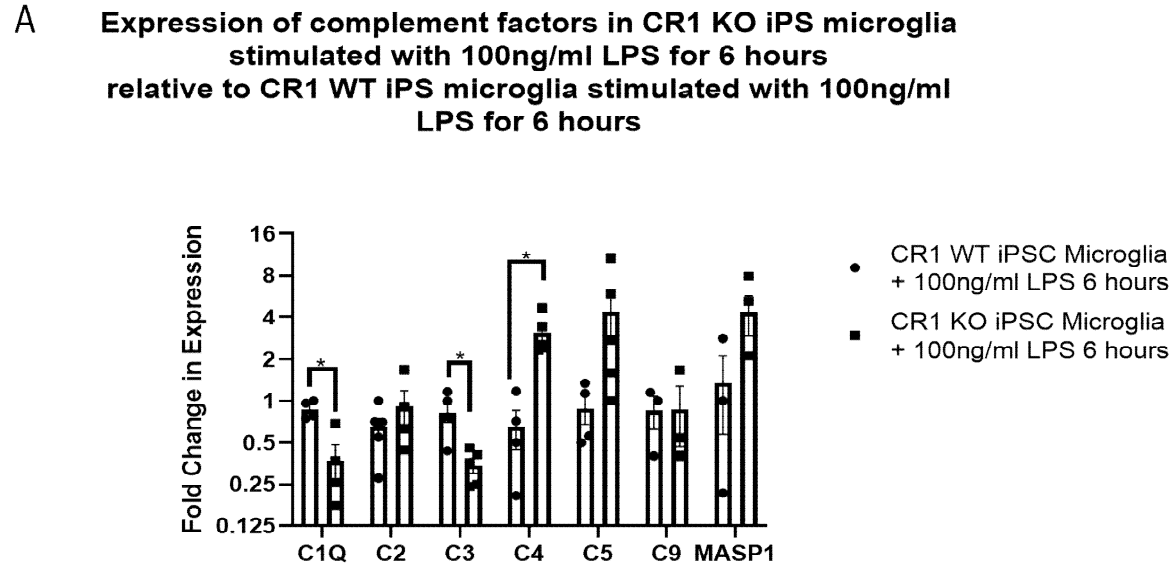

B

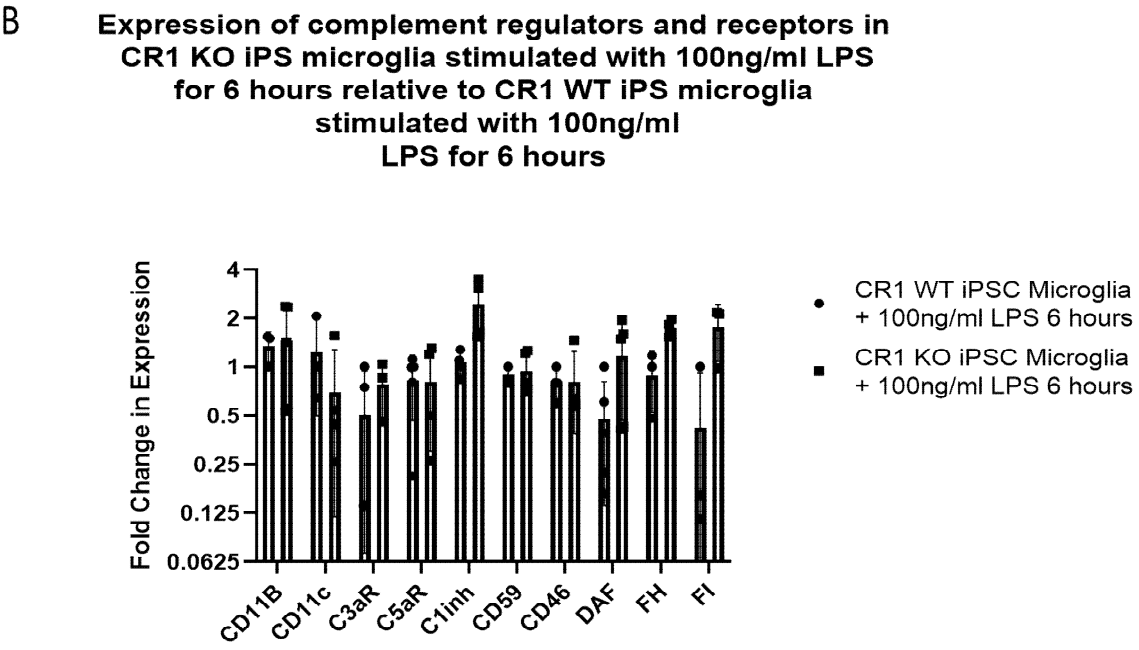

Figure 6.7: Complement factor, receptor and regulator message expression in CR1 KO iPS microglia stimulated with 100ng/ml LPS for 6 hours relative to CR1 WT iPS microglia stimulated with 100ng/ml LPS for 6 hours *A) Expression of complement factors reveal significant reductions in C1Q (P=0.04) and C3 expression (p=0.03) while expression of C4 is significantly increased (P=0.017) in stimulated CR1 KO iPS microglia relative to stimulated CR1 WT iPS microglia. B) Expression of complement receptors and regulators in stimulated CR1 KO iPS microglia were not significantly different to expression in stimulated CR1 WT iPS microglia. Error bars represent the SD. A multiple t-test with post hoc Holm-Sidak multiple comparison was performed with significance set at * P< 0.05; ** P < 0.001; *** P<0.001; ****P<0.0001. Absence of asterisk indicates no significant difference with P > 0.05.*

6.2.1.3 Effect of CR1 KO on expression of transcript for inflammatory mediators following LPS challenge

Activation of microglia elicits a series of events including the upregulation of key pro-inflammatory cytokines and transcription factors. Data in an earlier results chapter, (chapter 3; figure 3.19) showed that iPS microglia significantly increased pro-inflammatory cytokine and increases in mediator transcript following LPS treatment. The same panel was used to measure changes in transcript in CR1 KO iPS microglia relative to undifferentiated iPS cells. Figure 6.8 shows transcript levels for all four inflammatory mediators increased in response to LPS. *IL-6* and *TNFa* were. *NLRP3* and *NFKB* showed smaller increases. None of these changes was statistically significant.

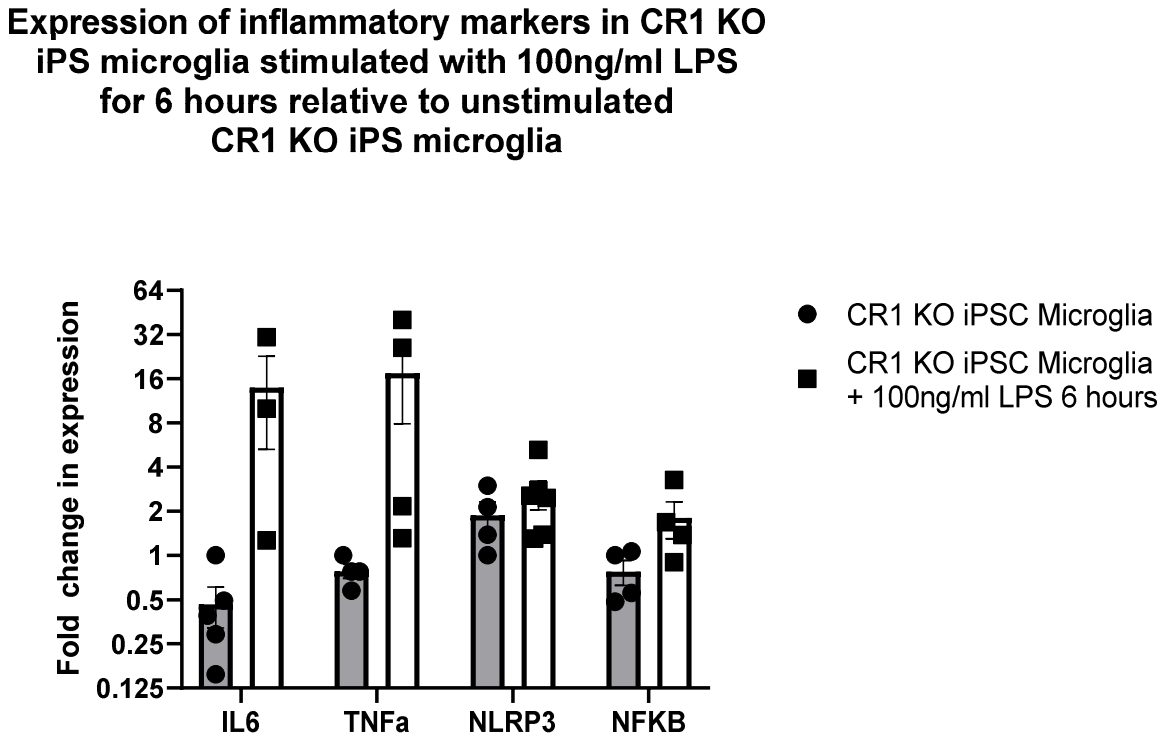

Figure 6.7: Message expression of inflammatory markers in CR1 KO iPS microglia stimulated with 100ng/ml LPS for 6 hours compared to expression in unstimulated CR1 KO iPS microglia.

*None of these markers were significantly upregulated with stimulation of CR1 KO iPS microglia. Error bars represent the SD. A multiple Mann Whitney test with Holm-Sidak post hoc was used with significance set to * P< 0.05; ** P < 0.01; *** P<0.001; ****P<0.0001. Absence of asterisk indicates no significant difference with P > 0.05.*

Comparison of inflammation markers transcript between stimulated CR1 KO iPS microglia and stimulated CR1 WT iPS microglia is shown in figure 6.8. This indicates the KO of CR1 to produce less transcript of activation products upon stimulation with LPS compared to WT CR1 iPS microglia. Statistical analysis revealed IL-6 transcript to be reduced 95% (P=0.01) and TNFα to be reduced 99.3% (P=0.02). Other inflammatory markers did not show significant differences.

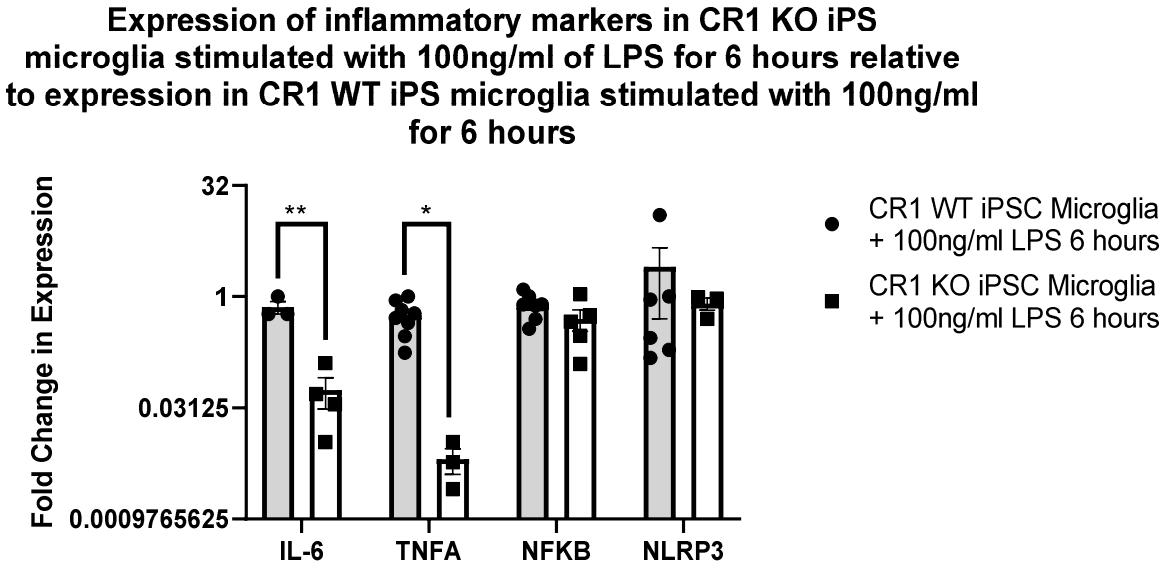

Figure 6.9: Message expression of inflammatory markers in CR1 KO iPS microglia stimulated with 100ng/ml LPS for 6 hours was increased compared to expression in stimulated CR1 WT iPS microglia. *Two key cytokines were shown to have reduced transciprt expression in stimulated CR1 KO iPS microglia relative to stimulated CR1 WT iPS microglia. Cytokine IL-6 was reduced 30% (P= 0.01) while TNFα was downregulated 50% (P=0.02) Error bars represent the SD. A multiple t-test Holm-Sidak post hoc was used with significance set to * P< 0.05; ** P < 0.01; *** P<0.001; ****P<0.0001. Absence of asterisk indicates no significant difference with P > 0.05.*

6.2.2 Measuring changes in protein expression of an cytokine IL-1β

The cytokine IL-1β was measured by ELISA in supernatants of one clone of iPS microglia CR1 WT (D2) and one clone of CR1 KO (G3) following a 24-hour 100ng/ml LPS stimulation. A longer time of LPS exposure was used to enable measurement of changes in protein expression. Figure 6.10 shows that significantly more IL-1β was produced by CR1 WT iPS microglia, averaging around 2.5pg/ml in cell supernatant, compared to homozygous CR1 KO clones where IL-1β levels were 0.06pg/ml (p=0.0059).

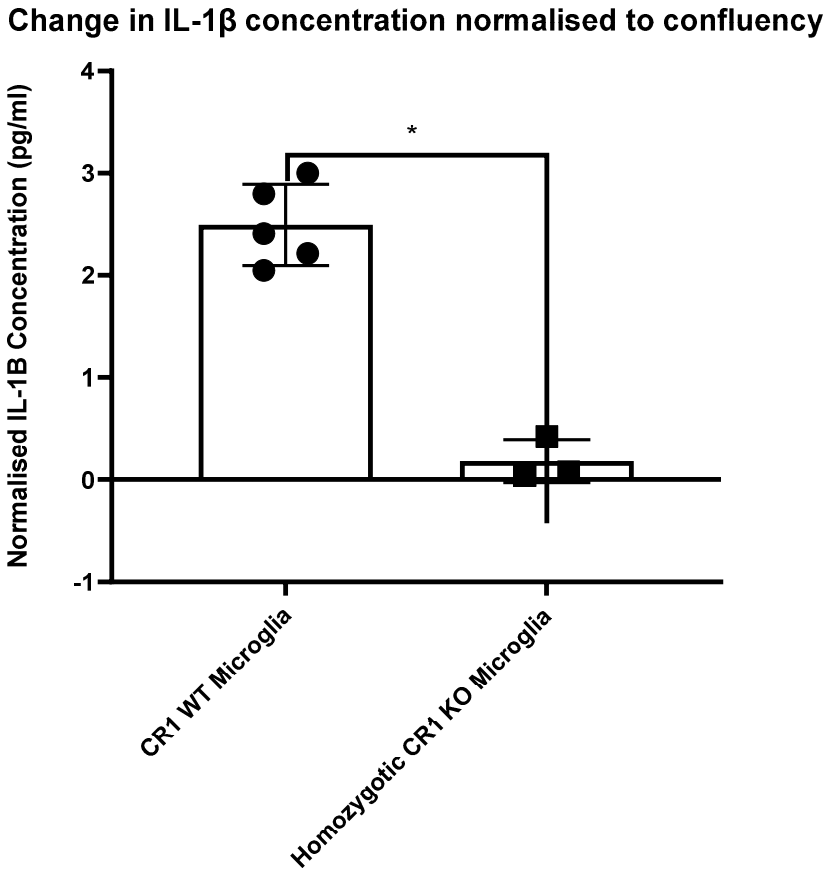

Figure 6.10: IL-1β concentration supernatant in CR1 WT and CR1 KO iPS microglia after stimulation with 100ng/ml for 24 hours.

*Almost no IL-1B was detected in supernatants of homozygotic CR1 KO cell line following stimulation with LPS but 2.5pg/ml was detected in CR1 WT. Values were normalised to confluency measurements collected using IncuCyte software. ANOVA was performed indicating significant difference between CR1 WT microglia and CR1 KO microglia to be significantly different (p=0.0059). Data represents one biological repeat performed in one clone of each, for CR1 WT this was D2 and one cone of homozygotic CR1 KO, G3.As data is non-parametric a Mann Whitney test was performed with significance set to * P< 0.05; ** P < 0.01; *** P<0.001; ****P<0.0001. Cells were all taken from one harvest and were terminally differentiated simultaneously.*

6.2.3 Phagocytosis

6.2.3.1 Phagocytosis of pH-rodo conjugated e-coli beads

In order to test the functional consequences of CR1 KO in iPS microglia, phagocytosis assays were performed using PH-rodo conjugated E coli; these fluoresce red when exposed to an acidic environment within the cell. Following phagocytic engulfment, fluorescence can be detected upon uptake into the acidic lysosome compartment. Phagocytosis was inhibited by treatment with 10µM Cytochalasin D (Cyto D), an actin inhibitor. Three particle opsonization protocols were used and phagocytic uptake between each is compared in CR1 WT iPS microglia in figure 6.11.

All groups showed increased fluorescence over the 4 hour time course with the lowest phagocytic uptake shown for the non-opsonized group, in which e-coli bioparticles were directly added onto iPS microglia cultures. The highest fluorescence magnitude was measured in the opsonized group in

which bioparticles were incubated with normal human serum (NHS) for one hour before being added into cultures. In between these was the third condition, FI depleted serum which used NHS depleted of all FI to opsonize bioparticles. In all cases. phagocytosis was completely inhibited by 10µM CytoD. Images for each condition shown in figure 6.11b represent the end point for each condition and mirror the data. Additionally, they illustrate that opsonizing the bioparticles produces reduced red background than when bioparticles are directly added to the dish.

Kruskal Wallis comparison of the mean of each group revealed significant differences in phagocytic uptake in opsonized Vs non opsonized (p= 0.0163) and cyto D (<0.0001, n= 3) to be significantly different as well as difference of FI depleted E.coli and cyto D groups (p=0.0381).

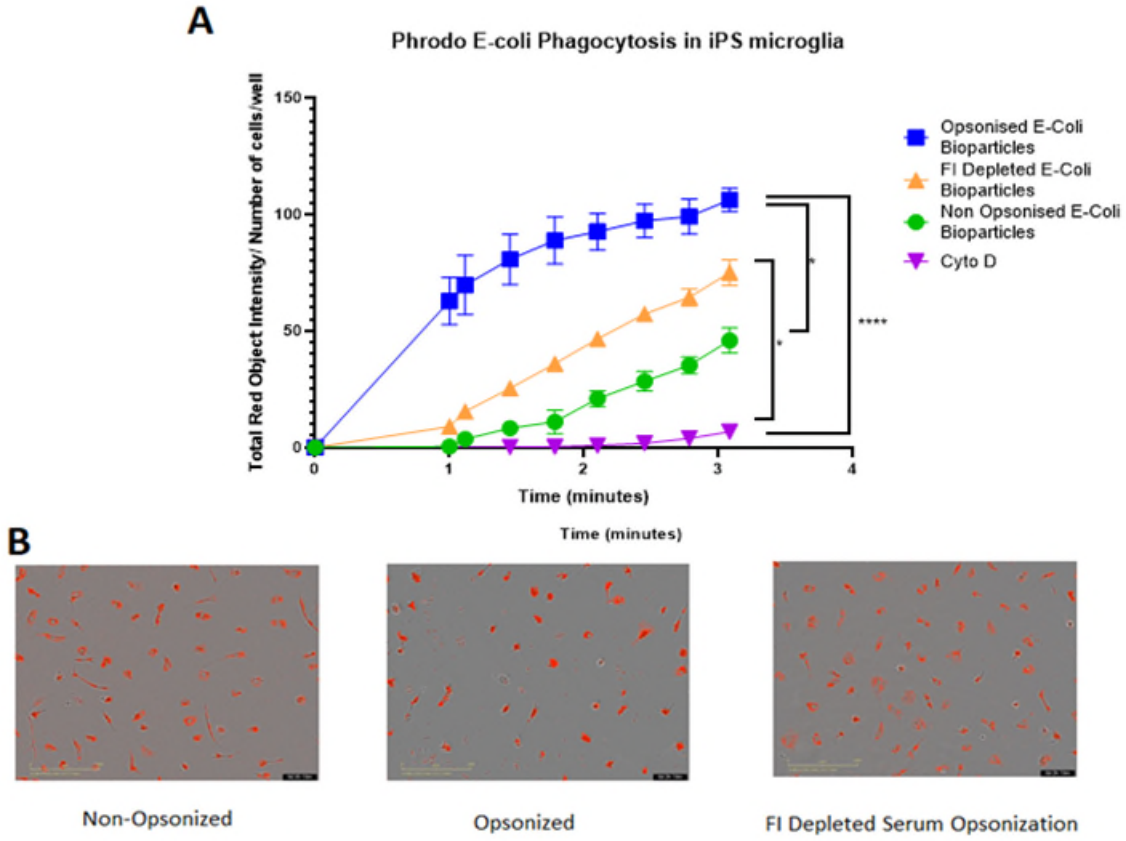

Figure 6.11: IPS microglia phagocytose e-coli beads in three separate conditions. *A) Total red object intensity, normalised to number cells/mm², increased when particles were incubated with IPS microglia over 3 hours. Three separate conditions were trialled; non-opsonized beads; beads opsonised by incubation with human serum and beads opsonised with factor I depleted serum. All three conditions had an increase in red fluorescence over 4 hours compared to the Cyto D control, with the non-opsonized beads having a general lower magnitude of red fluorescence relative to opsonized conditions. B) Images taken from each three conditions at the final time point show red fluorescence inside the cells, with the opsonized conditions showing a cleaner culture with less background. N=3 for all groups except Cyto D whichis n=1.. Kruskal Wallis comparison of the mean of each group revealed phagocytic uptake in opsonized Vs non opsonized (p= 0.0163) and cyto D (<0.0001,n= 3) to be significantly different alongside difference of FI depleted e-coli and cyto D groups (p=0.0381). Data in this figure is representative of 3 biological repeats and 3 technical repeats, except for Cyto D which is just 1 technical repeat.*

4.2.3.2 Phagocytosis of pHrodo e-coli beads in CR1 WT and CR1 KO iPS microglia

To test whether phagocytosis was impacted by CR1 KO, phagocytosis under all three conditions was compared between CR1 WT iPS microglia and CR1 KO iPS microglia. Figure 6.12a shows that non-

opsonized e-coli bead were taken up to a similar degree over 3 hours in CR1 KO and CR1 WT cells. Uptake was inhibited with 10uM Cyto-D. Representative images from the last time point of the CR1 WT and CR1 KO phagocytosis are shown in figure 6.12b.

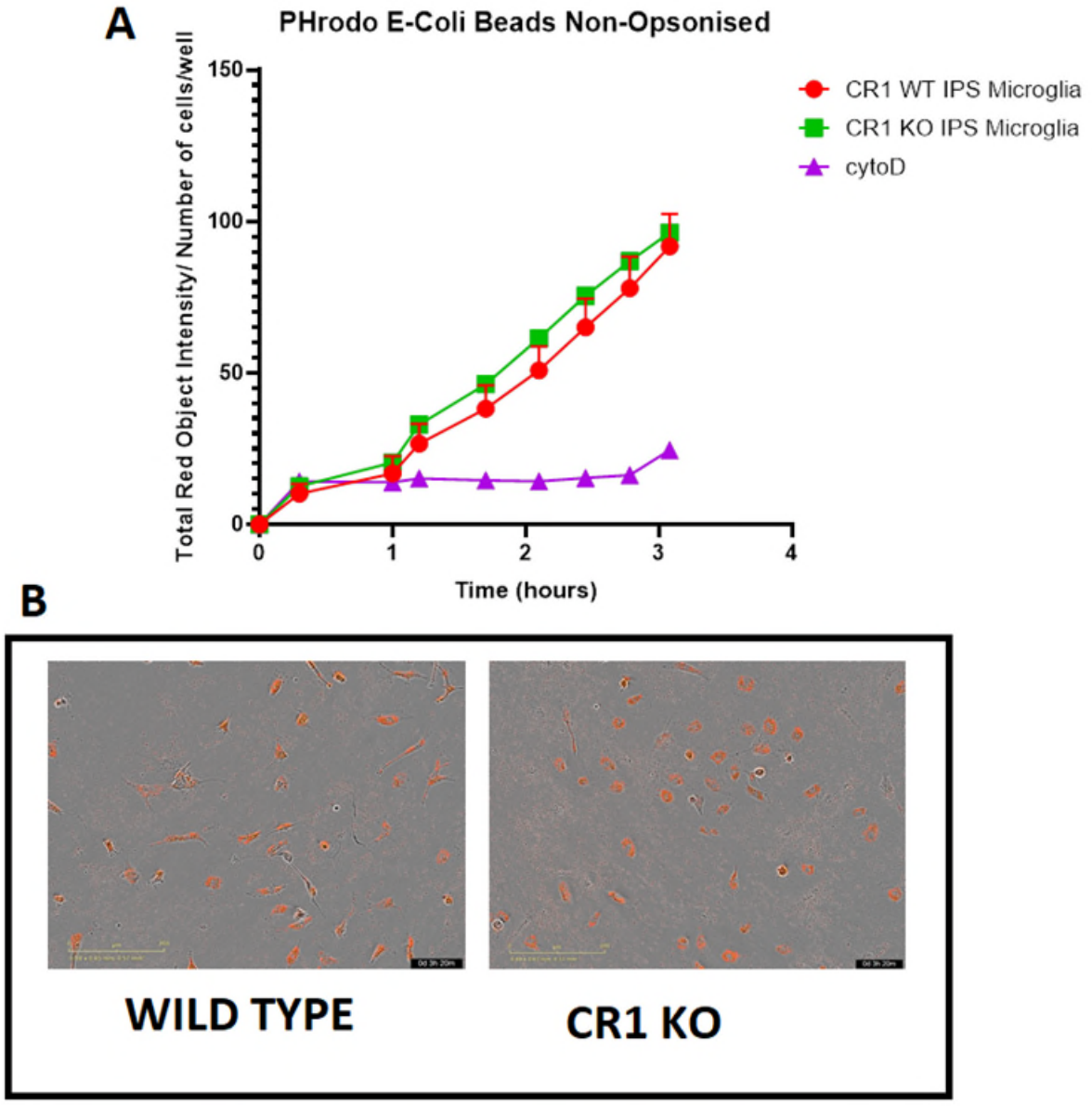

Figure 6.12: Non-opsonized e-coli beads were ingested by iPS microglia CR1 WT and CR1 KO. *A) Total red object intensity was normalised to number of cells/well and indicates a steady linear increase similar in both cell types. All groups have an n=3 except the Cyto-D control group which n=1, this was ran on CR1 WT. Error bars represent SEM. B) Representative images from the final time point in one WT and CR1 KO run. This data represents two biological repeats and three technical repeats, except for Cyto D which is just 1 technical repeat.*

I next compared phagocytosis of normal serum-opsonized beads (Figure 6.13a). Over the time course, CR1 KO iPS microglia showed a reduced red bead fluorescence compared to WT CR1 iPS microglia, demonstrating a reduced capacity to phagocytose opsonised particles. Two-way ANOVA indicates this difference to be significant for the last three time points. Figure 6.13b) shows representative images from the last time point of the run.

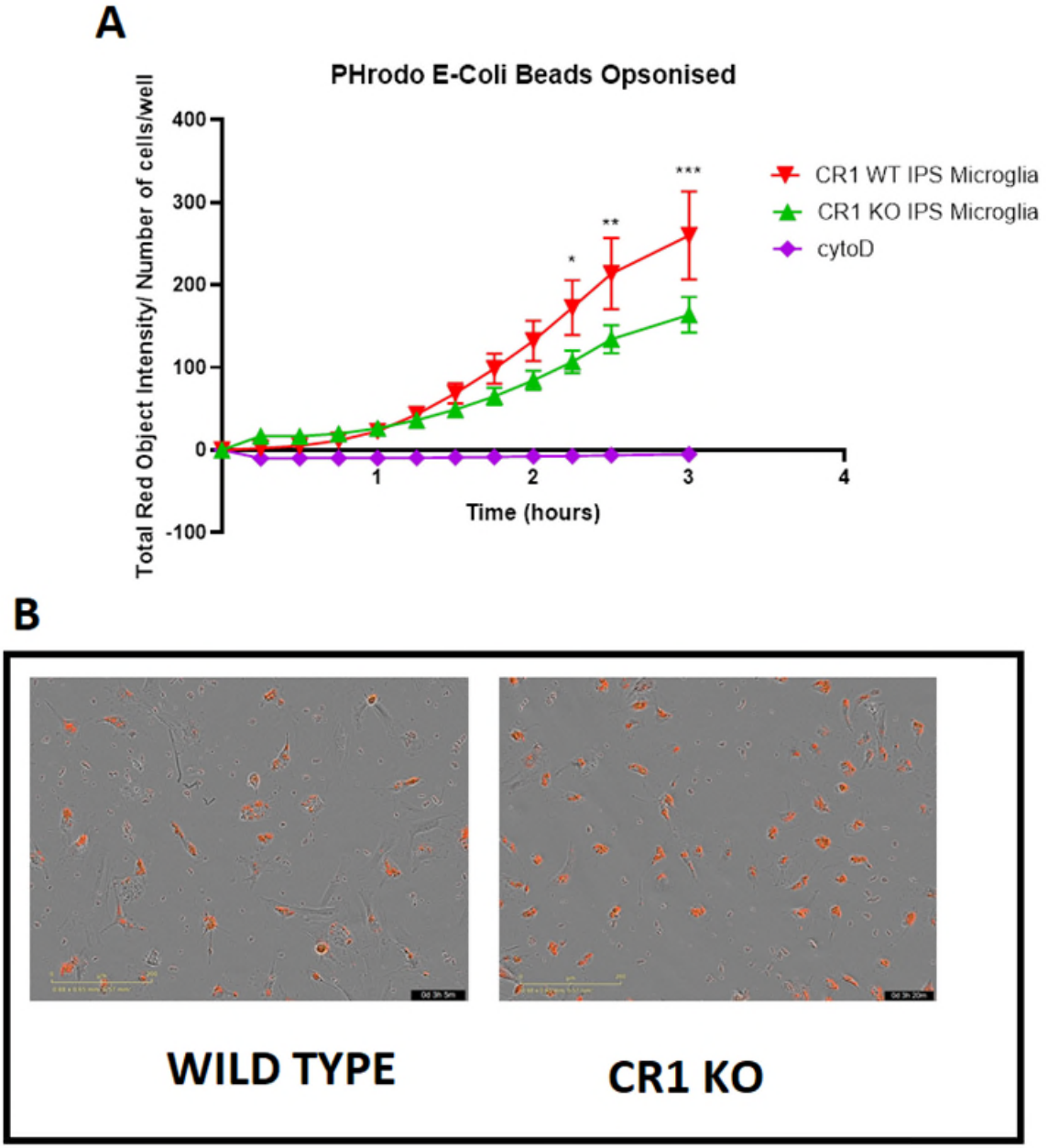

Figure 6.13: Phagocytosis of opsonized e-coli beads in CR1 KO IPS Microglia and CR1 WT IPS Microglia *Coating of beads was performed with normal human serum to coat beads with active complement fragments, making them easily detectable for cells. CR1 KO IPS microglia and CR1 WT IPS microglia showed significantly different bead uptake significant at later times as shown by two way ANOVA; time point 4 hours 40 minutes p= 0.0165, time point 5 hours p = 0.0028 and time point 5hours 30 minutes p=0.0003. n=3 for all groups except CytoD which n=1 this was ran on CR1 WT. Error bars represent SEM. B) Representative images from the final time point in one WT and CR1 KO run. This data represents two biological repeats and three technical repeats, except for Cyto D which is just 1 technical repeat.*

CR1 acts as co-factor for FI-mediated breakdown of complement opsonizing fragment C3b to iC3b, a ligand for the important microglial phagocytosis receptor CR3. In the absence of CR1, iC3b is not generated, meaning no ligand for CR3 to recognise. To test whether the differences observed for CR1 KO and CR1 WT iPS microglia were caused by failure to generate iC3b, I tested whether depletion of FI from the serum prior to incubation impacted phagocytosis in KO and WT cells. Figure 6.14 shows that when particles were opsonised using FI-depleted serum, uptake was identical in CR1 KO and CR1 WT cells, showing that the opsonic enhancement activity of CR1 is via its FI-cofactor activity to

generate iC3b, the ligand for CR3. Representative images in figure 6.14b) show the last time point from CR1 WT and CR1 KO runs in this condition.

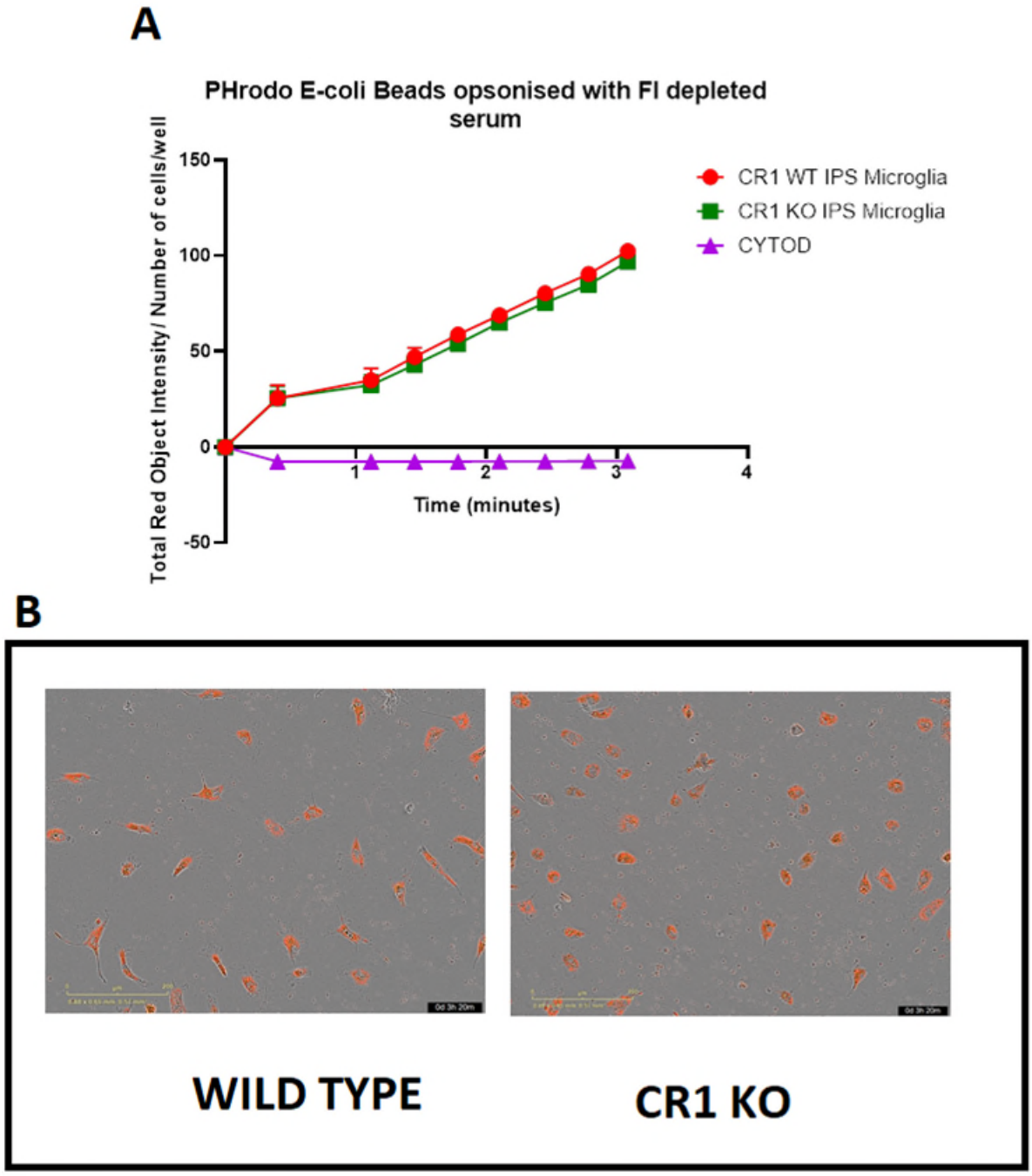

Figure 6.14: Phagocytosis of beads opsonized in FI depleted human serum *Total red object intensity normalised to number of cells/well indicates similar uptake of e-coli beads for the complete run in both cell types which was effectively inhibited with 10μM of Cyto this was ran on CR1 WT D. Error bars represent SEM. B) Representative images from the final time point in one WT and CR1 KO run. This data represents two biological repeats and three technical repeats, except for Cyto D which is just 1 technical repeat.*

6.3 Discussion

6.3.1 Comparison of complement transcript in three iPS brain cells and CR1 KO iPS microglia

Activation of iPS microglia was performed with LPS, which interacts with TLR4 resulting in a pro-inflammatory phenotype. Slight change in complement factors was observed with a significant increase in central molecule C3. Indeed, activation of microglia is often characterized by upregulation of CR3 and increased production of C1q.

Complement transcript in stimulated CR1 KO microglia relative to CR1 WT microglia reveal some complement production differences, indicating that absence of CR1 alters complement response to LPS. Notable is a significantly reduction of C3 transcript in CR1 KO microglia relative to CR1 WT microglia. Mouse models deficient in Crry also reveal reduced C3 protein in serum alongside reduced FB[268]; however, also saw an up regulation in C3 transcript. This was hypothesised to be due to chronic alternative pathway activation depleting available C3, an effect mirrored in FH deficient mouse model[248]. The difference in effect could be due to limitations in the study. Firstly, a 6 hour time point represents a very acute stimulation. Extending this to 24 hours may help to uncover more long term interactions. Furthermore, transcript only offers a small part of the story, future studies should investigate changes in protein expression between these cell types in these conditions. In addition to these first steps, a more specific look into the regulation of the AP in CR1 KO compared to CR1 WT may reveal some interesting results. This could be done using zymosan as a stimulant.

6.3.2 Absence of CR1 altered inflammatory phenotype of iPS microglia

Activation of microglia with LPS has shown to be a good model in studying neuroinflammation[63]. Production of cytokines is an essential component of microglia activation and increased production of pro-inflammatory markers has been shown in LOAD patient's CSF and post-mortem tissue[38]. For instance, cytokine TNFα is shown to be highly upregulated in LOAD patient's CSF compared to non-demented controls. Three polymorphisms within TNFα have been linked to increased risk in developing LOAD, two of which are linked to increased secretion of TNFα[269].

Data in this chapter reveal TNFα transcript to be upregulated following 100ng/ml 6 hour LPS in CR1 WT and CR1 KO iPS microglia (figures 3.19 and , respectively 6.7). Comparison of stimulated CR1 KO iPS microglia to stimulated CR1 WT iPS microglia reveal the absence of CR1 to significantly reduce the TNFα transcript generated. A similar effect on protein has been shown on isolated rat microglia, in which treatment of LPS with Crry blocking antibody resulted in lower TNFα protein secretion compared to groups in which LPS was added alone[162]. It is unclear how CR1 may be involved in cytokine production although a relationship between complement and TNFα has previously been shown. Most literature focus' on showing the effect of TNFα on complement secretion, with increases of C3 and FB shown alongside increases of TNFα. A relationship of complement on TNFα secretion has also been demonstrated[271]. Increased TNFα secretion has been shown when bacteria are added to isolated macrophages in C3 depleted serum or alongside a CR4 blocking antibody in a strain dependant manner, compared to addition with normal serum[272]. A role of C3 and complement in modulating TNFα requires further investigation. In this study absence of CR1 could increase C3 protein, due to loss of CR1 C3 convertase inhibitor action. Therefore, a reduction in TNFα transcript is accordance with previous data on C3 and TNFα production. Moving forward protein measurements of TNFα and other

cytokines should be made in addition to protein measurements for C3 and the individual C3 fragments and different time points following activation. Additional groups of CR3 and CR4 blocking antibodies should be added with LPS to aid in uncovering the role of C3 fragments in TNFα production.

A single IL-1β ELISA was conducted, indicating that while CR1 WT iPS microglia produced IL-1β in response to inflammatory challenge, CR1 KO iPS microglia produced almost none. IL-1 β is produced from the cleavage of pro-IL-1 β by caspase 1[68]. Previous studies have indicated that C1q suppresses pro-caspase and pro-IL-1 β activation which would reduce production of IL-1 β[273]. Indeed, C1q was shown to directly bind to CR1 within LHR-D; therefore absence of CR1 could increase the opportunity for C1q to bind to alternative ligands, blocking production of IL-1 β[102,148].

Future work would include repeating this data in the other CR1 KO clones to ensure the effect is due to removal of CR1, alongside additional measurements of other inflammatory markers, caspase-1 and C1q protein to aid in uncovering the mechanism involved.

6.3.3 Phagocytosis

Absence of CR1 had no effect on phagocytosis of non-opsonized beads but did cause a marked reduction in uptake when the bioparticles were opsonized with NHS. When pre-treated with NHS C3b binds to the e-coli bioparticles. In the presence of FI and one of its cofactors; CD46, FH or CR1 this is converted from C3b to iC3b[86]. iC3b is the ligand for phagocytosis receptor CR3 allowing for quick recognition and uptake of bioparticles. This is shown in figure 6.11, which shows opsonised bioparticles to produce the largest fluorescence. Comparison of opsonised bioparticle uptake between CR1 WT and CR1 KO iPS microglia in figure 6.13 shows the absence of CR1 to significantly reduce uptake. In the absence of CR1 less co-factors are available to engage with FI, therefore reducing conversion of C3b to iC3b and reducing ligand for CR3. This is supported by the FI depleted data which indicates the absence of FI within the serum to reduce the phagocytic capacity generally, as shown in figure 6.11, but to also be unaffected by the absence of CR1. This is because no iC3b can be generated in the absence of FI, regardless of whether the cells possess CR1. Future work should utilise C3 depleted serum as an alternative control to the FI depleted serum. This would restrict production of C3b and therefore not include the effect of alternative FI co-factors which could be present. Additionally, complement is not the only available opsonin, IgG and IgM have also shown to decorate microbes for enhanced detection by phagocytes via FCγIII receptors[139]. Therefore, it may be beneficial to asses opsonisation of other particles on beads, particularly as previous studies have shown IgM to also bind to CR3[274].

Although E. coli bioparticles have shown to present a good experimental paradigm for the investigation of neuroinflammation and phagocytosis, Aβ offers a far more relevant LOAD model. Previous studies have indicated Aβ is taken up through endocytosis, mainly micropinocytosis pathways by microglia[222].. Previous studies using soluble Aβ oligomer and isolated rat microglia showed a reduction in Aβ oligomer uptake when co-treated with Crry blocking antibody[162]. This indicates a potential role for crry in Aβ uptake and suggests a potential role for CR1 in this mechanisms. Further work would complete this data in the conditions used for e-coli beads and investigate a longer time course.

6.3.4 Conclusion

Although preliminary, these data indicate that knockout of CR1 impacts essential microglia functions. It is important to note complete removal of CR1 is a blunt model which does not capture the effect of

CR1 in LOAD. Investigating the expression and effect of different CR1 size polymorphism on microglia is required.

7.0 Discussion

7.1 Introduction

The work in this thesis has focused on the major GWAS hit, complement receptor 1 (CR1/CD35)[134,136]. A member of the complement system, Cr1 is located on chromosome 1q32, within the regulators of complement activation (RCA) gene cluster [86]. Multiple SNPs within Cr1 have been associated with LOAD including 8 intronic SNPs, rs6656401, rs3818361, rs1408077, rs48744610, rs646817, rs12034383, rs6701713 and rs6701710, and 2 in coding regions, rs116806456 and rs6691117[275]. The most consistent hit is rs6656401, which lies within close range of a linkage disequilibrium site in the gene[141]. It has been shown those with the risk allele (A) at rs6656401 have an 86% likelihood of expressing the longer, CR1-S phenotype[176]. Indeed, LOAD patients and non-demented age related elderly individuals with this allele both show increased plaque burden[276].

Investigation of the roles of CR1 at the cellular and biochemical level in LOAD remains limited. This is in part due to inconsistent data on the expression of CR1 within the CNS[141]. Investigations using cell models and primary cell cultures have revealed different expression profiles, with microglia, neurons and astrocytes all showing expression of CR1 in different reports[134,141]. Some have even shown complete absence of CR1 in post-mortem brain tissue[156].

The central aims of this project were to first establish a reliable iPS model for microglia, and fully characterize the cells for key microglia markers and functions. This would then provide an ideal human model for the investigation of CR1 expression and function on microglia. Another key glial cell type, iPS astrocytes, were investigated for expression of CR1 to complete an understanding of the expression of CR1 on CNS phagocytosing glia. Once expression was sufficiently confirmed, CR1 KO iPS lines were generated and fully characterized. Functional analysis was planned to investigate the impact of CR1 on key microglia actions, including phagocytosis, change in complement function, inflammatory cytokine production, ROS roduction and synaptic pruning. Additional aims included generation of isogenic iPS lines of two main CR1 isoforms, CR1-F and CR1-S to aid in understanding why the longer CR1 form has been associated with increased LOAD risk despite the variant conferring increased activity.

Unfortunately, due to difficulties in designing the CRISPR and time constraints caused by COVID-19, the final objective was not possible. COVID-19 work restrictions greatly limited lab time, cultures which had just been set up at the beginning of lockdown had to be destroyed and restarted months later significantly impacting the time to run functional experiments. For this reason, functional analysis between CR1 WT and CR1 KO iPS microglia was limited.

7.2 Main Findings and future experiments

7.2.1 Generation of human iPS models

iPS microglia were successfully generated following an EB based protocol adapted from Haensseler et al 2017[207] which was itself adapted from macrophage differentiation protocol in Van Wilgenberg et al 2013[277]. The original protocol terminally differentiated precursors in XVIVO-15 medium supplemented with IL-3 and GM-CSF[207]. Microglia grown in this medum express key markers CX3CR1 and TMEM119 but also possess large vacuoles throughout the cell body. Unpublished RT-qPCR

performed in the lab indicated that they had higher expression of inflammatory markers suggesting them to be slightly activated. To overcome this, in-house ACM was generated and used to terminally differentiate cells. ACM was produced from iPS astrocyte cultures and batches generated over multiple collections. Aliquots were diluted to a final concentration of 1ng/ml of CCL2, as has previously been done[227]. Cells differentiated with ACM showed high expression for CX3CR1 and TMEM119 and were highly branched, without the presence of the vacuoles seen with supplemented XVIVO differentiation. Previous studies have suggested the presence of TGFβ, cholesterols and M-CSF to be the essential factors within ACM for the differentiation to microglia[278,279]. Fully characterizing the expression of each component in ACM is required and may suggest a more robust approach using relevant molecule to batch control. Indeed, much work is needed to find the best terminal differentiation conditions to produce the most physiologically relevant microglia model. Current published protocols use a range of supplemented and conditioned medias with many claiming microglia are best produced in co-culture with neurons or astrocytes, highlighting the importance of neuron-glia and glia-glia signaling[200,207]. Moving forward, RNA sequencing of microglia produced with various supplemented media should be compared to each other and to extracted primary human microglia. This would aid in finding the best media to produce the most relevant microglia cells.

Many protocols for the differentiation of microglia exist; in this thesis two different protocols were followed. Only a brief comparison of produced microglia was done. A more extensive comparison comparing the transcript profile of each iPS cell alongside functional comparison of these cells including phagocytosis or response to inflammatory signals would be valuable. The EB method was chosen moving forward because it was technically favorable. This protocol produced more cells, for longer periods of time and did not have the added problem of unwanted non-iPS cells in the culture. Indeed, microglia cultures from the monolayer method often also contained continuously proliferating flat cells growing underneath the microglia and making these cultures unusable. Initially, it was considered that these cells were fibroblasts, likely present due to a bit of the monolayer detaching and being plated alongside the precursors; however, cell sorting the precursors for CD11b did not resolve the issue. Furthermore, immunofluorescence staining revealed these flat cells to be positive for the pan-macrophage marker IBA-1. It is possible that these cells are paraventricular macrophages, which are differentiated alongside microglia in utero[280,281]. However, a full characterization of these cells is required; this should include fibroblast marker CD49b and perivascular macrophage marker CD163[282,283].

7.2.2 Expression of CR1 on iPS glia

The primary objective of this work was to investigate the expression of CR1 on iPS glia cells. Expression of CR1 on iPS microglia was convincingly shown with a range of techniques. CR1 transcript was present and increased slightly following LPS stimulation. Previous studies reported upregulation of Crry, the rodent CR1 ortholog, in isolated rat microglia following LPS and oligomer Aβ treatment[162]. In addition to observing changes of CR1 in activated microglia, an ELISA for the detection of soluble CR1 in cell supernatants should be performed. A prelimary ELISA was performed but failed to find soluble CR1 within the range of the standards, suggesting supernatant should either be concentrated, or CR1 pulled down prior to the ELISA.

Other iPS cell types, iPS astrocytes and immature cortical neurons were also investigated for CR1 expression; these showed no protein or transcript. Cortical neurons are referred to as immature as they had not yet formed synapses or produce spontaneous action potentials, a key neuronal characterization. Therefore, to better understand the expression of CR1, these cells should undergo

a longer maturation period. Additionally, co-culture of iPS microglia with either/both iPS astrocytes and iPS neurons would aid in completing this work, firstly because more complicated co-cultures have been shown to produce more mature cells, and transcript analysis shows they are more like primary cells. Indeed, some studies have indicated that microglia are most 'microglia-like' when grown alongside either neurons or astrocytes[57,207]. Organoids containing neuronal, astrocytic and microglia cells in a 3D context would be hugely advantageous in confirming the expression of CR1 on each of these cell types. In addition to this, characterization of cells isolated from human live brain or post-mortem tissue for expression of CR1 is required.

7.2.3 Generation of CR1 KO clones

CR1 KO clones were generated using CRISPR Cas9 technology. Clones were picked and screened for those which had incorporated the edit. This identified multiple clones which did not take up the edit, along with seven heterozygotic and three homozygotic KO clones. Confirmation of a frame shift and introduction of PTC was shown following sequencing of KO clones. Additionally, absence of CR1 protein was shown with western blotting and immunofluorescence. All KO clones were shown to successfully differentiate into iPS microglia alongside WT cells and showed similar expression of key microglia transcripts IBA-1 and CX3CR1 and protein expression of CD11b. Knocking out of CR1 is useful in confirming expression and performing preliminary investigations into how CR1 may be involved in microglia functions. However, generating lines more relevant to the alterations seen in LOAD patients would be hugely beneficial. This would include the manipulation of isogenic lines for alternative CR1 size polymorphisms. Performing this CRISPR may require adapted Cas proteins due to the highly homologous nature of CR1 protein. For instance, use of Cas nickase would produce single stranded break allowing for more precise edits to be made[210]. Investigating whether different size polymorphism of CR1 affects expression and function on iPS microglia is necessary to understand how CR1 may be implicated in pathology.

7.2.4 Functional differences of CR1 KO iPS microglia and CR1 WT iPS microglia

7.2.4.1 Complement regulation

As CR1 is primarily a complement receptor/regulator, preliminary investigations into differences in complement transcript expression between CR1 WT and CR1 KO iPS microglia at baseline and after 6 hour 100ng/ml LPS stimulation was investigated using high throughput RT-qPCR. After LPS challenge, CR1 KO expressed significantly less C3 transcript relative to CR1 WT. This is contradictory to previous studies using crry KO rodent models, which showed increases in C3 transcript[268]. The difference in these findings could be due to too short a stimulation time course being investigated here. Longer stimulation times such as 24 hours and 48 hours may yielf very different results. Furthermore, protein characterization for complement factors and regulators is required either by ELISA or western blotting techniques. Understanding how the AP is altered is directly relevant to LOAD following in-situ studies of post-mortem LOAD tissue to possess increased alternative pathway regulators FH, FI and FB compared to non-demented tissues, suggesting increased alternative pathway activation in LOAD[266].

7.2.4.2 Microglia activation

The effect of CR1 KO on microglia activation was investigated by measuring changes in pro-inflammatory cytokine transcript expression. This reveals CR1 KO to produce significantly less

transcript for key pro-inflammatory cytokines TNFα and IL-6 compared to CR1 WT. The role of CR1 in this remains unclear. Previous studies have shown that blockage of Crry on isolated rat microglia stimulated with LPS reduced production of TNFα[162]. These results require repeating with protein measures in human cells.

A prelimary ELISA for IL-1β was performed after 24-hour LPS stimulation. This revealed significantly less IL-1β protein secreted in CR1 KO iPS microglia relative to CR1 WT cells. This indicates That CR1 expression impacts IL-1β secretion, through an unknown mechanism. Interaction of complement and the inflammasome, responsible for IL-1β production have been previously shown[284]. For instance, sub-lytic MAC attack triggered NLRP3 activation and IL-1β secretion through an influx of calcium ions[284]. The dysregulation of complement homeostasis caused by the lack of CR1 would be expected to produce an increase in C5 activation and therefore MAC formation. However, this would be expected to result in an increase of inflammasome activation and IL-1β secretion rather than a reduction. To fully understand the effect of CR1 on inflammasome activation, additional measurements such as NLRP3 protein, caspase-1 protein and formation of ASC should be compared between CR1 KO and CR1 WT cells after LPS stimulation or other challenges. Additionally, measurements of complement protein and sub-lytic MAC attack will provide invaluable information on how the inflammasome may be altered by the absence of CR1.

7.2.4.3 Phagocytosis

CR1 KO and CR1 WT iPS microglia showed no difference in phagocytosis of non-opsonized bioparticles or those opsonized in FI depleted serum to prevent degradation of C3b to iC3b. However, CR1 KO iPS microglia showed significantly reduced uptake of beads opsonized in NHS. This shows that lack of CR1, by reducing the capacity for production of iC3b (the ligand for CR3), significantly impacts uptake of opsonised e-coli beads, confirming an important role for CR1 in phagocytosis. Moving forward, full characterization of beads for C3b, iC3b and immunoglobulins is required. Firstly, to confirm the assumptions made above and secondly to provide information on the relative amount of opsonization between bioparticles coated with NHS and with FI depleted NHS. Blocking interactions of immunoglobulins with their relevant receptors and/or blockage of CR3 would help in uncovering the role of complement in this assay[274].

Knock out of CR1, while a useful tool, provides a blunt model for studying its role in microglia. More relevant to LOAD is generation of isogenic lines with alternative CR1 size polymorphisms. Indeed, the longer CR1-S isotype has been linked to LOAD[141]. This is interesting as this has an additional binding site for C3b, which in line with these findings would lead to increased formation of iC3b and therefore increased phagocytosis[141]. This lies in conflict with the accumulation of Aβ seen in LOAD. This makes comparing the capabilities of microglial CR1-F and CR1-S to facilitate phagocytosis of diverse cargos essential. In addition to this, the numbers of molecules expressed on microglia for each polymorphism should be compared as expression number for CR1-S has shown to be reduced compared to CR1-F receptors[141,285]. In this circumstance, reduced number of receptors could negate the advantage of an extra binding site.

Future experiments should also investigate alternative cargos. Prelimary data for phagocytosis of soluble Aβ oligomers conjugated to a permanent FITC dye was performed. This showed slight reductions of uptake in CR1 KO that failed to reach significance. However, this experiment was limited to non-opsonized conditions, and only two time points so may have missed a significant effect of CR1 KO and requires repeating with a larger range of conditions. Previous findings showed blockage of Crry in rat microglia reduced oligomer Aβ uptake[162]. Additionally, overexpression of soluble Crry in

brain in an AD mouse model caused increased Aβ aggregates and increased neuronal degeneration. These findings implicate Crry, the rodent CR1 ortholog, in Aβ pathology, in which a build up of aggregates is considered a major pathological hallmark of LOAD. Expanding this experiment to include a larger range of opsonization conditions and time course would provide date relevant to AD and might identify potential pathways to therapeutically target. However, it is important to note the Aβ used was oligomeric and should be fully characterized to ensure no fibrillization has occurred as multiple studies have highlighted multiple batch differences as a major caveat of using Aβ in cell cultures.

7.3 Additional experiments

Functional work in this thesis has focused on CR1 in complement regulation, phagocytosis and inflammation of iPS microglia cells. Much of this is prelimary, offering a starting point for exploring potential actions of CR1 in LOAD pathology; additional experiments have been mentioned in the previous section. Alongside strengthening and expanding these data, additional aspects of LOAD pathology should be investigated, such as tau pathology. Like Amyloid beta, hyperphosphorylated tau within neurons is a major hallmark for LOAD. In unpublished data from the Haroutunian lab a correlation between CR1 mRNA and neurofibrillar tangle density and phosphorylation abundance has been shown[180]. Additionally, mouse models with Crry deletion showed a significant and strong reduction of phosphorylation at serine 235 site, a marker of hyperphosphorylation[164]. How this relates to human CR1 should be investigated using human tissue and bioinformatics data, so as to investigate any links between the genetic hits and patient's pathology.

Another important aspect of CR1 in LOAD is its roles in synaptic pruning. Loss of synapse is a major hallmark in LOAD pathology, offering the best pathological correlate for cognitive decline[134]. Work on synaptic elimination has highlighted an important complement element with LOAD mouse models deficient for C3 and C1q showing defects in synaptic pruning[129,130]. Indeed, C1q deficient animals produced so many synapses they were prone to spontaneous seizures[286]. Staining studies have shown C3 and C1q to decorate synapses of the developing retina, targeting them for elimination[130]. The stimulus for synapse targeting is unclear, although synaptic activity has been considered as a potential factor for tagging. These complement tags are detected by microglia phagocytosis receptor CR3, allowing for microglia to engulf the unwanted connection. This is supported by LOAD mouse models; absence of CR3 protected from synaptic loss [287] .

A direct role for CR1 in synaptic pruning has not yet been shown. However, C1q directly binds CR1 through a binding site within LHR-D[141]. Indeed, CR1 GWAS hit rs4844609 (Ser1610Thr) has been linked to C1q binding. Individuals homozygotic or heterozygotic for this SNP show a small but significant increase in C1q binding to CR1[141,149]. It is possible that increased binding of C1q on synapses heavily expressing CR1 could exacerbate complement synaptic elimination, as seen in LOAD. Studying synaptic elimination is difficult with most recent experiments utilizing the developing mouse retina as a model. One alternative to this is utilizing synaptosomes, which are the isolated neuronal terminal and can be produced from iPS cortical neuronal cultures[288]. Conjugation of synaptosomes with a pHRodo-dye will allow for uptake by microglia to be measured, as described before with e-coli bioparticles[288]. Another alternative assay is the co-culture of iPS neurons with iPS microglia and the use of diOlistic dyes. DiOlistic dyes are non-specifically taken up into the majority of cells, and provide images with good resolution. Measuring the rate of synaptic uptake using the methods described in Bahrini et al 2015 and a CR3 blocking antibody as a control may provide a potential assay for measuring

synaptic elimination[289]. Using CR1 with varying rs4844609 phenotypes could uncover a role of CR1 in synapse elimination.

7.4 Limitations of iPS models

While iPS cells offer a robust source of human microglia cells they still have multiple limitations. Firstly, generation of iPS microglia is expensive and time demanding, taking several weeks-months before you know if the culture has been successful or not. Beyond this, differentiation to microglia cell type is still being optimized. Terminal media studies are currently ongoing, in search for the most suitable media to generate microglia. These problems are partly overcome by co-culturing of cells or organoids. However, these come with other difficulties and requires extensive optimization. Another limitation is the age of cells. This is particularly important to remember when considering neurodegenerative disorders like LOAD in-which the major risk factor is age[290]. This is partially overcome by chemical ageing of cells. One example of this is progerin treatment of iPS neurons which shortens telomers and has been used to study Parkinson's disease[291]. A third limitation of this study is the use of only one cell line, KOLF2. Previous studies have shown different stem cell clones to behave drastically different. Repeating these measurements in additional cell lines is essential.

iPS provide an invaluable human model for the study of CR1 which does not have the problems associated with post-mortem isolation of microglia. However, since beginning this project, chimeric animal models with humanized CR1-S have been developed by Jackson labs[163]. These animal models provide an important tool for understanding CR1 within the CNS and will be useful for multiple assays. Continued development of mice with CR1-F and crossing of them onto genetic LOAD backgrounds (such as the APP/PS1 mice) will aid in uncovering CR1 specific effects on LOAD via post-mortem tissue analysis. Furthermore, this offers an opportunity to investigate interaction of CR1 with other GWAS hits particularly APOE.

7.5 Concluding Remarks

The work performed in this thesis demonstrates that CR1 is present within iPS microglia, suggesting it to have a role within the CNS. Indeed, this work shows that CR1 expression impacts on microglia function, linking it to many disease processes key in LOAD pathogenesis. Continuing this work could provide important mechanistic information and will lead to a better understanding of the emerging role of complement in LOAD pathology. A more complete understanding of these process could allow for the development of therapeutic strategies.

8.0 References

1. Assal, F. History of Dementia. in 118–126 (2019). doi:10.1159/000494959.
2. Yang, H. D., Kim, D. H., Lee, S. B. & Young, L. D. History of Alzheimer's Disease. *Dement. Neurocognitive Disord.* **15**, 115 (2016).
3. Boller, F. & Forbes, M. M. History of dementia and dementia in history: An overview. *J. Neurol. Sci.* **158**, 125–133 (1998).
4. Murman, D. The Impact of Age on Cognition. *Semin. Hear.* **36**, 111–121 (2015).
5. Duong, S., Patel, T. & Chang, F. Dementia. *Can. Pharm. J. / Rev. des Pharm. du Canada* **150**, 118–129 (2017).
6. Escolme, B. When grief has mates: King Lear and the politics of happiness. *The Lancet Psychiatry* **5**, 621–622 (2018).
7. Sanderson, D. How King Lear teaches us about ageing and dementia. *The Times* (2016).
8. Schumacher, J. *et al.* Dysfunctional brain dynamics and their origin in Lewy body dementia. *Brain* **142**, 1767–1782 (2019).
9. Kane, J. P. M. *et al.* Clinical prevalence of Lewy body dementia. *Alzheimers. Res. Ther.* **10**, 19 (2018).
10. D.M., H., E., M. & D.J., S. Alzheimer disease in 2020. *Cold Spring Harb. Perspect. Med.* **2**, 1–5 (2012).
11. Ryan, N. S., Rossor, M. N. & Fox, N. C. Alzheimer's disease in the 100 years since Alzheimer's death. *Brain* **138**, 3816–3821 (2015).
12. Wittenberg, R., Hu, B. & Luis Barraza-Araiza, A. R. *Projections of older people with dementia and costs of dementia care in the United Kingdom, 2019–2040*. https://www.alzheimers.org.uk/sites/default/files/2019-11/cpec_report_november_2019.pdf (2019).
13. Reitz, C. Alzheimer's disease and the amyloid cascade hypothesis: A critical review. *Int. J. Alzheimers. Dis.* **2012**, (2012).
14. Hippius, H. & Neundörfer, G. The discovery of Alzheimer's disease. *Dialogues Clin. Neurosci.* **5**, 101–108 (2003).
15. Tanzi, R. E. & Bertram, L. Twenty Years of the Alzheimer's Disease Amyloid Hypothesis: A Genetic Perspective. *Cell* **120**, 545–555 (2005).
16. Masters, C. L. & Selkoe, D. J. Biochemistry of Amyloid -Protein and Amyloid Deposits in Alzheimer Disease. *Cold Spring Harb. Perspect. Med.* **2**, a006262–a006262 (2012).
17. Ricciarelli, R. & Fedele, E. The Amyloid Cascade Hypothesis in Alzheimer's Disease: It's Time to Change Our Mind. *Curr. Neuropharmacol.* **15**, (2017).
18. Uddin, M. S. *et al.* Revisiting the amyloid cascade hypothesis: From anti-aβ therapeutics to auspicious new ways for alzheimer's disease. *Int. J. Mol. Sci.* **21**, 1–33 (2020).
19. Karran, E., Mercken, M. & Strooper, B. De. The amyloid cascade hypothesis for Alzheimer's disease: An appraisal for the development of therapeutics. *Nat. Rev. Drug Discov.* **10**, 698–712 (2011).

20. Knopman, D. S., Petersen, R. C. & Jack, C. R. A brief history of “Alzheimer disease”. *Neurology* **92**, 1053–1059 (2019).

21. Ricciarelli, R. & Fedele, E. The Amyloid Cascade Hypothesis in Alzheimer’s Disease: It’s Time to Change Our Mind. *Curr. Neuropharmacol.* **15**, 926–935 (2017).

22. Selkoe, D. J. & Hardy, J. The amyloid hypothesis of Alzheimer’s disease at 25 years. *EMBO Mol. Med.* **8**, 595–608 (2016).

23. Hardy, J. A. & Higgins, G. A. Alzheimer’s Disease: The Amyloid Cascade Hypothesis. *Science (80-.).* **256**, 184–185 (1992).

24. Kim, H. Y., Lee, D. K., Chung, B. R., Kim, H. V. & Kim, Y. Intracerebroventricular injection of amyloid-# peptides in normal mice to acutely induce alzheimer-like cognitive deficits. *J. Vis. Exp.* **2016**, 1–6 (2016).

25. Drummond, E. & Wisniewski, T. Alzheimer’s disease: experimental models and reality. *Acta Neuropathol.* **133**, 155–175 (2017).

26. O’Brien, R. J. & Wong, P. C. Amyloid Precursor Protein Processing and Alzheimer’s Disease. *Annu. Rev. Neurosci.* **34**, 185–204 (2011).

27. Zhang, X. & Song, W. The role of APP and BACE1 trafficking in APP processing and amyloid-β generation. *Alzheimers. Res. Ther.* **5**, 46 (2013).

28. Chow, V. W., Mattson, M. P., Wong, P. C. & Gleichmann, M. An Overview of APP Processing Enzymes and Products. *NeuroMolecular Med.* **12**, 1–12 (2010).

29. Chen, G. *et al.* Amyloid beta: structure, biology and structure-based therapeutic development. *Acta Pharmacol. Sin.* **38**, 1205–1235 (2017).

30. Wolfe, M. S. Unlocking truths of γ-secretase in Alzheimer’s disease: what is the translational potential? *Future Neurol.* **9**, 419–429 (2014).

31. Guyon, A., Rousseau, J., Lamothe, G. & Tremblay, J. P. The protective mutation A673T in amyloid precursor protein gene decreases Aβ peptides production for 14 forms of Familial Alzheimer’s Disease in SH-SY5Y cells. *PLoS One* **15**, e0237122 (2020).

32. Jonsson, T. *et al.* A mutation in APP protects against Alzheimer’s disease and age-related cognitive decline. *Nature* **488**, 96–99 (2012).

33. TCW, J. & Goate, A. M. Genetics of β-Amyloid Precursor Protein in Alzheimer’s Disease. *Cold Spring Harb. Perspect. Med.* **7**, a024539 (2017).

34. Chételat, G. *et al.* Amyloid imaging in cognitively normal individuals, at-risk populations and preclinical Alzheimer’s disease. *NeuroImage Clin.* **2**, 356–365 (2013).

35. Iacono, D. *et al.* The Nun Study: Clinically silent AD, neuronal hypertrophy, and linguistic skills in early life. *Neurology* **73**, 665–673 (2009).

36. Nelson, P. T. *et al.* Brains With Medial Temporal Lobe Neurofibrillary Tangles But No Neuritic Amyloid Plaques Are a Diagnostic Dilemma But May Have Pathogenetic Aspects Distinct From Alzheimer Disease. *J. Neuropathol. Exp. Neurol.* **68**, 774–784 (2009).

37. Schönheit, B., Zarski, R. & Ohm, T. G. Spatial and temporal relationships between plaques and tangles in Alzheimer-pathology. *Neurobiol. Aging* **25**, 697–711 (2004).

38. Sudduth, T. L., Schmitt, F. A., Nelson, P. T. & Wilcock, D. M. Neuroinflammatory phenotype in early Alzheimer’s disease. *Neurobiol. Aging* **34**, 1051–1059 (2013).

39. Heneka, M. T. *et al.* HHS Public Access Neuroinflammation in Alzheimer ' s Disease. *Lancet Neurol* **14**, 388–405 (2018).

40. Yiannopoulou, K. G. & Papageorgiou, S. G. Current and future treatments for Alzheimer's disease. *Ther. Adv. Neurol. Disord.* **6**, 19–33 (2013).

41. CHEN, W.-W., ZHANG, X. & HUANG, W.-J. Role of neuroinflammation in neurodegenerative diseases (Review). *Mol. Med. Rep.* **13**, 3391–3396 (2016).

42. Leng, F. & Edison, P. Neuroinflammation and microglial activation in Alzheimer disease: where do we go from here? *Nat. Rev. Neurol.* **17**, 157–172 (2021).

43. Kinney, J. W. *et al.* Inflammation as a central mechanism in Alzheimer's disease. *Alzheimer's Dement. Transl. Res. Clin. Interv.* **4**, 575–590 (2018).

44. Kinney, J. W. *et al.* Inflammation as a central mechanism in Alzheimer's disease. *Alzheimer's Dement. Transl. Res. Clin. Interv.* **4**, 575–590 (2018).

45. Shen, X.-N. *et al.* Identification of inflammatory and vascular markers associated with mild cognitive impairment. *Aging (Albany. NY).* **11**, 2403–2419 (2019).

46. McGeer, P. L. & McGeer, E. G. NSAIDs and Alzheimer disease: Epidemiological, animal model and clinical studies. *Neurobiol. Aging* **28**, 639–647 (2007).

47. Aisen, P. S. & Davis, K. L. Inflammatory mechanisms in Alzheimer's disease: implications for therapy. *Am. J. Psychiatry* **151**, 1105–13 (1994).

48. McKee, A. C. *et al.* Ibuprofen reduces Aβ, hyperphosphorylated tau and memory deficits in Alzheimer mice. *Brain Res.* **1207**, 225–236 (2008).

49. Lim, G. P. *et al.* Ibuprofen Suppresses Plaque Pathology and Inflammation in a Mouse Model for Alzheimer's Disease. *J. Neurosci.* **20**, 5709–5714 (2000).

50. Chong, Y. Effect of a carboxy-terminal fragment of the alzheimer's amyloid precursor protein on expression of proinflammatory cytokines in rat glial cells. *Life Sci.* **61**, 2323–2333 (1997).

51. Quintanilla, R. A., Orellana, D. I., González-Billault, C. & Maccioni, R. B. Interleukin-6 induces Alzheimer-type phosphorylation of tau protein by deregulating the cdk5/p35 pathway. *Exp. Cell Res.* **295**, 245–257 (2004).

52. Giovannoni, F. & Quintana, F. J. The Role of Astrocytes in CNS Inflammation. *Trends Immunol.* **41**, 805–819 (2020).

53. Perez-Nievas, B. G. & Serrano-Pozo, A. Deciphering the astrocyte reaction in Alzheimer's disease. *Front. Aging Neurosci.* **10**, 1–23 (2018).

54. Kobayashi, K. *et al.* Apoptosis of astrocytes with enhanced lysosomal activity and oligodendrocytes in white matter lesions in Alzheimer's disease. *Neuropathol. Appl. Neurobiol.* **28**, 238–251 (2002).

55. Mouser, P. E., Head, E., Ha, K.-H. & Rohn, T. T. Caspase-Mediated Cleavage of Glial Fibrillary Acidic Protein within Degenerating Astrocytes of the Alzheimer's Disease Brain. *Am. J. Pathol.* **168**, 936–946 (2006).

56. Abdelhak, A. *et al.* Glial Activation Markers in CSF and Serum From Patients With Primary Progressive Multiple Sclerosis: Potential of Serum GFAP as Disease Severity Marker? *Front. Neurol.* **10**, (2019).

57. Timmerman, R., Burm, S. M. & Bajramovic, J. J. An overview of in vitro methods to study

microglia. *Front. Cell. Neurosci.* **12**, 1–12 (2018).

58. Egensperger, R., Kösel, S., Von Eitzen, U. & Graeber, M. B. Microglial activation in Alzheimer disease: Association with APOE genotype. *Brain Pathol.* **8**, 439–447 (1998).

59. Ulrich, J. D. *et al.* ApoE facilitates the microglial response to amyloid plaque pathology. *J. Exp. Med.* **215**, 1047–1058 (2018).

60. Condello, C., Yuan, P., Schain, A. & Grutzendler, J. Microglia constitute a barrier that prevents neurotoxic protofibrillar Aβ42 hotspots around plaques. *Nat. Commun.* **6**, 6176 (2015).

61. Baik, S. H., Kang, S., Son, S. M. & Mook-Jung, I. Microglia contributes to plaque growth by cell death due to uptake of amyloid β in the brain of Alzheimer's disease mouse model. *Glia* **64**, 2274–2290 (2016).

62. Lively, S. & Schlichter, L. C. Microglia Responses to Pro-inflammatory Stimuli (LPS, IFNγ+TNFα) and Reprogramming by Resolving Cytokines (IL-4, IL-10). *Front. Cell. Neurosci.* **12**, (2018).

63. Liu, Y. *et al.* LPS receptor (CD14): A receptor for phagocytosis of Alzheimer's amyloid peptide. *Brain* **128**, 1778–1789 (2005).

64. Hines, D. J., Choi, H. B., Hines, R. M., Phillips, A. G. & MacVicar, B. A. Prevention of LPS-Induced Microglia Activation, Cytokine Production and Sickness Behavior with TLR4 Receptor Interfering Peptides. *PLoS One* **8**, e60388 (2013).

65. Kang, J.-B., Park, D.-J., Shah, M.-A., Kim, M.-O. & Koh, P.-O. Lipopolysaccharide induces neuroglia activation and NF-κB activation in cerebral cortex of adult mice. *Lab. Anim. Res.* **35**, 19 (2019).

66. Zheng, D., Liwinski, T. & Elinav, E. Inflammasome activation and regulation: toward a better understanding of complex mechanisms. *Cell Discov.* **6**, (2020).

67. Hanslik, K. L. & Ulland, T. K. The Role of Microglia and the Nlrp3 Inflammasome in Alzheimer's Disease. *Front. Neurol.* **11**, (2020).

68. Heneka, M. T. *et al.* NLRP3 is activated in Alzheimer's disease and contributes to pathology in APP/PS1 mice. *Nature* **493**, 674–678 (2013).

69. Downs, K. P., Nguyen, H., Dorfleutner, A. & Stehlik, C. An overview of the non-canonical inflammasome. *Mol. Aspects Med.* **76**, 100924 (2020).

70. Couturier, J. *et al.* Activation of phagocytic activity in astrocytes by reduced expression of the inflammasome component ASC and its implication in a mouse model of Alzheimer disease. *J. Neuroinflammation* **13**, 20 (2016).

71. Halle, A. *et al.* The NALP3 inflammasome is involved in the innate immune response to amyloid-β. *Nat. Immunol.* **9**, 857–865 (2008).

72. Perry, R. The role of TNF and its receptors in Alzheimer's disease. *Neurobiol. Aging* **22**, 873–883 (2001).

73. Jiang, H. *et al.* Genetic deletion of TNFRII gene enhances the Alzheimer-like pathology in an APP transgenic mouse model via reduction of phosphorylated I B. *Hum. Mol. Genet.* **23**, 4906–4918 (2014).

74. Zhou, M., Xu, R., Kaelber, D. C. & Gurney, M. E. Tumor Necrosis Factor (TNF) blocking agents are associated with lower risk for Alzheimer's disease in patients with rheumatoid arthritis and psoriasis. *PLoS One* **15**, e0229819 (2020).

75. Decourt, B., Lahiri, D. K. & Sabbagh, M. N. Targeting Tumor Necrosis Factor Alpha for Alzheimer's Disease. *Curr. Alzheimer Res.* **14**, 412–425 (2017).

76. Kunkle, B. W. *et al.* Genetic meta-analysis of diagnosed Alzheimer's disease identifies new risk loci and implicates Aβ, tau, immunity and lipid processing. *Nat. Genet.* **51**, 414–430 (2019).

77. Lambert, J. C. *et al.* Implication of the immune system in Alzheimer's disease: evidence from genome-wide pathway analysis. *J. Alzheimer's Dis.* **20**, 1107–1118 (2010).

78. Harold, D. *et al.* Genome-wide association study identifies variants at CLU and PICALM associated with Alzheimer's disease. *Nat. Genet.* **41**, 1088–1093 (2009).

79. Squillario, M. *et al.* A telescope GWAS analysis strategy, based on SNPs-genes-pathways ensamble and on multivariate algorithms, to characterize late onset Alzheimer's disease. *Sci. Rep.* **10**, 1–12 (2020).

80. Baker, E. & Escott-Price, V. Polygenic Risk Scores in Alzheimer's Disease: Current Applications and Future Directions. *Front. Digit. Heal.* **2**, (2020).

81. Yamazaki, Y., Zhao, N., Caulfield, T. R., Liu, C.-C. & Bu, G. Apolipoprotein E and Alzheimer disease: pathobiology and targeting strategies. *Nat. Rev. Neurol.* **15**, 501–518 (2019).

82. Lumsden, A. L., Mulugeta, A., Zhou, A. & Hyppönen, E. Apolipoprotein E (APOE) genotype-associated disease risks: a phenome-wide, registry-based, case-control study utilising the UK Biobank. *EBioMedicine* **59**, 102954 (2020).

83. Kao, P. Y. P., Leung, K. H., Chan, L. W. C., Yip, S. P. & Yap, M. K. H. Pathway analysis of complex diseases for GWAS, extending to consider rare variants, multi-omics and interactions. *Biochim. Biophys. Acta - Gen. Subj.* **1861**, 335–353 (2017).

84. Robinson, M., Lee, B. Y. & Hane, F. T. Recent Progress in Alzheimer's Disease Research, Part 2: Genetics and Epidemiology. *J. Alzheimer's Dis.* **57**, 317–330 (2017).

85. Nesargikar, P., Spiller, B. & Chavez, R. The complement system: History, pathways, cascade and inhibitors. *Eur. J. Microbiol. Immunol.* **2**, 103–111 (2012).

86. Barnum, S. R. *Complement Factsbook*. (2018).

87. Moticka, E. J. Complement. in *A Historical Perspective on Evidence-Based Immunology* 95–103 (Elsevier, 2016). doi:10.1016/B978-0-12-398381-7.00012-5.

88. Zeipel, G., Hanson, H.-S. & Stedingk, L.-V. PURIFICATION FROM EUGLOBULIN OF THE FIRST COMPONENT (Cl) OF COMPLEMENT AND ITS SUBCOMPONENTS BY HEPARIN-SEPHAROSE CHROMATOGRAPHY. *Acta Pathol. Microbiol. Scand. Sect. C Immunol.* **85C**, 123–130 (2009).

89. Lepow, I. H., Naff, G. B., Todd, E. W., Pensky, J. & Hinz, C. F. CHROMATOGRAPHIC RESOLUTION OF THE FIRST COMPONENT OF HUMAN COMPLEMENT INTO THREE ACTIVITIES. *J. Exp. Med.* **117**, 983–1008 (1963).

90. Haihua, C., Wei, W., Kun, H., Yuanli, L. & Fei, L. Cobra Venom Factor-induced complement depletion protects against lung ischemia reperfusion injury through alleviating blood-air barrier damage. *Sci. Rep.* **8**, 1–8 (2018).

91. Fritzinger, D. C. *et al.* Functional characterization of human C3/cobra venom factor hybrid proteins for therapeutic complement depletion. *Dev. Comp. Immunol.* **33**, 105–116 (2009).

92. Gordon, J., Whitehead, H. R. & Wormall, A. The Action of Ammonia on Complement. The Fourth Component. *Biochem. J.* **20**, 1028–1035 (1926).

93. LEVINE, L., OSLER, A. G. & MAYER, M. M. Studies on the role of Ca++ and Mg++ in complement fixation and immune hemolysis. III. The respective roles of Ca++ and Mg++ in immune hemolysis. *J. Immunol.* **71**, 374–379 (1953).

94. Blatt, A. Z., Pathan, S. & Ferreira, V. P. Properdin: a tightly regulated critical inflammatory modulator. *Immunol. Rev.* **274**, 172–190 (2016).

95. SjÖHolm, A. G., Selander, B., ÖStenson, S., HolmstrÖM, E. & SÖDerstrÖM, C. Normal human serum depleted of Clq, factor D and properdin: its use in studies of complement activation. *APMIS* **99**, 1120–1128 (1991).

96. Fromell, K. *et al.* Assessment of the Role of C3(H2O) in the Alternative Pathway. *Front. Immunol.* **11**, (2020).

97. Thurman, J. M. & Holers, V. M. The Central Role of the Alternative Complement Pathway in Human Disease. *J. Immunol.* **176**, 1305–1310 (2006).

98. Merle, N. S., Church, S. E., Fremeaux-Bacchi, V. & Roumenina, L. T. Complement system part I - molecular mechanisms of activation and regulation. *Front. Immunol.* **6**, 1–30 (2015).

99. Nesargikar, P., Spiller, B. & Chavez, R. The complement system: History, pathways, cascade and inhibitors. *Eur. J. Microbiol. Immunol.* **2**, 103–111 (2012).

100. Cooper, N. R., Jensen, F. C., Welsh, R. M. & Oldstone, M. B. Lysis of RNA tumor viruses by human serum: direct antibody-independent triggering of the classical complement pathway. *J. Exp. Med.* **144**, 970–984 (1976).

101. Takahashi, M., Mori, S., Shigeta, S. & Fujita1, T. Role of MBL-associated Serine Protease (MASP) On Activation of the Lectin Complement Pathway. in *Current Topics in Innate Immunity* 93–104 (Springer New York). doi:10.1007/978-0-387-71767-8_8.

102. Jacquet, M. *et al.* C1q and mannose-binding lectin interact with CR1 in the same region on CCP24-25 modules. *Front. Immunol.* **9**, 1–11 (2018).

103. Beltrame, M. H., Catarino, S. J., Goeldner, I., Boldt, A. B. W. & de Messias-Reason, I. J. The Lectin Pathway of Complement and Rheumatic Heart Disease. *Front. Pediatr.* **2**, (2015).

104. Jiang, H., Wagner, E., Zhang, H. & Frank, M. M. Complement 1 Inhibitor Is a Regulator of the Alternative Complement Pathway. *J. Exp. Med.* **194**, 1609–1616 (2001).

105. Tenner, A. J., Stevens, B. & Woodruff, T. M. New tricks for an ancient system: Physiological and pathological roles of complement in the CNS. *Mol. Immunol.* **102**, 3–13 (2018).

106. Zipfel, P. F. & Skerka, C. Complement regulators and inhibitory proteins. *Nat. Rev. Immunol.* **9**, 729–740 (2009).

107. van Beek, J. *et al.* Decay-Accelerating Factor (CD55) Is Expressed by Neurons in Response to Chronic but Not Acute Autoimmune Central Nervous System Inflammation Associated with Complement Activation. *J. Immunol.* **174**, 2353–2365 (2005).

108. Liu, D. & Niu, Z. X. The structure, genetic polymorphisms, expression and biological functions of complement receptor type 1 (CR1/CD35). *Immunopharmacol. Immunotoxicol.* **31**, 524–535 (2009).

109. Farkas, I. *et al.* CD59 blocks not only the insertion of C9 into MAC but inhibits ion channel formation by homologous C5b-8 as well as C5b-9. *J. Physiol.* **539**, 537–545 (2002).

110. Ferrari, R. *et al.* Implication of common and disease specific variants in CLU, CR1, and PICALM.

Neurobiol. Aging **33**, 1846.e7-1846.e18 (2012).

111. Ormsby, R. J. *et al.* Functional and Structural Implications of the Complement Factor H Y402H Polymorphism Associated with Age-Related Macular Degeneration. *Investig. Opthalmology Vis. Sci.* **49**, 1763 (2008).

112. Abrera-Abeleda, M. A. Variations in the complement regulatory genes factor H (CFH) and factor H related 5 (CFHR5) are associated with membranoproliferative glomerulonephritis type II (dense deposit disease). *J. Med. Genet.* **43**, 582–589 (2005).

113. Dalakas, M. C., Alexopoulos, H. & Spaeth, P. J. Complement in neurological disorders and emerging complement-targeted therapeutics. *Nat. Rev. Neurol.* **16**, 601–617 (2020).

114. Johansson, J. U. *et al.* Peripheral complement interactions with amyloid β peptide in Alzheimer's disease: Polymorphisms, structure, and function of complement receptor 1. *Alzheimer's Dement.* **14**, 1438–1449 (2018).

115. Hansen, D. V., Hanson, J. E. & Sheng, M. Microglia in Alzheimer's disease. *J. Cell Biol.* **217**, 459–472 (2018).

116. Morgan, B. P. Complement in the pathogenesis of Alzheimer's disease. *Semin. Immunopathol.* **40**, 113–124 (2018).

117. Veerhuis, R., Nielsen, H. M. & Tenner, A. J. Complement in the brain. *Mol. Immunol.* **48**, 1592–1603 (2011).

118. Veerhuis, R., Janssen, I., Hack, C. E. & Eikelenboom, P. Early complement components in Alzheimer's disease brains. *Acta Neuropathol.* **91**, 53–60 (1995).

119. Wu, T. *et al.* Complement C3 Is Activated in Human AD Brain and Is Required for Neurodegeneration in Mouse Models of Amyloidosis and Tauopathy. *Cell Rep.* **28**, 2111-2123.e6 (2019).

120. Smyth, M. D. *et al.* Decreased levels of C1q in cerebrospinal fluid of living Alzheimer patients correlate with disease state. *Neurobiol. Aging* **15**, 609–614 (1994).

121. Daborg, J. *et al.* Cerebrospinal fluid levels of complement proteins C3, C4 and CR1 in Alzheimer's disease. *J. Neural Transm.* **119**, 789–797 (2012).

122. Davies, C. & Spires-Jones, T. L. Complementing Tau: New Data Show that the Complement System Is Involved in Degeneration in Tauopathies. *Neuron* **100**, 1267–1269 (2018).

123. Iqbal, K. *et al.* Animal Models of the Sporadic Form of Alzheimer's Disease: Focus on the Disease and Not Just the Lesions1. *J. Alzheimer's Dis.* **37**, 469–474 (2013).

124. LaFerla, F. M. & Green, K. N. Animal Models of Alzheimer Disease. *Cold Spring Harb. Perspect. Med.* **2**, a006320–a006320 (2012).

125. Maier, M. *et al.* Complement C3 Deficiency Leads to Accelerated Amyloid Plaque Deposition and Neurodegeneration and Modulation of the Microglia/Macrophage Phenotype in Amyloid Precursor Protein Transgenic Mice. *J. Neurosci.* **28**, 6333–6341 (2008).

126. Mukherjee, P. & Pasinetti, G. M. The role of complement anaphylatoxin C5a in neurodegeneration: Implications in Alzheimer's disease. *J. Neuroimmunol.* **105**, 124–130 (2000).

127. Fonseca, M. I. *et al.* Treatment with a C5aR Antagonist Decreases Pathology and Enhances Behavioral Performance in Murine Models of Alzheimer's Disease. *J. Immunol.* **183**, 1375–

1383 (2009).

128. Subramanian, J., Savage, J. C. & Tremblay, M. È. Synaptic Loss in Alzheimer's Disease: Mechanistic Insights Provided by Two-Photon in vivo Imaging of Transgenic Mouse Models. *Front. Cell. Neurosci.* **14**, 1–13 (2020).

129. Shi, Q. *et al.* Complement C3-deficient mice fail to display age-related hippocampal decline. *J. Neurosci.* **35**, 13029–13042 (2015).

130. Stevens, B. *et al.* The Classical Complement Cascade Mediates CNS Synapse Elimination. *Cell* **131**, 1164–1178 (2007).

131. Schafer, D. P. *et al.* Microglia Sculpt Postnatal Neural Circuits in an Activity and Complement-Dependent Manner. *Neuron* **74**, 691–705 (2012).

132. Efthymiou, A. G. & Goate, A. M. Late onset Alzheimer's disease genetics implicates microglial pathways in disease risk. *Mol. Neurodegener.* **12**, 1–12 (2017).

133. Carpanini, S. M. *et al.* The impact of complement genes on the risk of late-onset Alzheimer's disease. *Genes (Basel).* **12**, (2021).

134. Hazrati, L. N. *et al.* Genetic association of CR1 with Alzheimer's disease: A tentative disease mechanism. *Neurobiol. Aging* **33**, 2949.e5-2949.e12 (2012).

135. Tan, L. *et al.* Effect of CLU genetic variants on cerebrospinal fluid and neuroimaging markers in healthy, mild cognitive impairment and Alzheimer's disease cohorts. *Sci. Rep.* **6**, 1–12 (2016).

136. Crehan, H. *et al.* Complement receptor 1 (CR1) and Alzheimer's disease. *Immunobiology* **217**, 244–250 (2012).

137. Villegas-Llerena, C., Phillips, A., Reitboeck, P. G., Hardy, J. & Pocock, J. M. Microglial genes regulating neuroinflammation in the progression of Alzheimer's disease. *Curr. Opin. Neurobiol.* **36**, 74–81 (2016).

138. Morgan P.B. Complement in the Pathogenesis of Alzheimer's disease. *Semin. Immunopathol.* **5**, 113–124 (2018).

139. Craig, M. L., Waitumbi, J. N. & Taylor, R. P. Processing of C3b-Opsonized Immune Complexes Bound to Non-Complement Receptor 1 (CR1) Sites on Red Cells: Phagocytosis, Transfer, and Associations with CR1. *J. Immunol.* **174**, 3059–3066 (2005).

140. Krych-Goldberg, M. *et al.* Decay accelerating activity of complement receptor type 1 (CD35). Two active sites are required for dissociating C5 convertases. *J. Biol. Chem.* **274**, 31160–31168 (1999).

141. Fonseca, M. I. *et al.* Analysis of the putative role of CR1 in Alzheimer's disease: Genetic association, expression and function. *PLoS One* **11**, 1–21 (2016).

142. Danielsson, C., Pascual, M., French, L., Steiger, G. & Schifferli, J. -A. Soluble complement receptor type 1 (CD35) is released from leukocytes by surface cleavage. *Eur. J. Immunol.* **24**, 2725–2731 (1994).

143. Li, L. M., Li, J. B., Zhu, Y. & Fan, G. Y. Soluble complement receptor type 1 inhibits complement system activation and improves motor function in acute spinal cord injury. *Spinal Cord* **48**, 105–111 (2010).

144. Canova, C., Neal, J. W. & Gasque, P. Expression of innate immune complement regulators on

brain epithelial cells during human bacterial meningitis. *J. Neuroinflammation* **3**, 22 (2006).

145. Smith, B. O. *et al.* Structure of the C3b Binding Site of CR1 (CD35), the Immune Adherence Receptor. *Cell* **108**, 769–780 (2002).

146. Wong, W. W. *et al.* Structure of the human CR1 gene. Molecular basis of the structural and quantitative polymorphisms and identification of a new CR1-like allele. *J. Exp. Med.* **169**, 847–863 (1989).

147. Fonseca, M. I. *et al.* Analysis of the putative role of CR1 in Alzheimer's disease: Genetic association, expression and function. *PLoS One* **11**, (2016).

148. Klickstein, L. B., Barbashov, S. F., Liu, T., Jack, R. M. & Nicholson-Weller, A. Complement Receptor Type 1 (CR1, CD35) Is a Receptor for C1q. *Immunity* **7**, 345–355 (1997).

149. Jacquet, M. *et al.* C1q and Mannose-Binding Lectin Interact with CR1 in the Same Region on CCP24-25 Modules. *Front. Immunol.* **9**, (2018).

150. Moulds, J. M. The Knops blood group system: A review. *Immunohematology* **26**, 2–7 (2010).

151. Paccaud, J. -P, Carpentier, J. -L & Schifferli, J. A. Difference in the clustering of complement receptor type 1 (CR1) on polymorphonuclear leukocytes and erythrocytes: Effect on immune adherence. *Eur. J. Immunol.* **20**, 283–289 (1990).

152. Mahmoudi, R. *et al.* Inherited and acquired decrease in complement receptor 1 (CR1) density on red blood cells associated with high levels of soluble CR1 in Alzheimer's disease. *Int. J. Mol. Sci.* **19**, 1–18 (2018).

153. Chevalier, J. Distribution in clusters of complement receptor type one (CR1) on human erythrocytes . Why The JI ? Submit online . • Rapid Reviews ! 30 days * from submission to initial decision • No Triage ! Every submission reviewed by practicing scientists • Fast P. (2019).

154. Allen Human Brain Atlas; CR1. *Allen Human Brain Atlas* CR1: RNA in the brain https://www.proteinatlas.org/ENSG00000203710-CR1/brain.

155. Allen Brain Atlas: CR1 In situ. *Allen Brain Atlas* CR1: In Situ data https://www.proteinatlas.org/ENSG00000203710-CR1/tissue/cerebral+cortex#img.

156. Singhrao, S. K., Neal, J. W., Rushmere, N. K., Morgan, B. P. & Gasque, P. Differential expression of individual complement regulators in the brain and choroid plexus. *Lab. Invest.* **79**, 1247–59 (1999).

157. Gasque, P. *et al.* Identification and characterization of complement C3 receptors on human astrocytes. *J. Immunol.* **156**, 2247–55 (1996).

158. Brubaker, W. D. *et al.* Peripheral complement interactions with amyloid β peptide: Erythrocyte clearance mechanisms. *Alzheimer's Dement.* **13**, 1397–1409 (2017).

159. Davoust, N., Nataf, S., Holers, V. M. & Barnum, S. R. Expression of the murine complement regulatory protein Crry by glial cells and neurons. *Glia* **27**, 162–170 (1999).

160. Jacobson, A. C. & Weis, J. H. Comparative Functional Evolution of Human and Mouse CR1 and CR2. *J. Immunol.* **181**, 2953–2959 (2008).

161. Banadakoppa, M., Pennington, K., Balakrishnan, M. & Yallampalli, C. Complement inhibitor Crry expression in mouse placenta is essential for maintaining normal blood pressure and fetal growth. *PLoS One* **15**, 1–14 (2020).

162. Crehan, H., Hardy, J. & Pocock, J. Blockage of CR1 prevents activation of rodent microglia. *Neurobiol. Dis.* **54**, 139–149 (2013).

163. Jackson, H. M. *et al.* A novel mouse model expressing human forms for complement receptors CR1 and CR2. *BMC Genet.* **21**, 101 (2020).

164. Killick, R., Hughes, T. R., Morgan, B. P. & Lovestone, S. Deletion of Crry, the murine ortholog of the sporadic Alzheimer's disease risk gene CR1, impacts tau phosphorylation and brain CFH. *Neurosci. Lett.* **533**, 96–99 (2013).

165. Lambert, J. C. *et al.* Genome-wide association study identifies variants at CLU and CR1 associated with Alzheimer's disease. *Nat. Genet.* **41**, 1094–1099 (2009).

166. Lambert, J. C. *et al.* Meta-analysis of 74,046 individuals identifies 11 new susceptibility loci for Alzheimer's disease. *Nat. Genet.* **45**, 1452–1458 (2013).

167. Carrasquillo, M. M. *et al.* Replication of CLU, CR1, and PICALM Associations With Alzheimer Disease. *Arch. Neurol.* **67**, (2010).

168. Naj, A. C. *et al.* Common variants at MS4A4/MS4A6E, CD2AP, CD33 and EPHA1 are associated with late-onset Alzheimer's disease. *Nat. Genet.* **43**, 436–441 (2011).

169. Jun, G. Meta-analysis Confirms CR1, CLU, and PICALM as Alzheimer Disease Risk Loci and Reveals Interactions With APOE Genotypes. *Arch. Neurol.* **67**, 1473 (2010).

170. Schjeide, B.-M. M. *et al.* The Role of Clusterin, Complement Receptor 1, and Phosphatidylinositol Binding Clathrin Assembly Protein in Alzheimer Disease Risk and Cerebrospinal Fluid Biomarker Levels. *Arch. Gen. Psychiatry* **68**, 207 (2011).

171. Chen, L. H. *et al.* Polymorphisms of CR1, CLU and PICALM confer susceptibility of Alzheimer's disease in a southern Chinese population. *Neurobiol. Aging* **33**, 210.e1-210.e7 (2012).

172. Hazrati, L.-N. *et al.* Genetic association of CR1 with Alzheimer's disease: A tentative disease mechanism. *Neurobiol. Aging* **33**, 2949.e5-2949.e12 (2012).

173. Chung, S. J. *et al.* CR1, ABCA7, and APOE genes affect the features of cognitive impairment in Alzheimer's disease. *J. Neurol. Sci.* **339**, 91–96 (2014).

174. Ma, X.-Y. *et al.* Missense variants in CR1 are associated with increased risk of Alzheimer' disease in Han Chinese. *Neurobiol. Aging* **35**, 443.e17-443.e21 (2014).

175. Arvanitakis, Z. *et al.* Cerebral amyloid angiopathy pathology and cognitive domains in older persons. *Ann. Neurol.* **69**, 320–327 (2011).

176. Bralten, J. *et al.* CR1 genotype is associated with entorhinal cortex volume in young healthy adults. *Neurobiol. Aging* **32**, 2106.e7-2106.e11 (2011).

177. Biffi, A. Genetic Variation and Neuroimaging Measures in Alzheimer Disease. *Arch. Neurol.* **67**, 677 (2010).

178. Ruseva, M. M. *et al.* Crry deficiency in complement sufficient mice: C3 consumption occurs without associated renal injury. *Mol. Immunol.* **46**, 803–811 (2009).

179. Strohmeyer, R., Shen, Y. & Rogers, J. Detection of complement alternative pathway mRNA and proteins in the Alzheimer's disease brain. *Mol. Brain Res.* **81**, 7–18 (2000).

180. Gandy, S., Haroutunian, V., DeKosky, S. T., Sano, M. & Schadt, E. E. CR1 and the 'vanishing amyloid' hypothesis of Alzheimer's disease. *Biol. Psychiatry* **73**, 393–5 (2013).

181. Dello Russo, C. *et al.* The human microglial HMC3 cell line: Where do we stand? A systematic literature review. *J. Neuroinflammation* **15**, 1–24 (2018).

182. Boheler, R. K. Stem cell pluripotency: *J. cell Physiol.* **221**, 10–17 (2012).

183. Plusa, B. & Hadjantonakis, A.-K. Embryonic stem cell identity grounded in the embryo. *Nat. Cell Biol.* **16**, 502–504 (2014).

184. Xu, J. *et al.* A Simple and Effective Method for the Isolation of Inner Cell Mass Samples from Human Blastocysts for Gene Expression Analysis. *Vitr. Cell. Dev. Biol.* **50**, 232–36. (2014).

185. Evans, M. J. & Kaufman, M. H. Establishment in culture of pluripotential cells from mouse embryos. *Nature* **292**, 154–156 (1981).

186. Martin, G. R. Isolation of a pluripotent cell line from early mouse embryos cultured in medium conditioned by teratocarcinoma stem cells. *Proc. Natl. Acad. Sci.* **78**, 7634–7638 (1981).

187. Lai, D. *et al.* Derivation and characterization of human embryonic stem cells on human amnion epithelial cells. *Sci. Rep.* **5**, 10014 (2015).

188. Takahashi, K. & Yamanaka, S. Induction of Pluripotent Stem Cells from Mouse Embryonic and Adult Fibroblast Cultures by Defined Factors. *Cell* **126**, 663–676 (2006).

189. Shafa, M., Yang, F., Fellner, T., Rao, M. S. & Baghbaderani, B. A. Human-induced pluripotent stem cells manufactured using a current good manufacturing practice-compliant process differentiate into clinically relevant cells from three germ layers. *Front. Med.* **5**, 1–12 (2018).

190. Ohnuki, M. & Takahashi, K. Present and future challenges of induced pluripotent stem cells. *Philos. Trans. R. Soc. B Biol. Sci.* **370**, 20140367 (2015).

191. Yamanaka, S. Induced Pluripotent Stem Cells: Past, Present, and Future. *Cell Stem Cell* **10**, 678–684 (2012).

192. Xie, N. & Tang, B. The Application of Human iPSCs in Neurological Diseases: From Bench to Bedside. *Stem Cells Int.* **2016**, 23–27 (2016).

193. Mungenast, A. E., Siegert, S. & Tsai, L.-H. Modeling Alzheimer's disease with human induced pluripotent stem (iPS) cells. *Mol. Cell. Neurosci.* **73**, 13–31 (2016).

194. McQuade, A. *et al.* Development and validation of a simplified method to generate human microglia from pluripotent stem cells. *Mol. Neurodegener.* **13**, 1–13 (2018).

195. Kirabali, T. & Rust, R. iPS-derived pericytes for neurovascular regeneration. *Eur. J. Clin. Invest.* **51**, (2021).

196. Chambers, S. M. *et al.* Highly efficient neural conversion of human ES and iPS cells by dual inhibition of SMAD signaling. *Nat. Biotechnol.* **27**, 275–280 (2009).

197. Takata, K. *et al.* Induced-Pluripotent-Stem-Cell-Derived Primitive Macrophages Provide a Platform for Modeling Tissue-Resident Macrophage Differentiation and Function. *Immunity* **47**, 183-198.e6 (2017).

198. Lopez-Caraballo, L., Martorell-Marugan, J., Carmona-Sáez, P. & Gonzalez-Munoz, E. iPS-Derived Early Oligodendrocyte Progenitor Cells from SPMS Patients Reveal Deficient In Vitro Cell Migration Stimulation. *Cells* **9**, 1803 (2020).

199. Aflaki, E. *et al.* A characterization of Gaucher iPS-derived astrocytes: Potential implications for Parkinson's disease. *Neurobiol. Dis.* **134**, 104647 (2020).

200. Muffat, U. *et al.* Efficient derivation of microglia-like cells from human pluripotent stem cells HHS Public Access Author manuscript. *Nat Med* **22**, 1358–1367 (2016).

201. Iwasaki, H. *et al.* Distinctive and indispensable roles of PU.1 in maintenance of hematopoietic stem cells and their differentiation. *Blood* **106**, 1590–1600 (2005).

202. Taoudi, S. Haematopoiesis during embryonic development. *Exp. Hematol.* **41**, S4 (2013).

203. Ross, C. & Boroviak, T. E. Origin and function of the yolk sac in primate embryogenesis. *Nat. Commun.* **11**, 1–14 (2020).

204. Ginhoux, F. & Prinz, M. Origin of Microglia: Current Concepts and Past Controversies. *Cold Spring Harb. Perspect. Biol.* **7**, a020537 (2015).

205. Ginhoux, F. *et al.* Fate Mapping Analysis Reveals That Adult Microglia Derive from Primitive Macrophages. *Science (80-.).* **330**, 841–845 (2010).

206. Lu, S. J. *et al.* Robust generation of hemangioblastic progenitors from human embryonic stem cells. *Regen. Med.* **3**, 693–704 (2008).

207. Haenseler, W. *et al.* A Highly Efficient Human Pluripotent Stem Cell Microglia Model Displays a Neuronal-Co-culture-Specific Expression Profile and Inflammatory Response. *Stem Cell Reports* **8**, 1727–1742 (2017).

208. McQuade, A. *et al.* Development and validation of a simplified method to generate human microglia from pluripotent stem cells. *Mol. Neurodegener.* **13**, 67 (2018).

209. Ishino, Y., Krupovic, M. & Forterre, P. History of CRISPR-Cas from Encounter with a Mysterious. *J. Bacteriol.* **200**, e00580-17 (2018).

210. Adli, M. The CRISPR tool kit for genome editing and beyond. *Nat. Commun.* **9**, (2018).

211. Navarro-Guerrero, E. *et al.* Genome-wide CRISPR/Cas9-knockout in human induced Pluripotent Stem Cell (iPSC)-derived macrophages. *Sci. Rep.* **11**, (2021).

212. Shou, Y., Liang, F., Xu, S. & Li, X. The Application of Brain Organoids: From Neuronal Development to Neurological Diseases. *Front. Cell Dev. Biol.* **8**, (2020).

213. Byrne, R. A. J. *et al.* Novel Monoclonal Antibodies Against Mouse C1q: Characterisation and Development of a Quantitative ELISA for Mouse C1q. *Mol. Neurobiol.* **58**, 4323–4336 (2021).

214. Zelek, W. M., Taylor, P. R. & Morgan, B. P. Development and characterization of novel anti-C5 monoclonal antibodies capable of inhibiting complement in multiple species. *Immunology* **157**, 283–295 (2019).

215. Harris, C. L., Lublin, D. M. & Morgan, B. P. Efficient generation of monoclonal antibodies for specific protein domains using recombinant immunoglobulin fusion proteins: Pitfalls and solutions. *J. Immunol. Methods* **268**, 245–258 (2002).

216. Kucukkilic, E. *et al.* Complement receptor 1 gene (CR1) intragenic duplication and risk of Alzheimer's disease. *Hum. Genet.* **137**, 305–314 (2018).

217. Li, Q. & Barres, B. A. Microglia and macrophages in brain homeostasis and disease. *Nat. Rev. Immunol.* **18**, 225–242 (2018).

218. Mendes, M. S. & Majewska, A. K. An overview of microglia ontogeny and maturation in the homeostatic and pathological brain. *Eur. J. Neurosci.* **53**, 3525–3547 (2021).

219. Podleśny-Drabiniok, A., Marcora, E. & Goate, A. M. Microglial Phagocytosis: A Disease-

Associated Process Emerging from Alzheimer's Disease Genetics. *Trends Neurosci.* **43**, 965–979 (2020).

220. Onuska, K. M. The dual role of microglia in the progression of Alzheimer's disease. *J. Neurosci.* **40**, 1608–1610 (2020).

221. Correale, J. & Farez, M. F. The role of astrocytes in multiple sclerosis progression. *Front. Neurol.* **6**, 1–12 (2015).

222. Wesén, E., Jeffries, G. D. M., Dzebo, M. M. & Esbjörner, E. K. Endocytic uptake of monomeric amyloid-β peptides is clathrin- A nd dynamin-independent and results in selective accumulation of Aβ(1-42) compared to Aβ(1-40). *Sci. Rep.* **7**, 1–14 (2017).

223. Stansley, B., Post, J. & Hensley, K. A comparative review of cell culture systems for the study of microglial biology in Alzheimer's disease. *J. Neuroinflammation* **9**, 577 (2012).

224. Thion, M. S. & Garel, S. Microglial ontogeny, diversity and neurodevelopmental functions. *Curr. Opin. Genet. Dev.* **65**, 186–194 (2020).

225. Speicher, A. M., Wiendl, H., Meuth, S. G. & Pawlowski, M. Generating microglia from human pluripotent stem cells: Novel in vitro models for the study of neurodegeneration. *Mol. Neurodegener.* **14**, 1–16 (2019).

226. Serio, A. *et al.* Astrocyte pathology and the absence of non-cell autonomy in an induced pluripotent stem cell model of TDP-43 proteinopathy. *Proc. Natl. Acad. Sci. U. S. A.* **110**, 4697–4702 (2013).

227. Rushton, D. J., Mattis, V. B., Svendsen, C. N., Allen, N. D. & Kemp, P. J. Stimulation of GABA-induced Ca2+ influx enhances maturation of human induced pluripotent stem cell-derived neurons. *PLoS One* **8**, 1–16 (2013).

228. Frame, J. M., McGrath, K. E. & Palis, J. Erythro-myeloid progenitors: "Definitive" hematopoiesis in the conceptus prior to the emergence of hematopoietic stem cells. *Blood Cells, Mol. Dis.* **51**, 220–225 (2013).

229. Keller, G., Kennedy, M., Papayannopoulou, T. & Wiles, M. V. Hematopoietic commitment during embryonic stem cell differentiation in culture. *Mol. Cell. Biol.* **13**, 473–486 (1993).

230. Sturgeon, C. M., Ditadi, A., Awong, G., Kennedy, M. & Keller, G. Wnt signaling controls definitive and primitive. **32**, 554–561 (2014).

231. Ehman, E. C. *et al.* Diverse requirements for microglial survival, specification, and function revealed by defined-medium cultures Christopher. *Neuron* **46**, 1247–1262 (2017).

232. Easley-Neal, C., Foreman, O., Sharma, N., Zarrin, A. A. & Weimer, R. M. CSF1R Ligands IL-34 and CSF1 Are Differentially Required for Microglia Development and Maintenance in White and Gray Matter Brain Regions. *Front. Immunol.* **10**, (2019).

233. Re, F. *et al.* Granulocyte-Macrophage Colony-Stimulating Factor Induces an Expression Program in Neonatal Microglia That Primes Them for Antigen Presentation. *J. Immunol.* **169**, 2264–2273 (2002).

234. Esen, N. & Kielian, T. Effects of low dose GM-CSF on microglial inflammatory profiles to diverse pathogen-associated molecular patterns (PAMPs). *J. Neuroinflammation* **4**, 1–18 (2007).

235. Ngwa, C. & Liu, F. CD200-CD200R signaling and diseases: a potential therapeutic target? *Int. J. Physiol. Pathophysiol. Pharmacol.* **11**, 297–309 (2019).

236. Chamak, B. & Mallat, M. Fibronectin and laminin regulate the in vitro differentiation of microglial cells. *Neuroscience* **45**, 513–527 (1991).

237. Garcia-Alegria, E. *et al.* Early Human Hemogenic Endothelium Generates Primitive and Definitive Hematopoiesis In Vitro. *Stem Cell Reports* **11**, 1061–1074 (2018).

238. Jin, C., Li, W., Yuan, J., Xu, W. & Cheng, Z. Association of the CR1 polymorphism with late-onset Alzheimer's disease in Chinese Han populations: A meta-analysis. *Neurosci. Lett.* **527**, 46–49 (2012).

239. Shaltouki, A., Peng, J., Liu, Q., Rao, M. S. & Zeng, X. Efficient generation of astrocytes from human pluripotent stem cells in defined conditions. *Stem Cells* **31**, 941–952 (2013).

240. Yuan, S. H. *et al.* Cell-surface marker signatures for the Isolation of neural stem cells, glia and neurons derived from human pluripotent stem cells. *PLoS One* **6**, (2011).

241. Kawai, S., Kurganov, E. & Miyata, S. Transient increase of microglial C1q expression in the circumventricular organs of adult mouse during LPS-induced inflammation. *Cell Biochem. Funct.* **38**, 392–400 (2020).

242. Chevalier, J. Distribution in clusters of complement receptor type one (CR1) on human erythrocytes. *J. Immunol.* **142**, 2031–2036 (1989).

243. Matejuk, A. & Ransohoff, R. M. Crosstalk Between Astrocytes and Microglia: An Overview. *Front. Immunol.* **11**, 1–11 (2020).

244. Lian, H. *et al.* Astrocyte-Microglia Cross Talk through Complement Activation Modulates Amyloid Pathology in Mouse Models of Alzheimer's Disease. *J. Neurosci.* **36**, 577–589 (2016).

245. Lian, H. *et al.* Astrocyte-microglia cross talk through complement activation modulates amyloid pathology in mouse models of alzheimer's disease. *J. Neurosci.* **36**, 577–589 (2016).

246. Singhrao, S. K., Neal, J. W., Rushmere, N. K., Morgan, B. P. & Gasque, P. Differential expression of individual complement regulators in the brain and choroid plexus. *Lab. Invest.* **79**, 1247–59 (1999).

247. Brouwers, N. *et al.* Alzheimer risk associated with a copy number variation in the complement receptor 1 increasing C3b/C4b binding sites. *Mol. Psychiatry* **17**, 223–233 (2012).

248. Ruseva, M. M. *et al.* Crry deficiency in complement sufficient mice: C3 consumption occurs without associated renal injury. *Mol. Immunol.* **46**, 803–811 (2009).

249. Shi, M. *et al.* Premature termination codons are recognized in the nucleus in a reading-frame-dependent manner. *Cell Discov.* **1**, 1–20 (2015).

250. Brogna, S. & Wen, J. Nonsense-mediated mRNA decay (NMD) mechanisms. *Nat. Struct. Mol. Biol.* **16**, 107–113 (2009).

251. Karousis, E. D. & Mühlemann, O. Nonsense-mediated mRNA decay begins where translation ends. *Cold Spring Harb. Perspect. Biol.* **11**, 1–18 (2019).

252. Shah, N. J. *Recombinant DNA technology*. *Introduction to Basics of Pharmacology and Toxicology: Volume 1: General and Molecular Pharmacology: Principles of Drug Action* (2019). doi:10.1007/978-981-32-9779-1_34.

253. Joung, J. K. & Sander, J. D. TALENs: a widely applicable technology for targeted genome editing. *Nat. Rev. Mol. Cell Biol.* **14**, 49–55 (2013).

254. Han, X. *et al.* Nonsense-mediated mRNA decay: A 'nonsense' pathway makes sense in stem

cell biology. *Nucleic Acids Res.* **46**, 1038–1051 (2018).

255. Smits, A. H. *et al.* Biological plasticity rescues target activity in CRISPR knock outs. *Nat. Methods* **16**, 1087–1093 (2019).

256. Jo, H. Y. *et al.* Functional in vivo and in vitro effects of 20q11.21 genetic aberrations on hPSC differentiation. *Sci. Rep.* **10**, 1–14 (2020).

257. Amps, K. *et al.* Screening ethnically diverse human embryonic stem cells identifies a chromosome 20 minimal amplicon conferring growth advantage. *Nat. Biotechnol.* **29**, 1132–1144 (2011).

258. Brauer, R. B. *et al.* EXTRAHEPATIC SYNTHESIS OF C6 IN THE RAT IS SUFFICIENT FOR COMPLEMENT-MEDIATED HYPERACUTE REJECTION OF A GUINEA PIG CARDIAC XENOGRAFT. *Transplantation* **59**, 1073–1076 (1995).

259. MORGAN, B. P. & GASQUE, P. Extrahepatic complement biosynthesis: where, when and why? *Clin. Exp. Immunol.* **107**, 1–7 (1997).

260. Tang, S., Zhou, W., Sheerin, N. S., Vaughan, R. W. & Sacks, S. H. Contribution of renal secreted complement C3 to the circulating pool in humans. *J. Immunol.* **162**, 4336–41 (1999).

261. Lucchinetti, C. *et al.* Heterogeneity of multiple sclerosis lesions: implications for the pathogenesis of demyelination. *Ann. Neurol.* **47**, 707–17 (2000).

262. Carpanini, S. M., Torvell, M. & Morgan, B. P. Therapeutic Inhibition of the Complement System in Diseases of the Central Nervous System. *Front. Immunol.* **10**, (2019).

263. Hosokawa, M., Klegeris, A., Maguire, J. & McGeer, P. L. Expression of complement messenger RNAs and proteins by human oligodendroglial cells. *Glia* **42**, 417–423 (2003).

264. Luchena, C., Zuazo-Ibarra, J., Alberdi, E., Matute, C. & Capetillo-Zarate, E. Contribution of neurons and glial cells to complement-mediated synapse removal during development, aging and in Alzheimer's disease. *Mediators Inflamm.* **2018**, (2018).

265. Thomas, A., Gasque, P., Vaudry, D., Gonzalez, B. & Fontaine, M. Expression of a complete and functional complement system by human neuronal cells in vitro. *Int. Immunol.* **12**, 1015–1023 (2000).

266. Strohmeyer, R., Shen, Y. & Rogers, J. Detection of complement alternative pathway mRNA and proteins in the Alzheimer's disease brain. *Mol. Brain Res.* **81**, 7–18 (2000).

267. Cockburn, I. A. *et al.* A human complement receptor 1 polymorphism that reduces Plasmodium falciparum rosetting confers protection against severe malaria. *Proc. Natl. Acad. Sci. U. S. A.* **101**, 272–277 (2004).

268. Wu, X. *et al.* Membrane Protein Crry Maintains Homeostasis of the Complement System. *J. Immunol.* **181**, 2732–2740 (2008).

269. Laws, S. M. *et al.* TNF polymorphisms in Alzheimer disease and functional implications on CSF beta-amyloid levels. *Hum. Mutat.* **26**, 29–35 (2005).

270. Montgomery, S. L. *et al.* Chronic Neuron- and Age-Selective Down-Regulation of TNF Receptor Expression in Triple-Transgenic Alzheimer Disease Mice Leads to Significant Modulation of Amyloid- and Tau-Related Pathologies. *Am. J. Pathol.* **182**, 2285–2297 (2013).

271. Sartain, S. E., Turner, N. A. & Moake, J. L. TNF Regulates Essential Alternative Complement Pathway Components and Impairs Activation of Protein C in Human Glomerular Endothelial

Cells. *J. Immunol.* **196**, 832–845 (2016).

272. Irani, V. R. & Maslow, J. N. Induction of murine macrophage TNF-Î± synthesis by Mycobacterium avium is modulated through complement-dependent interaction via complement receptors 3 and 4 in relation to M. avium glycopeptidolipid. *FEMS Microbiol. Lett.* **246**, 221–228 (2005).

273. Benoit, M. E., Clarke, E. V., Morgado, P., Fraser, D. A. & Tenner, A. J. Complement Protein C1q Directs Macrophage Polarization and Limits Inflammasome Activity during the Uptake of Apoptotic Cells. *J. Immunol.* **188**, 5682–5693 (2012).

274. Weinstein, J. R. *et al.* IgM-Dependent Phagocytosis in Microglia Is Mediated by Complement Receptor 3, Not Fc / Receptor. *J. Immunol.* **195**, 5309–5317 (2015).

275. Ries, M. & Sastre, M. Mechanisms of Aβ clearance and degradation by glial cells. *Front. Aging Neurosci.* **8**, 1–9 (2016).

276. Thambisetty, M. *et al.* Effect of Complement CR1 on Brain Amyloid Burden During Aging and Its Modification by APOE Genotype. *Biol. Psychiatry* **73**, 422–428 (2013).

277. Wilgenburg, B. van, Browne, C., Vowles, J. & Cowley, S. A. Efficient, Long Term Production of Monocyte-Derived Macrophages from Human Pluripotent Stem Cells under Partly-Defined and Fully-Defined Conditions. *PLoS One* **8**, e71098 (2013).

278. Ji-wen, Y., Tong-yan, T. & Qi-lin, H. Protective effect of astrocyte-conditioned medium on neurons following hypoxia and mechanical injury. *Chinese J. Traumatol. - English Ed.* **16**, 3–9 (2013).

279. Zhang, J. *et al.* Mouse Astrocytes Promote Microglial Ramification by Releasing TGF-β and Forming Glial Fibers. *Front. Cell. Neurosci.* **14**, 1–15 (2020).

280. Li, Q. & Barres, B. A. Microglia and macrophages in brain homeostasis and disease. *Nat. Rev. Immunol.* **18**, 225–242 (2018).

281. Yang, T., Guo, R. & Zhang, F. Brain perivascular macrophages: Recent advances and implications in health and diseases. *CNS Neurosci. Ther.* **25**, 1318–1328 (2019).

282. LeBleu, V. S. & Neilson, E. G. Origin and functional heterogeneity of fibroblasts. *FASEB J.* **34**, 3519–3536 (2020).

283. Kim, W.-K. *et al.* CD163 Identifies Perivascular Macrophages in Normal and Viral Encephalitic Brains and Potential Precursors to Perivascular Macrophages in Blood. *Am. J. Pathol.* **168**, 822–834 (2006).

284. Triantafilou, K., Hughes, T. R., Triantafilou, M. & Morgan, B. P. The complement membrane attack complex triggers intracellular Ca2+ fluxes leading to NLRP3 inflammasome activation. *J. Cell Sci.* (2013) doi:10.1242/jcs.124388.

285. Mahmoudi, R. *et al.* Alzheimer's disease is associated with low density of the long CR1 isoform. *Neurobiol. Aging* **36**, 1766.e5-1766.e12 (2015).

286. Vukojicic, A. *et al.* The Classical Complement Pathway Mediates Microglia-Dependent Remodeling of Spinal Motor Circuits during Development and in SMA. *Cell Rep.* **29**, 3087-3100.e7 (2019).

287. Coulthard, L. G., Hawksworth, O. A. & Woodruff, T. M. Complement: The Emerging Architect of the Developing Brain. *Trends Neurosci.* **41**, 373–384 (2018).

288. Sellgren, C. M. *et al.* Increased synapse elimination by microglia in schizophrenia patient-derived models of synaptic pruning. *Nat. Neurosci.* **22**, 374–385 (2019).

289. Bahrini, I., Song, J., Diez, D. & Hanayama, R. Neuronal exosomes facilitate synaptic pruning by up-regulating complement factors in microglia. *Sci. Rep.* **5**, 7989 (2015).

290. Sansores-España, D., Carrillo-Avila, A., Melgar-Rodriguez, S., Díaz-Zuñiga, J. & Martínez-Aguilar, V. Periodontitis and Alzheimers disease. *Med. Oral Patol. Oral y Cir. Bucal* **26**, e43–e48 (2021).

291. Miller, J. D. *et al.* Human iPSC-Based Modeling of Late-Onset Disease via Progerin-Induced Aging. *Cell Stem Cell* **13**, 691–705 (2013).

1. Assal, F. History of Dementia. in 118–126 (2019). doi:10.1159/000494959.

2. Yang, H. D., Kim, D. H., Lee, S. B. & Young, L. D. History of Alzheimer's Disease. *Dement. Neurocognitive Disord.* **15**, 115 (2016).

3. Boller, F. & Forbes, M. M. History of dementia and dementia in history: An overview. *J. Neurol. Sci.* **158**, 125–133 (1998).

4. Murman, D. The Impact of Age on Cognition. *Semin. Hear.* **36**, 111–121 (2015).

5. Duong, S., Patel, T. & Chang, F. Dementia. *Can. Pharm. J. / Rev. des Pharm. du Canada* **150**, 118–129 (2017).

6. Escolme, B. When grief has mates: King Lear and the politics of happiness. *The Lancet Psychiatry* **5**, 621–622 (2018).

7. Sanderson, D. How King Lear teaches us about ageing and dementia. *The Times* (2016).

8. Schumacher, J. *et al.* Dysfunctional brain dynamics and their origin in Lewy body dementia. *Brain* **142**, 1767–1782 (2019).

9. Kane, J. P. M. *et al.* Clinical prevalence of Lewy body dementia. *Alzheimers. Res. Ther.* **10**, 19 (2018).

10. D.M., H., E., M. & D.J., S. Alzheimer disease in 2020. *Cold Spring Harb. Perspect. Med.* **2**, 1–5 (2012).

11. Ryan, N. S., Rossor, M. N. & Fox, N. C. Alzheimer's disease in the 100 years since Alzheimer's death. *Brain* **138**, 3816–3821 (2015).

12. Wittenberg, R., Hu, B. & Luis Barraza-Araiza, A. R. *Projections of older people with dementia and costs of dementia care in the United Kingdom, 2019–2040*. https://www.alzheimers.org.uk/sites/default/files/2019-11/cpec_report_november_2019.pdf (2019).

13. Reitz, C. Alzheimer's disease and the amyloid cascade hypothesis: A critical review. *Int. J. Alzheimers. Dis.* **2012**, (2012).

14. Hippius, H. & Neundörfer, G. The discovery of Alzheimer's disease. *Dialogues Clin. Neurosci.* **5**, 101–108 (2003).

15. Tanzi, R. E. & Bertram, L. Twenty Years of the Alzheimer's Disease Amyloid Hypothesis: A Genetic Perspective. *Cell* **120**, 545–555 (2005).

16. Masters, C. L. & Selkoe, D. J. Biochemistry of Amyloid -Protein and Amyloid Deposits in Alzheimer Disease. *Cold Spring Harb. Perspect. Med.* **2**, a006262–a006262 (2012).

17. Ricciarelli, R. & Fedele, E. The Amyloid Cascade Hypothesis in Alzheimer's Disease: It's Time to Change Our Mind. *Curr. Neuropharmacol.* **15**, (2017).

18. Uddin, M. S. *et al.* Revisiting the amyloid cascade hypothesis: From anti-aβ therapeutics to auspicious new ways for alzheimer's disease. *Int. J. Mol. Sci.* **21**, 1–33 (2020).

19. Karran, E., Mercken, M. & Strooper, B. De. The amyloid cascade hypothesis for Alzheimer's disease: An appraisal for the development of therapeutics. *Nat. Rev. Drug Discov.* **10**, 698–712 (2011).

20. Knopman, D. S., Petersen, R. C. & Jack, C. R. A brief history of "Alzheimer disease". *Neurology* **92**, 1053–1059 (2019).

21. Ricciarelli, R. & Fedele, E. The Amyloid Cascade Hypothesis in Alzheimer's Disease: It's Time to Change Our Mind. *Curr. Neuropharmacol.* **15**, 926–935 (2017).

22. Selkoe, D. J. & Hardy, J. The amyloid hypothesis of Alzheimer's disease at 25 years. *EMBO Mol. Med.* **8**, 595–608 (2016).

23. Hardy, J. A. & Higgins, G. A. Alzheimer's Disease: The Amyloid Cascade Hypothesis. *Science (80-.).* **256**, 184–185 (1992).

24. Kim, H. Y., Lee, D. K., Chung, B. R., Kim, H. V. & Kim, Y. Intracerebroventricular injection of amyloid-# peptides in normal mice to acutely induce alzheimer-like cognitive deficits. *J. Vis. Exp.* **2016**, 1–6 (2016).

25. Drummond, E. & Wisniewski, T. Alzheimer's disease: experimental models and reality. *Acta Neuropathol.* **133**, 155–175 (2017).

26. O'Brien, R. J. & Wong, P. C. Amyloid Precursor Protein Processing and Alzheimer's Disease. *Annu. Rev. Neurosci.* **34**, 185–204 (2011).

27. Zhang, X. & Song, W. The role of APP and BACE1 trafficking in APP processing and amyloid-β generation. *Alzheimers. Res. Ther.* **5**, 46 (2013).

28. Chow, V. W., Mattson, M. P., Wong, P. C. & Gleichmann, M. An Overview of APP Processing Enzymes and Products. *NeuroMolecular Med.* **12**, 1–12 (2010).

29. Chen, G. *et al.* Amyloid beta: structure, biology and structure-based therapeutic development. *Acta Pharmacol. Sin.* **38**, 1205–1235 (2017).

30. Wolfe, M. S. Unlocking truths of γ-secretase in Alzheimer's disease: what is the translational potential? *Future Neurol.* **9**, 419–429 (2014).

31. Guyon, A., Rousseau, J., Lamothe, G. & Tremblay, J. P. The protective mutation A673T in amyloid precursor protein gene decreases Aβ peptides production for 14 forms of Familial Alzheimer's Disease in SH-SY5Y cells. *PLoS One* **15**, e0237122 (2020).

32. Jonsson, T. *et al.* A mutation in APP protects against Alzheimer's disease and age-related cognitive decline. *Nature* **488**, 96–99 (2012).

33. TCW, J. & Goate, A. M. Genetics of β-Amyloid Precursor Protein in Alzheimer's Disease. *Cold Spring Harb. Perspect. Med.* **7**, a024539 (2017).

34. Chételat, G. *et al.* Amyloid imaging in cognitively normal individuals, at-risk populations and preclinical Alzheimer's disease. *NeuroImage Clin.* **2**, 356–365 (2013).

35. Iacono, D. *et al.* The Nun Study: Clinically silent AD, neuronal hypertrophy, and linguistic skills in early life. *Neurology* **73**, 665–673 (2009).

36. Nelson, P. T. *et al.* Brains With Medial Temporal Lobe Neurofibrillary Tangles But No Neuritic Amyloid Plaques Are a Diagnostic Dilemma But May Have Pathogenetic Aspects Distinct From Alzheimer Disease. *J. Neuropathol. Exp. Neurol.* **68**, 774–784 (2009).

37. Schönheit, B., Zarski, R. & Ohm, T. G. Spatial and temporal relationships between plaques and tangles in Alzheimer-pathology. *Neurobiol. Aging* **25**, 697–711 (2004).

38. Sudduth, T. L., Schmitt, F. A., Nelson, P. T. & Wilcock, D. M. Neuroinflammatory phenotype in early Alzheimer's disease. *Neurobiol. Aging* **34**, 1051–1059 (2013).

39. Heneka, M. T. *et al.* HHS Public Access Neuroinflammation in Alzheimer ' s Disease. *Lancet Neurol* **14**, 388–405 (2018).

40. Yiannopoulou, K. G. & Papageorgiou, S. G. Current and future treatments for Alzheimer's disease. *Ther. Adv. Neurol. Disord.* **6**, 19–33 (2013).

41. CHEN, W.-W., ZHANG, X. & HUANG, W.-J. Role of neuroinflammation in neurodegenerative diseases (Review). *Mol. Med. Rep.* **13**, 3391–3396 (2016).

42. Leng, F. & Edison, P. Neuroinflammation and microglial activation in Alzheimer disease: where do we go from here? *Nat. Rev. Neurol.* **17**, 157–172 (2021).

43. Kinney, J. W. *et al.* Inflammation as a central mechanism in Alzheimer's disease. *Alzheimer's Dement. Transl. Res. Clin. Interv.* **4**, 575–590 (2018).

44. Kinney, J. W. *et al.* Inflammation as a central mechanism in Alzheimer's disease. *Alzheimer's Dement. Transl. Res. Clin. Interv.* **4**, 575–590 (2018).

45. Shen, X.-N. *et al.* Identification of inflammatory and vascular markers associated with mild cognitive impairment. *Aging (Albany. NY).* **11**, 2403–2419 (2019).

46. McGeer, P. L. & McGeer, E. G. NSAIDs and Alzheimer disease: Epidemiological, animal model and clinical studies. *Neurobiol. Aging* **28**, 639–647 (2007).

47. Aisen, P. S. & Davis, K. L. Inflammatory mechanisms in Alzheimer's disease: implications for therapy. *Am. J. Psychiatry* **151**, 1105–13 (1994).

48. McKee, A. C. *et al.* Ibuprofen reduces Aβ, hyperphosphorylated tau and memory deficits in Alzheimer mice. *Brain Res.* **1207**, 225–236 (2008).

49. Lim, G. P. *et al.* Ibuprofen Suppresses Plaque Pathology and Inflammation in a Mouse Model for Alzheimer's Disease. *J. Neurosci.* **20**, 5709–5714 (2000).

50. Chong, Y. Effect of a carboxy-terminal fragment of the alzheimer's amyloid precursor protein on expression of proinflammatory cytokines in rat glial cells. *Life Sci.* **61**, 2323–2333 (1997).

51. Quintanilla, R. A., Orellana, D. I., González-Billault, C. & Maccioni, R. B. Interleukin-6 induces Alzheimer-type phosphorylation of tau protein by deregulating the cdk5/p35 pathway. *Exp. Cell Res.* **295**, 245–257 (2004).

52. Giovannoni, F. & Quintana, F. J. The Role of Astrocytes in CNS Inflammation. *Trends Immunol.* **41**, 805–819 (2020).

53. Perez-Nievas, B. G. & Serrano-Pozo, A. Deciphering the astrocyte reaction in Alzheimer's disease. *Front. Aging Neurosci.* **10**, 1–23 (2018).

54. Kobayashi, K. *et al.* Apoptosis of astrocytes with enhanced lysosomal activity and oligodendrocytes in white matter lesions in Alzheimer's disease. *Neuropathol. Appl. Neurobiol.* **28**, 238–251 (2002).

55. Mouser, P. E., Head, E., Ha, K.-H. & Rohn, T. T. Caspase-Mediated Cleavage of Glial Fibrillary Acidic Protein within Degenerating Astrocytes of the Alzheimer's Disease Brain. *Am. J. Pathol.* **168**, 936–946 (2006).

56. Abdelhak, A. *et al.* Glial Activation Markers in CSF and Serum From Patients With Primary Progressive Multiple Sclerosis: Potential of Serum GFAP as Disease Severity Marker? *Front. Neurol.* **10**, (2019).

57. Timmerman, R., Burm, S. M. & Bajramovic, J. J. An overview of in vitro methods to study microglia. *Front. Cell. Neurosci.* **12**, 1–12 (2018).

58. Egensperger, R., Kösel, S., Von Eitzen, U. & Graeber, M. B. Microglial activation in Alzheimer disease: Association with APOE genotype. *Brain Pathol.* **8**, 439–447 (1998).

59. Ulrich, J. D. *et al.* ApoE facilitates the microglial response to amyloid plaque pathology. *J. Exp. Med.* **215**, 1047–1058 (2018).

60. Condello, C., Yuan, P., Schain, A. & Grutzendler, J. Microglia constitute a barrier that prevents neurotoxic protofibrillar Aβ42 hotspots around plaques. *Nat. Commun.* **6**, 6176 (2015).

61. Baik, S. H., Kang, S., Son, S. M. & Mook-Jung, I. Microglia contributes to plaque growth by cell death due to uptake of amyloid β in the brain of Alzheimer's disease mouse model. *Glia* **64**, 2274–2290 (2016).

62. Lively, S. & Schlichter, L. C. Microglia Responses to Pro-inflammatory Stimuli (LPS, IFNγ+TNFα) and Reprogramming by Resolving Cytokines (IL-4, IL-10). *Front. Cell. Neurosci.* **12**, (2018).

63. Liu, Y. *et al.* LPS receptor (CD14): A receptor for phagocytosis of Alzheimer's amyloid peptide. *Brain* **128**, 1778–1789 (2005).

64. Hines, D. J., Choi, H. B., Hines, R. M., Phillips, A. G. & MacVicar, B. A. Prevention of LPS-Induced Microglia Activation, Cytokine Production and Sickness Behavior with TLR4 Receptor Interfering Peptides. *PLoS One* **8**, e60388 (2013).

65. Kang, J.-B., Park, D.-J., Shah, M.-A., Kim, M.-O. & Koh, P.-O. Lipopolysaccharide induces neuroglia activation and NF-κB activation in cerebral cortex of adult mice. *Lab. Anim. Res.* **35**, 19 (2019).

66. Zheng, D., Liwinski, T. & Elinav, E. Inflammasome activation and regulation: toward a better understanding of complex mechanisms. *Cell Discov.* **6**, (2020).

67. Hanslik, K. L. & Ulland, T. K. The Role of Microglia and the Nlrp3 Inflammasome in Alzheimer's Disease. *Front. Neurol.* **11**, (2020).

68. Heneka, M. T. *et al.* NLRP3 is activated in Alzheimer's disease and contributes to pathology in APP/PS1 mice. *Nature* **493**, 674–678 (2013).

69. Downs, K. P., Nguyen, H., Dorfleutner, A. & Stehlik, C. An overview of the non-canonical inflammasome. *Mol. Aspects Med.* **76**, 100924 (2020).

70. Couturier, J. *et al.* Activation of phagocytic activity in astrocytes by reduced expression of the inflammasome component ASC and its implication in a mouse model of Alzheimer disease. *J. Neuroinflammation* **13**, 20 (2016).

71. Halle, A. *et al.* The NALP3 inflammasome is involved in the innate immune response to amyloid-β. *Nat. Immunol.* **9**, 857–865 (2008).

72. Perry, R. The role of TNF and its receptors in Alzheimer's disease. *Neurobiol. Aging* **22**, 873–

883 (2001).

73. Jiang, H. *et al.* Genetic deletion of TNFRII gene enhances the Alzheimer-like pathology in an APP transgenic mouse model via reduction of phosphorylated I B. *Hum. Mol. Genet.* **23**, 4906–4918 (2014).

74. Zhou, M., Xu, R., Kaelber, D. C. & Gurney, M. E. Tumor Necrosis Factor (TNF) blocking agents are associated with lower risk for Alzheimer's disease in patients with rheumatoid arthritis and psoriasis. *PLoS One* **15**, e0229819 (2020).

75. Decourt, B., Lahiri, D. K. & Sabbagh, M. N. Targeting Tumor Necrosis Factor Alpha for Alzheimer's Disease. *Curr. Alzheimer Res.* **14**, 412–425 (2017).

76. Kunkle, B. W. *et al.* Genetic meta-analysis of diagnosed Alzheimer's disease identifies new risk loci and implicates Aβ, tau, immunity and lipid processing. *Nat. Genet.* **51**, 414–430 (2019).

77. Lambert, J. C. *et al.* Implication of the immune system in Alzheimer's disease: evidence from genome-wide pathway analysis. *J. Alzheimer's Dis.* **20**, 1107–1118 (2010).

78. Harold, D. *et al.* Genome-wide association study identifies variants at CLU and PICALM associated with Alzheimer's disease. *Nat. Genet.* **41**, 1088–1093 (2009).

79. Squillario, M. *et al.* A telescope GWAS analysis strategy, based on SNPs-genes-pathways ensamble and on multivariate algorithms, to characterize late onset Alzheimer's disease. *Sci. Rep.* **10**, 1–12 (2020).

80. Baker, E. & Escott-Price, V. Polygenic Risk Scores in Alzheimer's Disease: Current Applications and Future Directions. *Front. Digit. Heal.* **2**, (2020).

81. Yamazaki, Y., Zhao, N., Caulfield, T. R., Liu, C.-C. & Bu, G. Apolipoprotein E and Alzheimer disease: pathobiology and targeting strategies. *Nat. Rev. Neurol.* **15**, 501–518 (2019).

82. Lumsden, A. L., Mulugeta, A., Zhou, A. & Hyppönen, E. Apolipoprotein E (APOE) genotype-associated disease risks: a phenome-wide, registry-based, case-control study utilising the UK Biobank. *EBioMedicine* **59**, 102954 (2020).

83. Kao, P. Y. P., Leung, K. H., Chan, L. W. C., Yip, S. P. & Yap, M. K. H. Pathway analysis of complex diseases for GWAS, extending to consider rare variants, multi-omics and interactions. *Biochim. Biophys. Acta - Gen. Subj.* **1861**, 335–353 (2017).

84. Robinson, M., Lee, B. Y. & Hane, F. T. Recent Progress in Alzheimer's Disease Research, Part 2: Genetics and Epidemiology. *J. Alzheimer's Dis.* **57**, 317–330 (2017).

85. Nesargikar, P., Spiller, B. & Chavez, R. The complement system: History, pathways, cascade and inhibitors. *Eur. J. Microbiol. Immunol.* **2**, 103–111 (2012).

86. Barnum, S. R. *Complement Factsbook*. (2018).

87. Moticka, E. J. Complement. in *A Historical Perspective on Evidence-Based Immunology* 95–103 (Elsevier, 2016). doi:10.1016/B978-0-12-398381-7.00012-5.

88. Zeipel, G., Hanson, H.-S. & Stedingk, L.-V. PURIFICATION FROM EUGLOBULIN OF THE FIRST COMPONENT (Cl) OF COMPLEMENT AND ITS SUBCOMPONENTS BY HEPARIN-SEPHAROSE CHROMATOGRAPHY. *Acta Pathol. Microbiol. Scand. Sect. C Immunol.* **85C**, 123–130 (2009).

89. Lepow, I. H., Naff, G. B., Todd, E. W., Pensky, J. & Hinz, C. F. CHROMATOGRAPHIC RESOLUTION OF THE FIRST COMPONENT OF HUMAN COMPLEMENT INTO THREE ACTIVITIES. *J. Exp. Med.* **117**, 983–1008 (1963).

90. Haihua, C., Wei, W., Kun, H., Yuanli, L. & Fei, L. Cobra Venom Factor-induced complement depletion protects against lung ischemia reperfusion injury through alleviating blood-air barrier damage. *Sci. Rep.* **8**, 1–8 (2018).

91. Fritzinger, D. C. *et al.* Functional characterization of human C3/cobra venom factor hybrid proteins for therapeutic complement depletion. *Dev. Comp. Immunol.* **33**, 105–116 (2009).

92. Gordon, J., Whitehead, H. R. & Wormall, A. The Action of Ammonia on Complement. The Fourth Component. *Biochem. J.* **20**, 1028–1035 (1926).

93. LEVINE, L., OSLER, A. G. & MAYER, M. M. Studies on the role of Ca++ and Mg++ in complement fixation and immune hemolysis. III. The respective roles of Ca++ and Mg++ in immune hemolysis. *J. Immunol.* **71**, 374–379 (1953).

94. Blatt, A. Z., Pathan, S. & Ferreira, V. P. Properdin: a tightly regulated critical inflammatory modulator. *Immunol. Rev.* **274**, 172–190 (2016).

95. SjÖHolm, A. G., Selander, B., ÖStenson, S., HolmstrÖM, E. & SÖDerstrÖM, C. Normal human serum depleted of Clq, factor D and properdin: its use in studies of complement activation. *APMIS* **99**, 1120–1128 (1991).

96. Fromell, K. *et al.* Assessment of the Role of C3(H2O) in the Alternative Pathway. *Front. Immunol.* **11**, (2020).

97. Thurman, J. M. & Holers, V. M. The Central Role of the Alternative Complement Pathway in Human Disease. *J. Immunol.* **176**, 1305–1310 (2006).

98. Merle, N. S., Church, S. E., Fremeaux-Bacchi, V. & Roumenina, L. T. Complement system part I - molecular mechanisms of activation and regulation. *Front. Immunol.* **6**, 1–30 (2015).

99. Nesargikar, P., Spiller, B. & Chavez, R. The complement system: History, pathways, cascade and inhibitors. *Eur. J. Microbiol. Immunol.* **2**, 103–111 (2012).

100. Cooper, N. R., Jensen, F. C., Welsh, R. M. & Oldstone, M. B. Lysis of RNA tumor viruses by human serum: direct antibody-independent triggering of the classical complement pathway. *J. Exp. Med.* **144**, 970–984 (1976).

101. Takahashi, M., Mori, S., Shigeta, S. & Fujita1, T. Role of MBL-associated Serine Protease (MASP) On Activation of the Lectin Complement Pathway. in *Current Topics in Innate Immunity* 93–104 (Springer New York). doi:10.1007/978-0-387-71767-8_8.

102. Jacquet, M. *et al.* C1q and mannose-binding lectin interact with CR1 in the same region on CCP24-25 modules. *Front. Immunol.* **9**, 1–11 (2018).

103. Beltrame, M. H., Catarino, S. J., Goeldner, I., Boldt, A. B. W. & de Messias-Reason, I. J. The Lectin Pathway of Complement and Rheumatic Heart Disease. *Front. Pediatr.* **2**, (2015).

104. Jiang, H., Wagner, E., Zhang, H. & Frank, M. M. Complement 1 Inhibitor Is a Regulator of the Alternative Complement Pathway. *J. Exp. Med.* **194**, 1609–1616 (2001).

105. Tenner, A. J., Stevens, B. & Woodruff, T. M. New tricks for an ancient system: Physiological and pathological roles of complement in the CNS. *Mol. Immunol.* **102**, 3–13 (2018).

106. Zipfel, P. F. & Skerka, C. Complement regulators and inhibitory proteins. *Nat. Rev. Immunol.* **9**, 729–740 (2009).

107. van Beek, J. *et al.* Decay-Accelerating Factor (CD55) Is Expressed by Neurons in Response to Chronic but Not Acute Autoimmune Central Nervous System Inflammation Associated with

Complement Activation. *J. Immunol.* **174**, 2353–2365 (2005).

108. Liu, D. & Niu, Z. X. The structure, genetic polymorphisms, expression and biological functions of complement receptor type 1 (CR1/CD35). *Immunopharmacol. Immunotoxicol.* **31**, 524–535 (2009).

109. Farkas, I. *et al.* CD59 blocks not only the insertion of C9 into MAC but inhibits ion channel formation by homologous C5b-8 as well as C5b-9. *J. Physiol.* **539**, 537–545 (2002).

110. Ferrari, R. *et al.* Implication of common and disease specific variants in CLU, CR1, and PICALM. *Neurobiol. Aging* **33**, 1846.e7-1846.e18 (2012).

111. Ormsby, R. J. *et al.* Functional and Structural Implications of the Complement Factor H Y402H Polymorphism Associated with Age-Related Macular Degeneration. *Investig. Opthalmology Vis. Sci.* **49**, 1763 (2008).

112. Abrera-Abeleda, M. A. Variations in the complement regulatory genes factor H (CFH) and factor H related 5 (CFHR5) are associated with membranoproliferative glomerulonephritis type II (dense deposit disease). *J. Med. Genet.* **43**, 582–589 (2005).

113. Dalakas, M. C., Alexopoulos, H. & Spaeth, P. J. Complement in neurological disorders and emerging complement-targeted therapeutics. *Nat. Rev. Neurol.* **16**, 601–617 (2020).

114. Johansson, J. U. *et al.* Peripheral complement interactions with amyloid β peptide in Alzheimer's disease: Polymorphisms, structure, and function of complement receptor 1. *Alzheimer's Dement.* **14**, 1438–1449 (2018).

115. Hansen, D. V., Hanson, J. E. & Sheng, M. Microglia in Alzheimer's disease. *J. Cell Biol.* **217**, 459–472 (2018).

116. Morgan, B. P. Complement in the pathogenesis of Alzheimer's disease. *Semin. Immunopathol.* **40**, 113–124 (2018).

117. Veerhuis, R., Nielsen, H. M. & Tenner, A. J. Complement in the brain. *Mol. Immunol.* **48**, 1592–1603 (2011).

118. Veerhuis, R., Janssen, I., Hack, C. E. & Eikelenboom, P. Early complement components in Alzheimer's disease brains. *Acta Neuropathol.* **91**, 53–60 (1995).

119. Wu, T. *et al.* Complement C3 Is Activated in Human AD Brain and Is Required for Neurodegeneration in Mouse Models of Amyloidosis and Tauopathy. *Cell Rep.* **28**, 2111-2123.e6 (2019).

120. Smyth, M. D. *et al.* Decreased levels of C1q in cerebrospinal fluid of living Alzheimer patients correlate with disease state. *Neurobiol. Aging* **15**, 609–614 (1994).

121. Daborg, J. *et al.* Cerebrospinal fluid levels of complement proteins C3, C4 and CR1 in Alzheimer's disease. *J. Neural Transm.* **119**, 789–797 (2012).

122. Davies, C. & Spires-Jones, T. L. Complementing Tau: New Data Show that the Complement System Is Involved in Degeneration in Tauopathies. *Neuron* **100**, 1267–1269 (2018).

123. Iqbal, K. *et al.* Animal Models of the Sporadic Form of Alzheimer's Disease: Focus on the Disease and Not Just the Lesions1. *J. Alzheimer's Dis.* **37**, 469–474 (2013).

124. LaFerla, F. M. & Green, K. N. Animal Models of Alzheimer Disease. *Cold Spring Harb. Perspect. Med.* **2**, a006320–a006320 (2012).

125. Maier, M. *et al.* Complement C3 Deficiency Leads to Accelerated Amyloid Plaque Deposition

and Neurodegeneration and Modulation of the Microglia/Macrophage Phenotype in Amyloid Precursor Protein Transgenic Mice. *J. Neurosci.* **28**, 6333–6341 (2008).

126. Mukherjee, P. & Pasinetti, G. M. The role of complement anaphylatoxin C5a in neurodegeneration: Implications in Alzheimer's disease. *J. Neuroimmunol.* **105**, 124–130 (2000).

127. Fonseca, M. I. *et al.* Treatment with a C5aR Antagonist Decreases Pathology and Enhances Behavioral Performance in Murine Models of Alzheimer's Disease. *J. Immunol.* **183**, 1375–1383 (2009).

128. Subramanian, J., Savage, J. C. & Tremblay, M. È. Synaptic Loss in Alzheimer's Disease: Mechanistic Insights Provided by Two-Photon in vivo Imaging of Transgenic Mouse Models. *Front. Cell. Neurosci.* **14**, 1–13 (2020).

129. Shi, Q. *et al.* Complement C3-deficient mice fail to display age-related hippocampal decline. *J. Neurosci.* **35**, 13029–13042 (2015).

130. Stevens, B. *et al.* The Classical Complement Cascade Mediates CNS Synapse Elimination. *Cell* **131**, 1164–1178 (2007).

131. Schafer, D. P. *et al.* Microglia Sculpt Postnatal Neural Circuits in an Activity and Complement-Dependent Manner. *Neuron* **74**, 691–705 (2012).

132. Efthymiou, A. G. & Goate, A. M. Late onset Alzheimer's disease genetics implicates microglial pathways in disease risk. *Mol. Neurodegener.* **12**, 1–12 (2017).

133. Carpanini, S. M. *et al.* The impact of complement genes on the risk of late-onset Alzheimer's disease. *Genes (Basel).* **12**, (2021).

134. Hazrati, L. N. *et al.* Genetic association of CR1 with Alzheimer's disease: A tentative disease mechanism. *Neurobiol. Aging* **33**, 2949.e5-2949.e12 (2012).

135. Tan, L. *et al.* Effect of CLU genetic variants on cerebrospinal fluid and neuroimaging markers in healthy, mild cognitive impairment and Alzheimer's disease cohorts. *Sci. Rep.* **6**, 1–12 (2016).

136. Crehan, H. *et al.* Complement receptor 1 (CR1) and Alzheimer's disease. *Immunobiology* **217**, 244–250 (2012).

137. Villegas-Llerena, C., Phillips, A., Reitboeck, P. G., Hardy, J. & Pocock, J. M. Microglial genes regulating neuroinflammation in the progression of Alzheimer's disease. *Curr. Opin. Neurobiol.* **36**, 74–81 (2016).

138. Morgan P.B. Complement in the Pathogenesis of Alzheimer's disease. *Semin. Immunopathol.* **5**, 113–124 (2018).

139. Craig, M. L., Waitumbi, J. N. & Taylor, R. P. Processing of C3b-Opsonized Immune Complexes Bound to Non-Complement Receptor 1 (CR1) Sites on Red Cells: Phagocytosis, Transfer, and Associations with CR1. *J. Immunol.* **174**, 3059–3066 (2005).

140. Krych-Goldberg, M. *et al.* Decay accelerating activity of complement receptor type 1 (CD35). Two active sites are required for dissociating C5 convertases. *J. Biol. Chem.* **274**, 31160–31168 (1999).

141. Fonseca, M. I. *et al.* Analysis of the putative role of CR1 in Alzheimer's disease: Genetic association, expression and function. *PLoS One* **11**, 1–21 (2016).

142. Danielsson, C., Pascual, M., French, L., Steiger, G. & Schifferli, J. -A. Soluble complement receptor type 1 (CD35) is released from leukocytes by surface cleavage. *Eur. J. Immunol.* **24**, 2725–2731 (1994).

143. Li, L. M., Li, J. B., Zhu, Y. & Fan, G. Y. Soluble complement receptor type 1 inhibits complement system activation and improves motor function in acute spinal cord injury. *Spinal Cord* **48**, 105–111 (2010).

144. Canova, C., Neal, J. W. & Gasque, P. Expression of innate immune complement regulators on brain epithelial cells during human bacterial meningitis. *J. Neuroinflammation* **3**, 22 (2006).

145. Smith, B. O. *et al.* Structure of the C3b Binding Site of CR1 (CD35), the Immune Adherence Receptor. *Cell* **108**, 769–780 (2002).

146. Wong, W. W. *et al.* Structure of the human CR1 gene. Molecular basis of the structural and quantitative polymorphisms and identification of a new CR1-like allele. *J. Exp. Med.* **169**, 847–863 (1989).

147. Fonseca, M. I. *et al.* Analysis of the putative role of CR1 in Alzheimer's disease: Genetic association, expression and function. *PLoS One* **11**, (2016).

148. Klickstein, L. B., Barbashov, S. F., Liu, T., Jack, R. M. & Nicholson-Weller, A. Complement Receptor Type 1 (CR1, CD35) Is a Receptor for C1q. *Immunity* **7**, 345–355 (1997).

149. Jacquet, M. *et al.* C1q and Mannose-Binding Lectin Interact with CR1 in the Same Region on CCP24-25 Modules. *Front. Immunol.* **9**, (2018).

150. Moulds, J. M. The Knops blood group system: A review. *Immunohematology* **26**, 2–7 (2010).

151. Paccaud, J. -P, Carpentier, J. -L & Schifferli, J. A. Difference in the clustering of complement receptor type 1 (CR1) on polymorphonuclear leukocytes and erythrocytes: Effect on immune adherence. *Eur. J. Immunol.* **20**, 283–289 (1990).

152. Mahmoudi, R. *et al.* Inherited and acquired decrease in complement receptor 1 (CR1) density on red blood cells associated with high levels of soluble CR1 in Alzheimer's disease. *Int. J. Mol. Sci.* **19**, 1–18 (2018).

153. Chevalier, J. Distribution in clusters of complement receptor type one (CR1) on human erythrocytes . Why The JI ? Submit online . • Rapid Reviews ! 30 days * from submission to initial decision • No Triage ! Every submission reviewed by practicing scientists • Fast P. (2019).

154. Allen Human Brain Atlas; CR1. *Allen Human Brain Atlas* CR1: RNA in the brain https://www.proteinatlas.org/ENSG00000203710-CR1/brain.

155. Allen Brain Atlas: CR1 In situ. *Allen Brain Atlas* CR1: In Situ data https://www.proteinatlas.org/ENSG00000203710-CR1/tissue/cerebral+cortex#img.

156. Singhrao, S. K., Neal, J. W., Rushmere, N. K., Morgan, B. P. & Gasque, P. Differential expression of individual complement regulators in the brain and choroid plexus. *Lab. Invest.* **79**, 1247–59 (1999).

157. Gasque, P. *et al.* Identification and characterization of complement C3 receptors on human astrocytes. *J. Immunol.* **156**, 2247–55 (1996).

158. Brubaker, W. D. *et al.* Peripheral complement interactions with amyloid β peptide: Erythrocyte clearance mechanisms. *Alzheimer's Dement.* **13**, 1397–1409 (2017).

159. Davoust, N., Nataf, S., Holers, V. M. & Barnum, S. R. Expression of the murine complement regulatory protein Crry by glial cells and neurons. *Glia* **27**, 162–170 (1999).

160. Jacobson, A. C. & Weis, J. H. Comparative Functional Evolution of Human and Mouse CR1 and CR2. *J. Immunol.* **181**, 2953–2959 (2008).

161. Banadakoppa, M., Pennington, K., Balakrishnan, M. & Yallampalli, C. Complement inhibitor Crry expression in mouse placenta is essential for maintaining normal blood pressure and fetal growth. *PLoS One* **15**, 1–14 (2020).

162. Crehan, H., Hardy, J. & Pocock, J. Blockage of CR1 prevents activation of rodent microglia. *Neurobiol. Dis.* **54**, 139–149 (2013).

163. Jackson, H. M. *et al.* A novel mouse model expressing human forms for complement receptors CR1 and CR2. *BMC Genet.* **21**, 101 (2020).

164. Killick, R., Hughes, T. R., Morgan, B. P. & Lovestone, S. Deletion of Crry, the murine ortholog of the sporadic Alzheimer's disease risk gene CR1, impacts tau phosphorylation and brain CFH. *Neurosci. Lett.* **533**, 96–99 (2013).

165. Lambert, J. C. *et al.* Genome-wide association study identifies variants at CLU and CR1 associated with Alzheimer's disease. *Nat. Genet.* **41**, 1094–1099 (2009).

166. Lambert, J. C. *et al.* Meta-analysis of 74,046 individuals identifies 11 new susceptibility loci for Alzheimer's disease. *Nat. Genet.* **45**, 1452–1458 (2013).

167. Carrasquillo, M. M. *et al.* Replication of CLU, CR1, and PICALM Associations With Alzheimer Disease. *Arch. Neurol.* **67**, (2010).

168. Naj, A. C. *et al.* Common variants at MS4A4/MS4A6E, CD2AP, CD33 and EPHA1 are associated with late-onset Alzheimer's disease. *Nat. Genet.* **43**, 436–441 (2011).

169. Jun, G. Meta-analysis Confirms CR1, CLU, and PICALM as Alzheimer Disease Risk Loci and Reveals Interactions With APOE Genotypes. *Arch. Neurol.* **67**, 1473 (2010).

170. Schjeide, B.-M. M. *et al.* The Role of Clusterin, Complement Receptor 1, and Phosphatidylinositol Binding Clathrin Assembly Protein in Alzheimer Disease Risk and Cerebrospinal Fluid Biomarker Levels. *Arch. Gen. Psychiatry* **68**, 207 (2011).

171. Chen, L. H. *et al.* Polymorphisms of CR1, CLU and PICALM confer susceptibility of Alzheimer's disease in a southern Chinese population. *Neurobiol. Aging* **33**, 210.e1-210.e7 (2012).

172. Hazrati, L.-N. *et al.* Genetic association of CR1 with Alzheimer's disease: A tentative disease mechanism. *Neurobiol. Aging* **33**, 2949.e5-2949.e12 (2012).

173. Chung, S. J. *et al.* CR1, ABCA7, and APOE genes affect the features of cognitive impairment in Alzheimer's disease. *J. Neurol. Sci.* **339**, 91–96 (2014).

174. Ma, X.-Y. *et al.* Missense variants in CR1 are associated with increased risk of Alzheimer' disease in Han Chinese. *Neurobiol. Aging* **35**, 443.e17-443.e21 (2014).

175. Arvanitakis, Z. *et al.* Cerebral amyloid angiopathy pathology and cognitive domains in older persons. *Ann. Neurol.* **69**, 320–327 (2011).

176. Bralten, J. *et al.* CR1 genotype is associated with entorhinal cortex volume in young healthy adults. *Neurobiol. Aging* **32**, 2106.e7-2106.e11 (2011).

177. Biffi, A. Genetic Variation and Neuroimaging Measures in Alzheimer Disease. *Arch. Neurol.* **67**, 677 (2010).

178. Ruseva, M. M. *et al.* Crry deficiency in complement sufficient mice: C3 consumption occurs without associated renal injury. *Mol. Immunol.* **46**, 803–811 (2009).

179. Strohmeyer, R., Shen, Y. & Rogers, J. Detection of complement alternative pathway mRNA and proteins in the Alzheimer's disease brain. *Mol. Brain Res.* **81**, 7–18 (2000).

180. Gandy, S., Haroutunian, V., DeKosky, S. T., Sano, M. & Schadt, E. E. CR1 and the 'vanishing amyloid' hypothesis of Alzheimer's disease. *Biol. Psychiatry* **73**, 393–5 (2013).

181. Dello Russo, C. *et al.* The human microglial HMC3 cell line: Where do we stand? A systematic literature review. *J. Neuroinflammation* **15**, 1–24 (2018).

182. Boheler, R. K. Stem cell pluripotency: *J. cell Physiol.* **221**, 10–17 (2012).

183. Plusa, B. & Hadjantonakis, A.-K. Embryonic stem cell identity grounded in the embryo. *Nat. Cell Biol.* **16**, 502–504 (2014).

184. Xu, J. *et al.* A Simple and Effective Method for the Isolation of Inner Cell Mass Samples from Human Blastocysts for Gene Expression Analysis. *Vitr. Cell. Dev. Biol.* **50**, 232–36. (2014).

185. Evans, M. J. & Kaufman, M. H. Establishment in culture of pluripotential cells from mouse embryos. *Nature* **292**, 154–156 (1981).

186. Martin, G. R. Isolation of a pluripotent cell line from early mouse embryos cultured in medium conditioned by teratocarcinoma stem cells. *Proc. Natl. Acad. Sci.* **78**, 7634–7638 (1981).

187. Lai, D. *et al.* Derivation and characterization of human embryonic stem cells on human amnion epithelial cells. *Sci. Rep.* **5**, 10014 (2015).

188. Takahashi, K. & Yamanaka, S. Induction of Pluripotent Stem Cells from Mouse Embryonic and Adult Fibroblast Cultures by Defined Factors. *Cell* **126**, 663–676 (2006).

189. Shafa, M., Yang, F., Fellner, T., Rao, M. S. & Baghbaderani, B. A. Human-induced pluripotent stem cells manufactured using a current good manufacturing practice-compliant process differentiate into clinically relevant cells from three germ layers. *Front. Med.* **5**, 1–12 (2018).

190. Ohnuki, M. & Takahashi, K. Present and future challenges of induced pluripotent stem cells. *Philos. Trans. R. Soc. B Biol. Sci.* **370**, 20140367 (2015).

191. Yamanaka, S. Induced Pluripotent Stem Cells: Past, Present, and Future. *Cell Stem Cell* **10**, 678–684 (2012).

192. Xie, N. & Tang, B. The Application of Human iPSCs in Neurological Diseases: From Bench to Bedside. *Stem Cells Int.* **2016**, 23–27 (2016).

193. Mungenast, A. E., Siegert, S. & Tsai, L.-H. Modeling Alzheimer's disease with human induced pluripotent stem (iPS) cells. *Mol. Cell. Neurosci.* **73**, 13–31 (2016).

194. McQuade, A. *et al.* Development and validation of a simplified method to generate human microglia from pluripotent stem cells. *Mol. Neurodegener.* **13**, 1–13 (2018).

195. Kirabali, T. & Rust, R. iPS-derived pericytes for neurovascular regeneration. *Eur. J. Clin. Invest.* **51**, (2021).

196. Chambers, S. M. *et al.* Highly efficient neural conversion of human ES and iPS cells by dual inhibition of SMAD signaling. *Nat. Biotechnol.* **27**, 275–280 (2009).

197. Takata, K. *et al.* Induced-Pluripotent-Stem-Cell-Derived Primitive Macrophages Provide a

Platform for Modeling Tissue-Resident Macrophage Differentiation and Function. *Immunity* **47**, 183-198.e6 (2017).

198. Lopez-Caraballo, L., Martorell-Marugan, J., Carmona-Sáez, P. & Gonzalez-Munoz, E. iPS-Derived Early Oligodendrocyte Progenitor Cells from SPMS Patients Reveal Deficient In Vitro Cell Migration Stimulation. *Cells* **9**, 1803 (2020).

199. Aflaki, E. *et al.* A characterization of Gaucher iPS-derived astrocytes: Potential implications for Parkinson's disease. *Neurobiol. Dis.* **134**, 104647 (2020).

200. Muffat, U. *et al.* Efficient derivation of microglia-like cells from human pluripotent stem cells HHS Public Access Author manuscript. *Nat Med* **22**, 1358–1367 (2016).

201. Iwasaki, H. *et al.* Distinctive and indispensable roles of PU.1 in maintenance of hematopoietic stem cells and their differentiation. *Blood* **106**, 1590–1600 (2005).

202. Taoudi, S. Haematopoiesis during embryonic development. *Exp. Hematol.* **41**, S4 (2013).

203. Ross, C. & Boroviak, T. E. Origin and function of the yolk sac in primate embryogenesis. *Nat. Commun.* **11**, 1–14 (2020).

204. Ginhoux, F. & Prinz, M. Origin of Microglia: Current Concepts and Past Controversies. *Cold Spring Harb. Perspect. Biol.* **7**, a020537 (2015).

205. Ginhoux, F. *et al.* Fate Mapping Analysis Reveals That Adult Microglia Derive from Primitive Macrophages. *Science (80-.).* **330**, 841–845 (2010).

206. Lu, S. J. *et al.* Robust generation of hemangioblastic progenitors from human embryonic stem cells. *Regen. Med.* **3**, 693–704 (2008).

207. Haenseler, W. *et al.* A Highly Efficient Human Pluripotent Stem Cell Microglia Model Displays a Neuronal-Co-culture-Specific Expression Profile and Inflammatory Response. *Stem Cell Reports* **8**, 1727–1742 (2017).

208. McQuade, A. *et al.* Development and validation of a simplified method to generate human microglia from pluripotent stem cells. *Mol. Neurodegener.* **13**, 67 (2018).

209. Ishino, Y., Krupovic, M. & Forterre, P. History of CRISPR-Cas from Encounter with a Mysterious. *J. Bacteriol.* **200**, e00580-17 (2018).

210. Adli, M. The CRISPR tool kit for genome editing and beyond. *Nat. Commun.* **9**, (2018).

211. Navarro-Guerrero, E. *et al.* Genome-wide CRISPR/Cas9-knockout in human induced Pluripotent Stem Cell (iPSC)-derived macrophages. *Sci. Rep.* **11**, (2021).

212. Shou, Y., Liang, F., Xu, S. & Li, X. The Application of Brain Organoids: From Neuronal Development to Neurological Diseases. *Front. Cell Dev. Biol.* **8**, (2020).

213. Byrne, R. A. J. *et al.* Novel Monoclonal Antibodies Against Mouse C1q: Characterisation and Development of a Quantitative ELISA for Mouse C1q. *Mol. Neurobiol.* **58**, 4323–4336 (2021).

214. Zelek, W. M., Taylor, P. R. & Morgan, B. P. Development and characterization of novel anti-C5 monoclonal antibodies capable of inhibiting complement in multiple species. *Immunology* **157**, 283–295 (2019).

215. Harris, C. L., Lublin, D. M. & Morgan, B. P. Efficient generation of monoclonal antibodies for specific protein domains using recombinant immunoglobulin fusion proteins: Pitfalls and solutions. *J. Immunol. Methods* **268**, 245–258 (2002).

216. Kucukkilic, E. *et al.* Complement receptor 1 gene (CR1) intragenic duplication and risk of Alzheimer's disease. *Hum. Genet.* **137**, 305–314 (2018).

217. Li, Q. & Barres, B. A. Microglia and macrophages in brain homeostasis and disease. *Nat. Rev. Immunol.* **18**, 225–242 (2018).

218. Mendes, M. S. & Majewska, A. K. An overview of microglia ontogeny and maturation in the homeostatic and pathological brain. *Eur. J. Neurosci.* **53**, 3525–3547 (2021).

219. Podleśny-Drabiniok, A., Marcora, E. & Goate, A. M. Microglial Phagocytosis: A Disease-Associated Process Emerging from Alzheimer's Disease Genetics. *Trends Neurosci.* **43**, 965–979 (2020).

220. Onuska, K. M. The dual role of microglia in the progression of Alzheimer's disease. *J. Neurosci.* **40**, 1608–1610 (2020).

221. Correale, J. & Farez, M. F. The role of astrocytes in multiple sclerosis progression. *Front. Neurol.* **6**, 1–12 (2015).

222. Wesén, E., Jeffries, G. D. M., Dzebo, M. M. & Esbjörner, E. K. Endocytic uptake of monomeric amyloid-β peptides is clathrin- A nd dynamin-independent and results in selective accumulation of Aβ(1-42) compared to Aβ(1-40). *Sci. Rep.* **7**, 1–14 (2017).

223. Stansley, B., Post, J. & Hensley, K. A comparative review of cell culture systems for the study of microglial biology in Alzheimer's disease. *J. Neuroinflammation* **9**, 577 (2012).

224. Thion, M. S. & Garel, S. Microglial ontogeny, diversity and neurodevelopmental functions. *Curr. Opin. Genet. Dev.* **65**, 186–194 (2020).

225. Speicher, A. M., Wiendl, H., Meuth, S. G. & Pawlowski, M. Generating microglia from human pluripotent stem cells: Novel in vitro models for the study of neurodegeneration. *Mol. Neurodegener.* **14**, 1–16 (2019).

226. Serio, A. *et al.* Astrocyte pathology and the absence of non-cell autonomy in an induced pluripotent stem cell model of TDP-43 proteinopathy. *Proc. Natl. Acad. Sci. U. S. A.* **110**, 4697–4702 (2013).

227. Rushton, D. J., Mattis, V. B., Svendsen, C. N., Allen, N. D. & Kemp, P. J. Stimulation of GABA-induced Ca2+ influx enhances maturation of human induced pluripotent stem cell-derived neurons. *PLoS One* **8**, 1–16 (2013).

228. Frame, J. M., McGrath, K. E. & Palis, J. Erythro-myeloid progenitors: "Definitive" hematopoiesis in the conceptus prior to the emergence of hematopoietic stem cells. *Blood Cells, Mol. Dis.* **51**, 220–225 (2013).

229. Keller, G., Kennedy, M., Papayannopoulou, T. & Wiles, M. V. Hematopoietic commitment during embryonic stem cell differentiation in culture. *Mol. Cell. Biol.* **13**, 473–486 (1993).

230. Sturgeon, C. M., Ditadi, A., Awong, G., Kennedy, M. & Keller, G. Wnt signaling controls definitive and primitive. **32**, 554–561 (2014).

231. Ehman, E. C. *et al.* Diverse requirements for microglial survival, specification, and function revealed by defined-medium cultures Christopher. *Neuron* **46**, 1247–1262 (2017).

232. Easley-Neal, C., Foreman, O., Sharma, N., Zarrin, A. A. & Weimer, R. M. CSF1R Ligands IL-34 and CSF1 Are Differentially Required for Microglia Development and Maintenance in White and Gray Matter Brain Regions. *Front. Immunol.* **10**, (2019).

233. Re, F. *et al.* Granulocyte-Macrophage Colony-Stimulating Factor Induces an Expression Program in Neonatal Microglia That Primes Them for Antigen Presentation. *J. Immunol.* **169**, 2264–2273 (2002).

234. Esen, N. & Kielian, T. Effects of low dose GM-CSF on microglial inflammatory profiles to diverse pathogen-associated molecular patterns (PAMPs). *J. Neuroinflammation* **4**, 1–18 (2007).

235. Ngwa, C. & Liu, F. CD200-CD200R signaling and diseases: a potential therapeutic target? *Int. J. Physiol. Pathophysiol. Pharmacol.* **11**, 297–309 (2019).

236. Chamak, B. & Mallat, M. Fibronectin and laminin regulate the in vitro differentiation of microglial cells. *Neuroscience* **45**, 513–527 (1991).

237. Garcia-Alegria, E. *et al.* Early Human Hemogenic Endothelium Generates Primitive and Definitive Hematopoiesis In Vitro. *Stem Cell Reports* **11**, 1061–1074 (2018).

238. Jin, C., Li, W., Yuan, J., Xu, W. & Cheng, Z. Association of the CR1 polymorphism with late-onset Alzheimer's disease in Chinese Han populations: A meta-analysis. *Neurosci. Lett.* **527**, 46–49 (2012).

239. Shaltouki, A., Peng, J., Liu, Q., Rao, M. S. & Zeng, X. Efficient generation of astrocytes from human pluripotent stem cells in defined conditions. *Stem Cells* **31**, 941–952 (2013).

240. Yuan, S. H. *et al.* Cell-surface marker signatures for the Isolation of neural stem cells, glia and neurons derived from human pluripotent stem cells. *PLoS One* **6**, (2011).

241. Kawai, S., Kurganov, E. & Miyata, S. Transient increase of microglial C1q expression in the circumventricular organs of adult mouse during LPS-induced inflammation. *Cell Biochem. Funct.* **38**, 392–400 (2020).

242. Chevalier, J. Distribution in clusters of complement receptor type one (CR1) on human erythrocytes. *J. Immunol.* **142**, 2031–2036 (1989).

243. Matejuk, A. & Ransohoff, R. M. Crosstalk Between Astrocytes and Microglia: An Overview. *Front. Immunol.* **11**, 1–11 (2020).

244. Lian, H. *et al.* Astrocyte-Microglia Cross Talk through Complement Activation Modulates Amyloid Pathology in Mouse Models of Alzheimer's Disease. *J. Neurosci.* **36**, 577–589 (2016).

245. Lian, H. *et al.* Astrocyte-microglia cross talk through complement activation modulates amyloid pathology in mouse models of alzheimer's disease. *J. Neurosci.* **36**, 577–589 (2016).

246. Singhrao, S. K., Neal, J. W., Rushmere, N. K., Morgan, B. P. & Gasque, P. Differential expression of individual complement regulators in the brain and choroid plexus. *Lab. Invest.* **79**, 1247–59 (1999).

247. Brouwers, N. *et al.* Alzheimer risk associated with a copy number variation in the complement receptor 1 increasing C3b/C4b binding sites. *Mol. Psychiatry* **17**, 223–233 (2012).

248. Ruseva, M. M. *et al.* Crry deficiency in complement sufficient mice: C3 consumption occurs without associated renal injury. *Mol. Immunol.* **46**, 803–811 (2009).

249. Shi, M. *et al.* Premature termination codons are recognized in the nucleus in a reading-frame-dependent manner. *Cell Discov.* **1**, 1–20 (2015).

250. Brogna, S. & Wen, J. Nonsense-mediated mRNA decay (NMD) mechanisms. *Nat. Struct. Mol. Biol.* **16**, 107–113 (2009).

251. Karousis, E. D. & Mühlemann, O. Nonsense-mediated mRNA decay begins where translation ends. *Cold Spring Harb. Perspect. Biol.* **11**, 1–18 (2019).

252. Shah, N. J. *Recombinant DNA technology*. *Introduction to Basics of Pharmacology and Toxicology: Volume 1: General and Molecular Pharmacology: Principles of Drug Action* (2019). doi:10.1007/978-981-32-9779-1_34.

253. Joung, J. K. & Sander, J. D. TALENs: a widely applicable technology for targeted genome editing. *Nat. Rev. Mol. Cell Biol.* **14**, 49–55 (2013).

254. Han, X. *et al.* Nonsense-mediated mRNA decay: A 'nonsense' pathway makes sense in stem cell biology. *Nucleic Acids Res.* **46**, 1038–1051 (2018).

255. Smits, A. H. *et al.* Biological plasticity rescues target activity in CRISPR knock outs. *Nat. Methods* **16**, 1087–1093 (2019).

256. Jo, H. Y. *et al.* Functional in vivo and in vitro effects of 20q11.21 genetic aberrations on hPSC differentiation. *Sci. Rep.* **10**, 1–14 (2020).

257. Amps, K. *et al.* Screening ethnically diverse human embryonic stem cells identifies a chromosome 20 minimal amplicon conferring growth advantage. *Nat. Biotechnol.* **29**, 1132–1144 (2011).

258. Brauer, R. B. *et al.* EXTRAHEPATIC SYNTHESIS OF C6 IN THE RAT IS SUFFICIENT FOR COMPLEMENT-MEDIATED HYPERACUTE REJECTION OF A GUINEA PIG CARDIAC XENOGRAFT. *Transplantation* **59**, 1073–1076 (1995).

259. MORGAN, B. P. & GASQUE, P. Extrahepatic complement biosynthesis: where, when and why? *Clin. Exp. Immunol.* **107**, 1–7 (1997).

260. Tang, S., Zhou, W., Sheerin, N. S., Vaughan, R. W. & Sacks, S. H. Contribution of renal secreted complement C3 to the circulating pool in humans. *J. Immunol.* **162**, 4336–41 (1999).

261. Lucchinetti, C. *et al.* Heterogeneity of multiple sclerosis lesions: implications for the pathogenesis of demyelination. *Ann. Neurol.* **47**, 707–17 (2000).

262. Carpanini, S. M., Torvell, M. & Morgan, B. P. Therapeutic Inhibition of the Complement System in Diseases of the Central Nervous System. *Front. Immunol.* **10**, (2019).

263. Hosokawa, M., Klegeris, A., Maguire, J. & McGeer, P. L. Expression of complement messenger RNAs and proteins by human oligodendroglial cells. *Glia* **42**, 417–423 (2003).

264. Luchena, C., Zuazo-Ibarra, J., Alberdi, E., Matute, C. & Capetillo-Zarate, E. Contribution of neurons and glial cells to complement-mediated synapse removal during development, aging and in Alzheimer's disease. *Mediators Inflamm.* **2018**, (2018).

265. Thomas, A., Gasque, P., Vaudry, D., Gonzalez, B. & Fontaine, M. Expression of a complete and functional complement system by human neuronal cells in vitro. *Int. Immunol.* **12**, 1015–1023 (2000).

266. Strohmeyer, R., Shen, Y. & Rogers, J. Detection of complement alternative pathway mRNA and proteins in the Alzheimer's disease brain. *Mol. Brain Res.* **81**, 7–18 (2000).

267. Cockburn, I. A. *et al.* A human complement receptor 1 polymorphism that reduces Plasmodium falciparum rosetting confers protection against severe malaria. *Proc. Natl. Acad. Sci. U. S. A.* **101**, 272–277 (2004).

268. Wu, X. *et al.* Membrane Protein Crry Maintains Homeostasis of the Complement System. *J.*

Immunol. **181**, 2732–2740 (2008).

269. Laws, S. M. *et al.* TNF polymorphisms in Alzheimer disease and functional implications on CSF beta-amyloid levels. *Hum. Mutat.* **26**, 29–35 (2005).

270. Montgomery, S. L. *et al.* Chronic Neuron- and Age-Selective Down-Regulation of TNF Receptor Expression in Triple-Transgenic Alzheimer Disease Mice Leads to Significant Modulation of Amyloid- and Tau-Related Pathologies. *Am. J. Pathol.* **182**, 2285–2297 (2013).

271. Sartain, S. E., Turner, N. A. & Moake, J. L. TNF Regulates Essential Alternative Complement Pathway Components and Impairs Activation of Protein C in Human Glomerular Endothelial Cells. *J. Immunol.* **196**, 832–845 (2016).

272. Irani, V. R. & Maslow, J. N. Induction of murine macrophage TNF-Î± synthesis by Mycobacterium avium is modulated through complement-dependent interaction via complement receptors 3 and 4 in relation to M. avium glycopeptidolipid. *FEMS Microbiol. Lett.* **246**, 221–228 (2005).

273. Benoit, M. E., Clarke, E. V., Morgado, P., Fraser, D. A. & Tenner, A. J. Complement Protein C1q Directs Macrophage Polarization and Limits Inflammasome Activity during the Uptake of Apoptotic Cells. *J. Immunol.* **188**, 5682–5693 (2012).

274. Weinstein, J. R. *et al.* IgM-Dependent Phagocytosis in Microglia Is Mediated by Complement Receptor 3, Not Fc / Receptor. *J. Immunol.* **195**, 5309–5317 (2015).

275. Ries, M. & Sastre, M. Mechanisms of Aβ clearance and degradation by glial cells. *Front. Aging Neurosci.* **8**, 1–9 (2016).

276. Thambisetty, M. *et al.* Effect of Complement CR1 on Brain Amyloid Burden During Aging and Its Modification by APOE Genotype. *Biol. Psychiatry* **73**, 422–428 (2013).

277. Wilgenburg, B. van, Browne, C., Vowles, J. & Cowley, S. A. Efficient, Long Term Production of Monocyte-Derived Macrophages from Human Pluripotent Stem Cells under Partly-Defined and Fully-Defined Conditions. *PLoS One* **8**, e71098 (2013).

278. Ji-wen, Y., Tong-yan, T. & Qi-lin, H. Protective effect of astrocyte-conditioned medium on neurons following hypoxia and mechanical injury. *Chinese J. Traumatol. - English Ed.* **16**, 3–9 (2013).

279. Zhang, J. *et al.* Mouse Astrocytes Promote Microglial Ramification by Releasing TGF-β and Forming Glial Fibers. *Front. Cell. Neurosci.* **14**, 1–15 (2020).

280. Li, Q. & Barres, B. A. Microglia and macrophages in brain homeostasis and disease. *Nat. Rev. Immunol.* **18**, 225–242 (2018).

281. Yang, T., Guo, R. & Zhang, F. Brain perivascular macrophages: Recent advances and implications in health and diseases. *CNS Neurosci. Ther.* **25**, 1318–1328 (2019).

282. LeBleu, V. S. & Neilson, E. G. Origin and functional heterogeneity of fibroblasts. *FASEB J.* **34**, 3519–3536 (2020).

283. Kim, W.-K. *et al.* CD163 Identifies Perivascular Macrophages in Normal and Viral Encephalitic Brains and Potential Precursors to Perivascular Macrophages in Blood. *Am. J. Pathol.* **168**, 822–834 (2006).

284. Triantafilou, K., Hughes, T. R., Triantafilou, M. & Morgan, B. P. The complement membrane attack complex triggers intracellular Ca2+ fluxes leading to NLRP3 inflammasome activation. *J. Cell Sci.* (2013) doi:10.1242/jcs.124388.

285. Mahmoudi, R. *et al.* Alzheimer's disease is associated with low density of the long CR1 isoform. *Neurobiol. Aging* **36**, 1766.e5-1766.e12 (2015).

286. Vukojicic, A. *et al.* The Classical Complement Pathway Mediates Microglia-Dependent Remodeling of Spinal Motor Circuits during Development and in SMA. *Cell Rep.* **29**, 3087-3100.e7 (2019).

287. Coulthard, L. G., Hawksworth, O. A. & Woodruff, T. M. Complement: The Emerging Architect of the Developing Brain. *Trends Neurosci.* **41**, 373–384 (2018).

288. Sellgren, C. M. *et al.* Increased synapse elimination by microglia in schizophrenia patient-derived models of synaptic pruning. *Nat. Neurosci.* **22**, 374–385 (2019).

289. Bahrini, I., Song, J., Diez, D. & Hanayama, R. Neuronal exosomes facilitate synaptic pruning by up-regulating complement factors in microglia. *Sci. Rep.* **5**, 7989 (2015).

290. Sansores-España, D., Carrillo-Avila, A., Melgar-Rodriguez, S., Díaz-Zuñiga, J. & Martínez-Aguilar, V. Periodontitis and Alzheimers disease. *Med. Oral Patol. Oral y Cir. Bucal* **26**, e43–e48 (2021).

291. Miller, J. D. *et al.* Human iPSC-Based Modeling of Late-Onset Disease via Progerin-Induced Aging. *Cell Stem Cell* **13**, 691–705 (2013).

9.0 Appendix

9.1 Appendix 1 RT qPCR primers

Gene	Forward	Reverse
Housekeepers		
HPRT	CCTGGCGTCGTGATTAGTGA	CGAGCAAGACGTTCAGTCCT
SDHA	ACTGTTGCAGCACAGCTAGA	CCGCCCTTTCCAAACTTGAG
B ACTIN	GAGCACAGAGCCTCGCCTTT	TCATCATCCATGGTGAGCTGG
GAPDH	TGC ACC ACC AAC TGC TTA GC	GGC ATG GAC TGT GGT CAT GAG
UBC	CGG TGA ACG CCG ATG ATT AT	ATC TGC ATT GTC AAG TGA CGA
Differentiation Markers		
OCT3/4	TTCTGGCGCCGGTTACAGAACCA	GACAACAATGAAAATCTTCAGGAGA
Nanog	TTCTTGACCGGGACCTTGTC	TTCTTGACCGGGACCTTGTC
SOX2	ACTTTTGTCGGAGACGGAGA	GTTCATGTGCGCGTAACTGT
CD11b	CCCGGAAAACTCAGAGGTCA	CAGCATATTTCACCGGCAGC
CD45	CATTTGGCTTTGCCTTTCTG	TTCTCTTTCAAAGGTGCTTGC
CD14		
CD235a	GGCAATGCACACTTCAACTT	AATAATGAGTGTTATCTCGGTTTCC
TMEM119	AGGCCGTGGACTTAAACCAG	TGCCCCCAGGACCAGTT
CX3CR1	AGGCCGTGGACTTAAACCAG	CATGGTGAAGGCCCCACTG
IBA-1	GCTGAGCTATGAGCCAAACC	TCATCCAGCCTCTCTTCCTG
MERTK	TCC ATC CGT CCG GAG AGA AA	CCC TTG CCT CAG TGA TAG CTC
Complement		
FD	GACAGCTGCAAGGGTGACTC	TAGATCCCGGGCTTCTTGCG
CD46	CAAAATCTCCAGCGTCCAGTG	CTGCAACTCCAACAACTATGGC
C1Qa	GACAACAGGAGGCAGGCCC	CTTTCTTCCCGTCTGGTGCT
C1s	GCACCACCAAAGAAGGTGCT	CAGTGTCTCCTGAGATTATCACATC
C9	ACAGCAGGCTATGGGATCAAC	CACGTTCCAAGGTCTTCGGT
C5	TTACGAGTGGTGCCAGAAGG	TGGGAACTCCTTTCGTCTGC
CD59	TGGAAGAGGATCTTGGGCG	TGCAGGCTATGACCTGAATG
DAF	ACCACCACACCAAATGCTCA	AACACGTGTGCCCAGATAGA
MASP1	CAAGGCAGGAAAATGAGGTGG	ATCCGAAACCCATCTGGGAC
C1inh	CCAGAAGTTTGGAGTCCGCT	TGTTGTTGCGACCTTCCCTT
CSMD1	CGGGTGATTATTTGGCTCCG	CCACAGTTCTGACCCTTCGC
CR4	GCTGCAAGCATCATTCGTTA	CCAATCAGGACCAGGTCAGT
C3aR	ACTCGTGGAGACATCCAGGT	GAAGATTTCCCGGTACACGA
C5aR	GAGCCCAGGAGACCAGAACATG	TACATGTTGAGCAGGATGAGGGA
CR2	CTGCAGCAATACCACAAAGGACAG	AATCGGATCACCAATGGAACCC
C2	AAGACAAAGGATCATGAAAATGGAA	GAGAGCCACCCATATTGGACTT
C4	AGCTGCAGTTTTCCTTGGGC	GTGTACTCGACGTGGCCTTT
FB	TGCACCGAGGGAACAACTC	GGAGCAGCTCTTCCTTTTGTTG
FI	TGCATCTGTGGCTCAAGAAGAAAC	CATCCTTAATTGCCACCTGCCAT
FH	ATGTCAGAAAAGGCCCTGTGGA	CCATCTGTGTCACATTCACGGT
Activation		

IL-10	GGCACCCAGTCTGAGAACAG	GGCAACCCAGGTAACCCTTA
IL-6	TTCTCCACAAGCGCCTTC	AGAGGTGAGTGGCTGTCTGT
IL1β	CCTGAGCTCGCCAGTGAAA	TCCTGGAAGGAGCACTTCATCT
TNFA	CCCCAGGGACCTCTCTCTA	GCTTGAGGGTTTGCTACAACA
NFKB	TCCATATTTGGGAAGGCCTGA	TTGAAGGTATGGGCCATCTGT
NLRP3	AGGAGAACTTTCTGTGTGGACC	AGCCCTTCTGGGGAGGATAG
Astrocyte markers		
GFAP	GAGCAGGAGGAGCGGCAC	TAGTCGTTGGCTTCGTGCTT
EAAT2	TAACTCTGGCGGCCAATGGAAAGT	ACGCTGGGGAGTTTATTCAAGAAT

9.2 Appendix 2 Raw Fluidigm CT values

The following data has been directly extracted from the Fluidigm software post run. The CT value is the average cycle threshold for each sample and gen. The ΔCT is normalized to housekeepers GAPDH, UBC, ACTINβ, SDHA and HPRT and is performed by the Fludigm R package software. Results with 999 indicate a failed run. This is most likely due to absence of transcript for this marker but can also indicate a technical error. Data in the thesis text have undergone ΔΔCT analysis. All data is included in the appendix, included samples which were excluded later. RNA used in Fluidigm experiments were all from one differentiation but from multiple different harvests. Cells were taken and differentiated from as early as harvest 2. Future work would not differentiate precursor cells to microglia until at least harvest 4 as it has been suggested precursors require further maturation before terminal differentiation. . The same batch of ACM was used for all differentiations used for Fluidim RNA.

cDNA	Gene	CT	ΔCT
WT iPS 6	LIN28	4.019285	-5.95937
WT iPS 6	Oct-04	3.587261	-6.54033
WT iPS 6	BMP4	6.882567	-2.93797
WT iPS 6	CD34	8.175037	-3.90287
WT iPS 6	SOX2	14.70585	-0.52564
WT iPS 6	FLK1	11.17995	-0.9309
WT iPS 6	CD45	999	999
WT iPS 6	CD11B	11.97984	5.457886
WT iPS 6	CD235a	28.17664	17.46537
WT iPS 6	BRAC	11.63577	2.298888
WT iPS 6	MERTK	17.83321	999
WT iPS 6	RUNX1	11.16413	-8.04479
WT iPS 6	NESTIN	9.846737	0.188398
WT iPS 6	MAP2	15.58079	-2.45582
WT iPS 6	NFKB	19.26659	12.25212
WT iPS 6	NLRP3	29.80995	18.85971
WT iPS 6	TREM2	20.3087	7.197396
WT iPS 6	IBA1	10.3822	2.139541
WT iPS 6	CD14	17.3496	5.167787
WT iPS 6	VIMENTIN	6.808785	2.864818

WT iPS 6	GFAP	15.37587	7.506206
WT iPS 6	EAAT2	14.72063	999
WT iPS 6	ALDH1	10.40067	-0.01689
WT iPS 6	S100B	17.74853	0.528668
WT iPS 6	NEUN	21.35402	-3.28866
WT iPS 6	CX3CR1	11.24328	1.166221
WT iPS 6	BIN1	18.29617	1.731397
WT iPS 6	TGFB	12.77212	1.202417
WT iPS 6	TMEM119	11.15096	3.665714
WT iPS 6	ABCA7	24.99779	-0.13403
WT iPS 6	PICALM	7.308372	1.024825
WT iPS 6	INPP5D	9.549558	1.628273
WT iPS 6	APOE	10.34801	2.711352
WT iPS 6	EPHA1	11.44651	7.118427
WT iPS 6	HLA-DR	7.011793	-6.63633
WT iPS 6	PLCG2	5.862178	2.315856
WT iPS 6	CD33	22.91049	11.47505
WT iPS 6	CR1	20.07151	9.550288
WT iPS 6	CD59	9.858082	1.066649
WT iPS 6	MASP	23.13561	13.61449
WT iPS 6	CR1	12.18874	1.667519
WT iPS 6	CD46	12.58339	4.232385
WT iPS 6	C1IN	10.71281	-0.7868
WT iPS 6	C6	21.86437	3.271131
WT iPS 6	C3aR	10.61668	-0.48345
WT iPS 6	DAF	18.23502	9.117122
WT iPS 6	C2	7.608138	0.356601
WT iPS 6	C3	23.67804	15.39055
WT iPS 6	C1S	21.74743	1.358286
WT iPS 6	C1QA1	13.1603	7.206671
WT iPS 6	FH	20.32603	3.378897
WT iPS 6	CR4	17.93009	6.125591
WT iPS 6	FB	999	999
WT iPS 6	C9	21.53128	13.72319
WT iPS 6	C5aR	23.84003	16.38171
WT iPS 6	P2RY12	24.65374	13.19612
WT iPS 6	C4	16.11263	3.569204
WT iPS 6	FI	10.96976	0.659936
WT iPS 6	CSMD1	20.43272	6.473247
WT iPS 6	C5	13.14045	-0.2656
WT iPS 6	C1QB	14.43571	4.146799
WT iPS 6	CD68	12.93716	9.781925
WT iPS 6	NOS	21.17572	1.70763
WT iPS 6	IL1B	25.52396	999
WT iPS 6	NOS	999	999
WT iPS 6	IL6	999	999

WT iPS 6	TNFA	21.33631	6.565905
WT iPS 5	LIN28	10.23675	0.258099
WT iPS 5	Oct-04	10.839	0.711409
WT iPS 5	BMP4	8.578078	-1.24246
WT iPS 5	CD34	12.72096	0.643052
WT iPS 5	SOX2	15.78141	0.54992
WT iPS 5	FLK1	9.713198	-2.39765
WT iPS 5	CD45	18.60529	1.805923
WT iPS 5	CD11B	8.153081	1.631128
WT iPS 5	CD235a	12.22368	1.512404
WT iPS 5	BRAC	10.75685	1.419969
WT iPS 5	MERTK	25.22112	999
WT iPS 5	RUNX1	17.006	-2.20292
WT iPS 5	NESTIN	10.48381	0.825466
WT iPS 5	MAP2	17.85823	-0.17838
WT iPS 5	NFKB	8.657522	1.643059
WT iPS 5	NLRP3	12.84095	1.89071
WT iPS 5	TREM2	15.18352	2.072218
WT iPS 5	IBA1	10.032	1.78934
WT iPS 5	CD14	13.56643	1.384624
WT iPS 5	VIMENTIN	4.944814	1.000847
WT iPS 5	GFAP	9.453736	1.584076
WT iPS 5	EAAT2	21.13731	999
WT iPS 5	ALDH1	11.17164	0.754075
WT iPS 5	S100B	18.64394	1.424086
WT iPS 5	NEUN	24.81673	0.174054
WT iPS 5	CX3CR1	11.67815	1.601092
WT iPS 5	BIN1	17.99722	1.432452
WT iPS 5	TGFB	11.79466	0.224958
WT iPS 5	TMEM119	8.66726	1.182009
WT iPS 5	ABCA7	999	999
WT iPS 5	PICALM	7.615546	1.331999
WT iPS 5	INPP5D	9.579319	1.658035
WT iPS 5	APOE	9.51899	1.882331
WT iPS 5	EPHA1	5.827863	1.499778
WT iPS 5	HLA-DR	14.55993	0.91181
WT iPS 5	PLCG2	4.412082	0.86576
WT iPS 5	CD33	13.5828	2.147357
WT iPS 5	CR1	7.51132	-3.0099
WT iPS 5	CD59	9.925048	1.133615
WT iPS 5	MASP	9.247767	-0.27335
WT iPS 5	CR1	11.68191	1.160683
WT iPS 5	CD46	9.694557	1.343549
WT iPS 5	C1IN	11.1109	-0.38871
WT iPS 5	C6	18.43204	-0.16119

WT iPS 5	C3aR	10.70161	-0.39852
WT iPS 5	DAF	10.26603	1.148134
WT iPS 5	C2	8.580562	1.329025
WT iPS 5	C3	9.662887	1.375401
WT iPS 5	C1S	20.38881	-0.00033
WT iPS 5	C1QA1	7.190824	1.237195
WT iPS 5	FH	17.68028	0.733148
WT iPS 5	CR4	11.95758	0.153084
WT iPS 5	FB	999	999
WT iPS 5	C9	9.022499	1.214403
WT iPS 5	C5aR	8.395879	0.937554
WT iPS 5	P2RY12	13.00147	1.543848
WT iPS 5	C4	13.4769	0.933475
WT iPS 5	FI	11.20959	0.899762
WT iPS 5	CSMD1	10.66392	-3.29555
WT iPS 5	C5	10.28973	-3.11632
WT iPS 5	C1QB	11.11971	0.830795
WT iPS 5	CD68	3.982205	0.826969
WT iPS 5	NOS	19.32213	-0.14596
WT iPS 5	IL1B	999	999
WT iPS 5	NOS	999	999
WT iPS 5	IL6	13.13762	1.942783
WT iPS 5	TNFA	16.96261	2.192212
WT iPS 7	BMP4	19.8672	10.04667
WT iPS 7	CD34	19.80425	7.726344
WT iPS 7	SOX2	999	999
WT iPS 7	FLK1	999	999
WT iPS 7	CD45	999	999
WT iPS 7	CD11B	999	999
WT iPS 7	CD235a	999	999
WT iPS 7	BRAC	999	999
WT iPS 7	MERTK	22.75609	999
WT iPS 7	RUNX1	999	999
WT iPS 7	NESTIN	21.39486	11.73652
WT iPS 7	MAP2	999	999
WT iPS 7	NFKB	24.48639	17.47193
WT iPS 7	NLRP3	999	999
WT iPS 7	TREM2	999	999
WT iPS 7	IBA1	999	999
WT iPS 7	CD14	999	999
WT iPS 7	VIMENTIN	999	999
WT iPS 7	GFAP	24.48773	16.61807
WT iPS 7	EAAT2	999	999
WT iPS 7	ALDH1	999	999
WT iPS 7	S100B	27.62783	10.40797

WT iPS 7	NEUN	24.81584	0.173157
WT iPS 7	CX3CR1	26.60374	16.52669
WT iPS 7	BIN1	999	999
WT iPS 7	TGFB	999	999
WT iPS 7	TMEM119	999	999
WT iPS 7	ABCA7	999	999
WT iPS 7	PICALM	999	999
WT iPS 7	INPP5D	999	999
WT iPS 7	APOE	21.35164	13.71498
WT iPS 7	EPHA1	999	999
WT iPS 7	HLA-DR	999	999
WT iPS 7	PLCG2	28.20701	24.66068
WT iPS 7	CD33	999	999
WT iPS 7	CR1	999	999
WT iPS 7	CD59	29.60135	20.80991
WT iPS 7	MASP	999	999
WT iPS 7	CR1	999	999
WT iPS 7	CD46	999	999
WT iPS 7	C1IN	20.81706	9.317452
WT iPS 7	C6	999	999
WT iPS 7	C3aR	999	999
WT iPS 7	DAF	999	999
WT iPS 7	C2	17.60681	10.35528
WT iPS 7	C3	999	999
WT iPS 7	C1S	999	999
WT iPS 7	C1QA1	999	999
WT iPS 7	FH	999	999
WT iPS 7	CR4	999	999
WT iPS 7	FB	999	999
WT iPS 7	C9	999	999
WT iPS 7	C5aR	999	999
WT iPS 7	P2RY12	999	999
WT iPS 7	C4	999	999
WT iPS 7	FI	999	999
WT iPS 7	CSMD1	999	999
WT iPS 7	C5	21.75321	8.347157
WT iPS 7	C1QB	22.35831	12.0694
WT iPS 7	CD68	999	999
WT iPS 7	NOS	999	999
WT iPS 7	IL1B	999	999
WT iPS 7	NOS	999	999
WT iPS 7	IL6	999	999
WT iPS 7	TNFA	999	999
WT iPS 1	Oct-04	999	999
WT iPS 1	BMP4	999	999

WT iPS 1	CD34	999	999
WT iPS 1	SOX2	999	999
WT iPS 1	FLK1	999	999
WT iPS 1	CD45	999	999
WT iPS 1	CD11B	21.27754	14.75559
WT iPS 1	CD235a	999	999
WT iPS 1	BRAC	19.52244	10.18556
WT iPS 1	MERTK	999	999
WT iPS 1	RUNX1	999	999
WT iPS 1	NESTIN	24.89645	15.23811
WT iPS 1	MAP2	999	999
WT iPS 1	NFKB	18.5922	11.57774
WT iPS 1	NLRP3	999	999
WT iPS 1	TREM2	999	999
WT iPS 1	IBA1	999	999
WT iPS 1	CD14	999	999
WT iPS 1	VIMENTIN	16.98963	13.04566
WT iPS 1	GFAP	20.21478	12.34512
WT iPS 1	EAAT2	999	999
WT iPS 1	ALDH1	999	999
WT iPS 1	S100B	999	999
WT iPS 1	NEUN	25.56189	0.919209
WT iPS 1	CX3CR1	999	999
WT iPS 1	BIN1	999	999
WT iPS 1	TGFB	999	999
WT iPS 1	TMEM119	21.60528	14.12003
WT iPS 1	ABCA7	999	999
WT iPS 1	PICALM	999	999
WT iPS 1	INPP5D	999	999
WT iPS 1	APOE	999	999
WT iPS 1	EPHA1	19.41732	15.08923
WT iPS 1	HLA-DR	999	999
WT iPS 1	PLCG2	21.59681	18.05048
WT iPS 1	CD33	999	999
WT iPS 1	CR1	999	999
WT iPS 1	CD59	999	999
WT iPS 1	MASP	999	999
WT iPS 1	CR1	999	999
WT iPS 1	CD46	24.06687	15.71586
WT iPS 1	C1IN	21.2167	9.71709
WT iPS 1	C6	999	999
WT iPS 1	C3aR	999	999
WT iPS 1	DAF	25.04153	15.92364
WT iPS 1	C2	16.6173	9.365768
WT iPS 1	C3	23.95939	15.67191
WT iPS 1	C1S	999	999

WT iPS 1	C1QA1	22.73444	16.78081
WT iPS 1	FH	999	999
WT iPS 1	CR4	999	999
WT iPS 1	FB	999	999
WT iPS 1	C9	999	999
WT iPS 1	C5aR	999	999
WT iPS 1	P2RY12	20.72587	9.268248
WT iPS 1	C4	999	999
WT iPS 1	FI	999	999
WT iPS 1	CSMD1	999	999
WT iPS 1	C5	999	999
WT iPS 1	C1QB	22.86518	12.57627
WT iPS 1	CD68	16.71957	13.56433
WT iPS 1	NOS	999	999
WT iPS 1	IL1B	999	999
WT iPS 1	NOS	999	999
WT iPS 1	IL6	22.10475	10.90991
WT iPS 1	TNFA	999	999
WT iPS 2	BMP4	17.88499	8.064453
WT iPS 2	CD34	17.42575	5.347849
WT iPS 2	SOX2	22.32251	7.09102
WT iPS 2	FLK1	22.27764	10.16678
WT iPS 2	CD45	999	999
WT iPS 2	CD11B	21.22608	14.70413
WT iPS 2	CD235a	999	999
WT iPS 2	BRAC	21.25258	11.91569
WT iPS 2	MERTK	999	999
WT iPS 2	RUNX1	23.62395	4.415037
WT iPS 2	NESTIN	22.28991	12.63157
WT iPS 2	MAP2	28.04484	10.00823
WT iPS 2	NFKB	19.52897	12.51451
WT iPS 2	NLRP3	999	999
WT iPS 2	TREM2	999	999
WT iPS 2	IBA1	21.28225	13.03959
WT iPS 2	CD14	999	999
WT iPS 2	VIMENTIN	15.96914	12.02518
WT iPS 2	GFAP	18.13413	10.26447
WT iPS 2	EAAT2	999	999
WT iPS 2	ALDH1	999	999
WT iPS 2	S100B	999	999
WT iPS 2	NEUN	999	999
WT iPS 2	CX3CR1	24.33729	14.26023
WT iPS 2	BIN1	999	999
WT iPS 2	TGFB	999	999
WT iPS 2	TMEM119	19.79931	12.31406

WT iPS 2	ABCA7	999	999
WT iPS 2	PICALM	18.22159	11.93804
WT iPS 2	INPP5D	999	999
WT iPS 2	APOE	19.72842	12.09176
WT iPS 2	EPHA1	18.83069	14.5026
WT iPS 2	HLA-DR	18.79167	5.143545
WT iPS 2	PLCG2	19.89835	16.35202
WT iPS 2	CD33	999	999
WT iPS 2	CR1	21.75323	11.232
WT iPS 2	CD59	22.57384	13.78241
WT iPS 2	MASP	24.83175	15.31063
WT iPS 2	CR1	23.00053	12.47931
WT iPS 2	CD46	23.01821	14.6672
WT iPS 2	C1IN	19.93384	8.434237
WT iPS 2	C6	999	999
WT iPS 2	C3aR	23.23944	12.13931
WT iPS 2	DAF	22.73939	13.62149
WT iPS 2	C2	16.42115	9.169613
WT iPS 2	C3	999	999
WT iPS 2	C1S	999	999
WT iPS 2	C1QA1	21.53963	15.586
WT iPS 2	FH	999	999
WT iPS 2	CR4	21.58666	9.782162
WT iPS 2	FB	999	999
WT iPS 2	C9	999	999
WT iPS 2	C5aR	999	999
WT iPS 2	P2RY12	999	999
WT iPS 2	C4	999	999
WT iPS 2	FI	999	999
WT iPS 2	CSMD1	999	999
WT iPS 2	C5	999	999
WT iPS 2	C1QB	24.35093	14.06202
WT iPS 2	CD68	17.3159	14.16066
WT iPS 2	NOS	26.13951	6.67142
WT iPS 2	IL1B	999	999
WT iPS 2	NOS	999	999
WT iPS 2	IL6	999	999
WT iPS 2	TNFA	999	999
WT PRE 9	LIN28	18.95302	8.974365
WT PRE 9	Oct-04	13.93259	3.805001
WT PRE 9	BMP4	13.20743	3.386894
WT PRE 9	CD34	18.81783	6.739925
WT PRE 9	SOX2	19.7991	4.567608
WT PRE 9	FLK1	10.17104	-1.93981
WT PRE 9	CD45	19.48749	2.688129

WT PRE 9	CD11B	9.854636	3.332683
WT PRE 9	CD235a	11.60262	0.891347
WT PRE 9	BRAC	12.69045	3.353568
WT PRE 9	MERTK	999	999
WT PRE 9	RUNX1	16.78105	-2.42786
WT PRE 9	NESTIN	11.48602	1.827683
WT PRE 9	MAP2	15.91206	-2.12455
WT PRE 9	NFKB	9.001523	1.987061
WT PRE 9	NLRP3	13.81751	2.867271
WT PRE 9	TREM2	12.74561	-0.3657
WT PRE 9	IBA1	6.158995	-2.08367
WT PRE 9	CD14	14.33379	2.151983
WT PRE 9	VIMENTIN	3.206444	-0.73752
WT PRE 9	GFAP	6.484775	-1.38489
WT PRE 9	EAAT2	999	999
WT PRE 9	ALDH1	13.02456	2.606996
WT PRE 9	S100B	20.7033	3.483442
WT PRE 9	NEUN	23.57368	-1.069
WT PRE 9	CX3CR1	19.21855	9.141493
WT PRE 9	BIN1	19.68105	3.116281
WT PRE 9	TGFB	12.21108	0.641374
WT PRE 9	TMEM119	8.979625	1.494375
WT PRE 9	ABCA7	999	999
WT PRE 9	PICALM	6.55909	0.275543
WT PRE 9	INPP5D	11.29063	3.369341
WT PRE 9	APOE	10.59543	2.958766
WT PRE 9	EPHA1	4.699894	0.371809
WT PRE 9	HLA-DR	22.35255	8.704429
WT PRE 9	PLCG2	4.791748	1.245426
WT PRE 9	CD33	16.06699	4.631546
WT PRE 9	CR1	8.847676	-1.67355
WT PRE 9	CD59	9.549006	0.757573
WT PRE 9	MASP	10.63927	1.11815
WT PRE 9	CR1	11.93929	1.418061
WT PRE 9	CD46	9.48778	1.136771
WT PRE 9	C1IN	11.18135	-0.31826
WT PRE 9	C6	999	999
WT PRE 9	C3aR	7.623064	-3.47707
WT PRE 9	DAF	10.96182	1.843917
WT PRE 9	C2	7.268728	0.017191
WT PRE 9	C3	7.880177	-0.40731
WT PRE 9	C1S	15.91389	-4.47525
WT PRE 9	C1QA1	6.833819	0.88019
WT PRE 9	FH	17.62918	0.682046
WT PRE 9	CR4	9.061498	-2.743
WT PRE 9	FB	999	999

WT PRE 9	C9	8.722554	0.914458
WT PRE 9	C5aR	8.642701	1.184376
WT PRE 9	P2RY12	15.36902	3.911403
WT PRE 9	C4	14.79182	2.248398
WT PRE 9	FI	20.13913	9.829306
WT PRE 9	CSMD1	10.25532	-3.70415
WT PRE 9	C5	12.09278	-1.31327
WT PRE 9	C1QB	11.07364	0.784728
WT PRE 9	CD68	4.592811	1.437574
WT PRE 9	NOS	6.325441	-13.1426
WT PRE 9	IL1B	999	999
WT PRE 9	NOS	999	999
WT PRE 9	IL6	7.210164	-3.98467
WT PRE 9	TNFA	8.294192	-6.47621
WT PRE 7	LIN28	4.427013	-5.55164
WT PRE 7	Oct-04	3.998078	-6.12951
WT PRE 7	BMP4	6.827909	-2.99263
WT PRE 7	CD34	8.00244	-4.07546
WT PRE 7	SOX2	14.05834	-1.17315
WT PRE 7	FLK1	11.66882	-0.44203
WT PRE 7	CD45	999	999
WT PRE 7	CD11B	13.41519	6.89324
WT PRE 7	CD235a	18.92455	8.21328
WT PRE 7	BRAC	11.10646	1.769578
WT PRE 7	MERTK	17.77172	999
WT PRE 7	RUNX1	10.11955	-9.08936
WT PRE 7	NESTIN	11.47863	1.820294
WT PRE 7	MAP2	15.71337	-2.32324
WT PRE 7	NFKB	18.43833	11.42387
WT PRE 7	NLRP3	999	999
WT PRE 7	TREM2	21.48887	8.377565
WT PRE 7	IBA1	10.89256	2.649904
WT PRE 7	CD14	999	999
WT PRE 7	VIMENTIN	5.971593	2.027626
WT PRE 7	GFAP	16.1391	8.26944
WT PRE 7	EAAT2	16.29923	999
WT PRE 7	ALDH1	13.02101	2.603444
WT PRE 7	S100B	21.83648	4.616626
WT PRE 7	NEUN	24.2093	-0.43338
WT PRE 7	CX3CR1	17.68441	7.607354
WT PRE 7	BIN1	22.44933	5.884557
WT PRE 7	TGFB	19.9096	8.339895
WT PRE 7	TMEM119	10.91579	3.430541
WT PRE 7	ABCA7	999	999

WT PRE 7	PICALM	6.986709	0.703162
WT PRE 7	INPP5D	9.793234	1.87195
WT PRE 7	APOE	9.184126	1.547466
WT PRE 7	EPHA1	10.10137	5.773287
WT PRE 7	HLA-DR	7.470129	-6.17799
WT PRE 7	PLCG2	6.821579	3.275257
WT PRE 7	CD33	22.92981	11.49437
WT PRE 7	CR1	21.45091	10.92968
WT PRE 7	CD59	10.48368	1.692244
WT PRE 7	MASP	25.41169	15.89057
WT PRE 7	CR1	12.34913	1.827907
WT PRE 7	CD46	12.72493	4.373921
WT PRE 7	C1IN	9.570347	-1.92926
WT PRE 7	C6	999	999
WT PRE 7	C3aR	11.17163	0.071497
WT PRE 7	DAF	18.5868	9.468903
WT PRE 7	C2	6.551929	-0.69961
WT PRE 7	C3	999	999
WT PRE 7	C1S	21.45365	1.064512
WT PRE 7	C1QA1	24.31662	18.36299
WT PRE 7	FH	20.71476	3.767628
WT PRE 7	CR4	16.88325	5.078755
WT PRE 7	FB	999	999
WT PRE 7	C9	999	999
WT PRE 7	C5aR	21.81985	14.36153
WT PRE 7	P2RY12	999	999
WT PRE 7	C4	15.61624	3.072822
WT PRE 7	FI	999	999
WT PRE 7	CSMD1	999	999
WT PRE 7	C5	14.08802	0.68197
WT PRE 7	C1QB	17.98393	7.69502
WT PRE 7	CD68	12.78047	9.625236
WT PRE 7	NOS	22.35096	2.882867
WT PRE 7	IL1B	27.18039	999
WT PRE 7	NOS	999	999
WT PRE 7	IL6	999	999
WT PRE 7	TNFA	20.12247	5.35207
WT PRE 6	LIN28	19.14054	9.161887
WT PRE 6	Oct-04	21.55919	11.4316
WT PRE 6	BMP4	12.63629	2.815757
WT PRE 6	CD34	999	999
WT PRE 6	SOX2	21.95298	6.72149
WT PRE 6	FLK1	15.0717	2.960848
WT PRE 6	CD45	19.78933	2.989968
WT PRE 6	CD11B	10.32202	3.80007

WT PRE 6	CD235a	15.6472	4.935923
WT PRE 6	BRAC	11.47903	2.142152
WT PRE 6	MERTK	25.00244	999
WT PRE 6	RUNX1	20.81664	1.607727
WT PRE 6	NESTIN	17.48658	7.828245
WT PRE 6	MAP2	20.25162	2.215002
WT PRE 6	NFKB	8.498804	1.484342
WT PRE 6	NLRP3	17.46982	6.519576
WT PRE 6	TREM2	16.99717	3.885863
WT PRE 6	IBA1	11.96992	3.727258
WT PRE 6	CD14	17.06358	4.881767
WT PRE 6	VIMENTIN	5.987883	2.043916
WT PRE 6	GFAP	9.136543	1.266883
WT PRE 6	EAAT2	999	999
WT PRE 6	ALDH1	18.60264	8.185077
WT PRE 6	S100B	23.89447	6.67461
WT PRE 6	NEUN	999	999
WT PRE 6	CX3CR1	15.64376	5.566705
WT PRE 6	BIN1	999	999
WT PRE 6	TGFB	17.04138	5.471673
WT PRE 6	TMEM119	11.14889	3.663636
WT PRE 6	ABCA7	999	999
WT PRE 6	PICALM	8.465775	2.182228
WT PRE 6	INPP5D	12.17384	4.252557
WT PRE 6	APOE	10.58848	2.951823
WT PRE 6	EPHA1	6.281243	1.953159
WT PRE 6	HLA-DR	21.45661	7.808484
WT PRE 6	PLCG2	7.465116	3.918794
WT PRE 6	CD33	17.82238	6.386934
WT PRE 6	CR1	9.825121	-0.6961
WT PRE 6	CD59	12.36517	3.573736
WT PRE 6	MASP	11.41545	1.894325
WT PRE 6	CR1	17.43821	6.916982
WT PRE 6	CD46	10.23965	1.888645
WT PRE 6	C1IN	12.2423	0.742692
WT PRE 6	C6	999	999
WT PRE 6	C3aR	17.01971	5.919577
WT PRE 6	DAF	13.29562	4.177719
WT PRE 6	C2	7.993063	0.741526
WT PRE 6	C3	11.16753	2.880046
WT PRE 6	C1S	21.81018	1.421041
WT PRE 6	C1QA1	11.06417	5.110538
WT PRE 6	FH	20.02386	3.07672
WT PRE 6	CR4	13.6402	1.835709
WT PRE 6	FB	999	999
WT PRE 6	C9	9.576156	1.76806

WT PRE 6	C5aR	11.80986	4.351537
WT PRE 6	P2RY12	13.48008	2.022462
WT PRE 6	C4	14.97575	2.43233
WT PRE 6	FI	999	999
WT PRE 6	CSMD1	12.65475	-1.30472
WT PRE 6	C5	15.55259	2.146544
WT PRE 6	C1QB	14.50958	4.220664
WT PRE 6	CD68	5.136061	1.980825
WT PRE 6	NOS	21.12443	1.656343
WT PRE 6	IL1B	999	999
WT PRE 6	NOS	999	999
WT PRE 6	IL6	13.90458	2.709749
WT PRE 6	TNFA	19.1806	4.410197
WT PRE 4	BMP4	12.9064	3.085862
WT PRE 4	CD34	13.45573	1.377826
WT PRE 4	SOX2	20.46791	5.23642
WT PRE 4	FLK1	18.95689	6.846039
WT PRE 4	CD45	999	999
WT PRE 4	CD11B	17.91727	11.39531
WT PRE 4	CD235a	16.70258	5.99131
WT PRE 4	BRAC	19.78327	10.44639
WT PRE 4	MERTK	23.20438	999
WT PRE 4	RUNX1	17.43685	-1.77206
WT PRE 4	NESTIN	16.12435	6.466008
WT PRE 4	MAP2	16.06636	-1.97025
WT PRE 4	NFKB	19.41012	12.39566
WT PRE 4	NLRP3	12.3502	1.39996
WT PRE 4	TREM2	17.60767	4.496364
WT PRE 4	IBA1	13.85078	5.608117
WT PRE 4	CD14	14.92989	2.74808
WT PRE 4	VIMENTIN	14.91471	10.97075
WT PRE 4	GFAP	17.44148	9.571824
WT PRE 4	EAAT2	17.06605	999
WT PRE 4	ALDH1	17.06097	6.643403
WT PRE 4	S100B	15.82797	-1.39189
WT PRE 4	NEUN	17.59517	-7.0475
WT PRE 4	CX3CR1	17.32616	7.249099
WT PRE 4	BIN1	17.14081	0.57604
WT PRE 4	TGFB	13.65064	2.080934
WT PRE 4	TMEM119	15.86566	8.380414
WT PRE 4	ABCA7	13.35263	-11.7792
WT PRE 4	PICALM	13.98845	7.704905
WT PRE 4	INPP5D	16.44103	8.519744
WT PRE 4	APOE	13.75758	6.120918
WT PRE 4	EPHA1	12.77858	8.4505

WT PRE 4	HLA-DR	14.09745	0.449327
WT PRE 4	PLCG2	12.57343	9.027105
WT PRE 4	CD33	14.00075	2.565307
WT PRE 4	CR1	15.30589	4.784668
WT PRE 4	CD59	16.77757	7.986141
WT PRE 4	MASP	13.7255	4.20438
WT PRE 4	CR1	17.47922	6.957999
WT PRE 4	CD46	16.10097	7.74996
WT PRE 4	C1IN	15.62531	4.125706
WT PRE 4	C6	17.41458	-1.17866
WT PRE 4	C3aR	16.21925	5.11912
WT PRE 4	DAF	16.71712	7.599223
WT PRE 4	C2	15.97021	8.718674
WT PRE 4	C3	15.85859	7.571106
WT PRE 4	C1S	18.22135	-2.16779
WT PRE 4	C1QA1	16.7019	10.74828
WT PRE 4	FH	15.16104	-1.7861
WT PRE 4	CR4	17.28388	5.47938
WT PRE 4	FB	20.2161	999
WT PRE 4	C9	19.09968	11.29159
WT PRE 4	C5aR	16.76529	9.306967
WT PRE 4	P2RY12	18.35907	6.901451
WT PRE 4	C4	17.03255	4.48913
WT PRE 4	FI	16.89342	6.583596
WT PRE 4	CSMD1	11.52639	-2.43308
WT PRE 4	C5	16.55493	3.148884
WT PRE 4	C1QB	17.97395	7.685035
WT PRE 4	CD68	18.06114	14.9059
WT PRE 4	NOS	16.23829	-3.2298
WT PRE 4	IL1B	26.14994	999
WT PRE 4	NOS	16.68109	-2.78699
WT PRE 4	IL6	18.18043	6.985593
WT PRE 4	TNFA	17.20455	2.43415
WT PRE 5	BMP4	20.37423	10.5537
WT PRE 5	CD34	20.18256	8.10466
WT PRE 5	SOX2	26.89752	11.66603
WT PRE 5	FLK1	999	999
WT PRE 5	CD45	999	999
WT PRE 5	CD11B	20.89198	14.37003
WT PRE 5	CD235a	999	999
WT PRE 5	BRAC	999	999
WT PRE 5	MERTK	19.2067	999
WT PRE 5	RUNX1	999	999
WT PRE 5	NESTIN	20.82118	11.16284
WT PRE 5	MAP2	999	999

WT PRE 5	NFKB	22.70977	15.69531
WT PRE 5	NLRP3	999	999
WT PRE 5	TREM2	999	999
WT PRE 5	IBA1	999	999
WT PRE 5	CD14	999	999
WT PRE 5	VIMENTIN	999	999
WT PRE 5	GFAP	20.19678	12.32712
WT PRE 5	EAAT2	999	999
WT PRE 5	ALDH1	999	999
WT PRE 5	S100B	22.20269	4.982834
WT PRE 5	NEUN	999	999
WT PRE 5	CX3CR1	23.11305	13.03599
WT PRE 5	BIN1	999	999
WT PRE 5	TGFB	999	999
WT PRE 5	TMEM119	999	999
WT PRE 5	ABCA7	999	999
WT PRE 5	PICALM	999	999
WT PRE 5	INPP5D	999	999
WT PRE 5	APOE	999	999
WT PRE 5	EPHA1	999	999
WT PRE 5	HLA-DR	22.91837	9.270248
WT PRE 5	PLCG2	999	999
WT PRE 5	CD33	999	999
WT PRE 5	CR1	999	999
WT PRE 5	CD59	25.01156	16.22013
WT PRE 5	MASP	999	999
WT PRE 5	CR1	22.58396	12.06274
WT PRE 5	CD46	999	999
WT PRE 5	C1IN	999	999
WT PRE 5	C6	999	999
WT PRE 5	C3aR	999	999
WT PRE 5	DAF	999	999
WT PRE 5	C2	19.678	12.42646
WT PRE 5	C3	23.92895	15.64146
WT PRE 5	C1S	999	999
WT PRE 5	C1QA1	999	999
WT PRE 5	FH	999	999
WT PRE 5	CR4	999	999
WT PRE 5	FB	999	999
WT PRE 5	C9	22.64712	14.83902
WT PRE 5	C5aR	999	999
WT PRE 5	P2RY12	999	999
WT PRE 5	C4	999	999
WT PRE 5	FI	999	999
WT PRE 5	CSMD1	999	999
WT PRE 5	C5	20.66353	7.257477

WT PRE 5	C1QB	20.15748	9.868571
WT PRE 5	CD68	999	999
WT PRE 5	NOS	25.2179	5.749807
WT PRE 5	IL1B	999	999
WT PRE 5	NOS	999	999
WT PRE 5	IL6	999	999
WT PRE 5	TNFA	999	999
WT PRE 3	BMP4	11.42869	1.608157
WT PRE 3	CD34	14.23521	2.157311
WT PRE 3	SOX2	13.83124	-1.40025
WT PRE 3	FLK1	12.75868	0.647828
WT PRE 3	CD45	18.18013	1.380771
WT PRE 3	CD11B	6.109612	-0.41234
WT PRE 3	CD235a	8.519915	-2.19136
WT PRE 3	BRAC	8.626584	-0.7103
WT PRE 3	MERTK	20.71133	999
WT PRE 3	RUNX1	20.03676	0.827844
WT PRE 3	NESTIN	10.17969	0.521353
WT PRE 3	MAP2	25.93232	7.895705
WT PRE 3	NFKB	7.438439	0.423976
WT PRE 3	NLRP3	13.99624	3.045999
WT PRE 3	TREM2	12.5487	-0.5626
WT PRE 3	IBA1	8.243702	0.001041
WT PRE 3	CD14	11.43866	-0.74315
WT PRE 3	VIMENTIN	3.426164	-0.5178
WT PRE 3	GFAP	7.626765	-0.2429
WT PRE 3	EAAT2	999	999
WT PRE 3	ALDH1	11.43035	1.012788
WT PRE 3	S100B	17.86311	0.643256
WT PRE 3	NEUN	26.3669	1.724224
WT PRE 3	CX3CR1	9.320794	-0.75626
WT PRE 3	BIN1	17.87739	1.312623
WT PRE 3	TGFB	11.84067	0.270962
WT PRE 3	TMEM119	6.577149	-0.9081
WT PRE 3	ABCA7	24.81808	-0.31374
WT PRE 3	PICALM	6.406394	0.122847
WT PRE 3	INPP5D	6.966418	-0.95487
WT PRE 3	APOE	6.789996	-0.84666
WT PRE 3	EPHA1	3.744136	-0.58395
WT PRE 3	HLA-DR	13.98408	0.33596
WT PRE 3	PLCG2	6.767245	3.220923
WT PRE 3	CD33	11.28018	-0.15527
WT PRE 3	CR1	10.33219	-0.18903
WT PRE 3	CD59	8.275841	-0.51559
WT PRE 3	MASP	12.8701	3.348976

WT PRE 3	CR1	16.71025	6.189024
WT PRE 3	CD46	10.41781	2.066806
WT PRE 3	C1IN	9.453168	-2.04644
WT PRE 3	C6	999	999
WT PRE 3	C3aR	11.40989	0.30976
WT PRE 3	DAF	10.45019	1.332287
WT PRE 3	C2	7.336503	0.084966
WT PRE 3	C3	12.40483	4.117347
WT PRE 3	C1S	19.60254	-0.7866
WT PRE 3	C1QA1	7.156964	1.203335
WT PRE 3	FH	18.35349	1.406359
WT PRE 3	CR4	12.236	0.431507
WT PRE 3	FB	999	999
WT PRE 3	C9	7.320769	-0.48733
WT PRE 3	C5aR	9.726437	2.268112
WT PRE 3	P2RY12	9.930628	-1.52699
WT PRE 3	C4	10.19742	-2.346
WT PRE 3	FI	11.9454	1.635571
WT PRE 3	CSMD1	999	999
WT PRE 3	C5	12.01564	-1.39041
WT PRE 3	C1QB	8.986165	-1.30275
WT PRE 3	CD68	3.439888	0.284651
WT PRE 3	NOS	17.69663	-1.77146
WT PRE 3	IL1B	999	999
WT PRE 3	NOS	999	999
WT PRE 3	IL6	10.58981	-0.60503
WT PRE 3	TNFA	10.97121	-3.79919
WT PRE 1	LIN28	11.5741	1.595449
WT PRE 1	Oct-04	12.11831	1.990724
WT PRE 1	BMP4	7.814535	-2.006
WT PRE 1	CD34	14.06658	1.988675
WT PRE 1	SOX2	12.77616	-2.45534
WT PRE 1	FLK1	8.410935	-3.69992
WT PRE 1	CD45	19.79615	2.996789
WT PRE 1	CD11B	8.069776	1.547824
WT PRE 1	CD235a	13.58626	2.874992
WT PRE 1	BRAC	10.43492	1.09804
WT PRE 1	MERTK	999	999
WT PRE 1	RUNX1	14.90861	-4.3003
WT PRE 1	NESTIN	12.86398	3.205638
WT PRE 1	MAP2	15.91203	-2.12458
WT PRE 1	NFKB	8.802778	1.788315
WT PRE 1	NLRP3	12.6833	1.733064
WT PRE 1	TREM2	14.49331	1.382007
WT PRE 1	IBA1	9.990094	1.747434

WT PRE 1	CD14	13.80192	1.620106
WT PRE 1	VIMENTIN	4.48786	0.543893
WT PRE 1	GFAP	9.619488	1.749828
WT PRE 1	EAAT2	18.9506	999
WT PRE 1	ALDH1	12.2658	1.848239
WT PRE 1	S100B	21.26347	4.043609
WT PRE 1	NEUN	25.70478	1.062103
WT PRE 1	CX3CR1	12.42655	2.349497
WT PRE 1	BIN1	20.30689	3.742123
WT PRE 1	TGFB	12.42411	0.854405
WT PRE 1	TMEM119	7.530008	0.044757
WT PRE 1	ABCA7	999	999
WT PRE 1	PICALM	7.217533	0.933986
WT PRE 1	INPP5D	9.492544	1.57126
WT PRE 1	APOE	9.669277	2.032618
WT PRE 1	EPHA1	5.509902	1.181818
WT PRE 1	HLA-DR	14.83167	1.183545
WT PRE 1	PLCG2	5.150624	1.604302
WT PRE 1	CD33	13.52114	2.085689
WT PRE 1	CR1	7.573319	-2.94791
WT PRE 1	CD59	9.749164	0.957731
WT PRE 1	MASP	9.552316	0.031195
WT PRE 1	CR1	11.52934	1.008114
WT PRE 1	CD46	10.55235	2.201339
WT PRE 1	C1IN	10.41562	-1.08398
WT PRE 1	C6	17.34493	-1.2483
WT PRE 1	C3aR	9.623912	-1.47622
WT PRE 1	DAF	10.40873	1.290836
WT PRE 1	C2	8.542187	1.29065
WT PRE 1	C3	10.1541	1.866618
WT PRE 1	C1S	18.4952	-1.89394
WT PRE 1	C1QA1	7.117265	1.163636
WT PRE 1	FH	16.75481	-0.19232
WT PRE 1	CR4	11.13195	-0.67254
WT PRE 1	FB	999	999
WT PRE 1	C9	9.475226	1.66713
WT PRE 1	C5aR	9.37009	1.911764
WT PRE 1	P2RY12	12.99508	1.537455
WT PRE 1	C4	13.30803	0.764604
WT PRE 1	FI	12.27026	1.960436
WT PRE 1	CSMD1	9.50209	-4.45738
WT PRE 1	C5	8.997215	-4.40883
WT PRE 1	C1QB	9.962598	-0.32631
WT PRE 1	CD68	3.865537	0.710301
WT PRE 1	NOS	20.01271	0.544621
WT PRE 1	IL1B	999	999

WT PRE 1	NOS	999	999
WT PRE 1	IL6	13.30256	2.107723
WT PRE 1	TNFA	16.49353	1.723129
WT PRE 2	LIN28	17.04446	7.065805
WT PRE 2	Oct-04	17.38161	7.25402
WT PRE 2	BMP4	999	999
WT PRE 2	CD34	25.11676	13.03885
WT PRE 2	SOX2	999	999
WT PRE 2	FLK1	999	999
WT PRE 2	CD45	999	999
WT PRE 2	CD11B	999	999
WT PRE 2	CD235a	999	999
WT PRE 2	BRAC	999	999
WT PRE 2	MERTK	21.67027	999
WT PRE 2	RUNX1	999	999
WT PRE 2	NESTIN	21.29513	11.63679
WT PRE 2	MAP2	999	999
WT PRE 2	NFKB	999	999
WT PRE 2	NLRP3	999	999
WT PRE 2	TREM2	999	999
WT PRE 2	IBA1	23.73477	15.49211
WT PRE 2	CD14	999	999
WT PRE 2	VIMENTIN	20.42872	16.48475
WT PRE 2	GFAP	21.14987	13.28021
WT PRE 2	EAAT2	999	999
WT PRE 2	ALDH1	999	999
WT PRE 2	S100B	999	999
WT PRE 2	NEUN	25.37689	0.734209
WT PRE 2	CX3CR1	24.67709	14.60003
WT PRE 2	BIN1	999	999
WT PRE 2	TGFB	999	999
WT PRE 2	TMEM119	22.64308	15.15783
WT PRE 2	ABCA7	999	999
WT PRE 2	PICALM	999	999
WT PRE 2	INPP5D	999	999
WT PRE 2	APOE	999	999
WT PRE 2	EPHA1	999	999
WT PRE 2	HLA-DR	999	999
WT PRE 2	PLCG2	25.84548	22.29916
WT PRE 2	CD33	999	999
WT PRE 2	CR1	999	999
WT PRE 2	CD59	999	999
WT PRE 2	MASP	999	999
WT PRE 2	CR1	999	999
WT PRE 2	CD46	999	999

WT PRE 2	C1IN	999	999
WT PRE 2	C6	999	999
WT PRE 2	C3aR	999	999
WT PRE 2	DAF	999	999
WT PRE 2	C2	999	999
WT PRE 2	C3	25.78215	17.49466
WT PRE 2	C1S	999	999
WT PRE 2	C1QA1	999	999
WT PRE 2	FH	999	999
WT PRE 2	CR4	999	999
WT PRE 2	FB	999	999
WT PRE 2	C9	999	999
WT PRE 2	C5aR	26.22426	18.76594
WT PRE 2	P2RY12	999	999
WT PRE 2	C4	999	999
WT PRE 2	FI	999	999
WT PRE 2	CSMD1	999	999
WT PRE 2	C5	24.94572	11.53967
WT PRE 2	C1QB	21.22611	10.9372
WT PRE 2	CD68	999	999
WT PRE 2	NOS	28.799	9.330911
WT PRE 2	IL1B	999	999
WT PRE 2	NOS	999	999
WT PRE 2	IL6	999	999
WT PRE 2	TNFA	999	999
WT PRE 8	LIN28	6.390918	-3.58774
WT PRE 8	Oct-04	6.124769	-4.00282
WT PRE 8	BMP4	10.91001	1.089479
WT PRE 8	CD34	10.13782	-1.94008
WT PRE 8	SOX2	15.65727	0.425779
WT PRE 8	FLK1	15.89792	3.787067
WT PRE 8	CD45	999	999
WT PRE 8	CD11B	19.78879	13.26684
WT PRE 8	CD235a	999	999
WT PRE 8	BRAC	14.34847	5.01159
WT PRE 8	MERTK	19.61338	999
WT PRE 8	RUNX1	14.96393	-4.24499
WT PRE 8	NESTIN	17.1659	7.507559
WT PRE 8	MAP2	18.27018	0.233566
WT PRE 8	NFKB	19.6133	12.59884
WT PRE 8	NLRP3	999	999
WT PRE 8	TREM2	999	999
WT PRE 8	IBA1	14.46139	6.218726
WT PRE 8	CD14	999	999
WT PRE 8	VIMENTIN	9.305138	5.36117

WT PRE 8	GFAP	17.62161	9.751951
WT PRE 8	EAAT2	21.61594	999
WT PRE 8	ALDH1	16.42776	6.010198
WT PRE 8	S100B	999	999
WT PRE 8	NEUN	999	999
WT PRE 8	CX3CR1	19.83865	9.761594
WT PRE 8	BIN1	999	999
WT PRE 8	TGFB	19.77861	8.208907
WT PRE 8	TMEM119	13.10068	5.615427
WT PRE 8	ABCA7	999	999
WT PRE 8	PICALM	11.20389	4.920343
WT PRE 8	INPP5D	15.35664	7.435351
WT PRE 8	APOE	13.51391	5.877248
WT PRE 8	EPHA1	13.9189	9.590818
WT PRE 8	HLA-DR	11.51283	-2.13529
WT PRE 8	PLCG2	11.45023	7.903909
WT PRE 8	CD33	999	999
WT PRE 8	CR1	999	999
WT PRE 8	CD59	13.81143	5.019994
WT PRE 8	MASP	999	999
WT PRE 8	CR1	15.70782	5.186595
WT PRE 8	CD46	15.40391	7.052898
WT PRE 8	C1IN	12.35731	0.857705
WT PRE 8	C6	999	999
WT PRE 8	C3aR	17.8606	6.76047
WT PRE 8	DAF	23.69291	14.57501
WT PRE 8	C2	10.24934	2.9978
WT PRE 8	C3	999	999
WT PRE 8	C1S	999	999
WT PRE 8	C1QA1	999	999
WT PRE 8	FH	19.66576	2.718622
WT PRE 8	CR4	20.80897	9.004479
WT PRE 8	FB	999	999
WT PRE 8	C9	999	999
WT PRE 8	C5aR	999	999
WT PRE 8	P2RY12	999	999
WT PRE 8	C4	18.8647	6.321282
WT PRE 8	FI	999	999
WT PRE 8	CSMD1	999	999
WT PRE 8	C5	999	999
WT PRE 8	C1QB	21.91553	11.62662
WT PRE 8	CD68	18.16703	15.01179
WT PRE 8	NOS	23.55328	4.085187
WT PRE 8	IL1B	999	999
WT PRE 8	NOS	999	999
WT PRE 8	IL6	999	999

WT PRE 8	TNFA	999	999
WT MG 1	LIN28	999	999
WT MG 1	Oct-04	21.65519	11.5276
WT MG 1	BMP4	999	999
WT MG 1	CD34	17.3228	5.244897
WT MG 1	SOX2	27.23383	12.00233
WT MG 1	FLK1	19.09541	6.984556
WT MG 1	CD45	999	999
WT MG 1	CD11B	24.04541	17.52346
WT MG 1	CD235a	19.76095	9.049675
WT MG 1	BRAC	21.43108	12.0942
WT MG 1	MERTK	21.71176	999
WT MG 1	RUNX1	999	999
WT MG 1	NESTIN	20.41092	10.75258
WT MG 1	MAP2	19.81866	1.782045
WT MG 1	NFKB	21.81805	14.80359
WT MG 1	NLRP3	999	999
WT MG 1	TREM2	999	999
WT MG 1	IBA1	19.42054	11.17788
WT MG 1	CD14	999	999
WT MG 1	VIMENTIN	10.8934	6.949438
WT MG 1	GFAP	16.16642	8.296761
WT MG 1	EAAT2	999	999
WT MG 1	ALDH1	18.34336	7.925798
WT MG 1	S100B	22.64548	5.425627
WT MG 1	NEUN	20.21437	-4.42831
WT MG 1	CX3CR1	23.67499	13.59793
WT MG 1	BIN1	999	999
WT MG 1	TGFB	999	999
WT MG 1	TMEM119	17.36369	9.878438
WT MG 1	ABCA7	999	999
WT MG 1	PICALM	15.12812	8.844573
WT MG 1	INPP5D	999	999
WT MG 1	APOE	999	999
WT MG 1	EPHA1	19.21193	14.88384
WT MG 1	HLA-DR	999	999
WT MG 1	PLCG2	999	999
WT MG 1	CD33	999	999
WT MG 1	CR1	999	999
WT MG 1	CD59	20.92557	12.13413
WT MG 1	MASP	999	999
WT MG 1	CR1	999	999
WT MG 1	CD46	21.01209	12.66109
WT MG 1	C1IN	20.24092	8.741308
WT MG 1	C6	999	999

WT MG 1	C3aR	999	999
WT MG 1	DAF	999	999
WT MG 1	C2	21.62605	14.37451
WT MG 1	C3	21.53796	13.25047
WT MG 1	C1S	999	999
WT MG 1	C1QA1	999	999
WT MG 1	FH	999	999
WT MG 1	CR4	999	999
WT MG 1	FB	999	999
WT MG 1	C9	17.39765	9.589555
WT MG 1	C5aR	25.00748	17.54915
WT MG 1	P2RY12	999	999
WT MG 1	C4	24.69666	12.15324
WT MG 1	FI	999	999
WT MG 1	CSMD1	16.12938	2.169914
WT MG 1	C5	17.01338	3.607327
WT MG 1	C1QB	19.25304	8.964127
WT MG 1	CD68	20.84846	17.69322
WT MG 1	NOS	24.08518	4.617089
WT MG 1	IL1B	999	999
WT MG 1	NOS	999	999
WT MG 1	IL6	999	999
WT MG 1	TNFA	999	999
WT MG 5	LIN28	999	999
WT MG 5	Oct-04	999	999
WT MG 5	BMP4	999	999
WT MG 5	CD34	999	999
WT MG 5	SOX2	999	999
WT MG 5	FLK1	999	999
WT MG 5	CD45	999	999
WT MG 5	CD11B	16.04032	9.51837
WT MG 5	CD235a	22.41845	11.70718
WT MG 5	BRAC	20.61078	11.2739
WT MG 5	MERTK	999	999
WT MG 5	RUNX1	999	999
WT MG 5	NESTIN	20.89439	11.23605
WT MG 5	MAP2	999	999
WT MG 5	NFKB	18.2614	11.24694
WT MG 5	NLRP3	999	999
WT MG 5	TREM2	999	999
WT MG 5	IBA1	19.06739	10.82473
WT MG 5	CD14	999	999
WT MG 5	VIMENTIN	15.9244	11.98043
WT MG 5	GFAP	19.77125	11.90159
WT MG 5	EAAT2	999	999

WT MG 5	ALDH1	999	999
WT MG 5	S100B	999	999
WT MG 5	NEUN	999	999
WT MG 5	CX3CR1	999	999
WT MG 5	BIN1	999	999
WT MG 5	TGFB	22.95752	11.38781
WT MG 5	TMEM119	19.55364	12.06839
WT MG 5	ABCA7	999	999
WT MG 5	PICALM	999	999
WT MG 5	INPP5D	999	999
WT MG 5	APOE	999	999
WT MG 5	EPHA1	16.95889	12.63081
WT MG 5	HLA-DR	999	999
WT MG 5	PLCG2	16.28856	12.74224
WT MG 5	CD33	999	999
WT MG 5	CR1	999	999
WT MG 5	CD59	24.75791	15.96648
WT MG 5	MASP	999	999
WT MG 5	CR1	999	999
WT MG 5	CD46	999	999
WT MG 5	C1IN	999	999
WT MG 5	C6	999	999
WT MG 5	C3aR	999	999
WT MG 5	DAF	24.45707	15.33917
WT MG 5	C2	999	999
WT MG 5	C3	999	999
WT MG 5	C1S	999	999
WT MG 5	C1QA1	18.10081	12.14718
WT MG 5	FH	999	999
WT MG 5	CR4	23.98617	12.18167
WT MG 5	FB	999	999
WT MG 5	C9	999	999
WT MG 5	C5aR	999	999
WT MG 5	P2RY12	999	999
WT MG 5	C4	999	999
WT MG 5	FI	999	999
WT MG 5	CSMD1	999	999
WT MG 5	C5	999	999
WT MG 5	C1QB	17.92552	7.636607
WT MG 5	CD68	16.0337	12.87846
WT MG 5	NOS	999	999
WT MG 5	IL1B	999	999
WT MG 5	NOS	999	999
WT MG 5	IL6	999	999
WT MG 5	TNFA	999	999

WT MG 6	LIN28	999	999
WT MG 6	Oct-04	999	999
WT MG 6	BMP4	999	999
WT MG 6	CD34	999	999
WT MG 6	SOX2	999	999
WT MG 6	FLK1	999	999
WT MG 6	CD45	999	999
WT MG 6	CD11B	20.21899	13.69704
WT MG 6	CD235a	999	999
WT MG 6	BRAC	999	999
WT MG 6	MERTK	21.69348	999
WT MG 6	RUNX1	999	999
WT MG 6	NESTIN	19.52804	9.869705
WT MG 6	MAP2	999	999
WT MG 6	NFKB	999	999
WT MG 6	NLRP3	999	999
WT MG 6	TREM2	999	999
WT MG 6	IBA1	999	999
WT MG 6	CD14	999	999
WT MG 6	VIMENTIN	19.25421	15.31024
WT MG 6	GFAP	20.70013	12.83047
WT MG 6	EAAT2	999	999
WT MG 6	ALDH1	999	999
WT MG 6	S100B	999	999
WT MG 6	NEUN	999	999
WT MG 6	CX3CR1	999	999
WT MG 6	BIN1	999	999
WT MG 6	TGFB	999	999
WT MG 6	TMEM119	999	999
WT MG 6	ABCA7	999	999
WT MG 6	PICALM	26.26123	19.97768
WT MG 6	INPP5D	999	999
WT MG 6	APOE	999	999
WT MG 6	EPHA1	20.35685	16.02876
WT MG 6	HLA-DR	999	999
WT MG 6	PLCG2	20.09735	16.55103
WT MG 6	CD33	999	999
WT MG 6	CR1	999	999
WT MG 6	CD59	999	999
WT MG 6	MASP	999	999
WT MG 6	CR1	999	999
WT MG 6	CD46	999	999
WT MG 6	C1IN	999	999
WT MG 6	C6	999	999
WT MG 6	C3aR	999	999
WT MG 6	DAF	999	999

WT MG 6	C2	999	999
WT MG 6	C3	999	999
WT MG 6	C1S	999	999
WT MG 6	C1QA1	22.58924	16.63561
WT MG 6	FH	999	999
WT MG 6	CR4	999	999
WT MG 6	FB	999	999
WT MG 6	C9	999	999
WT MG 6	C5aR	999	999
WT MG 6	P2RY12	999	999
WT MG 6	C4	999	999
WT MG 6	FI	999	999
WT MG 6	CSMD1	999	999
WT MG 6	C5	23.16854	9.762496
WT MG 6	C1QB	21.78963	11.50072
WT MG 6	CD68	19.26872	16.11349
WT MG 6	NOS	999	999
WT MG 6	IL1B	999	999
WT MG 6	NOS	999	999
WT MG 6	IL6	999	999
WT MG 6	TNFA	999	999
WT MG 6	ACTB	999	999
WT MG 3	LIN28	16.78603	6.80737
WT MG 3	Oct-04	14.68505	4.557459
WT MG 3	BMP4	13.52124	3.700705
WT MG 3	CD34	18.87289	6.79499
WT MG 3	SOX2	999	999
WT MG 3	FLK1	11.14878	-0.96207
WT MG 3	CD45	20.3262	3.526841
WT MG 3	CD11B	10.91051	4.388556
WT MG 3	CD235a	13.62165	2.910382
WT MG 3	BRAC	14.52747	5.190593
WT MG 3	MERTK	999	999
WT MG 3	RUNX1	20.11553	0.90661
WT MG 3	NESTIN	13.84089	4.182548
WT MG 3	MAP2	17.52119	-0.51543
WT MG 3	NFKB	11.78417	4.769704
WT MG 3	NLRP3	16.65077	5.700526
WT MG 3	TREM2	17.00584	3.894532
WT MG 3	IBA1	7.865502	-0.37716
WT MG 3	CD14	16.13243	3.950622
WT MG 3	VIMENTIN	5.08949	1.145523
WT MG 3	GFAP	9.261951	1.392291
WT MG 3	EAAT2	999	999
WT MG 3	ALDH1	13.38649	2.968927

WT MG 3	S100B	21.94732	4.72746
WT MG 3	NEUN	25.38399	0.741309
WT MG 3	CX3CR1	20.6236	10.54654
WT MG 3	BIN1	22.90361	6.338842
WT MG 3	TGFB	13.25658	1.686876
WT MG 3	TMEM119	10.0734	2.588147
WT MG 3	ABCA7	999	999
WT MG 3	PICALM	8.785593	2.502046
WT MG 3	INPP5D	13.68478	5.763495
WT MG 3	APOE	12.88044	5.243777
WT MG 3	EPHA1	5.699612	1.371528
WT MG 3	HLA-DR	17.01638	3.368252
WT MG 3	PLCG2	6.663233	3.116911
WT MG 3	CD33	18.79596	7.360509
WT MG 3	CR1	11.91465	1.393426
WT MG 3	CD59	11.9171	3.125664
WT MG 3	MASP	13.93241	4.411287
WT MG 3	CR1	13.07837	2.557144
WT MG 3	CD46	11.79414	3.443127
WT MG 3	C1IN	13.29598	1.796369
WT MG 3	C6	999	999
WT MG 3	C3aR	9.490293	-1.60984
WT MG 3	DAF	12.89056	3.772662
WT MG 3	C2	9.789982	2.538445
WT MG 3	C3	11.27372	2.98623
WT MG 3	C1S	19.21908	-1.17006
WT MG 3	C1QA1	8.538191	2.584562
WT MG 3	FH	18.2547	1.30756
WT MG 3	CR4	12.60452	0.800023
WT MG 3	FB	999	999
WT MG 3	C9	10.6853	2.877207
WT MG 3	C5aR	10.50692	3.048596
WT MG 3	P2RY12	22.26077	10.80315
WT MG 3	C4	16.26222	3.718798
WT MG 3	FI	19.11841	8.80858
WT MG 3	CSMD1	15.28998	1.330507
WT MG 3	C5	14.03905	0.632999
WT MG 3	C1QB	12.34068	2.051769
WT MG 3	CD68	6.197942	3.042706
WT MG 3	NOS	9.493938	-9.97415
WT MG 3	IL1B	999	999
WT MG 3	NOS	999	999
WT MG 3	IL6	12.1785	0.983661
WT MG 3	TNFA	10.54453	-4.22588
WT MG 11	LIN28	999	999

WT MG 11	Oct-04	999	999
WT MG 11	BMP4	999	999
WT MG 11	CD34	999	999
WT MG 11	SOX2	29.53474	14.30324
WT MG 11	FLK1	999	999
WT MG 11	CD45	999	999
WT MG 11	CD11B	999	999
WT MG 11	CD235a	999	999
WT MG 11	BRAC	999	999
WT MG 11	MERTK	23.04838	999
WT MG 11	RUNX1	999	999
WT MG 11	NESTIN	999	999
WT MG 11	MAP2	999	999
WT MG 11	NFKB	999	999
WT MG 11	NLRP3	999	999
WT MG 11	TREM2	999	999
WT MG 11	IBA1	999	999
WT MG 11	CD14	999	999
WT MG 11	VIMENTIN	22.85986	18.91589
WT MG 11	GFAP	999	999
WT MG 11	EAAT2	999	999
WT MG 11	ALDH1	999	999
WT MG 11	S100B	999	999
WT MG 11	NEUN	999	999
WT MG 11	CX3CR1	999	999
WT MG 11	BIN1	999	999
WT MG 11	TGFB	999	999
WT MG 11	TMEM119	22.17218	14.68693
WT MG 11	ABCA7	999	999
WT MG 11	PICALM	999	999
WT MG 11	INPP5D	999	999
WT MG 11	APOE	999	999
WT MG 11	EPHA1	999	999
WT MG 11	HLA-DR	999	999
WT MG 11	PLCG2	22.44699	18.90067
WT MG 11	CD33	999	999
WT MG 11	CR1	999	999
WT MG 11	CD59	999	999
WT MG 11	MASP	999	999
WT MG 11	CR1	999	999
WT MG 11	CD46	999	999
WT MG 11	C1IN	999	999
WT MG 11	C6	999	999
WT MG 11	C3aR	999	999
WT MG 11	DAF	999	999
WT MG 11	C2	999	999

WT MG 11	C3	999	999
WT MG 11	C1S	999	999
WT MG 11	C1QA1	999	999
WT MG 11	FH	999	999
WT MG 11	CR4	999	999
WT MG 11	FB	999	999
WT MG 11	C9	999	999
WT MG 11	C5aR	999	999
WT MG 11	P2RY12	999	999
WT MG 11	C4	999	999
WT MG 11	FI	999	999
WT MG 11	CSMD1	999	999
WT MG 11	C5	999	999
WT MG 11	C1QB	20.83336	10.54445
WT MG 11	CD68	999	999
WT MG 11	NOS	25.44422	5.976128
WT MG 11	IL1B	999	999
WT MG 11	NOS	999	999
WT MG 11	IL6	999	999
WT MG 11	TNFA	999	999
WT MG 7	LIN28	999	999
WT MG 7	Oct-04	18.82794	8.700348
WT MG 7	BMP4	999	999
WT MG 7	CD34	999	999
WT MG 7	SOX2	999	999
WT MG 7	FLK1	19.95871	7.847856
WT MG 7	CD45	999	999
WT MG 7	CD11B	11.57674	5.054787
WT MG 7	CD235a	20.12289	9.411615
WT MG 7	BRAC	20.36996	11.03308
WT MG 7	MERTK	999	999
WT MG 7	RUNX1	999	999
WT MG 7	NESTIN	19.10949	9.451146
WT MG 7	MAP2	999	999
WT MG 7	NFKB	15.42478	8.410318
WT MG 7	NLRP3	23.1736	12.22336
WT MG 7	TREM2	999	999
WT MG 7	IBA1	18.56052	10.31786
WT MG 7	CD14	999	999
WT MG 7	VIMENTIN	10.96869	7.024718
WT MG 7	GFAP	19.65751	11.78785
WT MG 7	EAAT2	999	999
WT MG 7	ALDH1	20.11434	9.696773
WT MG 7	S100B	24.09824	6.878384
WT MG 7	NEUN	27.21218	2.569503

WT MG 7	CX3CR1	999	999
WT MG 7	BIN1	999	999
WT MG 7	TGFB	19.2576	7.687898
WT MG 7	TMEM119	14.20844	6.723185
WT MG 7	ABCA7	999	999
WT MG 7	PICALM	19.07889	12.79535
WT MG 7	INPP5D	21.24877	13.32749
WT MG 7	APOE	999	999
WT MG 7	EPHA1	16.1079	11.77981
WT MG 7	HLA-DR	999	999
WT MG 7	PLCG2	11.09399	7.547671
WT MG 7	CD33	24.75329	13.31784
WT MG 7	CR1	999	999
WT MG 7	CD59	22.37853	13.58709
WT MG 7	MASP	999	999
WT MG 7	CR1	19.73107	9.209848
WT MG 7	CD46	21.67624	13.32524
WT MG 7	C1IN	999	999
WT MG 7	C6	999	999
WT MG 7	C3aR	19.7762	8.67607
WT MG 7	DAF	21.48616	12.36827
WT MG 7	C2	17.347	10.09547
WT MG 7	C3	999	999
WT MG 7	C1S	999	999
WT MG 7	C1QA1	13.05159	7.097959
WT MG 7	FH	999	999
WT MG 7	CR4	15.95309	4.148591
WT MG 7	FB	999	999
WT MG 7	C9	21.37157	13.56348
WT MG 7	C5aR	999	999
WT MG 7	P2RY12	999	999
WT MG 7	C4	999	999
WT MG 7	FI	999	999
WT MG 7	CSMD1	19.05867	5.099205
WT MG 7	C5	999	999
WT MG 7	C1QB	15.62378	5.33487
WT MG 7	CD68	12.41112	9.25588
WT MG 7	NOS	22.05193	2.583836
WT MG 7	IL1B	999	999
WT MG 7	NOS	999	999
WT MG 7	IL6	20.79038	9.595544
WT MG 7	TNFA	999	999
WT MG 8	LIN28	14.6462	0
WT MG 8	Oct-04	14.26381	0
WT MG 8	BMP4	15.31357	0

WT MG 8	CD34	17.20542	0
WT MG 8	SOX2	21.13453	0
WT MG 8	FLK1	12.74424	0
WT MG 8	CD45	24.82919	0
WT MG 8	CD11B	11.12424	0
WT MG 8	CD235a	14.0774	0
WT MG 8	BRAC	11.95056	0
WT MG 8	MERTK	20.99617	0
WT MG 8	RUNX1	19.88239	0
WT MG 8	NESTIN	13.68622	0
WT MG 8	MAP2	19.96045	0
WT MG 8	NFKB	11.99625	0
WT MG 8	NLRP3	16.86232	0
WT MG 8	TREM2	18.12144	0
WT MG 8	IBA1	11.55349	0
WT MG 8	CD14	15.75573	0
WT MG 8	VIMENTIN	5.80311	0
WT MG 8	GFAP	10.28091	0
WT MG 8	EAAT2	24.06564	0
WT MG 8	ALDH1	13.86887	0
WT MG 8	S100B	21.76567	0
WT MG 8	NEUN	27.37512	0
WT MG 8	CX3CR1	15.61169	0
WT MG 8	BIN1	21.30491	0
WT MG 8	TGFB	13.31112	0
WT MG 8	TMEM119	10.69473	0
WT MG 8	ABCA7	999	999
WT MG 8	PICALM	9.841196	0
WT MG 8	INPP5D	12.30904	0
WT MG 8	APOE	12.96453	0
WT MG 8	EPHA1	8.110281	0
WT MG 8	HLA-DR	19.03151	0
WT MG 8	PLCG2	6.965343	0
WT MG 8	CD33	18.06604	0
WT MG 8	CR1	12.46044	-0.62976
WT MG 8	CD59	13.23917	0
WT MG 8	MASP	14.70159	0
WT MG 8	CR1	13.71997	0.629764
WT MG 8	CD46	13.16542	0
WT MG 8	C1IN	13.68479	0
WT MG 8	C6	26.20946	0
WT MG 8	C3aR	10.67282	0
WT MG 8	DAF	14.52233	0
WT MG 8	C2	10.82848	0
WT MG 8	C3	12.8789	0
WT MG 8	C1S	19.92222	0

WT MG 8	C1QA1	10.07251	0
WT MG 8	FH	20.4525	0
WT MG 8	CR4	14.59216	0
WT MG 8	FB	999	999
WT MG 8	C9	11.57204	0
WT MG 8	C5aR	12.28917	0
WT MG 8	P2RY12	17.52759	0
WT MG 8	C4	16.25756	0
WT MG 8	FI	15.55885	0
WT MG 8	CSMD1	12.57849	0
WT MG 8	C5	15.06188	0
WT MG 8	C1QB	13.80553	0
WT MG 8	CD68	6.987742	0
WT MG 8	NOS	16.9477	0
WT MG 8	IL1B	999	999
WT MG 8	NOS	999	999
WT MG 8	IL6	14.84606	0
WT MG 8	TNFA	18.40968	0
WT MG 9	LIN28	15.25031	5.271655
WT MG 9	Oct-04	14.31894	4.191346
WT MG 9	BMP4	14.39086	4.570324
WT MG 9	CD34	17.04946	4.971552
WT MG 9	SOX2	18.27788	3.046391
WT MG 9	FLK1	9.449106	-2.66174
WT MG 9	CD45	20.02334	3.223973
WT MG 9	CD11B	10.04485	3.5229
WT MG 9	CD235a	12.42819	1.716921
WT MG 9	BRAC	13.50984	4.172954
WT MG 9	MERTK	21.97904	999
WT MG 9	RUNX1	18.11055	-1.09837
WT MG 9	NESTIN	12.49271	2.834369
WT MG 9	MAP2	17.36957	-0.66704
WT MG 9	NFKB	9.334975	2.320513
WT MG 9	NLRP3	14.15123	3.200992
WT MG 9	TREM2	14.45678	1.345472
WT MG 9	IBA1	6.837093	-1.40557
WT MG 9	CD14	14.65895	2.47714
WT MG 9	VIMENTIN	3.688563	-0.2554
WT MG 9	GFAP	6.373375	-1.49629
WT MG 9	EAAT2	999	999
WT MG 9	ALDH1	13.20911	2.791548
WT MG 9	S100B	19.55689	2.337029
WT MG 9	NEUN	26.01503	1.372347
WT MG 9	CX3CR1	16.12217	6.04511
WT MG 9	BIN1	22.17586	5.611091

WT MG 9	TGFB	12.44051	0.870805
WT MG 9	TMEM119	9.433992	1.948742
WT MG 9	ABCA7	999	999
WT MG 9	PICALM	7.23982	0.956273
WT MG 9	INPP5D	12.36519	4.443908
WT MG 9	APOE	11.62269	3.986034
WT MG 9	EPHA1	5.171113	0.843028
WT MG 9	HLA-DR	21.66214	8.01402
WT MG 9	PLCG2	5.433563	1.887242
WT MG 9	CD33	16.0064	4.570957
WT MG 9	CR1	9.72561	-0.79561
WT MG 9	CD59	10.06283	1.271395
WT MG 9	MASP	11.1995	1.678377
WT MG 9	CR1	12.00215	1.480923
WT MG 9	CD46	9.776501	1.425492
WT MG 9	C1IN	12.3241	0.824494
WT MG 9	C6	999	999
WT MG 9	C3aR	8.423386	-2.67675
WT MG 9	DAF	11.91668	2.798779
WT MG 9	C2	8.398477	1.14694
WT MG 9	C3	8.849	0.561514
WT MG 9	C1S	16.94553	-3.44361
WT MG 9	C1QA1	6.936782	0.983153
WT MG 9	FH	17.47724	0.5301
WT MG 9	CR4	9.295126	-2.50937
WT MG 9	FB	999	999
WT MG 9	C9	9.244949	1.436853
WT MG 9	C5aR	9.192234	1.733909
WT MG 9	P2RY12	16.22644	4.768819
WT MG 9	C4	14.39956	1.856139
WT MG 9	FI	17.31014	7.000308
WT MG 9	CSMD1	10.67669	-3.28278
WT MG 9	C5	13.76351	0.357459
WT MG 9	C1QB	11.4267	1.13779
WT MG 9	CD68	5.138754	1.983517
WT MG 9	NOS	8.000468	-11.4676
WT MG 9	IL1B	999	999
WT MG 9	NOS	999	999
WT MG 9	IL6	9.884573	-1.31026
WT MG 9	TNFA	9.092183	-5.67822
WT MG 2	BMP4	10.10579	0.285258
WT MG 2	CD34	14.59329	2.515385
WT MG 2	SOX2	20.71333	5.481841
WT MG 2	FLK1	10.17032	-1.94053
WT MG 2	CD45	18.93244	2.133079

WT MG 2	CD11B	8.300934	1.778981
WT MG 2	CD235a	11.07158	0.360307
WT MG 2	BRAC	11.97996	2.643082
WT MG 2	MERTK	21.49273	999
WT MG 2	RUNX1	15.52079	-3.68813
WT MG 2	NESTIN	11.16554	1.507202
WT MG 2	MAP2	16.557	-1.47961
WT MG 2	NFKB	7.680979	0.666517
WT MG 2	NLRP3	11.73135	0.781113
WT MG 2	TREM2	11.37096	-1.74035
WT MG 2	IBA1	5.196422	-3.04624
WT MG 2	CD14	13.07193	0.890117
WT MG 2	VIMENTIN	2.5	-1.44397
WT MG 2	GFAP	5.121305	-2.74836
WT MG 2	EAAT2	999	999
WT MG 2	ALDH1	11.61332	1.195753
WT MG 2	S100B	20.2185	2.998643
WT MG 2	NEUN	27.20842	2.565742
WT MG 2	CX3CR1	15.85064	5.773578
WT MG 2	BIN1	22.5967	6.031929
WT MG 2	TGFB	13.18248	1.612774
WT MG 2	TMEM119	7.326375	-0.15888
WT MG 2	ABCA7	999	999
WT MG 2	PICALM	6.335954	0.052407
WT MG 2	INPP5D	10.7645	2.84322
WT MG 2	APOE	9.748046	2.111387
WT MG 2	EPHA1	3.331292	-0.99679
WT MG 2	HLA-DR	17.01054	3.362414
WT MG 2	PLCG2	4.205134	0.658812
WT MG 2	CD33	14.93348	3.498031
WT MG 2	CR1	8.581611	-1.93961
WT MG 2	CD59	9.681434	0.890001
WT MG 2	MASP	10.3278	0.806683
WT MG 2	CR1	11.37196	0.850734
WT MG 2	CD46	8.809003	0.457994
WT MG 2	C1IN	10.64777	-0.85184
WT MG 2	C6	999	999
WT MG 2	C3aR	6.331083	-4.76905
WT MG 2	DAF	9.795059	0.677159
WT MG 2	C2	6.694885	-0.55665
WT MG 2	C3	7.651046	-0.63644
WT MG 2	C1S	15.38506	-5.00408
WT MG 2	C1QA1	5.497547	-0.45608
WT MG 2	FH	17.14458	0.197449
WT MG 2	CR4	9.917839	-1.88666
WT MG 2	FB	999	999

WT MG 2	C9	8.611412	0.803316
WT MG 2	C5aR	7.342025	-0.1163
WT MG 2	P2RY12	14.37306	2.915439
WT MG 2	C4	14.97352	2.430102
WT MG 2	FI	14.47328	4.163451
WT MG 2	CSMD1	11.23455	-2.72492
WT MG 2	C5	11.72208	-1.68396
WT MG 2	C1QB	9.297138	-0.99177
WT MG 2	CD68	3.777499	0.622262
WT MG 2	NOS	5.464132	-14.004
WT MG 2	IL1B	999	999
WT MG 2	NOS	999	999
WT MG 2	IL6	6.315075	-4.87976
WT MG 2	TNFA	6.908696	-7.86171
WT MG 4	BMP4	16.10277	6.282231
WT MG 4	CD34	18.66203	6.584131
WT MG 4	SOX2	999	999
WT MG 4	FLK1	999	999
WT MG 4	CD45	999	999
WT MG 4	CD11B	23.01212	16.49016
WT MG 4	CD235a	999	999
WT MG 4	BRAC	999	999
WT MG 4	MERTK	999	999
WT MG 4	RUNX1	999	999
WT MG 4	NESTIN	19.65329	9.99495
WT MG 4	MAP2	999	999
WT MG 4	NFKB	29.38116	22.36669
WT MG 4	NLRP3	999	999
WT MG 4	TREM2	999	999
WT MG 4	IBA1	999	999
WT MG 4	CD14	999	999
WT MG 4	VIMENTIN	20.74774	16.80377
WT MG 4	GFAP	999	999
WT MG 4	EAAT2	999	999
WT MG 4	ALDH1	15.03165	4.614083
WT MG 4	S100B	999	999
WT MG 4	NEUN	999	999
WT MG 4	CX3CR1	18.02214	7.94508
WT MG 4	BIN1	999	999
WT MG 4	TGFB	17.52688	5.957177
WT MG 4	TMEM119	24.87743	17.39218
WT MG 4	ABCA7	999	999
WT MG 4	PICALM	999	999
WT MG 4	INPP5D	999	999
WT MG 4	APOE	19.10995	11.47329

WT MG 4	EPHA1	23.70597	19.37789
WT MG 4	HLA-DR	999	999
WT MG 4	PLCG2	24.8586	21.31227
WT MG 4	CD33	999	999
WT MG 4	CR1	999	999
WT MG 4	CD59	999	999
WT MG 4	MASP	999	999
WT MG 4	CR1	999	999
WT MG 4	CD46	999	999
WT MG 4	C1IN	999	999
WT MG 4	C6	999	999
WT MG 4	C3aR	999	999
WT MG 4	DAF	999	999
WT MG 4	C2	999	999
WT MG 4	C3	999	999
WT MG 4	C1S	999	999
WT MG 4	C1QA1	999	999
WT MG 4	FH	999	999
WT MG 4	CR4	999	999
WT MG 4	FB	999	999
WT MG 4	C9	999	999
WT MG 4	C5aR	999	999
WT MG 4	P2RY12	999	999
WT MG 4	C4	999	999
WT MG 4	FI	16.24354	5.933713
WT MG 4	CSMD1	999	999
WT MG 4	C5	999	999
WT MG 4	C1QB	23.17575	12.88684
WT MG 4	CD68	23.13305	19.97782
WT MG 4	NOS	28.90259	9.434504
WT MG 4	IL1B	999	999
WT MG 4	NOS	999	999
WT MG 4	IL6	999	999
WT MG 4	TNFA	999	999
WT MG LPS 6	Oct-04	17.91744	7.789853
WT MG LPS 6	BMP4	16.31798	6.49745
WT MG LPS 6	CD34	25.82633	13.74843
WT MG LPS 6	SOX2	999	999
WT MG LPS 6	FLK1	16.68384	4.57299
WT MG LPS 6	CD45	999	999
WT MG LPS 6	CD11B	11.17612	4.654172
WT MG LPS 6	CD235a	14.54262	3.83135
WT MG LPS 6	BRAC	15.88817	6.551286
WT MG LPS 6	MERTK	999	999
WT MG LPS 6	RUNX1	18.12867	-1.08025

WT MG LPS 6	NESTIN	18.17732	8.518984
WT MG LPS 6	MAP2	23.93696	5.900351
WT MG LPS 6	NFKB	11.83744	4.822974
WT MG LPS 6	NLRP3	18.82626	7.876018
WT MG LPS 6	TREM2	16.88326	3.771952
WT MG LPS 6	IBA1	11.00038	2.757721
WT MG LPS 6	CD14	17.43054	5.248734
WT MG LPS 6	VIMENTIN	6.689415	2.745448
WT MG LPS 6	GFAP	13.85701	5.987348
WT MG LPS 6	EAAT2	999	999
WT MG LPS 6	ALDH1	15.80639	5.388827
WT MG LPS 6	S100B	22.1969	4.977042
WT MG LPS 6	NEUN	999	999
WT MG LPS 6	CX3CR1	999	999
WT MG LPS 6	BIN1	999	999
WT MG LPS 6	TGFB	17.15203	5.58232
WT MG LPS 6	TMEM119	10.12079	2.63554
WT MG LPS 6	ABCA7	999	999
WT MG LPS 6	PICALM	12.36376	6.080213
WT MG LPS 6	INPP5D	16.5256	8.604319
WT MG LPS 6	APOE	14.98518	7.348526
WT MG LPS 6	EPHA1	8.127482	3.799398
WT MG LPS 6	HLA-DR	999	999
WT MG LPS 6	PLCG2	8.418796	4.872474
WT MG LPS 6	CD33	19.68301	8.247564
WT MG LPS 6	CR1	15.82703	5.305805
WT MG LPS 6	CD59	15.51179	6.720361
WT MG LPS 6	MASP	18.28689	8.765765
WT MG LPS 6	CR1	15.37403	4.852805
WT MG LPS 6	CD46	15.86829	7.517284
WT MG LPS 6	C1IN	16.93058	5.430974
WT MG LPS 6	C6	999	999
WT MG LPS 6	C3aR	12.97984	1.879707
WT MG LPS 6	DAF	15.93	6.8121
WT MG LPS 6	C2	12.62944	5.377904
WT MG LPS 6	C3	21.13009	12.8426
WT MG LPS 6	C1S	23.64069	3.251545
WT MG LPS 6	C1QA1	10.81334	4.859707
WT MG LPS 6	FH	999	999
WT MG LPS 6	CR4	11.89324	0.088745
WT MG LPS 6	FB	999	999
WT MG LPS 6	C9	13.42697	5.618875
WT MG LPS 6	C5aR	17.25827	9.799942
WT MG LPS 6	P2RY12	999	999
WT MG LPS 6	C4	18.5602	6.016782
WT MG LPS 6	FI	999	999

WT MG LPS 6	CSMD1	17.94004	3.980568
WT MG LPS 6	C5	17.26684	3.860796
WT MG LPS 6	C1QB	13.73127	3.442357
WT MG LPS 6	CD68	7.674898	4.519661
WT MG LPS 6	NOS	11.85917	-7.60892
WT MG LPS 6	IL1B	999	999
WT MG LPS 6	NOS	999	999
WT MG LPS 6	IL6	12.25374	1.058903
WT MG LPS 6	TNFA	12.19916	-2.57124
WT MG LPS 3	LIN28	12.88776	2.909108
WT MG LPS 3	Oct-04	12.42498	2.297391
WT MG LPS 3	BMP4	12.69901	2.87848
WT MG LPS 3	CD34	15.00663	2.928725
WT MG LPS 3	SOX2	23.55125	8.319755
WT MG LPS 3	FLK1	10.23328	-1.87757
WT MG LPS 3	CD45	18.69242	1.893061
WT MG LPS 3	CD11B	8.726139	2.204186
WT MG LPS 3	CD235a	11.89098	1.179711
WT MG LPS 3	BRAC	11.55077	2.213887
WT MG LPS 3	MERTK	22.2337	999
WT MG LPS 3	RUNX1	15.4116	-3.79731
WT MG LPS 3	NESTIN	12.83954	3.181205
WT MG LPS 3	MAP2	17.84224	-0.19438
WT MG LPS 3	NFKB	7.711659	0.697196
WT MG LPS 3	NLRP3	12.21896	1.268724
WT MG LPS 3	TREM2	11.59652	-1.51478
WT MG LPS 3	IBA1	5.986712	-2.25595
WT MG LPS 3	CD14	13.6264	1.444593
WT MG LPS 3	VIMENTIN	3.674848	-0.26912
WT MG LPS 3	GFAP	4.919602	-2.95006
WT MG LPS 3	EAAT2	999	999
WT MG LPS 3	ALDH1	12.17123	1.753664
WT MG LPS 3	S100B	20.94381	3.723952
WT MG LPS 3	NEUN	999	999
WT MG LPS 3	CX3CR1	14.12005	4.042988
WT MG LPS 3	BIN1	21.70887	5.144097
WT MG LPS 3	TGFB	13.38735	1.817642
WT MG LPS 3	TMEM119	7.317884	-0.16737
WT MG LPS 3	ABCA7	999	999
WT MG LPS 3	PICALM	6.277425	-0.00612
WT MG LPS 3	INPP5D	10.54195	2.620668
WT MG LPS 3	APOE	9.788496	2.151837
WT MG LPS 3	EPHA1	3.902621	-0.42546
WT MG LPS 3	HLA-DR	17.56999	3.921871
WT MG LPS 3	PLCG2	5.520766	1.974444

WT MG LPS 3	CD33	15.1888	3.753355
WT MG LPS 3	CR1	11.09511	0.573886
WT MG LPS 3	CD59	9.421636	0.630203
WT MG LPS 3	MASP	12.91382	3.392704
WT MG LPS 3	CR1	12.12373	1.602501
WT MG LPS 3	CD46	8.841246	0.490238
WT MG LPS 3	C1IN	12.06719	0.567583
WT MG LPS 3	C6	999	999
WT MG LPS 3	C3aR	7.441972	-3.65816
WT MG LPS 3	DAF	10.63708	1.519183
WT MG LPS 3	C2	7.269646	0.018109
WT MG LPS 3	C3	9.034392	0.746906
WT MG LPS 3	C1S	15.62305	-4.76609
WT MG LPS 3	C1QA1	6.261975	0.308346
WT MG LPS 3	FH	17.84687	0.899736
WT MG LPS 3	CR4	9.721753	-2.08274
WT MG LPS 3	FB	999	999
WT MG LPS 3	C9	9.02516	1.217064
WT MG LPS 3	C5aR	8.269893	0.811568
WT MG LPS 3	P2RY12	15.61526	4.157638
WT MG LPS 3	C4	15.38138	2.837959
WT MG LPS 3	FI	13.56914	3.259309
WT MG LPS 3	CSMD1	13.11842	-0.84105
WT MG LPS 3	C5	13.57065	0.164601
WT MG LPS 3	C1QB	10.02018	-0.26873
WT MG LPS 3	CD68	4.162162	1.006926
WT MG LPS 3	NOS	6.724368	-12.7437
WT MG LPS 3	IL1B	999	999
WT MG LPS 3	NOS	999	999
WT MG LPS 3	IL6	7.24469	-3.95015
WT MG LPS 3	TNFA	7.725292	-7.04511
WT MG LPS 5	LIN28	999	999
WT MG LPS 5	Oct-04	20.09193	9.964342
WT MG LPS 5	BMP4	19.52996	9.709422
WT MG LPS 5	CD34	23.74608	11.66818
WT MG LPS 5	SOX2	23.16046	7.928969
WT MG LPS 5	FLK1	15.741	3.630152
WT MG LPS 5	CD45	999	999
WT MG LPS 5	CD11B	13.70163	7.179674
WT MG LPS 5	CD235a	17.42806	6.71679
WT MG LPS 5	BRAC	999	999
WT MG LPS 5	MERTK	18.47296	999
WT MG LPS 5	RUNX1	999	999
WT MG LPS 5	NESTIN	17.36019	7.701852
WT MG LPS 5	MAP2	21.24141	3.204796

WT MG LPS 5	NFKB	15.12451	8.110044
WT MG LPS 5	NLRP3	22.06283	11.11259
WT MG LPS 5	TREM2	999	999
WT MG LPS 5	IBA1	13.86448	5.621817
WT MG LPS 5	CD14	21.25845	9.076643
WT MG LPS 5	VIMENTIN	10.55459	6.610624
WT MG LPS 5	GFAP	15.76438	7.894718
WT MG LPS 5	EAAT2	999	999
WT MG LPS 5	ALDH1	20.04312	9.625557
WT MG LPS 5	S100B	22.82922	5.609366
WT MG LPS 5	NEUN	21.10726	-3.53541
WT MG LPS 5	CX3CR1	22.4273	12.35024
WT MG LPS 5	BIN1	999	999
WT MG LPS 5	TGFB	16.94563	5.375921
WT MG LPS 5	TMEM119	13.65749	6.172236
WT MG LPS 5	ABCA7	999	999
WT MG LPS 5	PICALM	15.94752	9.66397
WT MG LPS 5	INPP5D	20.02455	12.10326
WT MG LPS 5	APOE	20.57936	12.94271
WT MG LPS 5	EPHA1	11.15244	6.824357
WT MG LPS 5	HLA-DR	23.1358	9.487674
WT MG LPS 5	PLCG2	12.06345	8.517132
WT MG LPS 5	CD33	24.49239	13.05694
WT MG LPS 5	CR1	19.09391	8.572683
WT MG LPS 5	CD59	18.53849	9.747056
WT MG LPS 5	MASP	21.50902	11.9879
WT MG LPS 5	CR1	18.82262	8.301391
WT MG LPS 5	CD46	18.11125	9.760243
WT MG LPS 5	C1IN	20.10097	8.601363
WT MG LPS 5	C6	999	999
WT MG LPS 5	C3aR	19.61985	8.519719
WT MG LPS 5	DAF	20.64263	11.52473
WT MG LPS 5	C2	16.40972	9.158179
WT MG LPS 5	C3	24.83042	16.54293
WT MG LPS 5	C1S	999	999
WT MG LPS 5	C1QA1	13.19332	7.239694
WT MG LPS 5	FH	999	999
WT MG LPS 5	CR4	16.96902	5.164525
WT MG LPS 5	FB	999	999
WT MG LPS 5	C9	15.88999	8.081891
WT MG LPS 5	C5aR	20.41659	12.95827
WT MG LPS 5	P2RY12	999	999
WT MG LPS 5	C4	23.2319	10.68848
WT MG LPS 5	FI	999	999
WT MG LPS 5	CSMD1	20.05773	6.09826
WT MG LPS 5	C5	22.71461	9.308557

WT MG LPS 5	C1QB	16.01719	5.728283
WT MG LPS 5	CD68	10.96174	7.806499
WT MG LPS 5	NOS	16.34507	-3.12301
WT MG LPS 5	IL1B	999	999
WT MG LPS 5	NOS	999	999
WT MG LPS 5	IL6	18.73819	7.543355
WT MG LPS 5	TNFA	15.8171	1.046696
WT MG LPS 13	LIN28	9.579602	-0.39905
WT MG LPS 13	Oct-04	9.454941	-0.67265
WT MG LPS 13	BMP4	9.532276	-0.28826
WT MG LPS 13	CD34	9.447798	-2.63011
WT MG LPS 13	SOX2	9.544237	-5.68726
WT MG LPS 13	FLK1	9.454212	-2.65664
WT MG LPS 13	CD45	9.532625	-7.26674
WT MG LPS 13	CD11B	9.523294	3.001341
WT MG LPS 13	CD235a	9.465727	-1.24555
WT MG LPS 13	BRAC	9.740424	0.403543
WT MG LPS 13	MERTK	9.373779	999
WT MG LPS 13	RUNX1	9.488297	-9.72062
WT MG LPS 13	NESTIN	9.60366	-0.05468
WT MG LPS 13	MAP2	9.624395	-8.41222
WT MG LPS 13	NFKB	9.554675	2.540212
WT MG LPS 13	NLRP3	9.398344	-1.5519
WT MG LPS 13	TREM2	9.456169	-3.65514
WT MG LPS 13	IBA1	9.67233	1.429669
WT MG LPS 13	CD14	9.573905	-2.6079
WT MG LPS 13	VIMENTIN	9.283557	5.33959
WT MG LPS 13	GFAP	9.418049	1.548389
WT MG LPS 13	EAAT2	9.69639	999
WT MG LPS 13	ALDH1	9.550328	-0.86723
WT MG LPS 13	S100B	9.61816	-7.6017
WT MG LPS 13	NEUN	9.444819	-15.1979
WT MG LPS 13	CX3CR1	9.526837	-0.55022
WT MG LPS 13	BIN1	9.460504	-7.10426
WT MG LPS 13	TGFB	9.491867	-2.07784
WT MG LPS 13	TMEM119	9.493641	2.008391
WT MG LPS 13	ABCA7	9.436059	-15.6958
WT MG LPS 13	PICALM	9.141431	2.857884
WT MG LPS 13	INPP5D	9.440722	1.519438
WT MG LPS 13	APOE	9.549447	1.912788
WT MG LPS 13	EPHA1	9.036354	4.708269
WT MG LPS 13	HLA-DR	9.466493	-4.18163
WT MG LPS 13	PLCG2	9.390071	5.843749
WT MG LPS 13	CD33	9.498705	-1.93674
WT MG LPS 13	CR1	9.350508	-1.17072

WT MG LPS 13	CD59	9.245714	0.454281
WT MG LPS 13	MASP	9.275995	-0.24513
WT MG LPS 13	CR1	9.393318	-1.12791
WT MG LPS 13	CD46	9.330867	0.979859
WT MG LPS 13	C1IN	9.368378	-2.13123
WT MG LPS 13	C6	9.420577	-9.17266
WT MG LPS 13	C3aR	9.304985	-1.79515
WT MG LPS 13	DAF	9.348295	0.230396
WT MG LPS 13	C2	9.266719	2.015182
WT MG LPS 13	C3	9.424956	1.137471
WT MG LPS 13	C1S	9.410181	-10.979
WT MG LPS 13	C1QA1	9.308561	3.354932
WT MG LPS 13	FH	9.454247	-7.49289
WT MG LPS 13	CR4	9.257355	-2.54714
WT MG LPS 13	FB	9.403585	999
WT MG LPS 13	C9	9.238784	1.430688
WT MG LPS 13	C5aR	9.34667	1.888345
WT MG LPS 13	P2RY12	9.235423	-2.2222
WT MG LPS 13	C4	9.437419	-3.106
WT MG LPS 13	FI	9.478187	-0.83164
WT MG LPS 13	CSMD1	9.311066	-4.6484
WT MG LPS 13	C5	9.269151	-4.1369
WT MG LPS 13	C1QB	9.35168	-0.93723
WT MG LPS 13	CD68	8.814958	5.659721
WT MG LPS 13	NOS	9.228626	-10.2395
WT MG LPS 13	IL1B	9.320861	999
WT MG LPS 13	NOS	9.280783	-10.1873
WT MG LPS 13	IL6	9.31419	-1.88065
WT MG LPS 13	TNFA	9.264592	-5.50581
WT MG LPS 14	LIN28	19.29304	9.314381
WT MG LPS 14	Oct-04	999	999
WT MG LPS 14	BMP4	999	999
WT MG LPS 14	CD34	999	999
WT MG LPS 14	SOX2	29.31447	14.08298
WT MG LPS 14	FLK1	999	999
WT MG LPS 14	CD45	999	999
WT MG LPS 14	CD11B	14.35404	7.832085
WT MG LPS 14	CD235a	999	999
WT MG LPS 14	BRAC	999	999
WT MG LPS 14	MERTK	20.9989	999
WT MG LPS 14	RUNX1	999	999
WT MG LPS 14	NESTIN	19.81115	10.15281
WT MG LPS 14	MAP2	999	999
WT MG LPS 14	NFKB	14.49891	7.484451
WT MG LPS 14	NLRP3	25.98758	15.03734

WT MG LPS 14	TREM2	999	999
WT MG LPS 14	IBA1	999	999
WT MG LPS 14	CD14	21.55176	9.369953
WT MG LPS 14	VIMENTIN	17.22384	13.27988
WT MG LPS 14	GFAP	20.17994	12.31028
WT MG LPS 14	EAAT2	999	999
WT MG LPS 14	ALDH1	999	999
WT MG LPS 14	S100B	29.7574	12.53754
WT MG LPS 14	NEUN	23.6411	-1.00158
WT MG LPS 14	CX3CR1	27.20856	17.13151
WT MG LPS 14	BIN1	999	999
WT MG LPS 14	TGFB	999	999
WT MG LPS 14	TMEM119	16.58786	9.102614
WT MG LPS 14	ABCA7	999	999
WT MG LPS 14	PICALM	19.97118	13.68764
WT MG LPS 14	INPP5D	999	999
WT MG LPS 14	APOE	999	999
WT MG LPS 14	EPHA1	19.02054	14.69246
WT MG LPS 14	HLA-DR	24.73828	11.09016
WT MG LPS 14	PLCG2	12.5261	8.979774
WT MG LPS 14	CD33	999	999
WT MG LPS 14	CR1	21.151	10.62977
WT MG LPS 14	CD59	23.9045	15.11306
WT MG LPS 14	MASP	25.22968	15.70855
WT MG LPS 14	CR1	999	999
WT MG LPS 14	CD46	22.14647	13.79546
WT MG LPS 14	C1IN	999	999
WT MG LPS 14	C6	999	999
WT MG LPS 14	C3aR	20.1117	9.011571
WT MG LPS 14	DAF	20.98531	11.86741
WT MG LPS 14	C2	999	999
WT MG LPS 14	C3	999	999
WT MG LPS 14	C1S	999	999
WT MG LPS 14	C1QA1	13.82923	7.875597
WT MG LPS 14	FH	999	999
WT MG LPS 14	CR4	19.73052	7.926025
WT MG LPS 14	FB	999	999
WT MG LPS 14	C9	23.60431	15.79622
WT MG LPS 14	C5aR	23.4695	16.01118
WT MG LPS 14	P2RY12	999	999
WT MG LPS 14	C4	24.91101	12.36759
WT MG LPS 14	FI	999	999
WT MG LPS 14	CSMD1	999	999
WT MG LPS 14	C5	24.1495	10.74345
WT MG LPS 14	C1QB	14.53352	4.244611
WT MG LPS 14	CD68	14.04078	10.88555

WT MG LPS 14	NOS	24.81052	5.342433
WT MG LPS 14	IL1B	999	999
WT MG LPS 14	NOS	999	999
WT MG LPS 14	IL6	18.37738	7.182541
WT MG LPS 14	TNFA	24.52738	9.756981
WT MG LPS 11	LIN28	999	999
WT MG LPS 11	Oct-04	20.21506	10.08747
WT MG LPS 11	BMP4	999	999
WT MG LPS 11	CD34	999	999
WT MG LPS 11	SOX2	26.16736	10.93587
WT MG LPS 11	FLK1	999	999
WT MG LPS 11	CD45	999	999
WT MG LPS 11	CD11B	999	999
WT MG LPS 11	CD235a	24.22153	13.51026
WT MG LPS 11	BRAC	999	999
WT MG LPS 11	MERTK	21.57461	999
WT MG LPS 11	RUNX1	999	999
WT MG LPS 11	NESTIN	20.15332	10.49498
WT MG LPS 11	MAP2	999	999
WT MG LPS 11	NFKB	999	999
WT MG LPS 11	NLRP3	999	999
WT MG LPS 11	TREM2	999	999
WT MG LPS 11	IBA1	25.36002	17.11736
WT MG LPS 11	CD14	999	999
WT MG LPS 11	VIMENTIN	21.08491	17.14094
WT MG LPS 11	GFAP	20.21677	12.34711
WT MG LPS 11	EAAT2	999	999
WT MG LPS 11	ALDH1	999	999
WT MG LPS 11	S100B	999	999
WT MG LPS 11	NEUN	999	999
WT MG LPS 11	CX3CR1	26.54476	16.4677
WT MG LPS 11	BIN1	999	999
WT MG LPS 11	TGFB	999	999
WT MG LPS 11	TMEM119	24.92456	17.43931
WT MG LPS 11	ABCA7	999	999
WT MG LPS 11	PICALM	999	999
WT MG LPS 11	INPP5D	999	999
WT MG LPS 11	APOE	999	999
WT MG LPS 11	EPHA1	999	999
WT MG LPS 11	HLA-DR	999	999
WT MG LPS 11	PLCG2	999	999
WT MG LPS 11	CD33	999	999
WT MG LPS 11	CR1	999	999
WT MG LPS 11	CD59	999	999
WT MG LPS 11	MASP	999	999

WT MG LPS 11	CR1	999	999
WT MG LPS 11	CD46	999	999
WT MG LPS 11	C1IN	999	999
WT MG LPS 11	C6	999	999
WT MG LPS 11	C3aR	999	999
WT MG LPS 11	DAF	999	999
WT MG LPS 11	C2	999	999
WT MG LPS 11	C3	999	999
WT MG LPS 11	C1S	999	999
WT MG LPS 11	C1QA1	999	999
WT MG LPS 11	FH	999	999
WT MG LPS 11	CR4	22.52983	10.72533
WT MG LPS 11	FB	999	999
WT MG LPS 11	C9	26.59951	18.79142
WT MG LPS 11	C5aR	999	999
WT MG LPS 11	P2RY12	999	999
WT MG LPS 11	C4	999	999
WT MG LPS 11	FI	999	999
WT MG LPS 11	CSMD1	23.81777	9.858298
WT MG LPS 11	C5	22.06848	8.662427
WT MG LPS 11	C1QB	21.37646	11.08755
WT MG LPS 11	CD68	999	999
WT MG LPS 11	NOS	999	999
WT MG LPS 11	IL1B	999	999
WT MG LPS 11	NOS	999	999
WT MG LPS 11	IL6	999	999
WT MG LPS 11	TNFA	999	999
WT MG LPS 15	LIN28	14.93695	4.9583
WT MG LPS 15	Oct-04	13.33412	3.206532
WT MG LPS 15	BMP4	15.15026	5.329728
WT MG LPS 15	CD34	17.11007	5.032167
WT MG LPS 15	SOX2	18.08251	2.851012
WT MG LPS 15	FLK1	9.16552	-2.94533
WT MG LPS 15	CD45	20.72005	3.920689
WT MG LPS 15	CD11B	10.0113	3.489348
WT MG LPS 15	CD235a	12.22529	1.51402
WT MG LPS 15	BRAC	13.32151	3.984631
WT MG LPS 15	MERTK	25.75896	999
WT MG LPS 15	RUNX1	17.45176	-1.75715
WT MG LPS 15	NESTIN	11.88323	2.224891
WT MG LPS 15	MAP2	16.93857	-1.09804
WT MG LPS 15	NFKB	9.600155	2.585693
WT MG LPS 15	NLRP3	13.86585	2.915612
WT MG LPS 15	TREM2	14.90743	1.796124
WT MG LPS 15	IBA1	6.822711	-1.41995

WT MG LPS 15	CD14	14.962	2.780188
WT MG LPS 15	VIMENTIN	3.744775	-0.19919
WT MG LPS 15	GFAP	6.70154	-1.16812
WT MG LPS 15	EAAT2	999	999
WT MG LPS 15	ALDH1	13.2577	2.840133
WT MG LPS 15	S100B	19.28947	2.069617
WT MG LPS 15	NEUN	23.08229	-1.56039
WT MG LPS 15	CX3CR1	16.56404	6.486981
WT MG LPS 15	BIN1	21.3357	4.770932
WT MG LPS 15	TGFB	11.97114	0.401439
WT MG LPS 15	TMEM119	9.285104	1.799854
WT MG LPS 15	ABCA7	24.98101	-0.15081
WT MG LPS 15	PICALM	7.353392	1.069845
WT MG LPS 15	INPP5D	12.31709	4.395807
WT MG LPS 15	APOE	11.53923	3.902572
WT MG LPS 15	EPHA1	5.018619	0.690534
WT MG LPS 15	HLA-DR	20.74915	7.101032
WT MG LPS 15	PLCG2	4.950798	1.404476
WT MG LPS 15	CD33	16.33725	4.9018
WT MG LPS 15	CR1	10.16628	-0.35494
WT MG LPS 15	CD59	9.985793	1.19436
WT MG LPS 15	MASP	11.85594	2.334822
WT MG LPS 15	CR1	12.11079	1.589569
WT MG LPS 15	CD46	9.964815	1.613806
WT MG LPS 15	C1IN	12.75373	1.254123
WT MG LPS 15	C6	999	999
WT MG LPS 15	C3aR	8.711049	-2.38909
WT MG LPS 15	DAF	11.78559	2.667686
WT MG LPS 15	C2	8.338182	1.086645
WT MG LPS 15	C3	9.254545	0.96706
WT MG LPS 15	C1S	17.54887	-2.84027
WT MG LPS 15	C1QA1	6.908271	0.954642
WT MG LPS 15	FH	18.05266	1.105527
WT MG LPS 15	CR4	10.79303	-1.01146
WT MG LPS 15	FB	999	999
WT MG LPS 15	C9	9.26459	1.456494
WT MG LPS 15	C5aR	8.552751	1.094426
WT MG LPS 15	P2RY12	15.62952	4.171901
WT MG LPS 15	C4	14.2003	1.656882
WT MG LPS 15	FI	16.64197	6.332146
WT MG LPS 15	CSMD1	12.53713	-1.42234
WT MG LPS 15	C5	13.8289	0.422849
WT MG LPS 15	C1QB	11.35612	1.067207
WT MG LPS 15	CD68	5.047975	1.892738
WT MG LPS 15	NOS	8.238814	-11.2293
WT MG LPS 15	IL1B	999	999

WT MG LPS 15	NOS	999	999
WT MG LPS 15	IL6	10.38061	-0.81422
WT MG LPS 15	TNFA	9.119166	-5.65124
WT MG LPS 12	LIN28	10.83852	0.859866
WT MG LPS 12	Oct-04	11.27399	1.146398
WT MG LPS 12	BMP4	9.219678	-0.60086
WT MG LPS 12	CD34	12.96008	0.88218
WT MG LPS 12	SOX2	15.07105	-0.16044
WT MG LPS 12	FLK1	10.69827	-1.41258
WT MG LPS 12	CD45	19.60497	2.805612
WT MG LPS 12	CD11B	8.778613	2.256661
WT MG LPS 12	CD235a	13.43238	2.721102
WT MG LPS 12	BRAC	11.39429	2.057412
WT MG LPS 12	MERTK	26.30332	999
WT MG LPS 12	RUNX1	19.33531	0.126396
WT MG LPS 12	NESTIN	10.86842	1.210078
WT MG LPS 12	MAP2	19.0071	0.970483
WT MG LPS 12	NFKB	9.026516	2.012053
WT MG LPS 12	NLRP3	13.25107	2.300834
WT MG LPS 12	TREM2	15.62932	2.518014
WT MG LPS 12	IBA1	9.894369	1.651708
WT MG LPS 12	CD14	13.93552	1.753713
WT MG LPS 12	VIMENTIN	4.992127	1.04816
WT MG LPS 12	GFAP	10.5784	2.708739
WT MG LPS 12	EAAT2	20.63723	999
WT MG LPS 12	ALDH1	11.4429	1.025337
WT MG LPS 12	S100B	20.275	3.055144
WT MG LPS 12	NEUN	22.49913	-2.14355
WT MG LPS 12	CX3CR1	11.75429	1.677233
WT MG LPS 12	BIN1	18.11918	1.554415
WT MG LPS 12	TGFB	12.19716	0.627458
WT MG LPS 12	TMEM119	8.975905	1.490655
WT MG LPS 12	ABCA7	24.08578	-1.04604
WT MG LPS 12	PICALM	8.021687	1.73814
WT MG LPS 12	INPP5D	9.921858	2.000574
WT MG LPS 12	APOE	9.793805	2.157146
WT MG LPS 12	EPHA1	5.802473	1.474389
WT MG LPS 12	HLA-DR	14.75497	1.106845
WT MG LPS 12	PLCG2	5.457112	1.91079
WT MG LPS 12	CD33	13.66365	2.228205
WT MG LPS 12	CR1	8.49753	-2.02369
WT MG LPS 12	CD59	10.66165	1.870218
WT MG LPS 12	MASP	10.26904	0.747918
WT MG LPS 12	CR1	12.25976	1.738531
WT MG LPS 12	CD46	10.0689	1.717894

WT MG LPS 12	C1IN	12.25364	0.75403
WT MG LPS 12	C6	18.31817	-0.27506
WT MG LPS 12	C3aR	11.62579	0.525657
WT MG LPS 12	DAF	10.58558	1.467686
WT MG LPS 12	C2	9.043051	1.791514
WT MG LPS 12	C3	10.33397	2.046484
WT MG LPS 12	C1S	19.9191	-0.47004
WT MG LPS 12	C1QA1	7.531064	1.577435
WT MG LPS 12	FH	17.36248	0.415345
WT MG LPS 12	CR4	12.87154	1.067042
WT MG LPS 12	FB	999	999
WT MG LPS 12	C9	9.861003	2.052907
WT MG LPS 12	C5aR	9.183796	1.725471
WT MG LPS 12	P2RY12	13.15457	1.696944
WT MG LPS 12	C4	13.98881	1.445383
WT MG LPS 12	FI	11.75086	1.441034
WT MG LPS 12	CSMD1	13.30089	-0.65858
WT MG LPS 12	C5	12.29713	-1.10892
WT MG LPS 12	C1QB	11.3494	1.060491
WT MG LPS 12	CD68	4.379593	1.224356
WT MG LPS 12	NOS	20.79491	1.326821
WT MG LPS 12	IL1B	999	999
WT MG LPS 12	NOS	999	999
WT MG LPS 12	IL6	13.63056	2.435729
WT MG LPS 12	TNFA	16.94361	2.173205
WT MG LPS 8	CD34	19.38074	7.302841
WT MG LPS 8	SOX2	999	999
WT MG LPS 8	FLK1	15.96328	3.852432
WT MG LPS 8	CD45	24.43319	7.633824
WT MG LPS 8	CD11B	10.5965	4.074544
WT MG LPS 8	CD235a	14.98481	4.273537
WT MG LPS 8	BRAC	11.69029	2.353413
WT MG LPS 8	MERTK	21.61922	999
WT MG LPS 8	RUNX1	999	999
WT MG LPS 8	NESTIN	16.22967	6.571326
WT MG LPS 8	MAP2	999	999
WT MG LPS 8	NFKB	10.32435	3.309884
WT MG LPS 8	NLRP3	17.01026	6.06002
WT MG LPS 8	TREM2	15.59528	2.483977
WT MG LPS 8	IBA1	11.37382	3.13116
WT MG LPS 8	CD14	14.76614	2.584332
WT MG LPS 8	VIMENTIN	7.40673	3.462763
WT MG LPS 8	GFAP	9.745927	1.876267
WT MG LPS 8	EAAT2	999	999
WT MG LPS 8	ALDH1	16.1858	5.768236

WT MG LPS 8	S100B	28.99253	11.77267
WT MG LPS 8	NEUN	999	999
WT MG LPS 8	CX3CR1	18.70646	8.629399
WT MG LPS 8	BIN1	24.06397	7.4992
WT MG LPS 8	TGFB	16.12685	4.557143
WT MG LPS 8	TMEM119	10.74623	3.260977
WT MG LPS 8	ABCA7	999	999
WT MG LPS 8	PICALM	10.90247	4.618922
WT MG LPS 8	INPP5D	11.94355	4.022266
WT MG LPS 8	APOE	12.13572	4.499065
WT MG LPS 8	EPHA1	8.554129	4.226045
WT MG LPS 8	HLA-DR	999	999
WT MG LPS 8	PLCG2	6.201492	2.65517
WT MG LPS 8	CD33	17.09278	5.657328
WT MG LPS 8	CR1	12.52307	2.001841
WT MG LPS 8	CD59	13.51343	4.721993
WT MG LPS 8	MASP	14.61541	5.094285
WT MG LPS 8	CR1	15.7145	5.193272
WT MG LPS 8	CD46	13.4713	5.120291
WT MG LPS 8	C1IN	12.70314	1.203528
WT MG LPS 8	C6	999	999
WT MG LPS 8	C3aR	11.57414	0.474006
WT MG LPS 8	DAF	14.91326	5.795365
WT MG LPS 8	C2	12.05355	4.802009
WT MG LPS 8	C3	14.62359	6.336106
WT MG LPS 8	C1S	19.86064	-0.5285
WT MG LPS 8	C1QA1	9.175101	3.221472
WT MG LPS 8	FH	999	999
WT MG LPS 8	CR4	13.60324	1.798744
WT MG LPS 8	FB	999	999
WT MG LPS 8	C9	13.18162	5.373524
WT MG LPS 8	C5aR	13.43825	5.979924
WT MG LPS 8	P2RY12	18.78535	7.327729
WT MG LPS 8	C4	16.71547	4.17205
WT MG LPS 8	FI	999	999
WT MG LPS 8	CSMD1	999	999
WT MG LPS 8	C5	17.33717	3.931117
WT MG LPS 8	C1QB	11.08306	0.794152
WT MG LPS 8	CD68	6.203478	3.048241
WT MG LPS 8	NOS	18.64144	-0.82664
WT MG LPS 8	IL1B	999	999
WT MG LPS 8	NOS	999	999
WT MG LPS 8	IL6	14.23117	3.03633
WT MG LPS 8	TNFA	17.68448	2.914074
KO LPS 4	BMP4	11.8957	2.075169

KO LPS 4	CD34	11.87045	-0.20745
KO LPS 4	SOX2	11.8484	-3.3831
KO LPS 4	FLK1	11.7322	-0.37865
KO LPS 4	CD45	11.97292	-4.82645
KO LPS 4	CD11B	8.563567	2.041615
KO LPS 4	CD235a	11.36	0.648724
KO LPS 4	BRAC	11.18605	1.84917
KO LPS 4	MERTK	11.62509	999
KO LPS 4	RUNX1	11.85805	-7.35086
KO LPS 4	NESTIN	11.26324	1.6049
KO LPS 4	MAP2	11.74847	-6.28815
KO LPS 4	NFKB	10.24319	3.228732
KO LPS 4	NLRP3	11.56055	0.610306
KO LPS 4	TREM2	11.67379	-1.43752
KO LPS 4	IBA1	9.367843	1.125182
KO LPS 4	CD14	11.32217	-0.85964
KO LPS 4	VIMENTIN	4.339269	0.395302
KO LPS 4	GFAP	8.0912	0.22154
KO LPS 4	EAAT2	11.66179	999
KO LPS 4	ALDH1	10.00658	-0.41099
KO LPS 4	S100B	11.84711	-5.37275
KO LPS 4	NEUN	11.84738	-12.7953
KO LPS 4	CX3CR1	11.70037	1.623314
KO LPS 4	BIN1	11.89859	-4.66618
KO LPS 4	TGFB	9.990369	-1.57934
KO LPS 4	TMEM119	8.957864	1.472614
KO LPS 4	ABCA7	11.82455	-13.3073
KO LPS 4	PICALM	8.717004	2.433457
KO LPS 4	INPP5D	11.69989	3.778609
KO LPS 4	APOE	10.57777	2.941113
KO LPS 4	EPHA1	8.926714	4.598629
KO LPS 4	HLA-DR	11.75181	-1.89631
KO LPS 4	PLCG2	4.76324	1.216918
KO LPS 4	CD33	11.73811	0.302662
KO LPS 4	CR1	11.421	0.899777
KO LPS 4	CD59	10.86299	2.071553
KO LPS 4	MASP	11.66255	2.141426
KO LPS 4	CR1	11.70732	1.186099
KO LPS 4	CD46	10.80906	2.458055
KO LPS 4	C1IN	11.28731	-0.2123
KO LPS 4	C6	11.571	-7.02224
KO LPS 4	C3aR	9.347706	-1.75243
KO LPS 4	DAF	11.59643	2.478533
KO LPS 4	C2	8.752376	1.500839
KO LPS 4	C3	10.07443	1.786946
KO LPS 4	C1S	11.82892	-8.56022

KO LPS 4	C1QA1	9.322095	3.368466
KO LPS 4	FH	11.78676	-5.16037
KO LPS 4	CR4	11.05149	-0.75301
KO LPS 4	FB	11.76046	999
KO LPS 4	C9	11.2501	3.442001
KO LPS 4	C5aR	9.856598	2.398273
KO LPS 4	P2RY12	11.79106	0.333443
KO LPS 4	C4	11.65054	-0.89289
KO LPS 4	FI	11.76794	1.458113
KO LPS 4	CSMD1	11.77794	-2.18153
KO LPS 4	C5	11.60673	-1.79931
KO LPS 4	C1QB	10.93297	0.644054
KO LPS 4	CD68	5.92799	2.772753
KO LPS 4	NOS	11.3199	-8.14819
KO LPS 4	IL1B	11.76362	999
KO LPS 4	NOS	11.81917	-7.64892
KO LPS 4	IL6	10.8831	-0.31174
KO LPS 4	TNFA	10.24171	-4.52869
KO LPS 5	BMP4	15.09618	5.275651
KO LPS 5	CD34	17.15735	5.079444
KO LPS 5	SOX2	999	999
KO LPS 5	FLK1	16.31465	4.203801
KO LPS 5	CD45	22.79181	5.992444
KO LPS 5	CD11B	10.79019	4.268234
KO LPS 5	CD235a	15.81383	5.102559
KO LPS 5	BRAC	11.09183	1.754948
KO LPS 5	MERTK	999	999
KO LPS 5	RUNX1	999	999
KO LPS 5	NESTIN	13.47732	3.818978
KO LPS 5	MAP2	23.53304	5.496424
KO LPS 5	NFKB	10.91692	3.902461
KO LPS 5	NLRP3	15.6086	4.658364
KO LPS 5	TREM2	17.9309	4.819598
KO LPS 5	IBA1	11.00945	2.766789
KO LPS 5	CD14	15.03849	2.856679
KO LPS 5	VIMENTIN	6.928496	2.984529
KO LPS 5	GFAP	9.985883	2.116223
KO LPS 5	EAAT2	999	999
KO LPS 5	ALDH1	13.72529	3.307731
KO LPS 5	S100B	23.46963	6.249774
KO LPS 5	NEUN	25.61004	0.967357
KO LPS 5	CX3CR1	15.59735	5.52029
KO LPS 5	BIN1	20.66437	4.099598
KO LPS 5	TGFB	16.17806	4.608358
KO LPS 5	TMEM119	10.87775	3.392497

KO LPS 5	ABCA7	999	999
KO LPS 5	PICALM	10.0142	3.730652
KO LPS 5	INPP5D	11.32311	3.401824
KO LPS 5	APOE	11.99371	4.357052
KO LPS 5	EPHA1	7.059999	2.731915
KO LPS 5	HLA-DR	19.21281	5.56469
KO LPS 5	PLCG2	5.320151	1.773829
KO LPS 5	CD33	17.02869	5.593244
KO LPS 5	CR1	10.90685	0.38563
KO LPS 5	CD59	12.4519	3.660465
KO LPS 5	MASP	12.74578	3.224663
KO LPS 5	CR1	16.98614	6.464914
KO LPS 5	CD46	12.79302	4.442009
KO LPS 5	C1IN	14.75407	3.254465
KO LPS 5	C6	999	999
KO LPS 5	C3aR	10.69594	-0.4042
KO LPS 5	DAF	12.98306	3.865162
KO LPS 5	C2	10.72116	3.469627
KO LPS 5	C3	12.23433	3.946843
KO LPS 5	C1S	20.49138	0.102243
KO LPS 5	C1QA1	8.879256	2.925627
KO LPS 5	FH	20.54819	3.601058
KO LPS 5	CR4	14.20902	2.40452
KO LPS 5	FB	999	999
KO LPS 5	C9	14.80118	6.993082
KO LPS 5	C5aR	11.19899	3.74067
KO LPS 5	P2RY12	16.16854	4.710915
KO LPS 5	C4	16.91746	4.374038
KO LPS 5	FI	15.76252	5.452695
KO LPS 5	CSMD1	17.74129	3.781816
KO LPS 5	C5	16.20459	2.798542
KO LPS 5	C1QB	11.97919	1.690278
KO LPS 5	CD68	5.521278	2.366042
KO LPS 5	NOS	18.90572	-0.56237
KO LPS 5	IL1B	999	999
KO LPS 5	NOS	999	999
KO LPS 5	IL6	13.54495	2.350119
KO LPS 5	TNFA	17.58126	2.810858
WT MG LPS 2	Oct-04	20.50279	10.3752
WT MG LPS 2	BMP4	999	999
WT MG LPS 2	CD34	24.12249	12.04458
WT MG LPS 2	SOX2	22.05564	6.824142
WT MG LPS 2	FLK1	19.73099	7.620137
WT MG LPS 2	CD45	999	999
WT MG LPS 2	CD11B	14.9935	8.471549

WT MG LPS 2	CD235a	18.6972	7.985929
WT MG LPS 2	BRAC	21.10378	11.7669
WT MG LPS 2	MERTK	22.17067	999
WT MG LPS 2	RUNX1	999	999
WT MG LPS 2	NESTIN	18.64769	8.989353
WT MG LPS 2	MAP2	22.48996	4.453349
WT MG LPS 2	NFKB	15.9526	8.938139
WT MG LPS 2	NLRP3	22.01775	11.06751
WT MG LPS 2	TREM2	21.3284	8.217093
WT MG LPS 2	IBA1	17.93777	9.695114
WT MG LPS 2	CD14	999	999
WT MG LPS 2	VIMENTIN	12.19637	8.2524
WT MG LPS 2	GFAP	17.65609	9.786432
WT MG LPS 2	EAAT2	999	999
WT MG LPS 2	ALDH1	999	999
WT MG LPS 2	S100B	19.82043	2.600571
WT MG LPS 2	NEUN	999	999
WT MG LPS 2	CX3CR1	23.73104	13.65398
WT MG LPS 2	BIN1	999	999
WT MG LPS 2	TGFB	21.31159	9.741888
WT MG LPS 2	TMEM119	15.07312	7.587874
WT MG LPS 2	ABCA7	999	999
WT MG LPS 2	PICALM	17.34088	11.05734
WT MG LPS 2	INPP5D	23.18214	15.26086
WT MG LPS 2	APOE	999	999
WT MG LPS 2	EPHA1	13.71376	9.385672
WT MG LPS 2	HLA-DR	999	999
WT MG LPS 2	PLCG2	13.12835	9.582024
WT MG LPS 2	CD33	999	999
WT MG LPS 2	CR1	999	999
WT MG LPS 2	CD59	21.64367	12.85224
WT MG LPS 2	MASP	999	999
WT MG LPS 2	CR1	20.19544	9.674213
WT MG LPS 2	CD46	20.39228	12.04127
WT MG LPS 2	C1IN	20.55919	9.059587
WT MG LPS 2	C6	999	999
WT MG LPS 2	C3aR	18.54055	7.440413
WT MG LPS 2	DAF	21.58419	12.46629
WT MG LPS 2	C2	18.33158	11.08004
WT MG LPS 2	C3	999	999
WT MG LPS 2	C1S	999	999
WT MG LPS 2	C1QA1	14.95708	9.003449
WT MG LPS 2	FH	999	999
WT MG LPS 2	CR4	17.36798	5.563485
WT MG LPS 2	FB	999	999
WT MG LPS 2	C9	20.31479	12.50669

WT MG LPS 2	C5aR	23.92832	16.47
WT MG LPS 2	P2RY12	999	999
WT MG LPS 2	C4	22.19037	9.646945
WT MG LPS 2	FI	999	999
WT MG LPS 2	CSMD1	999	999
WT MG LPS 2	C5	999	999
WT MG LPS 2	C1QB	17.25521	6.966302
WT MG LPS 2	CD68	12.17469	9.019453
WT MG LPS 2	NOS	14.90506	-4.56303
WT MG LPS 2	IL1B	999	999
WT MG LPS 2	NOS	999	999
WT MG LPS 2	IL6	19.04217	7.847335
WT MG LPS 2	TNFA	15.95126	1.18086
WT MG LPS 4	LIN28	999	999
WT MG LPS 4	Oct-04	999	999
WT MG LPS 4	BMP4	999	999
WT MG LPS 4	CD34	999	999
WT MG LPS 4	SOX2	22.67062	7.439131
WT MG LPS 4	FLK1	999	999
WT MG LPS 4	CD45	999	999
WT MG LPS 4	CD11B	16.08988	9.56793
WT MG LPS 4	CD235a	20.41569	9.704413
WT MG LPS 4	BRAC	999	999
WT MG LPS 4	MERTK	999	999
WT MG LPS 4	RUNX1	999	999
WT MG LPS 4	NESTIN	21.33288	11.67454
WT MG LPS 4	MAP2	999	999
WT MG LPS 4	NFKB	16.73958	9.725122
WT MG LPS 4	NLRP3	23.48077	12.53053
WT MG LPS 4	TREM2	23.53596	10.42466
WT MG LPS 4	IBA1	17.74002	9.497356
WT MG LPS 4	CD14	999	999
WT MG LPS 4	VIMENTIN	12.93066	8.986688
WT MG LPS 4	GFAP	19.57111	11.70145
WT MG LPS 4	EAAT2	999	999
WT MG LPS 4	ALDH1	999	999
WT MG LPS 4	S100B	999	999
WT MG LPS 4	NEUN	999	999
WT MG LPS 4	CX3CR1	25.76837	15.69131
WT MG LPS 4	BIN1	999	999
WT MG LPS 4	TGFB	21.43081	9.861108
WT MG LPS 4	TMEM119	16.87315	9.387905
WT MG LPS 4	ABCA7	999	999
WT MG LPS 4	PICALM	21.98275	15.6992
WT MG LPS 4	INPP5D	999	999

WT MG LPS 4	APOE	20.88504	13.24838
WT MG LPS 4	EPHA1	14.77941	10.45133
WT MG LPS 4	HLA-DR	999	999
WT MG LPS 4	PLCG2	13.87704	10.33072
WT MG LPS 4	CD33	25.42371	13.98826
WT MG LPS 4	CR1	21.36264	10.84142
WT MG LPS 4	CD59	22.18648	13.39505
WT MG LPS 4	MASP	23.99678	14.47566
WT MG LPS 4	CR1	999	999
WT MG LPS 4	CD46	22.57373	14.22272
WT MG LPS 4	C1IN	20.79461	9.295005
WT MG LPS 4	C6	999	999
WT MG LPS 4	C3aR	19.15423	8.054096
WT MG LPS 4	DAF	21.661	12.5431
WT MG LPS 4	C2	18.92465	11.67311
WT MG LPS 4	C3	999	999
WT MG LPS 4	C1S	999	999
WT MG LPS 4	C1QA1	14.89549	8.941861
WT MG LPS 4	FH	999	999
WT MG LPS 4	CR4	18.89697	7.092472
WT MG LPS 4	FB	999	999
WT MG LPS 4	C9	21.04955	13.24146
WT MG LPS 4	C5aR	999	999
WT MG LPS 4	P2RY12	999	999
WT MG LPS 4	C4	999	999
WT MG LPS 4	FI	999	999
WT MG LPS 4	CSMD1	999	999
WT MG LPS 4	C5	999	999
WT MG LPS 4	C1QB	18.39793	8.10902
WT MG LPS 4	CD68	13.37775	10.22251
WT MG LPS 4	NOS	15.96426	-3.50383
WT MG LPS 4	IL1B	999	999
WT MG LPS 4	NOS	999	999
WT MG LPS 4	IL6	20.55567	9.360839
WT MG LPS 4	TNFA	17.20332	2.432915
WT MG LPS 1	LIN28	19.9358	9.957141
WT MG LPS 1	Oct-04	15.77119	5.643598
WT MG LPS 1	BMP4	18.29023	8.469697
WT MG LPS 1	CD34	21.80677	9.728865
WT MG LPS 1	SOX2	20.04822	4.816724
WT MG LPS 1	FLK1	6.635424	-5.47543
WT MG LPS 1	CD45	22.06198	5.262618
WT MG LPS 1	CD11B	6.815978	0.294025
WT MG LPS 1	CD235a	7.155313	-3.55596
WT MG LPS 1	BRAC	14.25801	4.921128

WT MG LPS 1	MERTK	25.53743	999
WT MG LPS 1	RUNX1	18.30227	-0.90665
WT MG LPS 1	NESTIN	16.12156	6.46322
WT MG LPS 1	MAP2	18.45847	0.421856
WT MG LPS 1	NFKB	6.858302	-0.15616
WT MG LPS 1	NLRP3	7.264998	-3.68524
WT MG LPS 1	TREM2	16.19655	3.085243
WT MG LPS 1	IBA1	6.767439	-1.47522
WT MG LPS 1	CD14	16.88149	4.699676
WT MG LPS 1	VIMENTIN	4.541458	0.597491
WT MG LPS 1	GFAP	6.40303	-1.46663
WT MG LPS 1	EAAT2	6.742916	999
WT MG LPS 1	ALDH1	16.06072	5.643155
WT MG LPS 1	S100B	24.12337	6.903512
WT MG LPS 1	NEUN	6.751091	-17.8916
WT MG LPS 1	CX3CR1	6.788909	-3.28815
WT MG LPS 1	BIN1	6.807159	-9.75761
WT MG LPS 1	TGFB	6.653253	-4.91645
WT MG LPS 1	TMEM119	6.435744	-1.04951
WT MG LPS 1	ABCA7	6.475205	-18.6566
WT MG LPS 1	PICALM	6.420649	0.137102
WT MG LPS 1	INPP5D	6.831584	-1.0897
WT MG LPS 1	APOE	6.71467	-0.92199
WT MG LPS 1	EPHA1	5.706268	1.378184
WT MG LPS 1	HLA-DR	21.45677	7.80865
WT MG LPS 1	PLCG2	6.139014	2.592692
WT MG LPS 1	CD33	20.07499	8.639544
WT MG LPS 1	CR1	6.691259	-3.82997
WT MG LPS 1	CD59	6.490229	-2.3012
WT MG LPS 1	MASP	16.2829	6.761779
WT MG LPS 1	CR1	6.77819	-3.74303
WT MG LPS 1	CD46	6.584416	-1.76659
WT MG LPS 1	C1IN	6.382838	-5.11677
WT MG LPS 1	C6	7.008961	-11.5843
WT MG LPS 1	C3aR	6.557132	-4.543
WT MG LPS 1	DAF	6.578673	-2.53923
WT MG LPS 1	C2	6.480608	-0.77093
WT MG LPS 1	C3	6.837452	-1.45003
WT MG LPS 1	C1S	17.80633	-2.58281
WT MG LPS 1	C1QA1	6.514357	0.560728
WT MG LPS 1	FH	19.30098	2.353843
WT MG LPS 1	CR4	6.794448	-5.01005
WT MG LPS 1	FB	6.856778	999
WT MG LPS 1	C9	6.390573	-1.41752
WT MG LPS 1	C5aR	6.498194	-0.96013
WT MG LPS 1	P2RY12	20.34123	8.883613

WT MG LPS 1	C4	16.10844	3.565014
WT MG LPS 1	FI	6.98869	-3.32114
WT MG LPS 1	CSMD1	6.591458	-7.36801
WT MG LPS 1	C5	6.548309	-6.85774
WT MG LPS 1	C1QB	6.693878	-3.59503
WT MG LPS 1	CD68	5.684106	2.528869
WT MG LPS 1	NOS	6.38572	-13.0824
WT MG LPS 1	IL1B	6.570792	999
WT MG LPS 1	NOS	6.605638	-12.8625
WT MG LPS 1	IL6	6.731979	-4.46286
WT MG LPS 1	TNFA	6.599542	-8.17086
KO IPS 1	BMP4	9.820534	0
KO IPS 1	CD34	12.0779	0
KO IPS 1	SOX2	15.23149	0
KO IPS 1	FLK1	12.11085	0
KO IPS 1	CD45	16.79936	0
KO IPS 1	CD11B	6.521952	0
KO IPS 1	CD235a	10.71127	0
KO IPS 1	BRAC	9.336882	0
KO IPS 1	MERTK	999	999
KO IPS 1	RUNX1	19.20892	0
KO IPS 1	NESTIN	9.658339	0
KO IPS 1	MAP2	18.03661	0
KO IPS 1	NFKB	7.014463	0
KO IPS 1	NLRP3	10.95024	0
KO IPS 1	TREM2	13.1113	0
KO IPS 1	IBA1	8.242661	0
KO IPS 1	CD14	12.18181	0
KO IPS 1	VIMENTIN	3.943967	0
KO IPS 1	GFAP	7.86966	0
KO IPS 1	EAAT2	999	999
KO IPS 1	ALDH1	10.41756	0
KO IPS 1	S100B	17.21986	0
KO IPS 1	NEUN	24.64268	0
KO IPS 1	CX3CR1	10.07706	0
KO IPS 1	BIN1	16.56477	0
KO IPS 1	TGFB	11.56971	0
KO IPS 1	TMEM119	7.48525	0
KO IPS 1	ABCA7	25.13181	0
KO IPS 1	PICALM	6.283547	0
KO IPS 1	INPP5D	7.921284	0
KO IPS 1	APOE	7.636659	0
KO IPS 1	EPHA1	4.328084	0
KO IPS 1	HLA-DR	13.64812	0
KO IPS 1	PLCG2	3.546322	0

KO IPS 1	CD33	11.43545	0
KO IPS 1	CR1	7.424699	-3.09653
KO IPS 1	CD59	8.791433	0
KO IPS 1	MASP	9.521121	0
KO IPS 1	CR1	13.61775	3.096525
KO IPS 1	CD46	8.351009	0
KO IPS 1	C1IN	11.49961	0
KO IPS 1	C6	18.59324	0
KO IPS 1	C3aR	11.10013	0
KO IPS 1	DAF	9.117899	0
KO IPS 1	C2	7.251537	0
KO IPS 1	C3	8.287486	0
KO IPS 1	C1S	20.38914	0
KO IPS 1	C1QA1	5.953629	0
KO IPS 1	FH	16.94714	0
KO IPS 1	CR4	11.8045	0
KO IPS 1	FB	999	999
KO IPS 1	C9	7.808096	0
KO IPS 1	C5aR	7.458325	0
KO IPS 1	P2RY12	11.45762	0
KO IPS 1	C4	12.54342	0
KO IPS 1	FI	10.30983	0
KO IPS 1	CSMD1	13.95947	0
KO IPS 1	C5	13.40605	0
KO IPS 1	C1QB	10.28891	0
KO IPS 1	CD68	3.155237	0
KO IPS 1	NOS	19.46809	0
KO IPS 1	IL1B	999	999
KO IPS 1	NOS	999	999
KO IPS 1	IL6	11.19484	0
KO IPS 1	TNFA	14.7704	0
KO IPS 2	BMP4	999	999
KO IPS 2	CD34	21.3941	9.316199
KO IPS 2	SOX2	23.14982	7.918327
KO IPS 2	FLK1	23.15322	11.04237
KO IPS 2	CD45	999	999
KO IPS 2	CD11B	22.24035	15.7184
KO IPS 2	CD235a	999	999
KO IPS 2	BRAC	999	999
KO IPS 2	MERTK	21.36087	999
KO IPS 2	RUNX1	999	999
KO IPS 2	NESTIN	18.24896	8.590617
KO IPS 2	MAP2	999	999
KO IPS 2	NFKB	22.674	15.65954
KO IPS 2	NLRP3	999	999

KO IPS 2	TREM2	26.36984	13.25853
KO IPS 2	IBA1	21.18639	12.94373
KO IPS 2	CD14	999	999
KO IPS 2	VIMENTIN	999	999
KO IPS 2	GFAP	18.11356	10.2439
KO IPS 2	EAAT2	24.1887	999
KO IPS 2	ALDH1	999	999
KO IPS 2	S100B	999	999
KO IPS 2	NEUN	20.01416	-4.62852
KO IPS 2	CX3CR1	21.09874	11.02168
KO IPS 2	BIN1	999	999
KO IPS 2	TGFB	21.80441	10.2347
KO IPS 2	TMEM119	999	999
KO IPS 2	ABCA7	999	999
KO IPS 2	PICALM	23.2492	16.96565
KO IPS 2	INPP5D	21.4383	13.51702
KO IPS 2	APOE	22.37214	14.73548
KO IPS 2	EPHA1	999	999
KO IPS 2	HLA-DR	22.24091	8.592789
KO IPS 2	PLCG2	21.37379	17.82747
KO IPS 2	CD33	999	999
KO IPS 2	CR1	999	999
KO IPS 2	CD59	26.22677	17.43533
KO IPS 2	MASP	999	999
KO IPS 2	CR1	20.62893	10.1077
KO IPS 2	CD46	999	999
KO IPS 2	C1IN	22.04422	10.54461
KO IPS 2	C6	999	999
KO IPS 2	C3aR	999	999
KO IPS 2	DAF	999	999
KO IPS 2	C2	999	999
KO IPS 2	C3	24.21634	15.92885
KO IPS 2	C1S	999	999
KO IPS 2	C1QA1	21.50743	15.5538
KO IPS 2	FH	999	999
KO IPS 2	CR4	21.92608	10.12158
KO IPS 2	FB	999	999
KO IPS 2	C9	21.93112	14.12302
KO IPS 2	C5aR	25.64211	18.18378
KO IPS 2	P2RY12	999	999
KO IPS 2	C4	22.89337	10.34995
KO IPS 2	FI	999	999
KO IPS 2	CSMD1	999	999
KO IPS 2	C5	21.53766	8.131609
KO IPS 2	C1QB	19.12085	8.831942
KO IPS 2	CD68	24.45891	21.30367

KO IPS 2	NOS	25.39753	5.929437
KO IPS 2	IL1B	999	999
KO IPS 2	NOS	999	999
KO IPS 2	IL6	999	999
KO IPS 2	TNFA	999	999
KO IPS 4	BMP4	8.654107	-1.16643
KO IPS 4	CD34	7.569907	-4.508
KO IPS 4	SOX2	14.65798	-0.57352
KO IPS 4	FLK1	12.42707	0.316217
KO IPS 4	CD45	999	999
KO IPS 4	CD11B	17.12305	10.6011
KO IPS 4	CD235a	999	999
KO IPS 4	BRAC	12.86116	3.524277
KO IPS 4	MERTK	16.98819	999
KO IPS 4	RUNX1	11.81495	-7.39397
KO IPS 4	NESTIN	12.66367	3.005334
KO IPS 4	MAP2	18.41781	0.381198
KO IPS 4	NFKB	17.97823	10.96377
KO IPS 4	NLRP3	999	999
KO IPS 4	TREM2	26.93937	13.82807
KO IPS 4	IBA1	12.08732	3.844664
KO IPS 4	CD14	999	999
KO IPS 4	VIMENTIN	7.124454	3.180486
KO IPS 4	GFAP	15.36446	7.494796
KO IPS 4	EAAT2	20.64894	999
KO IPS 4	ALDH1	13.27533	2.857769
KO IPS 4	S100B	21.28693	4.067068
KO IPS 4	NEUN	25.70413	1.061451
KO IPS 4	CX3CR1	17.44381	7.366748
KO IPS 4	BIN1	999	999
KO IPS 4	TGFB	20.26565	8.695945
KO IPS 4	TMEM119	12.41603	4.930775
KO IPS 4	ABCA7	25.17572	0.043904
KO IPS 4	PICALM	8.905394	2.621847
KO IPS 4	INPP5D	13.53627	5.614986
KO IPS 4	APOE	10.78027	3.143608
KO IPS 4	EPHA1	11.1566	6.828514
KO IPS 4	HLA-DR	9.424817	-4.22331
KO IPS 4	PLCG2	9.490839	5.944517
KO IPS 4	CD33	999	999
KO IPS 4	CR1	22.38073	11.85951
KO IPS 4	CD59	10.90272	2.111292
KO IPS 4	MASP	26.52514	17.00402
KO IPS 4	CR1	13.28482	2.763595
KO IPS 4	CD46	999	999

KO IPS 4	C1IN	9.791127	-1.70848
KO IPS 4	C6	999	999
KO IPS 4	C3aR	14.89858	3.798446
KO IPS 4	DAF	21.48228	12.36438
KO IPS 4	C2	7.395585	0.144048
KO IPS 4	C3	999	999
KO IPS 4	C1S	20.53253	0.143385
KO IPS 4	C1QA1	22.15105	16.19742
KO IPS 4	FH	19.71763	2.770493
KO IPS 4	CR4	18.31166	6.507161
KO IPS 4	FB	999	999
KO IPS 4	C9	24.9848	17.17671
KO IPS 4	C5aR	999	999
KO IPS 4	P2RY12	999	999
KO IPS 4	C4	15.51687	2.973449
KO IPS 4	FI	999	999
KO IPS 4	CSMD1	999	999
KO IPS 4	C5	17.20963	3.803583
KO IPS 4	C1QB	18.39596	8.107046
KO IPS 4	CD68	15.57225	12.41702
KO IPS 4	NOS	22.63013	3.162036
KO IPS 4	IL1B	999	999
KO IPS 4	NOS	999	999
KO IPS 4	IL6	999	999
KO IPS 4	TNFA	25.83631	11.06591
KO IPS 3	BMP4	10.68963	0.869099
KO IPS 3	CD34	12.10401	0.026104
KO IPS 3	SOX2	16.47528	1.243786
KO IPS 3	FLK1	15.20359	3.092738
KO IPS 3	CD45	19.41747	2.618103
KO IPS 3	CD11B	8.541331	2.019379
KO IPS 3	CD235a	10.31216	-0.39911
KO IPS 3	BRAC	11.6646	2.32772
KO IPS 3	MERTK	21.9564	999
KO IPS 3	RUNX1	19.60898	0.400061
KO IPS 3	NESTIN	9.919799	0.261459
KO IPS 3	MAP2	999	999
KO IPS 3	NFKB	8.464373	1.44991
KO IPS 3	NLRP3	16.69103	5.740792
KO IPS 3	TREM2	14.66634	1.555038
KO IPS 3	IBA1	10.29936	2.056703
KO IPS 3	CD14	14.83792	2.656106
KO IPS 3	VIMENTIN	5.142521	1.198554
KO IPS 3	GFAP	9.258322	1.388662
KO IPS 3	EAAT2	999	999

KO IPS 3	ALDH1	10.32691	-0.09066
KO IPS 3	S100B	18.17616	0.956299
KO IPS 3	NEUN	21.93652	-2.70616
KO IPS 3	CX3CR1	9.505422	-0.57164
KO IPS 3	BIN1	16.53358	-0.03119
KO IPS 3	TGFB	11.49822	-0.07148
KO IPS 3	TMEM119	8.663247	1.177997
KO IPS 3	ABCA7	25.27038	0.138569
KO IPS 3	PICALM	8.121242	1.837695
KO IPS 3	INPP5D	8.811316	0.890032
KO IPS 3	APOE	8.981145	1.344486
KO IPS 3	EPHA1	5.253818	0.925734
KO IPS 3	HLA-DR	13.56067	-0.08745
KO IPS 3	PLCG2	8.296087	4.749765
KO IPS 3	CD33	13.11868	1.683228
KO IPS 3	CR1	10.66984	0.14862
KO IPS 3	CD59	10.04044	1.249012
KO IPS 3	MASP	12.36275	2.841627
KO IPS 3	CR1	23.90749	13.38627
KO IPS 3	CD46	11.33828	2.987274
KO IPS 3	C1IN	12.24492	0.745317
KO IPS 3	C6	21.3129	2.719657
KO IPS 3	C3aR	15.09652	3.996384
KO IPS 3	DAF	12.26009	3.142195
KO IPS 3	C2	9.597425	2.345888
KO IPS 3	C3	10.0458	1.758318
KO IPS 3	C1S	22.47684	2.087696
KO IPS 3	C1QA1	9.07597	3.122341
KO IPS 3	FH	20.2509	3.303767
KO IPS 3	CR4	14.60128	2.796781
KO IPS 3	FB	999	999
KO IPS 3	C9	8.885948	1.077852
KO IPS 3	C5aR	11.14925	3.690928
KO IPS 3	P2RY12	12.20756	0.749934
KO IPS 3	C4	11.6769	-0.86652
KO IPS 3	FI	9.850876	-0.45895
KO IPS 3	CSMD1	18.3537	4.394233
KO IPS 3	C5	14.11336	0.707315
KO IPS 3	C1QB	11.65128	1.362365
KO IPS 3	CD68	5.206335	2.051098
KO IPS 3	NOS	20.41406	0.945971
KO IPS 3	IL1B	999	999
KO IPS 3	NOS	999	999
KO IPS 3	IL6	13.63626	2.441429
KO IPS 3	TNFA	16.34008	1.569678

KO IPS 8	BMP4	9.389789	-0.43075
KO IPS 8	CD34	8.99133	-3.08657
KO IPS 8	SOX2	15.30553	0.074037
KO IPS 8	FLK1	13.37066	1.259813
KO IPS 8	CD45	999	999
KO IPS 8	CD11B	19.53078	13.00883
KO IPS 8	CD235a	999	999
KO IPS 8	BRAC	13.61761	4.280728
KO IPS 8	MERTK	17.32095	999
KO IPS 8	RUNX1	12.84837	-6.36055
KO IPS 8	NESTIN	13.66137	4.003031
KO IPS 8	MAP2	17.81597	-0.22064
KO IPS 8	NFKB	18.88214	11.86768
KO IPS 8	NLRP3	999	999
KO IPS 8	TREM2	23.55969	10.44838
KO IPS 8	IBA1	11.84611	3.60345
KO IPS 8	CD14	999	999
KO IPS 8	VIMENTIN	7.771673	3.827706
KO IPS 8	GFAP	15.93158	8.061917
KO IPS 8	EAAT2	19.59198	999
KO IPS 8	ALDH1	14.46381	4.04625
KO IPS 8	S100B	19.24199	2.022129
KO IPS 8	NEUN	22.05086	-2.59182
KO IPS 8	CX3CR1	18.69268	8.615622
KO IPS 8	BIN1	24.40276	7.837995
KO IPS 8	TGFB	20.89535	9.325641
KO IPS 8	TMEM119	12.09919	4.613938
KO IPS 8	ABCA7	999	999
KO IPS 8	PICALM	10.10871	3.825168
KO IPS 8	INPP5D	13.72264	5.801354
KO IPS 8	APOE	12.04475	4.40809
KO IPS 8	EPHA1	12.91415	8.58607
KO IPS 8	HLA-DR	9.523937	-4.12419
KO IPS 8	PLCG2	9.420752	5.87443
KO IPS 8	CD33	999	999
KO IPS 8	CR1	999	999
KO IPS 8	CD59	11.85823	3.0668
KO IPS 8	MASP	999	999
KO IPS 8	CR1	14.15428	3.633059
KO IPS 8	CD46	14.33713	5.98612
KO IPS 8	C1IN	11.88176	0.382151
KO IPS 8	C6	999	999
KO IPS 8	C3aR	16.04163	4.941494
KO IPS 8	DAF	23.84772	14.72982
KO IPS 8	C2	9.52588	2.274343
KO IPS 8	C3	999	999

KO IPS 8	C1S	24.05808	3.668936
KO IPS 8	C1QA1	22.13995	16.18632
KO IPS 8	FH	999	999
KO IPS 8	CR4	999	999
KO IPS 8	FB	999	999
KO IPS 8	C9	21.961	14.15291
KO IPS 8	C5aR	999	999
KO IPS 8	P2RY12	999	999
KO IPS 8	C4	17.66817	5.124752
KO IPS 8	FI	999	999
KO IPS 8	CSMD1	999	999
KO IPS 8	C5	17.46334	4.057288
KO IPS 8	C1QB	18.27148	7.982564
KO IPS 8	CD68	16.00599	12.85076
KO IPS 8	NOS	22.06413	2.596037
KO IPS 8	IL1B	999	999
KO IPS 8	NOS	999	999
KO IPS 8	IL6	999	999
KO IPS 8	TNFA	24.51988	9.749477
KO IPS 5	BMP4	20.64726	10.82673
KO IPS 5	CD34	999	999
KO IPS 5	SOX2	23.15925	7.927755
KO IPS 5	FLK1	999	999
KO IPS 5	CD45	999	999
KO IPS 5	CD11B	18.89386	12.37191
KO IPS 5	CD235a	999	999
KO IPS 5	BRAC	999	999
KO IPS 5	MERTK	22.78042	999
KO IPS 5	RUNX1	999	999
KO IPS 5	NESTIN	18.45528	8.796944
KO IPS 5	MAP2	999	999
KO IPS 5	NFKB	18.92583	11.91137
KO IPS 5	NLRP3	999	999
KO IPS 5	TREM2	999	999
KO IPS 5	IBA1	999	999
KO IPS 5	CD14	999	999
KO IPS 5	VIMENTIN	20.39112	16.44715
KO IPS 5	GFAP	18.57785	10.70819
KO IPS 5	EAAT2	999	999
KO IPS 5	ALDH1	999	999
KO IPS 5	S100B	999	999
KO IPS 5	NEUN	999	999
KO IPS 5	CX3CR1	23.52428	13.44722
KO IPS 5	BIN1	999	999
KO IPS 5	TGFB	20.45321	8.883504

KO IPS 5	TMEM119	999	999
KO IPS 5	ABCA7	999	999
KO IPS 5	PICALM	999	999
KO IPS 5	INPP5D	999	999
KO IPS 5	APOE	20.15606	12.5194
KO IPS 5	EPHA1	16.35266	12.02458
KO IPS 5	HLA-DR	999	999
KO IPS 5	PLCG2	23.8263	20.27998
KO IPS 5	CD33	999	999
KO IPS 5	CR1	999	999
KO IPS 5	CD59	999	999
KO IPS 5	MASP	999	999
KO IPS 5	CR1	26.64445	16.12323
KO IPS 5	CD46	24.22404	15.87303
KO IPS 5	C1IN	21.69526	10.19565
KO IPS 5	C6	999	999
KO IPS 5	C3aR	999	999
KO IPS 5	DAF	21.96541	12.84751
KO IPS 5	C2	17.21969	9.968151
KO IPS 5	C3	999	999
KO IPS 5	C1S	999	999
KO IPS 5	C1QA1	999	999
KO IPS 5	FH	999	999
KO IPS 5	CR4	22.14826	10.34377
KO IPS 5	FB	999	999
KO IPS 5	C9	18.25326	10.44517
KO IPS 5	C5aR	999	999
KO IPS 5	P2RY12	999	999
KO IPS 5	C4	999	999
KO IPS 5	FI	999	999
KO IPS 5	CSMD1	999	999
KO IPS 5	C5	23.01259	9.606546
KO IPS 5	C1QB	21.28219	10.99328
KO IPS 5	CD68	16.21911	13.06387
KO IPS 5	NOS	27.37656	7.908467
KO IPS 5	IL1B	999	999
KO IPS 5	NOS	999	999
KO IPS 5	IL6	999	999
KO IPS 5	TNFA	999	999
KO IPS 7	BMP4	999	999
KO IPS 7	CD34	999	999
KO IPS 7	SOX2	999	999
KO IPS 7	FLK1	999	999
KO IPS 7	CD45	999	999
KO IPS 7	CD11B	18.86806	12.34611

KO IPS 7	CD235a	999	999
KO IPS 7	BRAC	22.62378	13.2869
KO IPS 7	MERTK	999	999
KO IPS 7	RUNX1	999	999
KO IPS 7	NESTIN	21.58431	11.92597
KO IPS 7	MAP2	999	999
KO IPS 7	NFKB	16.84396	9.829498
KO IPS 7	NLRP3	28.53263	17.58239
KO IPS 7	TREM2	21.90678	8.795478
KO IPS 7	IBA1	20.12275	11.88009
KO IPS 7	CD14	999	999
KO IPS 7	VIMENTIN	15.12718	11.18321
KO IPS 7	GFAP	18.12197	10.25231
KO IPS 7	EAAT2	999	999
KO IPS 7	ALDH1	999	999
KO IPS 7	S100B	26.83528	9.615421
KO IPS 7	NEUN	999	999
KO IPS 7	CX3CR1	25.47119	15.39414
KO IPS 7	BIN1	999	999
KO IPS 7	TGFB	999	999
KO IPS 7	TMEM119	20.07989	12.59464
KO IPS 7	ABCA7	999	999
KO IPS 7	PICALM	17.96495	11.68141
KO IPS 7	INPP5D	999	999
KO IPS 7	APOE	999	999
KO IPS 7	EPHA1	13.92656	9.598479
KO IPS 7	HLA-DR	999	999
KO IPS 7	PLCG2	20.54277	16.99645
KO IPS 7	CD33	999	999
KO IPS 7	CR1	21.07529	10.55406
KO IPS 7	CD59	21.02359	12.23215
KO IPS 7	MASP	24.31699	14.79587
KO IPS 7	CR1	999	999
KO IPS 7	CD46	22.67096	14.31995
KO IPS 7	C1IN	21.2948	9.795195
KO IPS 7	C6	999	999
KO IPS 7	C3aR	999	999
KO IPS 7	DAF	22.46668	13.34878
KO IPS 7	C2	15.68927	8.43773
KO IPS 7	C3	999	999
KO IPS 7	C1S	999	999
KO IPS 7	C1QA1	21.01029	15.05666
KO IPS 7	FH	999	999
KO IPS 7	CR4	20.56584	8.761339
KO IPS 7	FB	999	999
KO IPS 7	C9	19.18234	11.37425

KO IPS 7	C5aR	999	999
KO IPS 7	P2RY12	999	999
KO IPS 7	C4	23.02583	10.48241
KO IPS 7	FI	999	999
KO IPS 7	CSMD1	999	999
KO IPS 7	C5	999	999
KO IPS 7	C1QB	23.39058	13.10167
KO IPS 7	CD68	14.63874	11.48351
KO IPS 7	NOS	999	999
KO IPS 7	IL1B	999	999
KO IPS 7	NOS	999	999
KO IPS 7	IL6	999	999
KO IPS 7	TNFA	999	999
KO PRE 1	BMP4	7.404161	-2.41637
KO PRE 1	CD34	8.282133	-3.79577
KO PRE 1	SOX2	15.69603	0.46454
KO PRE 1	FLK1	12.51471	0.403856
KO PRE 1	CD45	999	999
KO PRE 1	CD11B	13.47321	6.951261
KO PRE 1	CD235a	999	999
KO PRE 1	BRAC	13.14079	3.803911
KO PRE 1	MERTK	20.56235	999
KO PRE 1	RUNX1	13.45755	-5.75137
KO PRE 1	NESTIN	10.83384	1.175503
KO PRE 1	MAP2	15.3857	-2.65092
KO PRE 1	NFKB	19.24007	12.22561
KO PRE 1	NLRP3	999	999
KO PRE 1	TREM2	21.65186	8.540551
KO PRE 1	IBA1	12.06765	3.824985
KO PRE 1	CD14	18.54333	6.361521
KO PRE 1	VIMENTIN	7.901615	3.957648
KO PRE 1	GFAP	16.42906	8.559401
KO PRE 1	EAAT2	16.78437	999
KO PRE 1	ALDH1	11.77168	1.354122
KO PRE 1	S100B	19.64807	2.428215
KO PRE 1	NEUN	24.23954	-0.40314
KO PRE 1	CX3CR1	12.45737	2.380316
KO PRE 1	BIN1	18.6835	2.118735
KO PRE 1	TGFB	13.35738	1.787676
KO PRE 1	TMEM119	12.24562	4.76037
KO PRE 1	ABCA7	24.21782	-0.91399
KO PRE 1	PICALM	8.710996	2.427449
KO PRE 1	INPP5D	11.18869	3.267408
KO PRE 1	APOE	11.37124	3.734578
KO PRE 1	EPHA1	14.30264	9.974554

KO PRE 1	HLA-DR	8.69997	-4.94815
KO PRE 1	PLCG2	7.650406	4.104084
KO PRE 1	CD33	22.7075	11.27206
KO PRE 1	CR1	20.30046	9.779233
KO PRE 1	CD59	11.70008	2.908645
KO PRE 1	MASP	24.12278	14.60166
KO PRE 1	CR1	12.83347	2.312246
KO PRE 1	CD46	14.38094	6.029927
KO PRE 1	C1IN	11.99864	0.499032
KO PRE 1	C6	999	999
KO PRE 1	C3aR	12.81058	1.710446
KO PRE 1	DAF	19.76945	10.65155
KO PRE 1	C2	9.222375	1.970838
KO PRE 1	C3	24.60648	16.319
KO PRE 1	C1S	22.17634	1.7872
KO PRE 1	C1QA1	14.15657	8.202945
KO PRE 1	FH	999	999
KO PRE 1	CR4	19.12229	7.317789
KO PRE 1	FB	999	999
KO PRE 1	C9	23.87208	16.06398
KO PRE 1	C5aR	999	999
KO PRE 1	P2RY12	999	999
KO PRE 1	C4	16.89564	4.352223
KO PRE 1	FI	12.03955	1.729722
KO PRE 1	CSMD1	25.91019	11.95072
KO PRE 1	C5	16.77105	3.365002
KO PRE 1	C1QB	15.84302	5.554112
KO PRE 1	CD68	16.08349	12.92825
KO PRE 1	NOS	22.49287	3.024781
KO PRE 1	IL1B	29.88509	999
KO PRE 1	NOS	999	999
KO PRE 1	IL6	999	999
KO PRE 1	TNFA	999	999
KO PRE 4	Oct-04	4.412265	-5.71532
KO PRE 4	BMP4	7.595604	-2.22493
KO PRE 4	CD34	6.835379	-5.24252
KO PRE 4	SOX2	14.44278	-0.78871
KO PRE 4	FLK1	11.33118	-0.77967
KO PRE 4	CD45	999	999
KO PRE 4	CD11B	17.74948	11.22753
KO PRE 4	CD235a	999	999
KO PRE 4	BRAC	12.08847	2.751593
KO PRE 4	MERTK	16.52222	999
KO PRE 4	RUNX1	11.22298	-7.98593
KO PRE 4	NESTIN	12.10059	2.442255

KO PRE 4	MAP2	17.3301	-0.70651
KO PRE 4	NFKB	17.11639	10.10193
KO PRE 4	NLRP3	999	999
KO PRE 4	TREM2	22.28345	9.172147
KO PRE 4	IBA1	10.81484	2.572177
KO PRE 4	CD14	999	999
KO PRE 4	VIMENTIN	6.384703	2.440736
KO PRE 4	GFAP	14.91114	7.041478
KO PRE 4	EAAT2	17.97556	999
KO PRE 4	ALDH1	13.25558	2.838018
KO PRE 4	S100B	20.14444	2.92458
KO PRE 4	NEUN	24.23661	-0.40607
KO PRE 4	CX3CR1	16.81446	6.737402
KO PRE 4	BIN1	22.53281	5.968045
KO PRE 4	TGFB	19.256	7.686291
KO PRE 4	TMEM119	10.94078	3.455526
KO PRE 4	ABCA7	24.66199	-0.46982
KO PRE 4	PICALM	8.242622	1.959076
KO PRE 4	INPP5D	12.26259	4.341308
KO PRE 4	APOE	10.33684	2.700185
KO PRE 4	EPHA1	10.83651	6.508421
KO PRE 4	HLA-DR	8.008989	-5.63913
KO PRE 4	PLCG2	7.278988	3.732666
KO PRE 4	CD33	22.26143	10.82598
KO PRE 4	CR1	21.23603	10.7148
KO PRE 4	CD59	9.906586	1.115154
KO PRE 4	MASP	25.08102	15.55989
KO PRE 4	CR1	12.34547	1.824242
KO PRE 4	CD46	12.52887	4.177859
KO PRE 4	C1IN	9.528485	-1.97112
KO PRE 4	C6	999	999
KO PRE 4	C3aR	14.23274	3.132608
KO PRE 4	DAF	21.57292	12.45502
KO PRE 4	C2	7.237068	-0.01447
KO PRE 4	C3	999	999
KO PRE 4	C1S	20.68934	0.300197
KO PRE 4	C1QA1	21.80406	15.85043
KO PRE 4	FH	21.16158	4.21445
KO PRE 4	CR4	18.17393	6.369432
KO PRE 4	FB	999	999
KO PRE 4	C9	999	999
KO PRE 4	C5aR	23.30248	15.84415
KO PRE 4	P2RY12	999	999
KO PRE 4	C4	15.04341	2.499989
KO PRE 4	FI	999	999
KO PRE 4	CSMD1	25.86333	11.90386

KO PRE 4	C5	15.62364	2.217591
KO PRE 4	C1QB	18.05081	7.761903
KO PRE 4	CD68	14.7755	11.62026
KO PRE 4	NOS	21.31639	1.848296
KO PRE 4	IL1B	26.94531	999
KO PRE 4	NOS	999	999
KO PRE 4	IL6	999	999
KO PRE 4	TNFA	999	999
KO PRE 3	BMP4	10.66269	0.84216
KO PRE 3	CD34	11.89984	-0.17806
KO PRE 3	SOX2	16.27991	1.048419
KO PRE 3	FLK1	15.08132	2.970474
KO PRE 3	CD45	19.03429	2.234922
KO PRE 3	CD11B	8.567461	2.045509
KO PRE 3	CD235a	10.2221	-0.48917
KO PRE 3	BRAC	11.64235	2.305472
KO PRE 3	MERTK	24.8727	999
KO PRE 3	RUNX1	19.24143	0.032512
KO PRE 3	NESTIN	9.960905	0.302566
KO PRE 3	MAP2	999	999
KO PRE 3	NFKB	8.223864	1.209402
KO PRE 3	NLRP3	16.53945	5.589205
KO PRE 3	TREM2	14.2957	1.184397
KO PRE 3	IBA1	10.3129	2.070243
KO PRE 3	CD14	14.57353	2.391725
KO PRE 3	VIMENTIN	5.006337	1.06237
KO PRE 3	GFAP	9.121623	1.251963
KO PRE 3	EAAT2	999	999
KO PRE 3	ALDH1	10.32391	-0.09365
KO PRE 3	S100B	19.27094	2.051085
KO PRE 3	NEUN	23.61618	-1.0265
KO PRE 3	CX3CR1	9.628787	-0.44827
KO PRE 3	BIN1	16.35707	-0.2077
KO PRE 3	TGFB	11.49531	-0.07439
KO PRE 3	TMEM119	8.672647	1.187397
KO PRE 3	ABCA7	999	999
KO PRE 3	PICALM	8.099108	1.815561
KO PRE 3	INPP5D	8.829429	0.908145
KO PRE 3	APOE	8.935381	1.298722
KO PRE 3	EPHA1	5.029964	0.701879
KO PRE 3	HLA-DR	13.09565	-0.55247
KO PRE 3	PLCG2	8.674182	5.12786
KO PRE 3	CD33	13.12483	1.68938
KO PRE 3	CR1	10.42083	-0.10039
KO PRE 3	CD59	9.717429	0.925996

KO PRE 3	MASP	12.2675	2.746383
KO PRE 3	CR1	20.561	10.03978
KO PRE 3	CD46	11.23463	2.883626
KO PRE 3	C1IN	12.5401	1.040495
KO PRE 3	C6	21.94426	3.351023
KO PRE 3	C3aR	15.32565	4.225513
KO PRE 3	DAF	12.0767	2.958802
KO PRE 3	C2	9.268302	2.016765
KO PRE 3	C3	10.09763	1.810144
KO PRE 3	C1S	999	999
KO PRE 3	C1QA1	8.977354	3.023725
KO PRE 3	FH	19.96025	3.013112
KO PRE 3	CR4	14.69927	2.894776
KO PRE 3	FB	999	999
KO PRE 3	C9	8.689808	0.881712
KO PRE 3	C5aR	11.12974	3.671413
KO PRE 3	P2RY12	12.04685	0.589229
KO PRE 3	C4	11.50421	-1.03922
KO PRE 3	FI	9.890295	-0.41953
KO PRE 3	CSMD1	19.34333	5.383857
KO PRE 3	C5	14.38356	0.977513
KO PRE 3	C1QB	11.56775	1.278838
KO PRE 3	CD68	5.134639	1.979403
KO PRE 3	NOS	19.93856	0.470466
KO PRE 3	IL1B	999	999
KO PRE 3	NOS	999	999
KO PRE 3	IL6	13.33328	2.13844
KO PRE 3	TNFA	16.12674	1.356337
KO PRE 6	LIN28	5.070979	-4.90768
KO PRE 6	Oct-04	4.091795	-6.0358
KO PRE 6	BMP4	8.366765	-1.45377
KO PRE 6	CD34	7.51985	-4.55805
KO PRE 6	SOX2	14.08676	-1.14474
KO PRE 6	FLK1	12.4627	0.351852
KO PRE 6	CD45	999	999
KO PRE 6	CD11B	12.9249	6.40295
KO PRE 6	CD235a	19.88273	9.171458
KO PRE 6	BRAC	12.33157	2.994684
KO PRE 6	MERTK	19.20731	999
KO PRE 6	RUNX1	13.39011	-5.81881
KO PRE 6	NESTIN	9.768254	0.109914
KO PRE 6	MAP2	13.56164	-4.47498
KO PRE 6	NFKB	17.5603	10.54584
KO PRE 6	NLRP3	999	999
KO PRE 6	TREM2	22.36278	9.251475

KO PRE 6	IBA1	11.61358	3.370921
KO PRE 6	CD14	17.46223	5.280417
KO PRE 6	VIMENTIN	8.378056	4.434089
KO PRE 6	GFAP	15.45135	7.58169
KO PRE 6	EAAT2	19.45113	999
KO PRE 6	ALDH1	10.58718	0.169619
KO PRE 6	S100B	19.02096	1.801107
KO PRE 6	NEUN	20.22727	-4.41541
KO PRE 6	CX3CR1	11.632	1.554941
KO PRE 6	BIN1	20.57199	4.007224
KO PRE 6	TGFB	12.50995	0.940245
KO PRE 6	TMEM119	12.34685	4.861596
KO PRE 6	ABCA7	23.06886	-2.06295
KO PRE 6	PICALM	8.669321	2.385774
KO PRE 6	INPP5D	12.4053	4.484016
KO PRE 6	APOE	11.13875	3.502094
KO PRE 6	EPHA1	13.54268	9.214593
KO PRE 6	HLA-DR	8.85511	-4.79301
KO PRE 6	PLCG2	7.893237	4.346915
KO PRE 6	CD33	22.85955	11.4241
KO PRE 6	CR1	20.70585	10.18463
KO PRE 6	CD59	11.4078	2.616362
KO PRE 6	MASP	23.77509	14.25397
KO PRE 6	CR1	13.58917	3.067942
KO PRE 6	CD46	14.69265	6.341646
KO PRE 6	C1IN	11.11997	-0.37964
KO PRE 6	C6	999	999
KO PRE 6	C3aR	13.37224	2.272109
KO PRE 6	DAF	19.15604	10.03814
KO PRE 6	C2	8.319984	1.068447
KO PRE 6	C3	23.93234	15.64485
KO PRE 6	C1S	21.21277	0.823625
KO PRE 6	C1QA1	13.59326	7.639627
KO PRE 6	FH	18.59774	1.650607
KO PRE 6	CR4	18.6847	6.880204
KO PRE 6	FB	999	999
KO PRE 6	C9	21.35438	13.54629
KO PRE 6	C5aR	22.81541	15.35708
KO PRE 6	P2RY12	999	999
KO PRE 6	C4	16.22936	3.685943
KO PRE 6	FI	11.31579	1.005959
KO PRE 6	CSMD1	20.2765	6.31703
KO PRE 6	C5	15.61355	2.207501
KO PRE 6	C1QB	14.65916	4.370249
KO PRE 6	CD68	16.63596	13.48072
KO PRE 6	NOS	23.22425	3.756158

KO PRE 6	IL1B	999	999
KO PRE 6	NOS	999	999
KO PRE 6	IL6	999	999
KO PRE 6	TNFA	25.18087	10.41047
KO PRE 7	LIN28	15.28203	5.303376
KO PRE 7	Oct-04	15.94427	5.816676
KO PRE 7	BMP4	15.65319	5.832656
KO PRE 7	CD34	17.29372	5.215821
KO PRE 7	SOX2	999	999
KO PRE 7	FLK1	17.0115	4.900649
KO PRE 7	CD45	999	999
KO PRE 7	CD11B	16.11075	9.588798
KO PRE 7	CD235a	999	999
KO PRE 7	BRAC	19.12322	9.786339
KO PRE 7	MERTK	20.72274	999
KO PRE 7	RUNX1	999	999
KO PRE 7	NESTIN	15.77891	6.120568
KO PRE 7	MAP2	22.81223	4.775621
KO PRE 7	NFKB	18.8469	11.83243
KO PRE 7	NLRP3	25.91753	14.96729
KO PRE 7	TREM2	999	999
KO PRE 7	IBA1	17.98821	9.74555
KO PRE 7	CD14	21.79125	9.609435
KO PRE 7	VIMENTIN	12.42107	8.477106
KO PRE 7	GFAP	16.66669	8.797028
KO PRE 7	EAAT2	999	999
KO PRE 7	ALDH1	15.52742	5.109855
KO PRE 7	S100B	999	999
KO PRE 7	NEUN	999	999
KO PRE 7	CX3CR1	16.12829	6.051231
KO PRE 7	BIN1	25.86352	9.298749
KO PRE 7	TGFB	17.05778	5.488071
KO PRE 7	TMEM119	15.91082	8.425567
KO PRE 7	ABCA7	999	999
KO PRE 7	PICALM	16.68772	10.40417
KO PRE 7	INPP5D	19.79555	11.87427
KO PRE 7	APOE	19.6541	12.01744
KO PRE 7	EPHA1	14.88975	10.56167
KO PRE 7	HLA-DR	20.35784	6.70972
KO PRE 7	PLCG2	14.2112	10.66487
KO PRE 7	CD33	23.71471	12.27926
KO PRE 7	CR1	20.67863	10.1574
KO PRE 7	CD59	21.02226	12.23083
KO PRE 7	MASP	23.61892	14.0978
KO PRE 7	CR1	19.8208	9.29958

KO PRE 7	CD46	22.13854	13.78753
KO PRE 7	C1IN	19.9531	8.453488
KO PRE 7	C6	24.76469	6.171451
KO PRE 7	C3aR	17.63146	6.53133
KO PRE 7	DAF	21.41225	12.29435
KO PRE 7	C2	16.70429	9.452756
KO PRE 7	C3	20.95733	12.66985
KO PRE 7	C1S	999	999
KO PRE 7	C1QA1	15.278	9.324376
KO PRE 7	FH	999	999
KO PRE 7	CR4	21.14521	9.340717
KO PRE 7	FB	999	999
KO PRE 7	C9	17.91864	10.11054
KO PRE 7	C5aR	20.99313	13.53481
KO PRE 7	P2RY12	23.08026	11.62264
KO PRE 7	C4	20.48165	7.938228
KO PRE 7	FI	16.14653	5.836703
KO PRE 7	CSMD1	20.23919	6.279725
KO PRE 7	C5	19.89806	6.492014
KO PRE 7	C1QB	17.5928	7.303892
KO PRE 7	CD68	13.48864	10.3334
KO PRE 7	NOS	25.42395	5.955863
KO PRE 7	IL1B	999	999
KO PRE 7	NOS	999	999
KO PRE 7	IL6	23.74984	12.55501
KO PRE 7	TNFA	24.47658	9.706174
KO MG 4	BMP4	999	999
KO MG 4	CD34	999	999
KO MG 4	SOX2	999	999
KO MG 4	FLK1	10.69522	-1.41563
KO MG 4	CD45	999	999
KO MG 4	CD11B	11.708	5.18605
KO MG 4	CD235a	999	999
KO MG 4	BRAC	999	999
KO MG 4	MERTK	999	999
KO MG 4	RUNX1	11.47769	-7.73123
KO MG 4	NESTIN	999	999
KO MG 4	MAP2	13.90314	-4.13347
KO MG 4	NFKB	999	999
KO MG 4	NLRP3	12.54398	1.593743
KO MG 4	TREM2	999	999
KO MG 4	IBA1	999	999
KO MG 4	CD14	11.79832	-0.38349
KO MG 4	VIMENTIN	10.93915	6.995179
KO MG 4	GFAP	999	999

KO MG 4	EAAT2	11.89566	999
KO MG 4	ALDH1	999	999
KO MG 4	S100B	999	999
KO MG 4	NEUN	999	999
KO MG 4	CX3CR1	17.43159	7.354533
KO MG 4	BIN1	999	999
KO MG 4	TGFB	999	999
KO MG 4	TMEM119	999	999
KO MG 4	ABCA7	999	999
KO MG 4	PICALM	13.25609	6.972547
KO MG 4	INPP5D	11.63255	3.711264
KO MG 4	APOE	12.06774	4.431085
KO MG 4	EPHA1	14.88393	10.55585
KO MG 4	HLA-DR	13.87715	0.229031
KO MG 4	PLCG2	16.78132	13.235
KO MG 4	CD33	16.24928	4.813831
KO MG 4	CR1	10.22912	-0.2921
KO MG 4	CD59	13.59148	4.800049
KO MG 4	MASP	999	999
KO MG 4	CR1	999	999
KO MG 4	CD46	999	999
KO MG 4	C1IN	999	999
KO MG 4	C6	999	999
KO MG 4	C3aR	999	999
KO MG 4	DAF	999	999
KO MG 4	C2	13.97419	6.722648
KO MG 4	C3	15.04011	6.752622
KO MG 4	C1S	999	999
KO MG 4	C1QA1	17.94254	11.98891
KO MG 1	BMP4	11.6375	1.816966
KO MG 1	CD34	12.42968	0.351773
KO MG 1	SOX2	20.09588	4.864391
KO MG 1	FLK1	16.17412	4.063271
KO MG 1	CD45	20.97668	4.177317
KO MG 1	CD11B	11.04294	4.520988
KO MG 1	CD235a	15.46817	4.756899
KO MG 1	BRAC	13.95368	4.616799
KO MG 1	MERTK	23.16674	999
KO MG 1	RUNX1	17.04554	-2.16338
KO MG 1	NESTIN	14.22731	4.568973
KO MG 1	MAP2	22.53795	4.501337
KO MG 1	NFKB	11.90131	4.886844
KO MG 1	NLRP3	17.01338	6.063141
KO MG 1	TREM2	18.1283	5.016994
KO MG 1	IBA1	12.85052	4.607861

KO MG 1	CD14	16.78192	4.600109
KO MG 1	VIMENTIN	8.183389	4.239422
KO MG 1	GFAP	12.30835	4.438688
KO MG 1	EAAT2	999	999
KO MG 1	ALDH1	14.75522	4.337654
KO MG 1	S100B	21.39447	4.174617
KO MG 1	NEUN	23.37844	-1.26424
KO MG 1	CX3CR1	15.07175	4.994697
KO MG 1	BIN1	20.69071	4.125941
KO MG 1	TGFB	16.36344	4.793731
KO MG 1	TMEM119	11.92533	4.440076
KO MG 1	ABCA7	999	999
KO MG 1	PICALM	11.00414	4.720589
KO MG 1	INPP5D	12.59063	4.669341
KO MG 1	APOE	12.56778	4.931121
KO MG 1	EPHA1	8.735632	4.407547
KO MG 1	HLA-DR	12.6949	-0.95322
KO MG 1	PLCG2	7.694351	4.148029
KO MG 1	CD33	16.14412	4.708675
KO MG 1	CR1	12.17975	1.658525
KO MG 1	CD59	13.63522	4.843788
KO MG 1	MASP	14.34568	4.824564
KO MG 1	CR1	17.09695	6.575723
KO MG 1	CD46	14.07021	5.719206
KO MG 1	C1IN	15.97302	4.473413
KO MG 1	C6	999	999
KO MG 1	C3aR	15.87505	4.774917
KO MG 1	DAF	14.3033	5.185402
KO MG 1	C2	12.03758	4.786039
KO MG 1	C3	12.96136	4.673869
KO MG 1	C1S	25.86939	5.480245
KO MG 1	C1QA1	10.62556	4.671935
KO MG 1	FH	21.86269	4.915552
KO MG 1	CR4	16.7271	4.922603
KO MG 1	FB	999	999
KO MG 1	C9	13.10815	5.300057
KO MG 1	C5aR	12.94525	5.486924
KO MG 1	P2RY12	16.42908	4.971459
KO MG 1	C4	17.30703	4.76361
KO MG 1	FI	15.5895	5.279675
KO MG 1	CSMD1	19.03499	5.075517
KO MG 1	C5	18.26992	4.863872
KO MG 1	C1QB	15.04058	4.751669
KO MG 1	CD68	7.205657	4.05042
KO MG 1	NOS	22.46593	2.997838
KO MG 1	IL1B	999	999

KO MG 1	NOS	999	999
KO MG 1	IL6	16.38871	5.193873
KO MG 1	TNFA	20.36468	5.594275
KO MG 3	BMP4	14.50927	4.688734
KO MG 3	CD34	16.00182	3.923914
KO MG 3	SOX2	29.72884	14.49735
KO MG 3	FLK1	15.82168	3.710827
KO MG 3	CD45	999	999
KO MG 3	CD11B	15.18142	8.659472
KO MG 3	CD235a	999	999
KO MG 3	BRAC	19.07804	9.741159
KO MG 3	MERTK	21.70082	999
KO MG 3	RUNX1	999	999
KO MG 3	NESTIN	14.69336	5.035021
KO MG 3	MAP2	21.79245	3.755835
KO MG 3	NFKB	18.11939	11.10492
KO MG 3	NLRP3	25.16444	14.2142
KO MG 3	TREM2	999	999
KO MG 3	IBA1	16.68854	8.44588
KO MG 3	CD14	20.94167	8.759861
KO MG 3	VIMENTIN	12.04971	8.105741
KO MG 3	GFAP	16.61934	8.749682
KO MG 3	EAAT2	999	999
KO MG 3	ALDH1	14.33712	3.919553
KO MG 3	S100B	999	999
KO MG 3	NEUN	999	999
KO MG 3	CX3CR1	15.04337	4.966316
KO MG 3	BIN1	23.42639	6.861619
KO MG 3	TGFB	16.12167	4.551961
KO MG 3	TMEM119	14.85934	7.37409
KO MG 3	ABCA7	999	999
KO MG 3	PICALM	16.18337	9.899826
KO MG 3	INPP5D	19.14535	11.22406
KO MG 3	APOE	20.48851	12.85185
KO MG 3	EPHA1	14.26238	9.934298
KO MG 3	HLA-DR	18.98253	5.334405
KO MG 3	PLCG2	13.95366	10.40734
KO MG 3	CD33	23.33963	11.90418
KO MG 3	CR1	21.3196	10.79838
KO MG 3	CD59	19.95631	11.16488
KO MG 3	MASP	24.59205	15.07093
KO MG 3	CR1	18.54935	8.02813
KO MG 3	CD46	21.45402	13.10301
KO MG 3	C1IN	19.78176	8.282155

KO MG 3	C6	999	999
KO MG 3	C3aR	17.32087	6.220737
KO MG 3	DAF	21.07751	11.95961
KO MG 3	C2	16.14217	8.890637
KO MG 3	C3	23.75594	15.46846
KO MG 3	C1S	999	999
KO MG 3	C1QA1	14.37313	8.419502
KO MG 3	FH	999	999
KO MG 3	CR4	19.55919	7.75469
KO MG 3	FB	999	999
KO MG 3	C9	17.33983	9.531731
KO MG 3	C5aR	21.89975	14.44142
KO MG 3	P2RY12	999	999
KO MG 3	C4	18.51295	5.969531
KO MG 3	FI	14.66242	4.352591
KO MG 3	CSMD1	19.43358	5.474108
KO MG 3	C5	18.57052	5.164474
KO MG 3	C1QB	16.57126	6.28235
KO MG 3	CD68	12.89424	9.739008
KO MG 3	NOS	24.22544	4.757346
KO MG 3	IL1B	999	999
KO MG 3	NOS	999	999
KO MG 3	IL6	21.86423	10.66939
KO MG 3	TNFA	23.39936	8.628954
KO MG 2	BMP4	9.902565	0
KO MG 2	CD34	11.51471	0
KO MG 2	SOX2	11.73456	0
KO MG 2	FLK1	13.63986	0
KO MG 2	CD45	13.15964	0
KO MG 2	CD11B	12.77446	0
KO MG 2	CD235a	11.3509	0
KO MG 2	BRAC	12.7886	0
KO MG 2	MERTK	13.40321	0
KO MG 2	RUNX1	14.26232	0
KO MG 2	NESTIN	12.61879	0
KO MG 2	MAP2	12.8088	0
KO MG 2	NFKB	12.97886	0
KO MG 2	NLRP3	16.0624	0
KO MG 2	TREM2	13.92646	0
KO MG 2	IBA1	11.85795	0
KO MG 2	CD14	12.88651	0
KO MG 2	VIMENTIN	10.15612	0
KO MG 2	GFAP	10.20574	0
KO MG 2	EAAT2	13.02919	0
KO MG 2	ALDH1	13.35392	0

KO MG 2	S100B	14.11569	0
KO MG 2	NEUN	13.12497	0
KO MG 2	CX3CR1	14.27248	0
KO MG 2	BIN1	14.46627	0
KO MG 2	TGFB	12.70248	0
KO MG 2	TMEM119	11.4633	0
KO MG 2	ABCA7	11.27101	0
KO MG 2	PICALM	11.01507	0
KO MG 2	INPP5D	10.86898	0
KO MG 2	APOE	9.602792	0
KO MG 2	EPHA1	8.519294	0
KO MG 2	HLA-DR	8.268542	0
KO MG 2	PLCG2	9.096734	0
KO MG 2	CD33	8.611312	0
KO MG 2	CR1	12.29274	-0.19259
KO MG 2	CD59	11.42087	0
KO MG 2	MASP	12.64826	0
KO MG 2	CR1	12.67792	0.192587
KO MG 2	CD46	12.6429	0
KO MG 2	C1IN	12.98575	0
KO MG 2	C6	13.58089	0
KO MG 2	C3aR	12.91532	0
KO MG 2	DAF	11.86002	0
KO MG 2	C2	11.01396	0
KO MG 2	C3	12.46949	0
KO MG 2	C1S	12.28776	0
KO MG 2	C1QA1	12.08926	0
KO MG 2	FH	14.48984	0
KO MG 2	CR4	13.27344	0
KO MG 2	FB	14.16666	0
KO MG 2	C9	11.13528	0
KO MG 2	C5aR	13.32331	0
KO MG 2	P2RY12	13.53005	0
KO MG 2	C4	12.71033	0
KO MG 2	FI	13.70767	0
KO MG 2	CSMD1	13.03696	0
KO MG 2	C5	14.19631	0
KO MG 2	C1QB	13.29808	0
KO MG 2	CD68	12.54684	0
KO MG 2	NOS	26.0767	4.80369
KO MG 2	IL1B	11.46344	0
KO MG 2	NOS	16.46932	-4.80369
KO MG 2	IL6	12.63937	0
KO MG 2	TNFA	11.73757	0
KO MG 11	BMP4	999	999

KO MG 11	CD34	999	999
KO MG 11	SOX2	23.54456	8.313068
KO MG 11	FLK1	24.56449	12.45364
KO MG 11	CD45	999	999
KO MG 11	CD11B	18.1243	11.60235
KO MG 11	CD235a	21.28129	10.57002
KO MG 11	BRAC	21.82945	12.49257
KO MG 11	MERTK	21.01056	999
KO MG 11	RUNX1	999	999
KO MG 11	NESTIN	19.22393	9.565595
KO MG 11	MAP2	999	999
KO MG 11	NFKB	15.61098	8.596517
KO MG 11	NLRP3	999	999
KO MG 11	TREM2	999	999
KO MG 11	IBA1	18.75381	10.51115
KO MG 11	CD14	999	999
KO MG 11	VIMENTIN	14.48127	10.5373
KO MG 11	GFAP	13.83576	5.966103
KO MG 11	EAAT2	999	999
KO MG 11	ALDH1	18.44058	8.023018
KO MG 11	S100B	26.94228	9.722426
KO MG 11	NEUN	999	999
KO MG 11	CX3CR1	22.65282	12.57576
KO MG 11	BIN1	999	999
KO MG 11	TGFB	999	999
KO MG 11	TMEM119	19.73776	12.25251
KO MG 11	ABCA7	999	999
KO MG 11	PICALM	17.62985	11.34631
KO MG 11	INPP5D	22.3495	14.42821
KO MG 11	APOE	23.42422	15.78756
KO MG 11	EPHA1	13.78355	9.455467
KO MG 11	HLA-DR	999	999
KO MG 11	PLCG2	18.12135	14.57502
KO MG 11	CD33	999	999
KO MG 11	CR1	20.46953	9.948304
KO MG 11	CD59	22.31723	13.5258
KO MG 11	MASP	23.48152	13.9604
KO MG 11	CR1	999	999
KO MG 11	CD46	22.34115	13.99014
KO MG 11	C1IN	999	999
KO MG 11	C6	999	999
KO MG 11	C3aR	20.32897	9.228832
KO MG 11	DAF	999	999
KO MG 11	C2	15.84593	8.594397
KO MG 11	C3	21.85498	13.56749
KO MG 11	C1S	999	999

KO MG 11	C1QA1	19.96114	14.00751
KO MG 11	FH	999	999
KO MG 11	CR4	19.8305	8.026005
KO MG 11	FB	999	999
KO MG 11	C9	19.46376	11.65567
KO MG 11	C5aR	21.79658	14.33826
KO MG 11	P2RY12	999	999
KO MG 11	C4	999	999
KO MG 11	FI	999	999
KO MG 11	CSMD1	999	999
KO MG 11	C5	21.80002	8.393972
KO MG 11	C1QB	20.38571	10.0968
KO MG 11	CD68	14.68183	11.52659
KO MG 11	NOS	26.16162	6.693527
KO MG 11	IL1B	999	999
KO MG 11	NOS	999	999
KO MG 11	IL6	21.7939	10.59906
KO MG 11	TNFA	999	999
KO MG 9	BMP4	13.70291	3.882376
KO MG 9	CD34	15.84922	3.771316
KO MG 9	SOX2	20.61613	5.384638
KO MG 9	FLK1	14.88052	2.769665
KO MG 9	CD45	19.48239	2.683028
KO MG 9	CD11B	6.611659	0.089707
KO MG 9	CD235a	10.90206	0.190784
KO MG 9	BRAC	10.53267	1.195789
KO MG 9	MERTK	18.45917	999
KO MG 9	RUNX1	25.33666	6.127748
KO MG 9	NESTIN	10.7865	1.128156
KO MG 9	MAP2	21.57592	3.539303
KO MG 9	NFKB	8.78265	1.768187
KO MG 9	NLRP3	13.06854	2.118297
KO MG 9	TREM2	12.79764	-0.31367
KO MG 9	IBA1	6.986025	-1.25664
KO MG 9	CD14	12.5315	0.34969
KO MG 9	VIMENTIN	2.994419	-0.94955
KO MG 9	GFAP	6.161755	-1.70791
KO MG 9	EAAT2	999	999
KO MG 9	ALDH1	7.863801	-2.55376
KO MG 9	S100B	19.92588	2.706026
KO MG 9	NEUN	20.8984	-3.74427
KO MG 9	CX3CR1	13.78709	3.710036
KO MG 9	BIN1	19.47547	2.910697
KO MG 9	TGFB	8.461393	-3.10831
KO MG 9	TMEM119	7.445881	-0.03937

KO MG 9	ABCA7	25.25893	0.127113
KO MG 9	PICALM	6.215156	-0.06839
KO MG 9	INPP5D	9.427146	1.505862
KO MG 9	APOE	9.430799	1.79414
KO MG 9	EPHA1	6.668518	2.340434
KO MG 9	HLA-DR	14.92255	1.274422
KO MG 9	PLCG2	3.157858	-0.38846
KO MG 9	CD33	13.99177	2.556323
KO MG 9	CR1	11.54005	1.018825
KO MG 9	CD59	8.892134	0.100701
KO MG 9	MASP	13.45401	3.932887
KO MG 9	CR1	15.44933	4.928105
KO MG 9	CD46	10.10528	1.754266
KO MG 9	C1IN	12.09432	0.594712
KO MG 9	C6	999	999
KO MG 9	C3aR	6.770542	-4.32959
KO MG 9	DAF	12.54788	3.429976
KO MG 9	C2	6.744038	-0.5075
KO MG 9	C3	8.184988	-0.1025
KO MG 9	C1S	20.0087	-0.38044
KO MG 9	C1QA1	7.670034	1.716405
KO MG 9	FH	16.83387	-0.11326
KO MG 9	CR4	10.63546	-1.16904
KO MG 9	FB	999	999
KO MG 9	C9	11.45369	3.645591
KO MG 9	C5aR	8.231995	0.77367
KO MG 9	P2RY12	18.61023	7.152608
KO MG 9	C4	13.72245	1.179023
KO MG 9	FI	14.00121	3.69138
KO MG 9	CSMD1	14.95625	0.996783
KO MG 9	C5	14.32196	0.915911
KO MG 9	C1QB	11.20565	0.916738
KO MG 9	CD68	4.060963	0.905727
KO MG 9	NOS	11.38543	-8.08265
KO MG 9	IL1B	999	999
KO MG 9	NOS	999	999
KO MG 9	IL6	9.924936	-1.2699
KO MG 9	TNFA	8.691847	-6.07855
KO MG	BMP4	13.09814	3.277603
KO MG 9	CD34	16.13829	4.060387
KO MG 9	SOX2	23.5691	8.337604
KO MG 9	FLK1	11.6823	-0.42855
KO MG 9	CD45	17.87027	1.070904
KO MG 9	CD11B	9.066019	2.544066

KO MG 9	CD235a	12.84031	2.129034
KO MG 9	BRAC	11.26015	1.923273
KO MG 9	MERTK	18.30241	999
KO MG 9	RUNX1	999	999
KO MG 9	NESTIN	12.11148	2.45314
KO MG 9	MAP2	23.63221	5.595594
KO MG 9	NFKB	8.234136	1.219673
KO MG 9	NLRP3	11.51835	0.568112
KO MG 9	TREM2	13.05011	-0.0612
KO MG 9	IBA1	5.452859	-2.7898
KO MG 9	CD14	13.68912	1.507311
KO MG 9	VIMENTIN	3.129186	-0.81478
KO MG 9	GFAP	5.165002	-2.70466
KO MG 9	EAAT2	999	999
KO MG 9	ALDH1	12.04305	1.625491
KO MG 9	S100B	20.49192	3.272059
KO MG 9	NEUN	999	999
KO MG 9	CX3CR1	14.73418	4.65712
KO MG 9	BIN1	19.56948	3.004711
KO MG 9	TGFB	14.8238	3.254096
KO MG 9	TMEM119	7.789468	0.304218
KO MG 9	ABCA7	999	999
KO MG 9	PICALM	6.182218	-0.10133
KO MG 9	INPP5D	10.38435	2.463066
KO MG 9	APOE	9.705312	2.068653
KO MG 9	EPHA1	4.525712	0.197627
KO MG 9	HLA-DR	18.95738	5.309255
KO MG 9	PLCG2	3.436294	-0.11003
KO MG 9	CD33	14.88645	3.451007
KO MG 9	CR1	8.641156	-1.88007
KO MG 9	CD59	9.263113	0.47168
KO MG 9	MASP	10.20831	0.687188
KO MG 9	CR1	13.46013	2.938909
KO MG 9	CD46	8.840777	0.489769
KO MG 9	C1IN	12.12247	0.622866
KO MG 9	C6	999	999
KO MG 9	C3aR	6.905163	-4.19497
KO MG 9	DAF	11.35852	2.240619
KO MG 9	C2	7.459568	0.208031
KO MG 9	C3	7.709493	-0.57799
KO MG 9	C1S	19.55331	-0.83583
KO MG 9	C1QA1	5.856223	-0.09741
KO MG 9	FH	17.57747	0.630337
KO MG 9	CR4	11.77154	-0.03296
KO MG 9	FB	999	999
KO MG 9	C9	10.98932	3.181224

KO MG 9	C5aR	7.006359	-0.45197
KO MG 9	P2RY12	14.71929	3.261665
KO MG 9	C4	15.48066	2.93724
KO MG 9	FI	15.15742	4.847595
KO MG 9	CSMD1	16.39096	2.431487
KO MG 9	C5	14.43365	1.027605
KO MG 9	C1QB	9.551842	-0.73707
KO MG 9	CD68	3.413393	0.258156
KO MG 9	NOS	7.357574	-12.1105
KO MG 9	IL1B	999	999
KO MG 9	NOS	999	999
KO MG 9	IL6	10.09557	-1.09927
KO MG 9	TNFA	7.055419	-7.71498
KO MG 7	LIN28	9.680966	-0.29769
KO MG 7	Oct-04	9.569034	-0.55856
KO MG 7	BMP4	10.27457	0.45404
KO MG 7	CD34	11.51069	-0.56722
KO MG 7	SOX2	21.70335	6.471855
KO MG 7	FLK1	21.87766	9.766809
KO MG 7	CD45	999	999
KO MG 7	CD11B	12.9424	6.420446
KO MG 7	CD235a	999	999
KO MG 7	BRAC	19.34068	10.0038
KO MG 7	MERTK	22.80312	999
KO MG 7	RUNX1	22.55281	3.343895
KO MG 7	NESTIN	10.48193	0.823586
KO MG 7	MAP2	999	999
KO MG 7	NFKB	16.94095	9.926491
KO MG 7	NLRP3	28.946	17.99576
KO MG 7	TREM2	25.33515	12.22384
KO MG 7	IBA1	18.4294	10.18674
KO MG 7	CD14	17.90544	5.723626
KO MG 7	VIMENTIN	15.22837	11.28441
KO MG 7	GFAP	16.27725	8.407592
KO MG 7	EAAT2	999	999
KO MG 7	ALDH1	9.838059	-0.5795
KO MG 7	S100B	17.58346	0.363605
KO MG 7	NEUN	26.56241	1.91973
KO MG 7	CX3CR1	10.55504	0.477982
KO MG 7	BIN1	18.09662	1.531853
KO MG 7	TGFB	11.45302	-0.11668
KO MG 7	TMEM119	19.3677	11.88245
KO MG 7	ABCA7	24.58873	-0.54308
KO MG 7	PICALM	19.16409	12.88054
KO MG 7	INPP5D	20.97983	13.05855

KO MG 7	APOE	23.59207	15.95541
KO MG 7	EPHA1	16.39417	12.06608
KO MG 7	HLA-DR	15.13349	1.485372
KO MG 7	PLCG2	15.34933	11.80301
KO MG 7	CD33	19.81873	8.383284
KO MG 7	CR1	22.07673	11.55551
KO MG 7	CD59	20.98948	12.19805
KO MG 7	MASP	24.80847	15.28735
KO MG 7	CR1	22.00025	11.47902
KO MG 7	CD46	25.03048	16.67947
KO MG 7	C1IN	999	999
KO MG 7	C6	21.43106	2.837821
KO MG 7	C3aR	20.42907	9.328938
KO MG 7	DAF	20.45712	11.33922
KO MG 7	C2	16.49371	9.242178
KO MG 7	C3	999	999
KO MG 7	C1S	27.24886	6.859717
KO MG 7	C1QA1	12.58412	6.630489
KO MG 7	FH	999	999
KO MG 7	CR4	999	999
KO MG 7	FB	999	999
KO MG 7	C9	16.51788	8.709779
KO MG 7	C5aR	22.35591	14.89759
KO MG 7	P2RY12	999	999
KO MG 7	C4	23.77901	11.23559
KO MG 7	FI	10.47849	0.168659
KO MG 7	CSMD1	19.66341	5.703944
KO MG 7	C5	22.64898	9.242934
KO MG 7	C1QB	14.55339	4.264482
KO MG 7	CD68	15.11181	11.95657
KO MG 7	NOS	21.04656	1.578473
KO MG 5	BMP4	22.66238	12.84185
KO MG 5	CD34	999	999
KO MG 5	SOX2	21.06614	5.834644
KO MG 5	FLK1	21.28739	9.176539
KO MG 5	CD45	22.95041	6.151048
KO MG 5	CD11B	21.11502	14.59307
KO MG 5	CD235a	999	999
KO MG 5	BRAC	999	999
KO MG 5	MERTK	20.37324	999
KO MG 5	RUNX1	999	999
KO MG 5	NESTIN	18.61134	8.953005
KO MG 5	MAP2	23.13429	5.097672
KO MG 5	NFKB	20.42677	13.41231
KO MG 5	NLRP3	999	999

KO MG 5	TREM2	999	999
KO MG 5	IBA1	16.83708	8.594419
KO MG 5	CD14	999	999
KO MG 5	VIMENTIN	13.82945	9.88548
KO MG 5	GFAP	15.43618	7.566521
KO MG 5	EAAT2	999	999
KO MG 5	ALDH1	999	999
KO MG 5	S100B	25.8937	8.673839
KO MG 5	NEUN	20.53542	-4.10726
KO MG 5	CX3CR1	23.86497	13.78791
KO MG 5	BIN1	999	999
KO MG 5	TGFB	999	999
KO MG 5	TMEM119	999	999
KO MG 5	ABCA7	999	999
KO MG 5	PICALM	18.4548	12.17125
KO MG 5	INPP5D	999	999
KO MG 5	APOE	999	999
KO MG 5	EPHA1	16.44075	12.11266
KO MG 5	HLA-DR	999	999
KO MG 5	PLCG2	20.99415	17.44783
KO MG 5	CD33	999	999
KO MG 5	CR1	999	999
KO MG 5	CD59	999	999
KO MG 5	MASP	999	999
KO MG 5	CR1	999	999
KO MG 5	CD46	22.15881	13.80781
KO MG 5	C1IN	20.1852	8.685594
KO MG 5	C6	999	999
KO MG 5	C3aR	999	999
KO MG 5	DAF	999	999
KO MG 5	C2	14.62602	7.374483
KO MG 5	C3	999	999
KO MG 5	C1S	999	999
KO MG 5	C1QA1	999	999
KO MG 5	FH	999	999
KO MG 5	CR4	999	999
KO MG 5	FB	999	999
KO MG 5	C9	19.3963	11.5882
KO MG 5	C5aR	999	999
KO MG 5	P2RY12	999	999
KO MG 5	C4	22.84557	10.30215
KO MG 5	FI	999	999
KO MG 5	CSMD1	18.88553	4.926065
KO MG 5	C5	999	999
KO MG 5	C1QB	18.13611	7.847196
KO MG 5	CD68	20.77474	17.61951

KO MG 5	NOS	19.6967	0.228608
KO MG 5	IL1B	999	999
KO MG 5	NOS	999	999
KO MG 5	IL6	999	999
KO MG 5	TNFA	999	999
KO LPS 2	BMP4	12.57175	2.751213
KO LPS 2	CD34	13.08582	1.007919
KO LPS 2	SOX2	12.94245	-2.28905
KO LPS 2	FLK1	12.87192	0.761065
KO LPS 2	CD45	11.88746	-4.9119
KO LPS 2	CD11B	11.21884	4.69689
KO LPS 2	CD235a	11.94745	1.236178
KO LPS 2	BRAC	12.96051	3.623626
KO LPS 2	MERTK	13.65257	999
KO LPS 2	RUNX1	13.49179	-5.71713
KO LPS 2	NESTIN	12.27674	2.618396
KO LPS 2	MAP2	12.55911	-5.47751
KO LPS 2	NFKB	12.33383	5.319368
KO LPS 2	NLRP3	11.72975	0.779507
KO LPS 2	TREM2	11.72369	-1.38761
KO LPS 2	IBA1	11.67197	3.429308
KO LPS 2	CD14	9.91165	-2.27016
KO LPS 2	VIMENTIN	7.180624	3.236657
KO LPS 2	GFAP	7.308159	-0.5615
KO LPS 2	EAAT2	11.37476	999
KO LPS 2	ALDH1	13.92052	3.502955
KO LPS 2	S100B	18.46531	1.24545
KO LPS 2	NEUN	12.36566	-12.277
KO LPS 2	CX3CR1	13.47048	3.393426
KO LPS 2	BIN1	13.95897	-2.6058
KO LPS 2	TGFB	13.62183	2.052121
KO LPS 2	TMEM119	999	999
KO LPS 2	ABCA7	10.91251	-14.2193
KO LPS 2	PICALM	10.69267	4.409127
KO LPS 2	INPP5D	10.0904	2.169118
KO LPS 2	APOE	8.205437	0.568778
KO LPS 2	EPHA1	8.50714	4.179055
KO LPS 2	HLA-DR	10.51048	-3.13764
KO LPS 2	PLCG2	9.106169	5.559847
KO LPS 2	CD33	10.75041	-0.68504
KO LPS 2	CR1	27.57248	17.05125
KO LPS 2	CD59	11.50845	2.717013
KO LPS 2	MASP	11.5204	1.999276
KO LPS 2	CR1	14.92046	4.399237
KO LPS 2	CD46	999	999

KO LPS 2	C1IN	15.36748	3.86787
KO LPS 2	C6	23.59375	5.000509
KO LPS 2	C3aR	11.95509	0.854952
KO LPS 2	DAF	11.54944	2.431539
KO LPS 2	C2	11.59505	4.343514
KO LPS 2	C3	11.91132	3.623832
KO LPS 2	C1S	10.54112	-9.84802
KO LPS 2	C1QA1	11.58905	5.635425
KO LPS 2	FH	18.76762	1.820487
KO LPS 2	CR4	12.18571	0.381212
KO LPS 2	FB	10.45244	999
KO LPS 2	C9	11.49643	3.688338
KO LPS 2	C5aR	12.8322	5.373879
KO LPS 2	P2RY12	16.39165	4.934031
KO LPS 2	C4	15.69404	3.150613
KO LPS 2	FI	15.85963	5.549803
KO LPS 2	CSMD1	12.43545	-1.52402
KO LPS 2	C5	11.74196	-1.66409
KO LPS 2	C1QB	14.1254	3.836488
KO LPS 2	CD68	999	999
KO LPS 2	NOS	999	999
KO LPS 2	IL1B	999	999
KO LPS 2	NOS	999	999
KO LPS 2	IL6	13.21329	2.018459
KO LPS 2	TNFA	999	999
KO LPS 3	Oct-04	11.22967	1.10208
KO LPS 3	BMP4	12.3777	2.557168
KO LPS 3	CD34	14.1678	2.089898
KO LPS 3	SOX2	18.76523	3.533732
KO LPS 3	FLK1	9.506056	-2.60479
KO LPS 3	CD45	22.27328	5.473917
KO LPS 3	CD11B	8.460646	1.938694
KO LPS 3	CD235a	11.01442	0.303149
KO LPS 3	BRAC	9.223321	-0.11356
KO LPS 3	MERTK	24.20021	999
KO LPS 3	RUNX1	16.87317	-2.33575
KO LPS 3	NESTIN	10.89827	1.239931
KO LPS 3	MAP2	16.66418	-1.37243
KO LPS 3	NFKB	9.089744	2.075281
KO LPS 3	NLRP3	13.45797	2.507726
KO LPS 3	TREM2	14.86034	1.749034
KO LPS 3	IBA1	8.640846	0.398185
KO LPS 3	CD14	13.00731	0.825503
KO LPS 3	VIMENTIN	3.512753	-0.43121
KO LPS 3	GFAP	7.543943	-0.32572

KO LPS 3	EAAT2	23.85983	999
KO LPS 3	ALDH1	11.18775	0.770186
KO LPS 3	S100B	19.17838	1.958518
KO LPS 3	NEUN	24.92488	0.282202
KO LPS 3	CX3CR1	12.81212	2.735063
KO LPS 3	BIN1	19.0773	2.512526
KO LPS 3	TGFB	10.36945	-1.20025
KO LPS 3	TMEM119	7.927983	0.442733
KO LPS 3	ABCA7	999	999
KO LPS 3	PICALM	7.009027	0.72548
KO LPS 3	INPP5D	9.738922	1.817638
KO LPS 3	APOE	10.49428	2.857622
KO LPS 3	EPHA1	5.730857	1.402773
KO LPS 3	HLA-DR	16.16789	2.519768
KO LPS 3	PLCG2	4.558968	1.012646
KO LPS 3	CD33	15.72673	4.291285
KO LPS 3	CR1	10.16891	-0.35231
KO LPS 3	CD59	10.09967	1.308235
KO LPS 3	MASP	12.07519	2.554068
KO LPS 3	CR1	10.90745	0.386223
KO LPS 3	CD46	9.883832	1.532823
KO LPS 3	C1IN	10.69142	-0.80818
KO LPS 3	C6	27.02037	8.427135
KO LPS 3	C3aR	7.89266	-3.20747
KO LPS 3	DAF	12.09365	2.975752
KO LPS 3	C2	8.177094	0.925557
KO LPS 3	C3	11.28302	2.995535
KO LPS 3	C1S	17.07816	-3.31098
KO LPS 3	C1QA1	7.597338	1.64371
KO LPS 3	FH	17.21582	0.268683
KO LPS 3	CR4	11.91217	0.107672
KO LPS 3	FB	999	999
KO LPS 3	C9	8.524128	0.716032
KO LPS 3	C5aR	9.510266	2.051941
KO LPS 3	P2RY12	14.78409	3.326473
KO LPS 3	C4	13.40485	0.861431
KO LPS 3	FI	12.72389	2.414062
KO LPS 3	CSMD1	9.741729	-4.21774
KO LPS 3	C5	12.3478	-1.05825
KO LPS 3	C1QB	11.69847	1.409557
KO LPS 3	CD68	4.980337	1.8251
KO LPS 3	NOS	13.79673	-5.67136
KO LPS 3	IL1B	999	999
KO LPS 3	NOS	999	999
KO LPS 3	IL6	12.3331	1.138262
KO LPS 3	TNFA	15.41405	0.643648

KO MG LPS 1	LIN28	13.22768	3.249027
KO MG LPS 1	Oct-04	13.77977	3.652181
KO MG LPS 1	BMP4	11.18409	1.363556
KO MG LPS 1	CD34	15.54486	3.466956
KO MG LPS 1	SOX2	18.71707	3.485578
KO MG LPS 1	FLK1	13.3965	1.285645
KO MG LPS 1	CD45	20.74937	3.950004
KO MG LPS 1	CD11B	10.81093	4.288976
KO MG LPS 1	CD235a	15.99245	5.281173
KO MG LPS 1	BRAC	14.07303	4.736147
KO MG LPS 1	MERTK	19.22469	999
KO MG LPS 1	RUNX1	19.56465	0.355737
KO MG LPS 1	NESTIN	13.51596	3.857625
KO MG LPS 1	MAP2	18.89751	0.860892
KO MG LPS 1	NFKB	12.78479	5.770327
KO MG LPS 1	NLRP3	15.56454	4.614296
KO MG LPS 1	TREM2	21.09201	7.980708
KO MG LPS 1	IBA1	12.82229	4.579628
KO MG LPS 1	CD14	17.446	5.264194
KO MG LPS 1	VIMENTIN	6.938671	2.994704
KO MG LPS 1	GFAP	11.11472	3.245061
KO MG LPS 1	EAAT2	999	999
KO MG LPS 1	ALDH1	13.17884	2.761278
KO MG LPS 1	S100B	20.44007	3.220208
KO MG LPS 1	NEUN	22.80412	-1.83856
KO MG LPS 1	CX3CR1	14.64938	4.572321
KO MG LPS 1	BIN1	22.11989	5.555119
KO MG LPS 1	TGFB	14.18813	2.618427
KO MG LPS 1	TMEM119	11.31524	3.829986
KO MG LPS 1	ABCA7	23.64897	-1.48285
KO MG LPS 1	PICALM	10.77616	4.492612
KO MG LPS 1	INPP5D	13.06087	5.139584
KO MG LPS 1	APOE	12.82056	5.1839
KO MG LPS 1	EPHA1	8.209845	3.881761
KO MG LPS 1	HLA-DR	16.58944	2.941313
KO MG LPS 1	PLCG2	8.159824	4.613502
KO MG LPS 1	CD33	17.07813	5.642684
KO MG LPS 1	CR1	11.8358	1.314575
KO MG LPS 1	CD59	13.05526	4.263831
KO MG LPS 1	MASP	13.85192	4.330802
KO MG LPS 1	CR1	15.84335	5.322125
KO MG LPS 1	CD46	12.91789	4.566883
KO MG LPS 1	C1IN	14.67756	3.177953
KO MG LPS 1	C6	999	999
KO MG LPS 1	C3aR	14.82064	3.720507

KO MG LPS 1	DAF	13.38493	4.267036
KO MG LPS 1	C2	11.76505	4.513515
KO MG LPS 1	C3	14.41334	6.12585
KO MG LPS 1	C1S	999	999
KO MG LPS 1	C1QA1	10.55713	4.603502
KO MG LPS 1	FH	20.18549	3.238358
KO MG LPS 1	CR4	16.17931	4.374816
KO MG LPS 1	FB	999	999
KO MG LPS 1	C9	13.66826	5.860164
KO MG LPS 1	C5aR	11.32497	3.866641
KO MG LPS 1	P2RY12	17.56885	6.111225
KO MG LPS 1	C4	17.35282	4.809396
KO MG LPS 1	FI	13.98217	3.672337
KO MG LPS 1	CSMD1	15.73587	1.776399
KO MG LPS 1	C5	14.32805	0.922006
KO MG LPS 1	C1QB	13.88624	3.597325
KO MG LPS 1	CD68	6.25751	3.102273
KO MG LPS 1	NOS	21.47136	2.003274
KO MG LPS 1	IL1B	999	999
KO MG LPS 1	NOS	999	999
KO MG LPS 1	IL6	17.10561	5.910777
KO MG LPS 1	TNFA	19.69818	4.927774
KO LPS 4	BMP4	11.8957	2.075169
KO LPS 4	CD34	11.87045	-0.20745
KO LPS 4	SOX2	11.8484	-3.3831
KO LPS 4	FLK1	11.7322	-0.37865
KO LPS 4	CD45	11.97292	-4.82645
KO LPS 4	CD11B	8.563567	2.041615
KO LPS 4	CD235a	11.36	0.648724
KO LPS 4	BRAC	11.18605	1.84917
KO LPS 4	MERTK	11.62509	999
KO LPS 4	RUNX1	11.85805	-7.35086
KO LPS 4	NESTIN	11.26324	1.6049
KO LPS 4	MAP2	11.74847	-6.28815
KO LPS 4	NFKB	10.24319	3.228732
KO LPS 4	NLRP3	11.56055	0.610306
KO LPS 4	TREM2	11.67379	-1.43752
KO LPS 4	IBA1	9.367843	1.125182
KO LPS 4	CD14	11.32217	-0.85964
KO LPS 4	VIMENTIN	4.339269	0.395302
KO LPS 4	GFAP	8.0912	0.22154
KO LPS 4	EAAT2	11.66179	999
KO LPS 4	ALDH1	10.00658	-0.41099
KO LPS 4	S100B	11.84711	-5.37275
KO LPS 4	NEUN	11.84738	-12.7953

KO LPS 4	CX3CR1	11.70037	1.623314
KO LPS 4	BIN1	11.89859	-4.66618
KO LPS 4	TGFB	9.990369	-1.57934
KO LPS 4	TMEM119	8.957864	1.472614
KO LPS 4	ABCA7	11.82455	-13.3073
KO LPS 4	PICALM	8.717004	2.433457
KO LPS 4	INPP5D	11.69989	3.778609
KO LPS 4	APOE	10.57777	2.941113
KO LPS 4	EPHA1	8.926714	4.598629
KO LPS 4	HLA-DR	11.75181	-1.89631
KO LPS 4	PLCG2	4.76324	1.216918
KO LPS 4	CD33	11.73811	0.302662
KO LPS 4	CR1	11.421	0.899777
KO LPS 4	CD59	10.86299	2.071553
KO LPS 4	MASP	11.66255	2.141426
KO LPS 4	CR1	11.70732	1.186099
KO LPS 4	CD46	10.80906	2.458055
KO LPS 4	C1IN	11.28731	-0.2123
KO LPS 4	C6	11.571	-7.02224
KO LPS 4	C3aR	9.347706	-1.75243
KO LPS 4	DAF	11.59643	2.478533
KO LPS 4	C2	8.752376	1.500839
KO LPS 4	C3	10.07443	1.786946
KO LPS 4	C1S	11.82892	-8.56022
KO LPS 4	C1QA1	9.322095	3.368466
KO LPS 4	FH	11.78676	-5.16037
KO LPS 4	CR4	11.05149	-0.75301
KO LPS 4	FB	11.76046	999
KO LPS 4	C9	11.2501	3.442001
KO LPS 4	C5aR	9.856598	2.398273
KO LPS 4	P2RY12	11.79106	0.333443
KO LPS 4	C4	11.65054	-0.89289
KO LPS 4	FI	11.76794	1.458113
KO LPS 4	CSMD1	11.77794	-2.18153
KO LPS 4	C5	11.60673	-1.79931
KO LPS 4	C1QB	10.93297	0.644054
KO LPS 4	CD68	5.92799	2.772753
KO LPS 4	NOS	11.3199	-8.14819
KO LPS 4	IL1B	11.76362	999
KO LPS 4	NOS	11.81917	-7.64892
KO LPS 4	IL6	10.8831	-0.31174
KO LPS 4	TNFA	10.24171	-4.52869
Astro 1	LIN28	999	999
Astro 1	Oct-04	21.08757	10.95998
Astro 1	BMP4	999	999

Astro 1	CD34	14.8731	2.795197
Astro 1	SOX2	20.04572	4.81423
Astro 1	FLK1	17.20261	5.09176
Astro 1	CD45	999	999
Astro 1	CD11B	999	999
Astro 1	CD235a	16.89094	6.179663
Astro 1	BRAC	999	999
Astro 1	MERTK	21.51864	999
Astro 1	RUNX1	999	999
Astro 1	NESTIN	17.93269	8.274346
Astro 1	MAP2	19.46211	1.425497
Astro 1	NFKB	23.80656	16.7921
Astro 1	NLRP3	999	999
Astro 1	TREM2	999	999
Astro 1	IBA1	17.7352	9.492542
Astro 1	CD14	999	999
Astro 1	VIMENTIN	10.42455	6.480584
Astro 1	GFAP	15.73251	7.862852
Astro 1	EAAT2	999	999
Astro 1	ALDH1	17.19158	6.774018
Astro 1	S100B	20.24811	3.028254
Astro 1	NEUN	24.50745	-0.13523
Astro 1	CX3CR1	22.56565	12.48859
Astro 1	BIN1	25.60649	9.041717
Astro 1	TGFB	999	999
Astro 1	TMEM119	16.95421	9.468961
Astro 1	ABCA7	999	999
Astro 1	PICALM	14.01503	7.731481
Astro 1	INPP5D	19.98553	12.06424
Astro 1	APOE	999	999
Astro 1	EPHA1	17.56501	13.23693
Astro 1	HLA-DR	24.07963	10.4315
Astro 1	PLCG2	20.6041	17.05777
Astro 1	CD33	999	999
Astro 1	CR1	999	999
Astro 1	CD59	19.5104	10.71897
Astro 1	MASP	999	999
Astro 1	CR1	22.12371	11.60249
Astro 1	CD46	20.96857	12.61756
Astro 1	C1IN	19.93249	8.432878
Astro 1	C6	999	999
Astro 1	C3aR	999	999
Astro 1	DAF	999	999
Astro 1	C2	18.62141	11.36988
Astro 1	C3	22.18906	13.90157
Astro 1	C1S	999	999

Astro 1	C1QA1	24.10939	18.15576
Astro 1	FH	999	999
Astro 1	CR4	19.41999	7.615493
Astro 1	FB	999	999
Astro 1	C9	17.54812	9.740028
Astro 1	C5aR	999	999
Astro 1	P2RY12	999	999
Astro 1	C4	999	999
Astro 1	FI	999	999
Astro 1	CSMD1	14.7682	0.808734
Astro 1	C5	15.42352	2.01747
Astro 1	C1QB	19.88859	9.599682
Astro 1	CD68	18.0733	14.91806
Astro 1	NOS	26.52994	7.061852
Astro 1	IL1B	999	999
Astro 1	NOS	999	999
Astro 1	IL6	999	999
Astro 1	TNFA	999	999
Astro 2	LIN28	999	999
Astro 2	Oct-04	15.73533	5.60774
Astro 2	BMP4	15.4891	5.668568
Astro 2	CD34	6.806865	-5.27104
Astro 2	SOX2	17.65503	2.423534
Astro 2	FLK1	14.31422	2.203371
Astro 2	CD45	999	999
Astro 2	CD11B	22.04529	15.52334
Astro 2	CD235a	13.85407	3.142801
Astro 2	BRAC	13.60457	4.267689
Astro 2	MERTK	999	999
Astro 2	RUNX1	15.0244	-4.18452
Astro 2	NESTIN	12.70166	3.043318
Astro 2	MAP2	8.674743	-9.36187
Astro 2	NFKB	24.39378	17.37932
Astro 2	NLRP3	999	999
Astro 2	TREM2	999	999
Astro 2	IBA1	11.71181	3.469154
Astro 2	CD14	21.96758	9.78577
Astro 2	VIMENTIN	3.223559	-0.72041
Astro 2	GFAP	6.758041	-1.11162
Astro 2	EAAT2	16.86657	999
Astro 2	ALDH1	9.826711	-0.59085
Astro 2	S100B	13.78241	-3.43745
Astro 2	NEUN	26.16556	1.522886
Astro 2	CX3CR1	21.56308	11.48603
Astro 2	BIN1	22.58457	6.019802

Astro 2	TGFB	999	999
Astro 2	TMEM119	9.70945	2.224199
Astro 2	ABCA7	999	999
Astro 2	PICALM	8.489529	2.205982
Astro 2	INPP5D	15.26447	7.343182
Astro 2	APOE	17.74126	10.1046
Astro 2	EPHA1	8.613121	4.285037
Astro 2	HLA-DR	24.01094	10.36282
Astro 2	PLCG2	16.17987	12.63355
Astro 2	CD33	999	999
Astro 2	CR1	999	999
Astro 2	CD59	13.65629	4.864856
Astro 2	MASP	999	999
Astro 2	CR1	13.64397	3.122742
Astro 2	CD46	10.71934	2.368328
Astro 2	C1IN	15.50694	4.007333
Astro 2	C6	999	999
Astro 2	C3aR	21.16363	10.06349
Astro 2	DAF	20.22357	11.10567
Astro 2	C2	16.24121	8.989674
Astro 2	C3	21.08705	12.79956
Astro 2	C1S	20.87066	0.48152
Astro 2	C1QA1	999	999
Astro 2	FH	999	999
Astro 2	CR4	14.48059	2.676097
Astro 2	FB	999	999
Astro 2	C9	13.57197	5.763874
Astro 2	C5aR	999	999
Astro 2	P2RY12	999	999
Astro 2	C4	13.32616	0.782738
Astro 2	FI	18.68237	8.372545
Astro 2	CSMD1	6.664097	-7.29537
Astro 2	C5	7.24826	-6.15779
Astro 2	C1QB	17.45462	7.165704
Astro 2	CD68	12.97715	9.821917
Astro 2	NOS	25.2386	5.77051
Astro 2	IL1B	999	999
Astro 2	NOS	999	999
Astro 2	IL6	999	999
Astro 2	TNFA	999	999
Astro 3	LIN28	12.57014	2.591486
Astro 3	Oct-04	13.38552	3.257935
Astro 3	BMP4	16.00193	6.181399
Astro 3	CD34	17.01028	4.932375
Astro 3	SOX2	999	999

Astro 3	FLK1	999	999
Astro 3	CD45	999	999
Astro 3	CD11B	14.14102	7.61907
Astro 3	CD235a	19.81013	9.098853
Astro 3	BRAC	21.55528	12.2184
Astro 3	MERTK	23.93913	999
Astro 3	RUNX1	22.52951	3.320595
Astro 3	NESTIN	21.32498	11.66664
Astro 3	MAP2	24.42633	6.389713
Astro 3	NFKB	16.21507	9.200611
Astro 3	NLRP3	26.79081	15.84057
Astro 3	TREM2	999	999
Astro 3	IBA1	19.12246	10.87979
Astro 3	CD14	18.88912	6.707307
Astro 3	VIMENTIN	15.82028	11.87631
Astro 3	GFAP	23.06093	15.19127
Astro 3	EAAT2	999	999
Astro 3	ALDH1	23.28188	12.86431
Astro 3	S100B	999	999
Astro 3	NEUN	999	999
Astro 3	CX3CR1	999	999
Astro 3	BIN1	999	999
Astro 3	TGFB	21.83083	10.26113
Astro 3	TMEM119	17.16523	9.679983
Astro 3	ABCA7	999	999
Astro 3	PICALM	19.24823	12.96468
Astro 3	INPP5D	19.79961	11.87832
Astro 3	APOE	23.12958	15.49293
Astro 3	EPHA1	17.65779	13.32971
Astro 3	HLA-DR	17.23103	3.582909
Astro 3	PLCG2	13.48601	9.939683
Astro 3	CD33	23.59278	12.15734
Astro 3	CR1	999	999
Astro 3	CD59	21.04582	12.25439
Astro 3	MASP	999	999
Astro 3	CR1	23.31244	12.79121
Astro 3	CD46	22.12756	13.77656
Astro 3	C1IN	20.19102	8.691416
Astro 3	C6	999	999
Astro 3	C3aR	999	999
Astro 3	DAF	27.74799	18.63009
Astro 3	C2	19.22105	11.96951
Astro 3	C3	999	999
Astro 3	C1S	999	999
Astro 3	C1QA1	15.05997	9.10634
Astro 3	FH	999	999

Astro 3	CR4	22.23627	10.43177
Astro 3	FB	999	999
Astro 3	C9	999	999
Astro 3	C5aR	25.27164	17.81331
Astro 3	P2RY12	999	999
Astro 3	C4	20.85764	8.314222
Astro 3	FI	999	999
Astro 3	CSMD1	23.64425	9.684785
Astro 3	C5	999	999
Astro 3	C1QB	16.46373	6.174821
Astro 3	CD68	15.09109	11.93585
Astro 3	NOS	22.75463	3.286537
Astro 3	IL1B	999	999
Astro 3	NOS	999	999
Astro 3	IL6	19.91874	8.723901
Astro 3	TNFA	23.95517	9.184766
Neuronal 1	CD34	23.74055	11.66265
Neuronal 1	SOX2	21.60308	6.371588
Neuronal 1	FLK1	20.02915	7.918303
Neuronal 1	CD45	999	999
Neuronal 1	CD11B	13.83779	7.315833
Neuronal 1	CD235a	19.51171	8.800439
Neuronal 1	BRAC	16.65346	7.316577
Neuronal 1	MERTK	18.99205	999
Neuronal 1	RUNX1	999	999
Neuronal 1	NESTIN	17.97047	8.312129
Neuronal 1	MAP2	999	999
Neuronal 1	NFKB	15.82014	8.805674
Neuronal 1	NLRP3	20.1484	9.198163
Neuronal 1	TREM2	22.07485	8.963546
Neuronal 1	IBA1	16.91811	8.675453
Neuronal 1	CD14	19.39519	7.213381
Neuronal 1	VIMENTIN	11.67262	7.728657
Neuronal 1	GFAP	17.18524	9.315583
Neuronal 1	EAAT2	999	999
Neuronal 1	ALDH1	999	999
Neuronal 1	S100B	22.26107	5.041216
Neuronal 1	NEUN	22.41255	-2.23013
Neuronal 1	CX3CR1	22.34095	12.26389
Neuronal 1	BIN1	999	999
Neuronal 1	TGFB	19.46347	7.893766
Neuronal 1	TMEM119	14.41199	6.926741
Neuronal 1	ABCA7	999	999
Neuronal 1	PICALM	17.12519	10.84164
Neuronal 1	INPP5D	17.16762	9.246336

Neuronal 1	APOE	17.66344	10.02678
Neuronal 1	EPHA1	17.46721	13.13913
Neuronal 1	HLA-DR	22.91773	9.269611
Neuronal 1	PLCG2	11.23445	7.688125
Neuronal 1	CD33	20.92369	9.488244
Neuronal 1	CR1	999	999
Neuronal 1	CD59	20.04529	11.25386
Neuronal 1	MASP	20.29087	10.76975
Neuronal 1	CR1	23.72408	13.20285
Neuronal 1	CD46	19.55591	11.20491
Neuronal 1	C1IN	20.91423	9.414626
Neuronal 1	C6	999	999
Neuronal 1	C3aR	22.35951	11.25938
Neuronal 1	DAF	19.32306	10.20516
Neuronal 1	C2	18.76598	11.51444
Neuronal 1	C3	999	999
Neuronal 1	C1S	999	999
Neuronal 1	C1QA1	13.21974	7.266113
Neuronal 1	FH	999	999
Neuronal 1	CR4	19.17062	7.36612
Neuronal 1	FB	999	999
Neuronal 1	C9	21.04463	13.23654
Neuronal 1	C5aR	18.67712	11.21879
Neuronal 1	P2RY12	999	999
Neuronal 1	C4	19.79341	7.249983
Neuronal 1	FI	999	999
Neuronal 1	CSMD1	999	999
Neuronal 1	C5	999	999
Neuronal 1	C1QB	16.37466	6.085749
Neuronal 1	CD68	10.46049	7.305258
Neuronal 1	NOS	24.65882	5.19073
Neuronal 1	IL1B	999	999
Neuronal 1	NOS	999	999
Neuronal 1	IL6	19.97301	8.778176
Neuronal 1	TNFA	20.83784	6.067433
Neuronal 2	LIN28	13.27114	3.29249
Neuronal 2	Oct-04	8.614518	-1.51307
Neuronal 2	BMP4	12.33327	2.512737
Neuronal 2	CD34	6.820644	-5.25726
Neuronal 2	SOX2	16.25018	1.01869
Neuronal 2	FLK1	15.23925	3.128399
Neuronal 2	CD45	999	999
Neuronal 2	CD11B	16.58956	10.0676
Neuronal 2	CD235a	15.62406	4.912789
Neuronal 2	BRAC	14.86016	5.523278

Neuronal 2	MERTK	22.31042	999
Neuronal 2	RUNX1	9.947115	-9.2618
Neuronal 2	NESTIN	11.69751	2.039174
Neuronal 2	MAP2	6.55666	-11.48
Neuronal 2	NFKB	22.70844	15.69398
Neuronal 2	NLRP3	999	999
Neuronal 2	TREM2	18.53779	5.426487
Neuronal 2	IBA1	11.84142	3.598755
Neuronal 2	CD14	17.28096	5.099149
Neuronal 2	VIMENTIN	5.351146	1.407179
Neuronal 2	GFAP	10.91931	3.04965
Neuronal 2	EAAT2	16.46328	999
Neuronal 2	ALDH1	6.06384	-4.35372
Neuronal 2	S100B	15.11018	-2.10968
Neuronal 2	NEUN	20.61812	-4.02456
Neuronal 2	CX3CR1	15.23239	5.155328
Neuronal 2	BIN1	19.70947	3.144704
Neuronal 2	TGFB	15.65791	4.088204
Neuronal 2	TMEM119	11.78593	4.300684
Neuronal 2	ABCA7	999	999
Neuronal 2	PICALM	8.202546	1.918999
Neuronal 2	INPP5D	17.89494	9.973651
Neuronal 2	APOE	16.58055	8.943895
Neuronal 2	EPHA1	9.957725	5.629641
Neuronal 2	HLA-DR	19.52258	5.874458
Neuronal 2	PLCG2	11.48315	7.936824
Neuronal 2	CD33	999	999
Neuronal 2	CR1	999	999
Neuronal 2	CD59	11.93246	3.141027
Neuronal 2	MASP	22.22541	12.70429
Neuronal 2	CR1	999	999
Neuronal 2	CD46	10.60789	2.256882
Neuronal 2	C1IN	15.44518	3.945568
Neuronal 2	C6	16.47424	-2.119
Neuronal 2	C3aR	15.71057	4.610438
Neuronal 2	DAF	17.7051	8.587204
Neuronal 2	C2	13.52915	6.277608
Neuronal 2	C3	999	999
Neuronal 2	C1S	19.53953	-0.84961
Neuronal 2	C1QA1	18.39825	12.44462
Neuronal 2	FH	999	999
Neuronal 2	CR4	17.63045	5.82595
Neuronal 2	FB	999	999
Neuronal 2	C9	16.52169	8.713593
Neuronal 2	C5aR	24.26385	16.80553
Neuronal 2	P2RY12	999	999

Neuronal 2	C4	12.35991	-0.18352
Neuronal 2	FI	10.71552	0.405687
Neuronal 2	CSMD1	9.363064	-4.59641
Neuronal 2	C5	9.217148	-4.1889
Neuronal 2	C1QB	16.85455	6.565634
Neuronal 2	CD68	11.64695	8.491718
Neuronal 2	NOS	24.11017	4.64208
Neuronal 2	IL1B	26.21992	999
Neuronal 2	NOS	999	999
Neuronal 2	IL6	999	999
Neuronal 2	TNFA	20.88882	6.118415
Neuronal 3	LIN28	21.16381	11.18515
Neuronal 3	Oct-04	17.65418	7.526588
Neuronal 3	BMP4	16.15775	6.337216
Neuronal 3	CD34	22.05682	9.978915
Neuronal 3	SOX2	20.96011	5.728618
Neuronal 3	FLK1	17.61654	5.50569
Neuronal 3	CD45	26.91566	10.11629
Neuronal 3	CD11B	12.08479	5.562836
Neuronal 3	CD235a	17.74498	7.03371
Neuronal 3	BRAC	14.38431	5.047429
Neuronal 3	MERTK	21.2516	999
Neuronal 3	RUNX1	999	999
Neuronal 3	NESTIN	17.28236	7.624018
Neuronal 3	MAP2	22.54376	4.507144
Neuronal 3	NFKB	12.38189	5.367427
Neuronal 3	NLRP3	16.88625	5.936007
Neuronal 3	TREM2	20.01303	6.901726
Neuronal 3	IBA1	14.77775	6.535087
Neuronal 3	CD14	15.32284	3.141027
Neuronal 3	VIMENTIN	9.640454	5.696487
Neuronal 3	GFAP	15.42257	7.552912
Neuronal 3	EAAT2	999	999
Neuronal 3	ALDH1	19.63818	9.220614
Neuronal 3	S100B	24.13079	6.910936
Neuronal 3	NEUN	999	999
Neuronal 3	CX3CR1	20.66336	10.5863
Neuronal 3	BIN1	21.5678	5.003033
Neuronal 3	TGFB	17.06393	5.494223
Neuronal 3	TMEM119	12.23651	4.751264
Neuronal 3	ABCA7	999	999
Neuronal 3	PICALM	14.90853	8.624982
Neuronal 3	INPP5D	14.1069	6.185611
Neuronal 3	APOE	15.13626	7.499602
Neuronal 3	EPHA1	12.70996	8.381876

Neuronal 3	HLA-DR	999	999
Neuronal 3	PLCG2	10.54382	6.9975
Neuronal 3	CD33	19.88832	8.452873
Neuronal 3	CR1	999	999
Neuronal 3	CD59	15.54391	6.752475
Neuronal 3	MASP	18.56061	9.039489
Neuronal 3	CR1	999	999
Neuronal 3	CD46	16.6487	8.297694
Neuronal 3	C1IN	20.72628	9.226675
Neuronal 3	C6	999	999
Neuronal 3	C3aR	15.26255	4.162419
Neuronal 3	DAF	17.05865	7.940751
Neuronal 3	C2	15.18346	7.93192
Neuronal 3	C3	18.66728	10.37979
Neuronal 3	C1S	999	999
Neuronal 3	C1QA1	12.82575	6.872123
Neuronal 3	FH	999	999
Neuronal 3	CR4	17.15674	5.352242
Neuronal 3	FB	999	999
Neuronal 3	C9	18.48975	10.68166
Neuronal 3	C5aR	15.03342	7.575098
Neuronal 3	P2RY12	16.53124	5.073622
Neuronal 3	C4	17.06453	4.521107
Neuronal 3	FI	999	999
Neuronal 3	CSMD1	999	999
Neuronal 3	C5	19.7176	6.311553
Neuronal 3	C1QB	15.77203	5.48312
Neuronal 3	CD68	8.843244	5.688007
Neuronal 3	NOS	22.90617	3.438084
Neuronal 3	IL1B	999	999
Neuronal 3	NOS	999	999
Neuronal 3	IL6	19.72748	8.532644
Neuronal 3	TNFA	17.91669	3.146286

9.3 Appendix 3 HTA consent form

The following consent form was given to all individuals who donated blood for ghost pellet generation. Blood was not stored but was immediately processed as explained in the methods.

Medical / Dental School Research Ethics Committee

PARTICIPANT INFORMATION SHEET & CONSENT FORM

Project Title: Mechanisms of complement activation and regulation.

You are being invited to take part in a research study. Before you decide it is important for you to understand why the research is being done and what it will involve. Please take time to read the following information carefully and discuss it with others if you wish. Ask us if there is anything that is not clear or if you would like more information. Take time to decide whether or not you wish to take part.

What is the purpose of the study?

Complement is part of the immune system, present in blood, which helps fight infection by killing bacteria and other foreign organisms. However, sometimes it can go out of control and harm the body, causing disease. The reason for this lack of control is not always obvious. In order to understand how complement is involved in disease progression, it is essential to understand how complement works normally and how our body stops it causing any harm to ourselves. Once we know this, we can then start to understand how complement may be involved in disease in 'abnormal' conditions. We will take blood samples from normal, healthy volunteers and isolate individual complement components or regulators of complement (natural 'control' proteins) from plasma or from the membranes of red blood cells. **Purification of these proteins will enable in-depth analysis of their functional activity in the laboratory.** In addition, whole serum or cells (harvested form the blood) will be used in standard laboratory assays to analyse how active the complement is or how the cells are protecting themselves. Precise knowledge of the mechanisms by which C is normally activated and regulated, and the influence of these small variations or changes, will help us understand how disease is caused, how disease can be prevented, and help to design drugs to treat different diseases.

These studies are on-going and will take place over the next few years. However, your participation is required only as often as you wish and for as long as you wish. The studies do not focus on any one individual.

Why have I been chosen?

Our studies require proteins or cells which are present in blood of normal people, we can only do our research with samples of 'fresh' blood. We may use some cells from blood to isolate the genes which code for the complement proteins or regulators and then we will sequence parts of these genes (and only these genes). This is called 'genotyping'. There are lots of different sequences of these genes in normal people and all individuals have two different genes for each protein, these might be different. However, if both your genes encoding for one of your complement proteins are the same, we may be particularly interested in isolating the protein from

your blood or cells –this is because all your protein will be the same and it is easier for us to understand how it 'works' if there are no small changes or variations.

If we genotype your DNA, you will be given the option to know which form of these proteins you have.

Do I have to take part?

It is up to you to decide whether or not to take part. If you do decide to take part you will be given this information sheet to keep and be asked to sign a consent form. If you decide to take part you are still free to withdraw at any time and without giving a reason.

Participation in this research will be of no direct benefit to you, the proteins isolated from your blood will help us to better understand how the complement system works and may in the long-term help us to treat people who are suffering from diseases where complement is playing a role.

What will happen to me if I take part?

Blood will be taken from a vein in your arm. This is a standard procedure which takes place in hospitals every day. There may be some minor discomfort, and there are very small risks of bruising or a local infection which can be treated.

Once we have taken your blood –that is it! All the cells and proteins will be purified in the laboratory.

What about confidentiality?

We may sequence the genes which code for your complement proteins, this 'genotyping' information will not be made available to anyone outside of the research project without your consent.

In many instances the proteins purified from your blood will form part of a large 'pool' of these proteins where no one is specifically identified and the proteins from one person are not kept separate.

What do I have to do?

All that we require is a blood sample as described above.

What will happen to the results of the research study?

The results of the research will usually be published in biochemical or immunological research journals. No individuals will be identified in these publications. In many instances the proteins purified from your blood will form part of a large 'pool' of these proteins where no one is specifically identified and the proteins form one person are not kept separate. This pool of purified protein will be stored in freezers. The donors for any given pool may vary, in these cases the publications arising from use of these pools will not be specific to any individual. However, the research publications arising from the use of these purified complement proteins will be available on-line or from the individual investigators.

Who is organising and funding the research?

The research is being carried out by members of the 'Complement Biology Group', Systems Immunity Research Institute, Division of Infection and Immunity. A basic understanding of how complement works is an ongoing aim of this research group and the research is funded by different Charities and Research Councils. This might include The Wellcome Trust, the Medical Research Council, The Arthritis Research Campaign, Alzheimer Society, The Multiple Sclerosis Society, The Wales office of Research and Development and other such funding bodies.

Contact for Further Information

Professor B Paul Morgan, Dept Medical Biochemistry and Immunology, School of Medicine. Tel: 029 20742799; Email: morganbp@cardiff.ac.uk

Medical / Dental School Research Ethics Committee

CONSENT FORM

Title of Project:

Mechanisms of complement activation and regulation.

Name of Researcher:

Prof B. Paul Morgan

Complement Biology group, Systems Immunity Research Institute, Division of Infection and Immunity, Cardiff University, School of Medicine, Henry Welcome Building, 4F02, Heath Park, Cardiff CF14 4XN, UK

Please initialise next to statement

1. I confirm that I have read and understand the information sheet on the above project (version 2) and have had the opportunity to ask questions.

2. I understand that my participation is voluntary and that I am free to withdraw at any time, without giving any reason.

3. I agree to give a sample of blood for research in the above project and I understand how the sample will be collected.

4. I would like to be informed of any genotyping research results.

5. I understand that I will not benefit financially if this research leads to the development of new treatments or tests.

6. I know how to contact the research team if I need to.

7. I agree to take part in the above study.

_____	_____	_____
Name of Participant		Date Signature

_____	_____	_____
Name of Person taking consent (if different from researcher)	Date	Signature

_____	_____	_____